UNIVERSITAT DE BARCELONA

Identification and Fate of Known and Unknown Transformation Products of Pharmaceuticals in the Aquatic System

Božo Žonja

Programa de Doctorat

"Química Analítica del Medi Ambient i la Pol.lució"

IDENTIFICATION AND FATE OF KNOWN AND UNKNOWN TRANSFORMATION PRODUCTS OF PHARMACEUTICALS IN THE AQUATIC SYSTEM

Memòria presentada per optar al grau de Doctor per la Universitat de Barcelona per

Božo Žonja

Codirectora	**Codirectora**	**Tutora**
Dra. Sandra Pérez	**Dra. Mira Petrović**	**Dra. MªTeresa Galcerán**
Investigadora Distingida Dep. de Química Ambiental, IDAEA-CSIC	Professora d'investigació ICREA ICRA	Catedràtica Emèrita Facultat de Química Universitat de Barcelona

Barcelona 2016

Mojim herojima: materi Mari Kruvarovoj, ćali Leši Žonji i Franu

To my heroes: my mother Mare, my father Lešo and Fran

Als meus herois: la meva mare Mare, el meu pare Lešo i al Fran

A mis héroes: mi madre Mare, mi padre Lešo y Fran

"I tried out various experiments described in treatises on physics and chemistry, and the results were sometimes unexpected. At times, I would be encouraged by a little unhoped-for success; at others, I would be in the deepest despair because of accidents and failures resulting from my inexperience."

"Be less curious about people and more curious about ideas."

Marie Skłodowska Curie

This thesis was financially supported principally by the European Union's 7th Framework People Programme through Marie Curie Actions Initial Training Network CSI: EVIRONMENT (Isotope forensics meets biogeochemistry - linking sources and sinks of organic contaminants by compound specific isotope investigation. Grant agreement Nº: PITN-GA-2010-264329). Additional funding was received through EU FP7 projects CYTOTHREAT (Fate and effects of cytostatic pharmaceuticals in the environment and the identification of biomarkers for and improved risk assessment on environmental exposure. Grant agreement Nº: 265264) and SOLUTIONS (SOLUTIONS for present and future emerging pollutants in land and water resources management. Grant agreement Nº: 60343). Generalitat de Catalunya support is acknowledged via Consolidated Research Groups (2014 SGR 418-Water and Soil Quality Research Group, Instituto de Diagnóstico Ambiental y Estudios del agua).

Word cloud images used several times in this manuscript were generated using Wordclouds.com.

Acknowledgements

As it turns out, acknowledgements are the last thing to do to complete the rite of passage that has become this thesis. I was often baffled with the things and details people wrote here. Hopefully, these acknowledgments will not follow the same path. To give an abstract of the text that will follow, I will try to use this space only to acknowledge many people that were important for me during my PhD.

First of all, thanks to my supervisors Sandra and Mira for the chance to join them @IDAEA, and the time invested during my PhD years.

I am especially grateful to Sandra for introducing me to the field of environmental analytical chemistry, for sharing with me her experiences, her dedication, time and patience to see this thesis come to an end.

I am very thankful to Mira for making me part of IDAEA, and for being there for all the big decisions when I needed it.

I would also like to thank Damià for giving me so many opportunities, for the confidence to pursue my PhD and "post-doc" research, and beyond. He was, and still is an incredible mentor to me.

També m'agradaria donar les gràcies a la meva tutora de la UB, Prof. Maite Galcerán pel el seu interès genuí en ajudar que aquesta tesi arribi al final. Gràcies per la comprensió, consells i comentaris que van ajudar que el manuscrit d'aquesta tesi sigui més llegible i interessant.

Thank you Miren for the confidence and the chance to start my *post-doc* without the *doc* (or even without the *pre-doc*, depending on who you ask).

Special thanks goes for my Commisió de Seguiment: doctors Cristina Ariño, Francisco Javier Santos and Javier Saurina for following my work and progress over the past years, and to the president del programa de doctorat, doctor Miquel Vidal *per les bones notícies*. Finally, big thanks to my Thesis Committee, doctors Juan Lema, Encarna Moyano and Serge Chiron for accepting to be a part of the Tribunal dels Jutges.

Big thanks to all the fellows and supervisors involved with the CSI: Environment Marie Curie ITN. I've learnt a lot, but had fun even more at our meetings. To that end, thanks to all my co-authors for sharing their knowledge in our joint efforts towards publishing our results. This goes especially to Jordi for the incredibly imaginative ideas, and to Antonio D for his persistent patience and effectiveness. One day I might even learn the basics of organic chemistry.

Gracias a las lectoras lingüísticas de esta tesis; a la castellana Cristina i a la catalana Alicia.

Thanks to Antoni G for the brainstorming talks during coffee time.

Gracias a toda la administración del CID, tantas cosas durante la tesis fueron más fáciles gracias a su ayuda y apoyo.

Gracias sobre todo a tod@s l@s compañer@s del trabajo, mis Yugo-Barcelonin(a)s i prijatelji(ca)ma i familiji na Balkanu. Antes que todo tengo que decir (y agradecer) que, en todo el tiempo en Barcelona, nunca me he sentido como un extranjero (bueno, solo en las épocas de la incomprensible manía con la lotería de navidad). Siguiente, tengo que decir que me cuesta imaginar (empezar) un día al CSIC sin los *coffee breaks* y *piti breaks* con Àngels y Elena (a veces con Marinel.la también, cuando no anda por el mundo), acompañado con las conversaciones sobre el tiempo y la humedad, con las quejas de siempre y con risas. Después de la tesis, espero que continuaremos solo con los *coffee breaks* porque ya nos hacemos mayores y hay que cuidarse.

Seguramente esta tesis no se hubiera podido acabar sin la ayuda y paciencia de todos los amigos y compañeros de laboratorio. Agradezco, sobre todo, a los elefantes porque me enseñaron todo y a los no-tan elefantes por el buen rollo y por entender mis *nervios* en los últimos meses antes del depósito. Algunos se marcharon (Aleksandra, Paquislava, Kike, Vicky, Dani G, Giselle y much@s más), otros por los menos

los veo en vez en cuando (menos mal) (Jaume, Nicola, Cayo, Pablo y much@s más) pero muchos siguen en el CSIC (Cristina, Alicia, Josep, Marta, Marianne, Laia, Mar, y los no-tan elefantes - Danis, Alex, Cris B, Gabriella, Juan, Òscar, Simon, JCarlos, M.Pau, Ester, Micha, y much@s más. Majo, srića da skupa možemo grintati o svemu. Finalment, no puc acabar sense donar les gràcies a Roser y Dori, por siempre tener la puerta abierta.

Budući da Katalunja postaje glavno odredište znanstvenog gastarbajterstva (Balkan uključivo), nije nedostajalo porodice. Ne znam jel bi triba reći fala ili šta, jedino ća mogu reći je da ne mogu zamisliti Barćelonu sad i prije bez: Frana, Marka i Melanije (oni su bili stina), priko Petre, Antonije, Eve i Matije do Ane-Marije.

Na kraju oću iskoristit ovu priliku više od zahvale da se ispričan svima koje san zbog, em odlaska, em doktorata zapostavija (al ne zaboravija). Ima ih mnogo, al to su prije svega Matićka (sad i Boki), Žonjislava i Ivanica. Rodbinsko okupljanje uključeno, narafski.

Na kraju najvažnije, fala mojoj familiji, mojim roditeljsima, i sestri Miki, koji su u svakom trenu bili tu da uskoče di i kad triba. Fala van ća ste takvi kakvi jeste, jer bez vas ništa od ovog ne bi bilo moguće.

Add: I would like to apologise to anyone who felt left out. Surely, I can do a more proper *thank you* in person, with coffee or vino tinto.

Plus, I am no longer baffled.

Table of Contents


TPs
surface
human
identification
suspect
water
samples
photo
LMG-N2-G
hydrolysis
experiments
approach
showed
detection
screening
detected
concentration
profiling
metabolites
WWTPs
ZAN
degradation
OXO-LMG
wastewater
However
formed
sunlight
mass
batch
result
antiviral
structures
frequency
lab-scale
HRMS
neutral
products
three
transformed
following
found
stability
synthetic
median
environment
higher
performed
kinetics
reactors
chapter
parent
body
using
high
effluent
concentrations
Finally
media
elimination
properties
natural
relevant
days
time
related
combination
degraded
designed
simulated
suggesting
contrast
order
four
real
reaction
due
directly
amidine
deiodination
abiotic
Since
used
eleven
screened
depends
important
N2-glucuronide

Abstract

Pharmaceuticals which are used worldwide are designed to facilitate the life for the human society and have an important role in treatment and prevention of disease for both humans and animals. They are ubiquitous in the aquatic environment and are mainly derived from municipal wastewater treatment plants (WWTPs) due to their low removal rate. Therefore, their presence in the environment is directly linked to the human impact. Various biological and abiotic processes in the environment can transform them to transformation products (TPs). In many cases, transformation is already initiated in the human body by a variety of drug-metabolizing enzymes. The metabolites formed through human metabolism present some modifications in their chemical structures that can differ in physicochemical properties to their parent compound. Once they are excreted from the human body, both the unmetabolised parent drug and their metabolites enter WWTPs by means of the sewer system. Since the WWTPs are not designed to remove completely pharmaceutical residues, the fraction not removed after the treatment will eventually end up in the receiving water bodies. Consequently, due to pharmaceutical transformations in the human body, biotransformations in WWTPs and phototransformations in surface water, they can potentially produce a high number of TPs in real world samples which makes their identification a challenge.

In this thesis, two different approaches (TPs profiling and suspect screening) based on high resolution mass spectrometry (HRMS) for the detection and identification of TPs of pharmaceuticals were investigated. TPs profiling approach was applied for the identification of phototransformation products of an antiviral zanamivir (ZAN) in batch reactors filled with surface water. On the other hand, suspect screening approach was applied for evaluation of transformation, prioritization and identification of photoTPs of six iodinated contrast media in surface water. Finally, a combination of suspect and TPs profiling approach was applied for the detection of TPs of an anticonvulsant lamotrigine and its main human metabolite lamotrigine N2-glucuronide which were formed as the result of their degradation in both activated sludge and pH dependent hydrolysis.

The TPs profiling approach for evaluation of these transformations is illustrated in the example of photodegradation of an antiviral ZAN with identification of its TPs in surface water (Chapter 3.). Here a set of lab-scale experiments was performed in order to determine

the susceptibility of ZAN towards photodegradation under simulated and natural sunlight. The identification of the TPs was performed using hydrophilic interaction liquid chromatography coupled to high resolution mass spectrometry (HILIC-HRMS) where four photoTPs were tentatively identified and their proposed structures were rationalized by photolysis mechanisms. Kinetic experiments showed that photodegradation kinetics of ZAN in surface waters would proceed with slow kinetics since upon exposure of aqueous solutions of surface water (20 μg L^{-1}) to simulated sunlight, ZAN was degraded with $t_{1/2}$ of 3.6 h. Under natural sunlight irradiating surface water, about 30 % of the initial concentration of the antiviral disappeared within 18 days. However, when ZAN and its TPs were retrospectively screened from surface water extracts, neither the parent nor the TPs were detected. The results of this TP profiling used for the identification of TPs of ZAN, although straightforward, suggests that it is not suitable when dealing with a considerably elevated number of TPs formed in batch experiments.

However, time and effort needed to be optimised for the structure elucidation of 108 photoTPs of six iodinated contrast media (ICM) (Chapter 3.). Again, the photodegradation study was performed in surface water spiked with the ICMs using a sunlight lab-scale simulator. 108 TPs were generated and each photoTP was characterised by its unique exact mass of the molecular ion and retention time and added to a suspect list. Once the suspect list was generated, the photoTPs were searched in thirteen surface water samples which were extracted using a generic solid-phase extraction method (four cartridges of different chemistries in order to retain ample number of compounds with different chemical properties). Based on their detection frequency (those TPs with the frequency higher than 50 % were deemed important), eleven TPs were prioritized and their structures elucidated by HRMS and NMR (when possible). Out of the eleven prioritised TPs, ten were formed as the result of deiodination (either by deiodination, oxidative deiodination or intramolecular elimination). In the real surface water samples, median concentration of parent compounds was 110 ngL^{-1} reaching up to 6 μgL^{-1} for iomeprol while TPs were found at median concentration of 8 ngL^{-1}, reaching up to 0.4 μgL^{-1} for iomeprol TP651-B. Here detection-based prioritization served as a crucial step to reduce the number of TPs to be identified and thereby reducing costs and time for the subsequent target analysis. This time-effective approach not only guaranties that the degradation products elucidated would be found, but also that they are environmentally relevant. In summary, the proposed screening approach facilitates the evaluation of the degradation of polar compounds at a real scale with a fast detection of TPs without prior availability of the standards.

Approach used for detection and identification of TPs of ICM in Chapter 3 was an example of suspect screening where the suspect list of TPs was generated at lab-scale, In Chapter 4, the work started with a suspect screening of lamotrigine (LMG) and related compounds (its human metabolites, synthetic impurities and photoTPs) which were listed from the literature and searched in wastewater and surface water samples. As the result of suspect screening, LMG, three human metabolites and a LMG synthetic impurity (OXO-LMG) were detected in the screened samples. Preliminary results showed significantly higher concentrations of OXO-LMG in wastewater effluent, suggesting its formation in the WWTPs. However, biodegradation reactors amended with mixed liquor at neutral pH showed that LMG is resistant to biodegradation with only about 5 % elimination after 6 days. Since LMG is extensively and predominantly metabolised by phase II metabolism to its N2-glucuronide, this metabolite (LMG-N2-G) was degraded following the same experimental setup. Results showed that this metabolite was the actual source of the TP detected. Additionally, in batch experiments, LMG-N2-G was transformed, following pseudo-first kinetics, to three TPs as a result of i) deconjugation (to LMG), ii) oxidation of the glucuronic acid (to LMG-N2-G-TP430) and iii) amidine hydrolysis in combination with deconjugation (to OXO-LMG). In order to further rationalize the formation of the TP OXO-LMG, the stability of LMG-N2-G and related compounds was studied as a function of pH in the range of 4 – 9. Same as during biodegradation, LMG was stable across the entire pH range tested. However, LMG-N2-G was transformed to three TPs at neutral – basic pH. They were identified as TPs formed after hydrolysis of amidine and guanidine moieties. The third TP detected was an intermediated in the guanidine hydrolysis reaction. Kinetic experiments in wastewater samples at different concentration (20 and 200 nM) and pH (pH 6.5, 7, 8, 8.5 and 9) demonstrated that while the degradation constants were concentration independent, at higher pH, LMG-N2-G degraded at higher rate. The pH-dependent stability experiments of related compounds with different nitrogen N2-substituents on the 1,2,4-triazine ring showed that reaction of amidine and guanidine hydrolysis depends on imine tautomer equilibrium whose formation depends directly on the N2-supsitutent. LMG-N2-G major abiotic TP (amidine hydrolysis TP) was detected in hospital effluent and WWTP influent samples. Having in mind the concentrations of both biotic and abiotic TPs detected, a total mass balance at two-concentration levels batch reactors was closed at 86% and 102%, respectively. In three WWTPs total mass balance of LMG-N2-G ranged from 71-102%. Finally, LMG-N2-G and its TPs were detected in surface water samples with median concentration ranges of 23–186 ngL^{-1}. The work presented in this chapter gives a new insight into the behaviour of glucuronides of pharmaceuticals, suggesting that they might also be sources of yet undiscovered, but environmentally relevant TPs.

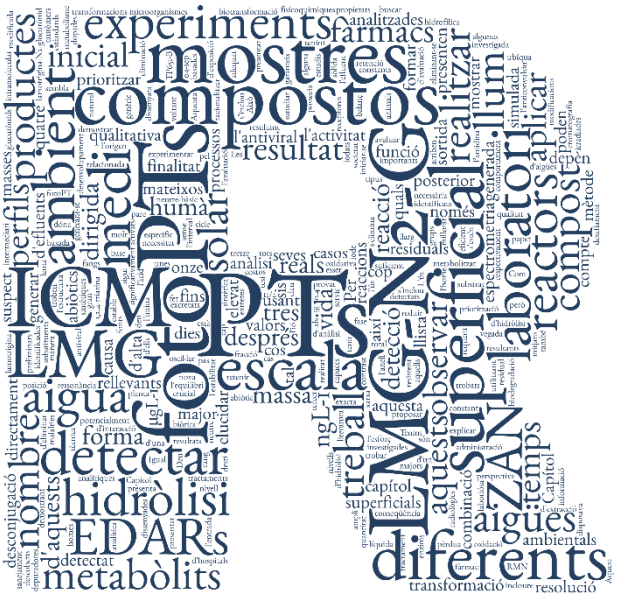
Resum

Els productes farmacèutics, l'ús dels quals s'estén a nivell mundial, estan dissenyats per millorar la qualitat de vida de la societat i juguen un paper clau en el tractament i la prevenció de malalties, tant en homes com en animals. Aquests compostos químics es troben de forma ubíqua en el medi ambient. Això es deu principalment a les estacions depuradores d'aigua residual (EDARs), les quals no són capaces d'eliminar de manera eficient aquest tipus de compostos, ja que no estan dissenyades amb aquesta finalitat. Per tant, la presència de fàrmacs en el medi ambient està directament relacionada amb l'activitat humana. Un cop al medi ambient, l'estructura d'aquests compostos pot ser modificada per diferents processos biològics i abiòtics, generant-se així els que es coneixen com a productes de transformació (PTs). De fet, la transformació dels fàrmacs pot iniciar-se en alguns casos en el cos humà, després de la seva administració a causa de l'activitat metabòlica dels diferents enzims que posseeix l'home. Els metabòlits formats en aquests processos presenten algunes modificacions en les seves estructures químiques pel que fa al compost original, i, en conseqüència, unes propietats fisicoquímiques diferents. Un cop excretats, tant el fàrmac original no metabolitzat com els seus metabòlits arriben a les EDARs mitjançant la xarxa de sanejament municipal d'aigües residuals. La fracció d'aquests compostos que no s'elimina en els diferents tractaments realitzats en l'EDAR, es descarrega juntament amb l'efluent de la planta als aigües receptores. El gran nombre de transformacions que poden experimentar els fàrmacs en el seu cicle de vida a causa del seu metabolisme en el cos humà, la seva biotransformació per microorganismes i la seva fototransformació per llum solar, pot generar un nombre molt elevat de PTs en el medi ambient, i, per tant, la identificació dels mateixos, necessària per avaluar el destí dels fàrmacs en el medi ambient, és un desafiament.

En el desenvolupament d'aquesta tesi es van aplicar dues aproximacions analítiques diferents: a)avaluació de perfils de PTs generats en experiments a escala de laboratori i b) anàlisi qualitativa dirigida *suspect screening* en mostres reals, tots dues basades en espectrometria de masses d'alta resolució (HRMS) per a la detecció i identificació de PTs de productes farmacèutics. L'aproximació d'avaluació de perfils de PTs en reactors a escala de laboratori es va aplicar per identificar productes de fototransformació (fotoPTs) de l'antiviral zanamivir (ZAN) en aigua superficial. L'aproximació de *suspect screening* es va aplicar per prioritzar i

identificar fotoPTs de sis mitjans de contrast radiològics iodats (ICM) en aigua superficial. Finalment, una combinació de les dues aproximacions es va aplicar per detectar PTs de l'anticonvulsiu lamotrigina (LMG) i del seu principal metabòlit humà, el lamotrigina-N2-glucurònid (LMG-N2-G), resultants de la seva degradació tant en fangs activats com a reaccions d'hidròlisi a diferents valors de pH.

En el Capítol 3 s'inclou la fotodegradació mitjançant llum solar natural i simulada de l'antiviral ZAN en aigua superficial evaluada amb els perfils de PTs obtinguts a partir de reactors a escala de laborator. La identificació dels fotoPTs es va realitzar mitjançant cromatografia líquida d'interacció hidrofílica acoblada a espectrometria de masses d'alta resolució (HILIC-HRMS). D'acord amb la informació generada amb aquesta tècnica analítica i tenint en compte les reaccions fotoquímiques identificades es van proposar estructures químiques temptatives per a quatre fotoPTs de ZAN. D'acord amb els experiments realitzats, ZAN es fotodegrada de forma lenta en aigües superficials. En aigua superficial irradiada amb llum solar simulada ZAN va presentar un temps de vida mitjana ($t_{1/2}$) de 3,6 h. No obstant això, en aigua superficial irradiada amb llum solar la concentració d'aquest antiviral només va disminuir al voltant d'un 30 % després de 18 dies d'exposició. La presència de ZAN i dels seus fotoPTs identificats va esser investigada posteriorment en mostres reals d'aigua superficial, però cap d'ells va ser detectat en les mostres analitzades. L'ús de l'aproximació de perfils de PTs formats en reactors a escala de laboratori, encara que és una aproximació simple, és laboriósa, i per tant, no sembla ser el mètode més adequat en aquells casos en els que el compost pare forma un nombre elevat de PTs.

En el treball posterior, el temps i l'esforç es van optimitzar per elucidar les estructures dels fotoPTs de sis ICM (Capítol 3). Una vegada més, els estudis de fotodegradació es van realitzar en aigua superficial dopades amb els ICM usant un simulador de llum solar. En les aigües irradiades es van detectar fins a 108 fotoPTs. La massa exacta de l'ió molecular i el temps de retenció específic de cada fotoPTs es van incloure en una llista de compostos amb la finalitat de buscar aquests compostos en tretze mostres d'aigua superficial extretes utilitzant un mètode genèric d'extracció en fase sòlida (usant quatre sorbents diferents per tal de retenir un ampli nombre de compostos). Es van prioritzar fins a onze fotoPTs en funció de la seva freqüència de detecció en les mostres (importants> 50%), i les seves estructures es van elucidar mitjançant HRMS i ressonància magnètica (RMN) (si es disposava d'una quantitat suficient). Deu d'aquests onze fotoPTs es van formar com a resultat de la pèrdua de iode (ja sigui per desiodació, desiodació oxidativa o eliminació intramolecular). Els ICM i els fotoPTs es van detectar a una concentració (mediana) de 110 ngL^{-1} i 8 ngL^{-1}, respectivament. Els valors màxims es van observar per omeprol (6 μgL-1) i el seu fotoPT iomeprol TP651-B (0.4

μgL^{-1}). En aquest cas, la priorització basada en la detecció va servir com un pas crucial per reduir el nombre de PTs a identificar, reduint així els costos i el temps de treball requerit per realitzar la posterior anàlisi dirigida. Aquesta aproximació garanteix la identificació de PTs rellevants per al medi ambient, i l'avaluació dels mateixos en mostres reals sense necessitat de tenir estàndards.

El treball del Capitol 3 és un exemple d'anàlisi qualitativa dirigida de fotoPTs en mostres ambientals a partir d' una llista de fotoPTs generada en base a experiments realitzats a escala de laboratori. En el capítol 4, s'inclou un treball que presenta una aproximació per detectar PTs de la LMG en mostres ambientals (aigües residuals i superficials) a partir de compostos relacionats trobats en la literatura (metabòlits humans, impureses sintètiques i fotoPTs). Com a resultat, es van detectar en les mostres analitzades el compost original LMG, tres metabòlits humans i una impuresa sintètica de la LMG (OXO-LMG). Els resultats preliminars apuntaven a la formació d'OXO-LMG a les EDARs, ja que es van trobar concentracions d'aquest compost significativament majors a la sortida que a l'entrada de les EDARs investigades. No obstant això, experiments a escala de laboratori amb reactors biològics a pH neutre amb LMG i el seu principal producte metabòlic, LMG-N2-G, van mostrar que la LMG és resistent a la biodegradació (eliminant-se només un 5 % de la concentració inicial després de 6 dies) i que el LMG-N2-G era en realitat l'origen de la OXO-LMG detectada a la sortida de les EDARs. En aquests experiments a escala laboratori, es va observar la generació de tres PTs a partir del LMG-N2-G, com a resultat de i) desconjugació (formant LMG), ii) oxidació de l'àcid glucurònic (formant LMG-N2-G - TP430) i iii) hidròlisi d'amidina en combinació amb desconjugació (formant OXO-LMG). Per tal de racionalitzar encara més la formació del PT OXO-LMG, es va estudiar l'estabilitat del LMG-N2-G i dels compostos relacionats en funció del valor de pH (en l'interval de 4-9). Igual que es va observar en els reactors biològics, la concentració de LMG es va mantenir estable al llarg del rang de pH provat. No obstant això, es van generar 3 PTs del LMG-N2-G a pH neutre-bàsic. Aquests PTs es van formar com a resultat de la hidròlisi dels grups amidina i guanidina. El tercer PT detectat va ser un intermediari en la reacció de la hidròlisi de la guanidina. Les constants de degradació per hidròlisi es van mostrar independents de la concentració inicial del compost original. No obstant això, a major pH, es va observar una major constant de reacció de degradació de LMG-N2-G. També es van realitzar experiments d' hidròlisi amb compostos relacionats que presenten diferents substituents en la posició N2 de l'anell 1,2,4-triazina. Aquest experiment va demostrar que la reacció d'hidròlisi d'amidina i guanidina depèn de l'equilibri dels tautòmers de l'imina, i la seva formació depèn directament del substrat N2. En mostres d'efluents d'hospitals i d'efluents d'EDAR es va detectar el PT abiòtic principal de LMG-N2-G (resultant de la hidròlisi de l'amidina). Tenint en compte les

concentracions dels PTs biòtics i abiòtics detectats, es va realitzar un balanç total de massa a dos nivells de concentració en reactors a escala de laboratori, obtenint un 86 % i un 102 % de la concentració inicial i en tres EDARs, on es va aconseguir explicar entre 71-102% de la massa inicial del LMG-N2-G. Finalment, LMG-N2-G i els seus PTs es van detectar en mostres d'aigua superficial amb concentracions (medianes) que van oscil·lar entre 23 i 186 ngL^{-1}. El treball presentat en aquest capítol dóna una nova perspectiva sobre el comportament dels metabòlits glucurònids dels productes farmacèutics en aigües mediambientals, demostrant que aquests compostos també poden ser fonts de PTs encara no descoberts, i potencialment rellevants per al medi ambient.


LMG-N2G
compuestos
concentración
foto
agua
muestras
reactores
medio
ambiente
productos
identificación
EDARs
aguas
laboratorio
metabolitos
estructuras
número
inicial
forma
antiviral
enfoque
escala
estos
partir
perfiles
detectaron
OXO-LMG
concentraciones
relacionados
farmacéuticos
reacción
fototransformación

Resumen

Los productos farmacéuticos, cuyo uso se extiende a nivel mundial, están diseñados para mejorar la calidad de vida de la sociedad y juegan un papel clave en el tratamiento y la prevención de enfermedades tanto en hombres como en animales. Estos compuestos químicos se encuentran de forma ubicua en el medio ambiente. Esto se debe principalmente a las estaciones depuradoras de agua residual (EDARs), las cuales no son capaces de eliminar de manera eficiente este tipo de compuestos, ya que no fueron diseñadas para este fin. Por lo tanto, la presencia de fármacos en el medio ambiente está directamente relacionada a la actividad humana. Una vez en el medio, la estructura de estos compuestos puede ser modificada por diferentes procesos biológicos y abióticos, generándose así lo que se conoce como productos de transformación (PTs). De hecho, la transformación de los fármacos puede iniciarse en algunos casos en el cuerpo humano después de su administración debido a la actividad metabólica de los diferentes enzimas que posee el hombre. Los metabolitos formados en estos procesos presentan algunas modificaciones en sus estructuras químicas con respecto al compuesto original, y, en consecuencia, unas propiedades fisicoquímicas diferentes. Una vez excretados, tanto el fármaco original no metabolizado como sus metabolitos llegan a las EDARs mediante la red de saneamiento municipal de aguas residuales. La fracción de estos compuestos que no se elimina en los diferentes tratamientos realizados en la EDAR, se descarga junto con el efluente de la planta en las aguas receptoras. El gran número de transformaciones que pueden experimentar los fármacos en su ciclo de vida debido a su metabolismo en el cuerpo humano, su biotransformación por microorganismos y su fototransformación por luz solar, puede generar un número muy elevado de PTs en el medio ambiente, y, por lo tanto, la identificación de los mismos, necesaria para evaluar el destino de los fármacos en el medio ambiente, es un desafío.

En el desarrollo de esta tesis se aplicaron dos enfoques analíticos diferentes (evaluación de perfiles de PTs generados en experimentos a escala de laboratorio y análisis cualitativo dirigido *suspect screening* en muestras reales) basados en espectrometría de masas de alta resolución (HRMS) para la detección e identificación de PTs de productos farmacéuticos. El enfoque de evaluación de perfiles de PTs en reactores a escala de laboratorio se aplicó para identificar productos de fototransformación (fotoPTs) del antiviral zanamivir (ZAN) en agua

superficial. El enfoque de *suspect screening* se aplicó para priorizar e identificar fotoPTs de seis medios de contraste radiológicos yodados (ICM) en agua superficial. Finalmente, una combinación de ambos enfoques se aplicó para detectar PTs del anticonvulsivo lamotrigina (LMG) y de su principal metabolito humano, el lamotrigina-N^2-glucurónido (LMG-N2-G), resultantes de su degradación tanto en lodos activados como en reacciones de hidrólisis a diferentes valores de pH.

La fotodegradación mediante luz solar natural y simulada del antiviral ZAN en agua superficial investigada a partir de los perfiles de PTs obtenidos a partir de reactores a escala de laboratorio se incluye en el Capítulo 3. La identificación de los fotoPTs se realizó mediante cromatografía líquida de interacción hidrofílica acoplada a espectrometría de masas de alta resolución (HILIC-HRMS). En base a la información generada con esta técnica analítica y teniendo en cuenta las reacciones fotoquímicas que pudieron acontecer se propusieron estructuras químicas de forma tentativa para cuatro fotoPTs de ZAN. De acuerdo a los experimentos realizados, ZAN se fotodegrada en aguas superficiales de forma lenta. En agua superficial irradiada con luz solar simulada ZAN presentó un tiempo de vida media ($t_{1/2}$) de 3,6 h. Sin embargo, en agua superficial irradiada con luz solar la concentración de este antiviral sólo disminuyó alrededor de un 30 % después de 18 días de exposición. La presencia de ZAN y de los fotoPTs identificados fue investigada posteriormente en muestras reales de agua superficial, pero ninguno de ellos fue detectado en las muestras analizadas. El uso de perfiles de PTs formados en reactores a escala de laboratorio, aunque es un enfoque simple, es laborioso, y por lo tanto, no parece ser el método más adecuado en casos cuando el compuesto padre forma un número elevado de los PTs.

En el trabajo posterior, el tiempo y el esfuerzo se optimizaron para elucidar las estructuras de los fotoPTs de seis ICM (Capítulo 3). Una vez más, los estudios de fotodegradación se realizaron en agua superficial fortificadas con los ICM usando un simulador de la luz solar. En las aguas irradiadas se detectaron hasta 108 fotoPTs. La masa exacta del ion molecular y el tiempo de retención especifico de cada fotoPTs se incluyeron en una lista de compuestos con el fin de buscar estos compuestos en trece muestras de agua superficial extraídas utilizando un método genérico de extracción en fase sólida (usando cuatro sorbentes diferentes con el fin de retener un amplio número de compuestos). Se priorizaron hasta once fotoPTs en función de su frecuencia de detección en las muestras (importantes>50%), y sus estructuras se elucidaron mediante HRMS y resonancia mágnética (RMN) (si se disponía de una cantidad suficiente). Diez de estos once fotoPTs se formaron como resultado de la pérdida de yodo (ya sea por desyodación, desyodación oxidativa o eliminación intramolecular). Los ICM y los fotoPTs se detectaron a una concentración (mediana) de 110

ngL^{-1} y 8 ngL^{-1}, respectivamente. Los valores máximos se observaron para iomeprol (6 μgL^{-1}) y su fotoPT iomeprol TP651-B (0.4 μgL^{-1}). En este caso, la priorización basada en la detección sirvió como un paso crucial para reducir el número de PTs a identificar, reduciendo así los costes y el tiempo de trabajo requerido para realizar el posterior análisis dirigido. Este enfoque garantiza la identificación de PTs relevantes para el medio ambiente, y la evaluación de los mismos en muestras reales sin necesidad de tener estándares.

El anterior trabajo, es un ejemplo de análisis cualitativo dirigido de fotoPTs en muestras ambientales usando una lista de fotoPTs generada a partir de experimentos realizados a escala de laboratorio. En el Capítulo 4, se incluye un trabajo que presenta un enfoque para detectar PTs de la LMG en muestras ambientales (aguas residuales y superficiales) a partir de compuestos relacionados encontrados en la literatura (metabolitos humanos, impurezas sintéticas y fotoPTs). Como resultado, se detectaron en las muestras analizadas el compuesto original LMG, tres metabolitos humanos y una impureza sintética de la LMG (OXO-LMG). Los resultados preliminares apuntaban a la formación de OXO-LMG en las EDARs, ya que se encontraron concentraciones de este compuesto significativamente mayores a la salida que a la entrada de las EDARs investigadas. Sin embargo, experimentos a escala de laboratorio con reactores biológicos a pH neutro con LMG y su principal producto metabólico, LMG-N2-G, mostraron que la LMG es resistente a la biodegradación (eliminándose sólo un 5% de la concentración inicial después de 6 días) y que el LMG-N2-G era en realidad el origen de la OXO-LMG detectada a la salida de las EDARs. En estos experimentos a escala laboratorio, se observó la generación de tres PTs a partir del LMG-N2-G, como resultado de i) desconjugación (formando LMG), ii) oxidación del ácido glucurónico (formando LMG-N2-G - TP430) y iii) hidrólisis de amidina en combinación con desconjugación (formando OXO-LMG). Con el fin de racionalizar aún más la formación del PT OXO-LMG, se estudió la estabilidad del LMG-N2-G y compuestos relacionados en función del valor de pH (en el intervalo de 4 - 9). Al igual que se observó en los reactores biológicos, la concentración de LMG se mantuvo estable a lo largo del rango de pH probado. Sin embargo, se generaron tres PTs del LMG-N2-G a pH neutro-básico. Estos PTs se formaron como resultado del hidrólisis de los grupos amidina y guanidina. El tercer PT detectado fue un intermediario en la reacción de hidrólisis de la guanidina. Las constantes de degradación por hidrólisis se mostraron independientes la concentración inicial del compuesto original. Sin embargo, a mayor pH, se observó una mayor constante de reacción de degradación de LMG-N2-G. Se realizaron experimentos de hidrólisis también con compuestos relacionados que presentan diferentes sustituyentes en la posición N2 del anillo 1,2,4-triazina. Este experimento demostró que la reacción de hidrólisis de amidina y guanidina depende del equilibrio de los tautómeros de la imina, cuya formación depende directamente del sustrato N2. En muestras

de efluentes de hospitales y de efluentes de EDARs se detectó el PT abiótico principal de LMG-N2-G (resultante del hidrólisis de la amidina). Teniendo en cuenta las concentraciones de los PTs bióticos y abióticos detectados, se realizó un balance total de masa a dos niveles de concentración en reactores a escala de laboratorio, obteniéndose un 86% y un 102% de la concentración inicial y en tres EDARs, donde se consiguió explicar entre 71-102% de la masa inicial del LMG-N2-G. Finalmente, LMG-N2-G y sus PTs se detectaron en muestras de agua superficial con concentraciones (medianas) que oscilaron entre 23 y 186 ngL^{-1}. El trabajo presentado en este capítulo da una nueva perspectiva sobre el comportamiento de los metabolitos glucurónidos de los productos farmacéuticos en aguas medioambientales, demostrando que estos compuestos también pueden ser fuentes de PTs aún no descubiertos, y potencialmente relevantes para el medio ambiente.

Chapter 1. Introduction

1.1. Pharmaceuticals and their transformation products in the aquatic environment

More than 30,000 synthetic chemical substances are in wide commercial use and their production and use have exponentially increased in modern societies due to demographic, social and economic factors (Howard and Muir 2010). Pharmaceuticals and other chemicals used worldwide are designed to facilitate the life for the human society. There are more than 10,000 prescriptions and over-the-counter pharmaceuticals with more than 1,300 unique active ingredients registered and approved for usage (FDA 2016a). Consumption of pharmaceuticals is typically given as Defined Daily Dose (DDD) unit, as recommended by the World Health Organisation (WHO). Although this number is an estimate, still it is independent of price and dosage forms. **Figure 1.1.** shows DDD per 1,000 inhabitants in Spain which has constantly grow up until 2009. and thereafter has been set at 230 DDD/1,000 inhabitants. On a global scale, global medicines doses consumption is expected to grow in most world regions (**Figure 1.2.**).

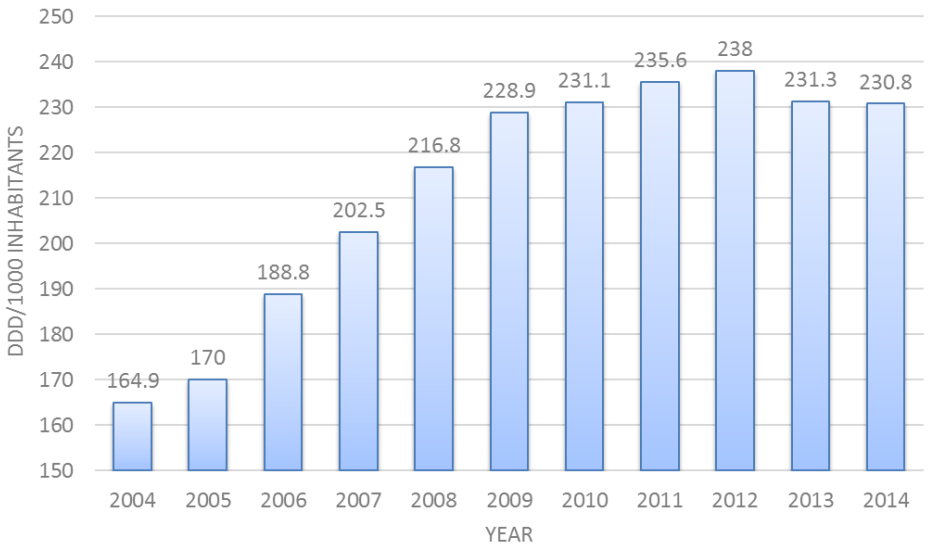

Figure 1.1. Consumption of alimentary tract and metabolism pharmaceuticals per 1,000 inhabitants per day in Spain from 2004 to 2014. Source of the data: OECD (OECD 2016) and Statista (Statista 2016).

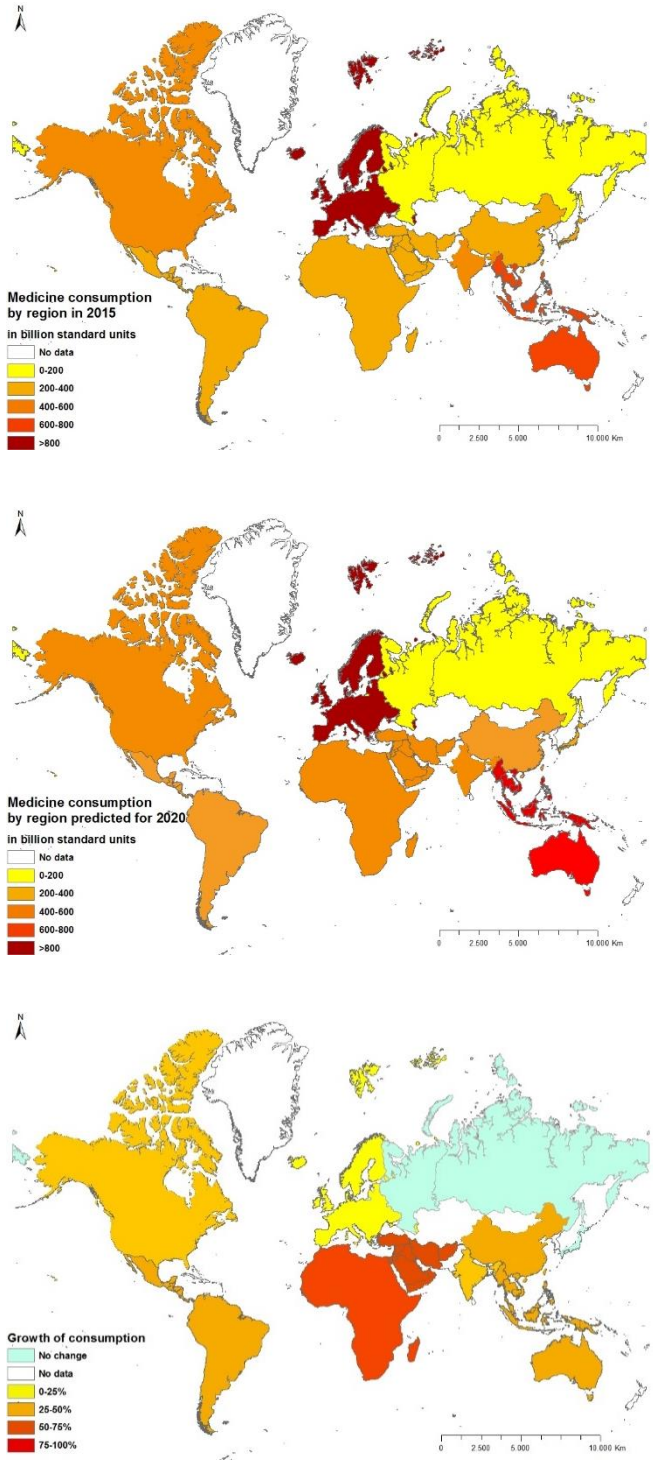

Figure 1.2. Global medicines doses consumption by world regions in 2015 and 2020 forecast. Source of the data: IMS Health (IMSHealth 2015) and Statista (Statista 2016).

Occurrence of pharmaceutical residues in the environment as a consequence of human or animal treatment is of major concern due to their inherent pharmacological activity and their continuous discharge into the aquatic environment (Barceló and Petrovic 2007, Ternes 1998). Their presence can produce unforeseen adverse or even deleterious effects on human health and environment. Due to the advances in the sensitivity and selectivity of analytical instrumentation a variety of previously not monitored chemicals have been detected in many environmental compartments (Zonja et al. 2014a). Pharmaceuticals are only one of the classes of the organic micro-pollutant chemicals, the so-called pollutants of emerging contaminates (ECs). This term encompasses a wide group of contaminants such as brominated flame retardants, drugs of abuse and their metabolites, hormones and other endocrine disrupting compounds, nanomaterials, organophosphate flame-retardant, plasticizers, perfluorinated compounds, polar pesticides and - pharmaceuticals and personal care products.

Although there is a recognized public and scientific concern regarding the presence and chronical exposure to drug residues in the environment, less attention was focused on the

evaluation of their transformation. These chemicals additionally have the potential to be transformed through various processes and the formed transformation products (TPs) can be more mobile, polar and toxic than the parent compound. In case of bioactive compounds their effect can be retained because the pharmaceutically active part of the molecule can remain unmodified. The transformation of pharmaceuticals in most cases starts in the human body where they are metabolized via phase I. or phase II. metabolism. These metabolites are typically more polar than their parent compound in order to be excreted via urine of faeces. The extent of metabolism defers between different pharmaceuticals and the metabolites can make a large fraction in the total mass balance of the administered drug. On the other hand, other pharmaceuticals are less prone to metabolic clearance and are typically excreted unchanged (Kasprzyk-Hordern et al. 2008, Upton et al. 1980). Recently, a new approach into the design of pharmaceuticals was suggested by Rastogi et al. (Rastogi et al. 2015). This approach was shown on the examples of propranolol, a beta blocker, and takes into an account the environmental degradability of a compound versus its pharmacological activity in order to ensure environmental attenuation (Rastogi et al. 2015). They generated new derivatives of the compound with photolysis and the ones whose drug moieties were intact were screened for both aerobic degradability and pharmacological potency. From the compounds detected, they found that a hydroxylated derivative of propranolol (4-OH-propranolol) maintained pharmacological activity but was completely degraded in a closed-bottle test (CBT) after 28 days making it more environmentally friendly that the original parent compound (propranolol), which did not degrade (Rastogi et al. 2015).

As said previously, the term transformation products (TPs) in general is applied to structurally related, but modified compounds that were changed (transformed) in some sort of a natural or engineered process. For pharmaceuticals, in the aquatic system we can classify the presence and modification of TPs considering either i) type of transformation or ii) the site where the transformation is occurring. For the type of transformation process, typically is divided into two groups: a) biotic and b) abiotic. Biotic transformations are typically reactions of human metabolism and microbial degradation. On the other hand, abiotic reactions can range from hydrolysis, reduction, chemical degradation (like chlorination) to oxidation (like ozonation and advanced oxidation processes) and photolysis (natural or simulated – photocatalisys). Apart from the type of transformation, we can categorize transformation according to site were a compound can undergo those modifications. In

general, they could be classified into a) natural systems or b) engineered systems. Natural systems are sites like human body, water bodies (lakes, rivers, oceans) or land bodies (soil, sediment). Contrary to the natural systems, engineered systems are systems where a certain treatment can provoke transformations. Most known systems include waste water treatment plants (WWTPs) or waterworks (like tap water production facilities). All these possible transformation types and sites lead to complex mixtures of parent compounds and their TPs that are present in the aquatic environment. These modifications are still poorly characterized; however, a lot of effort has been made toward their characterization and identification in recent years. Detailed and current status of the TPs research can be found in the following introductory chapters of this thesis.

1.2. Formation of transformation products through (bio)chemical processes

The following chapter will address the more recent examples of batch studies which had an aim to identify the TPs forming from both abiotic and biotic processes, simulating real conditions that can be encountered in the environment. In the section of abiotic transformations, different chemical degradations will be discussed like chemical hydrolysis, chlorination reactions, advanced oxidation (reduction) processes and photodegradation under both natural and simulated sunlight. The subsequent section will cover the most important biological processes that can transform pharmaceutical compounds in the environment, starting with the metabolism in the human body and microbial transformations in WWTPs. For each of the degradation processes, a brief description will be given with the special emphasis on the phototranformation under natural sunlight in surface water and microbial biodegradation during activated sludge treatment in WWTPs. Special emphasis has been given describe and discuss the different reaction types and pathways of both of these processes which were addressed in a separate chapter, respectively, and supported with tables summarising the current knowledge on the subject.

1.2.1. Abiotic Transformations

Chemical hydrolysis

Chemical hydrolysis is one of the major reactions that can transform organic contaminants in the aquatic environment because water is a ubiquitous reactant in the environment that can initiate consecutive reactions (Hirte et al. 2016). Although hydrolysis happens as the function of pH and temperature, other substances present in the real environment like dissolved organic matter or metals can influence the hydrolysis of organic contaminants in the aqueous systems (Macalady et al. 1988, Noblet et al. 1996, Whitacre 2012). Molecular structures of many pharmaceuticals contain hydrolysable functional groups like ester, amide, imide and halogens which are involved in the hydrolytic degradation (Zhang et al. 2015). These hydrolysable groups are especially frequent in many classes of antibiotics and cytostatic drugs like vinca alkaloids. Perhaps the most comprehensive and standardized laboratory test guidelines for abiotic hydrolytic transformation of chemicals in aquatic system at a certain pH was published by Organization for Economic Cooperation and Development (OECD) (OECD-Test-N°111). They suggest performing experiments at pH values normally found in the environment (pH 4- 9), a temperature range of 10 – 70 ^{0}C, and without presence of oxygen or light. Several studies focused their attention to detection of hydrolytic TPs in the environment. Pérez-Parada et al. (Pérez-Parada et al. 2011) and Hirte et al. (Hirte et al. 2016) studied the transformation of a beta-lactam antibiotic amoxicillin as a function of pH (all acidic, natural and basic pH). In both cases, several new TPs were identified. They found the hydrolysis rate is strongly pH-dependent and that the main TP was the result of opening of the lactam ring. Hirte et al. (Hirte et al. 2016) showed that the previously reported TPs by Pérez-Parada et al. (Pérez-Parada et al. 2011) are rather intermediates and that they further degrade to more stable end-products (Hirte et al. 2016). Both studies used the knowledge gained from the degradation experiments and screened wastewater and surface water samples in order to detect the TPs. They detected similar TPs (intermediaries defined by Hirte et al.) since their formation to the stable end-products proceeds with slow kinetics (Hirte et al. 2016). Hydrolysis, naturally, is not limited only to antibiotics. Benzoylecgonine, a main human metabolite of cocaine was also found to form via hydrolysis of ester bond (Bijlsma et al. 2013, Postigo et al. 2011b). Although in this case it is not straightforward to conclude whether a detected compound is a human metabolite of hydrolytic TP, a demethylated

hydrolysis TP of cocaine that was detected in WWTPs effluent formed only as the result of hydrolysis (Boix et al. 2014).

Chlorination reactions

Chlorination is a disinfection process applied in water treatment processes in WWTPs, drinking water facilities or in hospital effluents which use either chlorine, chloramines or chlorine dioxide as disinfectant. Although generally considered an engineered-driven process that serves for water disinfection, high usage of chlorine-based chemicals such as sodium hypochlorite (liquid bleach; NaOCl) in hospitals can also lead to formation of chlorination TPs in hospital effluents with no designed treatment. Chlorine disinfectants in the wastewater can react with the organic matter present and can form organochlorine compounds like halogenated organic compounds absorbable on the activated carbon (AOX) which were found to be toxic for aquatic organisms and, likewise persistent in the environment (Emmanuel et al. 2004). Due to its relatively low cost, chlorine is widely spread and most used chemical oxidant for disinfection of drinking water. In drinking water treatment, both initial pre-treatment used to start initial disinfection and the post-treatment which is done in order to limit the growth of heterotrophic organisms in the distribution systems are used (Deborde and von Gunten 2008).

Both gaseous chlorine and hypochlorite are typically used in water treatment. When either are dissolved in water they form a weak acid - hypochlorous acid which can partially dissociate to form hypochlorite ions. The presence of one or the other species is pH dependent (Lopez et al. 2001). Although both species can react with organic micropollutants, hypochlorous acid is the dominant reactive species during chlorination (Deborde and von Gunten 2008). Debrode and von Gunten (Deborde and von Gunten 2008) classified reactions of hypochlorous acid with organic compounds to three transformation pathways: i) oxidation reaction; ii) addition reactions to the unsaturated bond and iii) electrophilic substitution reactions. Having these pathways in mind, they concluded that the hypochlorous acid has high selectivity towards organic compounds. However, aqueous chlorine is a mild oxidant which cannot completely mineralize organic contaminates. Consequently, various TPs can be formed as the result of oxidation, addition or substitution reactions. The TPs that form in the disinfection process have been intensively studied since the discovery that they can be even more toxic that their parent compounds (Bedner and MacCrehan 2006) or

can form highly toxic so-called disinfection byproducts (DBPs) (Richardson 2005). One of the best examples for this are the generally non-toxic iodinated X-ray contrast media (ICM) which can form the most genotoxic and cytotoxic DBPs known (iodo-DBPs) during treatment with chlorine (or monochloramine) (Duirk et al. 2011, Plewa et al. 2004, Postigo and Richardson 2014, Richardson et al. 2008). Many DBPs will form as the result of chlorine interaction with natural/dissolved organic matter (NOM). However, they can be easily generated from micropollutants like pharmaceuticals since many of them have activated aromatic ring that can react with oxidants like chlorine (Postigo and Richardson 2014). Some of the most studied examples include antibiotics like sulfamethoxazole (Dodd and Huang 2004, Huang et al. 2008), anti-inflammatory drug diclofenac (Quintana et al. 2010, Soufan et al. 2012), lipid regulator gemfibrozil (Bulloch et al. 2012, Krkošek et al. 2011), antacids like cimetidine (Buth et al. 2007) or, more recently, antineoplastics like etoposide (Negreira et al. 2015a), erlotinib (Negreira et al. 2015b), tamoxifen (Negreira et al. 2015c) or vinca alkaloids (Negreira et al. 2016). In the case of the reactivity of the antineoplastic etoposide (Negreira et al. 2015a), although no halogenated TPs were detected as the result of chlorination and no DBPs were monitored, one demethylated TP (3'-O-desmethyl etoposide) was detected in surface water up to 33 ngL^{-1} concentration. Although this chlorinated TP is a known minor human metabolite of etoposide, it wasn't possible to undoubtedly demonstrate process involved in its formation (human metabolism vs. chlorination) which resulted in its detection in surface water.

As mentioned before, as alternatives to chlorination, chloramine and chlorine dioxide are also used for waster disinfection as well. **Chloramination** was selected as alternative to chlorination in order to reduce the formation of trihalometanes (THMs) and haloacetic acids (HAAs) (Krasner et al. 2013). But it is directly linked with the formation of nitrozamines like N-nitrosodimethylamine (NDMA) which are carcinogenic. Although, as in the case of chlorination, they can be generated from natural organic matter precursors, several studies have shown that pharmaceuticals that have dimethylamine groups can form NDMA under chloramination (Postigo and Richardson 2014, Richardson et al. 2007, Richardson and Ternes 2011). For example, out of the many pharmaceuticals precursors investigated containing dimethylamine group, an antacid ranitidine demonstrated to have a strong potential to form NDMA via nucleophilic substitution (Le Roux et al. 2011, Shen and Andrews 2011). Opposite to chlorination and chloramination, chlorine dioxide tends to form

few halogenated DBPs. As the result, when pharmaceuticals are exposed to chlorine dioxide, the majority of TPs are formed via oxidation and not halogenation (Postigo and Richardson 2014). There are limitations to the use of chlorine dioxide as disinfectant. It has been reported that oxidation with chlorine dioxide in drinking water may not reduce the antibiotic activity of fluoroquinolone pharmaceuticals since chlorine dioxide does not react with quinolone ring (Wang et al. 2010).

Advanced oxidation processes

Advanced oxidation processes (AOPs) are oxidation methods primarily based on formation of hydroxyl radicals (•OH) in aqueous phase that are involved in the degradation of pollutants either by transformation or mineralization. They have gained popularity in the past couple of decades since they are able to degrade more recalcitrant compounds that pass the conventional treatments like biodegradation in activated sludge in the WWTPs. The term AOPs includes a diversity of technological processes that can be applied like photolysis, ozonation, electrolysis, heterogeneous or homogenous catalysis based on ultraviolet (UV), near UV or visible light, the use of Fenton's reagent (solution of hydrogen peroxide with ferrous ions as a catalyst), ultrasound or wet air oxidation. Which process in the end will be used depends on the objective of the treatment and characteristics of the source water (Klavarioti et al. 2009). Likewise, the AOPs can be applied in combination with other processes like the combination of ozone (O_3) and hydrogen peroxide (H_2O_2), O_3 and UV, UV/H_2O_2 or the combination of the three. Other coupled processes include titanium oxide (TiO_2) in combination with UV and H_2O_2, ultrasound in combination with the Fenton reagent, Photo-Fenton, electrolysis with Fenton or wet air oxidation with H_2O_2 (Fatta-Kassinos et al. 2010). These oxidation processes have been extensively studied and have, in general, shown to be effective in removal of pharmaceuticals (Klavarioti et al. 2009). However, as with other removal methods, the disappearance of the parent compound does not imply efficient mineralization and special attention should be payed to the formation of TPs. Since AOPs typically rely on formation of radicals that are involved in non-specific reactions, this may lead to complex reaction pathways and an elevated number of TPs. But resulting reaction pathways in pharmaceuticals should lead to the loss of pharmacological activity, due to the increase in number of OH functional groups, and hence, the polarity of the molecule. This however, should be tested by analysing the activity of the TPs (Ternes et

al. 2003) since in some cases even after the degradation, newly formed TPs could contain functional pharmacophores (Zhu et al. 2015). AOPs, although environmentally friendly, still are expensive since for full mineralization of organic compounds like pharmaceuticals in wastewater, high energy and economic resources are needed. As a more sustainable AOP could be solar photocatalysis (Klavarioti et al. 2009) or to be used as a pre-treatment followed by biodegradation (Jelić et al. 2012, Osorio 2015).

Solar photodegradation

Solar photodegradation is a process which uses/evaluates the sunlight potential to degrade and transform microcontaminants like pharmaceuticals in, for instance, surface water. In sunlit natural waters, photochemical degradation can occur via two principal processes either as i) direct or ii) indirect. In direct photolysis, a molecule absorbs light (solar radiation), becomes unstable and subsequently degrades or transforms by bond cleavage. Therefore, in order to be able to absorb light, it is necessary that electronic absorption spectrum of a compound overlaps with the irradiation wavelengths. However, even with this overlap, whether or not a molecule will undergo photolysis depends on its structure and the photo-liable molecular features (Albini and Fasani 2004, Yan and Song 2014).

In indirect photochemical reactions, a compound is transformed as the result of sun-induced generation of reactive intermediaries from naturally present species like dissolved organic matter (DOM) or nitrates. Absorption of sun radiation by these natural constituents generates reactive and oxidative species like hydroxyl radicals (•OH), singlet oxygen ($^1O_2$), alkyl peroxy radicals (•OOR), carbonate radical ($•CO_3^-$) or solvated electrons (e_{aq}^-) which are generated by the ionization of a water molecule (Andreozzi et al. 2003, Boreen et al. 2003, Fatta-Kassinos et al. 2011b, Lam and Mabury 2005, Lin and Reinhard 2005, Petrovic et al. 2007). Nitrate, nitrite and DOM can typically generate all of these species. However, carbonate radical is formed as the result of hydroxyl reaction with bicarbonate/bicarbonate ion and thus can act as scavenger of hydroxyl ions (Fatta-Kassinos et al. 2011b, Lam and Mabury 2005). Additionally, light-absorbing species can absorb energy in a triple state and transfer it to an organic species at a ground state and invoke reaction via photosensitization. The prevalence of one over the other process (direct or indirect) will depend on the absorption spectrum of the chemicals and on the quantum yield of their photolysis(Doll and Frimmel 2003).

Out of the mentioned reactive species, hydroxyl radical is the most reactive one because of its non-selective and high electrophilic nature (Lam et al. 2005). The degree of photodegradation in surface water depends on many factors like water column depth, turbidity of the water, pH, temperature, latitude, salinity and, of course, season and hours of direct sunlight. However, other constituents present in the water can inhibit photodegradation like humic acids.

In naturally sunlit waters, photodegradation is deemed as the major abiotic transformation process that can naturally attenuate concentration of pharmaceuticals due to their design to resist another important abiotic process - hydrolysis (Boreen et al. 2003, Doll and Frimmel 2003, Fatta-Kassinos et al. 2011b, Lam and Mabury 2005, Nikolaou et al. 2007, Petrovic et al. 2007).

Solar photodegradation of pharmaceuticals and reaction pathways

Solar photodegradation of many pharmaceutical classes and compounds have been studied in the last decades. Many pharmaceuticals have aromatic rings, heteroatoms, and other functional groups in their structure that can absorb solar radiation or react with transients generated by solar irradiation in surface water (Boreen et al. 2003). Boreen et al. (Boreen et al. 2003) also noticed that many pharmaceuticals contain similar structural moieties as pesticides (like phenol, nitro and naphoxyl groups) which were previously found to undergo photodegradation.

A special attention was paid to the ones that were either found to pass the conventional water treatment or those whose concentrations detected in surface water were high. Examples of the most recent studies where photodegradation TPs of pharmaceuticals were identified can be found in **Table 1.1**.

In general, method of choice used for photodegradation of pharmaceuticals is degradation with a sunlight simulator over exposure of batch reactors to natural sunlight in order to accelerate photochemical reactions. However, both methods have been reported to be used, and in some cases a comparison between the two experiments is discussed (Goncalves et al. 2011, Tong et al. 2011).

As mentioned previously, pharmaceuticals are a large heterogeneous group structurally-wise. Therefore, it would be unlikely that a single reaction mechanism can be proposed for all of them or even in a specific pharmacological group.

Table 1.1. Phototransformation products of pharmaceuticals identified in batch reactors.

Compound	Process type	Nº TP	Primary pathways	MS-MS / HRMS method	Identification based on	Complementary method(s)	Environmental detection	Reference
4 analogues of sildenafil	Photolysis under simulated sunlight	15	Stepwise destruction of the piperazine ring producing a sulfonic acid derivative	LC-QExactive-MS (Thermo)	Fragmentation pattern, data dependent MS^2	Degradation of isotopically labelled compound	Yes	(Aceña et al. 2014)
5 Cephalosporin antibiotics	Photolysis under simulated sunlight	4-9	Oxidation of 1,4-cyclohexadiene to benzene, decarboxylation, amide cleavage	LC-LIT-MS/MS, (ABSciex)	LowRes Fragmentation pattern	-	N/A	(Wang and Lin 2012)
5-fluorouracil	Photolysis under simulated sunlight	1	Ring breakage, acid formation	LC-LIT-MS/MS, (ABSciex)	LowRes Fragmentation pattern	-	N/A	(Lin et al. 2013)
6 fluoroquinolone antibiotics	Photolysis under natural sunlight	34	Fluorine substitution and reductive elimination	LC-LIT-MS/MS (LXQ, Thermo)	LowRes Fragmentation pattern	-	N/A	(Sturini et al. 2012)
Amisulpride	Photolysis under simulated solar light	9	Desulfonylation, pyrrolidine and/or sulfonyl group, S-hydroxylation,	LC-LTQ-Orbitrap-MS	Fragmentation pattern, MS^2	Suspect screening for known TPs, SIEVE, Mass Frontier (prediction of fragmentation)	Yes, 1 TP	(Gros et al. 2015b)
Amlodipine	Photolysis under simulated sunlight	16	Aromatization of the dihydropiridine moiety (pyridine derivatives), dechlorination, hydroxylation of the benzene ring and dealkylation	LC-QToF-MS (Agilent)	Fragmentation pattern	-	Yes, 1 TP in WWTP effluent	(Jakimska et al. 2014b)
Azithromycin	Photolysis under simulated sunlight	7	(bis)-N-demethylation on the desosamine sugar, O-demethylationin the cladinose sugar, hydrolytic cleavages of the desosamineand/or cladinose residue.	LC-QToF-MS (Micromass)	Fragmentation pattern	-	N/A	(Tong et al. 2011b)

Compound	Process type	N° TP	Primary pathways	MS-MS / HRMS method	Identification based on	Complementary method(s)	Environmental detection	Reference
Ciprofloxacin	Photolysis and photocatalysis	8	Not oxidative to the quinolone ring	LC-QToF-MS	Fragmentation pattern	-	N/A	(Paul et al. 2010)
Cocaine	Photolysis under natural sunlight	10	Ester bond cleavage, hydroxylation, and demethylation	LC-QToF-MS (Micromass)	Fragmetnation pattern	Two TP standards available	N/A	(Postigo et al. 2011b)
Cyclophosphamide	Photolysis under simulated sunlight	0	No degradation observed	LC-LTQ-Orbitrap-MS (Thermo)	N/A	N/A	N/A	(Lutterbeck et al. 2016)
Desipramine	Photolysis under simulated solar light	10	Hydroxylation, Deamination, N-dealkylation	LC-LTQ-Orbitrap-MS	Fragmentation pattern, MS^2	SIEVE, Mass Fronteir (prediction of fragmentation)	Yes, none detected	(Gros et al. 2015b)
Diazepam and human metabolites	Photolysis under simulated sunlight	14	Formation of benzophenones, acridinones and quinazolinones or quinazolines	LC-LIT-MS/MS, MAT LCQ (Thermo)	Fragmentation pattern, MS^n	Benzophenine TP standards available	N/A	(West and Rowland 2012)
Four benzodiazepines	Photolysis under simulated sunlight	19	Opening of the diazepinone seven-membered ring, rearrangement into a highly stabilized six-membered ring	LC-QToF-MS (Micromass)	Fragmentation pattern	-	N/A	(Calisto et al. 2011)
Methadone	Photolysis under natural sunlight	5	Hydroxylation, fragmentation and cyclization	LC-QToF-MS (Micromass)	Fragmetnation pattern	One TP standard available	N/A	(Postigo et al. 2011a)
Norfloxacin, Enrofloxacin, Ciprofloxacin	Photolysis under simulated sunlight		Cyclopropane ring cleavage and oxidative photodegradation, fluorine solvolysis,	LC-MS/MS	LowRes Fragmentation pattern	-	N/A	(Babic et al. 2013)
Oseltamivir ester, Oseltamivir carboxylate	Photolysis under simulated and natural sunlight	5	Hydroxylation of the cyclohexene ring, ester hydrolysis, intramolecular cyclization involving the ester, cleavage of the ethylpropoxy side chain	LC-QToF-MS (Micromass)	Fragmentation pattern	-	Two TPs of OE were detected, but not quantified	(Goncalves et al. 2011b)

Compound	Process type	Nº TP	Primary pathways	MS-MS / HRMS method	Identification based on	Complementary method(s)	Environmental detection	Reference
Sertraline	Photolysis under simulated sunlight	10	Hydroxylation of the aromatic ring, dechlorination, and N-demethylation followed by amide hydrolysis	LC-QToF-MS (Agilent)	Fragmentation pattern	-	None detected, neither the parent	(Jakimska et al. 2014a)
Sildenafil, N-demethyl sildenafil	Photolysis under simulated sunlight	14	Degradation of the aliphatic heterocyclicmoiety until reaching the sulfonic acid intermediate	LC-QToF-MS (Micromass)	Fragmentation pattern	H/D exchange	N/A	(Eichhorn et al. 2012b)
Sulfamethazine, sulfapyridine and acetylated metabolites	Photolysis under simulated sunlight	21	Desulfonation, hydroxylation	LC-QToF-MS (Micromass)	Fragmentation pattern	-	N/A	(García-Galán et al. 2012)
Sulfamethoxazole	Photolysis	9	Cleavage of the sulfonamide bond and the photoisomerization by rearrangement of the isoxazole ring	LC-QToF-MS (Agilent)	Fragmentation pattern	-	N/A	(Trovo et al. 2009)
β-blockers	Photolysis with simulated sunlight	6	Ring oxidation, rearrangement, and deoxygenation	LC-MS/MS (TSQ, Thermo)	Fragmetnation pattern, NMR	NMR	N/A	(Liu and Williams 2007)

"-" – not reported; "N/A" – not analysed

Therefore, photodegradation pathways should be determined on an individual basis (or within a group of structurally – related compounds, like, for example, sulphonamide antibiotics). However, since the major reactive species in (in)direct photolysis are the hydroxyl radicals, many pharmaceuticals will form hydroxylated TPs. This was seen in a variety of pharmaceutical compounds like antiviral oseltamivir (Goncalves et al. 2011), antidepressants amisulpiride and despramine (Gros et al. 2015), fluoroquinolone antibiotic moxifloxacin (Sturini et al. 2012), nonsteroidal anti-inflammatory drug diclofenac (Aguera et al. 2005), antihypertensive atorvastatin (Lam and Mabury 2005) or synthetic opioid methadone (Postigo et al. 2011a) (see **Table 1.1**.)

Hydroxylation can occur either on the benzene ring or on the alkyl chain. However, the photodegradation can also form heteroatom oxides like S-oxide as seen in case of sulfamethoxazole (Trovo et al. 2009) and amisulpiride (Gros et al. 2015); or N-oxides in sildenafil and its related compounds (Aceña et al. 2014, Eichhorn et al. 2012a) (**Table 1.1.**). Depending on the functional groups or moieties of the pharmaceutical, a compound specific reactions have been reported, likewise. For the molecules containing halogens, dehalogenation (reductive halogenation) is seen with or without hydroxylation on the position from which the halogen is lost (oxidative dehalogenation). There are many individual examples to this like clofibric acid (Doll and Frimmel 2003) or diclofenac (Aguera et al. 2005), and group of structurally related compounds like defluorination of fluoroquinolone antibiotics (Babic et al. 2013, Sturini et al. 2012), dechlorination of benzodiazepines (West and Rowland 2012) or deiodination of iodinated contrast media (Perez et al. 2009). Furthermore, decarboxylation or dealkylation is a common reaction pathway. N-dealkylation or O-dealkylation are seen in formation of phototransfromation products of fluoroquinolone antibiotics enrofloxacin or levofloxacin (Sturini et al. 2012), antihypertensive atorvastatin (Lam and Mabury 2005), antibiotic azithromycin (Tong et al. 2011) or illicit drug cocaine (Postigo et al. 2011b) (**Table 1.1.**). Nevertheless, specific moieties will render specific reaction pathways, and thus TPs. Some examples are the epoxidation in the case of carbamazepine (Lam and Mabury 2005), the isomerization and cyclization of tamoxifen (DellaGreca et al. 2007) or the formation of benzophenones, acridinones, quinazolinones and quinazolines in the case of diazepam and its human metabolites (West and Rowland 2012)

1.2.2. Biotic Transformations

Human metabolism

Many pharmaceuticals get transformed even before they are discharged to wastewater by **human metabolism**. In the human body they are transformed by enzyme-catalysed reactions in order to detoxify pharmaceuticals. This is typically done by changing the physicochemical properties of the drug making it more hydrophilic. In this way, pharmacologically inactive metabolites are formed in order to be more easily excreted from the human body.

Human metabolism of pharmaceuticals can be principally divided in three groups called: phase I (modification), phase II (conjugation), followed by further modifications and excretion metabolism. Biotransformation of the pharmaceutical can occur in many tissues but the most important organ is the liver which is a rich source of enzymes like CYP450 which are directly involved in phase I oxidation reactions (Asha and Vidyavathi 2010). In phase I principal biochemical reactions taking place are oxidation, reduction or hydrolysis via cytochrome P450 *monooxydase* (CYP), NADPH-cytochrome P450 *reductase* or *esterase* and *amidase*. These reactions expose (unmask) or introduce reactive functional groups in the molecule of the parent drug, creating more hydrophilic compounds or creating active sites for conjugation in the phase II (Holčapek et al. 2008). Some of the typical functional groups are hydroxyl (-OH), amino (-NH_2, -NH-), carboxy (-COOH), or thiols (-SH). Apart from detoxification action of phase I metabolism, it is sometimes used to create pharmacologically active compounds from prodrugs like the hydrolytic conversion of enalapril to its active metabolite enalaprilat, or oseltamivir ester to oseltamivir carboxylate (Asha and Vidyavathi 2010).

In phase II metabolites either parent drugs or phase I metabolites are transformed to more hydrophilic molecules by conjugation which promotes excretion from the body. These biochemical reactions again are catalysed by different enzymes and the most important phase II reactions include glucuronidation, glutathione conjugation, amino acid conjugation, methylation, sulphation, and acetylation. Although, methylation and acetylation form more lipophilic metabolites, they serve to detoxify irritant groups on the molecule. Finally, the last phase of the xenobiotic metabolism is principally related to the excretion of the drug.

The reactions and rate of transformation of pharmaceuticals vary from compound to compound (or a family of structurally similar compounds) and can be quite different. Some pharmaceuticals are not metabolized at all like ICM or the antiviral zanamivir. On the other hand, other pharmaceuticals like diclofenac or lamotrigine are extensively metabolized. In the case of diclofenac, only about 15 % of the original parent compound is excreted unchanged while the dominant metabolite is the 4-hydroxydiclofenac (Stierlin and Faigle 1979, Stierlin et al. 1979). Since the metabolism of pharmaceuticals is incomplete (or in some cases non-existent), this mixture of compounds will be excreted via urine and/or feces and finally end up in the wastewater where they can be further transformed by microbial degradation.

Microbial degradation

Microbial degradation is likely the dominant transformation process for compounds like pharmaceuticals in WWTPs. In general, these transformations use chemical reactions which are catalysed by growing or resting microbial cells or enzymes isolated from microorganisms as the result of different chemical reactions which are activated during metabolism of microorganisms.

Transformation of pharmaceuticals can happen in the sewage system even before they reach WWTPs. For example, the deconjugation of glucuronide metabolites could be achieved by the enzymes present in the wastewater like *β- glucuronidases* which are produced by Escherichia coli (Bitton 2005, Dray et al. 1972, Jelic et al. 2015). However, main transformation, by both quality and quantity, is expected to occur in the WWTPs biological reactors filled with activated sludge.

In WWTPs pharmaceuticals are principally removed by aerobic or anaerobic transformation, as well as sorption. Volatilization, another removal mechanism in WWTPs for organic compounds, is not expected to remove pharmaceuticals since they typically exhibit low volatility. Moreover, sludge sorption is less relevant removal mechanism for polar compounds, and the decrease of pharmaceutical concentration in influent and effluent from WWTPs is usually attributed to biological transformation (Joss et al. 2006, Kagle et al. 2009). However, removal of the pharmaceuticals during conventional treatment depends on many operating parameters which affect sorption and biotransformation like hydraulic retention

time (HRT), solid retention time (SRT), redox conditions and temperature (Suárez et al. 2008). For example, longer SRT will improve elimination of many pharmaceuticals during treatment (Suárez et al. 2005). During biological treatment biodegradation occurs either as the result of anabolic or catabolic activity. Anabolic metabolism applies biodegradation in order to use a compound as carbon or energy source (used for the growth of the biomass), while catabolic refers to reactions where the compound undergoes concomitant transformation without being used as a carbon or energy source (it is transformed, but not used for growth) (Alexander 1999, Kagle et al. 2009). Due to low concentration of pharmaceuticals to support substantial biomass growth, it is likely that their transformation proceeds via catabolic metabolism during the active degradation of the substrate present in wastewater (Taewoo et al. 2007).

Biodegradation can occur in the aerobic and anaerobic zone of the activated sludge reactor or anaerobically during sludge digestion. Although some pharmaceuticals are degraded during anaerobic sludge digestion, the biodegradation under aerobic conditions is considered as the main removal process (Fent et al. 2006). Additionally, many WWTPs nowadays perform nitrogen removal using nitrification-denitrification over nitrite nitrogen species, or nitrification combined with anaerobic ammonium oxidation (Anammox) during nitrifying activated sludge treatment (Rodriguez-Caballero and Pijuan 2013). During the treatment mono (di) oxidase enzymes from bacteria present in the nitrifying activated sludge can aerobically catabolize pharmaceuticals. Different microorganisms, like ammonia oxidizing bacteria (AOB), form reactive nitrogen species like nitric oxide (•NO), peroxynitrite ($ONOO^-$) or nitrogen dioxide radicals (•NO2) (Chiron et al. 2010, Gunaydin and Houk 2009). As the result, these reactive nitrogen species can interact with pharmaceuticals and possibly form nitro ($-NO_2$) and nitroso (-NO) TPs (Pérez and Barceló 2008).

As commented before, biodegradation of pharmaceuticals is not limited to reactions during wastewater treatment. Once they are discharged from the WWTP they can be naturally attenuated by various abiotic and biotic processes such as: i) dilution in surface water, ii) sorption onto the suspended particulate matter or partition to sediment, iii) photodegradation under natural sunlight, iv) bioaccumulation in biota and – v) biodegradation by microorganism in water/sediment interface or bed sediment. There, the degree of biotransformation by natural attenuation will depend on the concentration and

type of microorganisms present and the physicochemical properties of the pharmaceuticals (Fent et al. 2006, Radke and Maier 2014).

Biotransformation reactions of pharmaceuticals in the aquatic system

In general, biological processes usually lead to only a limited degree and number of transformation of pharmaceuticals. For some pharmaceuticals that are metabolically stable and are excreted intact, this may eventually translate into stability toward microbial degradation in the environment (Jones et al. 2002). However, a few exceptions have been reported for some pharmaceuticals like carbamazepine (Pérez and Barceló 2007a). Nevertheless; microbial degradation is the most important process for the removal of pollutants in the environment where specific enzymes and corresponding specific transformation pathways are governed by biochemical reactions. As discussed before, transformations of pharmaceuticals in aerobic activated sludge are not limited only to parent compounds. Therefore, its human metabolites are also expected to either degrade or transform.

Over the last couple of decades many studies have studied biodegradation of pharmaceuticals, primarily in aerobic activated sludge, which was accompanied with the structural elucidation of the TPs detected. **Table 1.2.** summarizes the available recent works on the study and identification of microbial biodegradation products of pharmaceuticals. The majority of these studies report identification of biodegradation products of antibiotics, analgesics, antiviral agents, anti-inflammatory agents, iodinated X-ray contrast media, anticonvulsants, and psychiatric drugs, which are among the most frequently detected drugs for human use in wastewater and surface water.

Biotransformation of a pharmaceutical is structurally related and depends on the available functional moieties on the molecule and the enzymes present. The major biodegradation pathway of pharmaceuticals is the oxidative one and involves reactions like hydroxylation, oxidation and dealkylation. In detail, the reactions involve oxidation and/or hydrolytic cleavages such as: mono- and dihydroxylation, oxidation of alcohols, reduction of ketone groups, ester and amide hydrolysis, N-dealkylation, N-deacetylation, and oxidative decarboxylation (**Table 1.2**.). The metabolic enzymes involved in these mechanisms are very different, ranging from mixed-function oxidases such as P450 up to *esterases*, *hydrolases*,

reductases, and *transferases*. Hydroxylation is the most common pathway and has been reported for anticonvulsant oxcarbazepine (Kaiser et al. 2014), antidiabetic glibenclamide (Radjenović et al. 2008), antineoplastics like methotrexate or etoposide (Kosjek et al. 2015, Kosjek et al. 2016), benzodiazepines (Kosjek et al. 2012), β-blocker metoprolol (Rubirola et al. 2014), NSAID diclofenac (Kosjek et al. 2008), or opioid codeine (Wick et al. 2011). Another pathway is the oxidation of the primary alcohols followed by carboxylic acid formation (Kormos et al. 2010, Kormos et al. 2009, Pérez et al. 2006, Prasse et al. 2011). In the case of secondary or tertiary amines, alkyl ethers, or alkyl sulphides, the most common reaction pathway is the delkylation, and was observed during biodegradation of verapamil and metoprolol (Rubirola et al. 2014, Trautwein et al. 2008). However, other types have been reported as well. These include the oxidative cleavage of amine (Helbling et al. 2010b), amidine hydrolysis (Trautwein and Kummerer 2011) or ring cleavage (Kosjek et al. 2016). For the glucuronide human metabolites of pharmaceuticals, hydrolysis of the conjugate mostly in the presence of enzymes, like *β- glucuronidase,* (Kumar et al. 2012, Lee et al. 2012) is common (**Table 1.2.**).

Under nitrifying/denitrifying conditions, other reactions are possible. Pérez et al. (Pérez and Barceló 2008) identified a nitro-derivative of diclofenac which was formed in the nitrifying activated sludge (with the addition of ammonia). In this case, the TP was formed by nitration of the benzene ring. Besides, other studies have showed that other compounds like acetaminophen or sulfamethoxazole will form nitro TPs as well (Chiron et al. 2010, Osorio et al. 2014). Nitrogen species will not exclusively react via nitration. Diclofenac and several related NSAIDs also followed N-nitrosation or O-nitrosation pathway, and formed homonymous TPs (Osorio 2015, Pérez and Barceló 2008). However, the reactions of denitrification are not exclusively enzymatic but can mediate abiotic reactions by formation of reactive nitrogen species (NO and nitrite) (Nödler et al. 2012). Nodler et al.(Nödler et al. 2012) found that sulfamethoxazole in an anoxic water-sediment batch test under denitrifying conditions will form nitro and desamino TPs but in the absence of the nitrite, they observed the reversal of the nitro TP to the parent sulfamethoxazole (**Table 1.2.**).

Table 1.2. Biotransformation products of pharmaceuticals identified in batch reactors.

Compound	Process type	Nº TP	Primary pathways	MS-MS / HRMS method	Identification based on	Complementary method(s)	Environmental detection	Reference
19 amine containing compounds	Acrobic activated sludge	144	N-oxidation, N-dealkylation, N-acetylation, and N-succinylatio	LC-QExactive-MS (Thermo)	Fragmentation pattern, data dependent MS^2	Compound Discoverer 1.0. and SIEVE 2.2.for suspect and non-target screening, dozens of TPs confirmed with standard	N/A	(Gulde et al. 2016)
30 Amide containing compounds	Activated sludge batch system from a pilot scale membrane reactor	53	Series of reactions: amide hydrolysis and N-dealkylation, hydroxylation, oxidation, ester hydrolysis, dehalogenation, nitro reduction, and glutathione conjugation	LC-LTQ-Orbitrap-MS (Thermo)	Fragmentation pattern, data dependent MS^2	UM-PPS (now EAWAG-PPS)	N/A	(Helbling et al. 2010a)
2 acetylated metabolites of sulfapyridine and sulfamethazine	Aerobic effluent wastewater	2	Reversal reactions to the parent compound	LC-QToF-MS (Micromass)	Fragmentation pattern, available standards	-	Yes	(Garcia-Galan et al. 2012)
3 benzodiazepines (diazepam, oxazepam and bromazepam)	Biodegradation in flow-through pilot bioreactors	5	Formation of oxazepam,nordazepam, temazepam from diazepam,	LC-QToF-MS (Premier),	Fragmentation pattern,	-	N/A	(Kosjek et al. 2012)
3 ICM (Iohexol, Imeprol, Iopamidol)	Biodegradation (soil/water system)	27	Transformations at the side chains containing either, carboxylic moieties and/or primary and secondary amide moieties, the triiodoisophthalic acid structure remained unaltered	Qq-LIT-MS (4000 Q Trap, AbSciex)	Fragmentation pattern, MS^n NMR	Several TP standard isolated, NMR	Yes, several TP were detected	(Kormos et al. 2009)

Compound	Process type	Nº TP	Primary pathways	MS-MS / HRMS method	Identification based on	Complementary method(s)	Environmental detection	Reference
4 ICM (Iohexol, Imeprol, Iopamidol, Diatrizoate)	Biodegradation (soil/water system)	27+7	New TPs: oxidation, cleavage of the N-C bond and decarboxylation	Qq-LIT-MS (4000 Q Trap, AbSciex)	Fragmentation pattern, MS^n NMR	Several TP standard isolated, NMR	Yes, several TP were detected	(Kormos et al. 2010)
6 structurally-related NSAIDs	Aerobic activated sludge under nitrifying conditions	10+	Nitration and nitrozation	LC-QExactive-MS (Thermo)	Fragmentation pattern, data dependent MS^2	Chlorine isotopic pattern	N/A	(Osorio 2015)
Acetaminophen	Aerobic activated sludge under nitrifying conditions	2	Hydroxylation and nitration	LC-LIT-MS (Bruker Daltonic Esquire6000)	Fragmentation pattern of the standards	TP synthesis	Yes	(Chiron et al. 2010)
Acyclovir, Penciclovir	Biodegradation in activated sludge	8	Oxidation of the primary and terminal hydroxyl groups, β-oxidation followed by acetate cleavage	LC-LTQ-Orbitrap-MS (Thermo)	Fragmentation pattern, MS^n	1D and 2D NMR	Yes	(Prasse et al. 2011)
Azithromycin, Ciprofloxacin, Norfloxacin, Roxitromycin	MBR treatment using activated sludge	1+2+2 +1	Phosphorylation and acylation of macrolides and fluoroquinolones	LC-QToF-MS Premier (Micromass)	Fragmentation pattern	-	N/A	(Terzic et al. 2011)
Citalopram	Aerobic activated sludge	14	Oxidative reactions, such as hydroxylation, oxidation, N-oxidation and N-demethylation as the primary biotransformation mechanisms; nitrile hydrolysis and amide hydrolysis.	LC-QTOF-MS (Maxis impact, Bruker)	Fragmentation pattern, MS^2	LC-HILIC, EAWAG-BBD, Metabolite Tools, RT prediction using QSPR	Yes, 5 TPs detected in WWTP effluent	(Beretsou et al. 2016)
Codeine	Aerobic activated sludge	18	Double bond shifts, introduction of hydroxyl groups, amine demethylation.	LC-LIT-MS LC-LTQ-Orbitrap-MS	Fragmentation pattern, MS^2, NMR	Several TP standard isolated, NMR	Yes, several TP were detected	(Wick et al. 2011)

Compound	Process type	Nº TP	Primary pathways	MS-MS / HRMS method	Identification based on	Complementary method(s)	Environmental detection	Reference
Diclofenac	Aerobic activated sludge	3	Nitration, nitrozation, N-dealkylation and subsequent carboxylation	LC-QToF-MS (Micromass)	Fragmentation pattern	H/D-exchange experiments	N/A	(Pérez and Barceló 2008)
Diclofenac	Biodegradation	4	Hydroxylation, benzoquinone imine and nitro analogues	LC-QToF-MS	Fragmentation pattern	-	N/A	(Kosjek et al. 2008b)
Etoposide	Aerobic activated sludge	5	Glycoside bond hydrolysis, dehydrogenation, oxidation of dioxolane ring, ring cleavage with hydroxylation in the glycoside moiety	LC-QExactive-MS (Thermo)	Fragmentation pattern, data dependent MS^2	MZmine v. 2.18.3 used for detection of TPs-	N/A	(Kosjek et al. 2016)
Glibenclamide	Aerobic activated sludge	1	Hydroxylation of the cyclohexyl ring	LC-QToF-MS (Micromass)	Fragmentation pattern	-	None detected	(Radjenović et al. 2008)
Metformin	Biodegradation (Closed Bottle OECD301D and Zahn-Wellens OECD302B, Manometric Respiratory test (OEDC 301 F)	1	Amidine hydrolysis to guanylurea	LC-LIT-MS (Bruker Daltonic Esquire3000)	Fragmentation pattern, MS^n	-	Yes	(Trautwein and Kummerer 2011)
Methotrexate	Aerobic activated sludge	9	Demethylation, oxidative cleavage of amine, cleavage of C–N bond, aldehyde to carboxylate and hydroxylation	LC-QExactive-MS (Thermo)	Fragmentation pattern, data dependent MS^2	SIEVE used for detection of TPs	N/A	(Kosjek et al. 2015)
Metoprolol	Aerobic activated sludge	5	O-demethylation, hydroxylation	LC-LTQ-Orbitrap-MS (Thermo)	Fragmentation pattern, data-dependent	SIEVE, Mass Fronteir (prediction of fragmentation)	None (of the newly identified)	(Rubirola et al. 2014b)
Oxcarbazepine, and human metabolites of oxcarbazepine and carbamazepine	Aerobic activated sludge	7	Oxidation, α-ketol rearrangement, and benzylic acid rearrangement	LC-LTQ-Orbitrap-MS (Thermo)	Fragmentation pattern, data dependent MS^2, NMR	TP isolation, NMR	Yes, three TPs detected	(Kaiser et al. 2014)

Compound	Process type	N° TP	Primary pathways	MS-MS / HRMS method	Identification based on	Complementary method(s)	Environmental detection	Reference
Sulfamethoxazole	Anoxic water/sediment test under denitrification	2	Nitration, deamination and reversible reactions	LC-MS/MS (Varian)	Fragmentation pattern of the standards	TP synthesis	N/A	(Nödler et al. 2012)
Verapamil	Biodegradation (Closed Bottle OECD301D and Zahn-Wellens OECD302B	3	O- and N-demethylation	LC-LIT-MS (Bruker Daltonic Esquire3000)	Fragmentation pattern, MS^n	-	N/A	(Trautwein et al. 2008)

"-" – not reported; "N/A" – not analysed

Most comprehensive studies for biotransformation pathways elucidation have been reported for pharmaceuticals (among other compounds) by focusing on compounds which had either an amide (Helbling et al. 2010a) or amine (Gulde et al. 2016) moieties. There, instead of looking at the single compound, a list of amide or amine containing contaminants have been degraded and their behaviour studied. Helbling et al. (Helbling et al. 2010a), degraded 30 amide-containing compounds in activated sludge which formed 57 TPs. These generated TPs were identified, and the results of structural elucidation were translated to propose common pathways like amide hydrolysis and N-dealkylation, hydroxylation, oxidation, ester hydrolysis, dehalogenation, nitro reduction, and glutathione conjugation. Due to an elevated list of degraded parent compounds, which included primary, secondary and tertiary amides, additional information could be concluded for each subset of compounds. For example, primary amides hydrolysed rapidly while the hydrolysis rate of the secondary amides was influenced by steric effects. Tertiary amides followed the N-dealkylation pathway, conditioned that other specific structural moieties on the molecule are not more readily enzyme-catalysed (Helbling et al. 2010a). Similarly as with studying amide containing compounds, Gulde et al. (Gulde et al. 2016) systematically explored the biotransformation pathways of 19 amine (primary, secondary and tertiary) containing compounds which generated a total of 144 TPs (out of which 101 were identified). As the result, principal reactions for amides in activated sludge during biotransformation were identified as N-oxidation, N-dealkylation, N-acetylation and N-succinylation.

As in the case of Helbling et al. (Helbling et al. 2010a), the proposed biotransformation pathways were based on proper structural elucidation of the TPs generated which was crucial for understanding how these compounds behave under aerobic activated sludge biodegradation. Another crucial step was the detection of the TPs since the objective of both studies was to elucidate all possible pathways. In order to achieve this, in both cases both automated suspect and non-target screening were performed. Suspect screening was performed with a list of plausible TPs and was generated using biotransformation reaction prediction software EAWAG-BBD. Non-target screening was performed in order to account for all not predicted, but present TPs. Additionally, in Gulde et al. (Gulde et al. 2016), they candidly presented the confidence levels for all of the identified TPs using Schymanski guidelines (Schymanski et al. 2014a) making the evaluation of the reaction pathways even more comprehensive. Both of these studies were systematic in their approach

which afforded not only the identification of novel pathways, but also the probability of prediction on how other pharmaceuticals (or other micropollutans) with amide or amine substructure will transform by biodegradation. Consequently, the following chapters of the introduction section will focus precisely on the different identification approaches for reliable structural elucidation of the detected/formed TPs.

1.3. Identification of transformation products with liquid chromatography coupled to mass spectrometry

1.3.1. Instruments based on mass spectrometry used for analysis of transformation products

Structural elucidation of TPs is still one of the most used procedures for evaluation of the fate of emerging contaminants and is essential for the characterisation of their transformation pathways. However, this is still a complex and challenging task and requires an array of sophisticated instrumental techniques for a reliable identification of all TPs formed from selected compounds, such as gas chromatography-MS (GC-MS), liquid chromatography-MS (LC-MS), and nuclear magnetic resonance (NMR). Technological advances and developments in the field of LC-MS over the last decades has expanded its popularity and it has become one of the favourite techniques for structural identification of TPs (Zonja et al. 2014a). This is more so true for the identification of metabolites and TPs of pharmaceuticals, due to the polar nature of the most parent compounds and especially their TPs. Analysis with GC-MS is much less popular since polar compounds usually need to be derivatised at the functional group in order to reduce polarity and increase thermal stability and volatility (Dettmer et al. 2007).

Liquid chromatography (or ultra-performance liquid chromatography (UPLC)) is typically coupled with a mass spectrometer using different ionization sources. The (heated) electrospray ionization ((H)ESI) is the most applicable since it is the most versatile ionization source for a wide range of polar to very polar compounds and a wide m/z range. However, other ionization sources like atmospheric pressure photoionization (APPI) or atmospheric pressure chemical ionization (APCI) are also used for non-polar to medium polar compounds. The most widely used platforms with MS analysers for structural elucidation of

pharmaceutical TPs are quadrupole ion trap (IT) (or the quadrupole-linear ion trap (QqLIT)), time-of-flight (ToF) (or quadrupole time-of-flight (QToF)), and more recently, Orbitrap (either with or without a quadrupole or LIT used for preselection) (Rodriguez-Aller et al. 2013). Each of them are characterised by the resolution obtainable (resolving power), mass accuracy/precision, mass range, sensitivity, selectivity, linear/dynamic range, acquisition modes, acquisition speed, size and price, and the use will depend on application. High-resolution instruments afford the most straightforward route towards the reliable characterization of TPs because the determination of elemental formulae is based on the measurement of exact masses with accuracies better (lower) than 1-2 ppm in relative mass error. The high resolving power of the MS on some instruments is now exceeding even 100,000- which enables the determination of accurate masses even in complex samples which contain potentially interfering compounds with identical nominal masses (Zonja et al. 2014a).

Good starting point in the elucidation of unknown structures have been the IT-MS instruments. IT-MS is an analyser that uses a combination of electric or magnetic fields in order to trap ions in a small volume. Its relatively low cost, compact size and the possibility to trap and accumulate ions which increases signal-to-noise ratio is advantageous. However, their MS^n capabilities are particularly attractive for the identification of TPs because this sequential fragmentation allows identification of fragmentation pathways that may not be as obvious in the MS^2 instruments like triple-quad (QqQ), QTOF or Q-Orbitrap (Tozuka et al. 2003). On the other hand, due to their small trapping volume, IT-MS have a limited capacity for ion storage and the overfill of the trap results in deterioration in the mass spectrum and loss of the dynamic response range due to space charging (Hopfgartner et al. 2004). Linear ion traps can also be used for ion trapping with the benefit of a larger ion storage capacity and higher trapping efficiency over the conventional ion traps. Q-LIT system (trademark QTRAP) is similar to triple quadrupole MS (Q1, the collision cell, Q3) with the difference that the third quadrupole (LIT) can be operated either as the trap or as conventional quadrupole (RF/DC mode). If the LIT mode is used, the trapped ions are ejected axially in a mass-selective fashion using fringe field effect and are detected by the standard detector of the system (Guillarme et al. 2012).

Identification of TPs become more confident and expedited with the arrival of the of affordable, benchtop HRMS with improved selectivity like TOF and Orbitrap-MS. TOF MS measure the time that is needed for an ion to travel from the ion source to the detector where

they have been orthogonally accelerated in a pulsed fashion in a field-free region (Pavlović et al. 2007). The time that is needed for the ion to travel depends on the velocity of the ion which is m/z dependent. Hybrid QTOF-MS analysers advanced the confirmation of the compounds analysed since it allowed the use of the MS^2 experiments with prior selection of the parent ion m/z using a quadrupole and, thus, providing a compound specific fragmentation patter together with the accurate mass measurements of the fragment ions.

An alternative to TOF is the Orbitrap analyser from Thermo Scientific. Orbitrap is an ion trap analyser that uses Fourier transformation in order to produce m/z spectrum. The ionized ions that enter the system are injected via C-trap into the Orbitrap analyser. There, an electric field applied pushes the ions towards the central electrode where axial oscillations are initiated and the rotation around the central electrode which keeps ions from falling onto the central electrode. The ions that entered the Orbitrap analyser form thin rotating ring which oscillates along the central electrode with a period proportional to the square root of m/z which produces an image current on the outer Orbitrap electrodes. These signals are converted using Fourier transformation into frequency, and subsequently into a m/z spectrum(Hu et al. 2005, Makarov and Scigelova 2010, Zubarev and Makarov 2013). There are several instruments that are based on the Orbitrap technology, but the most used in the environmental analysis are the QExactive (Q-Orbitrap-MS) and LTQ-Orbitrap (LIT-Orbitrap-MS). The LTQ-Orbitrap is a hybrid instrument that uses LIT as an analyser and an orbitrap as an accurate mass detector. In the case of Q-Exactive, the LIT is "replaced" by a quadrupole mass filter. In both cases, high mass accuracy (1 – 2 ppm error), resolution (up to 140,000 for m/z 400) and the possibility for MS^n (MS^2 in the case of QExactive) make the Orbitrap line of instruments likewise attractive for elucidation of TPs.

1.3.2. Identification Schemes for structural elucidation of transformation products

A typical workflow for identification of TPs consists of five steps: i) generation, ii) extraction, iii) detection, iv) identification, and finally v) confirmation, if possible (**Figure 1.3.)**. In the initial step of the workflow, in order to describe TPs of pharmaceuticals, it is necessary to *generate* them in laboratory conditions, simulating an investigated process. For evaluation of biodegradability of a compound, several standardized tests are given by the OECD guidelines. The most used in literature are: i) Closed Bottle test (CBT, OECD 301 D) (OECD-Test-N°301); ii) manometric

respirometry test (MRT, OECD 301 F) (OECD-Test-N°301), and iii) Zahn-Wellens test (ZWT, OECD 302 B) (OECD-Test-N°302B). CBT test is designed to test compounds in the presence of low bacterial intensity, low nutrient content and constant temperature thus simulating surface water conditions. MRT and ZWT test are characterized by medium and high bacterial intensity, respectively and serve to simulate conditions in wastewater effluents. Trautwein et al. (Trautwein et al. 2008) used CBT and ZWT for biodegradation of calcium channel antagonist verapamil. They found that while verapamil was not biodegraded in the CBT test, after nine days in the ZWT reactor, it was completely eliminated. The authors studied the formation of the new peaks and found three N- and O-demethylated TPs. Similarly, the transformation of antidiabetic metformin to guanylurea, or antipsychotic chlorpromazine to its TPs was only seen in the medium-high bacterial density test using the three mentioned OECD tests (Trautwein and Kummerer 2011, Trautwein and Kümmerer 2012).

All of the OECD tests mentioned apply small doses of wastewater or activated sludge (compared to secondary treatment in the WWTP) to degrade a compound which may result in prolonged degradation time and provide no kinetics (Bletsou et al. 2015). As an alternative many degradation studies used aerated activated sludge (mixed liquor) from WWTPs (**Table 1.2.).** Typical concentration of solids in the activated sludge is between 4 – 5 gss/L. Batch reactors that use activated sludge for biodegradation can use either concentrated or diluted sludge (to 0.5 – 1 gss/L) in order to reduce the effect of sorption or to avoid matrix effects (Luft et al. 2014). For aerobic degradation, the batch reactors are typically aerated with the combination of carbon dioxide in order to maintain stable pH. Degradation under anaerobic conditions is performed under nitrogen atmosphere. In addition, control batch reactors have to be monitored in order to exclude formation of TPs from other, abiotic, processes like hydrolysis or the loss of parent compound through sorption to the particulate matter. Activated sludge batch reactors are a test of choice for degradation and identification of TPs for many pharmaceuticals since it allows a direct link with the biodegradation that will occur during secondary treatment in the WWTP with relatively good simulation of biotransformation pathways and kinetics (Helbling et al. 2012). Examples of biodegradation batch studies can be found in **Table 1.2.**

In order to assess the photodegradation of pharmaceuticals, batch experiments rely on exposure of an aqueous solution containing the compound to either natural or simulated sunlight.

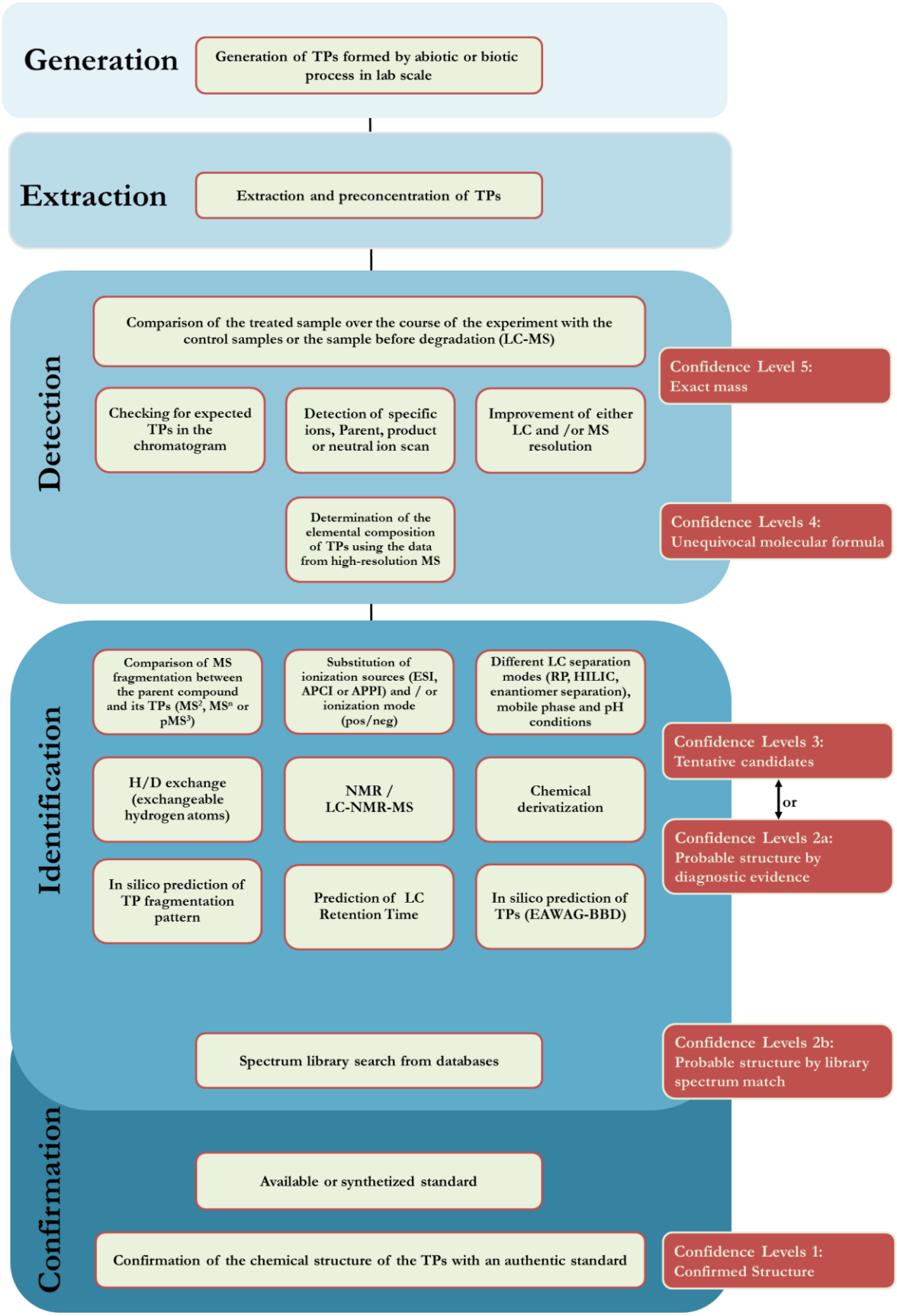

Figure 1.3. 5-step workflow for identification of TPs for polar compounds (Aceña et al. 2015b, Zonja et al. 2014a) with 5-identification confidence levels from Schymanski guidelines (Schymanski et al. 2014a).

The latter has the advantage that due to higher irradiance, photochemical reactions rates are faster and this reduced experiment time (in the range of hours), compared to exposure to natural sunlight which normally requires days to transform a compound. Gonçalves et al. (Goncalves et al. 2011) degraded an antiviral oseltamivir (ester) and its main human metabolite oseltamivir acid (formed via ester dealkylation) under both natural and simulated sunlight. Degradation of both compounds in surface water followed first order kinetics under simulated sunlight with the degradation half-life of 2.9 and 12 h, respectively. However, in surface water under natural sunlight, those half-lives were higher by two orders of magnitude.

Once the TPs are generated in laboratory conditions at low concentration, they may need to be *extracted* and preconcentrated from the solution using solid phase extraction (SPE) or by lyophilisation of the sample (**Figure 1.3.**). However, this is usually not necessary since the degradations are (or can be) performed at high initial concentrations of the parent compound.

Next, the *detection* of TPs is achieved by the comparison of the treated sample over the course of the experiment with the control samples or the sample before degradation (**Figure 1.3.**). This can be performed manually (visually) by studying the newly visible peaks in the chromatogram. Apart from peak-picking, it is possible to directly check for "expected" TPs in the chromatogram or detect some specific ions, or by using precursor or natural ion scan. However, more convenient recent trend is to use some peak-picking software in order to aid detection and reduce possibility of visual errors (Beretsou et al. 2016, Gros et al. 2015, Kosjek et al. 2016, Negreira et al. 2015b, 2016, Rubirola et al. 2014). Currently, many vendor software include data-treatment package.

As mentioned in the previous sections, the structural *identification* of TPs is performed by examination of their fragmentation pattern in comparison with the fragmentation pattern of the parent compound (**Tables 1.1.** and **1.2.**). However, prior to structural elucidation it is important to define what is the confidence level of the compound to be identified (**Figure 1.3.**). Schymanski et al (Schymanski et al. 2014a) proposed a five level identification confidence scheme which starts with a selection of an exact mass of interest (lowest level of confidence), and moves up through unequivocal molecular formula (level 4), tentative candidate (level 3), and probable structure (level 2), before reaching the level 1 which is a confirmation of a structure with a reference standard (highest degree of confidence). This not only assures the information on structural probability of a TP, but also helps

communicate identification confidence across the scientific community in order to give a general platform between different studies (Schymanski et al. 2014a). In essence, while the bottom two levels (4 and 5) are related only to MS detection (exact mass from full scan and MS isotopes/adducts), level three and up focus on structural identification. Moving up the scale can be achieved by either fragmentation experiments or additional complementary methods that can aid elucidation of an exact modification. As an example, in case of methylation of a parent compound, Schymanski guidelines make distinction between the tentative structure (a methyl group was added somewhere on the parent molecule – level 3) and a probable structure (a methyl group was added on a particular moiety of the parent molecule) which can be confirmed by a diagnostic evidence (level 2).

Additional MS-related strategies that can help in elucidation, by providing diagnostic evidences, is substituting the ionization source of the MS instrument from the most common (H)ESI to APPI or APCI. Eichhorn et al (Eichhorn et al. 2012a) were able to identify an N-oxide photoTP of sildenafil formed under simulated sunlight in aqueous solution using APCI. Contrary to the ESI source, in the full-scan mass spectrum using APCI they observed the characteristic loss of oxygen atom from the molecular ion due to thermal deoxygenation in the ion source, a neutral loss characteristic for many other N-oxide metabolites of pharmaceuticals.

Nevertheless, compound specific fragmentation is crucial for reliable identification. However, MS platforms like TOF or Orbitrap without the initial quadrupole filter can only generate full-scan MS spectra, or full-fragment-scan MS spectra where ions that are detected have already been fragmented using in-source fragmentation. With the addition of quadrupole, the preselection of the m/z generates an MS^2 spectrum that is highly selective towards the fragmented m/z. However, the addition of the quadrupole only allows the MS^2 degree of fragmentation while the MS^n is still option for the ITs. A hybrid experiment can be used to extend the degree of fragmentation to MS^3 using the combination of in-source fragmentation and the fragmentation in the collision cell. This type of experiment is called pseudo-MS^3 (pMS^3). The high fragmentation voltage in the ion source is used in order to produce a certain m/z ion fragments (pMS^2) which simulate parent ions and are later isolated in the quadrupole before being broken in the collision cell to produce pMS^3. In this case, the pMS^3 spectrum needs to be compared with MS^2 spectrum of the proposed TP in the sample at the corresponding retention time in order to ensure that the given m/z does come from

the parent TP and thus provide a more reliable confirmation (Padilla-Sanchez et al. 2012, Perez et al. 2009).

Complementary methods used for identification of transformation products

In many cases it is not possible to identify which part of the molecule was modified or to distinguish different positional isomers with MS^2 spectra. Many studies use several complementary techniques in order to additionally corroborate the structure of the detected TP (**Figure 1.3.**). Some of the most common methods used are based on different LC separation modes (chromatographic columns), exchange of the liable hydrogens with deuterium (H/D exchange), NMR, prediction of retention time (RT) or prediction of transformation products using *in-silico* prediction.

In general, pharmaceuticals are polar and low volatile compounds that are better retained on reverse-phased (RP) columns with, for example, C_{18}, C_8 or high strength silica (HSS). Modifications in the **chromatography column stationary phase** made possible for different groups of compounds to be better retained using fluorinated reversed phase, amide, porous graphitic carbon, phenyl, mix-mode or hydrophilic interaction chromatography (HILIC) columns. TPs of pharmaceuticals are normally even more polar that their parent compound and in some cases can be poorly retained on the RP columns. This can often be solved using HILIC chromatographic separation mode which uses polar stationary phases (bared silica, aminopropyl, diol and zwitterionic phases bonded to silica or polymeric supports) in combination with the mobile phases with prevailing composition of organic solvent. Typical organic solvent used is acetonitrile, but other solvents are possible to use like methanol or the combination of both. In HILIC, liquid-liquid partitioning between the bulk mobile phase and the adsorbed water layer is achieved when at least 1 % of water is used in the mobile phase and water serves as a strong eluting solvent. However, retention is not only governed by partitioning and other interactions influence separation like ion-exchange, H-bonding and dipole-dipole interactions (Hemström and Irgum 2006, Ikegami et al. 2008, Núñez et al. 2012, Petrovic et al. 2010). Advantages of using HILIC include reversal order of elution of the compounds (in comparison to RP chromatography), no need for ion-pairing agents, and the ionic strength which affects retention. Due to high percentage of organic solvent used for the mobile phase, it is can expected the increase in ionization

efficiency and, thus, sensitivity (Núñez et al. 2012). Beretsou et al. (Beretsou et al. 2016) reported the benefits of using HILIC chromatography for detection of some of the TPs of an antidepressant drug citalopram formed during degradation in aerated activated sludge. They detected and identified thirteen TPs using RP chromatography, but were able to detect an additional one (TP 360 B which was the result of amide hydrolysis) only by using HILIC, since RPLC was not able to separate isomers (amide hydrolysis vs. loss of water, followed by N-oxidation).

In addition, changing the **pH of the mobile phase** can help detect TPs with the acid functional groups. In RP chromatography, ion-exchange mechanism due to ion attraction between positively charged surface of charged surface hybrid (CSH) stationary phase and an acid molecule, at acidic pH will increase the retention (Nováková et al. 2012). Therefore, pH-dependent retention behaviour of compounds with acid moieties like carboxylic acids can additionally confirm or disprove their presence in the compound's structure (Eichhorn et al. 2012a).

Hydrogen/deuterium exchange (H/D exchange) is a reaction where covalently bonded hydrogen is exchanged by deuterium. For TP identification, this is typically performed on-line by replacing standard mobile phases with the deuterated ones (Eichhorn et al. 2005, Eichhorn et al. 2012a, Pérez and Barceló 2008, Perez et al. 2009, Pérez et al. 2006). This H/D exchange can be used to pinpoint if the group with the exchangeable protons and deuterons (hydroxylated or amino groups) is still present or not in the formed TP. This approach was used for confirmation purposes in studies that aimed at identification of TPs generated from biotransformation of trimethoprim (Eichhorn et al. 2005), iopromide (Pérez et al. 2006) or diclofenac (Pérez and Barceló 2008), and photoransformation of iopromide (Perez et al. 2009) or sildenafil (Eichhorn et al. 2012a).

Additional methods using **spectrophotometric detection** techniques (UV) can also help identify TPs but are not nearly as informative as other identification techniques like MS or NMR. However, instruments with diode array detection (DAD) or florescence can be used coupled with MS detection. In the matrix free environment, LC can be coupled with the UV or fluorescence detectors which can prevalently be used as a tool for isolation of generated TPs due to a non-destructive nature of these detectors.

In an ideal case, a detected TP will be available as an authentic standard that can be used to corroborate the structure. In some cases, it is possible to find commercially available standards of pharmaceutical human metabolites, but they are scarcely available for the environmental TPs. Due to some similarities between the human metabolism and microbial degradation, the two processes can yield the same metabolite/TP, thus making the commercialized standard available for environmental TPs. However, the overlap is not as common. This is why many environmental degradation studies currently focus their attention on either chemical synthesis of the standards or isolation of the standard from the transformed mixture. This affords not only the possibility to run NMR experiment for additional structural characterization but provides also the benefit of having the authentic standard that can be used for target method developments and, ultimately, serve for quantification of TPs in real-world samples.

Nuclear magnetic resonance plays an invaluable role for structural characterisation of TPs since it allows the unambiguous determination of a compound's structure and stereochemistry by generating unique resonance of various functional groups from the two most commonly used nuclei: the most receptive isotope at natural abundance (^{1}H) and ^{13}C. However, other isotopes of other heteroatom nuclei can also be used (^{19}F and ^{31}P). In addition, combination of one dimensional (1D) and 2D homo- and heteronuclear techniques (C-H and C-C) can be used for even more precise identification of the structure (Pérez et al. 2008, Prakash et al. 2007, Zonja et al. 2014a). On the negative side, NMR does not have the capability to separate compounds, and sample preparation is time-consuming due to high amounts needed of the compounds because of the limited sensitivity. Therefore, regularly amounts higher than 1 mg are needed reliable measurements. Coupling of LC to NMR can be a significant advantage because of abbreviated sample preparation, but nonetheless lacks in sensitivity for low concentrations which TPs are normally found in environmental samples (Celiz et al. 2009, Durand et al. 2010, Fatta-Kassinos et al. 2011a, Pan et al. 2006). Still, due to advances in instrumentation, higher sensitivity can be achieved using cryoprobe technology which improves signal to noise ratio by reducing the operating temperature of some components of the NMR spectrometer and hence, lower amount of compound are needed (Pellecchia et al. 2002, Spraul et al. 2003).

A comprehensive multistep approach which consists of using both NMR and MS for the identification of TPs was developed for many pharmaceuticals by Ternes group. This

included biotransformation products of several ICM (Kormos et al. 2010, Kormos et al. 2009, Schulz et al. 2008), antivirals acyclovir and penciclovir (Prasse et al. 2011), opiate codeine (Wick et al. 2011) and anticonvulsant oxcarbazepine and its human metabolites (Kaiser et al. 2014). In all of these studies, TPs generated under laboratory conditions were isolated using a semi-preparative LC chromatography. For those TPs that were successfully isolated in sufficient quantities additional experiments with NMR were performed and structures were later elucidated using both $MS^{(2 \text{ or } n)}$ fragmentation and NMR spectra. As the result, not only were the compounds identified up to the level 1 but also could be directly used in order to measure environmental concentrations of real-world samples. However, it is not always possible to use semi-preparative chromatography for TP isolation because of unsatisfying chromatographic separation due to large number of detected and overlapped peaks. Likewise, if the parent compound or its TP act as biocides to the biological system, large quantities cannot be used for generation of the TP making it inefficient for quantitative isolation (Luft et al. 2014).

As an example of a workflow used for identification of TPs, Perez et al. (Pérez et al. 2006) started with the degradation of an ICM iopromide (IOP) in both activated sludge and nitrifying activated sludge. They found that IOP was transformed primarily via oxidation of primary alcohols on the identical side chain. Several experiments have been performed in order to elucidate the structures of the detected TPs. They have studied initially a detailed fragmentation pattern of the TPs and the parent, which was followed by complementary experiments of an H/D-exchange and derivatisation (carboxylic acid to methyl ester) experiments in order to eliminate the O-methylation as a reaction pathway, and confirm the oxidation of the primary alcohol. Although in their case they did not have an authentic standard nor was it isolated or synthetized, the authors were able to move from the identification level 3 (tentative candidate) to level 2b /diagnostic evidence) for some TPs using complementary methods. However, Schulz et al (Schulz et al. 2008) advanced the knowledge on biotransformation pathways of IOP in a soil/water system to the highest level 1 (confirmed structure by reference standard) by isolating the formed TPs using semi-preparative chromatography and by studying the NMR spectra of each isolated compound.

1.4. Detection of TPs and pharmaceuticals in environmental samples using liquid chromatography coupled to low or high resolution mass spectrometry

Environmental samples contain a complex mixture of many water constituents, including substances which can interfere with the analysis of target compounds. In order to avoid interferences, a good separation method using LC is important for successful analysis of pharmaceuticals, their metabolites and TPs even when contemporary MS analysers are used. In the last couple of decades, a great number of research publications have been dedicated to development of multi-residue methods for quantification of pharmaceuticals in various environmental samples. Currently most analytical methods for the analysis of pharmaceuticals in environmental samples are based on LC-MS(/MS) since it offers improved selectivity and sensitivity, which is especially important for the analysis of TPs. In general, triple quadrupole (QqQ-MS) and QTRAP-MS analysers are the ones mostly used because they are robust and exhibit a large linear dynamic range for quantitative work (Zonja et al. 2014a).

Recent methods developed are based predominantly on the low resolution (LR) LC-MS/MS (Cerqueira et al. 2014, Grabic et al. 2012, Gros et al. 2012, 2013, Huerta et al. 2014, López-Serna et al. 2013, Negreira et al. 2013, Paíga et al. 2015, Pérez-Carrera et al. 2010, Petrie et al. 2016, Prasse et al. 2010, Togunde et al. 2012, Wille et al. 2010, Yuan et al. 2013). As with the case of mentioned TPs, pharmaceuticals are also present at low concentration levels depending on the type of aqueous samples. Therefore, prior to the analysis using LC-MS, it is necessary to purify the samples in order to remove interferences and to concentrate the target compounds. Many methods have been used for preconcentration of aqueous samples, but the SPE is the most ubiquitously used sample preparation technique, replacing laborious liquid-liquid extraction methods that use high amounts of organic solvent (Richardson 2011, Richardson and Ternes 2011, Richardson and Ternes 2014).

However, SPE is foremost a preconcentration method and SPE sorbents often lack selectivity and can concentrate other matrix compounds present that can interfere with the analysis. Still, many SPE sorbents have been developed for efficient extraction of pharmaceuticals. Oasis HLB is a hydrophilic-lipophilic balanced, polymeric, reversed-phase sorbent which is ubiquitously used and most commonly applied for simultaneous extraction of acidic, basic and neutral compounds at wide pH range of the samples, typically with enrichment factors between 100 and 10,000. (Gros et al. 2008) SPE can be performed off-

line (manually and separated from chromatographic run), or on-line, where the preconcentration step is part of the LC-MS/MS method, hence it is directly integrated into the analytical system. Although the method of choice is still the use of an off-line SPE method due to availability of the equipment, on-line SPE is growing in popularity for the analysis of pharmaceuticals and TPs because of high sensitivity and selectivity, minimum sample preparation, superior reproducibility, and automation (Anumol and Snyder 2015, Bourdat-Deschamps et al. 2014, Lindberg et al. 2015, López-Serna et al. 2010, Panditi et al. 2013, Richardson 2009). For reliable determination of extraction efficiency (and eventually the analysis itself), it is essential to add isotopically labelled compounds prior to the SPE step. The use of isotopically labelled compounds has become a standard procedure and has risen in the recent years due to their abundant availability and reasonable pricing. As for the TPs, analytical method developed for the tentative analysis of TPs in environmental samples can be achieved even without the isolated, synthetized or commercially available standards since compound specific MS/MS parameters can be optimized from the mixture of the generated TPs. Additionally, sample pretreatment can be assumed similar to the parent compounds since they are usually chemically similar to the target analytes and structurally related to their parent compounds. In this case, TPs cannot be quantified from the samples due to lack of genuine calibration cure but rather semi-quantitative concentrations are reported using the parent compound validation parameters (Aceña et al. 2014, Goncalves et al. 2011, Gros et al. 2015, Radjenović et al. 2008, Rubirola et al. 2014). Naturally, more superior approach which involves procurement of the TP either by isolation/synthesis or by purchasing can give reliable measured concentration of the TPs detected in the environmental samples. This is crucial for a realistic assessment of the environmental fate of pharmaceuticals and their associated environmental risk. (Chiron et al. 2010, Garcia-Galan et al. 2012, Kaiser et al. 2014, Kormos et al. 2010, Kormos et al. 2009, Nödler et al. 2012, Prasse et al. 2011, Schulz et al. 2008, Wick et al. 2011). Another benefit of having an isolated standard is that they can be used furthermore for structural confirmation by analysing the compound with some complementary techniques like NMR (Chapter 1.3.).

In the examples on both photo and biodegradation experiments shown in **Table 1.1 and 1.2**, only a couple of studies tested the results of their batch experiments with the analysis of the environmental samples in order to confirm occurrence. Out of the ones that did develop additional methods for quantification of TPs concentrations, vast majority used LRMS

method for which it was necessary to develop an additional method by optimizing compound specific parameters needed for determination. Although this is considered as the best option for reliable quantification, nonetheless, it was necessary to change from instrument used for identification (typically HRMS) to LRMS, which is time consuming.

Still, as an alternative, HRMS instruments can be used for quantification of compounds, especially due to recent reported superior sensitivity over older generation of HRMS instruments (**Table 1.3.**). In this case, not only is it not necessary to optimize compound-specific parameters, but both identification method and screening from the real-world samples can be done used the same method, and, in some cases, in the same run.

1.4. Target high resolution mass spectrometry methods for detection and quantification of pharmaceuticals, metabolites and transformation products

HRMS has historically been used for qualitative analysis, but in recent years a growing number of validated HRMS targeted methods have been reported (Aceña et al. 2015a, Aceña et al. 2015b, Hernández et al. 2014, Leendert et al. 2015). Some of the recent examples are reported in **Table 1.3**. Principally the advantage of HRMS has over the more classical LR triple quadrupole (QqQ) mass spectrometer is that in a single run it is possible to obtain the information on both target and non-target compounds. In quantitative analysis by LC-MS/MS, using the selected reaction monitoring (SRM) mode has been shown to be very selective if at least two SRM transitions of the target compound are selected (when possible) for quantification and confirmation purposes. For a LRMS method the use of SRM of a QqQ offers a reliable quantification of a compound after a series of a rules are met. However, in order to be able to use the SRM on target compounds it is necessary to optimize compound-specific MS parameters like determination of fragment ion masses and collision energies. On the other hand, high selectivity of a full MS scan mode of a HRMS renders the pre-knowledge of a specific mass (compound) unnecessary and, theoretically, an unlimited number of analytes can be detected without compromising sensitivity (Aceña et al. 2015a).

For reliable confirmation of a compound using LRMS, EU Commission Decision 2002/657/EC published an identification point (IP) system covering different ion selection criteria and giving it a certain IP which in total have to be at least four. In SRM mode of a triple-quad instruments, this is achieved with one precursor selection (1 IP) and two product

ions transition (1.5 IP each). In HRMS, this requirement is already fulfilled with the selection of one precursor (2 IP if resolution higher than 20 000 FWHM) and one fragment ion (2.5 IP), totalling in 4.5 IPs. However, this IP system only has in mind the MS aspects for compound confirmation, whereas the LC parameters like retention time (RT) always have to be fulfilled. Although not as common, still false positives are possible when SRM is used for quantification of compounds, especially in complex matrices. This can often happen with coelution of isobaric compounds (i.e. the same nominal mass) which may share the same fragments monitored due to lack of selective fragmentation (like loss of water, ammonia or acid). Additionally, these isobaric interferences can induce the change in the ratio between two SRM transitions which in principle cannot be superior to 20 % in the sample vs. the calibration curve (Kaufmann et al. 2009, Schürmann et al. 2009). Typical solution to this problem would be to select alternative transitions even at the cost of lower intensity. Even so, this is not always possible and the use of HRMS is advised if a compound yields only two fragments or less (Gallart-Ayala et al. 2011).

Table 1.3. presents a chronological list of methods that have been developed and validated for detection and quantification of pharmaceuticals, metabolites and TPs in environmental samples using LC-HRMS. In general, all methods reported for acquisition used either full scan MS, full scan MS followed by selective MS^2 fragmentation, or full scan MS in parallel with (non-selective) MS^2 scan. While full scan MS is always used for peak integration and thus quantification purposes, the latter two modes are usually needed for confirmation of compounds. The difference between them is in the preselection of ions that will produce fragments. In the case of selective MS^2 fragmentation, an m/z is selected either by user (from the inclusion list) or can be generated by the instrument depending if the m/z has met some certain criteria (thus data-dependent) like the highest abundancy. The non-selective fragmentation refers to alternating spectra acquisition of both full scan MS and full scan MS after a certain collision energy is applied. With TOF instruments this experiment is called MS^E and both scans are run with the applied collision energy, low and high, respectively. In Orbitrap based instruments, the term used is all ion fragmentation (AIF). In this case the combination of full scan MS and scan after the collision in high-energy collisional dissociation cell (HCD) is coupled to produce the AIF.

Table 1.3. Target analysis of pharmaceuticals in environmental waters using LC-HRMS.

Number of compounds analysed	Matrix	Pre-concentration method	LOD range [ngL^{-1}]	LOQ range [ngL^{-1}]	HRMS instrument and resolving power	Ionization mode	MS method mode	Quantification	Confirmation with MS^2 fragmentation	Reference
29	Surface water and WWTP influent and effluent	SPE (Oasis HLB)	10 – 500	-	QTOF (Waters Micro TOF), 5000 FWHM at 556 m/z	ESI+ and ESI-	Two methods: Full scan MS and MS^2	Full scan MS data, 20 mD window	Yes, manually	(Petrovic et al. 2006)
20	Hospital wastewater	SPE (Oasis HLB)	4 - 115	14 - 384	QTOF (Agilent 1100), 9500 FWHM at 922 m/z	ESI+	Two methods: Full scan MS and MS^2	Full scan MS data, 10 mDa	Yes, manually	(José Gómez et al. 2007)
32	Drinking and Surface water, WWTP influent and effluent	SPE (Oasis HLB)	0.04 - 300	-	QTOF (Waters Micro TOF), 5000 FWHM at 556 m/z	ESI+ and ESI-	Two methods: Full scan MS and MS^2	Full scan MS data, 20 mD window	Yes, manually	(Farré et al. 2008)
15	WWTP influent and effluent	SPE (Oasis MCX and MAX)	2.1 - 285	7 - 940	QTOF (Waters Micro TOF), 5000 FWHM at 556 m/z	ESI+ and ESI-	Low and High collision energy/ MS^E	Full scan MS data, 30 mD window	Yes, manually – one fragment confirmation	(Lavén et al. 2009)
87	Surface water and WWTP effluent	SPE (Oasis HLB)	<5 - 50	-	QTOF (Agilent 6530), 19500 FWHM at 922 m/z	ESI+ and ESI-	Two methods: Full scan MS and MS^2	-	Yes, automatically matched against a database	(del Mar Gómez-Ramos et al. 2011)
16	WWTP effluent	SPE (Oasis MCX and Strata-X)	4 - 91	11 - 190	QTOF (Waters Micromass LCT Premier TOF), >11000 FWHM	ESI+ and ESI-	Full scan MS	Full scan MS data, 60 mDa	None	(Nurmi and Pellinen 2011)
17	Seawater	Passive sampler (polydimethylsiloxane)	0.5 – 5 [ng sheet-1]	1 – 10 [ng sheet-1]	Orbitrap (Thermo Exactive), 50000 FWHM at 400 m/z	ESI+ and ESI	Full scan MS	Full scan MS, 10 ppm	None	(Wille et al. 2011)
5	WWTP influent	SPE (Oasisi HLB)	0.7 – 8.8	2.1 - 27	Linear ion trap Orbitrap (Thermo LTQ-Orbitrap), 30000 FWHM at 400 m/z	ESI-	Full scan MS, MS^2, data-dependent (LTQ)	Full scan MS, 10 ppm	Yes, manually	(Cahill et al. 2012)

Number of compounds analysed	Matrix	Pre-concentration method	LOD range [ngL^{-1}]	LOQ range [ngL^{-1}]	HRMS instrument and resolving power	Ionization mode	MS method mode	Quantification	Confirmation with MS^2 fragmentation	Reference
100	Drinking, surface, groundwater, WWTP influent and effluent	SPE (Oasis HLB)	<10 - >1000	-	QTOF (Agilent 6540), 30000 FWHM at 1522 m/z	ESI+ and ESI-	Full scan MS[1]	Full scan MS, 50 mDa	None	(Ferrer and Thurman 2012)
24	WWTP influent and effluent	SPE (Oasis MCX)	-	2 - 50	QTOF (Agilent 6520), 4750 - 20000 FWHM at 113 - 980 m/z	ESI+ and ESI-	Full scan MS, MS^2	Full scan MS and MS^2, 20 and 40 ppm, respectively	Yes, automatically	(González-Mariño et al. 2012)
5	Drinking and Surface water, WWTP effluent	SPE (Chromabond Tetracycline)	-	0.6 - 32	QTOF (Agilent 6520), 20000 FWHM at 1522 m/z	ESI+ and ESI-	Full scan MS, data-dependent	Full scan MS, or SIM	Yes? unclear	(Martín et al. 2012)
10	Surface water	Direct injection	3 - 10	10 - 30	QTOF (AB Sciex, Triple TOF 5600), 20000 FWHM at 609 m/z	ESI+	Full scan MS, MS^2, data-dependent	Full scan MS, 50 ppm	Yes, automatically matched against a database	(Martínez Bueno et al. 2012)
24	Drinking, Surface water and wastewater	Online SPE (C18 column)	3 - 227	10 - 750	Orbitrap (Thermo Exactive), 25000 FWHM	ESI+ and ESI-	Full scan MS	Full scan MS, 10 ppm	None[2]	(Wode et al. 2012)
24	WWTP influent and effluent	SPE (Oasis HLB)	-	2 - 360	Linear ion trap Orbitrao (Thermo LTQ-Orbitrap), 30000 FWHM at 400 m/z	ESI+	Full scan MS, MS^2, data-dependent (LTQ)	Full scan MS, 10 ppm	Yes, manually	(Bijlsma et al. 2013b)
150 (including pesticides)	WWTP effluent	SPE (Oasis HLB)	-	-	QTOF (Waters Premier TOF), 10000 FWHM at 556 m/z	ESI+ and ESI-	Low and High collision energy/ MS^E	Full scan MS, 20 mDa	Yes, manually	(Diaz et al. 2013)
27	WWTP influent	Online SPE (C18 column)	-	Full Scan: 0.5 – 54 MS^2: 1.5 - 23	Q-Orbitrap (Thermo Q-Exactive), 70000 FWHM at 400 m/z	ESI+	Full scan MS, targeted - MS^2	Full scan MS and MS^2, 10 ppm	Yes, automatically	(Fedorova et al. 2013)

1 MS^2 used for isobaric compounds and transformation products
2 For confirmation, a ^{13}C isotope, ^{37}Cl isotope, or adduct mass match was used

Number of compounds analysed	Matrix	Pre-concentration method	LOD range [ngL^{-1}]	LOQ range [ngL^{-1}]	HRMS instrument and resolving power	Ionization mode	MS method mode	Quantification	Confirmation with MS^2 fragmentation	Reference
11	Drinking and Surface water, WWTP influent and effluent	SPE (Oasis HLB)	-	0.4 - 182	TOF (Bruker microTOF-Q), 20000 FWHM	ESI+ and ESI-	Full scan MS	Full scan MS, 20 mDa	None	(Al-Qaim et al. 2014)
7	Surface water, WWTP influent and effluent	SPE (Oasis MCX)	-	2 - 15	QTOF (Agilent 6520), 5000 FWHM at 120 m/z	ESI+	Full scan MS, MS^2	Full scan MS, 20 ppm	Yes, automatically	(Casado et al. 2014)
26	Untreated wastewater (Hospital and WWTP)	SPE (Oasis HLB)	-	0.7 - 356	Orbitrap (Thermo Exactive), 50000 FWHM at m/z 200	ESI+	Full scan MS	Full scan MS, 20 ppm	None	(Gomez-Canela et al. 2014)
32	Surface water and WWTP effluent	Direct injection	3 - 100	5 - 500	QTOF (AB Sciex, Triple TOF 5600)	ESI+	Full scan MS, MS^2, data-dependent	Full scan MS, 20 mDa	Yes, library search	(López et al. 2014)
69	Drinking and Surface water	Direct injection	20 - > 5000	50 - >5000	QTOF (Waters Xevo G2 QTOF), 20000 FWHM	ESI+ and ESI-	Low and High collision energy/ MS^E	Full scan MS and MS^2, 50 ppm	Yes	(Vergeynst et al. 2014)
67	Surface water	SPE (Strata X)	0.5 – 31.1	1 - 94	Q-Orbitrap (Thermo Q-Exactive), Full Scan: 70000 FWHM at 200 m/z, MS^2: 17500 at 200 m/z	ESI+ and ESI-	Full scan MS, targeted - MS^2	Full scan MS, 5 ppm	Yes, manually	(Chitescu et al. 2015)
43	WWTP influent and effluent	SPE (Oasis HLB)	0.5 - >2500	1.8 - >2500	Double focusing magnetic sector HRMS (MAT95XP-TRAP, Thermo Finnigan), 10000 resolving power	ESI+ and ESI-	Multiple ion detection (MID)	Multiple ion detection (MID)	None, istopic ratio used	(Vergeynst et al. 2015)
51	WWTP influent	SPE-DEX (Oasis HLB discs)	-	0.4 - 187	Q-TOF (Waters Xevo G2-S)	ESI+	Low and High collision energy/ MS^E	Full scan MS and MS^2, 10 ppm	Yes, automatically	(Baz-Lomba et al. 2016)

"-" – not reported; "FWHM" - Full width at half maximum

The benefit of using non-selective fragmentation is that that every ion that enters the MS (from a certain abundancy and up) will be fragmented, and this can be used for confirmation or interpretation aim even at a later stage for retrospective analysis. However, since this fragmentation is compound specific, one value most likely will not be accommodating for all ions, and application of a collision-energy ramp is advised. Selective MS^2, on the other hand, offers a compound specific fragmentation that can be directly matched either with local or on-line spectral libraries which aids confirmation. For target analysis this is matched typically with the local library using software designed to facilitate data-mining.

Despite the acknowledged advantages, confirmation with selective MS^2 is not always used in methods based on HRMS (**Table 1.3.**). This is most likely because higher intensities are needed of a certain m/z in order to be selected and broken down which translates, consequently to higher LOQ ascertained. This was more so true for studies case where the older generation of HRMS instruments were used for the analysis.

A particular challenge using HRMS instruments for target method development is the definition of LODs and LOQs. A classical approach using signal-to-noise ratio is often useless since often no noise is present in the extracted ion chromatogram (XIC) for the selected m/z. Several authors have proposed alternative ways on how to determine LOD and LOQ. In some cases, LOD was determined by using statistical or semi-statistical approach taking into account low concentration measurement variability (Casado et al. 2014, Fedorova et al. 2013, Leendert et al. 2015, Vergeynst et al. 2014). Others have used instrumental limits of detection (iLOD) for the calculation of method limits of detection (mLOD) by correcting for the matrix effect and sample extraction enrichment factor (Al-Qaim et al. 2014, Moschet et al. 2013). Moschet et al. (Moschet et al. 2013) calculated the LOQs of 45 pesticides by dividing the iLOQ of each substance in ultrapure water with the matrix factor. In their case, the matrix factor corrected for both ion suppression/enhancement and for compound recovery. Additionally, LODs were calculated based on signal intensity or peak area cut-offs (Gomez-Canela et al. 2014, Masia et al. 2014).

Like in the triple quad instruments, matrix effects due to ESI ionization were observed for ESI-HRMS. Moreover, in full-scan orbitrap MS an enhanced mass suppression was reported, likely due to post-interface matrix suppression when too many ions trapped (Fedorova et al. 2013, Kaufmann et al. 2010, Leendert et al. 2015). Also, there are some limitations if using HRMS coupled with ultra-performance liquid chromatography (UPLC)

and FT Orbitrap MS since faster scan times are needed in order to provide sufficient data points across narrow chromatographic peaks (Cahill et al. 2012, Dunn et al. 2008). In order to compensate for this, scan cycle time and LC peak width need to be optimized accordingly (Hogenboom et al. 2009).

1.5. Novel approaches for detection and identification of transformation products

As mentioned in the previous sections, in recent years, a growing attention has been paid to identification and evaluation of TPs of pharmaceuticals. However, the process of identifying and detecting them in the real aquatic samples is not straightforward. The most general, common approach is the TPs profiling which consists of degradation of a certain compound at lab-scale conditions at elevated concentration followed by TP detection, identification and quantification has been explained in the section 1.3. The main challenge associated with the quantification of TPs in environmental matrices is the low concentrations they are commonly detected, making very sensitive analytical techniques a requirement for reliable quantification. Likewise, complexity of the matrix can affect performance and kinetics which translates typically to the need to use elevated concentrations of compounds to be degraded in laboratory scale. Results of degradation studies can be used to assess the applied process however, conclusions drawn from the controlled experiments need to be validated in monitoring studies dedicated at detection of TPs in the real-world samples. Much of the target methodology and approaches for identification of compounds have been covered in chapters 1.2. and 1.3. In some cases, the reaction mechanism can be proposed together with kinetic studies. In this kind of approach, typically the last step would be the detection of the parent and TPs in the real aquatic system samples. Regarding of this final step, the detection in real samples can have four type of outcomes ie. parent and the TPs are a) all or majority detected in the samples (Kormos et al. 2010, Kormos et al. 2009, Prasse et al. 2011, Schulz et al. 2008, Wick et al. 2011), b) not detected or not reported (Kosjek et al. 2015, Rubirola et al. 2014, Zonja et al. 2014b), c) detected at low concentration or d) only parent and small number of TPs are detected (Kosjek et al. 2012). The latter three possibilities do pose an open question whether the need for a uniform approach should be considered. Here it will be discussed the two possible options that can be considered as alternatives to the TPs profiling; a) suspect screening in order to prioritize the parent and TPs based on

their detection, and/or b) non-target screening approach applicable for unknowns or unpredictable transformations (**Figure 1.4.**).

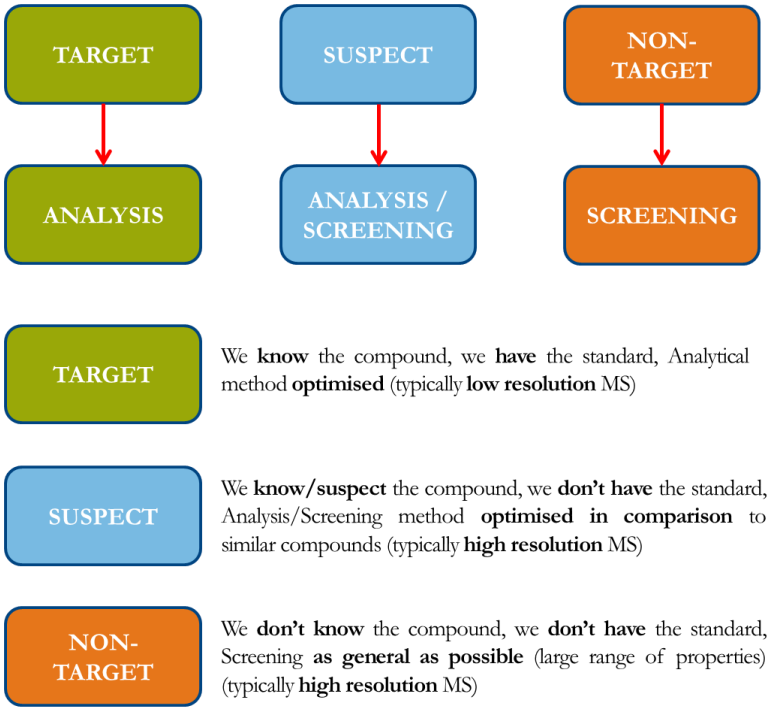

Figure 1.4. Differences between target, suspect and non-target analysis/screening.

1.5.1. Suspect screening approach

Suspect screening approach is a good alternative to TPs profiling approach because it allows for *a priori* detection of the suspected molecules in the real aquatic samples. They can either be predicted or generated in laboratory experiments without the need of a reference standard since molecular formula and/or structure are known. In a way, suspect screening is used for making sure that the compounds that will be identified and characterised, whether by a reaction mechanism or by a kinetic study, are already present in the aquatic samples that are monitored. In essence, the real-world detection step is forwarded right after the degradation and peak detection but prior to identification (**Figure 1.3.**). There are more than a few possibilities how to build a suspect list to be used for suspect screening of TPs (or metabolites or related compounds). This will ultimately depend on which process gives the resulting product. For suspect screening of TPs, the important step is the prediction of plausible TPs using *in silico* prediction tools based on computational algorithms. For

environmental analysis, several commercial and free software can be used for prediction of either biotic or abiotic TPs. One of the most widely used software for prediction in the environmental field is the University of Minnesota Pathway Prediction System (UM-PPS) (Gao et al. 2010, UM-PPS 2016). UM-PPS is a free software that predicts plausible pathways for microbial degradation of chemical compounds by using biotransformation rules based on reactions from their database and the ones found in the scientific literature. There are some limitations to the extent of the usefulness of the software. On one hand the addition of new pathways increases the number of possible degradation products and, thus high number of false positives are predicted as well (Bletsou et al. 2015). Additionally, UM-PPS has collected data from the degradation of pure cultures which do not automatically translate to the identical transformation pathways in the environmental systems (Helbling et al. 2010a). Apart from the UM-PPS prediction software, several others are available for prediction of either microbial metabolic reactions (CATABOL 2016), mammalian biotransformation reactions of usual functional groups (Meteor 2016), or biodegradation pathways of enzyme-catalysed reaction pathways of xenobiotic using KEGG database pathways and chemical structure alignments of substrate-product pairs (PathPred 2016). As for the abiotic processes, Zeneth software (Zeneth 2016) for prediction of degradation pathways derived from small molecule active pharmaceutical ingredients (APIs) like photochemical degradation or hydrolysis (Kleinman et al. 2014).

Once the suspect list is created from the predicted or generated TPs, HRMS analysis is performed which can provide a comprehensive picture of the overall contamination of samples with pharmaceuticals and their TPs. Successful suspect analysis relies on the application of HRMS for unequivocal determination of molecular ion exact masses and isotopic patterns. Furthermore, manual or automated data mining of fragmentation pattern plausibility or the pattern from spectral libraries is crucial for valid and meaningful results. However, as in the case of TPs profiling, different confidence levels can be applied for the identification of TPs (Schymanski et al. 2014a). The level the compound will be identified ultimately depends on the diagnostic evidence at hand. Several studies have tested computer-aided prediction of TPs for a comprehensive screening schemes. Kern et al. (Kern et al. 2009) used computer aided prediction to generate a list of TPs possibly forming from microbial metabolism. This list was joined with the list of predicted TPs with the ones reported in the scientific literature. Suspect screening was based on extracting the accurate mass from the

total ion chromatogram (TIC) with a very narrow extraction window, checking other parameters like plausible RT, and interpretation of each fragmentation pattern to communicate tentative detection of the target analyte(s). Although they did not have a standard of any of the TPs on the suspect list for quantification, they were able to detect nineteen TPs in several surface waters in Switzerland. Later on, Gómez Ramos et al. (Gomez-Ramos Mdel et al. 2011) developed an analytical method for the analysis of TPs of several pharmaceuticals in wastewater. They used an approach based on the use of fragmentation pattern of a compound during MS^2 and the relationship and consistency with the transformations experimented by these chemicals in the environment or during water treatment processes. Finally, eight TPs were detected in the samples analysed, three of which were confirmed and quantified by an analytical standard. This structure-fragment relationship between the parent and potential TP reported by Gomez Ramos et al. has been used in several more studies. Perhaps the most comprehensive assessment was performed by Schollée et al. (Schollée et al. 2015). There, they analysed influent and effluent wastewater where WWTP influent was spiked with parent compounds and human metabolites and WWTP effluent have been spiked with commercially available biotransformation TPs. In essence, they studied whether it would be possible to link the parent compound with its TP formed during WWTP secondary treatment. Except for one compound, all the others were statistically significant. However, many compounds did not show difference of more than one order of magnitude between influent and effluent. Finally, out of the 42 compounds investigated, 17 did not meet the threshold (Schollée et al. 2015). In addition to screening for confirmation purposes, there have been several attempts to define the suspect screening detection limits (SDL) and identification detection limits (IDL). Diaz et al. (Diaz et al. 2013) analysed nine water samples which were spiked at two concentration levels. They defined SNL as the lowest concentration level where a compound was detected in all samples using the most abundant ion. On the other hand, the IDL was defined as the lowest concentration for which a compound was satisfactorily identified in all spiked samples (presence of, at least, two m/z ions, expected retention time and minimum peak width of 5 and maximum mass error of 2 mDa). However, these two validation parameters clash with common understanding of suspect screening which takes a known-unknown as a must without the reference standard. If the standard exists, that the more appropriate term would be target analysis and these parameters would be the standard LODs/LOQs.

1.5.2. Non-target approach: detection of unknowns

Compared to suspect screening, non-target is a more complex approach since there is no previous information available on the compounds that are detected when used for evaluation of degradation. If the detected compound does not match any known compound (e.g. from a library) then a task of identifying its structure and linking its pre-degradation predecessor is necessary and helpful. The potential TP detected can be matched for example with the parent compound's fragmentation pattern, molecular ion or RT which can help filter the possible structures and, hence, facilitate the identification of the TP. In non-target screening, in order to achieve sufficient mass accuracy for confirmation of the elemental composition, HRMS is advised. Alternative to this is the search in available prediction systems (described in **section 1.5.2.**) which can help give an estimate whether a reaction linking it with the parent compound is feasible or not.

When working with HRMS, a large sets of data are generated and post-acquisition data processing tools are needed for efficient and rapid data treatment. In recent years, several commercial and freely available software have been developed for non-target data mining. Commercial software are mainly vendor software which are adapted to be used depending on the instrument sold. Additionally, the following open source software are available, and most commonly used: ENVIPY (ENVYPY 2016) or MZmine (MZmine_2 2016). These software are used for many steps needed for filtering of the detected mass of interest. The first step is peak picking which is followed by removal of noise peaks in comparison with control or blank samples. Following componentisation of isotopes and adducts, the crucial step is to determine the correct elemental composition of the exact mass detected which is typically performed by using the heuristic rules like seven golden rules by Kind and Fiehn (Kind and Fiehn 2007). Final step, in this workflow would be then the search of different chemical databases like Chemspider, NIST or PubChem which can give a candidate structures matched to the molecular formula determined in the previous step. Unfortunately, a large number of compounds are still typically suggested which can create big noise around the correct structure with the additional drawback that many databases have only included the parent compounds and not TPs in their library. However, if some information exists of the parent compound (which can be related to its TP), this can go long way and aid filtering to lesser number of candidates (Huntscha et al. 2014). Nonetheless, when no information can be matched to the parent compound, the most common strategy for peaks selection (in

service of time and effort effectiveness) is prioritisation by the most intense peaks (Schymanski et al. 2014b). In this case, the ranking of the most plausible candidate structure is performed by matching the fragmentation pattern of the mass of interest with the *in silico* mass fragmentation software like MassFrontier (MassFrontier 2016) which typically use fragmentation rules. Other option would be matching the fragmentation pattern with the ones in the spectral libraries like MassBank (MassBank 2016).

Chapter 2. Objectives of the thesis

In view of the limited information on formation and whereabouts of the transformation products in the environment, the overall objective of this thesis was to generate detailed knowledge on the transformation of the selected human pharmaceuticals: (an antiviral zanamivir, several iodinated contrast media compounds and an anticonvulsant lamotrigine) which had been only marginally addressed in the scientific literature. Using at the early stages well-established approaches for transformation products profiling, standard approaches were then refined, and ultimately innovative approaches were devised to streamline and automate the process of transformation products detection, characterisation, prioritisation and quantification in the aquatic system.

The specific objectives of this thesis were the following:

a) To evaluate the phototransformation of the antiviral zanamivir in surface water during 2008 influenza A epidemic.

The phototransformation products were identified using the well-established approach relying on manual peak search for emerging peaks in the LC-MS data (TPs profiling).

b) To evaluate the phototransformation of the highly prominent iodinated X-ray contrast media in surface water.

In contrast to the workflow used to achieve objective a), a combination of laboratory degradation experiments and suspect screening of real-world samples was used to prioritize surface water – relevant transformation products. This was expected to optimise the efforts required for time-intensive structural elucidations.

c) To investigate the fate of the poorly studied anticonvulsant lamotrigine in wastewater treatment plants.

Here, mass balance studies were carried out in the laboratory batch reactors as well as in real, raw and treated sewage samples from wastewater treatment plants in order to ensure that all relevant transformation products involved in the degradation pathways were qualified.

Chapter 3. Zanamivir and Iodinated Contrast Media: Phototransformation in Surface Water

3.1. Occurrence and fate of Zanamivir in the aquatic environment

Zanamivir (ZAN) is a highly potent and selective neuraminidase inhibitor recommended by world health organisation (WHO) for the treatment of influenza virus A and B during pandemics since it is preventing the infection of further healthy cells. Chemically, ZAN is a guanidine derivative of neuraminic acid, it is soluble in water and highly polar compound with the logP of -5.83. **Figure 3.1.** summarises some physico-chemical and pharmaco-kinetic properties of ZAN.

The use of ZAN rose as an alternative to another antiviral compound, Tamiflu (oseltamivir) which showed resistance to H1N1 virus during the 2008–09 flu season in Japan (Azuma et al. 2012). Likewise, in the eventual case of a pandemic caused by a viral infection it can be expected elevated and more concentrated use of ZAN since some other strains of virus already showed resistance to the oseltamivir as well (Nidzworski et al. 2014, Renzette et al. 2014, Woche et al. 2016).

Sanderson et al. (Sanderson et al. 2004) used quantitative structure–activity relationship (QSAR) modelling to predict most hazardous therapeutic classes with regards to their toxicity towards algae, daphnia and fish. Of almost 3000 compounds investigated, the antiviral drugs were placed among the eighth most hazardous drugs according to the investigated toxicity (Sanderson et al. 2004). On the other hand, as reported by Cunningham et al. (Cunningham et al. 2009), ZAN does not appear to pose an appreciable risk to human health from potential environmental exposure through consumption of, for example, contaminated drinking water and fish. They calculated the predicted environmental concentration (PEC) of ZAN and was estimated to be 0.1 ng L^{-1} in surface waters. However, although the worst-case scenario parameters were used, some uncertainties with the human health and the chronic exposures to mixtures of pharmaceuticals remain. In the case of oseltamivir, its PEC in case of a pandemic was reported to be up to 12 μgL^{-1} in the wastewater (Singer et al. 2007, Slater et al. 2011, Woche et al. 2016).

A

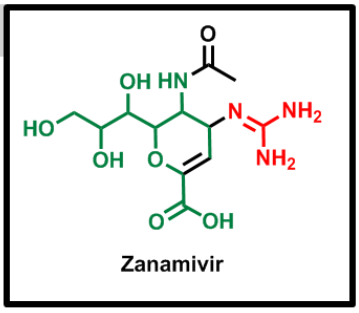

Zanamivir

B

Physico-chemical and pharmaco-kinetic properties of Zanamivir	
Names	Relenza, Zanamivir
MW	332.31 g/mol
Formula	$C_{12}H_{20}N_4O_7$
CAS	139110-80-8
Water solubility	7.31 mg/mL (25°C)
logP	- 5.83
pKa (strongest acidic/basic)	3.25 / 11.93
Dosage	5 – 20 mg
Excretion	renal in 24 h
Half life	2.5 – 5.1 h
Metabolims	Not metabolised

Figure 3.1. The structure of the antiviral Zanamivir (A), a guanidine derivative of neuraminic acid. Guanidine moiety is shown in red and the remaining structure of neuraminic acid in green. The table (B) shows basic physico-chemical and pharmaco-kinetic properties of Zanamivir. The data shown here have been collected from: Chemaxon platform (Chemaxon 2016), PubChem (PubChem 2016), FDA (FDA 2016b) and DrugBank (DrugBank 2016).

Antiviral drugs, in general, are administered in the early stages of an outbreak if there is no suitable vaccine available. Therefore, high amounts of these drugs would be consumed worldwide and could, thus, reach the environment either via human excretions or improper disposal (Bosch et al. 2007, Cunningham et al. 2009, Chan et al. 2011).

Cunningham et al. (Cunningham et al. 2009) also reported that ZAN suffers negligible metabolism in the human body and almost 100 % is renally excreted within 24 h (**Figure 3.1.**). Given the negative logD of ZAN this is to be expected. Therefore, only small amounts of the compound are absorbed by the human body. Since the ZAN in not transformed in the liver, the remainder of the drug is excreted intact in urine (Woche et al. 2016). As a consequence, high amounts of the compound would reach wastewater, and, since the removal by both primary and secondary wastewater treatments is also insignificant (Cunningham et al. 2009), ZAN could easily end up in surface water.

Only a couple of studies reported the occurrence of ZAN in wastewater and surface water. Azuma et al. (Azuma et al. 2012) reported concentrations of ZAN in WWTPs and surface water with the concentration of up to 15 ng L^{-1} in surface water. Another study found ZAN in the WWTP effluent at the concentration up to 46.5 ngL^{-1} and up to 58.8 ngL^{-1} in surface water (Takanami et al. 2012). However, up to date of the Article N°1, and to the best of the authors knowledge there were no studies that investigated the photolytic fate of ZAN in surface water.

3.2. Fate and transformation of iodinated contrast media in the aquatic environment

Iodinated X-ray contrast media (ICM) are pharmaceuticals used in human medicine for soft tissue imaging (organs or blood vessels) during diagnostic test (Pérez and Barceló 2007b). Chemically, the ICM studied in this thesis (**Figure 3.2**) are derivatives of 2,4,6-triiodobenzoic acid with polar carboxyl, amide and hydroxyl moieties in their sidechains (positions 1,3 and 5 in **Figure 3.2.**). In general, all ICM have iodine atoms in their structure which will absorb the X-rays during diagnostic testing. They are water soluble and polar compounds that can be either ionic, like diatrizoate (DTZ) (i.e. it has one free carboxyl group), while most of the other ICM are neutral compounds (i.e. all side chains are amide derivatives). **Table 3.1.** summarises some physico-chemical and pharmaco-kinetic properties of the ICM.

In the human body, ICM are metabolically very stable and are considered as chemically inert drugs which are rapidly eliminated from the body via urine or faeces (typically within one day) (**Table 3.1.**). Having in mind that they are not metabolised, and the relative high doses used per diagnostic test (up to 200 g), ICM are typically detected in raw wastewater at μgL^{-1} concentrations (Kormos et al. 2011, Pérez and Barceló 2007b, Ternes and Hirsch 2000).

Over the years multitude of methods based on LC-MS/MS have been developed and/or applied to study the occurrence of the ICM in wastewater and surface water (Echeverría et al. 2013, Ens et al. 2014, Hirsch et al. 2000, Kormos et al. 2011, Seitz et al. 2006, Ternes and Hirsch 2000, Watanabe et al. 2015, Yoon et al. 2010). One of the most comprehensive monitoring study on occurrence of ICM was reported by Loos et al. (Loos et al. 2013). In that study, 90 European WWTPs were sampled and analysed for the presence of 156 polar organic contaminates. They ranked the targeted compounds by detection frequency. With this broad scale study, reported detection frequencies of ICM were below expected: from 15 – 47 % in WWTP effluents. Based on their list, they were in the mid detection frequency range, topped by corrosion inhibitors (benzotriazoles), organophosphate ester flame retardants and plasticizers, and other pharmaceuticals like gandolinum (a non-iodinated contrast media) or risperidone, an antipsychotic. The rank order slightly changed when the compounds were sorted by median concentration. In this case, pharmaceuticals (e.g. carbamazepine) and artificial sweeteners joined the benzatriazoles and organophosphates as the compounds with the highest median concentration (Loos et al. 2013). However, regarding ICM detection with

the LC-MS/MS, it has to be noted that the LOQs for these compounds were on average 10 times higher than those of other compounds investigated. Most likely, if lower LOQ would have been achieved, ICM would have ended up higher on the list of the most frequently detected compounds.

A

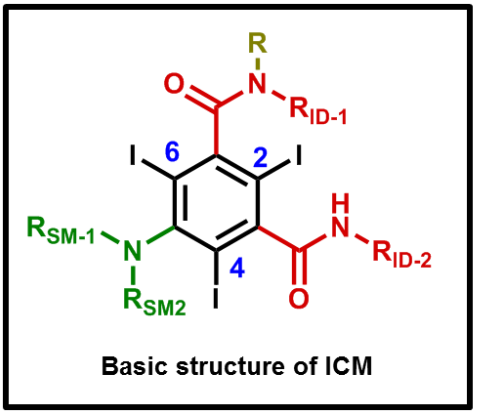

B

Name	R_{SM-1}	R_{SM-2}	R_{ID-1-2}	R	Abb
Iomeprol		H	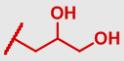	H	IMP
Iopamidol		CH_3	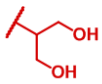	H	IPM
Iopromide	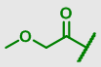	H	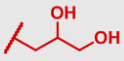	CH_3	IOP
Iohexol	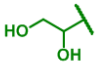		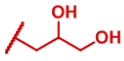	H	IOX
Iodixanol[a]	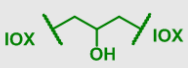		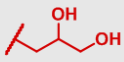	H	IDX
Diatrizoate[b]	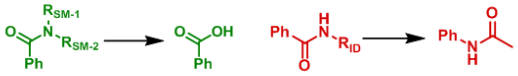				DTZ

Figure 3.2. The structures of ICM (A) where R_{ID} stands for substituents on the identical side chain (ID) for the two lateral chains in position 1 and 3 (drawn in red); R_{SM} stands for substituents on the similar side chain (SM) in position 5 (drawn in green); R stands for the substituent on one of the ID side chains (drawn in dark yellow).

The table (B) shows the substituents that are specific to each ICM studied in this thesis; [a]Iodixanol is a dimer of two iohexol molecules connected over a bridge in the ID side chain; [b]Diatrizoate has a SM side chain which is carboxylic acid (not an amide) and the ID side chains are phenylacetamide (not benzamide)

As mentioned in the introduction chapter, microbial degradation and adsorption to sludge are the most important processes in removal of pharmaceuticals in WWTPs. Although ICM do not undergo metabolism in the human body, they have been shown to be degraded in batch reactors with activated sludge (Pérez and Barceló 2007b, Pérez et al. 2006). Perez et al. (Pérez et al. 2006) reported degradation of iopromide (IOP) in batch reactors containing WWTP activated sludge or nitrifying activated sludge. They reported a 90 % removal after 9 days and identified three biodegradation TPs which were mainly the result of oxidation of primary alcohols by formation of carboxylates (Pérez et al. 2006). In another study by Schulz et al. (Schulz et al. 2008), again IOP was degraded in a water/soil system (soil was taken from a wastewater irrigation area and mixed with groundwater) over the course of 103 days. In this case, twelve TPs were detected and their structures elucidated. This was the first time that a TP of an ICM was screened and detected in wastewater. One TP was detected at a concentration as high as 3.7 μgL^{-1} in WWTP effluent (Schulz et al. 2008).

	IMP	IPM	IOP	IOX	IDX	DTZ
Names	Iomeron, Imeron, Accudenz	Iopamiro, Iopamigita, Scanlux	Ultravist, Clarograf, Iopromid	Omnipaque, Histodenz, Nitigraf	Visipaque, OptiPrep, Indixanol	Gastrolux, Pielograf, Urografin
MW	777.09 $gmol^{-1}$	777.09 $gmol^{-1}$	791.11 $gmol^{-1}$	821.14 $gmol^{-1}$	1550.19 $gmol^{-1}$	613.92 $gmol^{-1}$
Formula	$C_{17}H_{22}N_3I_3O_8$	$C_{17}H_{22}N_3I_3O_8$	$C_{18}H_{24}N_3I_3O_8$	$C_{19}H_{26}N_3I_3O_9$	$C_{35}H_{44}N_6I_6O_{15}$	$C_{11}H_9N_2I_3O_4$
CAS	78649-41-9	60166-93-0	73334-07-3	66108-95-0	92339-11-2	117-96-4
Water solubility	0.117 $mgmL^{-1}$	0.117 $mgmL^{-1}$	0.092 $mgmL^{-1}$	0.796 $mgmL^{-1}$	0.185 $mgmL^{-1}$	0.107 $mgmL^{-1}$
logP	-1.45	-0.74	-0.44	-1.95	-2.06	2.89
pKa (strongest acidic/basic)	11.73 / -1.36	11.00 / -1.55	11.09 / -1.40	11.73 / -1.36	11.44 / -1.06	2.17 / -4.2
Dosage	Dosage of ICM strongly depends on the type of X-ray based imaging techniques and the type of tissue to be visualised. They are typically used at concentrations of ~ 350 $mgmL^{-1}$ of iodine content.					
Excretion	In healthy subjects, these ICM are excreted renally. 90 % of the dose is recovered in urine between 24 and 96 h. 2 % of the dose is recovered in faeces					
Half life	0.5 – 1.9 h	~ 2 h	~ 2 h	2 - 3.4 h	~ 2.1 h	0.5 – 2 h
Metabolims	No significant metabolism, deiodination, or biotransformation occurs.					

Table 3.1. Physicochemical properties of ICM. The data shown have been taken from: Chemaxon platform (Chemaxon 2016), PubChem (PubChem 2016), FDA (FDA 2016b) and DrugBank (DrugBank 2016).

Follow-up studies by Ternes group (Kormos et al. 2010, Kormos et al. 2011, Kormos et al. 2009), expanded the degradation in water/soil system to four other ICM (DTZ, IOX, IPM and IMP). In the study on the occurrence of ICM and TPs in the water cycle, Kormos et al. (Kormos et al. 2011) developed a method for the determination of four iodinated X-ray contrast media (ICM) and 46 ICM biotransformation products (bioTPs) in raw and treated wastewater, surface water, groundwater, and drinking water. Out of the 46 TPs, 26 were detected in wastewater above their LOQ and several were detected in drinking water at levels as high as 0.5 μgL^{-1}.

Although ICM are partially removed in WWTPs, they are not readily mineralised but are rather transformed. In addition to biological elimination, ICM could be removed from wastewater by the application of advanced oxidation processes (AOPs) or advanced reduction processes (ARPs) which use the reactive species to degrade recalcitrant compounds (AOPs use hydroxyl radicals (·OH) while in ARPs, either reducing hydrated electron (e^-_{aq}) or hydrogen atom (H·) are used) (Jeong et al. 2010, Rosenfeldt and Linden 2004, Song et al. 2008).Several studies applied these processes to investigate the degradation of ICM using either UV photolysis, the combination of UV and peroxide (UV/H_2O_2), UV/TiO_2, UV-Vis/Fe(II)-oxalate/H_2O_2 or ozonation (Altmann et al. 2014, Doll and Frimmel 2004, Huber et al. 2003, Jeong et al. 2010, Rastogi et al. 2014, Seitz et al. 2008, Ternes et al. 2003, Zhao et al. 2014). Jeong et al. (Jeong et al. 2010) applied both AOPs and ARPs in the degradation of five ICM (DTZ, IOX, IOP, IPM and IMP) under γ-irradiation. The efficiencies of e^-_{aq} reaction with the five ICM ranged from 69 to 87 % and for ·OH reaction ranged from 68 to 79 % except for the ionic ICM - DTZ (40 %) (Jeong et al. 2010). Tian et al. (Tian et al. 2014) reported that IPM can be effectively decomposed by UV irradiation at 254 nm which followed pseudo-first order reaction kinetics. They achieved almost complete removal of IPM in 5 min. In a study by Chan et al. (Chan et al. 2010), near-complete mineralisation of IOP was achieved in less than 80 min. with the combination of UV (254 nm) and potassium peroxydisulfate. As reported, the degradation is believed to be caused principally by the combination of direct photolysis and sulphate radical attack. In a follow-up study (Chu et al. 2011), a > 80 % removal of IOP was achieved after 30 min. with the combination of sulphate and hydroxyl radicals attacks at acidic pH (in a $UV/S_2O_8^{2-}/H_2O_2$ system).

One of the most comprehensive studies on removal of ICM (together with other micro-contaminants) in hospital wastewater was reported by Kovalova et al. (Kovalova et al. 2013) where in a pilot-scale WWTP, five different post-treatment technologies (ozone (O_3), O_3/H_2O_2, powdered activated carbon (PAC), and low pressure UV light with and without TiO_2) were evaluated as to their elimination efficiency. ICM accounted for 95 % of the mass load of all compounds analysed. Although the elimination of non-ionic ICM with the post-treatment technologies was between 50 and 65 %, an ionic ICM – DTZ was recalcitrant and could be substantially removed only with high doses of UV. They also report that combined treatments (O_3/H_2O_2 and UV/TiO_2) did not improve the elimination compared to the single treatments (O_3 or UV) (Kovalova et al. 2013).

Radjenovic et al. (Radjenovic et al. 2013) studied degradation of DTZ by electrochemical reduction (graphite felt doped with palladium nanoparticles) and oxidation (boron-doped diamond anode) in a continuous–mode, three-compartment reactor. In hospital effluent, around 60 % of DTZ was removed after approximately 2 h of electrolysis (Radjenovic et al. 2013). More recently, electrooxidation at boron-doped diamond anode using sulphate and inert nitrate analyte proved efficient for deiodination of DTZ and IOP (Radjenovic and Petrovic 2016).

Apart from the engineered processes which are mainly tested for elimination of ICM from wastewater, solar degradation is a process of natural attenuation where sunlight could potentially degrade polar compounds in the environment and especially in surface water. Up until now, there have only been a couple of studies evaluating the degradation of ICM using either simulated or natural sunlight (Doll and Frimmel 2003, Pérez and Barceló 2007b, Perez et al. 2009, Steger-Hartmann et al. 2002). Doll and Frimmel (Doll and Frimmel 2003) evaluated the degradation of IMP and Pérez et al. (Perez et al. 2009) the degradation of IOP in water using simulated sunlight. The former study showed that IMP was degraded in the batch experiments and, in parallel, iodide detection provided evidence of deiodination. Unfortunately, no efforts were made to identify deiodianted TPs. In the latter study, Perez et al. (Perez et al. 2009) showed that IOP was almost completely degraded after 2 h of irradiation in aqueous solution using a Suntest solar simulator. The degradation of IOP was led to the formation of eight TPs which were identified using QqTOF-MS. However, neither the photoTPs of IOP nor other photoTPs from other ICM have been searched in real environmental samples. Thus their concentrations in real-world aquatic environment still have not been reported.

3.3. Chapter objectives

3.3.1. To evaluate the phototransformation of the antiviral zanamivir in surface water during 2008 influenza A epidemic.

The phototransformation products were identified using the well-established approach relying on manual peak search for emerging peaks in the LC-MS data (TPs profiling).

Since ZAN is not metabolised in the human body and is not readily biodegradable in WWTPs, and is, therefore, is released in the surface waters (Woche et al. 2016), in the **Article Nº1** entitled ***Evaluation of the phototransformation of the antiviral zanamivir in surface waters through identification of transformation products,*** we explore the susceptibility of ZAN to photodegrade in surface waters where photochemical degradation is likely to be the key process governing the whereabouts of organic micro-pollutants in surface waters (Aguera et al. 2005, Andreozzi et al. 2003, Doll and Frimmel 2003).

3.3.2. To evaluate the phototransformation of the highly prominent iodinated X-ray contrast media in surface water.

In contrast to the workflow used to achieve objective a), a combination of laboratory degradation experiments and suspect screening of real-world samples was used to prioritize surface water – relevant transformation products. This was expected to optimise the efforts required for time-intensive structural elucidations.

Due to the relevant surface water concentrations of ICMs, known phototransformation of IOP (Perez et al. 2009), their contribution to adsorbable organohalogens (AOX) (Putschew et al. 2000) and possible formation of highly toxic iodinated disinfection by-products in waterworks (Duirk et al. 2011), in the **Article Nº2** entitled ***LC-HRMS suspect screening for detection-based prioritization of iodinated contrast media photodegradates in surface waters***, we investigated the photodegradation of six ICM (IDX, IOP, IOX, IMP, IPM and DTZ) in surface waters by identification of their most relevant TPs based on their detection in river water samples collected and analysed.

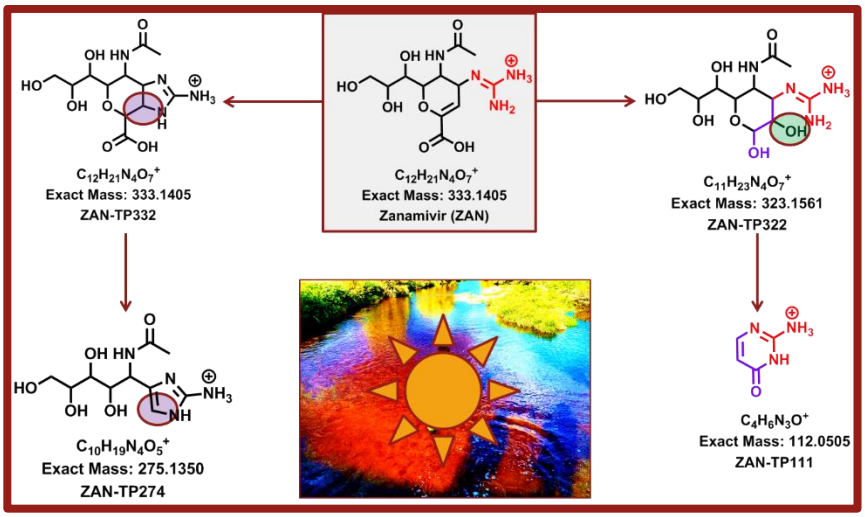

Article N°1:

<u>Zonja, B.</u>, Goncalves, C., Perez, S., Delgado, A., Petrovic, M., Alpendurada, M.F. and Barcelo, D.

Evaluation of the phototransformation of the antiviral zanamivir in surface waters through identification of transformation products.

(2014.) J Hazard Mater 265, 296-304.

Journal of Hazardous Materials 265 (2014) 296–304

Contents lists available at ScienceDirect

Journal of Hazardous Materials

journal homepage: www.elsevier.com/locate/jhazmat

Evaluation of the phototransformation of the antiviral zanamivir in surface waters through identification of transformation products

Bozo Zonja[a], Carlos Gonçalves[b,c], Sandra Pérez[a,*], Antonio Delgado[d,e], Mira Petrovic[f,g], Maria Fátima Alpendurada[b,c], Damià Barceló[a,g]

[a] Water and Soil Quality Research Group, IDAEA-CSIC, c/ Jordi Girona, 18-26, 08034 Barcelona, Spain
[b] IAREN – Water Institute of the Northern Region, Rua Dr. Eduardo Torres, 229, 4450-113 Matosinhos, Portugal
[c] Laboratory of Hydrology, Faculty of Pharmacy, University of Porto, Rua Aníbal Cunha, 164, 4050-047 Porto, Portugal
[d] University of Barcelona (UB), Faculty of Pharmacy; Unit of Medicinal Chemistry (Associated to CSIC), Avda. Joan XXIII, s/n, 08028 Barcelona, Spain
[e] Institute of Advanced Chemistry of Catalonia (IQAC-CSIC), Research Unit on Bioactive Molecules (RUBAM), Department of Biomedicinal Chemistry, Jordi Girona 18-26, 08034 Barcelona, Spain
[f] ICREA, Passeig Lluis Companys 23, 08010 Barcelona, Spain
[g] ICRA, C/ Emili Grahit, 101, Edifici H2O, 17003 Girona, Spain

HIGHLIGHTS

- Sunlight photodegradation of zanamivir in surface waters was investigated.
- Four new TPs were tentatively identified of which one was persistent.
- A new methodology using HILIC-LTQ Orbitrap-MS for identification of the TPs was established.
- Phototransformation pathways of zanamivir were mechanistically explained.

ARTICLE INFO

Article history:
Received 29 August 2013
Received in revised form 2 October 2013
Accepted 4 October 2013
Available online 24 October 2013

Keywords:
Photodegradation
Pharmaceutical
LC–MS
High resolution
Transformation products and pathways

ABSTRACT

The antiviral zanamivir has been recently reported to occur in surface waters where its presence may lead to the selection of resistant strains of virus in aquatic fauna. In order to evaluate the fate of zanamivir in surface waters, its susceptibility to phototransformation was evaluated using simulated and natural sunlight. Upon exposure of aqueous solutions (20 μg L^{-1}) to simulated sunlight, zanamivir in surface water degraded at $t_{1/2}$ 3.6 h. Under natural sunlight in surface water about 30% of the initial concentration of the antiviral disappeared within 18 days. The experiments with surface water showed similar effect as humic acid addition with expected decreasing effect on degradation while nitrate addition showed increasing effect. In the experiments with artificial sunlight at high concentrations of zanamivir, four photoproducts were tentatively identified by hydrophilic interaction chromatography-LTQ-Orbitrap-MS, showing $[M+H]^+$ ions at *m/z* 112 (TP111), *m/z* 275 (TP274), *m/z* 323 (TP322), and *m/z* 333 (TP332). However at 20 μg L^{-1} only the formation of the recalcitrant TP111 was observed. The proposed structures were rationalized by photolysis mechanisms. Photoproduct TP111 was confirmed with a commercially available standard (isocytosine). In summary, the findings suggest that the photodegradation of zanamivir in surface waters proceeds with slow kinetics.

1. Introduction

Zanamivir is a highly potent and selective neuraminidase inhibitor recommended by WHO for the treatment and prophylaxis of influenza virus A and B during pandemias. Several countries increased the stockpiles of zanamivir as an alternative to oseltamivir following the 2009 influenza pandemia [1]. For instance, the use of zanamivir rose as Tamiflu (oseltamivir)-resistant H1N1 virus was recorded during the 2008–09 flu season in Japan [2]. Furthermore, in the absence of suitable vaccines in the early stages of influenza outbreaks, the first line of defence is antiviral drugs. Large amounts of these drugs are, thus, consumed worldwide and may reach the environment via human excretions or improper disposal [3–5]. The effectiveness of these drugs will diminish with the emergence of resistant strains of the virus caused by improper human use and undesired high levels of antivirals in the aquatic environment in contact with wildfowl [4].

* Corresponding author at: IDAEA-CSIC, Department of Environmental Chemistry, Jordi Girona 18-26, Barcelona 08034, Spain. Tel.: +34 93 400 6100x5310; fax: +34 93 204 5904.
E-mail addresses: spsqam@cid.csic.es, spsqam@idaea.csic.es (S. Pérez).

0304-3894/$ – see front matter © 2013 Elsevier B.V. All rights reserved.
http://dx.doi.org/10.1016/j.jhazmat.2013.10.008

Using Q(SAR) modelling for 2986 different compounds, Sanderson et al. [6] ranked the antiviral drugs among the eighth predicted most hazardous therapeutic classes with regard to their toxicity towards algae, daphnia and fish. The reports of Cunningham et al. [5] showed that zanamivir suffers negligible metabolism in human body (almost 100% is renally excreted) and removal by both primary and secondary wastewater treatments is also insignificant. Based on the modelling carried out by these authors, zanamivir did not appear to pose an appreciable risk to human health from potential environmental exposure through consumption of contaminated drinking water and fish. Even though worst case scenarios were used for several variables, the predicted environmental concentrations (PEC) are average figures, not taking into account neither peak seasonal or pandemic disease nor seasonal decrease of river flow rates. Furthermore, indirect risks from development of antiviral resistance were not taken into account. The PEC for zanamivir was estimated to be 0.1 ng L^{-1} in surface waters [5]. The same authors reckon that a number of uncertainties remain, including: the assessment of the human health risk of chronic exposures to mixtures of pharmaceuticals; relative susceptibility of individuals and the effectiveness of existing water treatment technologies in removing pharmaceutical residues [5].

Due to its high polarity, the analytical determination of zanamivir is challenging and, as of today, few liquid chromatography–mass spectrometry (LC–MS)-based methods have been developed. Most of them deal with the analysis of the antiviral agent in biological matrices. Column chemistries varied from normal phase LC [7], reversed-phase (RP) LC [8] and hydrophilic interaction liquid chromatography (HILIC) [9]. The attractiveness of the latter variant arises from the fact that the mobile phase composition is fully compatible with electrospray ionization (ESI) with an elevated percentage of organic solvent in the mobile phase enhancing ionization efficiency and thus detection sensitivity [10].

A recent study from 2012 on the presence of zanamivir in samples from wastewater treatment plants and surface waters showed that it was detectable in river water (up to 15 ng L^{-1}) [2]. Despite these low levels awareness should be kept on the selection of resistant strains of virus in the aquatic fauna. In future years it is possible that the general usage of the drug will increase, since some influenza virus showed resistance to alternative drugs [11]. As reported [12–14] in surface waters, photochemical degradation is likely to be the most important mechanism for many pharmaceutical pollutants loss, which would make the knowledge of the photodegradation pathways and kinetics essential to predict the behaviour and the environmental impact of these pollutants in natural waters. To date, there is no information about the photodegradation mechanisms of zanamivir in surface waters and in view of the presence of zanamivir in surface waters and having in mind its possible increasing usage, in this work we studied the susceptibility of zanamivir to photodegradation in surface waters, which is considered a key process governing the whereabouts of organic micro-pollutants in surface waters. Irradiation experiments were carried out under simulated solar irradiation using a Suntest apparatus as well as by exposure to natural sunlight during autumn of 2009. Identification of transformation products were assessed by HILIC coupled to high-resolution LTQ-Orbitrap-MS. Low resolution tandem MS on a triple quadrupole MS was employed for studying the photolysis kinetics in different synthetic and natural matrices.

2. Experimental

2.1. Chemicals and reagents

Zanamivir (CAS 139110-80-8) was purchased from Toronto Research Chemicals (Ontario, Canada) and Isocytosine (CAS 108-53-2), purity ≥99%, was purchased from Sigma–Aldrich (Bellefonte, PA, USA). Water and acetonitrile for the LTQ-Orbitrap-MS analysis were purchased from Fischer Scientific in case of analysis while methanol was Baker analyzed LC–MS reagent (JTBaker, Deventer, Netherlands). Water, acetonitrile and methanol for UPLC–tandem MS analysis were LiChrosolv grade from Merck (Darmstadt, Germany). Formic acid Suprapur (>98%) was obtained also from Merck. The chemical actinometer 2-nitrobenzaldehyde (CAS 552-89-6, 98% purity) was obtained from Sigma–Aldrich.

2.2. Measurement of UV spectra and quantum yield calculation

Measurement of the UV–vis spectra is included in the supporting information. The quantum yield was calculated using 2-Nitrobenzaldehyde as a reference, for more detail see supporting information (SI-9).

2.3. Photodegradation experiments

The photodegradation experiments conducted under simulated solar irradiation conditions were performed in a Suntest CPS simulator (Heraeus, Hanau, Germany). The system was equipped with a Xenon arc lamp and appropriate glass filters to restrict the transmission of irradiation wavelengths below 290 nm, giving a wavelength spectrum closely resembling solar light. The lamp intensity was adjusted to an irradiance of 500 W m^{-2} corresponding to a light dose of 1800 kJ m^{-2} h^{-1}. The samples irradiated in the Suntest apparatus and the direct sunlight assays were contained in crimp-cap 20-mL quartz vials. At pre-defined time points 2 mL aliquots were withdrawn from the vials and frozen immediately. Control solutions preserved in the dark with aluminium foil in the suntest and were sampled at the same time points as the irradiation experiments to account for any light-independent breakdown processes. Before LC–MS analysis, the samples were freeze-dried overnight and thereafter reconstituted in 100 μL of CH_3CN/H_2O (3:2) for the determination of zanamivir. The experiments intended for the identification of the phototransformation products were carried out at a concentration of 40 mg L^{-1} to assure the generation of product ion spectra with sufficient intensity, whereas the kinetic studies were performed with zanamivir spiked at 1 mg L^{-1} and 20 μg L^{-1}respectively. The low concentration was sufficient to monitor the disappearance of the test compound until 99% was photolysed. For the laboratory studies and natural sunlight, zanamivir was added to surface water matrices: (i) artificial fresh water (AFW) resembling a moderately hard water (96 mg L^{-1} NaHCO3, 60 mg L^{-1} CaSO4·2H2O, 60 mg L^{-1} MgSO4 and 4 mg L^{-1} KCl; pH: 6.6), (ii) AFW containing 5 mg L^{-1} of NO_3 (pH: 6.6) and (iii) AFW water containing humic acids with an absorbance of 0.670 (equivalent to 5 mg L^{-1}; pH: 7.3). (iv) river water collected from the Llobregat river (Table S1 [15]). The stock solution of humic acids was prepared in water as described in the literature [15]. The latter set of experiments was conducted on the roof terrace of the CSIC building for a period of 21 days (starting on November 9, 2009; total accumulated radiation: 164 MJ m^{-2}) for spiked and before mentioned surface water collected from LLobregat river. The radiation conditions in the period of October to December 2009 are given in Fig. S1. Prior to spiking, the river water was sterilized by filtration with 0.22 μm (Durapore) filters to prevent any microbial degradation of zanamivir.

2.4. UPLC-LTQ-Orbitrap-MS, and UPLC-QqQ MS analysis

LTQ-Orbitrap Velos (ThermoFisher, San José, CA) was used for the identification of the photoproducts. The parameters of the electrospray ionization source were adjusted as follows: polarity (+)ESI, spray voltage +3.0 kV, heater temperature 350 °C, and

capillary temperature 350 °C. The chromatographic separation of the samples was performed on a Waters Acquity UPLC BEH HILIC column (50 mm × 2.1 mm, 1.7 μm) (Waters, Milford, USA) preceded by a pre-column of the same packing material (5 mm × 2.1 mm, 1.7 μm). The mobile phases employed were: (A) acetonitrile with 0.1% formic acid and (B) water (0.1% formic acid). Elution was accomplished with the following solvent gradient: 0 min (95% A) – 1 min (85% A) – 6 min (60% A), – 8 min (60% A) – 10 min (95% A) and stabilizing until 13 min. The flow rate was 300 μL min^{-1} and the column temperature was held at 35 °C. The injection volume was 10 μL.

Following the tentative identification of the major phototransformation products of zanamivir, a quantitative method was established to describe the reaction kinetics in artificial and natural water samples. A Waters TQD triple quadrupole MS connected to an Acquity UPLC system were used for that purpose. The parameters of the ESI source were set as follows: polarity (+)ESI, capillary voltage 3.0 kV, source temperature 120 °C, nebulizer gas 50 L h^{-1}, desolvation gas 600 L h^{-1}, and desolvation gas temperature 350 °C. The chromatographic separation of the samples was performed on a Waters Acquity UPLC binary solvent manager equipped with a BEH HILIC column (50 mm × 2.1 mm, 1.7 μm) (Waters, Milford, USA) preceded by a pre-column of the same packing material (10 mm × 2.1 mm, 3 μm). The mobile phases and chromatographic gradient is the same as LTQ Orbitrap Velos. The MS/MS parameters used for the acquisitions in MRM mode were individually optimized for zanamivir, and its respective photoproducts (see Table S2 in Supporting Information). Instrument control and data management were performed by MassLynx V4.1 software (Waters) and Xcalibur (Thermo Scientific).

3. Results and discussion

3.1. Optimization of the chromatographic separation

The chromatographic analysis of zanamivir was initially attempted employing an RP-C_{18} column (Fig. S2). Due to the high polarity of the analyte, however, no retention was achieved (t_r of 0.54 min) even at a methanol percentage in the mobile phase of as low as 2% at starting conditions. Furthermore, such conditions were far from optimal in view of minimizing potential interferences from matrix components. Therefore, the alternative suggested in the literature [9] was to use a HILIC column as this was expected to accommodate not only the parent compound but also for the first time any photoproducts being potentially more polar than zanamivir. As seen in Fig. S2 the HILIC column (B) substantially improves the retention of zanamivir in comparison to a C_{18} column (A) but also reveals the presence of an isobaric transformation product TP332 (D) that elutes at the same retention time on a C_{18} column (C). Fig. 1 illustrates the chromatographic separation on a HILIC column achieved for zanamivir and its transformation products.

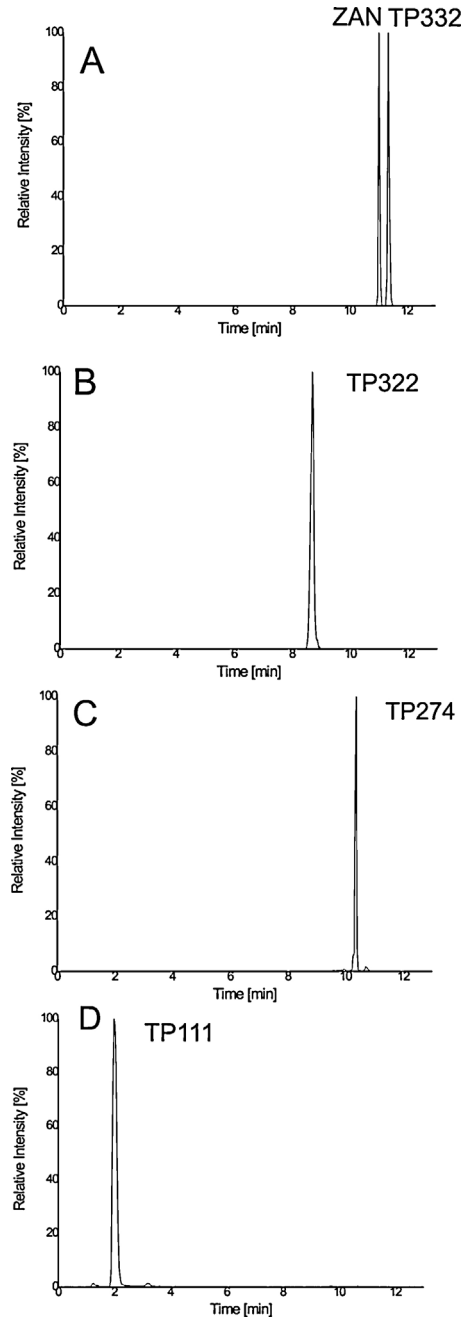

Fig. 1. Extracted ion chromatograms corresponding to UPLC separation of zanamivir and its photoproducts on HILIC column (acquired on LTQ-Orbitrap-MS) present in irradiated HPLC water sample (initial zanamivir concentration of 40 mg L^{-1}). The figure shows depicts the ion traces of the molecular ions of (A) zanamivir (*m/z* 333) and TP332 (m/z 333), (B) TP 322 (m/z 323), (C) TP 274 (m/z 275) and (D) TP 111 (*m/z* 112).

3.2. Identification of the phototransformation products

For the identification of zanamivir' photoproducts individual aqueous solutions (40 mg L^{-1}) were exposed in the Suntest apparatus for different time periods. The solutions were lyophilized and solvent-exchanged to LC method initial conditions for HILIC analysis. The chromatograms recorded in LTQ-Orbitrap-MS mode were examined for the appearance of new peaks concomitantly with the decrease of the parent compound (Fig. 1). In the light-exposed zanamivir samples, an intense peak was observed at 1.98 min with a molecular ion $[M+H]^+$ at *m/z* 112 (denoted as TP111). More discrete peaks were detected at 8.70 min (*m/z* 323; TP322), at 10.37 min (*m/z* 275, TP274) and at 11.35 min (*m/z* 333; TP332). The product ion mass spectra of zanamivir and its photoproducts were recorded on the LTQ-Orbitrap-MS to elucidate the respective chemical structures (Fig. 2) with the corresponding accurate mass measurement data compiled in Table 1.

The (+)ESI-mass spectra of zanamivir acquired by Orbitrap-MS are depicted in Figs. 2A and S3 respectively, using the Orbitrap' Higher-energy collisional dissociation (HCD) cell for collision-induced dissociation instead of resonance excitation of the isolated precursor ion in LTQ ion trap (data not shown), The fragmentation of zanamivir starts with the heterolytic cleavage of the C—N bond between the guanidine residue and the dihydropyrane ring

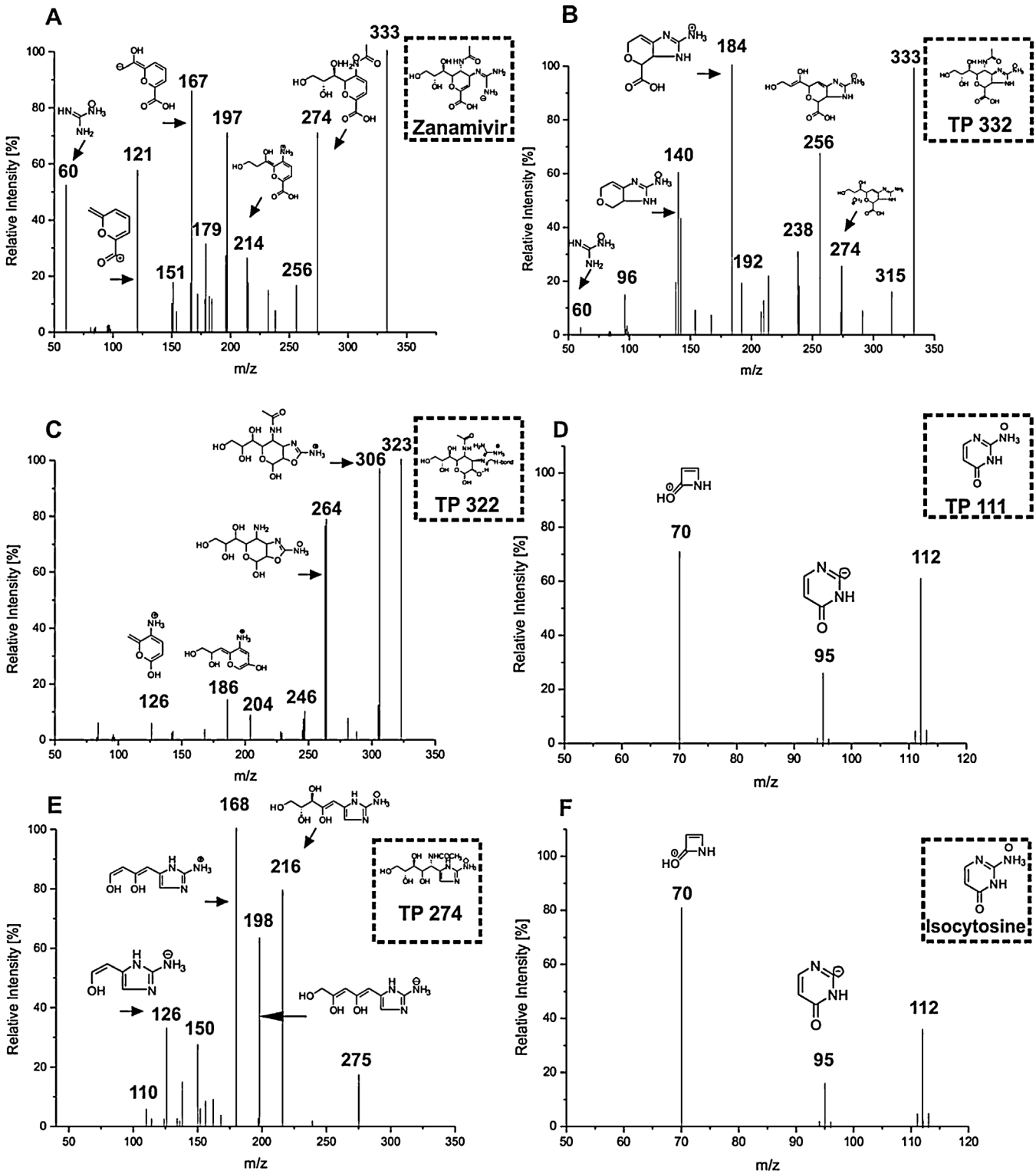

Fig. 2. (+)ESI-LTQ Orbitrap-MS spectra of zanamivir (A) and its photoproducts TP332 (B), TP322 (C), TP111 (D), TP274 (E) and isocytosine standard (F).

giving rise to the fragment ions at *m*/*z* 274 and *m*/*z* 60. The subsequent loss of water from the former structure produces the ion *m*/*z* 256, which then undergoes amide bond cleavage (−H_2C=CO) to yield *m*/*z* 214. Once this fragment ion loses ammonia, thereby generating *m*/*z* 197, a series of odd mass-to-charge fragment ions are formed corresponding to dehydrations and gradual breakdown of the hydroxylated aliphatic side chain. The structure of the base peak in the mass spectrum of zanamivir (*m*/*z* 121) is attributed to the conjugated monocyclic structure depicted in Fig. 2A.

The photoproduct TP332 is identical in elemental composition to zanamivir ($C_{12}H_{20}N_4O_7$; Table 1). The fact that it is among the detected transformation products the one with the least retention time shift with respect to the parent compound (Fig. 1) is in agreement with the hypothesis of a structurally closely related

Table 1
Accurate mass measurements of protonated zanamivir and photoproducts as determined by LC-LTQ-Orbitrap-MS in MS or MS/MS mode.

Nominal ion mass	Measured mass (*m*/*z*)	Mass error (ppm)	Elemental composition	Calculated mass (*m*/*z*)	DBE[a]
$[M+H]^+$	333.1406	+0.3	$C_{12}H_{21}N_4O_7$	333.1405	4.5
274	274.0922	+0.3	$C_{11}H_{16}NO_7$	274.0921	4.5
256	256.0818	±0.0	$C_{11}H_{14}NO_6$	256.0816	5.5
214	214.0710	−0.1	$C_9H_{12}NO_5$	214.0710	4.5
197	197.0444	−0.1	$C_9H_9O_5$	197.0444	5.5
179	179.0339	+0.2	$C_9H_7O_4$	179.0339	6.5
167	167.0339	+0.2	$C_8H_7O_4$	167.0339	5.5
151	151.0390	+0.5	$C_8H_7O_3$	151.0390	5.5
121	121.0285	+0.1	$C_7H_5O_2$	121.0284	5.5
60	60.0552	−6.7	CH6N3	60.0556	0.5
$[M+H]^+$	333.1409	+1.3	$C_{12}H_{21}N_4O_7$	333.1405	4.5
315	315.1303	+1.4	$C_{12}H_{19}N_4O_6$	315.1299	5.5
274	274.1036	+0.9	$C_{10}H_{16}N_3O_6$	274.1034	4.5
256	256.0930	+1.0	$C_{10}H_{14}N_3O_5$	256.0928	5.5
238	238.0825	+1.2	$C_{10}H_{12}N_3O_4$	238.0822	6.5
214	214.0712	+0.7	$C_9H_{12}NO_5$	214.0710	4.5
192	192.0769	+0.9	$C_9H_{10}N_3O_2$	192.0768	6.5
184	184.0719	+1.2	$C_7H_{10}N_3O_3$	184.0717	4.5
140	140.0820	+1.4	$C_6H_{10}N_3O$	140.0818	3.5
121	121.0398	+1.6	$C_6H_5ON_2$	121.0396	0.5
60	60.0550	−9.9	CH_6N_3	60.0556	0.5
$[M+H]^+$	323.1561	±0.0	$C_{11}H_{23}N_4O_7$	323.1561	2.5
306	306.1296	±0.0	$C_{11}H_{20}N_3O_7$	306.1296	3.5
264	264.1190	−0.1	$C_9H_{18}N_3O_6$	264.1190	2.5
263	263.1239	+0.5	$C_{10}H_{19}N_2O_6$	263.1238	2.5
246	246.1085	+0.1	$C_9H_{16}N_3O_5$	246.1084	3.5
204	204.0866	−0.2	$C_8H_{14}NO_5$	204.0866	2.5
186	186.0760	−0.2	$C_8H_{12}NO_4$	186.0761	3.5
$[M+H]^+$	275.1351	0.2	$C_{10}H_{19}N_4O_5$	275.1350	3.5
239	239.1139	0.0	$C_{10}H_{15}N_4O_3$	239.1139	5.5
216	216.0979	0.0	$C_8H_{14}N_3O_4$	216.0979	3.5
198	198.0873	0.0	$C_8H_{12}N_3O_3$	198.0873	4.5
180	180.0768	0.0	$C_8H_{10}N_3O_2$	180.0768	5.5
150	150.0662	0.0	$C_7H_8N_3O$	150.0662	5.5
138	138.0661	−0.3	$C_6H_8N_3O$	138.0662	4.5
126	126.0662	0.1	$C_5H_8N_3O$	126.0662	3.5
110	110.0714	0.8	$C_5H_8N_3$	110.0713	3.5
$[M+H]^+$	112.0506	+0.9	$C_4H_6N_3O$	112.0505	3.5
95	95.0241	+1.7	$C_4H_3N_2O$	95.0240	4.5
70	70.0289	+2.3	C_3H_4NO	70.0287	2.5

[a] Double-bond equivalents.

Scheme 1.

compound. The formation of TP332 can be explained as a result of an intramolecular Michael-type addition of the guanidine moiety upon the conjugated double bond in zanamivir (Scheme 1)

Quick inspection of the mass spectrum of TP332 in Fig. 2B reveals a striking difference between the two isobaric compounds: all major fragment ions of TP332 are even-mass ions. On the assumption that only even-electron species are formed – which is consistent with the chemical formula calculated in Table 1 – structures with an odd number of nitrogen atoms are prevailing. Low resolution MS would likely have led to postulate the same initial loss of the guanidine moiety, but the accurate mass measurements actually revealed that the ion *m*/*z* 274 ($C_{10}H_{16}N_3O_6$) differs in elemental composition from the nominally isobaric fragment ion in the (+)ESI mass spectrum of zanamivir (Fig. 2B; $C_{11}H_{16}NO_7$). In case of TP332 the formation of *m*/*z* 274 implies the loss of $H_2N{-}CO{-}CH_3$ from the protonated molecule. To conserve the guanidine residue in most of the fragment ions (*m*/*z* 256, 238, 214, 192, 184, 140) during the dissociation process, formation of a bicyclic structure was proposed (Fig. 2B), thereby substantially increasing the energy needed for cleaving off the guanidine moiety. As with zanamivir, gradual dehydration (*m*/*z* 274 → 256 → 238) and cleavage along the initially aliphatic side chain then produces a series of even-mass fragment ions. The base peak in Fig. 2B is proposed to completely lack the carbon side chain. Using the same collision energy settings for the generation of the product ion spectra of zanamivir and TP332, the large difference in relative intensities of the fragments ion at *m*/*z* 60 ($HN{=}CH(NH_2)_2$) is a good indicator of the less favourable guanidine cleavage in the latter compound.

As far as TP322 (t_r: 3.77 min) is concerned, its sum formula differs from zanamivir by the nominal replacement of a carbon atom by two hydrogen atoms ($C_{11}H_{23}N_4O_7$ as compared to $C_{12}H_{21}N_4O_7$; Table 1). The mass spectrum of TP322 (Fig. 2C) displays two distinct features: on the one hand it completely lacks an ion at *m*/*z* 60, whose presence would have reflected the easy to break the carbon–nitrogen bond between the guanidine; on the other hand, there is a nominal loss of 59 Da (*m*/*z* 323 → 264). As in case of TP332 (*m*/*z* 333 → 274), this process corresponds to the elimination of $H_2N{-}CO{-}CH_3$ rather than to the loss of $HN{=}CH(NH_2)_2$ as observed for zanamivir. However, unlike TP332, the overall loss of 59 Da can be interpreted as a result of a loss of ammonia (to give *m*/*z* 306) followed by a loss of acetyl, leading to the *m*/*z* 264 fragment (see Fig. S4 for the complete fragmentation pattern). Overall, these findings are indicative of structural modifications involving the guanidine group. A plausible structure consistent with these observations, and the fragmentation pattern as a whole, is the one

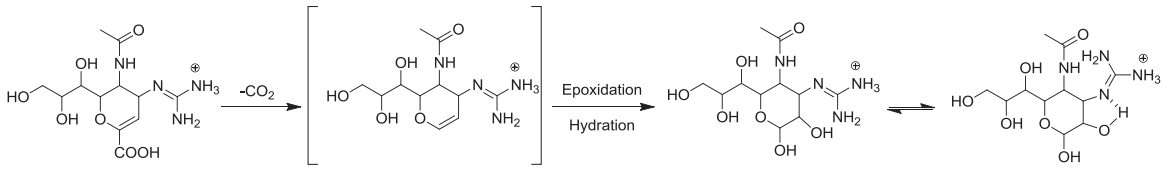

Scheme 2.

shown in Fig. 2C. The formation of TP322 can be explained by initial decarboxylation of zanamivir, followed by photochemical double bond epoxidation and subsequent hydration of this transient, highly reactive electrophilic species, as shown in Scheme 2 (for a related example of photochemical epoxidation, see [16]). The stability of the guanidine moiety could be explained, in part, to the possibility of intramolecular hydrogen bond formation between the guanidine moiety and one of the adjacent hydroxyl groups of the tetrahydropyrane system.

A third photoproduct was identified as TP274 where the sum formula differs from zanamivir by the nominal loss of $C_2H_2O_2$ ($C_{10}H_{19}N_4O_5$ as to $C_{12}H_{21}N_4O_7$; Table 1). The mass spectrum of TP274 (Fig. 2E) displays the same characteristic as TP322; complete lack of an ion at *m/z* 60 indicating cyclisation of the lateral chain differing from TP322 in breaking the guanidine ring. After the loss of C_2H_4NO, subsequent losses of water (18 Da) indicate highly hydroxylated side chain. Detailed fragmentation is the one shown in Fig. S6. The formation of TP274 can be tentatively explained by the series of successive decarboxylation and oxidation processes shown in Scheme 3. Despite the speculative nature of this interpretation, the aromaticity of the resulting photodegradation product could account for the suggested reaction pathway.

A fourth photoproduct was detected at *m/z* 112 with an elemental composition of $C_4H_6N_3O$ (Table 1) thus suggesting the guanidine residue to be conserved. Its (+)ESI-MS^2 spectrum (Fig. 2D) only displayed two fragment ions at *m/z* 95 and 70, corresponding to sequential losses of ammonia and HCN. This fragmentation pattern was consistent with the structure of isocytosine shown in Fig. 2F. Its formation can be explained from TP322, as shown in Scheme 4. Thus, oxidation of the hemiacetalic aldehyde to the corresponding carboxylic acid, followed by lactamization affords the key pyrimidin-4-one intermediate A. Radical formation and subsequent side chain elimination from "A" affords isocytosine (TP 111) [17].

Once the major photoproducts of zanamivir were identified, an analytical method was established based on UPLC-QqQ-MS for quantitative determination of these entities in the irradiated samples in order to construct the degradation profiles.

3.3. Degradation profiles and kinetics

The UV–vis spectra of zanamivir showed that it absorbed most intensively radiation below the filter cut-off of the used xenon lamp (Supporting Information Fig. S9A). The quantum yield was determined to amount to 0.0301 (see Supporting Information Fig. S9) which indicates the susceptibility of zanamivir to photochemical reactions.

The photodegradation experiments aimed to assess the photolysis of zanamivir at different concentrations in surface water under both simulated and natural sunlight. Fig. 3 shows the degradation of zanamivir at 40 mg L^{-1} under simulated sunlight. It can be seen that under artificial sunlight (Fig. 3) zanamivir is converted to all four photoproducts. Under natural sunlight, however (Fig. 4) only two transformation products (TP322 and TP111) are detectable. Fig. 5A shows the respective degradation profile upon irradiation of the 20 μg L^{-1} solutions in the sunlight simulator. Although the primary degradation of zanamivir was essentially complete within 24 h, the exposure time was extended in order to monitor the time course of the aforementioned photoproducts. Concurrently, control experiments were carried out in the dark for seven days to assess the relevance of hydrolytic composition (Fig. 5A). These results demonstrated that the zanamivir solution was chemically stable

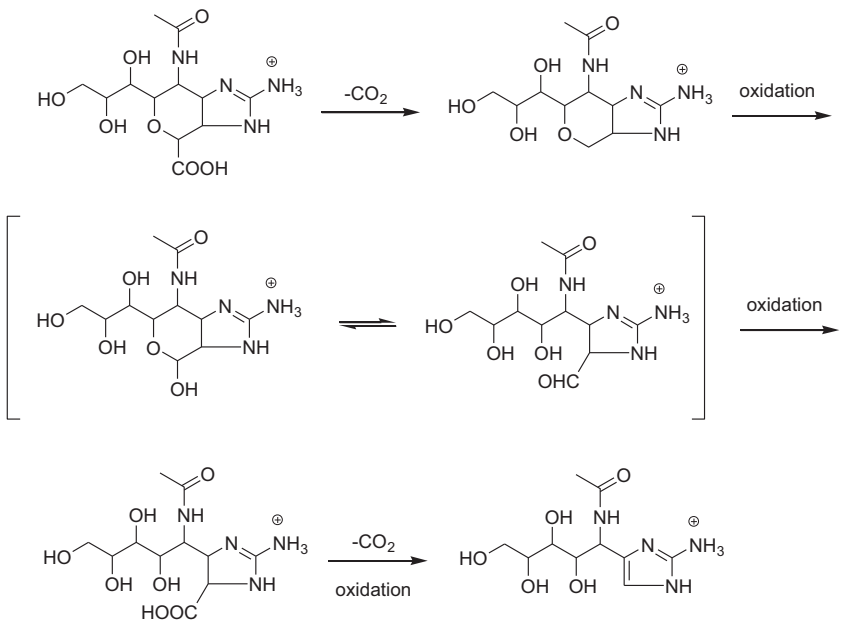

Scheme 3.

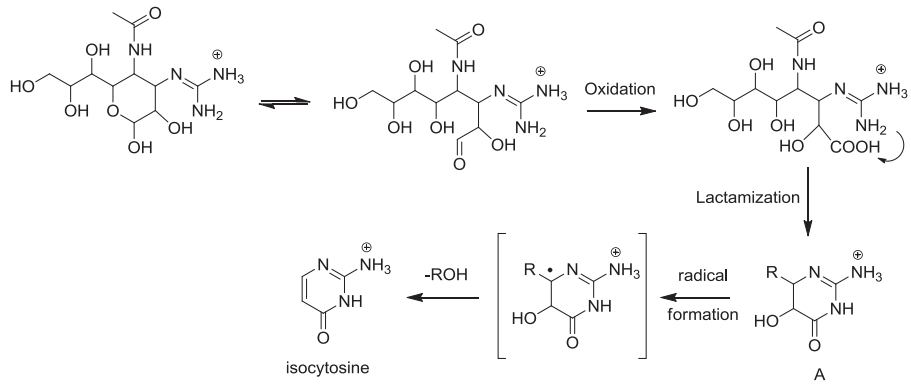

Scheme 4.

in the absence of light. However, under the influence of simulated sunlight zanamivir photodegraded with a half-life time of 3.6 h.

3.4. Effect of natural surface waters constituents in the degradation of zanamivir

In order to evaluate the influence of natural water constituents on the photodegradation of zanamivir a set of experiments mimicking the environmental conditions under both artificial and natural sunlight were performed (Fig. 4) in surface water taken from LLobregat river (Table S1). The kinetics of zanamivir (1 mg L^{-1}) was investigated in natural surface water of known composition showing slower photodegradation (detailed kinetic data obtained from fitting to first-order models are compiled in Table S3 in Supporting Information). Similar findings were observed for the degradation of zanamivir (1 mg L^{-1}) under natural irradiation conditions in early autumn at Barcelona latitude (irradiance intensities between 500 and 800 W m^{-2}) (see Fig. 4B). In experiments involving different water matrices (artificial freshwater, humic acids or nitrates) under artificial irradiation conditions, profiles showed that the natural surface water had similar profile to the addition of humic acids in artificial freshwater (Fig. S8). On the contrary, the degradation of zanamivir in artificial freshwater with nitrate constituents was faster. Results are also in accordance with the physico-chemical characterization of the surface water with lower nitrate concentration and higher total organic carbon concentration (Table S1).

Furthermore, the evolution of the transformation products, characterized by high-resolution MS in the first part of this study (see Section 3.3), was monitored over the irradiation period. Whereas four photoproducts had been detected under simulated sunlight experiments at a test compound concentration of 40 mg L^{-1} (Fig. 3), used to increase the detection sensitivity in identifying the photoproducts, in the kinetic studies at low concentration of zanamivir only the course of TP111 could be determined

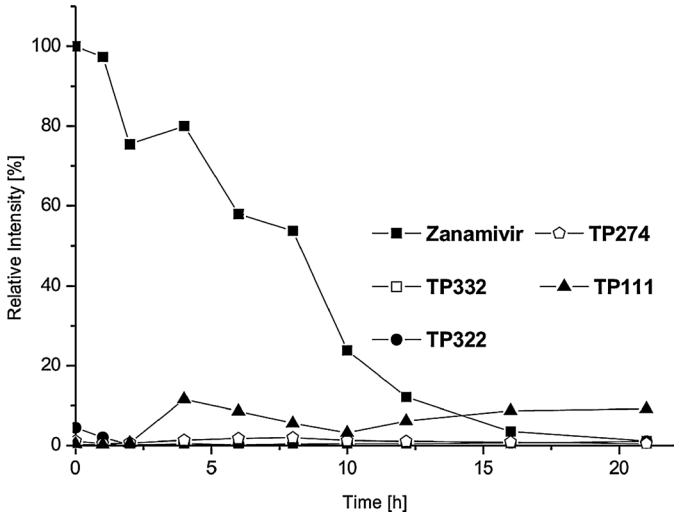

Fig. 3. Degradation profiles of zanamivir at 40 mg L^{-1} upon exposure to simulated sunlight in surface water. The intensity of the photoproducts is normalized to the maximum peak intensity of zanamivir recorded.

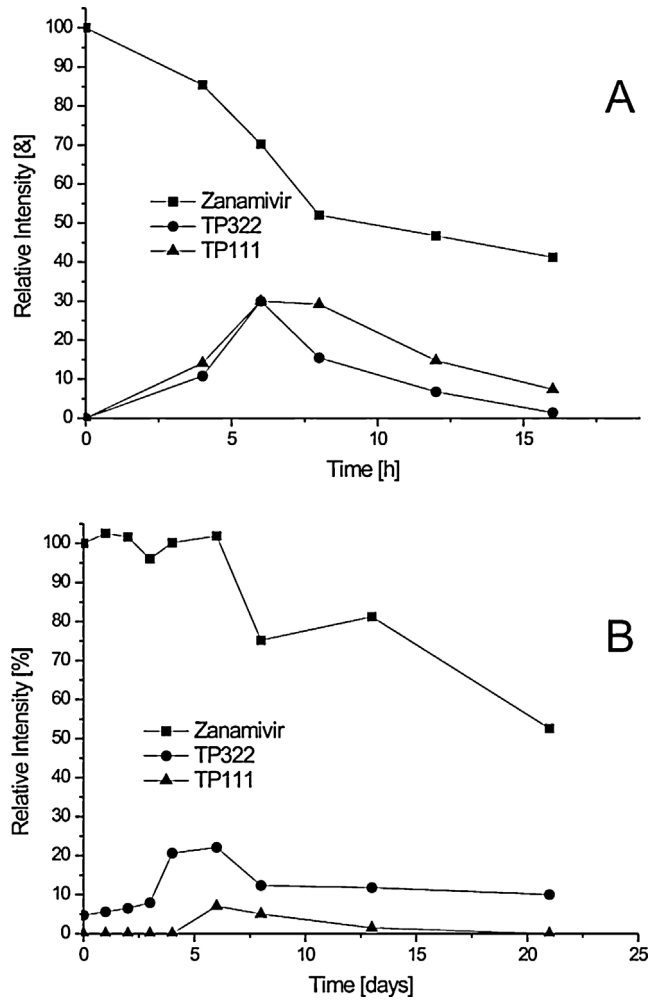

Fig. 4. Degradation profiles of zanamivir at 1 mg L^{-1} in surface water (SW) upon exposure to (A) simulated sunlight and (B) natural sunlight. The intensity of the photoproducts is normalized to the maximum peak intensity of the corresponding photoproduct recorded.

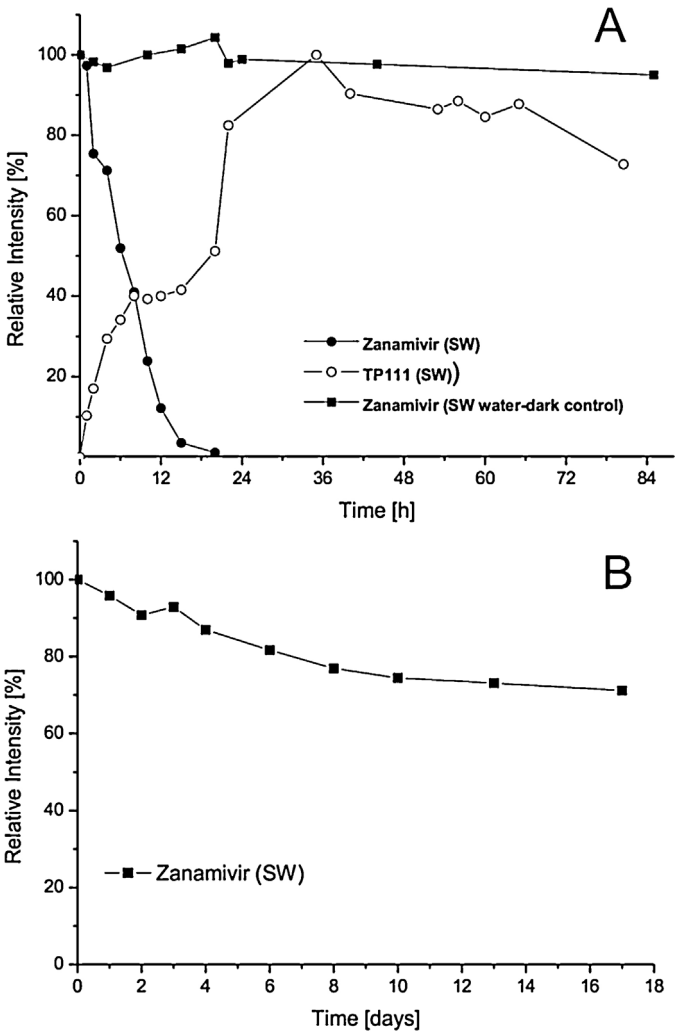

Fig. 5. Degradation profiles of zanamivir (20 μg L^{-1}) in surface water (SW) under (A) simulated sunlight and (B) natural sunlight. Intensity of the photoproduct TP111 is normalized to its maximum peak intensity recorded and zanamivir to its own.

at measurable levels (Fig. 5A). However, under natural sunlight (Fig. 5B) this concentration yielded no measurable transformation products. Since the photodegradation of zanamivir under simulated conditions proceeded at much faster rate, the nondetectability of TP111 (Fig. 5) is possibly related to the lower amounts formed under natural conditions also observed in the photodegradation of the antiviral oseltamivir in Gonçalves et al. [15]. Lack of detectable transformation products in concentrations of 1 mg L^{-1} as well as at 20 μg L^{-1} could suggest instrument detection limits problems but also photodegradation kinetics depending on the light-source [18]. Regarding the differences in photodegradation with natural vs. simulated sunlight, a possible explanation is a different intensity of various wavelengths in one vs. the other spectrum – in other words, the simulated sunlight not being a perfect proxy for the real one. In previous work, others have also noted somewhat different outcomes from the two approaches [18,19]. Both of these experimental methods should be viewed as complementary and proxies for the processes that occur in real rivers which can provide a better understanding of the photodegradation actually occurring in nature. The evolution of the relative abundance of TP111 in the degradation profiles recorded for surface water suggested that this compound was stable towards subsequent reactions, because it is the lightest among the four transformation products of zanamivir. After building up within the first day, relatively constant levels were measured over the next two days.

4. Conclusions

The findings in the photolysis studies under artificial sunlight suggested that zanamivir had an intrinsic potential to be broken down when exposed to light. The usage of a HILIC column proved to be essential for the retention and separation of the phototransformation products of zanamivir. LTQ-Orbitrap-MS served as a very powerful tool in elucidating the transformation products. The analyser afforded very robust accurate mass measurements with relative errors being below 2 ppm for all of the ions >m/z 100. Suntest experiments suggests that humic acid constituents influence zanamivir degradation profile in surface water. The experiments under natural sunlight were carried out in autumn, i.e. at the beginning of the influenza season. Conducted at low zanamivir concentrations, the outcomes indicated that its attenuation in environmental waters is likely to proceed with slow kinetics. Given the likely increase in influenza cases being treated with Relenza (zanamivir) instead of oseltamivir, further investigations are warranted on the occurrence and fate of zanamivir in the aquatic environment. This may include controlled studies on the photolysis of zanamivir in surface waters collected at different sites as well as experiments carried during different seasons.

Acknowledgements

B. Z. acknowledges the Marie Curie Actions ITN CSI: Environment PITN-GA-2010-264329 for the Early Stage Researcher contract and funding. SP acknowledges the contract from the Ramón y Cajal Programme of the Spanish Ministry of Economy and Competitiveness. The studies have partly been supported by the Spanish Ministry of Economy and Competitiveness [64551/HID and Consolider-Ingenio 2010 Scarce CSD2009-00065]. This work was partly supported by the Generalitat de Catalunya (Consolidated Research Group: Water and Soil Quality Unit 2009-SGR-965). Fundação para a Ciência e Tecnologia is greatly acknowledged for the Post-Doc grant SFRH/BPD/39650/2007. This work is also integrated in the project NORTE-01-0162-FEDER-000023 co-funded by ON.2 O Novo Norte.

Appendix A. Supplementary data

Supplementary data associated with this article can be found, in the online version, at http://dx.doi.org/10.1016/j.jhazmat.2013.10.008.

References

[1] V. Soundararajan, K. Tharakaraman, R. Raman, S. Raguram, Z. Shriver, V. Sasisekharan, R. Sasisekharan, Extrapolating from sequence the 2009 H1N1 'swine' influenza virus, Nat. Biotechnol. 27 (2009) 510–513.
[2] T. Azuma, N. Nakada, N. Yamashita, H. Tanaka, Synchronous dynamics of observed and predicted values of anti-influenza drugs in environmental waters during a seasonal influenza outbreak, Environ. Sci. Technol. 46 (2012) 12873–12881.
[3] M.E. Bosch, A.J.R. Sánchez, F.S. Rojas, C.B. Ojeda, Ribavirin analytical determinations since the origin until today, J. Pharm. Biomed. 45 (2007) 185–193.
[4] D. Chan, J. Tarbin, M. Sharman, M. Carson, M. Smith, S. Smith, Screening method for the analysis of antiviral drugs in poultry tissues using zwitterionic hydrophilic interaction liquid chromatography/tandem mass spectrometry, Anal. Chim. Acta 700 (2011) 194–200.
[5] V.L. Cunningham, S.P. Binks, M.J. Olson, Human health risk assessment from the presence of human pharmaceuticals in the aquatic environment, Regul. Toxicol. Pharmacol. 53 (2009) 39–45.
[6] H. Sanderson, D.J. Johnson, T. Reitsma, R.A. Brain, C.J. Wilson, K.R. Solomon, Ranking and prioritization of environmental risks of pharmaceuticals in surface waters, Regul. Toxicol. Pharmacol. 39 (2004) 158–183.

[7] J. Ge, F. Liu, E.H. Holmes, G.K. Ostrander, Q.X. Li, Aqueous normal phase liquid chromatography coupled with tandem time-of-flight quadrupole mass spectrometry for determination of zanamivir in human serum, J. Chromatogr. B: Analyt. Technol. Biomed. Life Sci. 906 (2012) 58–62.
[8] G.D. Allen, S.T. Brookes, A. Barrow, J.A. Dunn, C.M. Grosse, Liquid chromatographic–tandem mass spectrometric method for the determination of the neuraminidase inhibitor zanamivir (GG167) in human serum, J. Chromatogr. B: Biomed. Sci. Appl. 732 (1999) 383–393.
[9] T.M. Baughman, W.L. Wright, K.A. Hutton, Determination of zanamivir in rat and monkey plasma by positive ion hydrophilic interaction chromatography (HILIC)/tandem mass spectrometry, J. Chromatogr. B: Analyt. Technol. Biomed. Life Sci. 852 (2007) 505–511.
[10] Y. Hsieh, Potential of HILIC–MS in quantitative bioanalysis of drugs and drug metabolites, J. Sep. Sci. 31 (2008) 1481–1491.
[11] P.J. Collins, L.F. Haire, Y.P. Lin, J. Liu, R.J. Russell, P.A. Walker, J.J. Skehel, S.R. Martin, A.J. Hay, S.J. Gamblin, Crystal structures of oseltamivir-resistant influenza virus neuraminidase mutants, Nature 453 (2008) 1258–1261.
[12] R. Andreozzi, R. Marotta, N. Paxéus, Pharmaceuticals in STP effluents and their solar photodegradation in aquatic environment, Chemosphere 50 (2003) 1319–1330.
[13] T.E. Doll, F.H. Frimmel, Fate of pharmaceuticals – photodegradation by simulated solar UV-light, Chemosphere 52 (2003) 1757–1769.
[14] A. Aguera, L.A. Perez Estrada, I. Ferrer, E.M. Thurman, S. Malato, A.R. Fernandez-Alba, Application of time-of-flight mass spectrometry to the analysis of phototransformation products of diclofenac in water under natural sunlight, J. Mass Spectrom. 40 (2005) 908–915.
[15] C. Goncalves, S. Perez, V. Osorio, M. Petrovic, M.F. Alpendurada, D. Barcelo, Photofate of oseltamivir (Tamiflu) and oseltamivir carboxylate under natural and simulated solar irradiation: kinetics, identification of the transformation products, and environmental occurrence, Environ. Sci. Technol. 45 (2011) 4307–4314.
[16] G. Büchi, K.W. Fowler, A.M. Nadzan, Photochemical epoxidation of aflatoxin B1 and sterigmatocystin: synthesis of guanine-containing adducts, J. Am. Chem. Soc. 104 (1982) 544–547.
[17] V. Jagannadham, S. Steenken, One-electron reduction of nitrobenzenes by OH and H radical adducts to 6-methyluracil and 6-methylisocytosine via electron transfer and addition/elimination. Effect of substituents on rates and activation parameters for formation and heterolysis of nitroxyl-type tetrahedral intermediates, J. Phys. Chem. 92 (1988) 111–118.
[18] L. Ge, J. Chen, X. Qiao, J. Lin, X. Cai, Light-source-dependent effects of main water constituents on photodegradation of phenicol antibiotics: mechanism and kinetics, Environ. Sci. Technol. 43 (2009) 3101–3107.
[19] J. Niu, Y. Li, W. Wang, Light-source-dependent role of nitrate and humic acid in tetracycline photolysis: kinetics and mechanism, Chemosphere 92 (2013) 1423–1429.

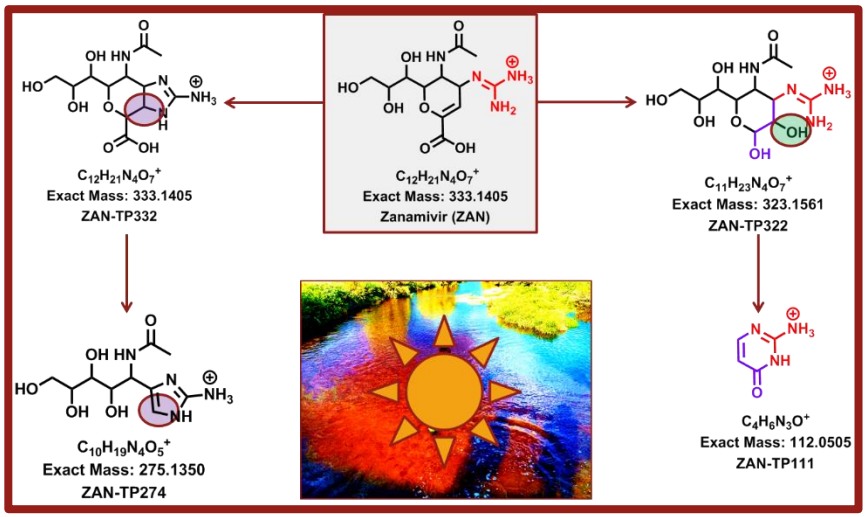

Article N°1:

Zonja, B., Goncalves, C., Perez, S., Delgado, A., Petrovic, M., Alpendurada, M.F. and Barcelo, D.

Evaluation of the phototransformation of the antiviral zanamivir in surface waters through identification of transformation products.

(2014.) J Hazard Mater 265, 296-304.

SUPPORTING INFORMATION

Total content: **Figures** – 9, and **Tables** – 3

Supporting information has been reformatted to match the style of the thesis, and in this article only, a Table of Contents was added.

Table of Contents

Table S-1: Physico-chemical characterization of the surface waters from Llobregat river used in the photodegradation studies.

Metals were determined by ICP-MS, nitrate by molecular absorbance spectophotometry (EAM) in the UV-vis region and total organic carbon (TOC) by a Shimadzu TOC-V CPH analyzer.

Parameter	LLobregat
pH	7.6
Conductivity [µS/cm]	1440
Na^+ [mg/L]	182
K^+ [mg/L]	34
Ca^{2+} [mg/L]	116
Mg^{2+} [mg/L]	32
Sr^{2+} [mg/L]	2.0
Fe^{3+} [µg/L]	<20
NO_3^- [mg/L]	<5
Cl^- [mg/L]	379
TOC [mg/L]	7.5

LOD: limit of detection

Table S-2: UPLC-QqQ-MS conditions for the determination of the zanamivir and its photoproducts.

Compound	Retention time [min]	MRM transition	Dwell time [s]	Cone voltage [V]	Collision energy [eV]
TP111	1.98	112 > 70	0.180	15	20
TP322	8.70	323 > 264	0.180	25	25
TP275	10.37	275>168	0.180	25	20
Zanamivir	11.03	333 > 60	0.180	30	25
TP332	11.35	333 > 184	0.180	25	25

Table S-3: Photodegradation kinetic parameters assuming a pseudo-first order model. k_{app}. – pseudo-first order degradation rate. Under direct solar irradiation $t_{1/2}$ are empirical estimations.

Matrix	$t_{1/2}$	k_{app}	r^2
Simulated solar irradiation [h]			
Surface water	3.6	0.19	0.925
Direct solar irradiation [days]			
Surface water	≈ 48	-	-

Figure S-1: Irradiation conditions found in Barcelona during the period of the irradiation studies performed under direct sunlight exposure, October to December 2009

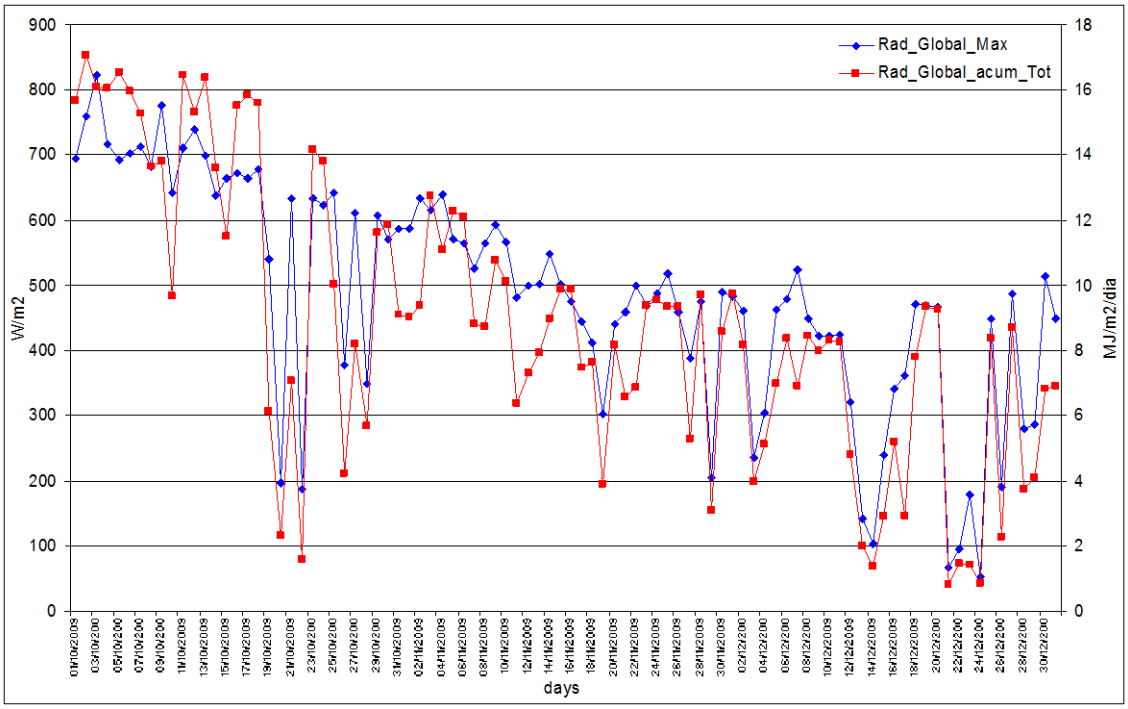

Figure S-2: Comparison of the extracted chromatograms corresponding to HPLC separation of zanamivir and TP332 using C18 (BEH C18, 100mmx 2.1 mm 1.7 µm- Waters, Milford, USA) and HILIC (Atlantis HILIC silica column, 100mm × 2.1 mm, 3 µm- Waters, Milford, USA) columns, respectively.

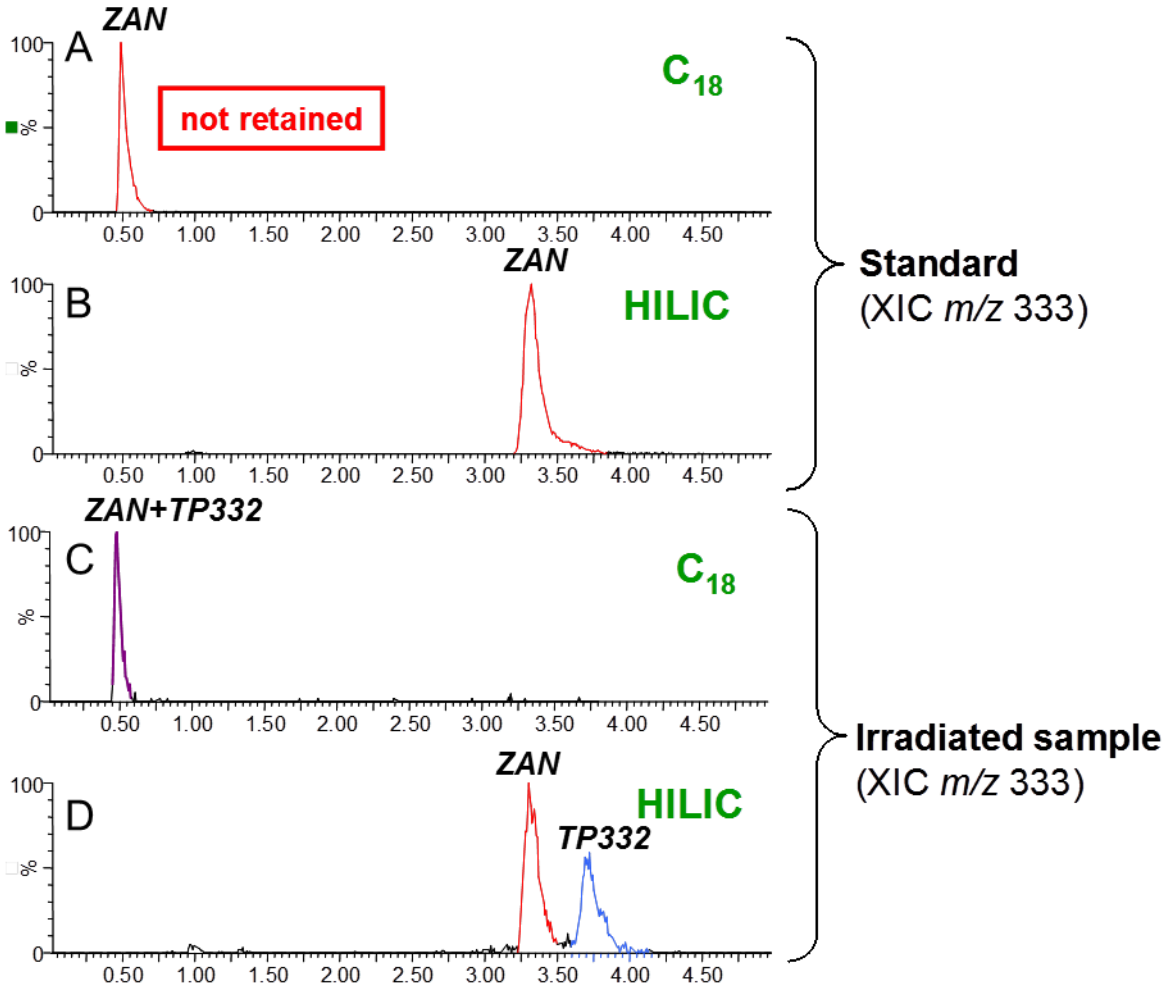

Figure S-3: Proposed fragmentation pattern of zanamivir in (+)ESI-MS.

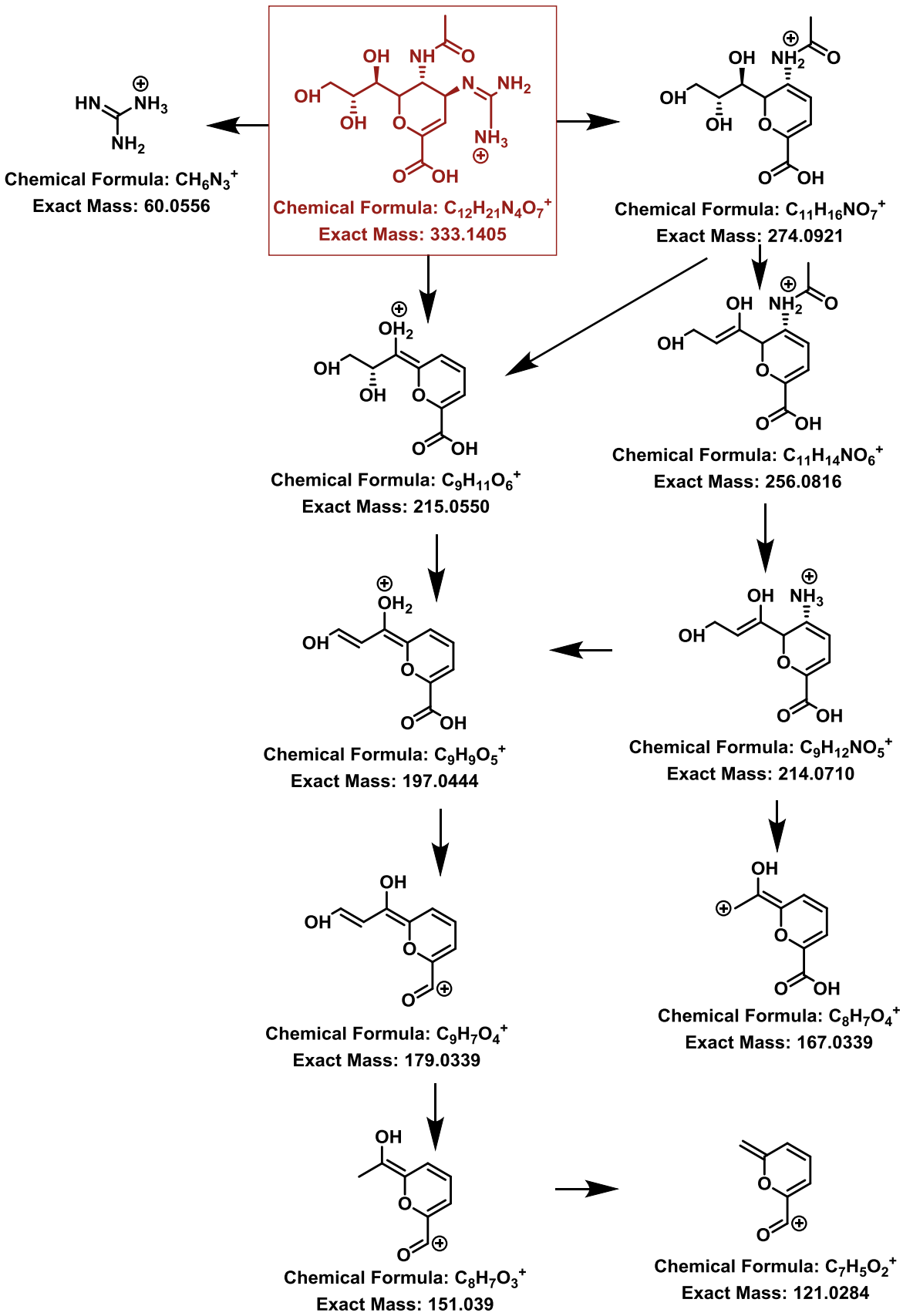

Figure S-4: Proposed fragmentation pattern of TP332 in (+)ESI-MS.

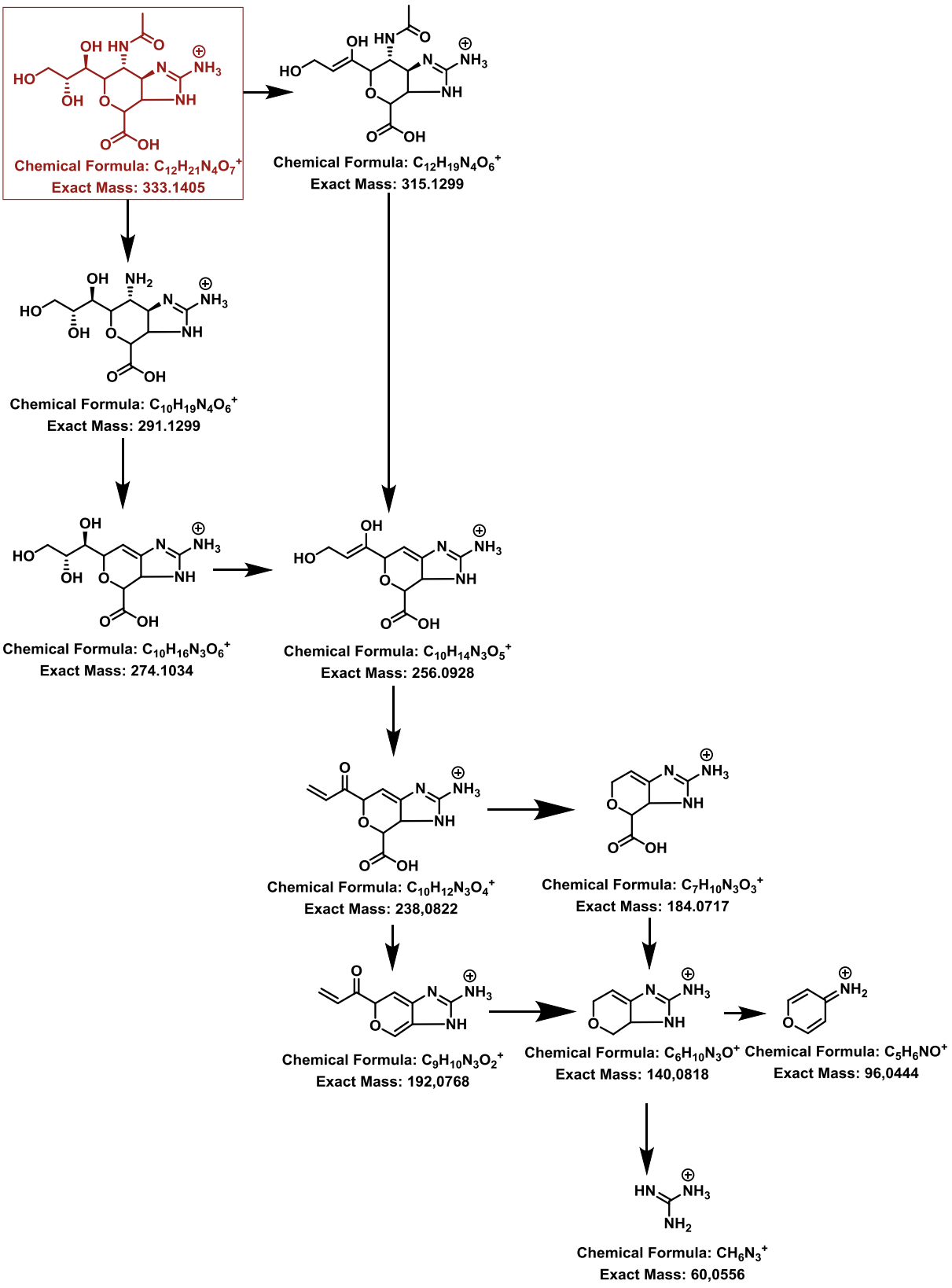

Figure S-5: Proposed fragmentation pattern of TP322 in (+)ESI-MS.

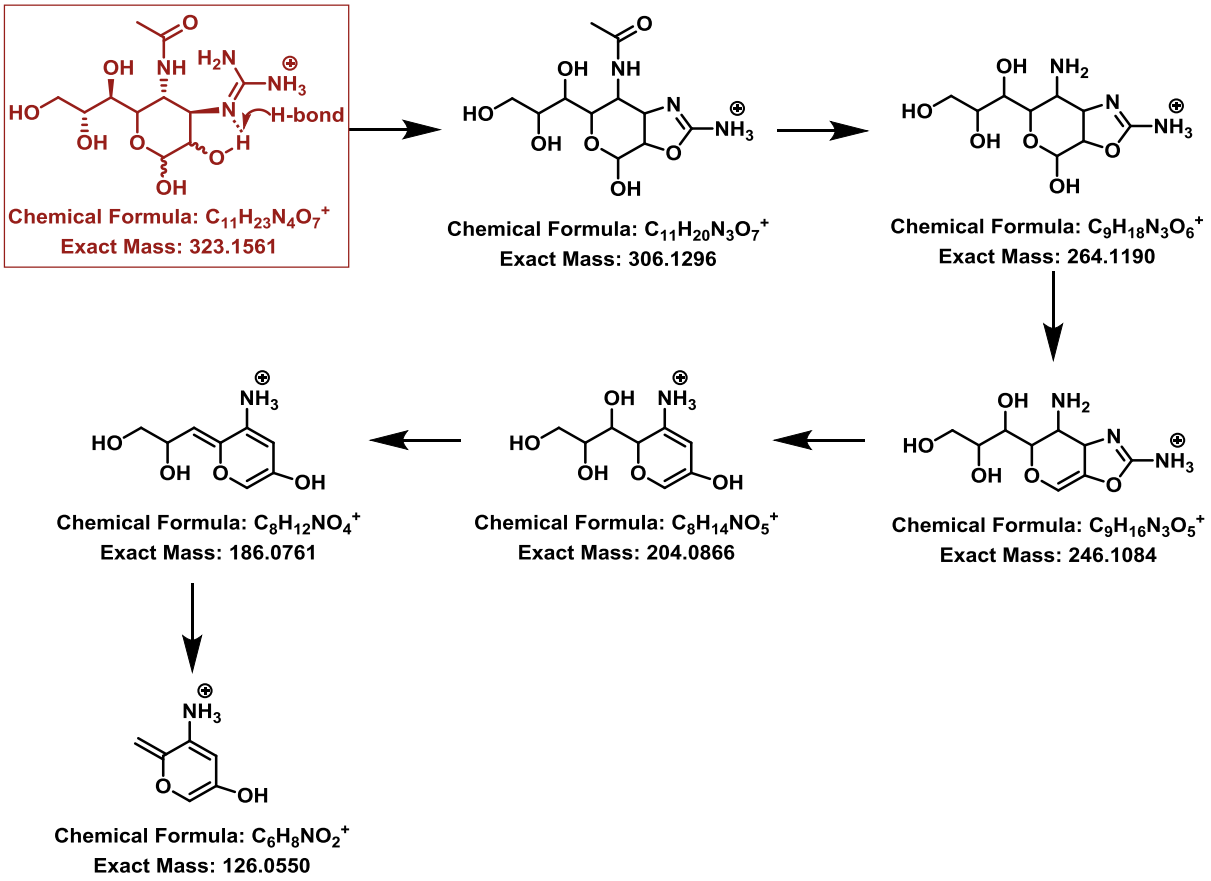

Figure S-6: Proposed fragmentation pattern of TP274 in (+)ESI-MS.

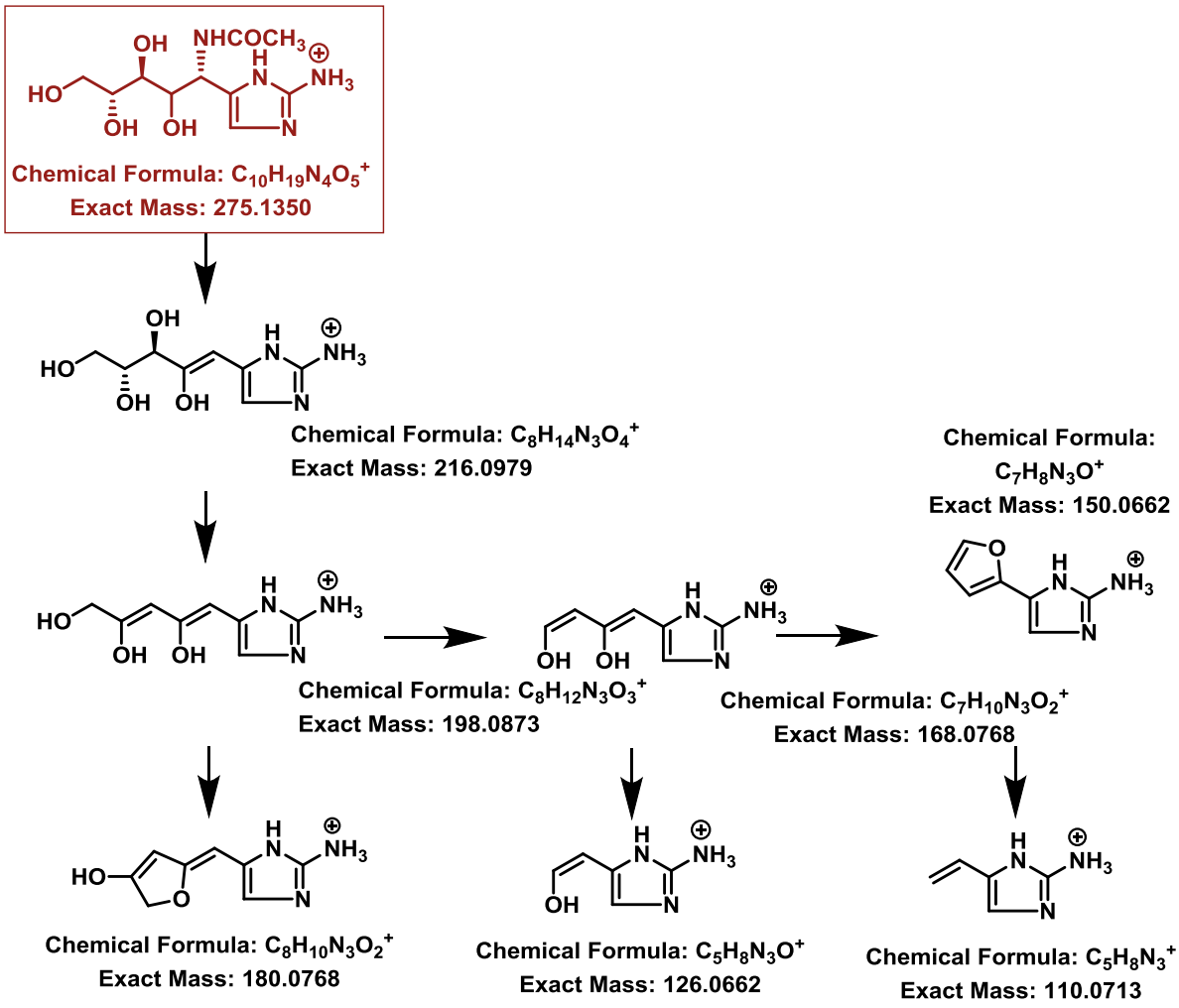

Figure S-7: Proposed fragmentation pattern of TP111 in (+)ESI-MS.

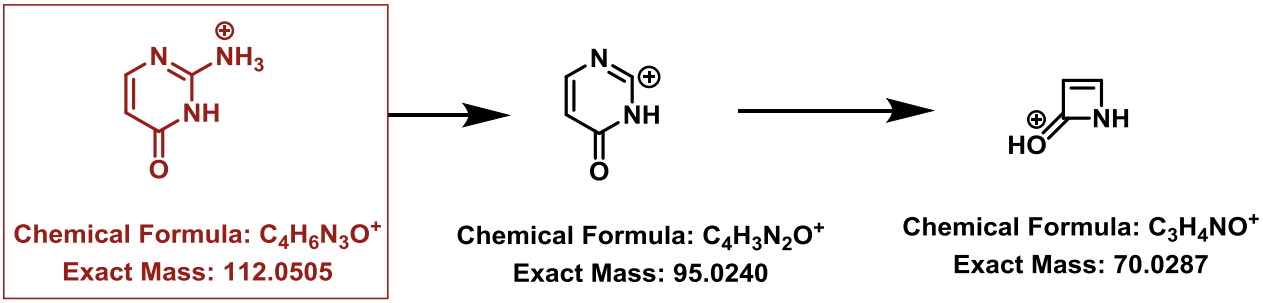

Figure S-8: Photodegradation profiles of Zanamivir in several water matrices under artificial irradiation conditions.

Artificial and natural water matrices of different composition spiked with zanamivir were assayed to evaluate the role of natural water constituents on the photodegradation rate.(Goncalves et al. 2011)

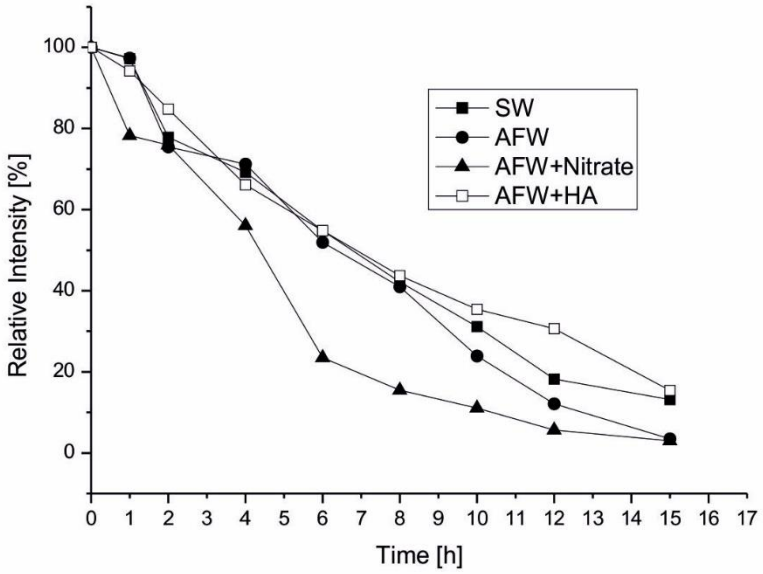

UV-Vis and calculation of quantum yield

UV-vis spectra were recorded on a Hitachi U3100 spectrophotometer where the scan was set from 190 – 800nm.

Figure S-9a. UV spectrum of Zanamivir

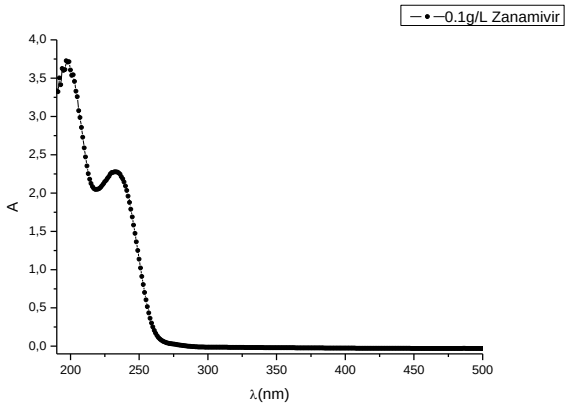

Chemical actinometry

The incident light intensity was determined using 2-nitrobenzaldehyde (2-NB) according to the methodologies described in Willett and Hites, and Galbavy et al.(Galbavy et al. 2010, Willett and Hites 2000)

Figure S-9b: Decay plot of 2-NB measured in suntest operator

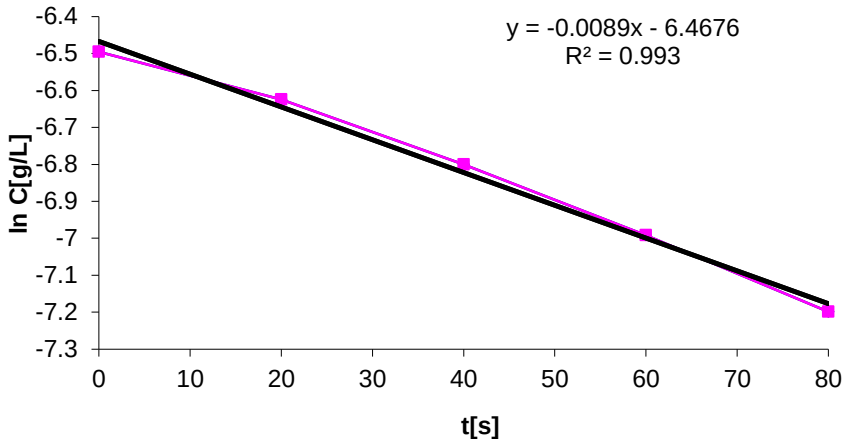

Equation for quantum yield calculation ($f_{2\text{-NB}}$:0.5)

$$\phi_{zan} = \frac{k_{zan}}{k_{2-NB}} \times \frac{\sum L_\lambda \varepsilon_\lambda^{2-NB}}{\sum L_\lambda \varepsilon_\lambda^{zan}} \phi_{2-NB}$$

$\phi_{zan,2-NB}$	Quantum yield of zanamivir and 2-NB
$k_{zan,2-NB}$	Constant rate of zanamivir and 2-NB
L_λ	Irradiance
$\varepsilon_\lambda^{zan,2-NB,}$	Molar absorption coefficient of zanamivir and 2-NB

SI – Reference:

C. Goncalves, S. Perez, V. Osorio, M. Petrovic, M.F. Alpendurada, D. Barcelo, Photofate of oseltamivir (Tamiflu) and oseltamivir carboxylate under natural and simulated solar irradiation: kinetics, identification of the transformation products, and environmental occurrence, Environ Sci Technol, 45 (2011) 4307-4314.

K.L. Willett, R.A. Hites, Chemical Actinometry: Using o-Nitrobenzaldehyde to Measure Light Intensity in Photochemical Experiments, J Chem Educ, 77 (2000) 900-902.

E.S. Galbavy, K. Ram, C. Anastasio, 2-Nitrobenzaldehyde as a chemical actinometer for solution and ice photochemistry, J Photoch Photobio A 209 (2010) 186-192.

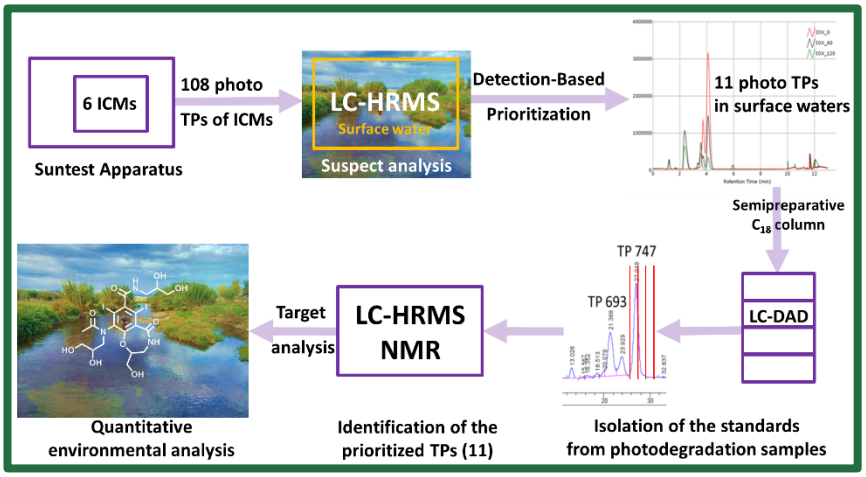

Article Nº2:

Zonja, B., Delgado, A., Pérez, S. and Barceló, D.

LC-HRMS Suspect Screening for Detection-Based Prioritization of Iodinated Contrast Media Photodegradates in Surface Waters.

(2015.) Environ Sci Technol 49(6), 3464-3472.

Environmental Science & Technology

Article

pubs.acs.org/est

LC-HRMS Suspect Screening for Detection-Based Prioritization of Iodinated Contrast Media Photodegradates in Surface Waters

Bozo Zonja,[†] Antonio Delgado,[‡,§] Sandra Pérez,*[,†] and Damià Barceló[†,∥]

[†]Water and Soil Quality Research Group, Department of Environmental Chemistry, IDAEA-CSIC, c/Jordi Girona, 18-26, 08034 Barcelona, Spain

[‡]University of Barcelona (UB), Faculty of Pharmacy, Department of Pharmacology and Medicinal Chemistry, Avga. Joan XXIII s/n, E-08028 Barcelona, Spain

[§]Department of Biomedicinal Chemistry, Research Unit on BioActive Molecules (RUBAM), IQAC−CSIC, c/Jordi Girona, 18-26, 08034 Barcelona, Spain

[∥]Catalan Institute of Water Research, c/Emili Grahit, 101, Edifici H_2O, Parc Científic i Tecnològic de la Universitat de Girona, E-17003 Girona, Spain

Supporting Information

ABSTRACT: The objective of the study was to demonstrate the applicability of suspect screening for the detection of six iodinated contrast media (ICM) and their phototransformation products (TPs) in surface waters. First, a photodegradation study of ICM in surface water using a sunlight lab-scale simulator was performed. By means of a guided differential sample analysis, the exact masses of the molecular ions and the retention times of TPs were identified. Positive findings were filtered manually generating a suspect list of 108 photoproducts. Following a generic solid-phase extraction of surface water samples, LC-HRMS was used to screen for the presence of the compounds previously detected in the photodegradation samples. On the basis of detection frequencies (>50% of the samples), 11 TPs were prioritized and their structures elucidated by HRMS and NMR. In the real surface water samples, median concentration of parent compounds was 110 ng/L reaching up to 6 μg/L for iomeprol, while TPs were found at median concentration of 8 ng/L, reaching up to 0.4 μg/L for iomeprol TP651-B. In summary, the proposed screening approach facilitates the evaluation of the degradation of polar compounds at a real scale with a fast detection of TPs without prior availability of the standards.

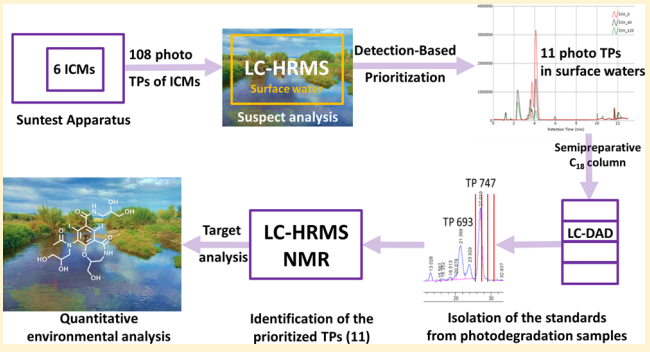

INTRODUCTION

One of the most frequently detected compounds in surface waters are iodinated contrast media (ICM). They are widely used in human medicine as imaging agents for organs or blood vessels during diagnostic tests.[1] Since they are metabolically very stable in the human body and are used in relatively high doses (up to 200 g per test), it does not come as a surprise that they can break through sewage treatment plants and reach surface waters in high concentrations.[1,2] Once in the surface water, ICM could be transformed through different processes and form a high number of transformation products (TPs).

A new generation and the affordability of high resolution mass spectrometers (HRMS) like orbitrap or time-of-flight-MS allows exploration of new approaches for detection of ICMs in environmental samples. Krauss et al.[3] introduced the terms target analysis, suspect, and nontarget screening. The main difference among the three analytical approaches is that target implies using a reference standard as a starting point for the method development, while suspect uses a list of suspected compounds with their exact masses, and nontarget refers to screening without any starting a priori information on the compound to be detected. While it can be appreciated that the latter two approaches provide a broader picture of the compound distribution of an environmental sample, still much further effort has to be dedicated to confirm and, if possible, quantify the detected compounds[4] (the process which precedes the target screening). Schymanski et. al.[5] proposed five identification confidence levels in HRMS analyses, with the starting point of filtering the exact mass of interest and the end point ideally being a confirmation of the structure using the reference standard. However, a special end point may be applied for detection and qualification of newly identified TPs, formed from biotic or abiotic processes, in cases when reference

Received: October 27, 2014
Revised: February 3, 2015
Accepted: February 11, 2015
Published: February 11, 2015

DOI: 10.1021/es505250q
Environ. Sci. Technol. 2015, 49, 3464−3472

standards cannot be procured. For instance, in Zonja et al.,[6] only one out of four phototransformation products of an antiviral Zanamivir was marketed. In such cases, a qualitative-reference standard may exist in the form of a mixture of parent compound and its TPs resulting from a transformation performed at the lab scale. For instance, Goncalves et al.[7] used a qualitative-reference standard for the detection of oseltamivir and its TPs in real surface waters since the standards were not available. Other approaches rely on obtaining the standards from semipreparative liquid chromatography or chemical synthesis when the standards are not commercially available. Kormos et.al.[8] isolated biotransformation products of several ICM by semipreparative chromatography and, after confirming the structures with MS^n and nuclear magnetic resonance (NMR), created a target method for their detection in the environmental samples. Another possibility is illustrated by the case of Osorio et al.,[9] where the biotransformation products of diclofenac were synthesized instead of isolated in order to confirm their structures.

Commonly, the suspect analysis has been used only to detect a wide range of parent compounds and their TPs, but only a few TP concentrations were determined because of the limited availability of TP standards.[10−12] Previous publications on suspect analysis were focused on detection of TPs rather than their determination of concentrations or their prioritization.[13]

This study uses existing approaches like isolation of the TPs by semipreparative HPLC and/or identification and structural elucidation of TPs, and combines them with the suspect screening analysis applied for surface water TP prioritization of ICM. Due to the relevant surface water concentrations of ICMs[1], known phototransformation of iopromide (IOP),[14] their contribution to adsorbable organohalogens (AOX),[15] and possible formation of highly toxic iodinated disinfection byproducts in waterworks,[16] the aim is to investigate a comprehensive and rapid approach for the evaluation of the phototransformation of polar compounds, ICM, in real surface waters using a detailed analytical workflow (Figure 1).

EXPERIMENTAL SECTION

Chemicals and Standards. Parent compounds diatrizoate (DTZ) and iohexol (IOX) were purchased from Sigma-Aldrich (Schnelldorf, Germany) and Iodixanol (IDX), iomeprol (IMP), iopamidol (IPM), and iopromide (IOP) for the analysis were purchased from Toronto Research Chemicals (Toronto, Canada). IMP and IPM were also purchased as formulated products (trademarks Iomeron and Iopamiro, respectively) and the active pharmaceutical ingredient isolated by semipreparative HPLC. Internal standards: iopamidol-d_3, iopromide-d_3, iohexol-d_5, and iomeprol-d_3 were purchased from Toronto Research Chemicals and iodixanol impurity C from LGC standards (Wesel, Germany). Actinometer used was 2-Nitrobenzaldehyde was purchased from Sigma-Aldrich. All solvents used (methanol, acetonitrile, and water) were purchased from Fisher Scientific (Geel, Belgium), except ethyl acetate which was from Merck. Formic acid (98%−100%) was ACS grade and purchased from Sigma-Aldrich (Schnelldorf, Germany).

SPE cartridges Oasis HLB (500 mg), MCX and MAX (both 200 mg) were bought from Waters (Waters Milford, U.S.A.) and Bond Elut PPL (500 mg) from Agilent Technologies (Waghaeusel/Wiesental, Germany). Calibration of the Q-Exactive was done with ESI positive ion calibration solution from Thermo Scientific (Dresden, Germany).

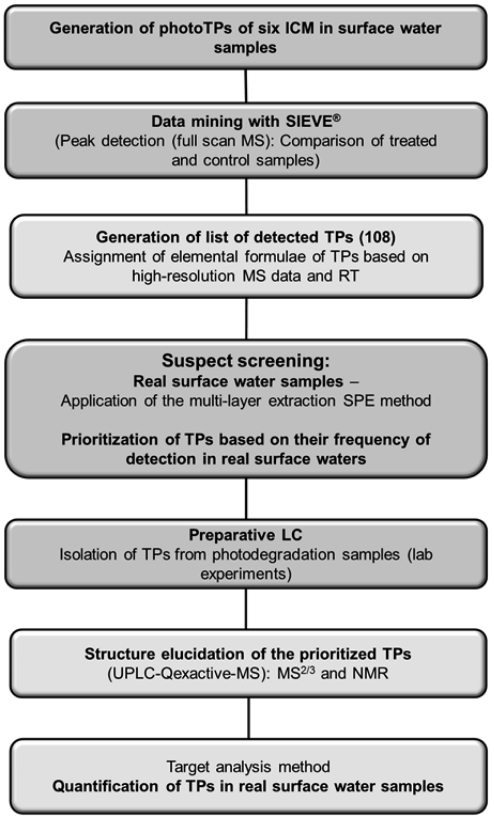

Figure 1. Analytical workflow for generation, prioritization, identification, and quantification of transformation products of ICM in surface waters.

Photodegradation Experiments. The photodegradation experiments were conducted under simulated solar radiation in a Suntest CPS simulator (Heraeus, Hanau, Germany). The system was equipped with a Xenon arc lamp and appropriate glass filters to restrict the transmission of wavelengths below 290 nm, giving a wavelength spectrum closely resembling solar light. The lamp intensity was adjusted to an irradiance of 500 W m^{-2} corresponding to a light dose of 1800 kJ m^{-2} h^{-1}. For the identification of potential TPs, each compound was irradiated separately at a concentration of 1 μg/mL in surface water collected from Llobregat river (pH 6.5; conductivity 1809 μS cm^{-1}; dissolved oxygen 4.13 mg L^{-1}). Test solutions were irradiated in the Suntest apparatus in crimp-cap 20 mL quartz vials. At predefined time points, 1 mL aliquots were withdrawn with a syringe from the vials and frozen immediately. For our control solutions, we also spiked individual surface water samples with the concentration of 1 μg/mL of standards. These solutions were wrapped with aluminum foil, exposed in Suntest and sampled in the same way and at the same time as the treated solutions. This allowed us to account for any dark reactions.

Screening Method for TP Detection in Photodegradation Samples and Suspect Screening Method for Surface Water Samples. In order to detect the parent compounds and any potential TPs from lab generated photodegradation as well as for a suspect screening of surface water samples, a method was developed using an Acquity UPLC coupled to Q-Exactive (Thermo Scientific, Bremen, Germany). Electrospray ionization interface (ESI) was operated in the positive ion mode to obtain the exact masses of the TPs

DOI: 10.1021/es505250q
Environ. Sci. Technol. 2015, 49, 3464−3472

and parent compounds. Only ESI positive mode was used because it was previously reported that ESI negative ion mode showed poor ionization efficiencies of the photoproducts of iopromide.[14] Likewise, other works analyzing ICM degradates found that the presence of amine, amide, and/or hydroxyl groups in the molecule of the ICM TP afforded protonation using acid mobile phase.[8,14,17] The chromatographic separation of the photodegradation samples was performed using an Acquity UPLC C_{18} column (100 mm × 2.1 mm, 1.7 μm) proceeded by a precolumn of the same packing material (5 mm × 2.1 mm, 1.7 μm) to obtain information regarding the chromatographic retention of the TPs. Detailed information on chromatographic and MS conditions as well as data-dependent parameters is provided in the Supporting Information (SI).

Environmental Samples from Surface Water. Thirteen Surface water grab samples were taken from the Besos and Llobregat rivers in the vicinity of the city of Barcelona (Spain) (SI Table SI-1 and Figure SI-1). Besos samples were taken in November (daily average solar irradiation of 2.30 $kWhm^{-2}$) and Llobregat samples in December 2013. (daily average solar irradiation of 1.88 $kWhm^{-2}$), both before heavy rain and during dry weather conditions with at least 9 h of daylight. Four different cartridges were used to enrich the samples; Oasis HLB, Bond Elut PPL, Oasis MAX, and Oasis MCX. (details: see *environmental samples from surface water* in the SI).

Isolation of Transformation Products via Semipreparative HPLC-DAD. Agilent HPLC-UV system with 1200 series DAD and analyte fraction collector were used in order to separate and isolate the prioritized TPs. The semipreparative analysis was accomplished with a Synergi Fusion RP column (250 mm × 21.20 mm, 10 μm Phenomenex, Aschaffenburg, Germany). (detailed description can be found in the SI, *isolation of transformation products via semipreparative HPLC-DAD*)

Identification of TPs with the Combination of MS and NMR. Exact mass measurements of the ICM and their TPs obtained from the purification of the photodegradation samples were carried out in full-scan and product ion mode using a Q-Exactive-MS interfaced with an ACQUITY UPLC system.

NMR experiments were carried out on a 600 MHz Bruker Avance III spectrometer, equipped with a TCI cryogenic probe and a Z-gradient coil. The 1D 1H, 1D 13C, and 2D 1H-13C sensitivity-enhanced and multiplicity-edited HSQC were measured at 298 K. Compounds were dissolved in CH_3OD or D_2O.

Determination of ICM and Their Prioritized TPs in Surface Water. The surface water extracts were reanalyzed for determination of the concentrations of ICM and their prioritized TPs using using an Acquity UPLC coupled to Q-Exactive. The method was slightly modified compared to suspect screening method and details can be found in *determination of ICM and their prioritized TPs in surface waters* in the SI

RESULTS AND DISCUSSION

In conventional strategies, which do not include suspect screening, the chemical structures of all the TPs generated under controlled conditions are first characterized and then searched for in environmental samples using LC-MS/MS-based target analysis. In contrast, the present approach selects the environmentally relevant TPs for subsequent structure elucidation based on their detection frequency in real samples. This largely reduces the number of compounds potentially detectable in the environment, and filters out only those TPs which deserve further attention and structure elucidation. This approach allowed for prioritizing 11 TPs out of 108 generated in the suntest apparatus mimicking environmental conditions and can have a wide application in the evaluation of the degradation of any polar compound at real scale.

Photolysis Studies of ICM in Surface Waters. Following the analytical workflow depicted in Figure 1, the first step was to photodegrade the six ICMs in order to generate the TPs that served as a starting point in the suspect screening method (see next section). Degradation profiles of the ICMs in surface water at the concentration of 1 μg/mL are shown in (SI Figure SI- 2).

Generation of Suspect Screening List and Prioritization of the TPs. Once the degradation samples had been run in the HRMS, the mass spectral data were processed with differential sample analysis software (SIEVE, Thermo Scientific). This created a list of exact masses of TPs. Since Perez et al.[14] previously identified the four photodegradation pathways of IOP, they were used as complementary information in order to determine whether these modifications happened in other ICM. Those reactions were as follows: (a) deiodination of the aromatic ring (Δ125.8966 Da relative to parent mass); (b) substitution of iodine by a hydroxyl group (Δ109.9017 Da); (c) N-demethylation of the amide in the hydroxylated side chain (specific loss only possible for IOP and IMP); and (d) oxidation of a methylene group in the hydroxylated side chain to the corresponding ketone (+ m/z 13.9790). On the basis of this, we produced a suspect list comprising 108 TPs (31 TP of IDX, 15 TPs of IOP (compared to the eight detected by Perez et.al.[14]), 23 TPs of IOX, 17 TPs of IMP, 13 TPs of IOM, and 9 TPs of DTZ). SI Table SI-2 lists all TPs detected in any of the photolysis samples taken between 0 and 160 min of exposure, which exhibited a peak intensity cutoff set to 5 E^5. This list was then applied to screen real surface water samples for the suspect TPs. The outcomes are also reported in SI Table SI-2 in which a finding is considered positive if the peak intensity was at least 1 E^5 counts. TPs detected in at least seven samples were deemed prioritized and advanced into the next step of the analytical workflow (Figure 1). TPs marked in bold in the SI Table SI-2 are the 11 prioritized TPs. Although photodegradation of DTZ yielded 9 TPs (SI Table SI-2) in our laboratory experiments, none of them were found in suspect screening of the surface water samples (SI Table SI-2—YES/NO). This led DTZ's TPs to be discarded from subsequent steps of the analytical workflow.

Four of the prioritized TPs had been reported earlier. They were formed under different oxidation/reduction processes.[14,18,19] However, in those studies, their structures were only tentatively identified and/or have not been considered as environmentally present compounds. Among the four compounds, IMP-TP651 and IOP-TP 665 were found when IMP and IOP, respectively, were degraded using γ-irradiation,[18] IOP-TP651 under simulated sun irradiation conditions[14] and IPM-TP667 using UV for the degradation of IPM.[19]

Isolation of Standards with Semipreparative-LC. Once the prioritization of the TPs was completed, the photodegradation of IDX, IOP, IOX, IMP, and IPM were repeated at a higher test concentration in order to synthesize and isolate the prioritized TPs. The majority of TPs eluted earlier than the respective parent compound, indicating enhanced polarity. The only TPs eluting later than the corresponding ICM were IOP-TP665 A, B, and C, IMP-TP651-B, and IOX-TP695-B. IDX and IOX formed a TP with identical retention time and exact

DOI: 10.1021/es505250q
Environ. Sci. Technol. 2015, 49, 3464−3472

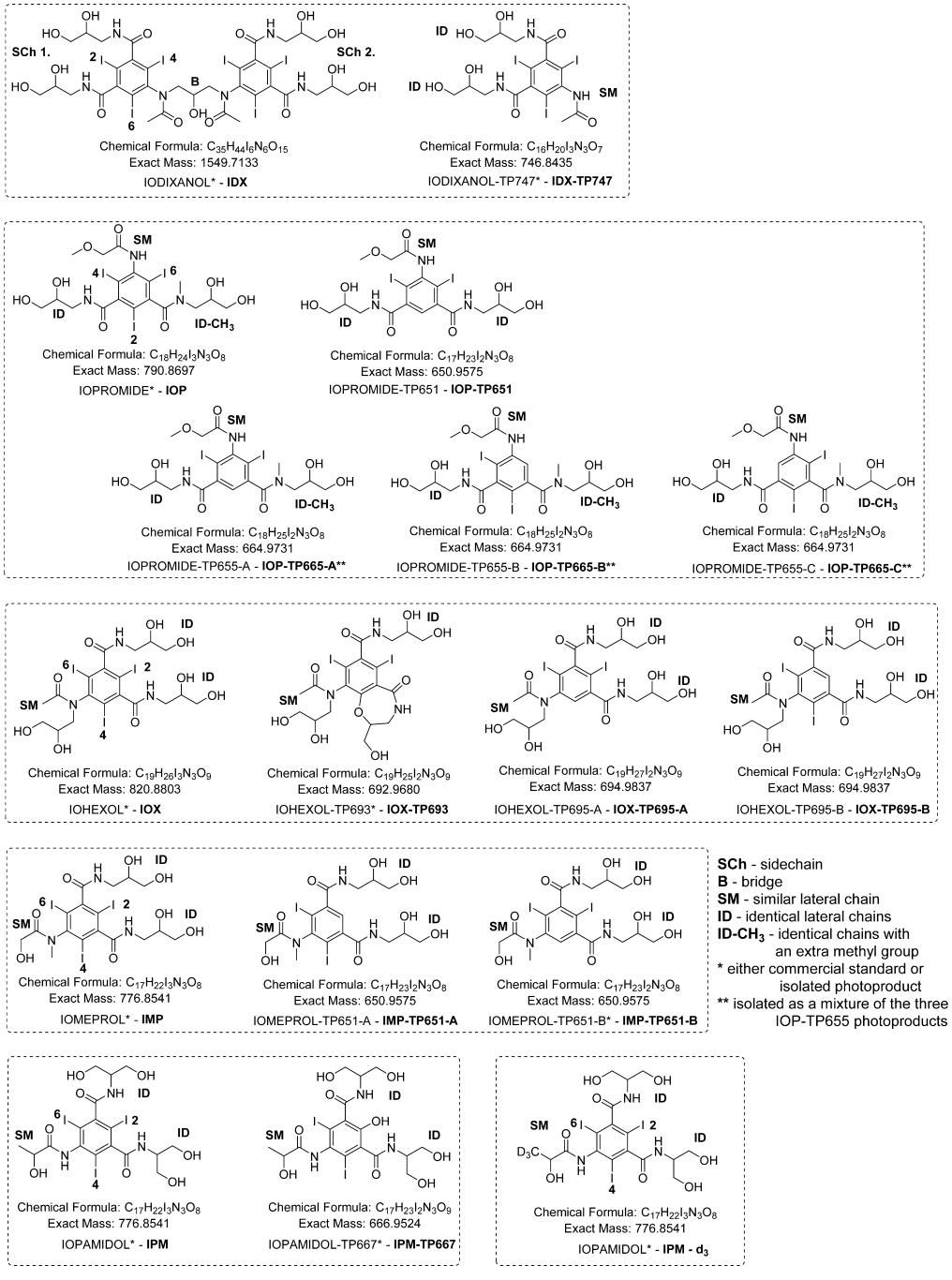

Figure 2. Structures of the parent ICM compounds and their prioritized TPs.

mass (TP693) suggesting the formation of a structurally identical species (Figure 2). Apart from matching retention times and exact masses of the molecular ions, the MS^2 spectra of these two TPs were identical (SI Figure SI-3). Although it was not possible to identify the precursor of TP693 detected in real water samples (it may originate from both IOX and IDX), for the sake of simplicity, it is referred to as IOX-TP693. Among the IDX-TPs peaks, TP693 coeluted with another TP, and it was thus not possible to obtain the purified standard by semipreparative LC. However, for the photolysis sample of IOX, chromatographic resolution was sufficient to isolate TP693 (SI Figure SI-4A,B). The TPs of IMP presented a similar problem. While it was possible to isolate TP651-B, which eluted after the parent peak, TP651-A coeluted with another TP of IMP, and it was thus not possible to purify and isolate it. After the isolation of the TP standards (four isolated as pure substances and three as mixture—IOP-TPs665-A-C) (SI Table SI-2), their structures were elucidated by HRMS and corroborated by high-field NMR experiments, as detailed in the following sections. Structures of the TPs that were not possible to isolate were elucidated by HRMS in the mixture.

Identification and Confirmation of the TP Structures with HRMS and NMR. Eleven TPs were designated as prioritized TPs of ICM based on their detection frequency in the real surface water samples: IDX-TP747, IOP-TPs 665A, B, and C, IOP-TP651, IOX-TP693, IOX-TP695A and B, IMP-TP651A and B, and IPM-TP667 (Figure 2). For their identification, the MS^2 and pseudo-MS^3 (pMS^3) product ion

DOI: 10.1021/es505250q
Environ. Sci. Technol. 2015, 49, 3464−3472

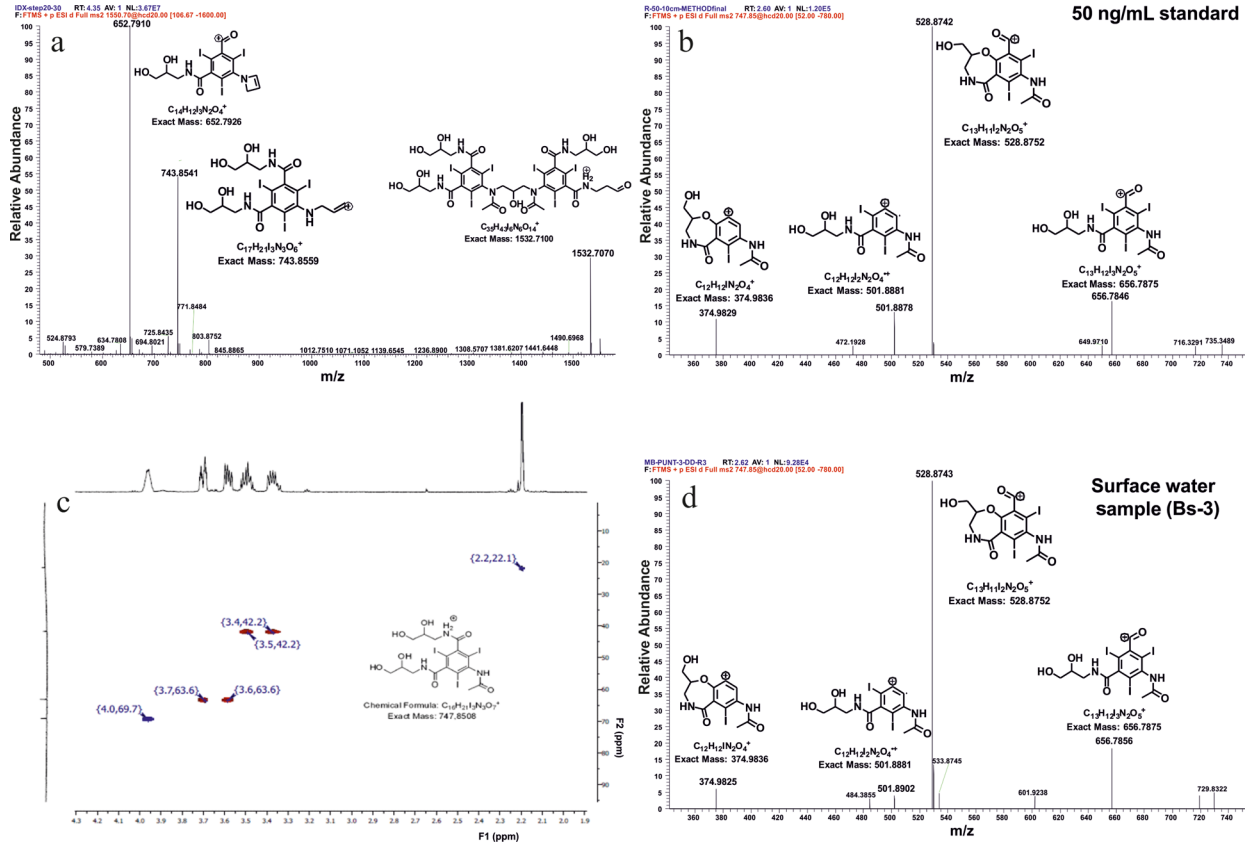

Figure 3. Example of the identification protocol (IDX-IDX-TP747) with (a) MS^2 spectrum of IDX at NCE 20 with the ramp of 30%; (b) MS^2 spectrum of isolated IDX-TP747 at NCE 20; (c) (HSQC)-NMR spectrum of isolated IDX-TP747; and (d) MS^2 spectrum of a IDX-TP747 found in surface water at NCE 20.

spectra of the five parent compounds and the 11 photodegradates were recorded to determine the plausible elemental compositions and structures of the fragment ions (see SI Table SI-3 for elemental compositions and SI Figures SI-5 for the fragmentation pathways and spectra). An example (IDX-TP747) of identification of TPs and matching the spectra with the suspect analytes in surface water is given in Figure 3.

General Aspects on the Fragmentation of ICM and Their TPs. In general, the fragmentation pathways of IMP, IPM, and IOP were very comparable, showing a number of identical cleavages, while the fragmentation of the IOX was slightly different because it bears more functional groups amenable to protonation. Related observations were reported by Kormos et al.[2] for ICM fragmentations using an ion trap-MS. On the whole, the losses of HI, I, and the loss of side chains are present in the fragmentation of the five ICMs (SI Figures SI-5). In particular, a specific loss of 91.0633 and 73.0528 Da for IMP, IPM, and IOP was observed with the compositional difference from the parent ion of $C_3H_9O_2N$ and C_3H_7ON, respectively. These losses were attributed to the loss of 2,3-dihydroxypropylamine and the subsequent spontaneous and reversible water addition. (SI Figures SI-5.3, 5.9, and 5.11). This unusual fragmentation behavior was previously reported by Beuch et al.,[20] where methyleneamine elimination was followed by instantaneous gas-phase water addition via an acylium ion intermediate. In the present study, additional information was obtained from the fragmentation of deuterated IPM (SI Figure SI-5.13), confirming that one of the *identical* side chains was modified rather than the *similar* deuterated chain, yielding *m/z* 707 in the case of IPM-d_3. The same pattern was observed in the respective TPs of these parent compounds (SI Figure-SI-5.4, 5.5, 5.10, and 5.12). For simplicity's sake, each ICM's side chains are described as *similar* and *identical* (*identical-CH*$_3$ in case of IOP), which refer to the annotations made in Figure 2. *Identical* side chain stands for the two lateral chains in position **1** and **3**, while the term *similar* refers to slightly modified chain in the position **5** (Figure 2.).

Identification of the Prioritized ICM TPs. The following section describes the structural elucidation of the prioritized TPs that were isolated by a semipreparative LC. More information on elucidation of the prioritized, but non-isolated TPs as well as additional information on the isolated ones, please refer to SI Figure SI-5, where a short introduction on TP identification is given before the corresponding fragmentation scheme.

IDX-TP747. The key photoproduct originating from IDX is TP747 (Figure 3). Its chemical formula ($C_{16}H_{21}O_7N_3I_3$) strongly suggests N-dealkylation at the central hydroxypropylene group, which serves as a linker between the two structurally identical triiodinated ring systems side chains (SCh 1 and SCh 2 from Figure 2). Fragmentation of the $[M + H]^+$ of TP747 (SI Figure SI-5.2-A and B) then follows the typical pattern of dehydration (*m/z* 729.8402), cleavage of the amide bond with a reversible water addition (like IPM, IMP, and IOP) in the *identical* chain (*m/z* 674.7980 vs *m/z* 656.7875), and elimination of HI (*m/z* 528.8752). The structure of this photoproduct TP747 was further confirmed by NMR (SI Figure SI-5.2-C), where the reduced number of carbon signals is indicative of the symmetry of the molecule. In addition, the Heteronuclear Single Quantum Coherence

DOI: 10.1021/es505250q
Environ. Sci. Technol. 2015, 49, 3464−3472

(HSQC) spectra allowed the unambiguous assignment of the methyne and methylene groups of the *identical* N (2,3 dihydroxypropyl)benzamide moieties (SI Figure SI-5.2-C).

IOX-TP693 (or IDX-TP693). For TP693 formed by IOX, the overall change in chemical composition corresponds to the net elimination of HI. The presence of a fragment ion with m/z 602.9120 in its product ion spectrum (SI Figure SI-5.7) indicates that one of the two amide side chains in IOX has been preserved. In addition, detection of m/z 560.9014 in the pMS^3 spectrum on the ion m/z 651.9647 shows that the *identical* side chain remains unchanged in the fragment m/z 651.9647. Indication that the *similar* side chain remained intact is the fragment m/z 432.9891 formed by loss of HI and cyclization of the *similar* side chain from fragment m/z 560.9014 (possible only if the *similar* side chain was not cyclized already). The most plausible route leading to the generation of TP693 involves substitution of one ring-bound iodine atom by the terminal primary hydroxyl group located in *similar* or *identical* side chain, giving rise to the 7-membered ring depicted in SI Figure SI-5.7-A. The NMR data of the isolated IOX-TP693 confirmed that the *identical* side chain cyclizes in IOX to give the TP693 (SI Figure SI-5.7-C). In particular, the HSQC spectrum showed a diagnostic CH group with chemical shifts of 4.85 ppm for a heavily coupled H atom and 89.8 ppm for the C atom. The chemical shift of the C atom is indicative of the preferred formation of a 7 membered ring system over an alternative 6 membered one, arising from cyclization of the secondary hydroxyl group of side chain *identical* or terminal primary hydroxyl from the *similar* side chain.

IMP-TP651-A and IMP-TP651-B. In contrast to IOX-TP693, where a single TP is formed from two different parent compounds, two TPs from IMP (TP651-A, 2.70 min, and TP651-B, 5.66 min) with identical exact mass and thus elemental composition were found in surface water samples. The $[M + H]^+$ with m/z 651.9647 corresponded to the replacement of iodine by hydrogen (SI Figure SI-5.10-A). This dehalogenation could occur at three different positions of the aromatic ring which, by considering the equivalence of positions **4** and **6**, it results in two different TPs (SI Scheme SI-1). The (+)ESI mass spectra of IMP-TP651-A and IMP-TP651-B (SI Figure SI-5.10-B) exhibited no qualitative differences. There were, however, noticeable differences in the relative intensities of all fragment ions. In an attempt to identify the structures of the two photoproducts, compound IMP-TP651-B was studied by NMR. Analysis of its HSQC spectrum (SI Figure SI-5.10-C) showed the presence of correlations for two different side chain CHOH and CH_2OH groups, an indication of the nonmagnetic equivalence of the hydroxybenzamido side chains and, hence, of the asymmetric nature of TP651-B with elimination of the iodine from the position **4** or **6**. Since we were not able to isolate the isomeric TP651-A (see in semipreparative isolation section), its structure was inferred from to correspond to reductive deiodination at position **2**.

IMP-TP667. The only TP of IPM detected in surface waters was IPM-TP667, originating from deiodination and hydroxylation. Taking into account that the *identical* and *similar* side chains were intact as indicated in the product ion spectrum (SI Figure SI-5.12-A-B) by the neutral loss of m/z 91.0633, the most likely structure corresponds to a phenolic structure with one iodine replaced by a hydroxyl group. HSQC-NMR analysis of TP667 was indicative of a symmetric structure since only one type of CH-N, one type of CH—O, and one type of CH_2—O moieties was observed (SI Figure SI-5.12-C). This would indicate that the more photolabile iodine would be the one located between the two benzamido groups in the original IPM structure.

Photodegradation Pathways. After the structure elucidation of the 11 prioritized TPs, the principal reactions are summarized in Scheme -1. They are (a) deiodination of parent

Scheme 1. Photodegradation Pathways of Prioritized ICM TPs

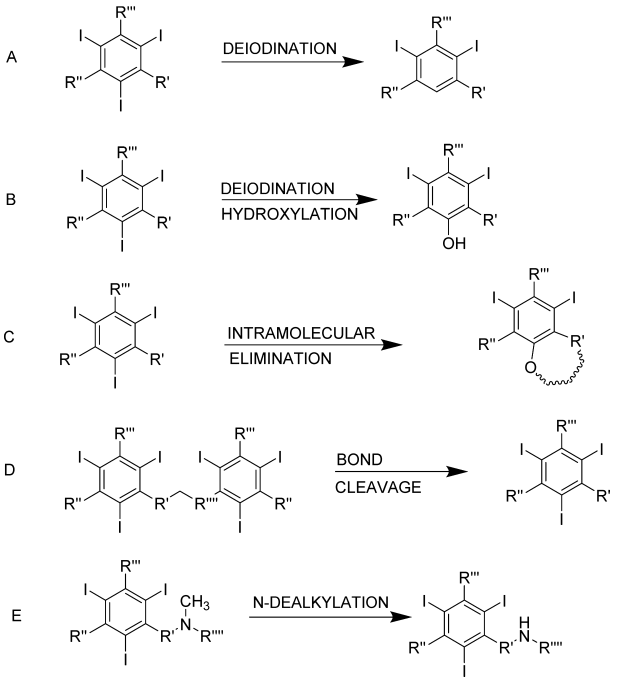

ICM with or without N-dealkylation of the amide in the hydroxylated side chain); (b) oxidative deiodination; (c) intramolecular elimination; (d) N-dealkylation of the hydroxypropylene group in the IDX; and (e) N-demethylation and concomitant deiodination (specific for IOP).

Validation of the LC-HRMS Method and Environmental Occurrence. Following the prioritization and mass spectral identification of the TPs, the surface water extracts previously interrogated in the prioritization process were reanalyzed using the validated method for quantitative determinations (See *determination of ICM and their prioritized TPs in surface waters* section with details on recovery and ion suppression measurement in the SI). ICM and their TPs absolute recoveries are shown in Table 1 with all target compounds between 71% (for DTZ) and 128% (for IOP). Ion suppression ranged from 44% (for IMP) and 130% (for IPM-TP667). LOQ was defined as the lowest scan peak with at least five data points, matched retention time (± 0.2 min), exact mass accuracy <5 ppm, and where it was possible to perform a MS^2 on a given mass. LOQ measurements were performed in HPLC water and corrected with recovery factor for the MLOQ (method limits of quantification, see matrix factor in Moschet et al.[4]). Measured LOQ ranged from 0.5 ng/L (IMP-TP651-B) up to 4.3 ng/L (for IDX- TP747).

A representative chromatogram of the detected parent compounds and TPs in nonspiked raw surface water samples is shown in SI Figure SI-6 (Besos-3). As can be seen from the SI Figure SI-6-TPs651, five peaks were detected for m/z

DOI: 10.1021/es505250q
Environ. Sci. Technol. 2015, 49, 3464−3472

Table 1. Occurrence of ICM in Llobregat (Ll) and Besos (Bs) Grab Surface Water Samples with Method Validation Parameters[a]

parameter	IDX	IDX-TP747	IOP	IOP-TPs665[e]	IOP-TP651[f]	IOX	IOX TP693	IOX TP695-A[f]
Ll-1	<LOQ	<LOQ	13.8 ± 0.3	4.4 ± 0.4	1.9 ± 0.1	26.1 ± 3.2	<LOQ	<LOQ
Ll-2	4.3 ± 0.4	5.2 ± 0.9	17.0 ± 0.3	<LOQ	2.1 ± 0.2	68.8 ± 7.1	2.2 ± 0.9	<LOQ
Ll-3	<LOQ	10.0 ± 1.2	18.7 ± 0.3	<LOQ	1.5 ± 0.1	159 ± 18	<LOQ	<LOQ
Ll-4	54.5 ± 0.8	11.5 ± 1.1	39.8 ± 3.0	4.3 ± 0.3	1.6 ± 0.0	160 ± 8	<LOQ	<LOQ
Ll-5	96.7 ± 3.1	8.1 ± 0.3	1785 ± 28	60.6 ± 1.7	30.2 ± 1.7	109 ± 3	<LOQ	<LOQ
Ll-6	129 ± 2	12.3 ± 1.6	192 ± 5	14.4 ± 0.6	5.3 ± 1.3	165 ± 16	<LOQ	<LOQ
Ll-7	129 ± 1	11.9 ± 1.7	214 ± 1	18.9 ± 0.9	4.0 ± 1.6	148 ± 17	<LOQ	<LOQ
Bs-1	240 ± 37	33.0 ± 0.3	655 ± 29	212 ± 2	298 ± 12.6	1286 ± 81	97.5 ± 1.0	110 ± 1
Bs-2	12.7 ± 2.4	81.9 ± 1.9	30.6 ± 3.5	12.4 ± 0.4	7.8 ± 0.4	1033 ± 61	69.1 ± 1.1	77.5 ± 2.0
Bs-3	287 ± 6	18.0 ± 0.3	836 ± 40	262 ± 3	471 ± 22	1326 ± 47	143 ± 3	55.2 ± 0.5
Bs-4	4050 ± 18	13.8 ± 1.9	372 ± 16	24.8 ± 4.1	35.5 ± 5.1	642 ± 10	12.1 ± 0.3	11.6 ± 2.2
Bs-5	1976 ± 37	15.1 ± 0.7	294 ± 13	38.1 ± 2.2	38.9 ± 7.2	754 ± 39	12.4 ± 1.0	23.9 ± 2.7
Bs-6	504 ± 33	6.6 ± 1.0	149 ± 4	16.8 ± 0.2	190 ± 4	221 ± 13	<LOQ	n.d.
LOQ [ng/L]	2.5	4.3	3.9	IOP[g]	IMP-651-B[g]	5.6	2.1	IOX[g]
NCE [%]	25	20	25	20	35	10	35	30
RT[b] [min]	4.34−4.65	2.63	3.93−4.08	4.14−4.62	3.61	2.89	1.94	2.45
R^2	0.9994	0.9998	0.9997	IOP[g]	IMP-651-B[g]	0.9998	0.9990	IOX[g]
recovery[c] [%]	102 ± 10	116 ± 4	128 ± 13	N/A	N/A	89 ± 3	120 ± 5	N/A
IS[d] [%]	74	62	45	N/A	N/A	76	68	N/A

parameter	IOX TP695-B[f]	IMP	IMP TP651-A[f]	IMP TP651-B	IPM	IPM TP667	DTZ
Ll-1	<LOQ	23.6 ± 1.4	3.2 ± 1	2.1 ± 0.4	8.9 ± 0.3	n.d.	15.1 ± 1.9
Ll-2	<LOQ	38.3 ± 4.5	2.7 ± 0.5	1.8 ± 0.3	15.4 ± 0.1	<LOQ	12.7 ± 5
Ll-3	<LOQ	41.6 ± 8.5	2.1 ± 0.2	1.4 ± 0.1	18.9 ± 0.1	<LOQ	4.8 ± 0.9
Ll-4	<LOQ	171 ± 18	4.7 ± 0.5	2.8 ± 0.5	17.0 ± 0.1	<LOQ	4.9 ± 0.6
Ll-5	<LOQ	1595 ± 78	37.3 ± 0.8	19.9 ± 0.5	65.7 ± 0.4	<LOQ	27.2 ± 3.4
Ll-6	<LOQ	686 ± 78	21.7 ± 1.8	10.9 ± 0.9	18.7 ± 0.3	<LOQ	8.6 ± 1.0
Ll-7	<LOQ	651 ± 65	22.8 ± 2.7	12.9 ± 1.5	20.4 ± 0.3	<LOQ	7.9 ± 0.4
Bs-1	93.1 ± 0.4	3519 ± 34	403 ± 11	293 ± 12	52.1 ± 2.0	2.3 ± 0.1	117 ± 6
Bs-2	56.4 ± 0.8	379 ± 15	42.9 ± 1.0	32.9 ± 2.4	14.0 ± 0.9	<LOQ	200 ± 6
Bs-3	71.6 ± 11.6	6100 ± 57	489 ± 23	394 ± 20	61.7 ± 1.9	3.1 ± 0.1	110 ± 6
Bs-4	15.1 ± 2.1	1693 ± 131	42.2 ± 8.1	50.4 ± 4.4	63.1 ± 3.0	n.d.	175 ± 33
Bs-5	20.3 ± 0.5	1526 ± 47	103 ± 7	54.9 ± 4.8	50.5 ± 3.4	n.d.	196 ± 30
Bs-6	n.d.	768 ± 46	22.7 ± 3.6	18.2 ± 1.0	15.8 ± 1.5	<LOQ	57.5 ± 10.2
LOQ [ng/L]	IOX[g]	0.6	IMP-651-B[g]	0.5	2.4	1.5	3.5
NCE [%]	30	30	35	35	30	10	20
RT[b] [min]	3.07	3.09	2.26	3.31	1.86	1.71	2.62
R^2	IOX[g]	0.9998	IMP-651-B[g]	0.9999	0.9998	0.9982	0.9994
recovery[c] [%]	N/A	78 ± 11	N/A	109 ± 8	106 ± 10	86 ± 1	71 ± 7
IS[d] [%]	N/A	44	N/A	77	108	130	73

[a]All concentrations are given in ng/L and the statistical errors are calculated based on three separate measurements and given as standard deviation (SD). [b]Retention times are given as a range for diastereoisomer peaks. [c]Recovery calculated for 250 ng spike. [d]Ion suppression calculated for 100 ng spike. [e]Concentration given as mixture of IOP TP665-A, B, and C. [f]Analytes which were not isolated and thus their concentrations are semiquantitative. [g]States which compound parameters were used for semiquantification.

651.9645. While the IMP-651-A and -B and IOP-TP651 were identified as such, the other two peaks (NL-IPM and NL-IMP; NL-neutral loss) had exactly the same retention time as the parent compounds IPM and IMP, respectively. The NL-peaks were also detected in standard solution. Hvattum et.al.[21] investigated this behavior and found that formic acid induces deiodination in the ESI capillary of the MS instrument. The same was observed for IOX-TP695-A and B, where (apart from the two TPs) a neutral loss of iodine from IOX shows a peak at 2.89 min which is the same retention time as IOX. The concentrations of the six ICM and the 11 TPs are given in Table 1.

When cross-referencing, there was no similarity of these prioritized TPs with known aerobic biodegradation ICM products found in previous studies.[2,8,17] Moreover, to the best of the authors' knowledge, deiodination has not been reported as an activated sludge biodegradation process of ICM. However, it should be noted that Redeker et.al.[22] found that DTZ can undergo deiodination (together with deacetylations) under anaerobic conditions. Parent compounds were detected in 100% of the samples and could be quantified in more than 97% of the samples. The only ICM not quantifiable in all samples was IDX, measured in 85% (11 out of 13) of the samples. TPs of the ICMs displayed different percentages regarding detection frequencies. They were detected in 96% with quantifiable levels in 70% of the samples. IDX-TP747 which was detected in all samples eluted at RT 2.68 min. However, an isobaric compound eluting at RT 2.79 min was also detected (SI Figure SI-6-IDX-TP747). Due to its proximity to the retention time of IDX-TP747, its fragmentation pattern

DOI: 10.1021/es505250q
Environ. Sci. Technol. 2015, 49, 3464−3472

was checked, and it was confirmed that it did not match the fragmentation pattern (data not shown) of IDX-TP747 (Figure 3). It was discarded from further analysis. IMP presented the highest concentrations, reaching in several samples levels above 1 μg/L with a maximum of 6 μg/L (river point Besos-3, SI Figure SI-1). Similarly, TP 651-B from IMP presented the highest levels of concentration but at the same sampling point reaching almost 400 ng/L, with the lowest concentration found in Llobregat-4 (1.4 ng/L). The lowest concentration of ICM in the surface water samples was for IPM, with a maximum concentration of 65.7 ng/L (approximately 100 times lower than the max. concentration of its positional isomer IMP) suggesting the lowest usage of this ICM in hospitals or higher elimination rates in WWTPs. Due to the low presence of the parent compound IPM, its TP667 was found at very low ng/L concentration and, in most of the cases, close to the LOQ. It was only possible to determine the concentration of IPM-TP667 in two river samples (Table 1).

■ ASSOCIATED CONTENT

Supporting Information

Analytical workflow scheme for TP detection and characterization; environmental samples from surface water; Photodegradation experiments; screening method for photodegradation samples and suspect screening method for surface water samples; isolation of transformation products via semipreparative HPLC-DAD; identification of TPs with the combination of MS and NMR; LC-HRMS method for determination of ICM and their prioritized TPs in surface waters; and additional figures, graphs, and tables. This material is available free of charge via the Internet at http://pubs.acs.org.

■ AUTHOR INFORMATION

Corresponding Author

*Phone: +34934006100; e-mail: spsqam@cid.csic.es (S.P.).

Author Contributions

The manuscript was written through contributions of all authors. All authors have given approval to the final version of the manuscript.

Notes

The authors declare no competing financial interest.

■ ACKNOWLEDGMENTS

B.Z. acknowledges the Marie Curie Actions ITN CSI:Environment PITN-GA-2010-264329 for the early stage researcher contract and funding. S.P. acknowledges the contract from the Ramon y Cajal Program of the Spanish Ministry of Economy and Competitiveness. This work has been financially supported by the Generalitat de Catalunya (Consolidated Research Groups "2014 SGR 418—Water and Soil Quality Unit", 2014 SGR 291—ICRA and 2014-SGR109— Research Unit on Bioactive Molecules). The authors acknowledge M. Gairi and Y. Perez for running the NMR experiments and J. Lopez and M. Fonatal for the use of the semipreparative LC. R. Chaler and D. Fanjul are acknowledged for the maintenance and help within the Mass spectrometry unit at IDAEA-CSIC. C. Martins from Thermo Fisher Scientific is acknowledged for the help with Thermo Software and M. Kuzmanovic for ArcGis figures. The authors appreciate a helpful discussion with E. Hvattum. This work reflects only the authors' views and the European Community is not liable for any use that may be made of the information contained therein.

■ REFERENCES

(1) Pérez, S.; Barceló, D. Fate and occurrence of X-ray contrast media in the environment. *Anal. Bioanal. Chem.* **2007**, *387* (4), 1235−1246.

(2) Kormos, J. L.; Schulz, M.; Ternes, T. A. Occurrence of iodinated X-ray contrast media and their biotransformation products in the urban water cycle. *Environ. Sci. Technol.* **2011**, *45* (20), 8723−32.

(3) Krauss, M.; Singer, H.; Hollender, J. LC-high resolution MS in environmental analysis: from target screening to the identification of unknowns. *Anal Bioanal Chem.* **2010**, *397* (3), 943−51.

(4) Moschet, C.; Piazzoli, A.; Singer, H.; Hollender, J. Alleviating the reference standard dilemma using a systematic exact mass suspect screening approach with liquid chromatography-high resolution mass spectrometry. *Anal. Chem.* **2013**, *85* (21), 10312−20.

(5) Schymanski, E. L.; Jeon, J.; Gulde, R.; Fenner, K.; Ruff, M.; Singer, H. P.; Hollender, J. Identifying small molecules via high resolution mass spectrometry: communicating confidence. *Environ. Sci. Technol.* **2014**, *48* (4), 2097−8.

(6) Zonja, B.; Goncalves, C.; Perez, S.; Delgado, A.; Petrovic, M.; Alpendurada, M. F.; Barcelo, D. Evaluation of the phototransformation of the antiviral zanamivir in surface waters through identification of transformation products. *J. Hazard Mater.* **2014**, *265*, 296−304.

(7) Goncalves, C.; Perez, S.; Osorio, V.; Petrovic, M.; Alpendurada, M. F.; Barcelo, D. Photofate of oseltamivir (Tamiflu) and oseltamivir carboxylate under natural and simulated solar irradiation: kinetics, identification of the transformation products, and environmental occurrence. *Environ. Sci. Technol.* **2011**, *45* (10), 4307−14.

(8) Kormos, J. L.; Schulz, M.; Wagner, M.; Ternes, T. A. Multistep approach for the structural identification of biotransformation products of iodinated X-ray contrast media by liquid chromatography/hybrid triple quadrupole linear ion trap mass spectrometry and 1H and 13C nuclear magnetic resonance. *Anal. Chem.* **2009**, *81* (22), 9216−9224.

(9) Osorio, V.; Imbert-Bouchard, M.; Zonja, B.; Abad, J. L.; Perez, S.; Barcelo, D. Simultaneous determination of diclofenac, its human metabolites and microbial nitration/nitrosation transformation products in wastewaters by liquid chromatography/quadrupole-linear ion trap mass spectrometry. *J. Chromatogr A* **2014**, *1347*, 63−71.

(10) Gómez-Ramos, M. M.; Ferrer, C.; Malato, O.; Agüera, A.; Fernández-Alba, A. R. Liquid chromatography-high-resolution mass spectrometry for pesticide residue analysis in fruit and vegetables: Screening and quantitative studies. *J. Chromatogr. A* **2013**, *1287*, 24−37.

(11) Rajski, T.; Gómez-Ramos, M. D. M.; Fernández-Alba, A. R. Large pesticide multiresidue screening method by liquid chromatography-Orbitrap mass spectrometry in full scan mode applied to fruit and vegetables. *J. Chromatogr. A* **2014**, *1360*, 119−127.

(12) Portolés, T.; Mol, J. G. J.; Sancho, J. V.; Hernández, F. Use of electron ionization and atmospheric pressure chemical ionization in gas chromatography coupled to time-of-flight mass spectrometry for screening and identification of organic pollutants in waters. *J. Chromatogr. A* **2014**, *1339*, 145−153.

(13) Kern, S.; Fenner, K.; Singer, H. P.; Schwarzenbach, R. P.; Hollender, J. Identification of transformation products of organic contaminants in natural waters by computer-aided prediction and high-resolution mass spectrometry. *Environ. Sci. Technol.* **2009**, *43* (18), 7039−7046.

(14) Perez, S.; Eichhorn, P.; Ceballos, V.; Barcelo, D. Elucidation of phototransformation reactions of the X-ray contrast medium iopromide under simulated solar radiation using UPLC-ESI-QqTOF-MS. *J. Mass Spectrom* **2009**, *44* (9), 1308−17.

(15) Putschew, A.; Wischnack, S.; Jekel, M. Occurrence of triiodinated X-ray contrast agents in the aquatic environment. *Sci. Total Environ.* **2000**, *255* (1−3), 129−134.

(16) Duirk, S. E.; Lindell, C.; Cornelison, C. C.; Kormos, J.; Ternes, T. A.; Attene-Ramos, M.; Osiol, J.; Wagner, E. D.; Plewa, M. J.; Richardson, S. D. Formation of toxic iodinated disinfection by-products from compounds used in medical imaging. *Environ. Sci. Technol.* **2011**, *45* (16), 6845−54.

DOI: 10.1021/es505250q
Environ. Sci. Technol. 2015, 49, 3464−3472

(17) Schulz, M.; Löffler, D.; Wagner, M.; Ternes, T. A. Transformation of the X-ray Contrast Medium Iopromide In Soil and Biological Wastewater Treatment. *Environ. Sci. Technol.* **2008**, *42* (19), 7207−7217.
(18) Jeong, J.; Jung, J.; Cooper, W. J.; Song, W. Degradation mechanisms and kinetic studies for the treatment of X-ray contrast media compounds by advanced oxidation/reduction processes. *Water Res.* **2010**, *44* (15), 4391−4398.
(19) Tian, F. X.; Xu, B.; Lin, Y. L.; Hu, C. Y.; Zhang, T. Y.; Gao, N. Y. Photodegradation kinetics of iopamidol by UV irradiation and enhanced formation of iodinated disinfection by-products in sequential oxidation processes. *Water Res.* **2014**, *58*, 198−208.
(20) Beuck, S.; Schwabe, T.; Grimme, S.; Schlorer, N.; Kamber, M.; Schanzer, W.; Thevis, M. Unusual mass spectrometric dissociation pathway of protonated isoquinoline-3-carboxamides due to multiple reversible water adduct formation in the gas phase. *J. Am. Soc. Mass Spectrom.* **2009**, *20* (11), 2034−48.
(21) Hvattum, E.; Priebe, H. Deiodination of iodinated aromatic compounds with electrospray ionization mass spectrometry. *Rapid Commun. Mass Spectrom.* **2013**, *27* (21), 2504−14.
(22) Redeker, M.; Wick, A.; Meermann, B.; Ternes, T. A. Removal of the iodinated X-ray contrast medium diatrizoate by anaerobic transformation. *Environ. Sci. Technol.* **2014**, *48* (17), 10145−10154.

DOI: 10.1021/es505250q
Environ. Sci. Technol. 2015, 49, 3464−3472

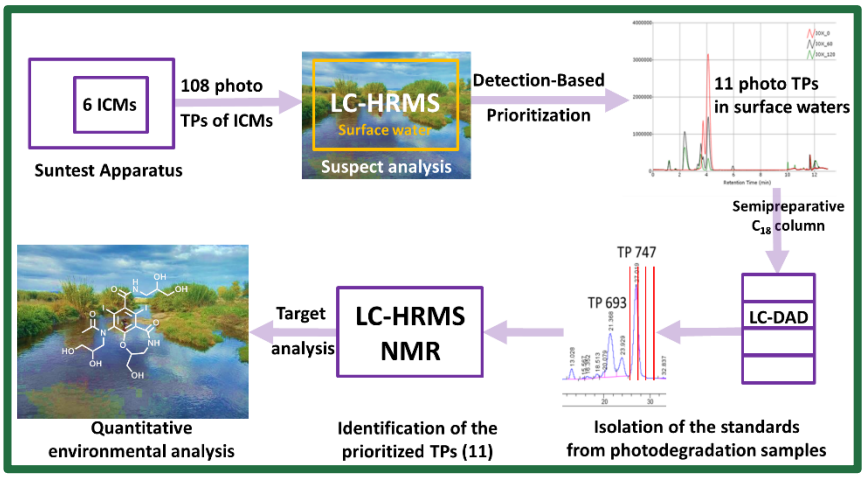

Article Nº2:

Zonja, B., Delgado, A., Pérez, S. and Barceló, D.

LC-HRMS Suspect Screening for Detection-Based Prioritization of Iodinated Contrast Media Photodegradates in Surface Waters.

(2015.) Environ Sci Technol 49(6), 3464-3472.

SUPPORTING INFORMATION

Total content: **Figures** – 36, **Tables** – 3 and **Schemes**-1

Supporting information has been reformatted to match the style of the thesis.

Table of Contents

Analytical workflow scheme for TP detection and characterization

The analytical workflow of the study starts with a generation of TPs in surface water spiked with ICM using a sunlight simulator. Next, a suspect analyte list was created including: (i) MS data mining with SIEVE and (ii) cross referencing it with IOP phototransformation reactions based on literature and our previous knowledge. Every compound is defined by a name, elemental formula and retention time. The three descriptors will serve as initial criteria of confirmation. After the list was established, a multi-layer SPE method was applied using cartridges with different retention mechanisms to account for different chemical properties. A total of 13 real surface water samples were collected, extracted and analysed with LC-MS for suspected analytes. The suspect analyte list was then condensed to a list of priority target analytes based on the detection frequencies in the surface water samples. Next, the TPs were isolated from photodegradation samples using semipreparative LC and their structures were elucidated using detailed HRMS analysis alongside with NMR. Finally, a target method was set up in order to quantify these prioritized and parent compounds in real surface water samples in cases when it was possible to separate the TPs with semipreparative LC. Remaining prioritized compounds were semi-quantified using similar standard for quantification.

Environmental samples from surface water

All samples were collected in 2.5 L-amber, solvent-rinsed glass bottles and filtered immediately through 0.7 μm glassfiber filters and spiked with 100 ng of internal standards. The samples were then stored at -20^{o}C until analysis. The enrichment of 800 mL of surface water samples (pH was adjusted to 6.3 - 6.7) was performed on SPE cartridges. For this step, four different cartridges were used; Oasis HLB, Bond Elut PPL, Oasis MAX and Oasis MCX. The four cartridges were connected in series and then conditioned with 5 ml of methanol: ethyl acetate (1:1) and 5 mL of water. The samples were then passed through the conditioned cartridges at a flow rate of about 10 mL min^{-1}. After drying with a vacuum pump, the enriched cartridges were eluted separately. Compounds retained on Oasis HLB and Bond Elute PPL were eluted with 3x3 mL of methanol/ethyl acetate (1:1) while the MAX and MCX cartridges were first eluted with 3 mL methanol: ethyl acetate (1:1) followed by 2x3 mL of 2 % formic acid in methanol (MAX) or 5 % of ammonia in methanol (MCX). Finally, the four extracts were combined and evaporated to dryness under a stream of nitrogen and

reconstituted in 400 µL of the initial mobile phase conditions (acetonitrile/water – 3:97). 20 µL of the final extract were injected into the UPLC-QExactive-MS.

Figure SI-1. 13 sampling sites of Besos and Llobregat rivers.

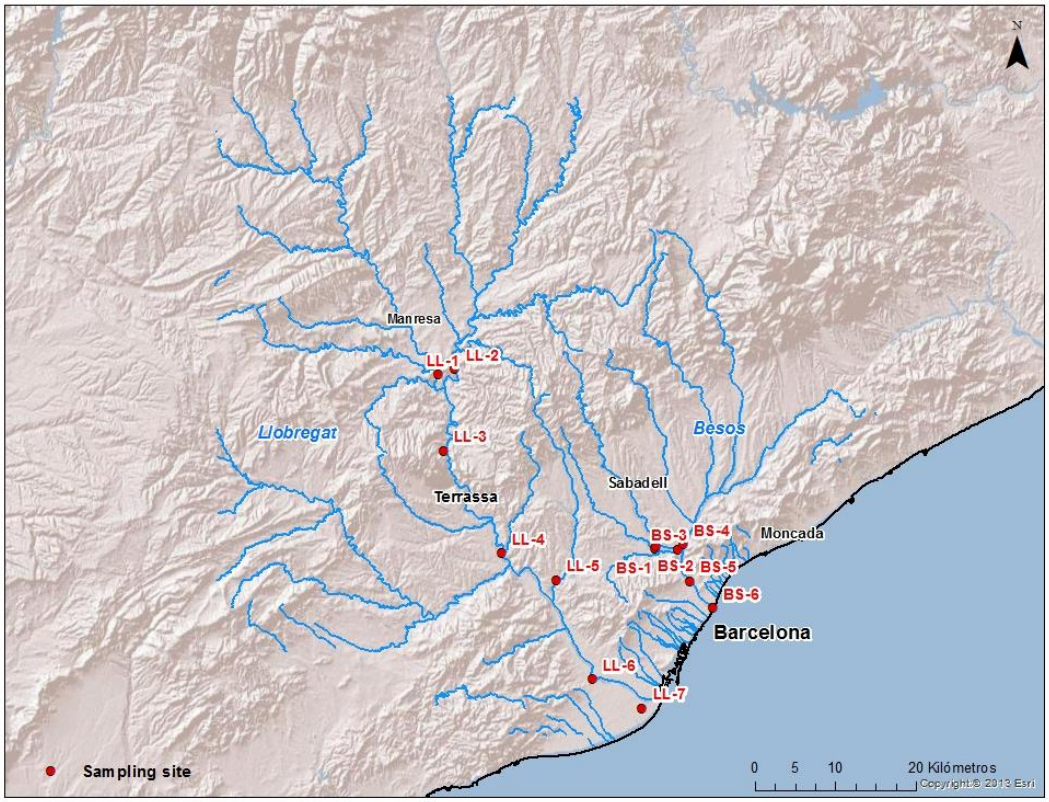

Table SI-1. Physico-chemical properties and location of the samples

SL	pH	T	O_2		σ	UTM coordinates		
		[ºC]	[mg/L]	[%]	[µS/cm]	Zone	X	Y
BS-1	8.3	16.1	8.30	86.2	1484	31	429192	4593550
BS-2	8.0	14.0	8.71	91.4	1165	31	429307	4593848
BS-3	8.3	13.5	9.25	96.2	838	31	432000	4593213
BS-4	8.1	15.3	9.10	95.4	1447	31	432651	4593766
BS-5	7.9	17.2	7.04	86.2	1388	31	433154	4589203
BS-6	7.8	16.8	6.33	80.5	35009	31	435804	4585677
LL-1	7.9	8.2	8.99	91.6	757	31	403881	4616871
LL-2	7.9	9.2	9.30	96.2	1087	31	405907	4617415
LL-3	7.8	7.9	9.04	92.8	1139	31	403792	4607459
LL-4	8.1	8.9	8.96	92.4	1220	31	410078	4594291
LL-5	8.1	14.2	8.72	90.4	1407	31	416614	4590452
LL-6	8.0	10.3	9.09	94.7	1395	31	420247	4577928
LL-7	7.3	12.1	*	*	6050	31	426109	4573894

BS - Besos river, LL – Llobregat river, SL - sampling location, T – temperature, σ – conductivity; * probe malfunctioned

Photodegradation experiments

Degradation profiles are shown in the **Figure SI-2** with the degradation half-times.

Figure SI-2. Degradation profiles of ICM in surface water at concentration of 1 µg/mL

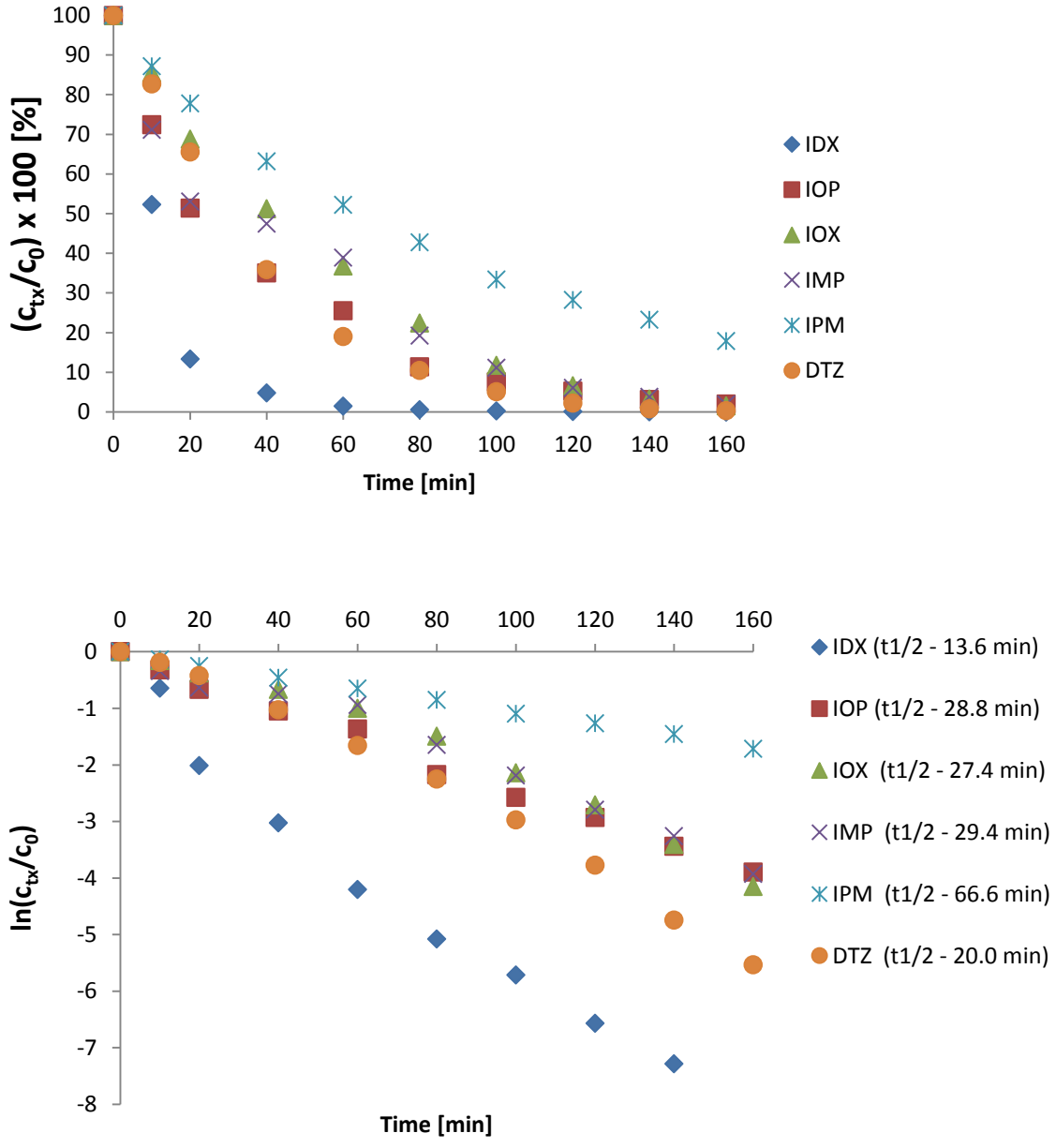

Screening method for photodegradation samples and suspect screening method for surface water samples

Screening method for photodegradated, lab generated samples

Electrospray ionization interface (ESI) was operated in the positive ion mode with the following settings: spray voltage +3.0 kV, heater temperature 250 ºC, and capillary temperature 350 ºC. The mobile phases employed were: (A) acetonitrile with 0.1 % formic acid and (B) water (0.1 % formic acid). Elution was accomplished with the following solvent gradient: 0 min (3 % A) - 1 min (3 % A) – 9 min (40 % A), - 10 min (95 % A) – 11 min (95 % A) – 12 min (3 % A) and stabilized until 15 min. The flow rate was 300 μL min^{-1} and the column temperature was held at 40 ºC.

For the detection method, a data dependent scan was applied with the following parameters; Full scan and data dependent-MS^2 were set to resolution of 35 000 [full width at half maximum (FWHM)], with the full scan range of m/z 200-1650. In the data dependent scan the isolation window was m/z 2 and the normalized collision energy was (NCE) 35.

Detailed list of all detected TPs (**Table SI-2**.) with the peak intensity cut-off set to $5e^5$ ie. all peak intensities above $5e^5$ in any of the degradation times (0-160 min) were included in the suspect list. Every TP is defined with a name (first part abbreviation of which parent compound it derived from and the second part nominal mass. In case of isobaric compounds additional A or B was added), retention time, measured mass and elemental composition (in comparison with the calculated one). The table also shows the mass difference form the parent compound as well as elemental composition difference. In case of iodixanol, for simplification reasons the elemental and mass differences are given both as difference from IDX (TP 1438, TP 1422 and TP 1312) and IDX-TP747 (the rest of the IDX TPs).

Suspect screening method for surface water samples

Once the TPs formed in photodegradation experiments have been catalogued and put in the table (first seven columns of **Table SI-2.**), the same LC-HRMS method as explained in the previous section has been applied to extracted surface water samples. At this point only retention time and exact mass have been used for confirmation of a suspected substance. Once the peak of a matching RT and exact mass was found in surface water samples, additional confirmation of MS^2 fragmentation, when possible, was also performed in order to confirm with certainty that it is the compound from our suspect list.

Finally, following the results of the suspect screening, two more columns were added. The first one, the Yes/No column states whether the compound was found in any of the real samples (peak intensity cut-off was set to 1e4 ie. all peaks with the intensity below 1e4 were set to NO – not found). The last column states the frequency of detection.

Table SI-2. Suspect analyte list generated from photodegradation experiments. Compounds detected in surface water samples (YES/NO column) and prioritized by their frequency of detection are written in bold

Compound Name	Retention time[a]	Measured mass	Elemental composition	DBE	Error [ppm]	Calculated mass	Δ mass from parent	Elemental Difference[b]	YES NO?	Frequency
IODIXANOL	**9.62**	**1550.7216**	**$C_{35}H_{45}O_{15}N_6I_6$**	**13.5**	**0.7**	**1550.7205**	**0.0000**		**YES**	**13**
IDX-TP 1438	9.54 - 9.75	1438.8040	$C_{35}H_{44}O_{16}N_6I_5$	14.5	0.5	1438.8032	111.9174	(-I) (+H_2O)	NO	N/A
IDX-TP 1422	9.57	1422.8093	$C_{35}H_{44}O_{15}N_6I_5$	14.5	0.8	1422.8083	127.9123	(-HI)	NO	N/A
IDX-TP 1312	9.54	1312.9063	$C_{35}H_{45}O_{16}N_6I_4$	14.5	-0.2	1312.9065	237.8140	(-I) (+O)	NO	N/A
IDX-TP 747	**3.24**	**747.8508**	**$C_{16}H_{21}O_7N_3I_3$**	**6.5**	**0.0**	**747.8508**	**0.0000**		**YES**	**13**
IDX-TP 862A	2.96	862.9143	$C_{21}H_{30}O_9N_4I_3$	7.5	0.2	862.9141	-115.0633	(+$C_5H_9O_2N$)	NO	N/A
IDX-TP 862B	7.40	862.9141	$C_{21}H_{30}O_9N_4I_3$	7.5	0.1	862.9141	-115.0633	(+$C_5H_9O_2N$)	NO	N/A
IDX-TP 825	1.43	825.8461	$C_{17}H_{23}O_{11}N_3I_3$	6.5	-0.6	825.8461	-77.9953	(+CH_2O_4)	NO	N/A
IDX-TP 805	3.93	805.8561	$C_{18}H_{23}O_9N_3I_3$	7.5	0.0	805.8563	-58.0055	(+CH_3COO)	YES	5
IDX-TP 751	7.03	751.9805	$C_{21}H_{28}O_{11}N_3I_2$	8.5	-0.5	751.9808	-4.1300	(+$C_4H_7O_4N$) (-I)	NO	N/A
IDX-TP 750	5.99	750.9971	$C_{21}H_{29}O_{10}N_4I_2$	8.5	-0.2	750.9968	-3.1460	(+$C_4H_8O_4N$) (-I)	NO	N/A
IDX-TP 745A	2.54	745.8352	$C_{16}H_{19}O_7N_3I_3$	7.5	0.0	745.8352	2.0157	(-H_2)	NO	N/A
IDX-TP 745B	3.70	745.8352	$C_{16}H_{19}O_7N_3I_3$	7.5	0.0	745.8352	2.0157	(-H_2)	NO	N/A
IDX-TP 735	5.85	735.0014	$C_{21}H_{29}O_9N_4I_2$	8.5	-0.6	735.0018	12.8490	(+$C_5H_8O_2N$) (-I)	NO	N/A
IDX-TP 707	2.46	707.9544	$C_{19}H_{24}O_{10}N_3I_2$	8.5	-1.0	707.9546	39.8962	(+CH_3O_3) (-I)	NO	N/A
IDX-TP 705	5.00	705.8404	$C_{14}H_{19}O_6N_3I_3$	5.5	0.2	705.8402	42.0106	(-CH_2CO)	NO	N/A
IDX-TP 699	1.50	699.9495	$C_{17}H_{24}O_{11}N_3I_2$	6.5	-0.6	699.9495	47.9013	(+CH_3+O_4) (-I)	NO	N/A
IDX-TP 693	**2.35**	**693.9750**	**$C_{19}H_{26}O_9N_3I_2$**	**7.5**	**-0.4**	**693.9753**	**52.8677**	**(+$C_3H_5O_2$) (-I)**	**YES**	**13**
IDX-TP 691	9.40	691.9598	$C_{19}H_{24}O_9N_3I_2$	8.5	0.2	691.9596	55.8912	(+$C_3H_3O_2$) (-I)	NO	N/A
IDX-TP 679	4.29	679.9597	$C_{18}H_{24}O_9N_3I_2$	7.5	0.0	679.9596	67.8912	(+$C_2H_3O_2$) (-I)	NO	N/A
IDX-TP 663	2.70	663.9645	$C_{18}H_{24}O_8N_3I_2$	7.5	0.0	663.9647	83.8861	(+C_2H_3O) (-I)	NO	N/A
IDX-TP 637	1.95	637.9492	$C_{16}H_{22}O_8N_3I_2$	6.5	0.2	637.9491	109.9017	(-I) (+OH)	NO	N/A
IDX-TP 621A	2.74	621.9540	$C_{16}H_{22}O_7N_3I_2$	6.5	-0.2	621.9542	125.8966	(-I+H)	YES	4
IDX-TP 621B	3.50	621.9540	$C_{16}H_{22}O_7N_3I_2$	6.5	-0.2	621.9542	125.8966	(-I+H)	YES	4
IDX-TP 619	5.35	619.9383	$C_{16}H_{20}O_7N_3I_2$	7.5	-0.4	619.9385	127.9123	(-HI)	NO	N/A
IDX-TP 596	1.68	596.9226	$C_{14}H_{19}O_8N_2I_2$	5.5	0.1	596.9225	150.9283	(-C_2H_2I+O)	NO	N/A
IDX-TP 570	1.83	570.0580	$C_{18}H_{25}O_{10}N_3I$	7.5	-0.8	570.0579	177.7929	(+$C_2H_4O_3$) (-I_2)	NO	N/A
IDX-TP 528A	1.69	528.0474	$C_{16}H_{23}O_9N_3I$	6.5	0.0	528.0473	219.8035	(+H_2O) (-I_2)	NO	N/A
IDX-TP 528B	2.84	528.0474	$C_{16}H_{23}O_9N_3I$	6.5	0.0	528.0473	219.8035	(+H_2O) (-I_2)	NO	N/A
IDX-TP 512A	1.86 - 2.99	512.0524	$C_{16}H_{23}O_8N_3I$	6.5	0.0	512.0524	235.7984	(-I_2) (H_2O)	NO	N/A
IDX-TP 512B	4.04	512.0524	$C_{16}H_{23}O_8N_3I$	6.5	0.0	512.0524	235.7984	(-I_2) (H_2O)	NO	N/A
IDX-TP 496	3.64	496.0578	$C_{16}H_{23}O_7N_3I$	6.5	0.5	496.0575	251.7933	(-I_2) (+H_2)	NO	N/A

Compound Name	Retention time[a]	Measured mass	Elemental composition	DBE	Error [ppm]	Calculated mass	Δ mass from parent	Elemental Difference[b]	YES NO?	Frequency
IOPROMIDE	**3.32 - 3.50**	**791.8765**	**$C_{18}H_{25}O_8N_3I_3$**	**6.5**	**-0.7**	**791.8770**	**0.0000**		**YES**	**13**
IOP-TP 719	3.03	719.8602	$C_{15}H_{21}O_6N_3I_3$	5.5	0.3	719.8559	72.0211	(CH_3CHCOO)	NO	N/A
IOP-TP 681	2.59 - 2.83	681.9751	$C_{18}H_{26}O_9N_3I_2$	6.5	-0.3	681.9759	109.9011	(-I) (+OH)	YES	4
IOP-TP 665-A-C	**3.57 - 4.32**	**665.9798**	**$C_{18}H_{26}O_8N_3I_2$**	**6.5**	**-0.9**	**665.9804**	**125.8966**	**(-I)**	**YES**	**13**
IOP-TP 651	**2.90**	**651.9645**	**$C_{17}H_{24}O_8N_3I_2$**	**6.5**	**-0.4**	**651.9647**	**139.9123**	**-CH (-I)**	**YES**	**13**
IOP-TP 649-A	2.59	649.9484	$C_{17}H_{22}O_8N_3I_2$	7.5	-1.0	649.9490	141.9280	-CH (-HI)	NO	N/A
IOP-TP 649-B	3.13	649.9490	$C_{17}H_{22}O_8N_3I_2$	7.5	-0.1	649.9490	141.9280	-CH (-HI)	NO	N/A
IOP-TP 554	4.73	554.0630	$C_{18}H_{25}O_9N_3I$	7.5	0.0	554.0630	237.8140	(-I) (+O)	YES	1
IOP-TP 526	3.72	526.0680	$C_{17}H_{25}O_8N_3I$	6.5	-0.2	526.0681	265.8089	($-C_2H_6I_2$)	YES	2
IOP-TP 482	4.42	482.0420	$C_{15}H_{21}O_7N_3I$	6.5	0.3	482.0419	309.8351	($-C_3H_5O_2I_2$)	NO	N/A
IOP-TP 466	4.15	466.0474	$C_{15}H_{21}O_6N_3I$	6.5	1.0	466.0470	325.8300	($-C_3H_5O_3I_2$)	NO	N/A
IOP-TP 452	3.60	452.0311	$C_{14}H_{19}O_6N_3I$	6.5	-0.5	452.0313	339.8457	($-C_4H_7O_3I_2$)	NO	N/A
IOP-TP 442	5.20	442.1459	$C_{18}H_{24}O_{10}N_3$	8.5	0.6	442.1456	349.7314	(- H_2I_3) (+O)	NO	N/A
IOP-TP 428	5.02	428.1662	$C_{18}H_{26}O_9N_3$	7.5	-0.4	428.1664	363.7106	(- I_3)	NO	N/A
IOHEXOL	**3.73 - 4.10**	**821.8874**	**$C_{19}H_{27}O_9N_3I_3$**	**6.5**	**-0.9**	**821.8876**	**0.0000**		**YES**	**13**
IOX-TP 779	3.16	779.8768	$C_{17}H_{25}O_8N_3I_3$	5.5	-0.9	779.8770	42.0106	($-CH_2CO$)	NO	N/A
IOX-TP 749	2.25	749.8660	$C_{16}H_{23}O_7N_3I_3$	5.5	-0.7	749.8665	72.0211	($-CH_3CHCOO$)	NO	N/A
IOX-TP 711	3.33	711.9857	$C_{19}H_{28}O_{10}N_3I_2$	6.5	-1.0	711.9859	109.9017	(-I) (+OH)	NO	N/A
IOX-TP 709	5.92	709.9702	$C_{19}H_{26}O_{10}N_3I_2$	7.5	-0.9	709.9702	111.9174	(-I) (+H_2O)	YES	1
IOX-TP 707A	4.66	707.9545	$C_{19}H_{24}O_{10}N_3I_2$	8.5	-0.8	707.9546	113.9330	(- H_3I) (+O)	NO	N/A
IOX-TP 707B	10.38	707.9545	$C_{19}H_{24}O_{10}N_3I_2$	8.5	-0.8	707.9546	113.9330	(- H_3I) (+O)	NO	N/A
IOX-TP 705	5.01	705.8402	$C_{14}H_{19}O_6N_3I_3$	5.5	0.0	705.8402	116.0473	($-C_5H_8O_3$)	NO	N/A
IOX-TP 695-A	**3.35**	**695.9926**	**$C_{19}H_{28}O_9N_3I_2$**	**6.5**	**2.4**	**695.9909**	**125.8967**	**(-I)**	**YES**	**12**
IOX-TP 695-B	**4.67**	**695.9927**	**$C_{19}H_{28}O_9N_3I_2$**	**6.5**	**2.4**	**695.9909**	**125.8967**	**(-I)**	**YES**	**12**
IOX-TP 693	**2.35**	**693.9752**	**$C_{19}H_{26}O_9N_3I_2$**	**7.5**	**-1.0**	**693.9753**	**127.9123**	**(-HI)**	**YES**	**13**
IOX-TP 693-B	3.55	693.9752	$C_{19}H_{26}O_9N_3I_2$	7.5	-1.0	693.9753	127.9123	(-HI)	YES	2
IOX-TP 677	5.09	677.9442	$C_{18}H_{22}O_9N_3I_2$	8.5	-0.5	677.9440	143.9436	(- CH_5I)	NO	N/A
IOX-TP 675A	7.16	675.9648	$C_{19}H_{24}O_8N_3I_2$	8.5	-0.6	675.9647	145.9229	(- H_3OI)	NO	N/A
IOX-TP 675B	8.75	675.9648	$C_{19}H_{24}O_8N_3I_2$	8.5	-0.6	675.9647	145.9229	(- H_3OI)	NO	N/A
IOX-TP 663	2.72	663.9649	$C_{18}H_{24}O_8N_3I_2$	7.5	-0.5	663.9647	157.9229	(- CH_3OI)	NO	N/A
IOX-TP 637	2.91	637.9487	$C_{16}H_{22}O_8N_3I_2$	6.5	-0.5	637.9491	183.9385	($-C_3H_5OI$)	NO	N/A

Compound Name	Retention time[a]	Measured mass	Elemental composition	DBE	Error [ppm]	Calculated mass	Δ mass from parent	Elemental Difference[b]	YES NO?	Frequency
IOX-TP 621	2.77	621.9542	$C_{16}H_{22}O_7N_3I_2$	6.5	-0.8	621.9542	199.9334	($-C_3H_5O_2I$)	YES	4
IOX-TP 602A	2.51 - 3.46	602.9122	$C_{16}H_{17}O_7N_2I_2$	8.5	-0.4	602.9120	218.9756	($-C_3H_{10}O_2NI$)	NO	N/A
IOX-TP 602B	3.91	602.9122	$C_{16}H_{17}O_7N_2I_2$	8.5	-0.4	602.9120	218.9756	($-C_3H_{10}O_2NI$)	NO	N/A
IOX-TP 600	1.71	600.0685	$C_{19}H_{27}O_{11}N_3I$	7.5	-0.9	600.0685	221.8191	($-I_2$) ($+O_2$)	NO	N/A
IOX-TP 570	1.85	570.0582	$C_{18}H_{25}O_{10}N_3I$	7.5	-0.5	570.0579	251.8297	($-CH_2I_2$) ($+O$)	NO	N/A
IOX-TP 556	1.43	556.0424	$C_{17}H_{23}O_{10}N_3I$	7.5	-0.7	556.0423	265.8453	($-C_2H_4I_2$) ($+O$)	NO	N/A
IOX-TP 538	1.47	538.0319	$C_{17}H_{21}O_9N_3I$	8.5	-0.6	538.0317	283.8559	($-C_2H_6I_2$)	NO	N/A
IOMEPROL	**4.42**	**777.8611**	**$C_{17}H_{23}O_8N_3I_3$**	**6.5**	**-1.1**	**777.8614**	**0.0000**		**YES**	**13**
IMP-TP 763	1.85	763.8456	$C_{16}H_{21}O_8N_3I_3$	6.5	-0.1	763.8457	14.0157	($-CH_2$)	YES	2
IMP-TP 719	10.56	719.8558	$C_{15}H_{21}O_6N_3I_3$	5.5	-0.1	719.8559	58.0055	($-CH_2COO$)	NO	N/A
IMP-TP 705	4.82	705.8401	$C_{14}H_{19}O_6N_3I_3$	5.5	-0.2	705.8402	72.0211	(CH_3CHCOO)	YES	3
IMP-TP 667A	1.99	667.9597	$C_{17}H_{24}O_9N_3I_2$	6.5	0.1	667.9596	109.9017	($-I$) ($+OH$)	NO	N/A
IMP-TP 667B	3.74	667.9597	$C_{17}H_{24}O_9N_3I_2$	6.5	0.1	667.9596	109.9017	($-I$) ($+OH$)	NO	N/A
IMP-TP 665	9.47	665.9438	$C_{17}H_{22}O_9N_3I_2$	7.5	-0.2	665.9440	111.9174	($-I$) ($+H_2O$)	NO	N/A
IMP-TP 651A	**2.70**	**651.9645**	**$C_{17}H_{24}O_8N_3I_2$**	**6.5**	**-0.3**	**651.9647**	**125.8966**	**(-I +H)**	**YES**	**13**
IMP-TP 651B	**5.66**	**651.9645**	**$C_{17}H_{24}O_8N_3I_2$**	**6.5**	**-0.3**	**651.9647**	**125.8966**	**(-I +H)**	**YES**	**13**
IMP-TP 649	2.40	649.9490	$C_{17}H_{22}O_8N_3I_2$	7.5	-0.2	649.9491	127.9123	($-HI$)	NO	N/A
IMP-TP 635	6.38	635.9334	$C_{16}H_{20}O_8N_3I_2$	7.5	0.0	637.9334	139.9123	($-CHI$)	NO	N/A
IMP-TP 605	10.13 - 10.21	605.9232	$C_{15}H_{18}O_7N_3I_2$	7.5	0.4	605.9229	171.9385	($-C_2H_5OI$)	NO	N/A
IMP-TP 574	2.54	574.0531	$C_{17}H_{25}O_{11}N_3I$	6.5	0.5	574.0528	203.8085	($-I_2$) ($+HI_3O_3$)	NO	N/A
IMP-TP 556A	2.74	556.0421	$C_{17}H_{23}O_{10}N_3I$	7.5	-0.3	556.0423	221.8191	($-I_2$) ($+O_2$)	NO	N/A
IMP-TP 556B	11.02	556.0421	$C_{17}H_{23}O_{10}N_3I$	7.5	-0.3	556.0423	221.8191	($-I_2$) ($+O_2$)	NO	N/A
IMP-TP 540	2.28	540.0474	$C_{17}H_{23}O_9N_3I$	7.5	0.0	540.0473	237.8140	($-I$) ($+O$)	YES	3
IMP-TP 512	10.48	512.0161	$C_{15}H_{19}O_9N_3I$	7.5	0.1	512.0160	265.8453	($-C_2H_6I_2$)	NO	N/A
IMP-TP 496	1.71	496.0577	$C_{16}H_{23}O_7N_3I$	6.5	0.3	496.0575	281.8039	($-COI_2$)	NO	N/A
IOPAMIDOL	**2.18**	**777.8619**	**$C_{17}H_{23}O_8N_3I_3$**	**6.5**	**0.7**	**777.8614**	**0.0000**		**YES**	**13**
IPM-TP 775	1.84	775.8456	$C_{17}H_{21}O_8N_3I_3$	7.5	-0.1	775.8457	2.0157	($-H_2$)	NO	N/A
IPM-TP 705	4.08	705.8401	$C_{14}H_{19}O_6N_3I_3$	5.5	0.1	705.8402	72.0211	($-CH_3CHCOO$)	NO	N/A
IPM-TP 667	**1.75**	**667.9598**	**$C_{17}H_{24}O_9N_3I_2$**	**6.5**	**0.3**	**667.9596**	**109.9017**	**(-I) (+OH)**	**YES**	**7**
IPM-TP 665	1.66 - 2.34	665.9446	$C_{17}H_{22}O_9N_3I_2$	7.5	1.0	665.9440	111.9174	($-I$) ($+H_2O$)	NO	N/A
IPM-TP 651	2.21 - 2.65	651.9650	$C_{17}H_{24}O_8N_3I_2$	6.5	0.5	651.9647	125.8966	($-I+H$)	NO	N/A

Compound Name	Retention time[a]	Measured mass	Elemental composition	DBE	Error [ppm]	Calculated mass	Δ mass from parent	Elemental Difference[b]	YES NO?	Frequency
IPM-TP 649	4.18	649.9492	$C_{17}H_{22}O_8N_3I_2$	7.5	0.2	649.9491	127.9123	(-HI)	NO	N/A
IPM-TP 635	3.04	635.9339	$C_{16}H_{20}O_8N_3I_2$	7.5	0.7	635.9334	141.9279	(- CH_3I)	NO	N/A
IPM-TP 621	1.88	621.9182	$C_{15}H_{18}O_8N_3I_2$	7.5	0.7	621.9178	155.9436	(- C_2H_5I)	NO	N/A
IPM-TP 577	2.74	577.9279	$C_{14}H_{18}O_6N_3I_2$	6.5	0.1	577.9279	199.9334	(- $C_3H_5O_2I$)	NO	N/A
IPM-TP 556	2.43 - 3.20	556.0426	$C_{17}H_{23}O_{10}N_3I$	7.5	0.6	556.0423	221.8191	(-I_2) (+O_2)	NO	N/A
IPM-TP 540	1.75 - 1.92	540.0475	$C_{17}H_{23}O_9N_3I$	7.5	0.4	540.0473	237.8140	(-I) (+O)	NO	N/A
IPM-TP 487	3.92	487.0207	$C_{14}H_{20}O_9N_2I$	5.5	0.1	487.0208	290.8406	(- $C_3H_3NI_2$) (+O)	NO	N/A
IPM-TP 480	5.21	480.9739	$C_{14}H_{14}O_9N_2I$	8.5	0.8	480.9738	296.8875	(- $C_3H_9NI_2$) (+O)	NO	N/A
DIATRIZOATE	**3.34**	**614.7767**	**$C_{11}H_{10}O_4N_2I_3$**	**6.5**	**-0.3**	**614.7769**	**0.0000**		**YES**	**13**
DTZ TP 504	1.66 - 2.56	504.8754	$C_{11}H_{11}O_5N_2I_2$	6.5	0.4	504.8752	109.9017	(-I) (+OH)	NO	N/A
DTZ TP 488	2.48	488.8802	$C_{11}H_{11}O_4N_2I_2$	6.5	-0.1	488.8803	125.8966	(-I.)	NO	N/A
DTZ TP 486A	1.66	486.8649	$C_{11}H_9O_4N_2I_2$	7.5	0.6	486.8646	127.9123	(-HI)	NO	N/A
DTZ TP 486B	5.58	486.8649	$C_{11}H_9O_4N_2I_2$	7.5	0.6	486.8646	127.9123	(-HI)	NO	N/A
DTZ TP 376A	4.60	376.9630	$C_{11}H_{10}O_5N_2I$	7.5	0.2	376.9629	237.8140	(- I_2) (+O)	NO	N/A
DTZ TP 376B	6.72	376.9630	$C_{11}H_{10}O_5N_2I$	7.5	0.2	376.9629	237.8140	(- I_2) (+O)	NO	N/A
DTZ TP 358	11.91	358.9524	$C_{11}H_8O_4N_2I$	8.5	0.2	358.9523	255.8246	(- H_2I_2)	NO	N/A
DTZ TP 350A	3.53	350.9837	$C_{10}H_{12}O_4N_2I$	5.5	0.3	350.9836	263.7933	(-COI+H)	NO	N/A
DTZ TP 350B	9.49	350.9837	$C_{10}H_{12}O_4N_2I$	5.5	0.3	350.9836	263.7933	(-COI+H)	NO	N/A

[a] Retention times are given as a range for diastereoisomer peaks; [b]Elemental composition difference in the case of IDX-TPs with only one benzene ring was calculated as difference from IDX-TP747

Isolation of transformation products via semipreparative HPLC-DAD

HPLC water test solutions were spiked with purchased IOP, IOX, IDX standards at 50 mg L^{-1}. In the case of IMP and IPM, they were first isolated from purchased formulated products (trademarks Iomeron and Iopamiro, respectively) and later spiked at the concentration of 50 mg L^{-1} in HPLC water. The spiked solutions were then photodegraded and ultimately used to isolate their corresponding TPs. After 120 minute of exposure of 50 mg L^{-1} solutions, the samples were freeze dried and reconstituted in 2 mL of HPLC water. 20 runs of 100 μL of these samples were injected onto Agilent HPLC-UV system Flow rate was set to 7.5 mL min^{-1} with isocratic conditions of acetonitrile/0.1 % of formic acid (1:9). The total run time varied from 60 to 100 min depending on the compound.

Peak detection was accomplished by DAD set at the nm range of 190 - 400 with the 2 nm step. Fraction collection was programmed based on preliminary experiments where narrow time fractions were screened for TP content (usually 4-5 fractions per observed peak). Aliquots of each fraction were first analyzed by UPLC-Q-Exactive-MS to check for purity. The fractions of the same compound were joined together, freeze-dried, weighted and sent to NMR analysis before being used as standards for the detection of TPs in real surface water samples.

Figure SI-3. shows the identical spectra of IOX TP693 and IDX TP693
Figure SI-4 shows the separation of IDX TPs and IOX TPs. As can be seen from the **Figure SI-4-A**, TP693 coeluted with another compound which was better separated among IOX-TPs shown in **Figure SI-4-B**.

Figure SI-3 Comparison between fragmentation pattern of Iohexol TP693 and Iodixanol TP-693

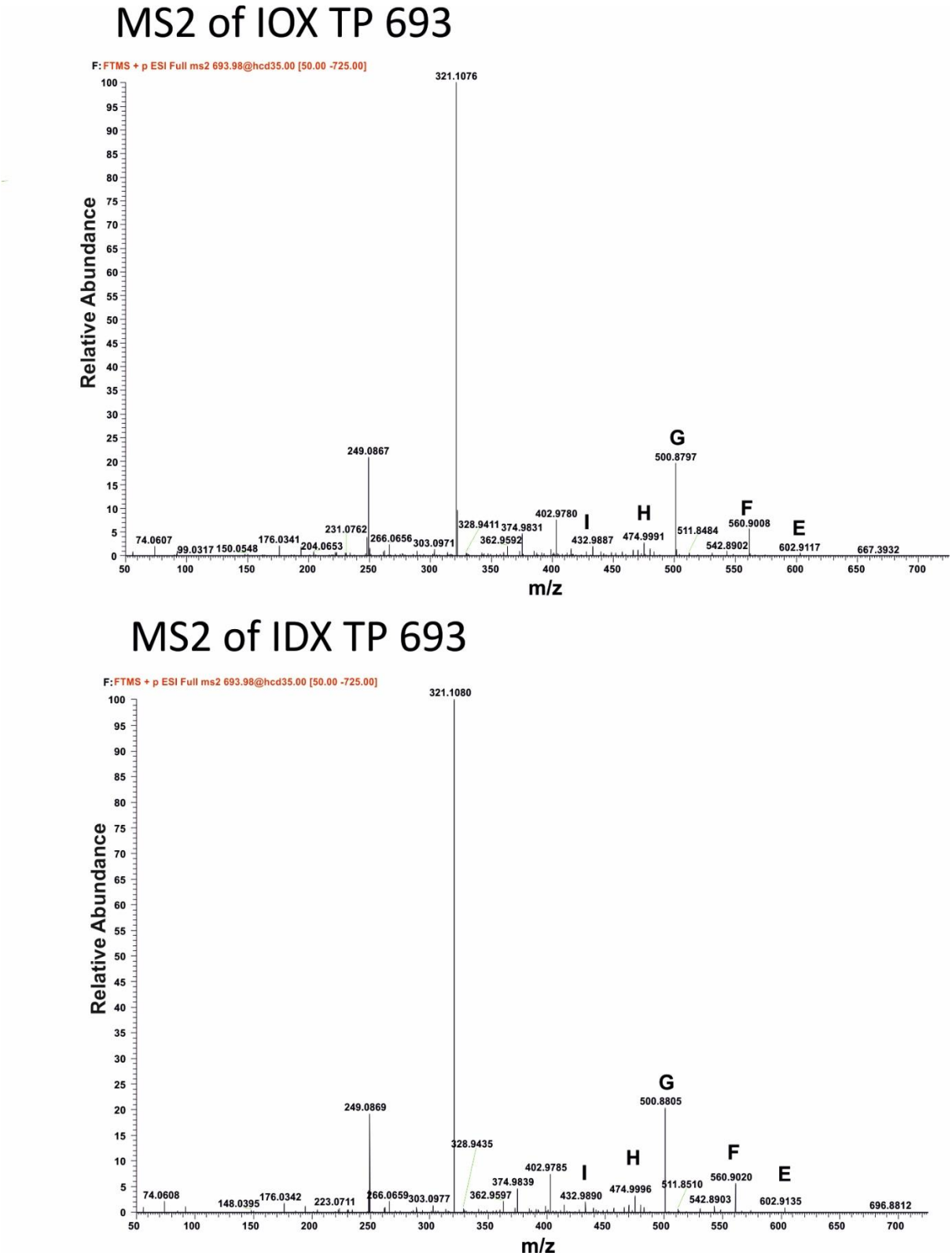

Figure SI-4 Semipreparative chromatographic separation of A) IDX-TP-747 and IDX-TP693 and B) IOX-TP693

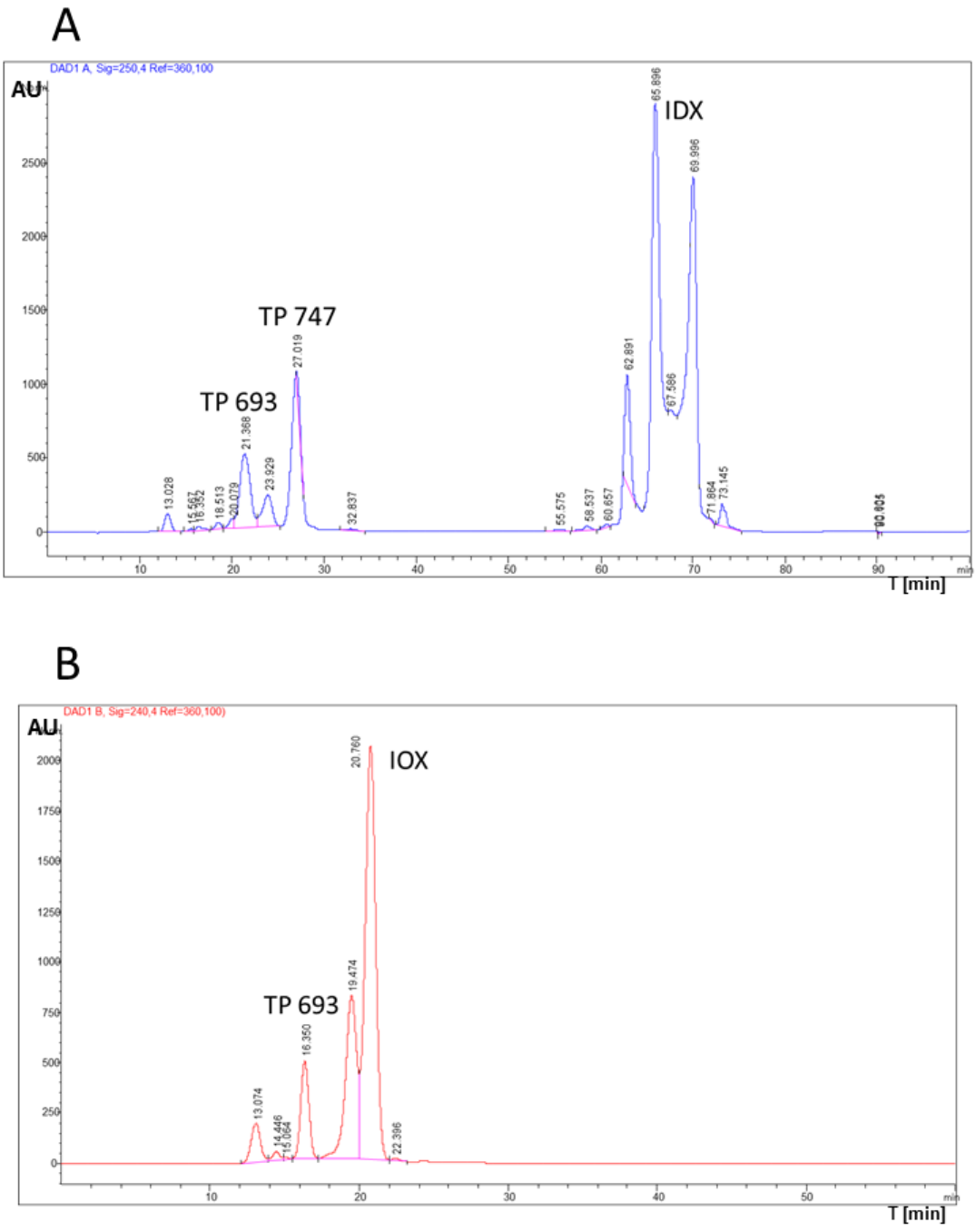

Identification of TPs with the combination of MS and NMR

The LC-MS parameters were similar to the ones for suspect analysis but with shorter run. The Q-Exactive-MS was operated at a resolution of 70,000 in scan mode while for MS/MS experiments resolution was set to 35,000 calculated based on external mass calibration with a standard mix for Thermo Scientific (see in chemicals and standards section) once a week.

Electrospray ionization interface (ESI) was operated in the positive ion mode with the following settings: spray voltage +3.0 kV, heater temperature 250 ºC, and capillary temperature 350 ºC. The mobile phases employed were: (A) acetonitrile with 0.1 % formic acid and (B) water (0.1 % formic acid). Elution was accomplished with the following solvent gradient: 0 min (3 % A) - 1 min (3 % A) – 6 min (20 % A), - 7 min (95 % A) – 8 min (95 % A) – 8.5 min (3 % A) and stabilized until 10 min. The flow rate was 300 μL min^{-1} and the column temperature was held at 40 ºC.

For the detection method, a data dependent scan was applied with the following parameters; Full scan and data dependent-MS^2 were set to resolution of 70 000, with the full scan range of depending on the compound identified (general range m/z 200 – 1600). Isolation window was m/z 2 and inclusion list turned on and filled with the list of investigated masses.

Pseudo- MS^3 (pMS^3) experiments were employed using *In-source ionization* in order to produce the given m/z fragment before breaking the ion in the HCD to obtain its pMS^3.

Figure SI-5 shows the fragmentation pattern (named: Figure SI-5.X-**A**., X = 1 - 13), MS^2 and pMS^3 spectra (named: Figure SI-5.X-**B**., X = 1 - 13) and, when possible, (HSQC)-NMR spectra (named: Figure SI-5.X-**C**., X = 2, 4, 7, 10 and 12) of a compound described.

Fragmentation pattern for IOP-TP665 A-C (**Figure SI-5.4-A**), IOX-TP695 A and B (**Figure SI-5.8-A**) and IMP-TP651 A and B (**Figure SI-5.10-A**) is drawn as a mixture of the corresponding isobaric compound(s) i.e. only one pattern is given per these three mixture of compounds. Iodine which is cleaved is marked in parenthesis. Final difference in fragmentation is marked above the arrows which show diagnostic fragments.

Fragmentation pattern in general is drawn with **black** and **red** arrows in which the **black** stands that a certain fragment has been seen in a pMS^3 spectrum of its direct predecessor and the **red** arrow states that the fragment was seen in the spectrum of its indirect predecessor. **Red** arrow was used only in cases when it was not possible to do a pMS^3 experiment on a given mass.

Details of a specific MS^2 and pMS^3 performed can be found in the header of each spectrum. Example below is given for IDX – MS^2 and IDX – 1508 pMS^3.

	Analyzer	Ionization	In-source	Experiment type	Selected mass	NCE	Mass range
IDX–MS^2	**FTMS**	**p ESI**	**-**	**Full ms2**	**1550.70**	**@hcd 10**	**106.67-1600.0**
IDX–1508 pMS^3	**FTMS**	**p ESI**	**sid=35**	**Full ms2**	**1508.71**	**@hcd 15**	**103.67-1550.0**

NCE (normalized collision energy) used throughout the experiments were 10, 15, 20 and 35. Unless otherwise stated, the NCEs 15 and 20 were used with the ramp of 30%.

Accurate mass measurements of protonated ICM photoproducts as determined by LC-QExactive-MS in MS^2 or pseudo MS^3 modes can be found in **Table SI-3.**

IODIXANOL (IDX)

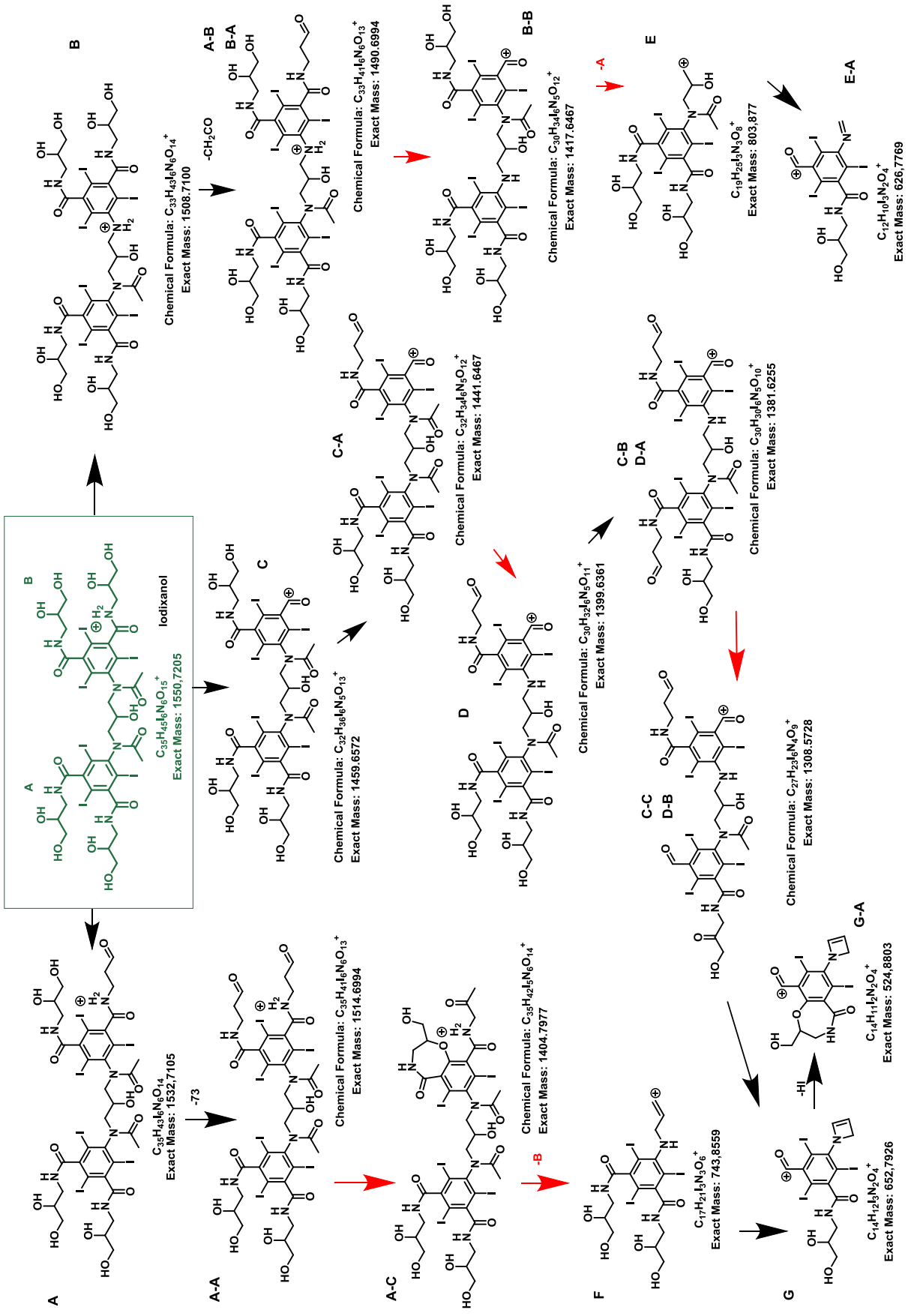

Figure SI-5.1-A. Fragmentation pattern of Iodixanol (IDX)

Figure SI-5.1-B. MS² and pMS³ spectra of Iodixanol (IDX)

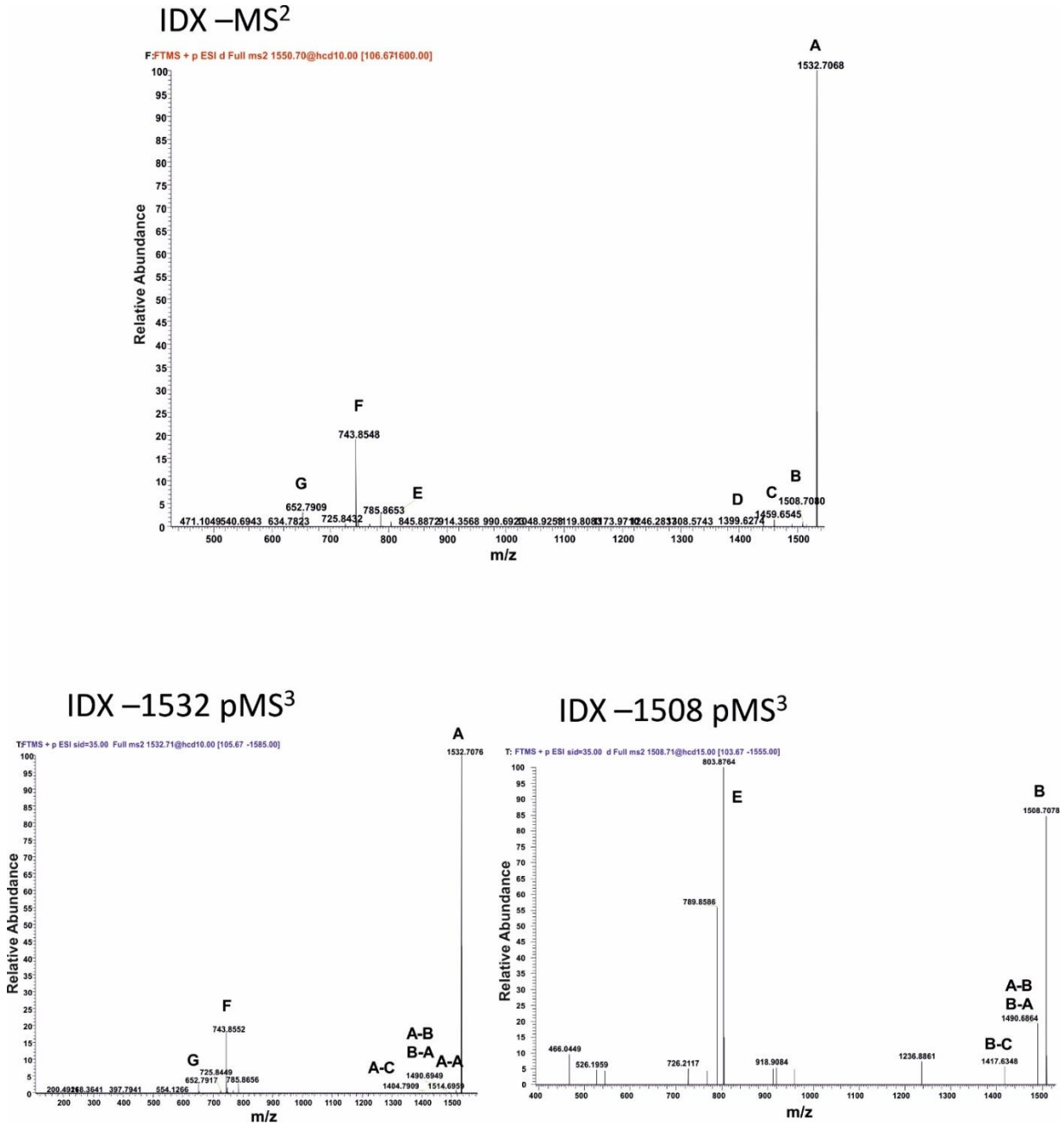

Figure SI-5.1-B. MS^2 and pMS^3 spectra of Iodixanol (IDX) - *continued*

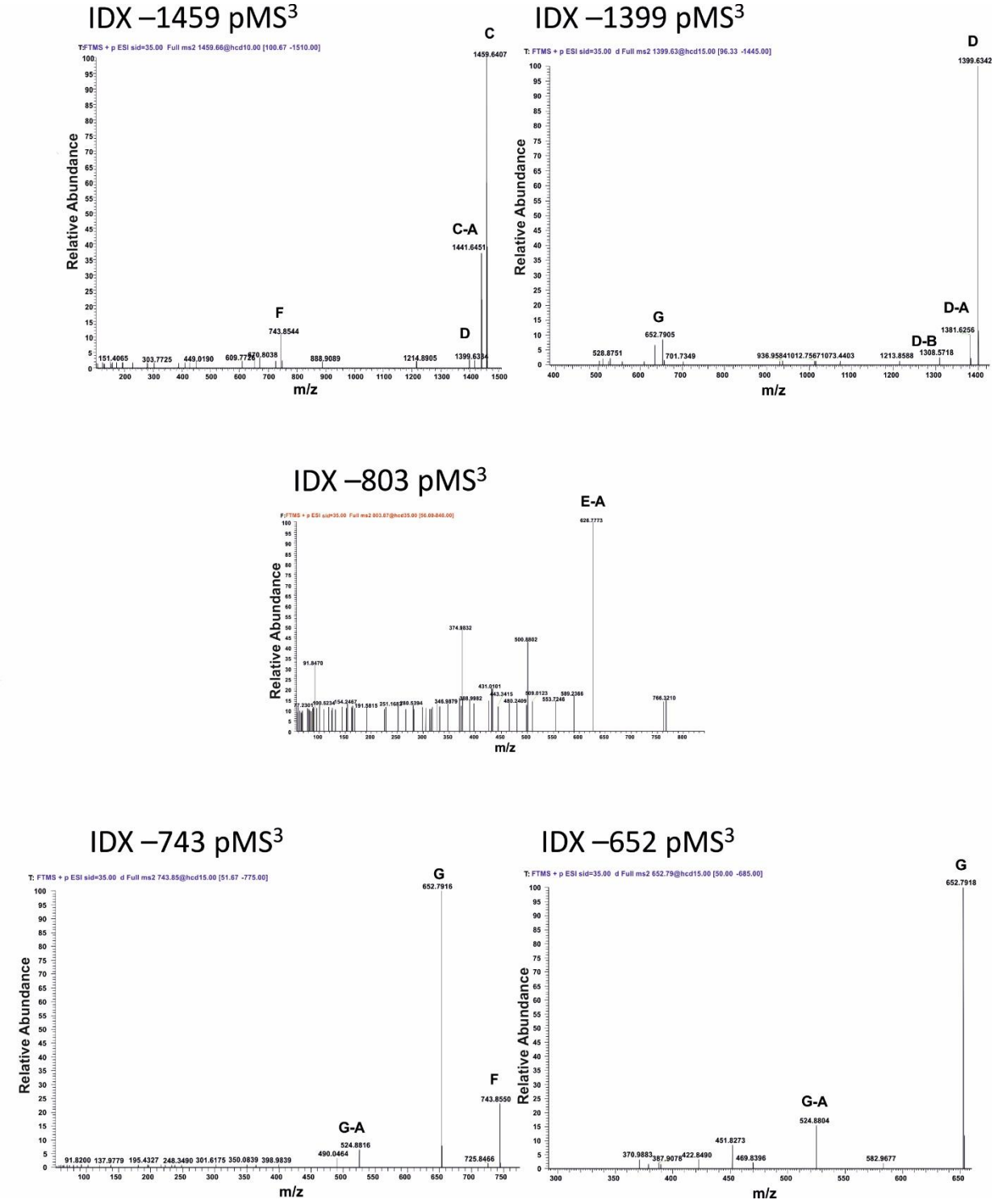

IODIXANOL TP-747 (IDX TP747)

Figure SI-5.2-A. Fragmentation pattern of Iodixanol – TP747 (IDX-TP747)

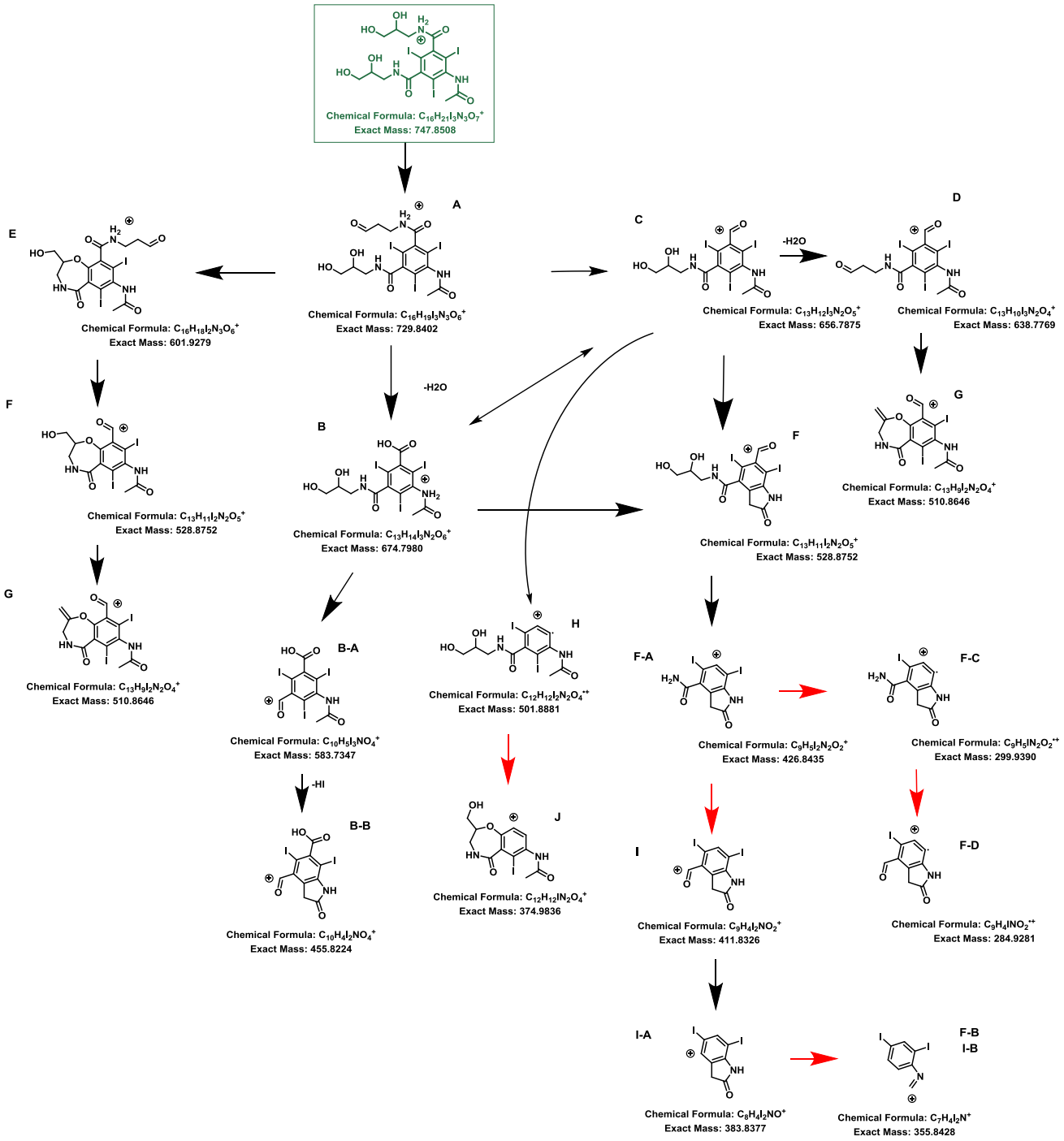

Figure SI-5.2-B. MS^2 and pMS^3 spectra of Iodixanol – TP747 (IDX-TP747)

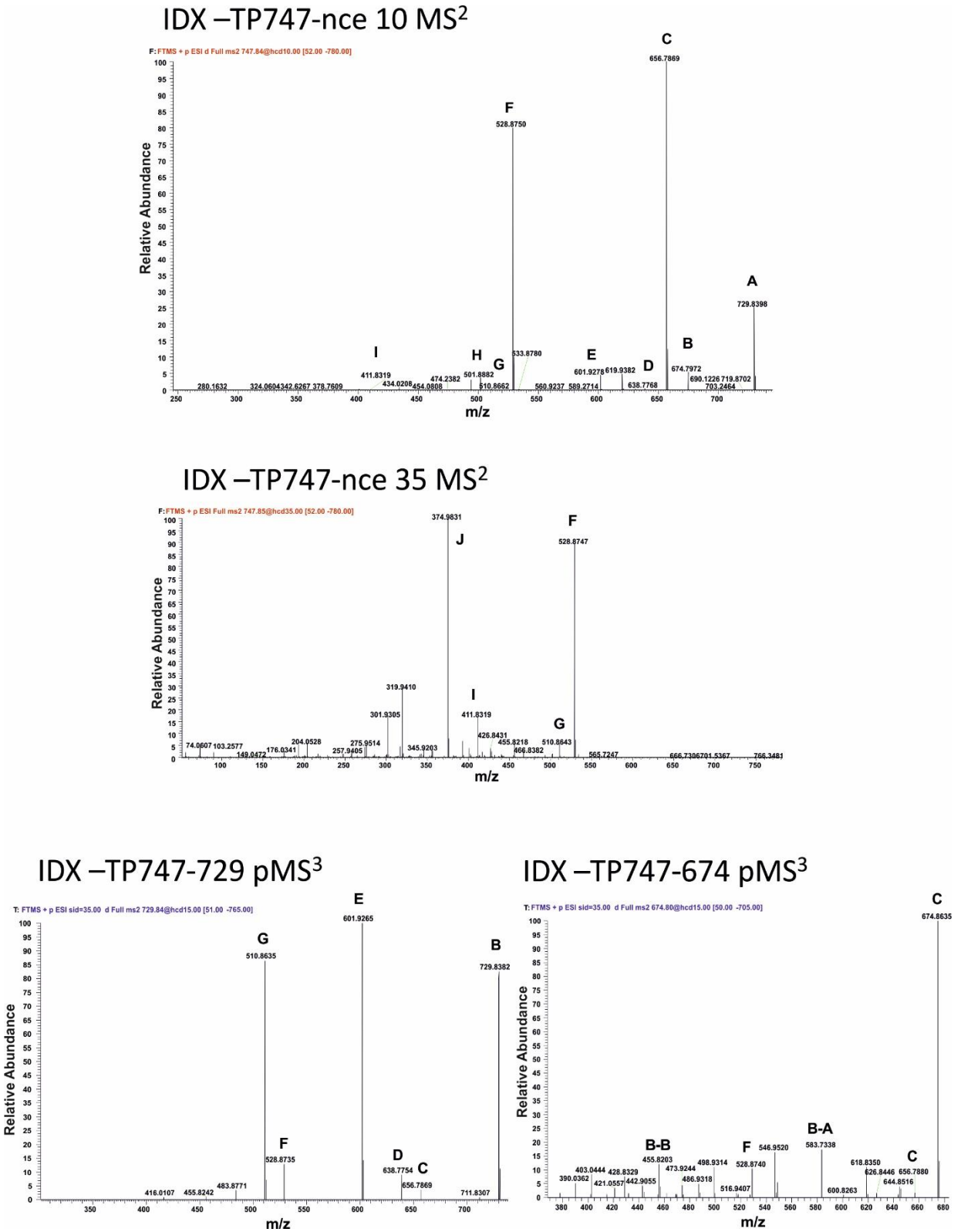

Figure SI-5.2-B. MS^2 and pMS^3 spectra of Iodixanol – TP747 (IDX-TP747) – *continued*

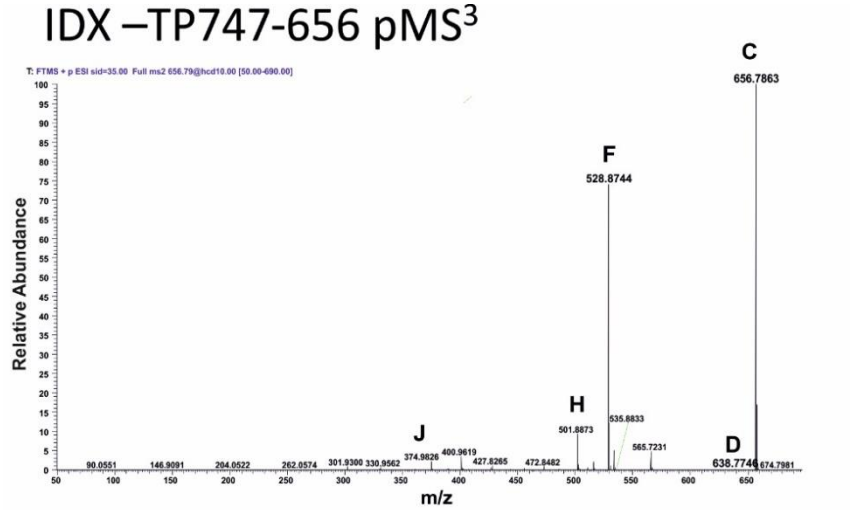

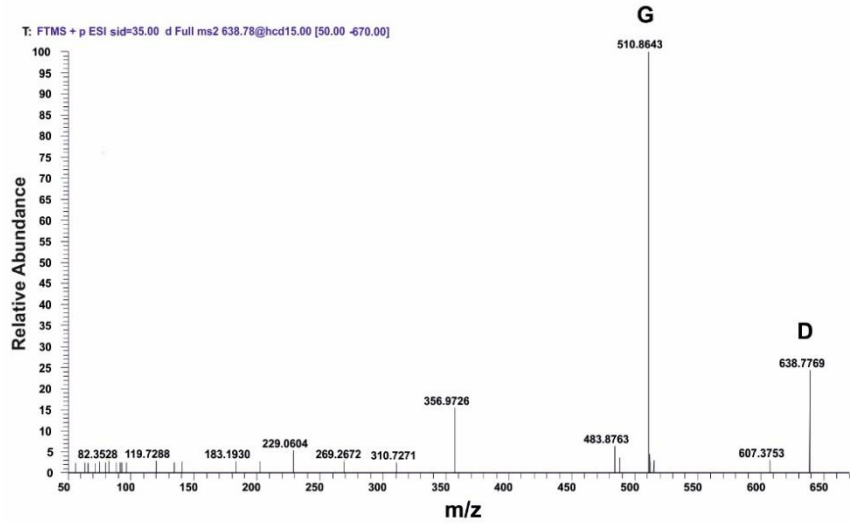

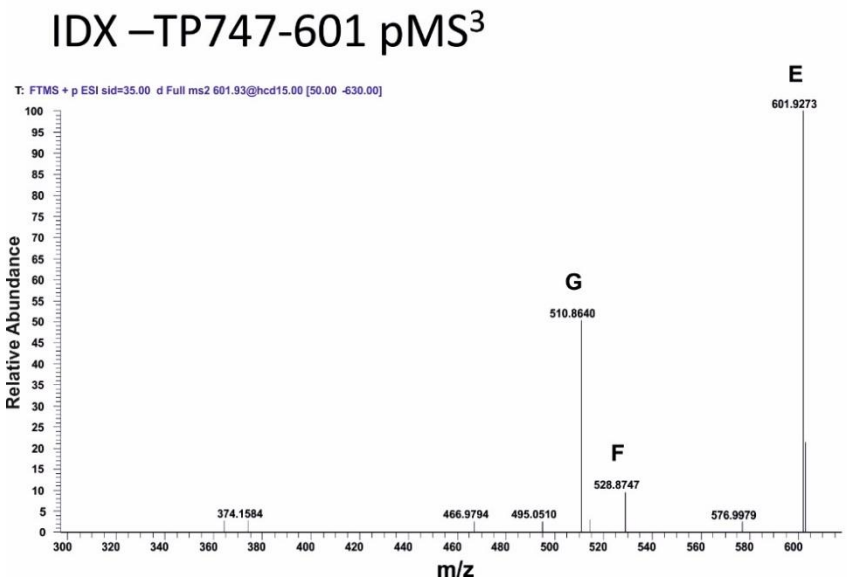

Figure SI-5.2-B. MS^2 and pMS^3 spectra of Iodixanol – TP747 (IDX-TP747) – *continued*

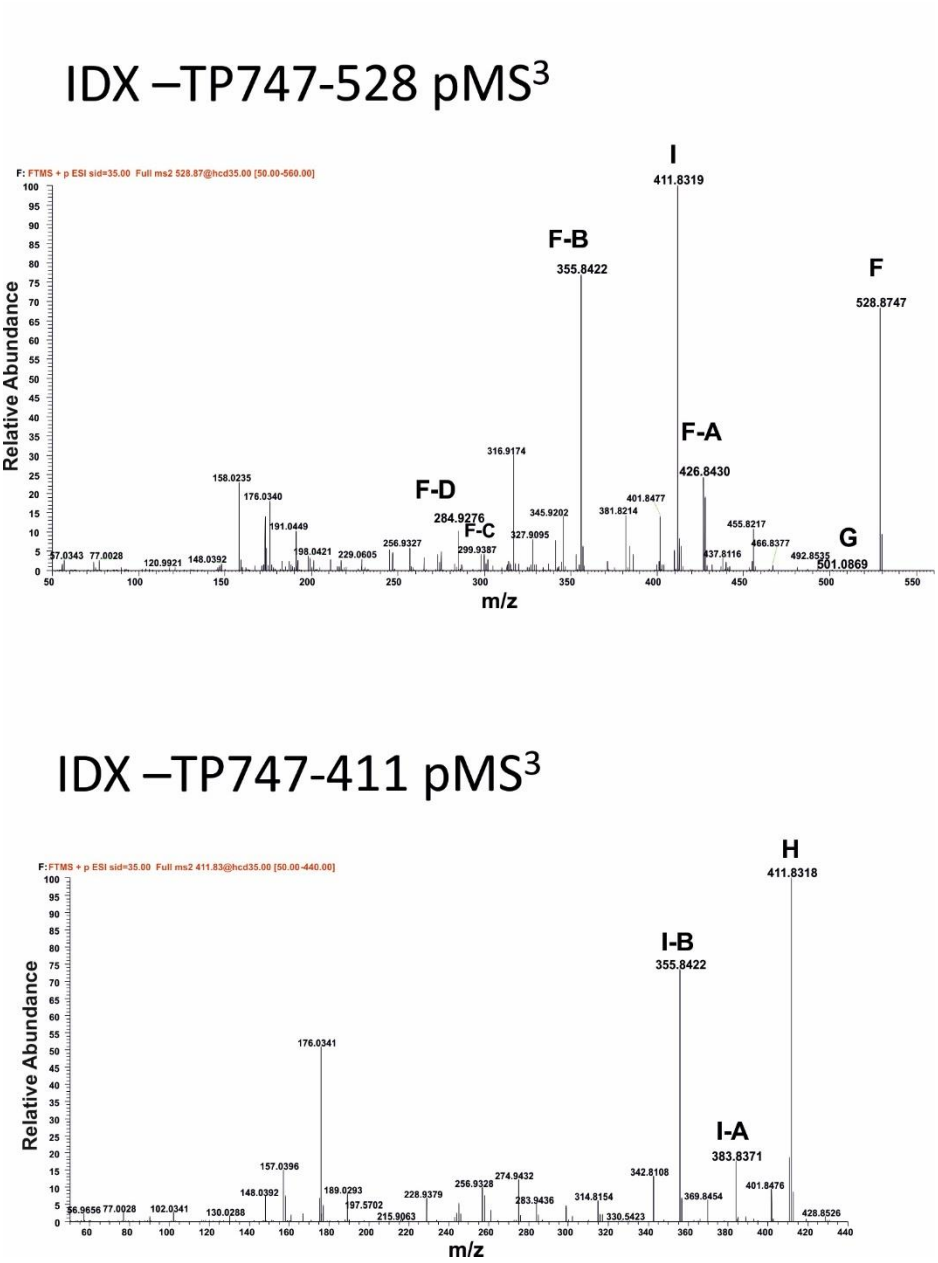

Figure SI-5.2-C. Proton and (HSQC)-NMR spectra of IDX-TP747

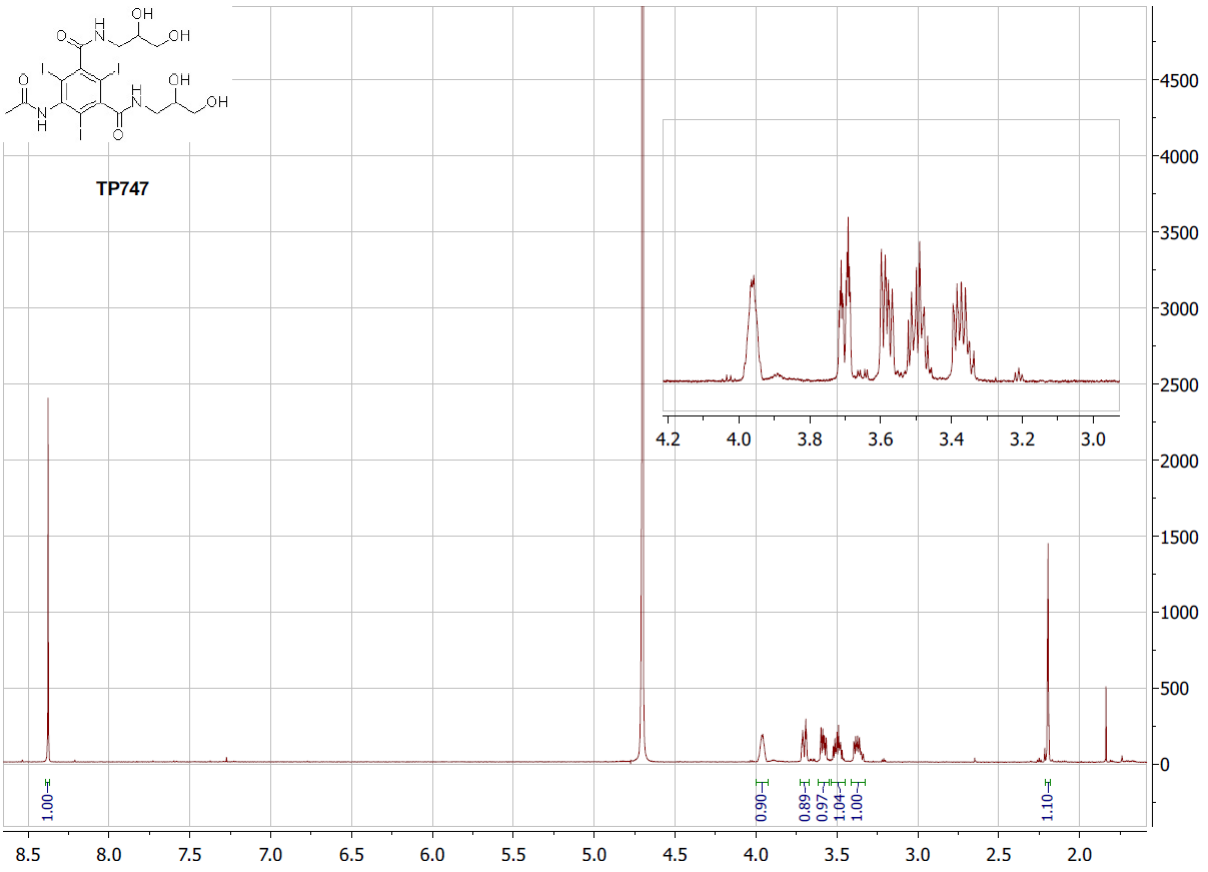

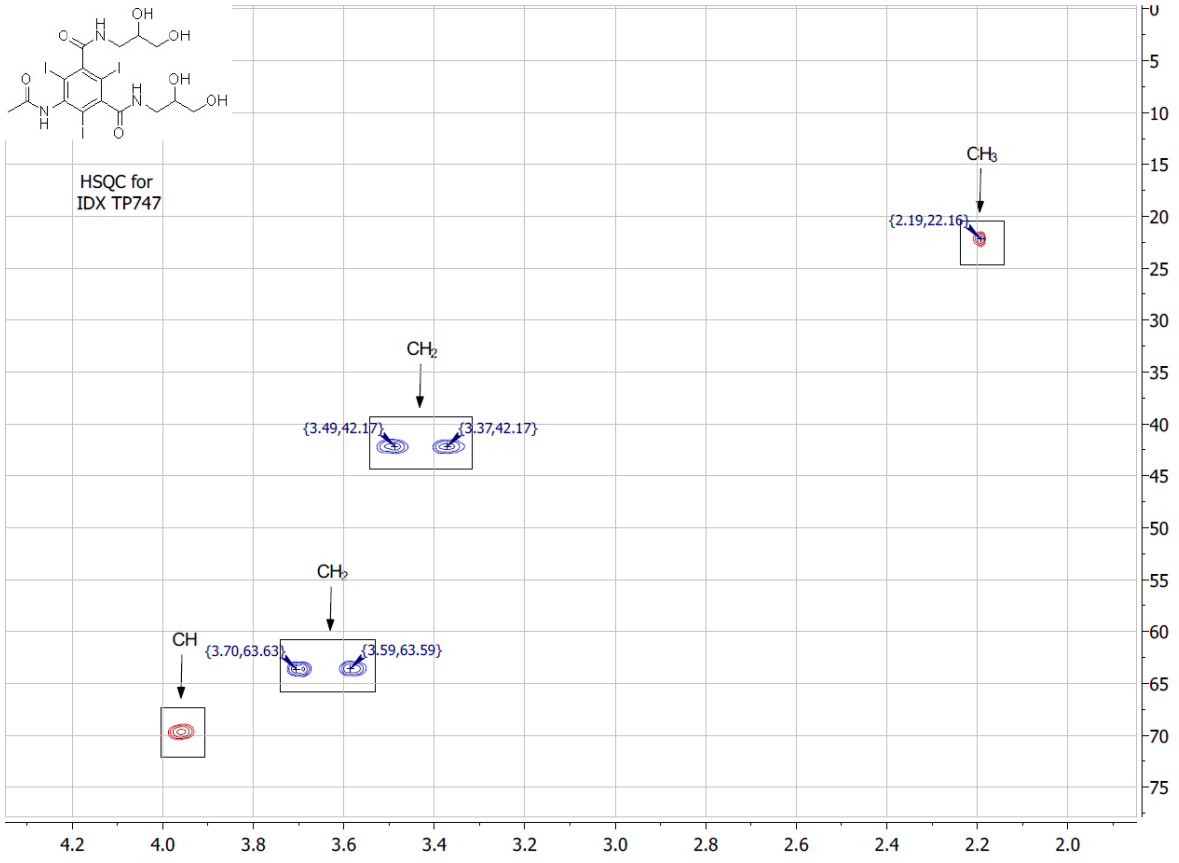

IOPROMIDE (IOP)

Figure SI-5.3-A. Fragmentation pattern of Iopromide (IOP)

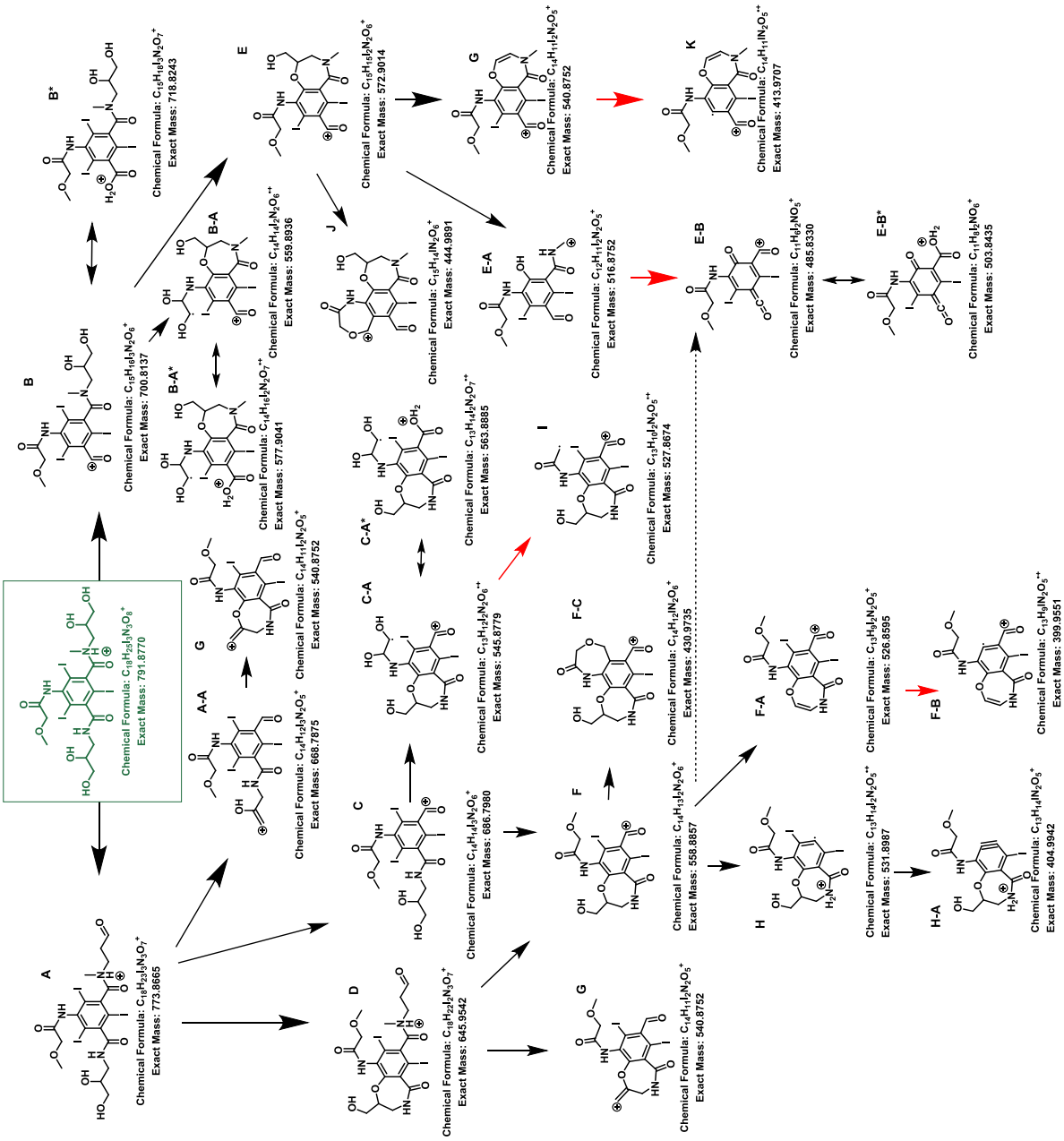

Figure SI-5.3-B. MS^2 and pMS^3 spectra of Iopromide (IOP)

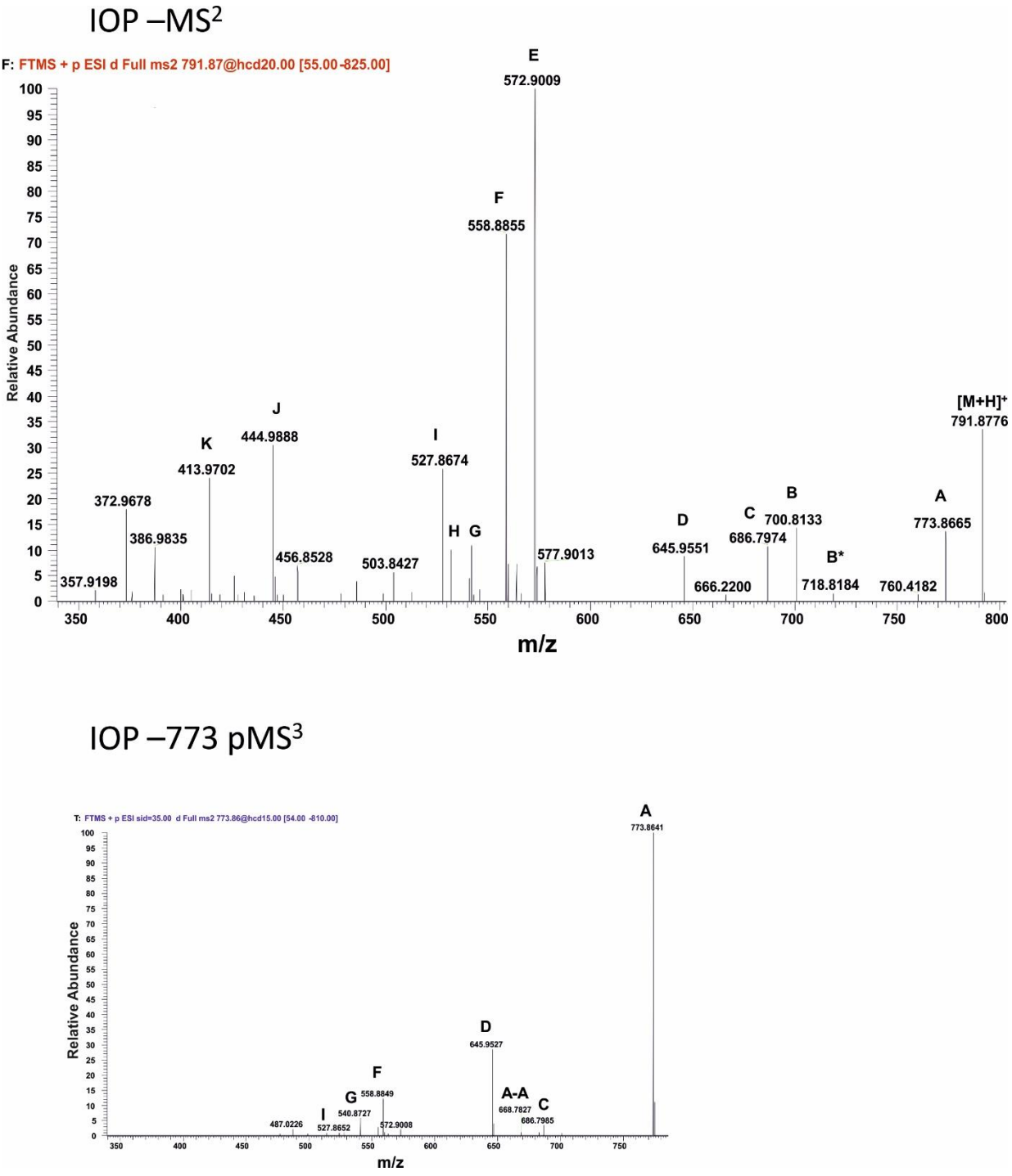

Figure SI-5.3-B. MS^2 and pMS^3 spectra of Iopromide (IOP) – *continued*

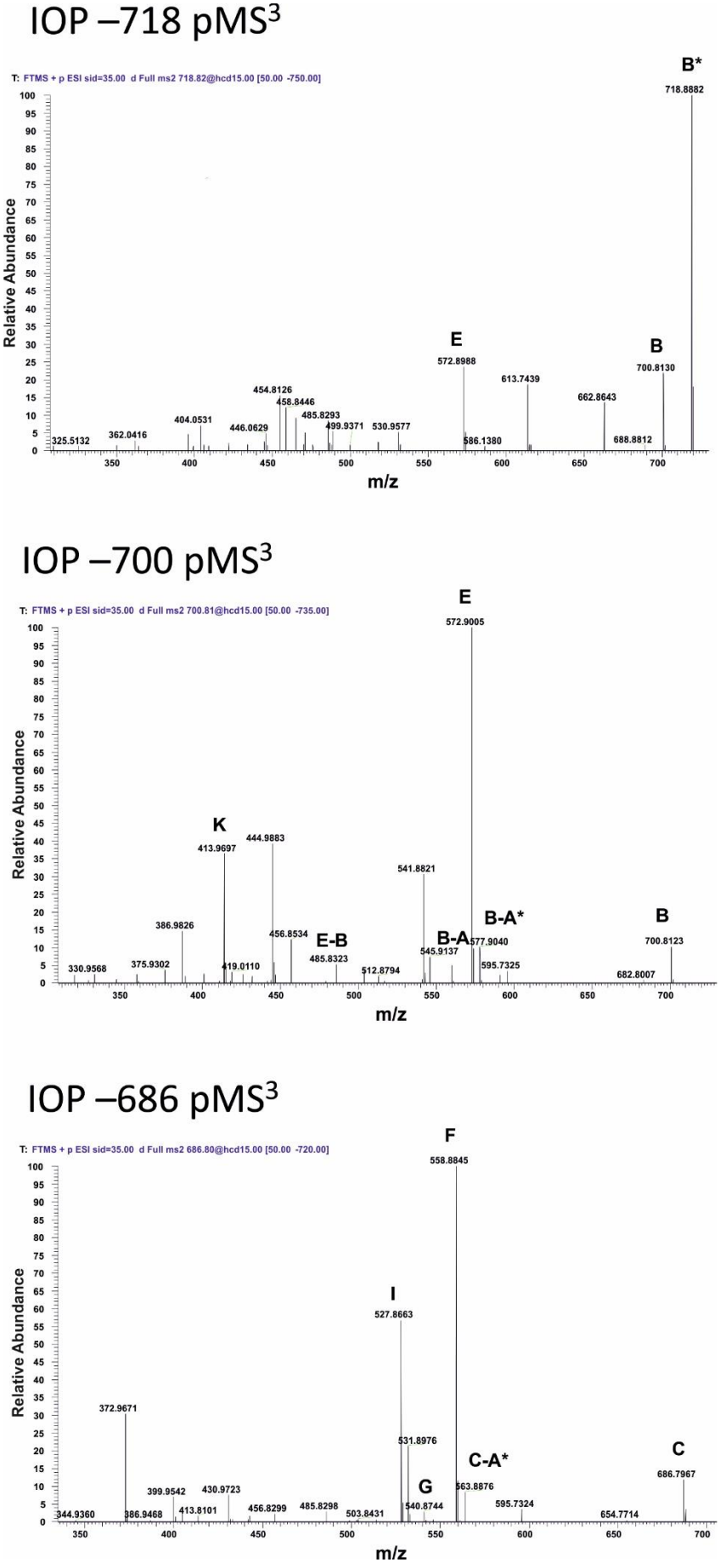

Figure SI-5.3-B. MS^2 and pMS^3 spectra of Iopromide (IOP) – *continued*

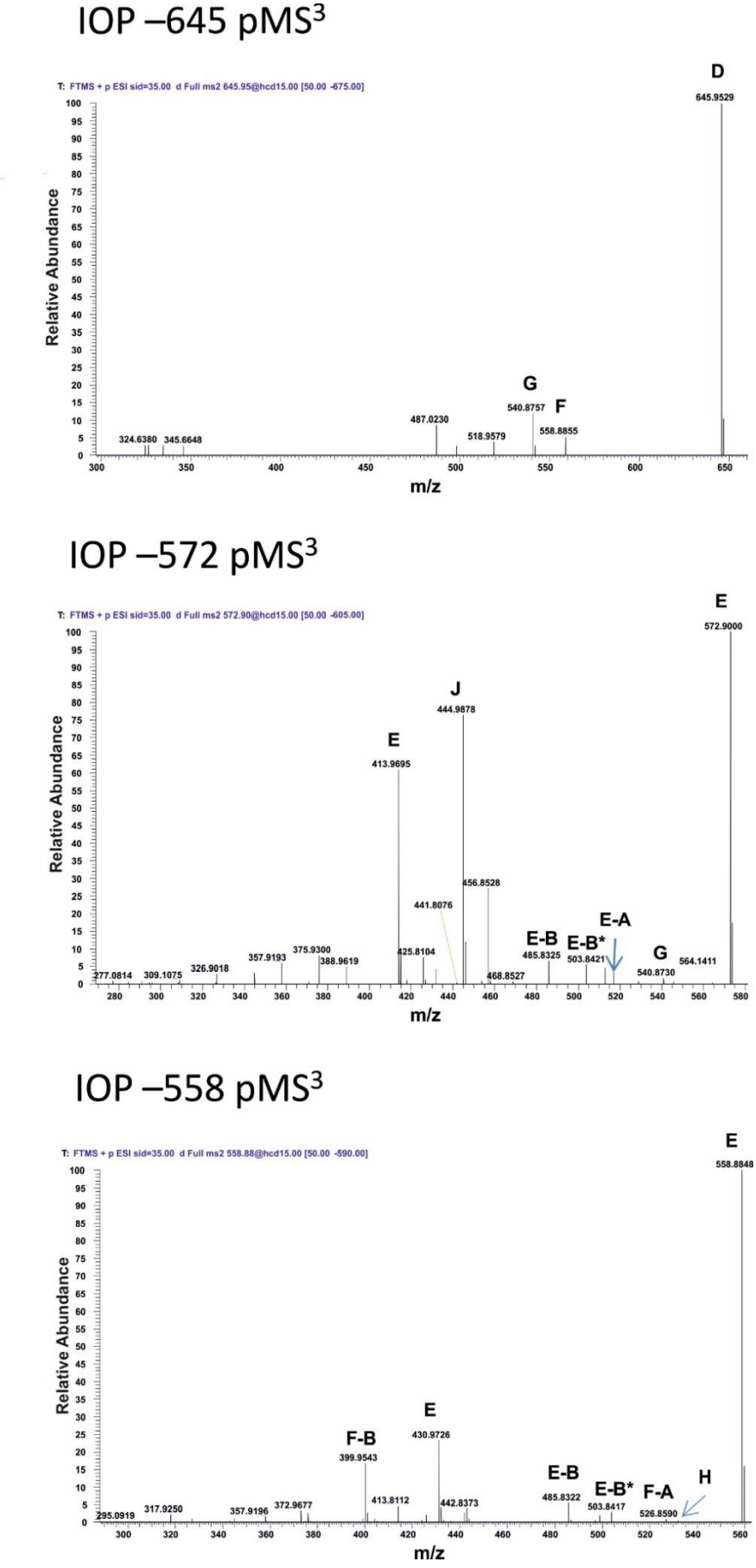

Figure SI-5.3-B. MS^2 and pMS^3 spectra of Iopromide (IOP) – *continued*

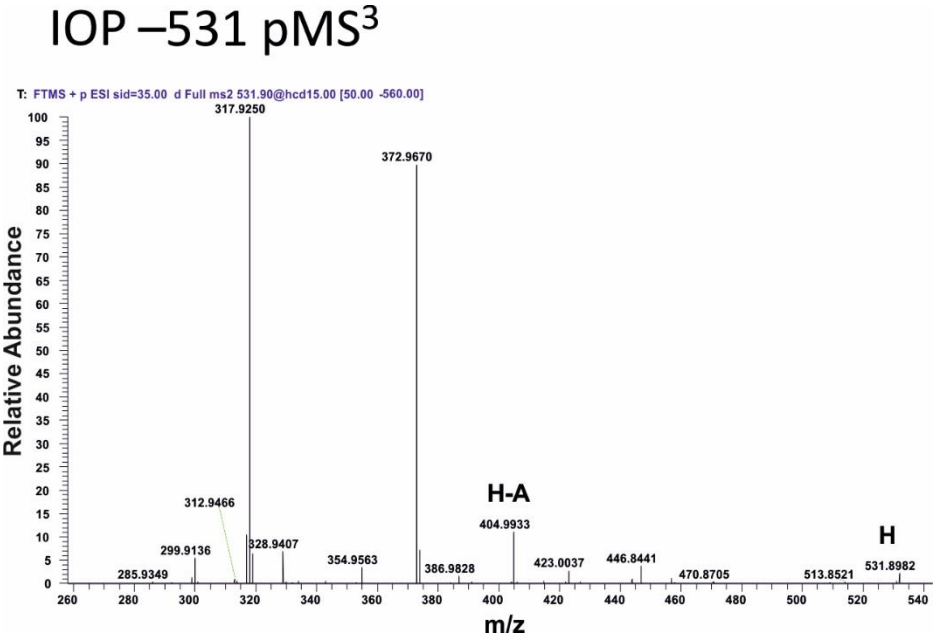

IOPROMIDE TP665 A-C (IOP TP665 A-C)

With respect to the photoproducts IOP-TP665-A, B and C (**Figure 2.**), their elemental composition differed from that of their parent compounds by the substitution of one iodine atom by hydrogen. This photolytic reductive deiodination, was suggested previously[14] and turned out to be non regioselective, producing a mixture of monodeiodinated photoproducts (**Figure 2.**). Here we have also detected a peak cluster of monodeiodinated IOP TPs. Upon analysis of the MS^2 (**Figure SI-5.4-B**), three different fragmentation patterns were observed. The separation of the three IOP products was not possible in the UPLC column and they were detected as a peak cluster (as mixture of diastereoisomers). Only IOP-TP665-C, the most retained TP, was partially separated. Moreover, it was not possible to separate IOP-TP665-A-C by semipreparative-LC and thus they were isolated together. The presence of the three IOP-TP665 (IOP-TP665-A, B and C) could also be inferred by NMR. Three $N-CH_3$ groups, belonging to three different *identical*-CH_3 type chains are observed in the HSQC experiment (**Figure SI-5.4-C**; peaks **a**). On the other hand, only two different *similar* chains were observed, as evidenced by the duplicity of the methylene group (**Figure SI-5.4-C**; peaks **f** and **f'**), whereas no additional multiplicities were observed for the remaining signals.

Detailed analysis of MS^2 spectra of the three compounds showed that they differed in the intensities of diagnostic fragments ions m/z 447.0048 and m/z 432.9891. While they display equal intensity for TP665-A, fragment m/z 432.9891 is more abundant in the spectrum of TP665-B and fragment ion m/z 447.0048 is more prominent in TP665-C. These product ions correspond to the cyclization of the *identical* (or *identical-*CH_3) side chain (with the loss of HI) once the other *identical* side chain has been cleaved (**Figure SI-5.4-B**). These differences in abundance would suggest that the cyclization would be equally favoured (both of these two fragments with the equal intensity), if the iodine is in the position **4** and **6**. On the other hand, when the formation of the fragment ion m/z 432.9891 is favoured, then the iodine is likely lost from the position **6** (and from position **4** in case of m/z 447.0048). However, information gathered from the pMS^3 spectra of the two fragments (m/z 432.9891 and 447.0048) is not as straightforward. If we attribute the differences in abundance to likelihood of cyclization of the two fragments, there is no reason why there would be differences in pMS^3 of these fragments between IOP-TP665-A-C. Lack of fragment m/z 305.0768 in pMS^3 of m/z 432.9891 of IOP-TP665-B and lack of m/z 319.0925 in pMS^3 of m/z 447.0048 of IOP-TP665-C makes these two IOP TPs (IOP-TP665-B and C) only tentatively identified. (**Figure SI-5.4-A and B**)

Figure SI-5.4-A. Fragmentation pattern of Iopromide – TP665 (IOP-TP665)

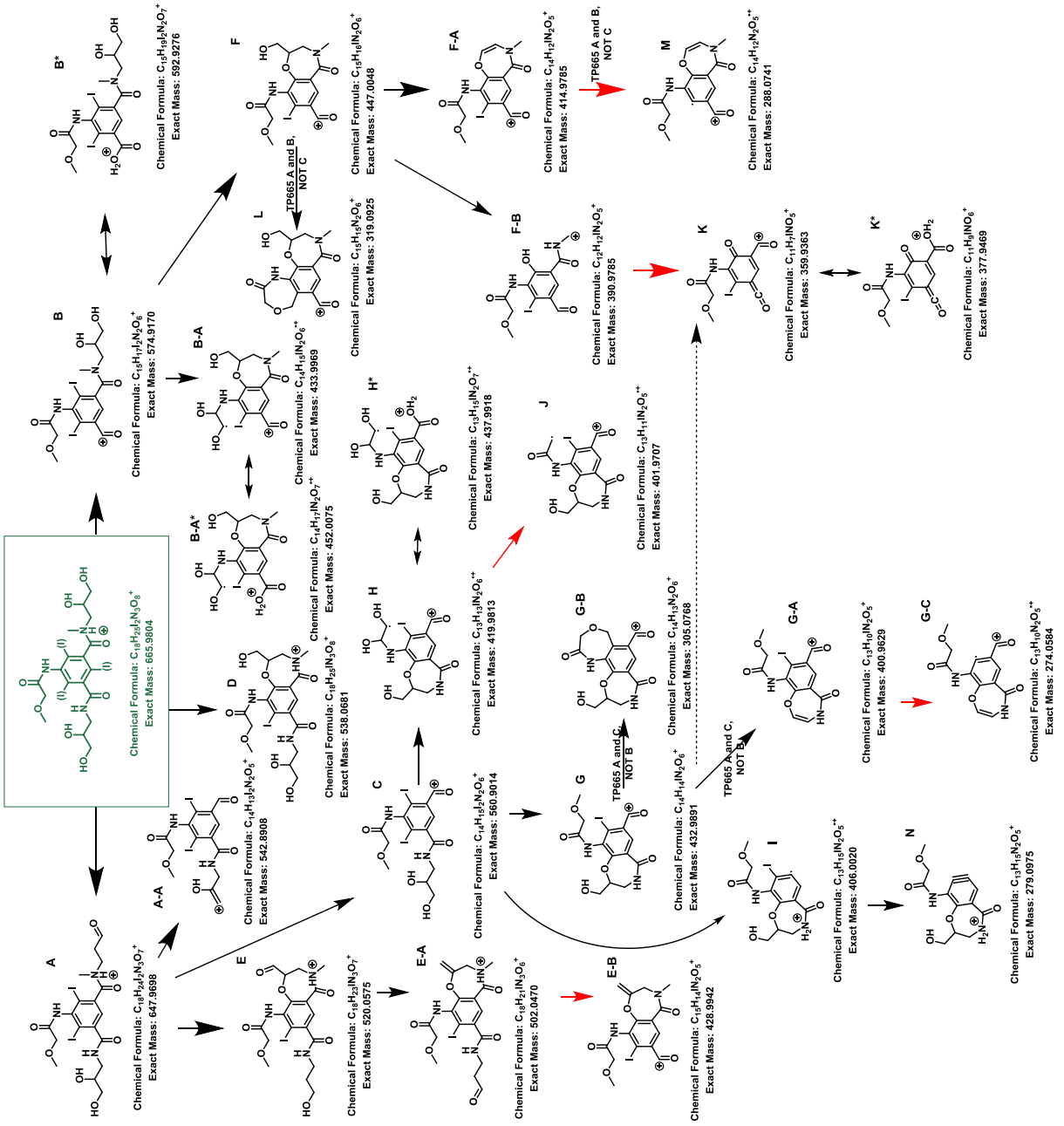

Figure SI-5.4-B. MS² and pMS³ spectra of Iopromide – TP665 A-C (IOP-TP665-A-C)

IOP –TP665-A
MS²

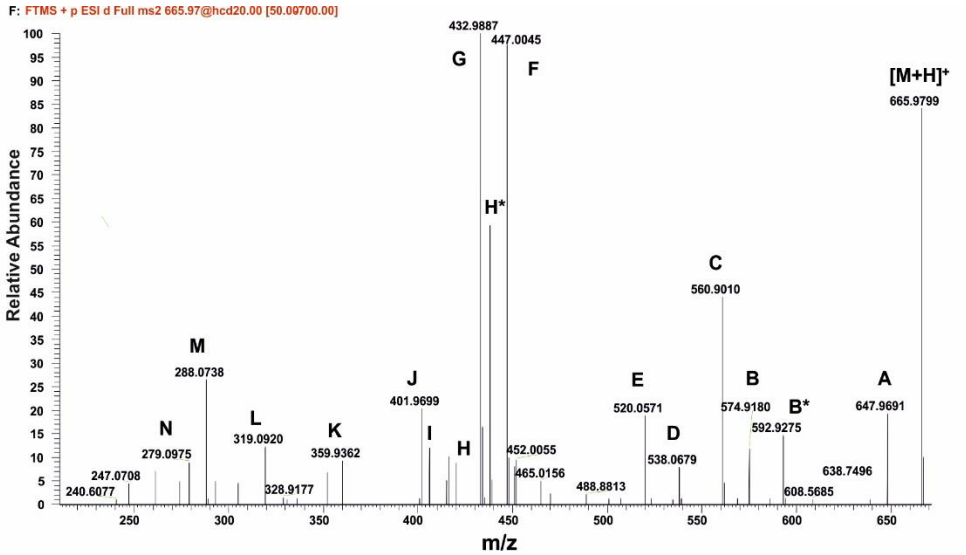

IOP –TP665-B
MS²

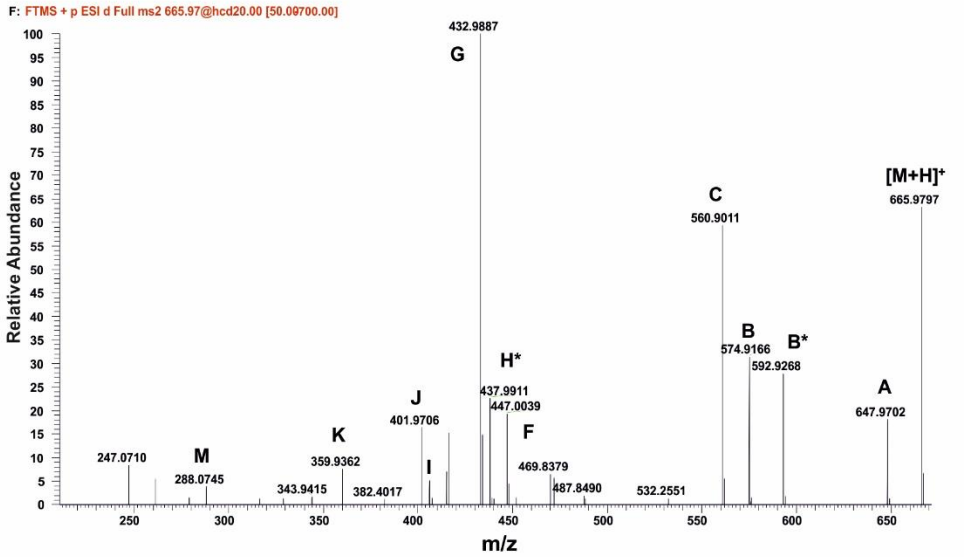

IOP –TP665-C
MS²

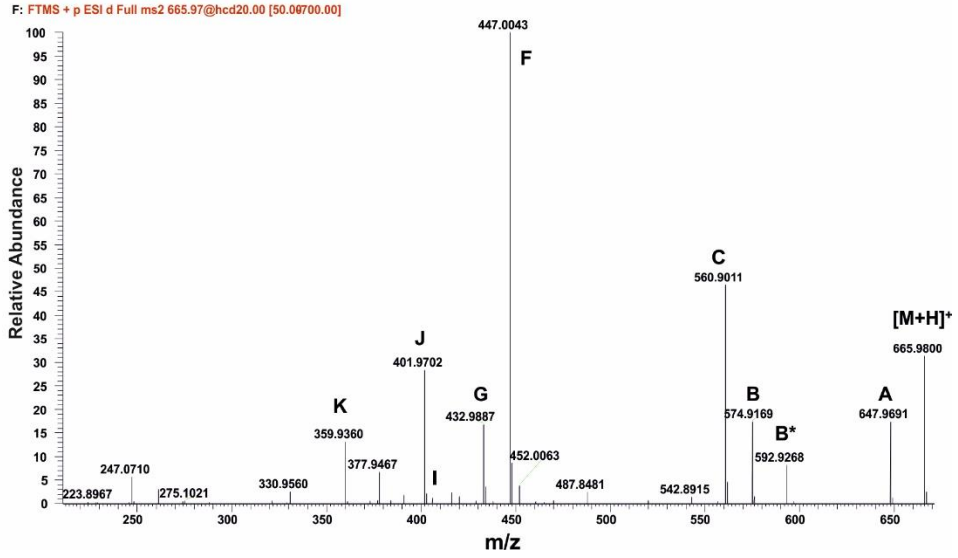

Figure SI-5.4-B. MS^2 and pMS^3 spectra of Iopromide – TP665 A-C (IOP-TP665-A-C) – *continued*

IOP –TP665-A
647 pMS^3

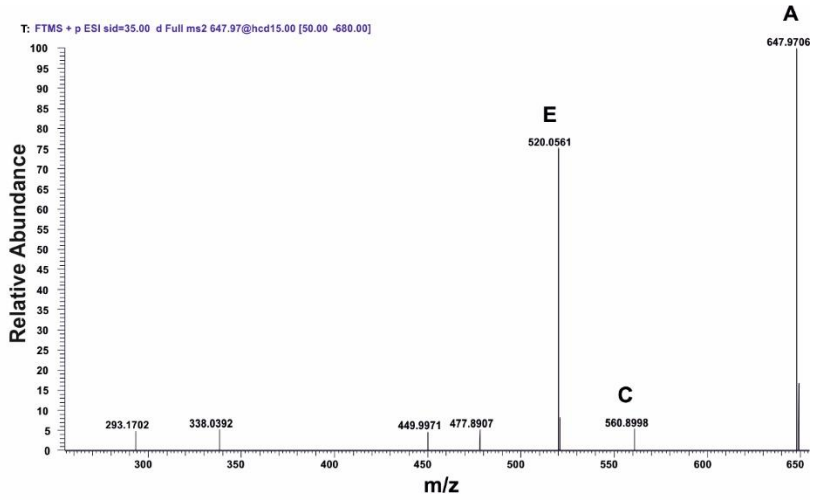

IOP –TP665-C
647 pMS^3

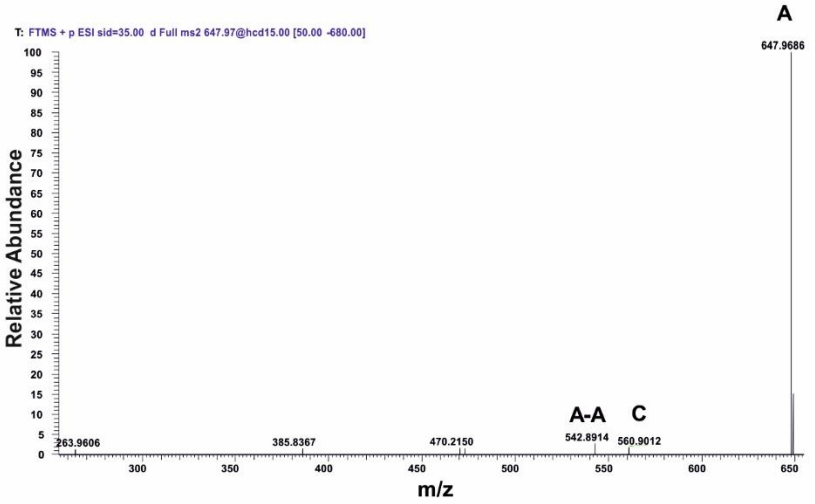

IOP –TP665-
592 PMS^3

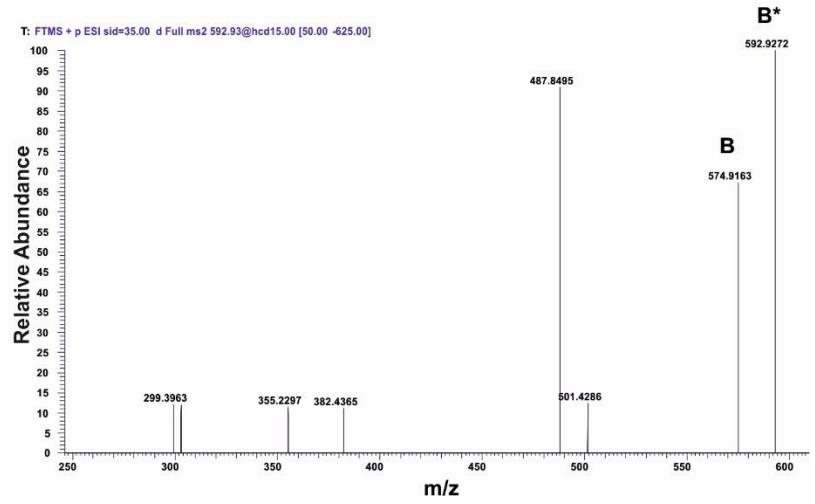

Figure SI-5.4-B. MS² and pMS³ spectra of Iopromide – TP665 A-C (IOP-TP665-A-C) – *continued*

IOP –TP665-A
574 pMS³

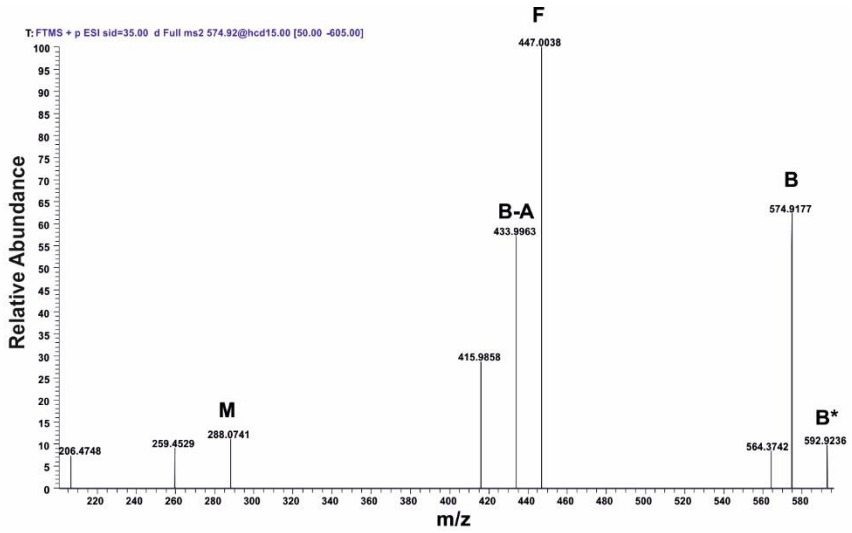

IOP –TP665-B
574 pMS³

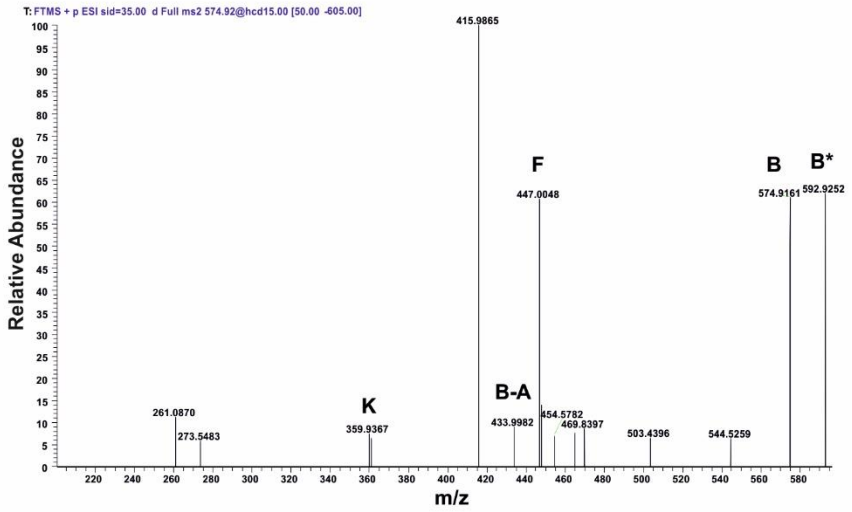

IOP –TP665-C
574 PMS³

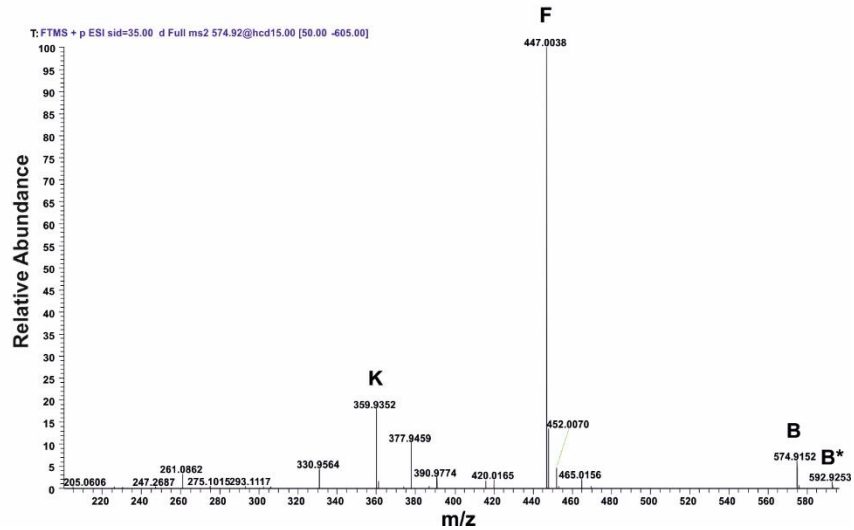

Figure SI-5.4-B. MS^2 and pMS^3 spectra of Iopromide – TP665 A-C (IOP-TP665-A-C) – *continued*

IOP –TP665-A
560 pMS^3

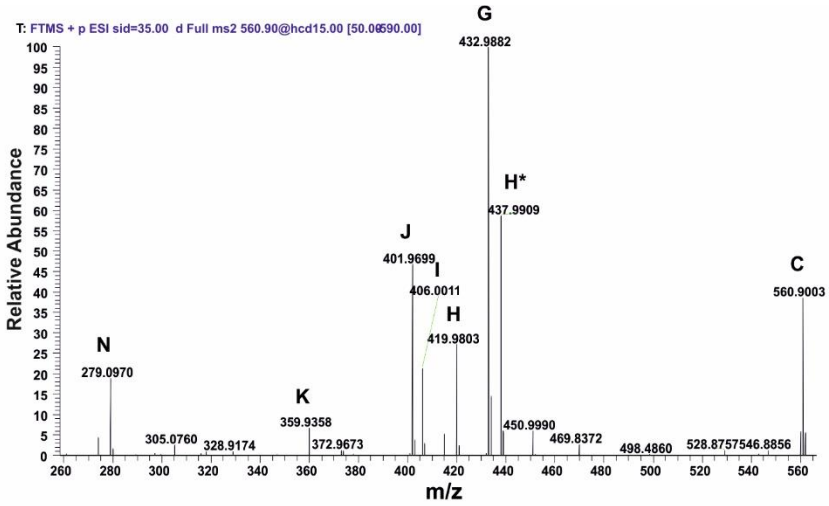

IOP –TP665-B
560 pMS^3

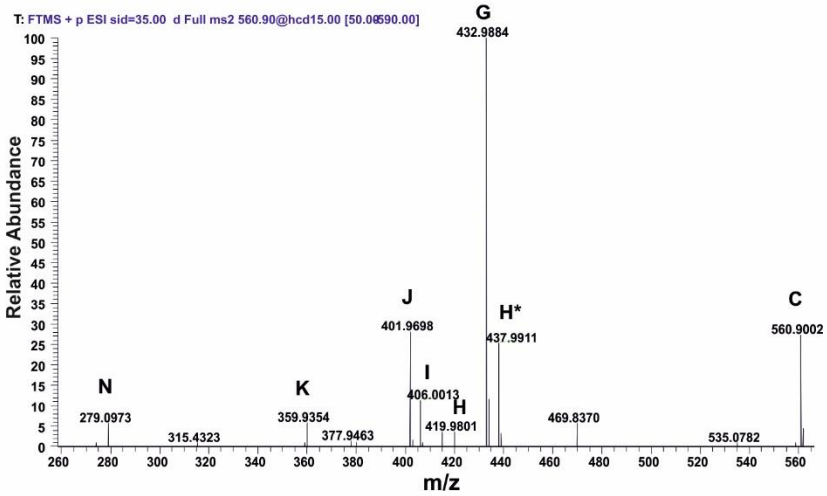

IOP –TP665-C
560 PMS^3

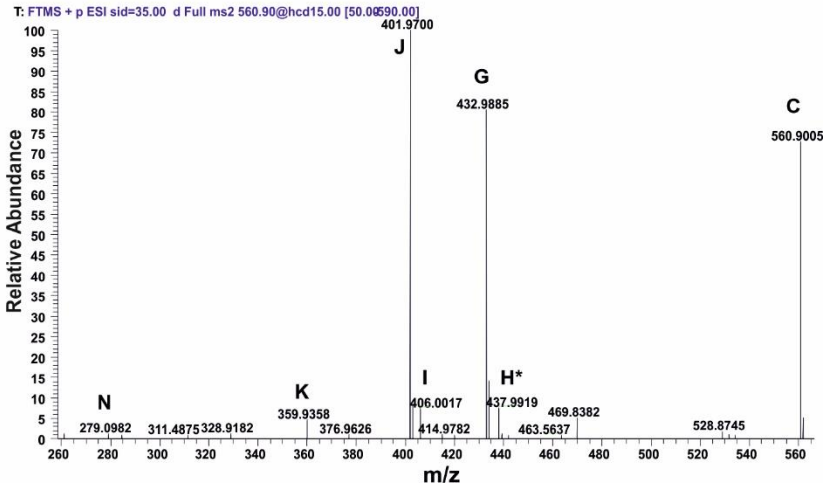

Figure SI-5.4-B. MS² and pMS³ spectra of Iopromide – TP665 A-C (IOP-TP665-A-C) - *continued*

IOP –TP665-A
447 pMS³

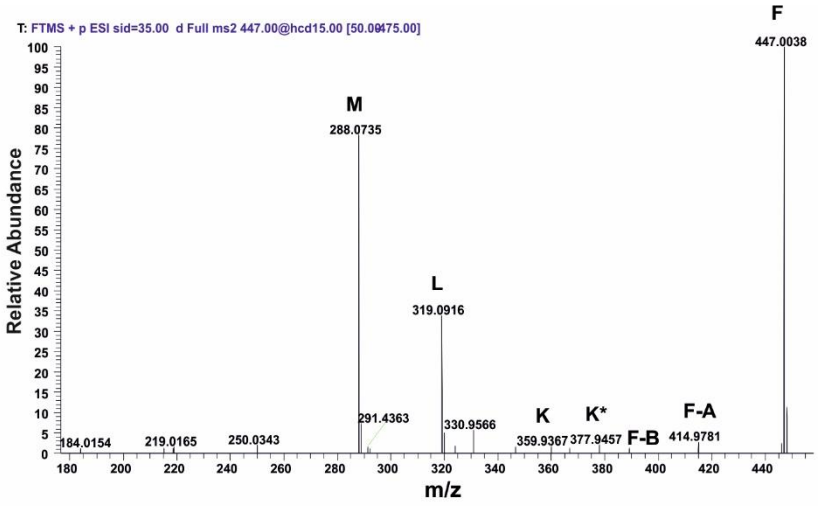

IOP –TP665-B
447 pMS³

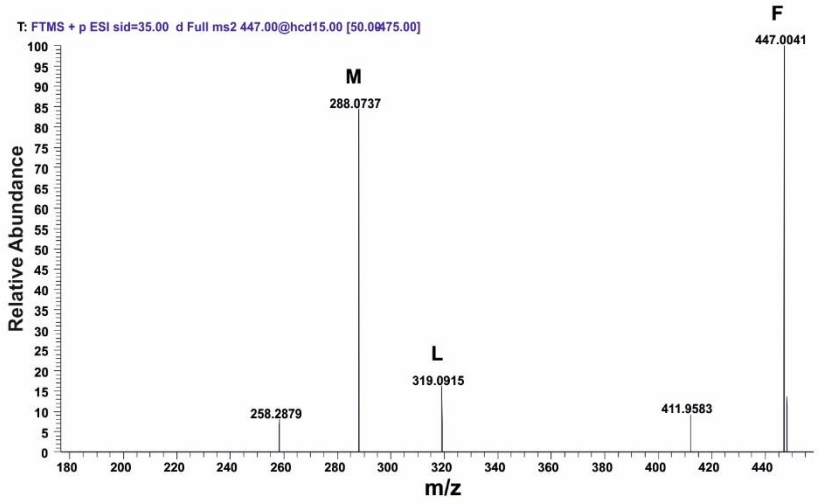

IOP –TP665-C
447 PMS³

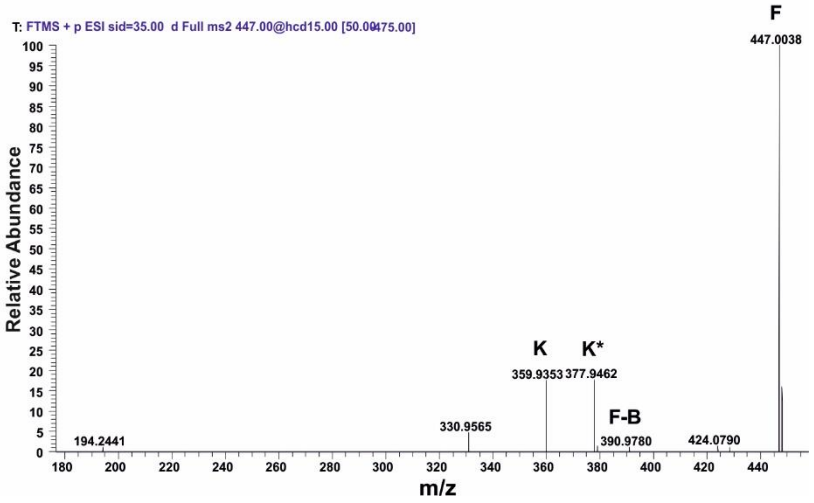

Figure SI-5.4-B. MS^2 and pMS^3 spectra of Iopromide – TP665 A-C (IOP-TP665-A-C) – *continued*

IOP –TP665-A
432 pMS^3

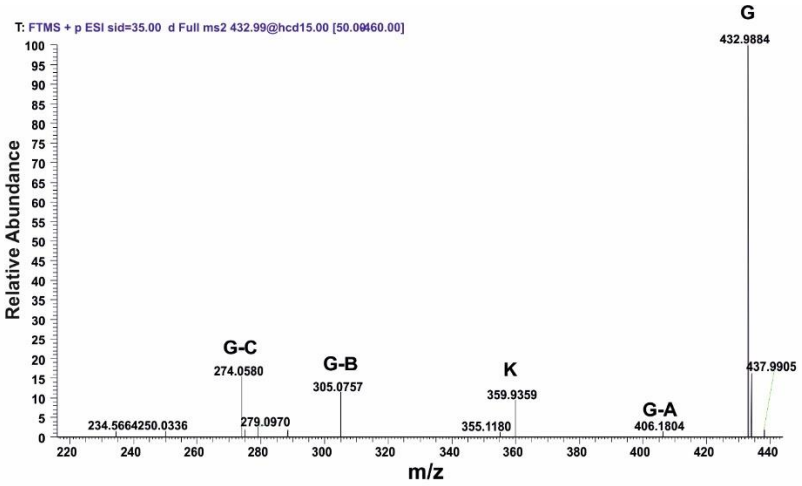

IOP –TP665-B
432 pMS^3

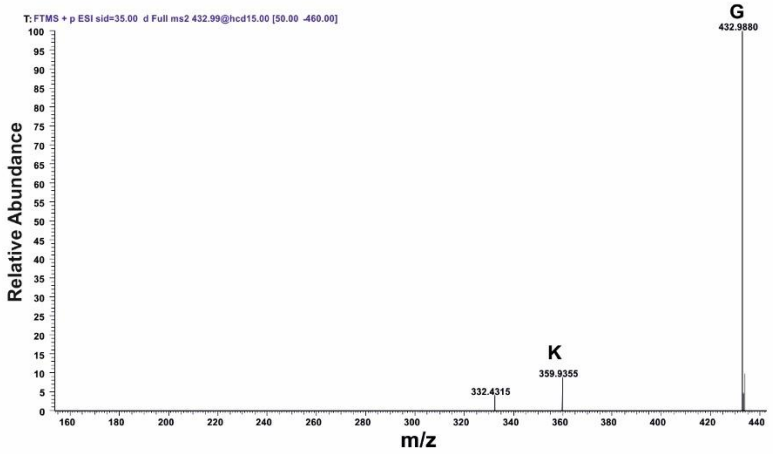

IOP –TP665-C
432 pMS^3

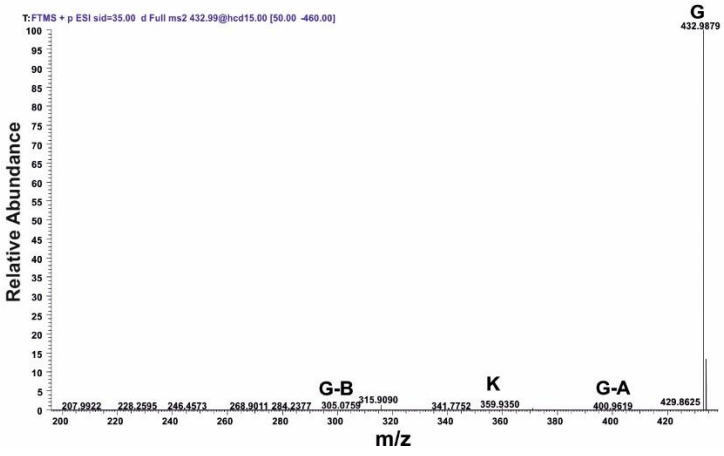

Figure SI-5.4-B. MS^2 and pMS^3 spectra of Iopromide – TP665 A-C (IOP-TP665-A-C) – *continued*

IOP –TP665-A
520 pMS^3

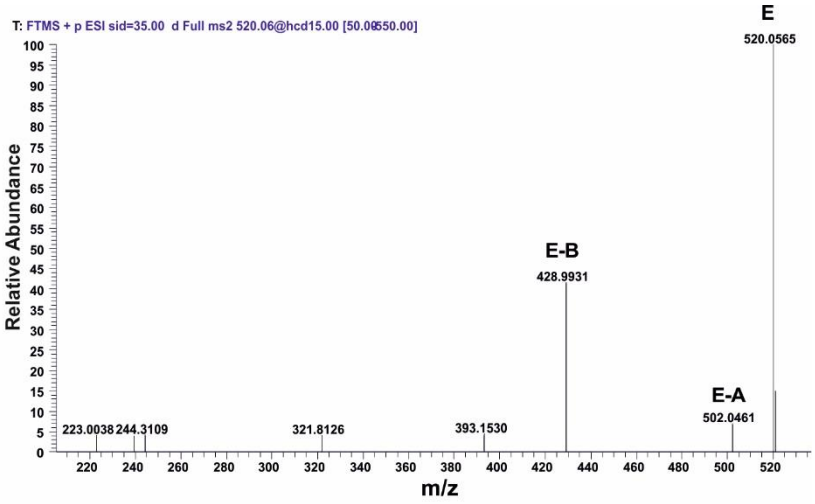

IOP –TP665-A
406 pMS^3

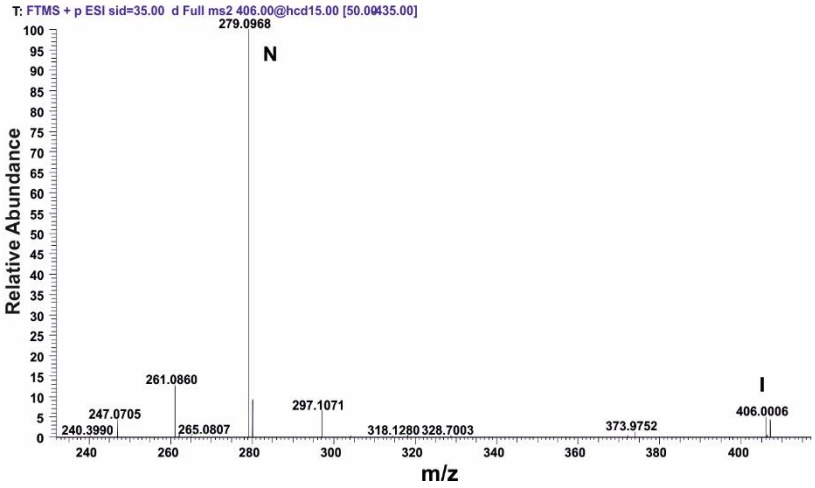

Figure SI-5.4-C. (HSQC)-NMR spectra of the sum of IOP-TP665-A-C.

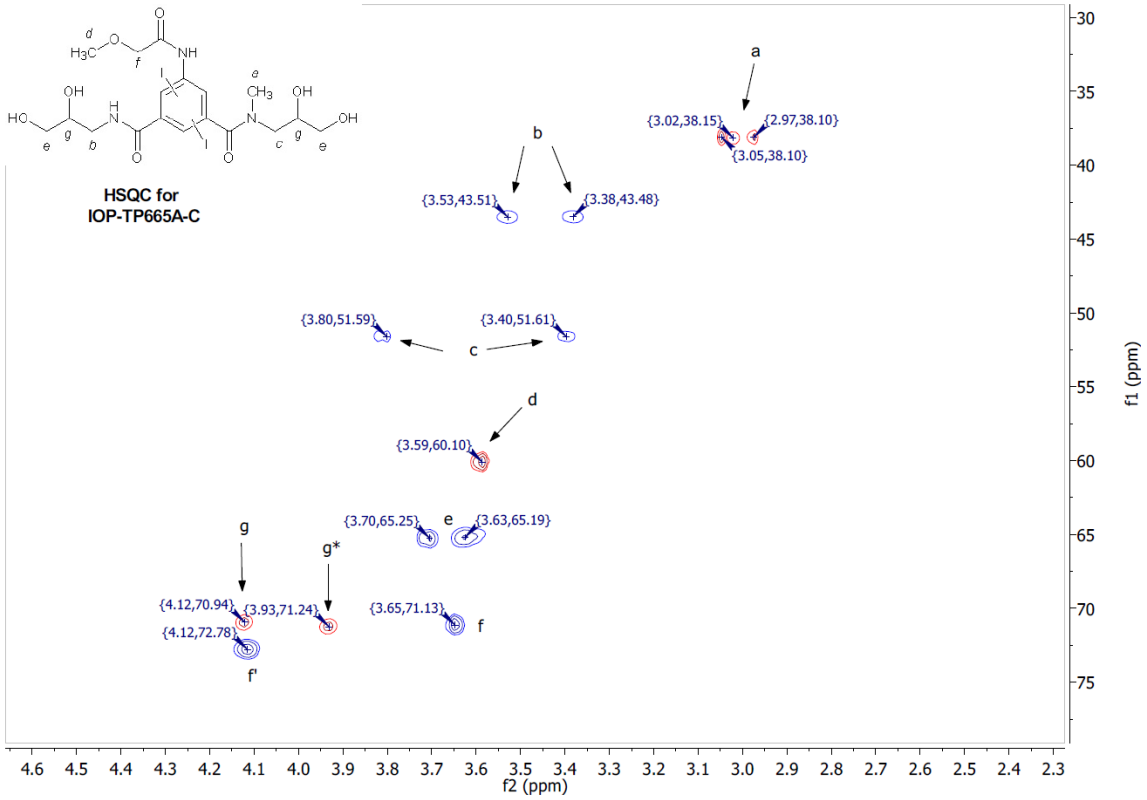

IOPROMIDE TP651 (IOP TP651)

Deiodination of IOP was found to be the key mechanism leading to the four TPs (IOP-TP665-A, B and C and IOP-TP651) that were detected in surface samples.

IOP-TP651 had been tentatively identified by Perez et.al.[14] by H/D exchange experiments on Q-TOF-MS which confirmed the deiodination and N-demethylation pathways. However, uncertainty remained of the exact position of the loss of iodine. Following N-demethylation, both side chains (*identical* and *identical-CH₃*) became undistinguishable, which suggests that there are only two possible sites for deiodination (like in the case of IMP-TP651-A and –B). The structure of the IOP-TP651 was inferred by comparing the pMS^3 spectra of the two fragments (m/z 560.9014 and m/z 432.9891) that IOP-TP651 has in common with the IOP-TP665-A-C. The fragment ion m/z 560.9014 and, particularly, the fragment m/z 432.9891 strongly suggest that the structure of this TP arises from the loss of iodine from position **2** (between two *identical* chains).

Figure SI-5.5-A. Fragmentation pattern Iopromide – TP651 (IOP-TP651)

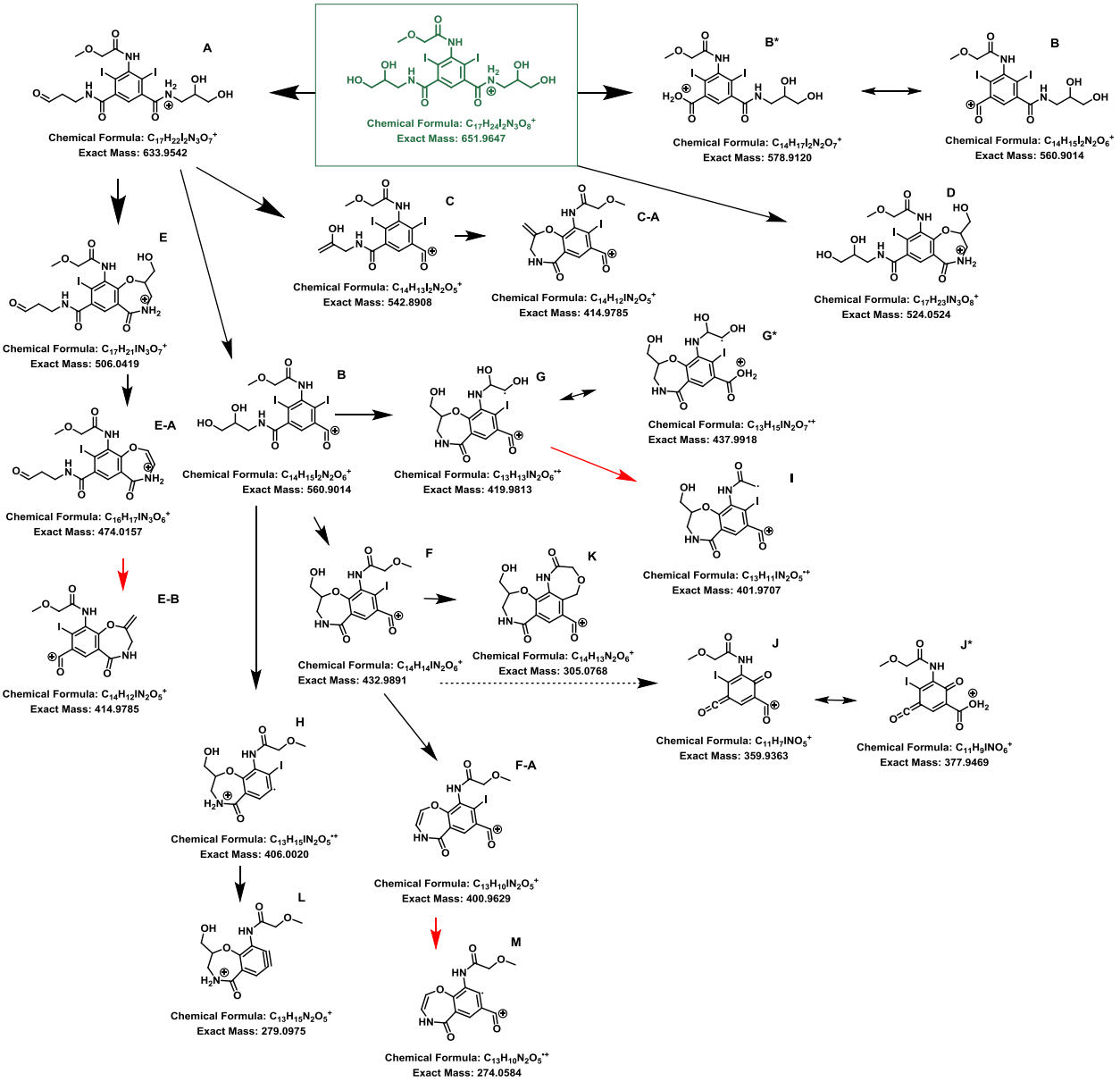

Figure SI-5.5-B. MS^2 and pMS^3 spectra of Iopromide – TP651 (IOP-TP651)

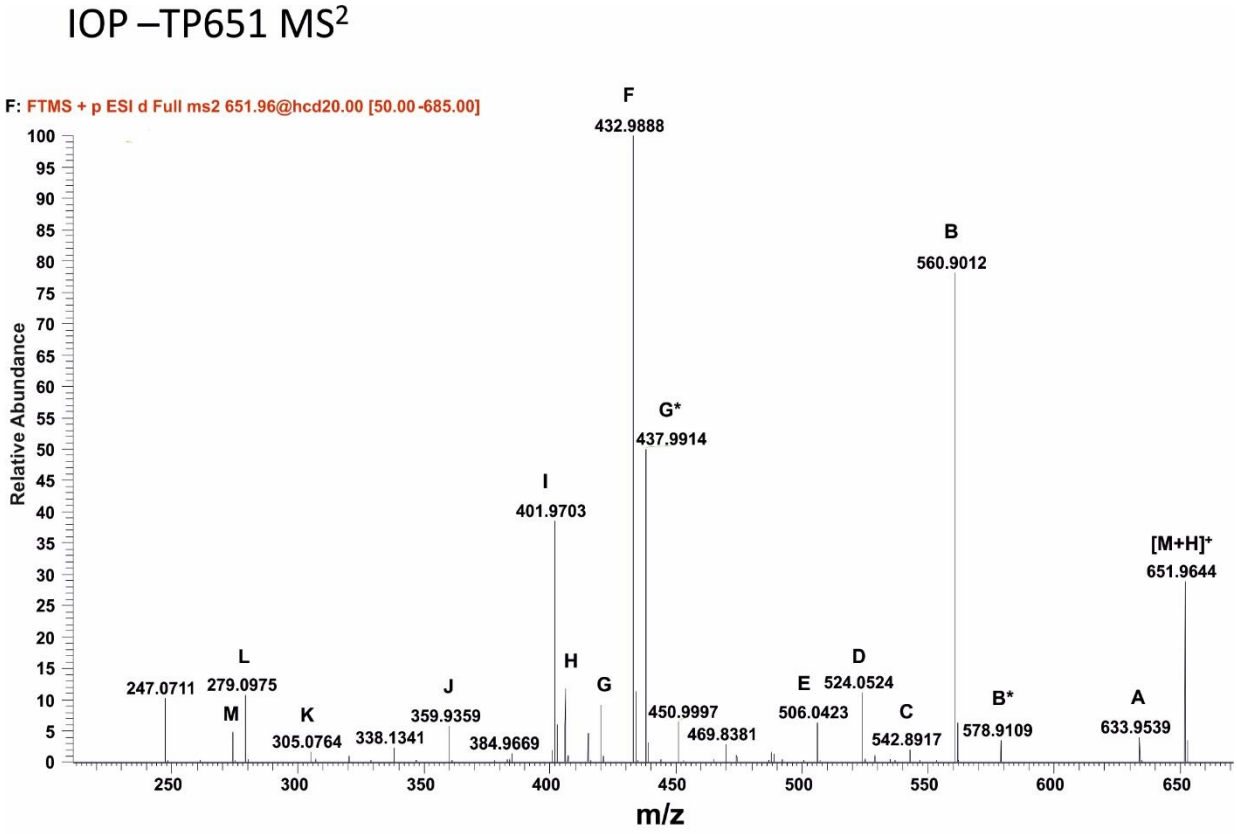

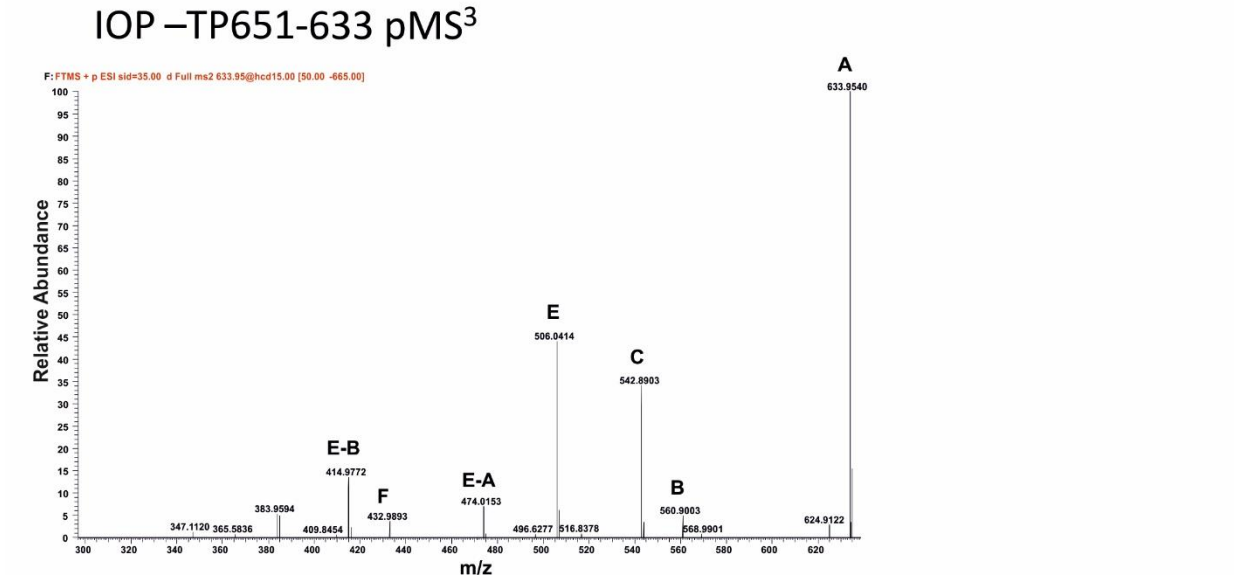

Figure SI-5.5-B. MS^2 and pMS^3 spectra of Iopromide – TP651 (IOP-TP651) – *continued*

IOP –TP651-578 pMS^3

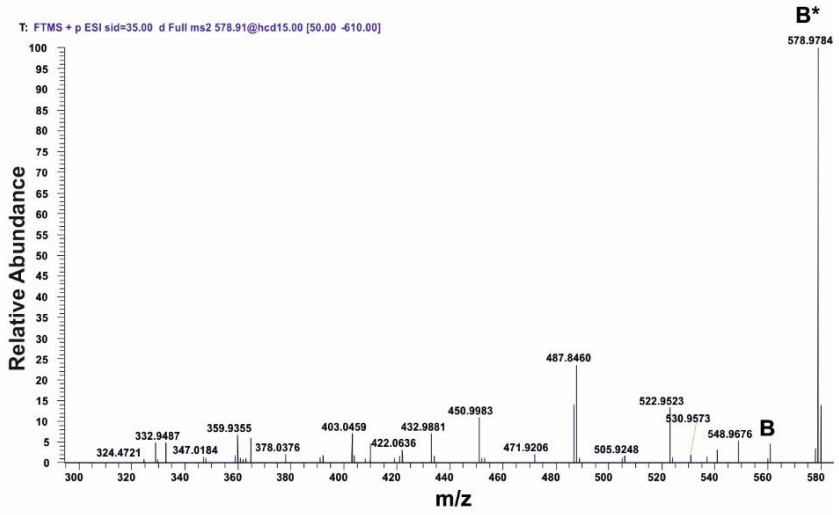

IOP –TP651-560 pMS^3

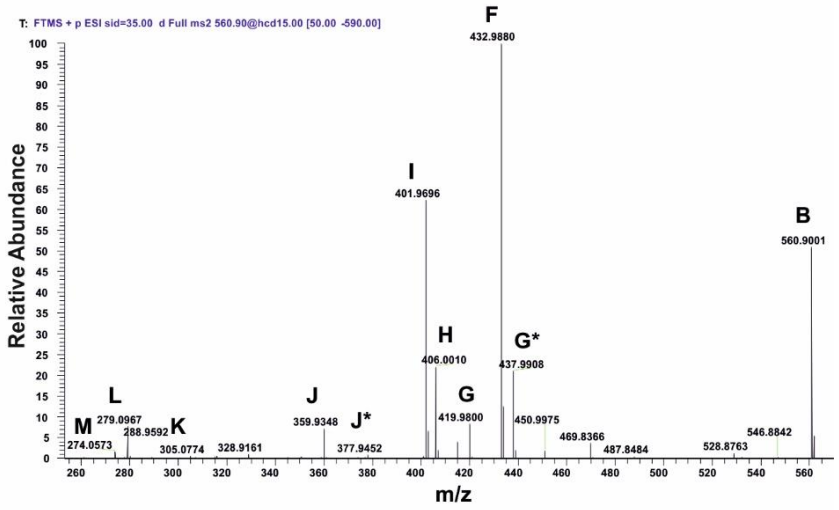

IOP –TP651-542 pMS^3

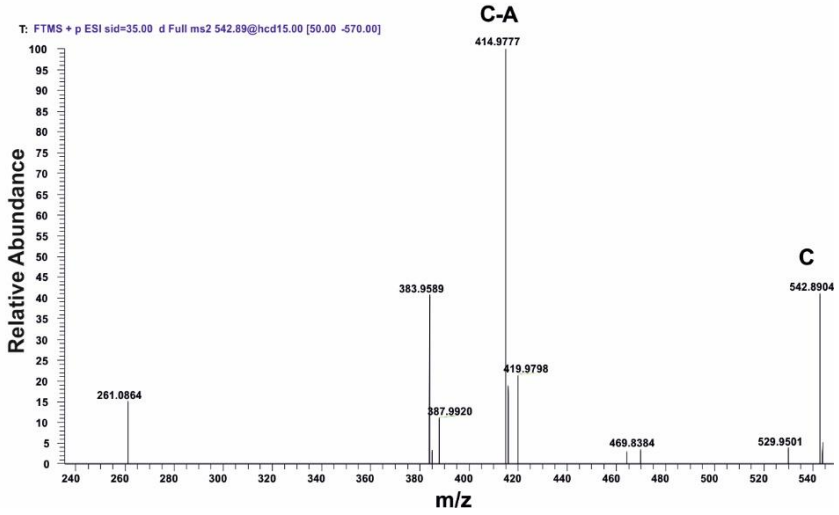

Figure SI-5.5-B. MS² and pMS³ spectra of Iopromide – TP651 (IOP-TP651) – *continued*

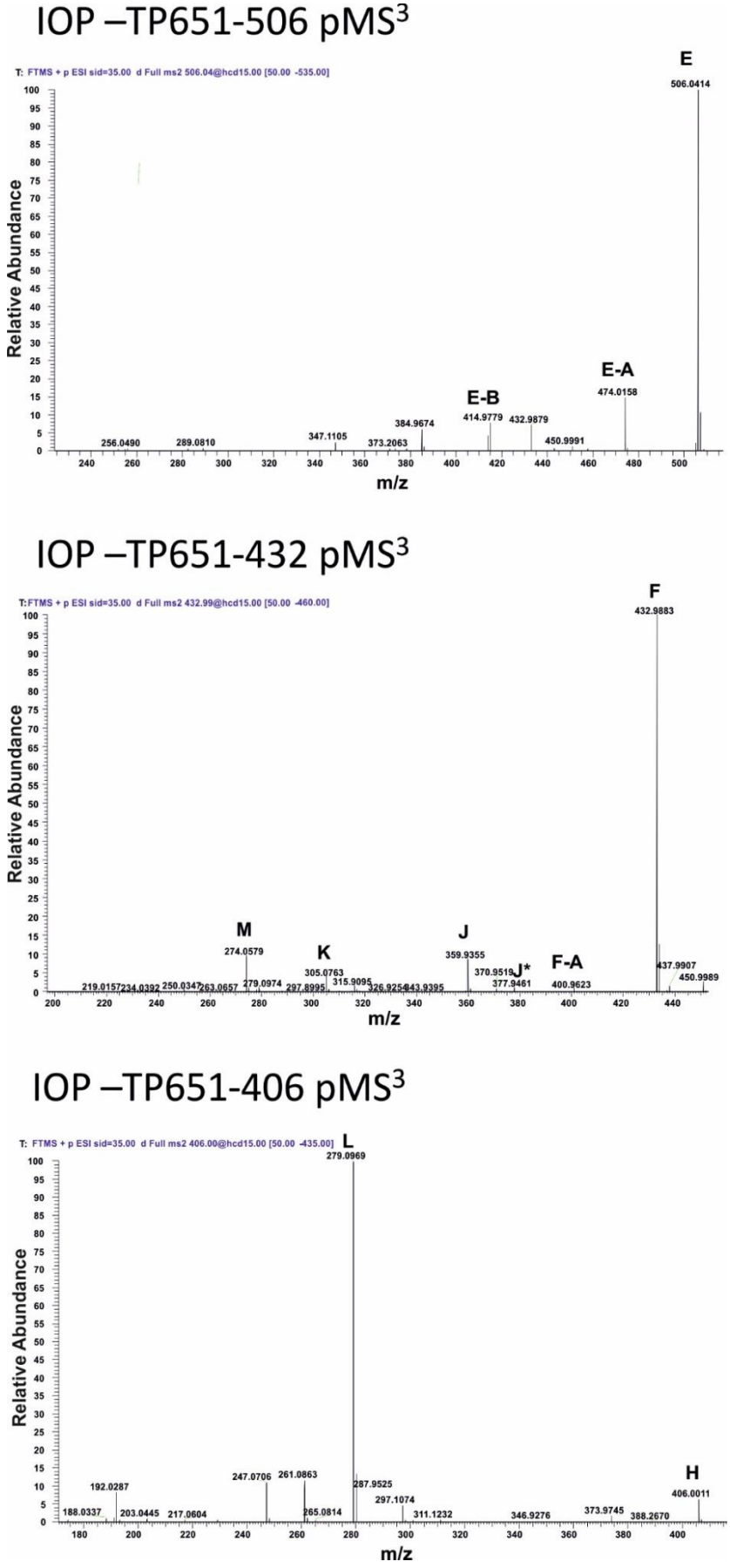

IOHEXOL (IOX)

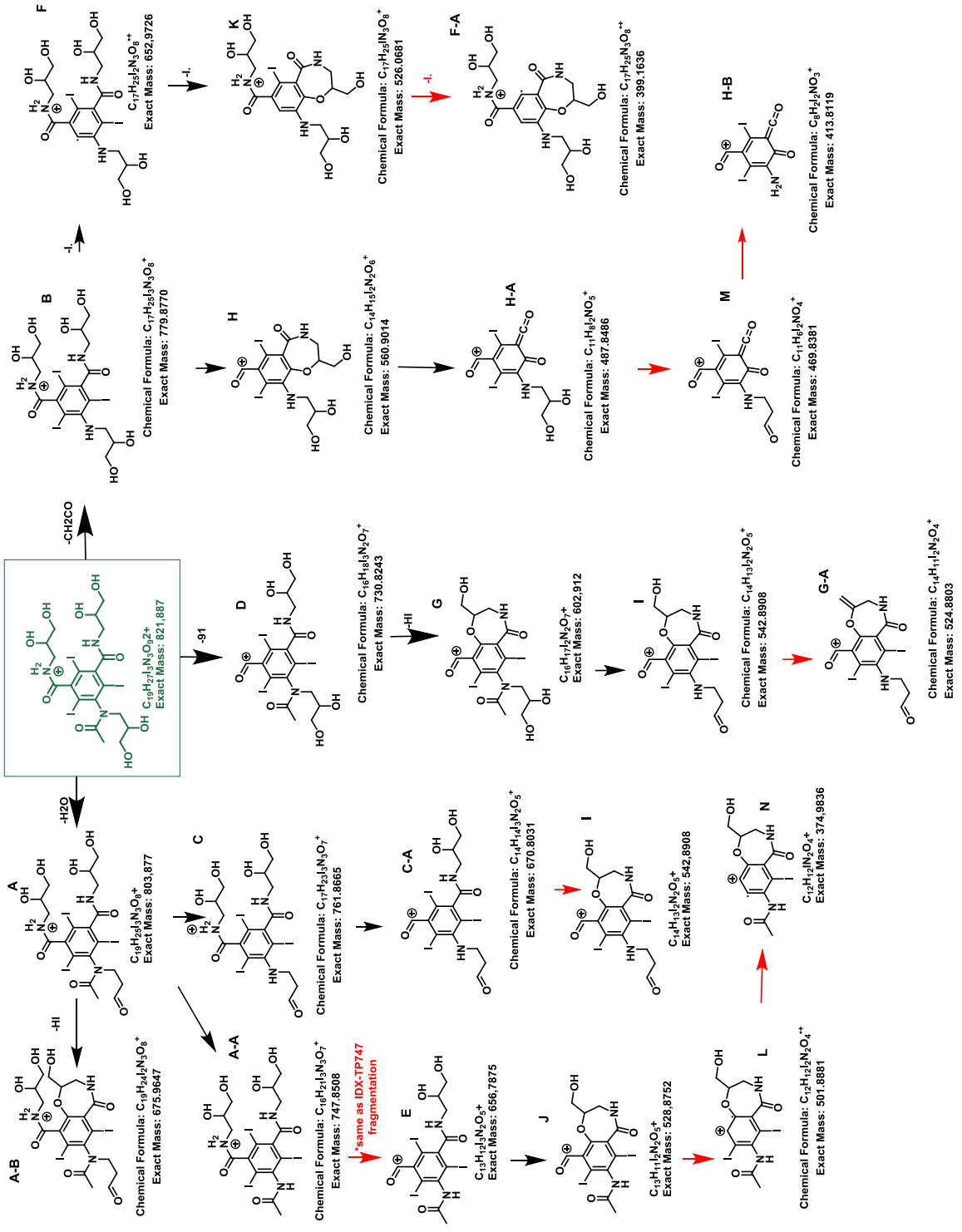

Figure SI-5.6-A. Fragmentation pattern of Iohexol (IOX)

Figure SI-5.6-B. MS^2 and pMS^3 spectra of Iohexol (IOX)

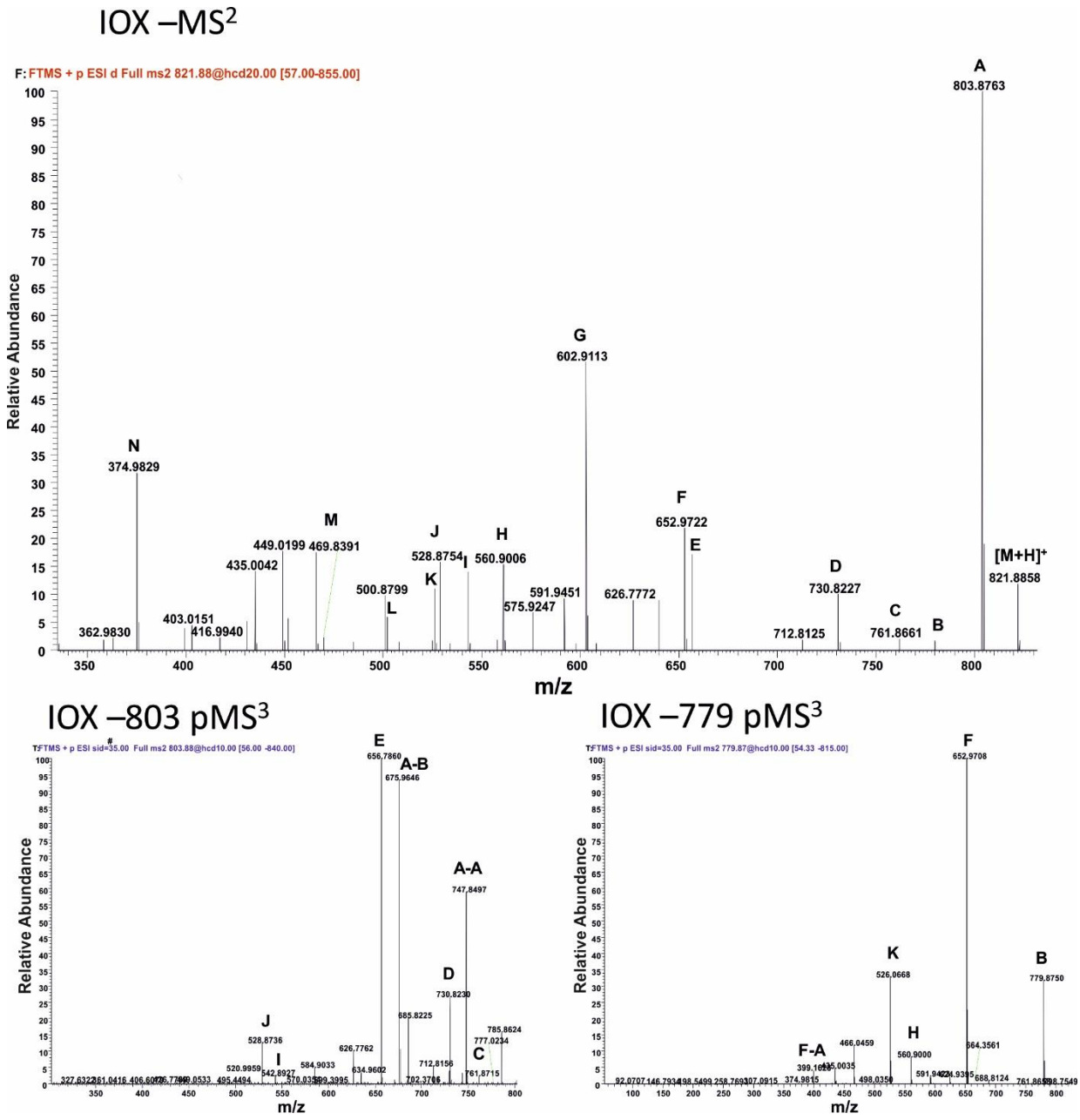

Figure SI-5.6-B. MS^2 and pMS^3 spectra of Iohexol (IOX) – *continued*

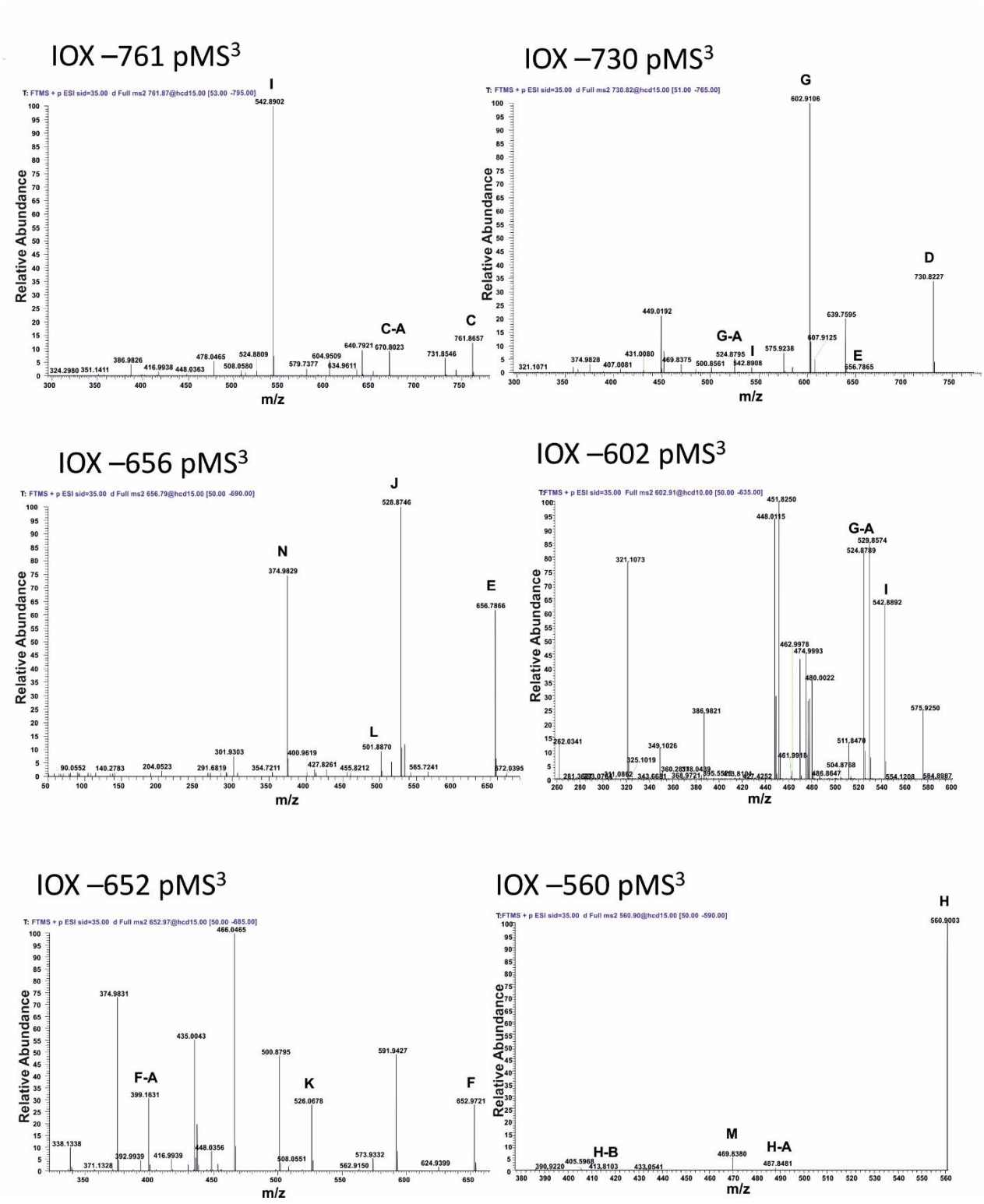

IOHEXOL TP693 (IOX-TP693)

Initially it was postulated that the *similar* side chain is involved in the formation of IOX-TP693 comparing the IOX degradation with IOP, IMP and IPM degradation. IOP did not produce any photoproduct with net elimination of HI (hypothetical m/z 663.9647); however, two non-prioritized TPs with m/z 649.9490 were detected (loss of HI and CH). So, when the molecule of IOP is bearing its C-methyl group in the *similar* side chain, no cyclization occurs. However, after a methyl is lost from the IOP, two photoproducts are formed (if it was an N-dealkylation, there would only be one TP649 since the *identical-CH_3* chain would be the same as the *identical* one). This suggested that the cyclization only occurs when a similar chain is involved and has hydroxyl groups (all IMP, IPM and IOX have hydroxylated similar chain). However, the NMR data of the isolated IOX-TP693 showed that it is actually the *identica*l side chain that cyclizes in IOX to give the TP693 (**Figure SI-5.7-C**).

Figure SI-5.7-A. Fragmentation pattern of Iohexol –TP693 (IOX-TP693)

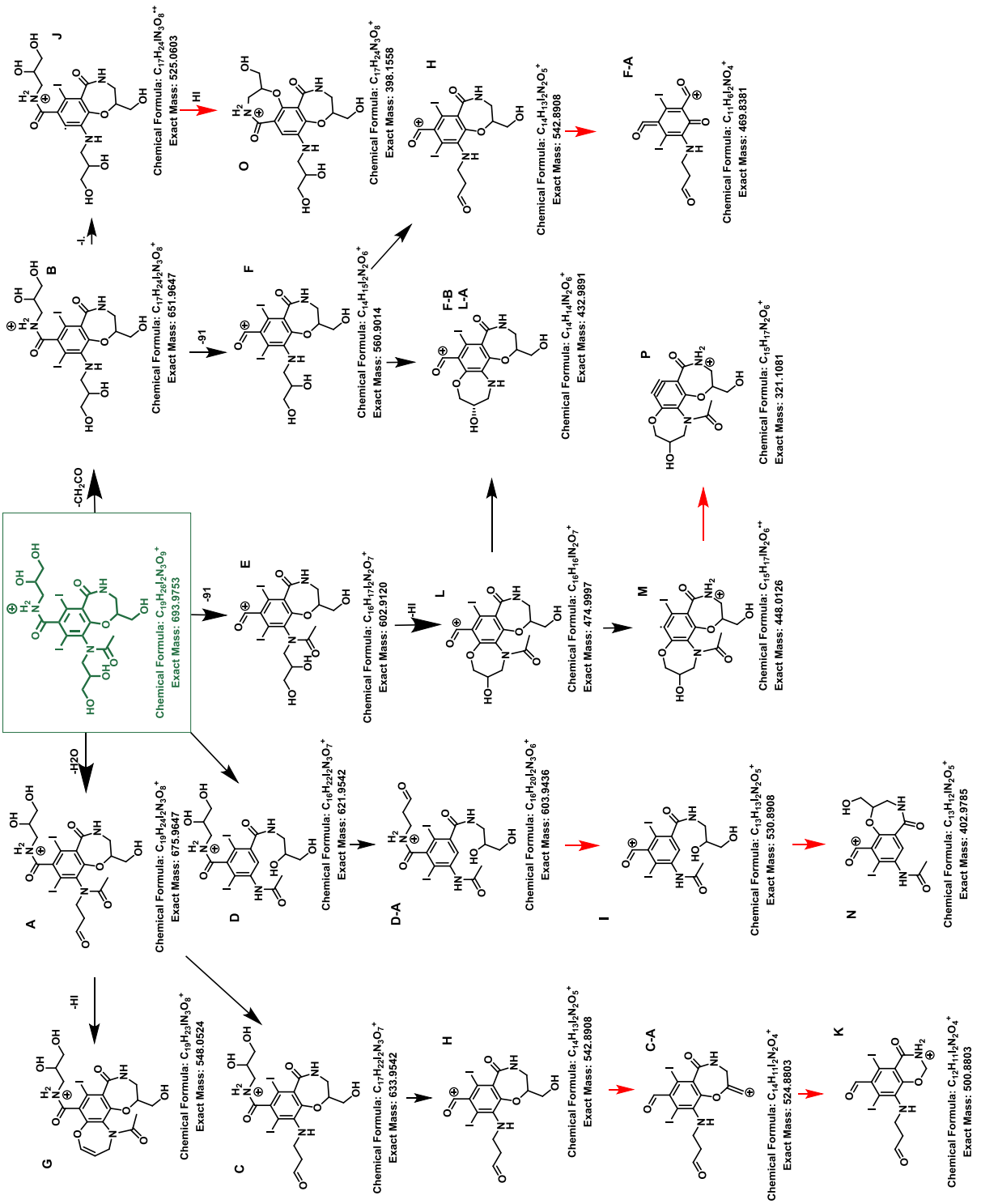

Figure SI-5.7-B. MS^2 and pMS^3 spectra of Iohexol –TP693 (IOX-TP693)

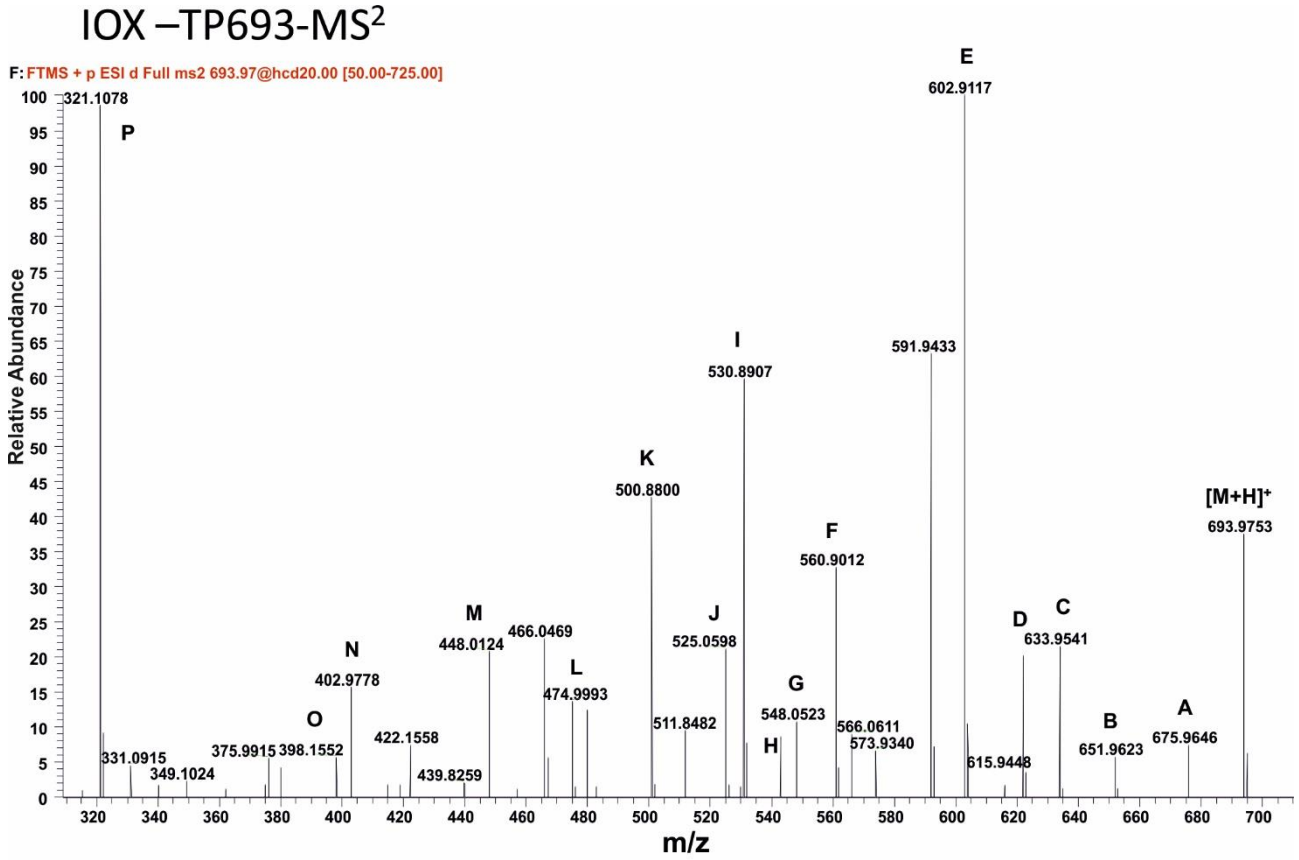

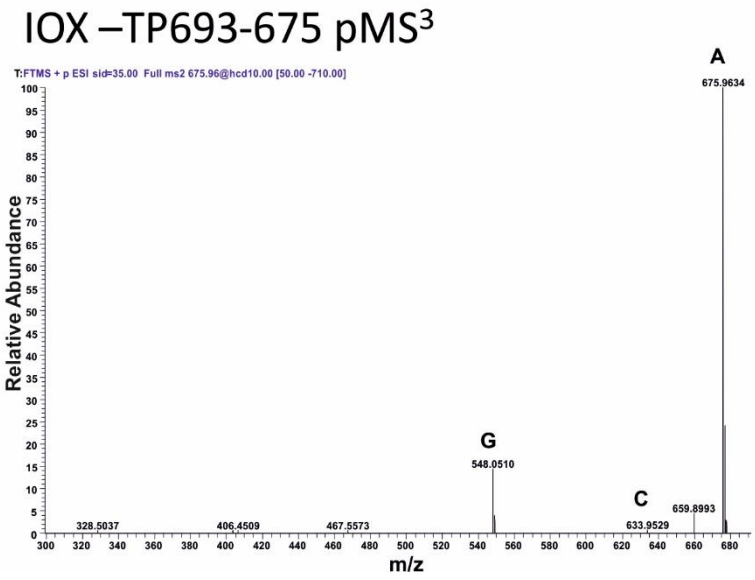

Figure SI-5.7-B. MS^2 and pMS^3 spectra of Iohexol –TP693 (IOX-TP693) – *continued*

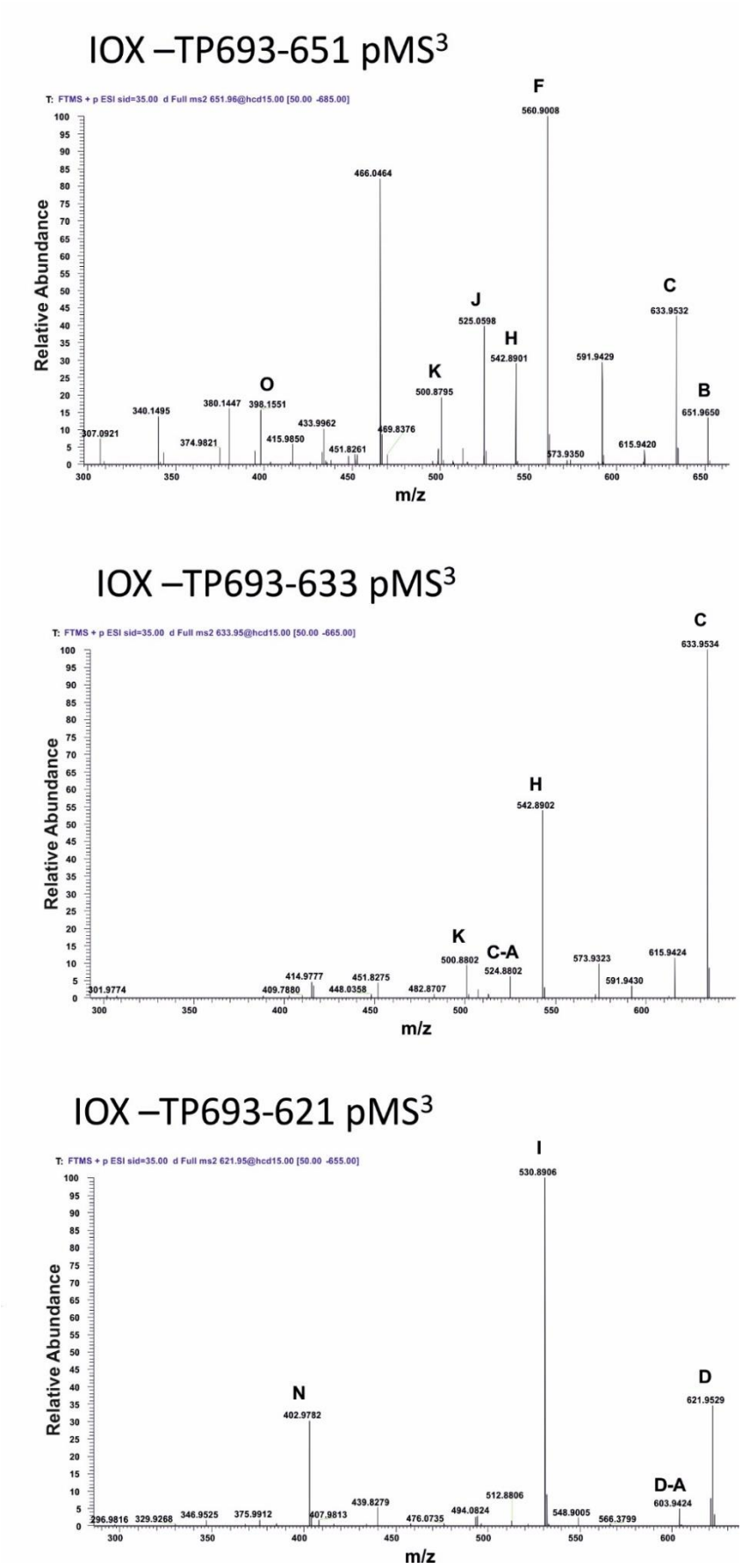

Figure SI-5.7-B. MS^2 and pMS^3 spectra of Iohexol –TP693 (IOX-TP693) – *continued*

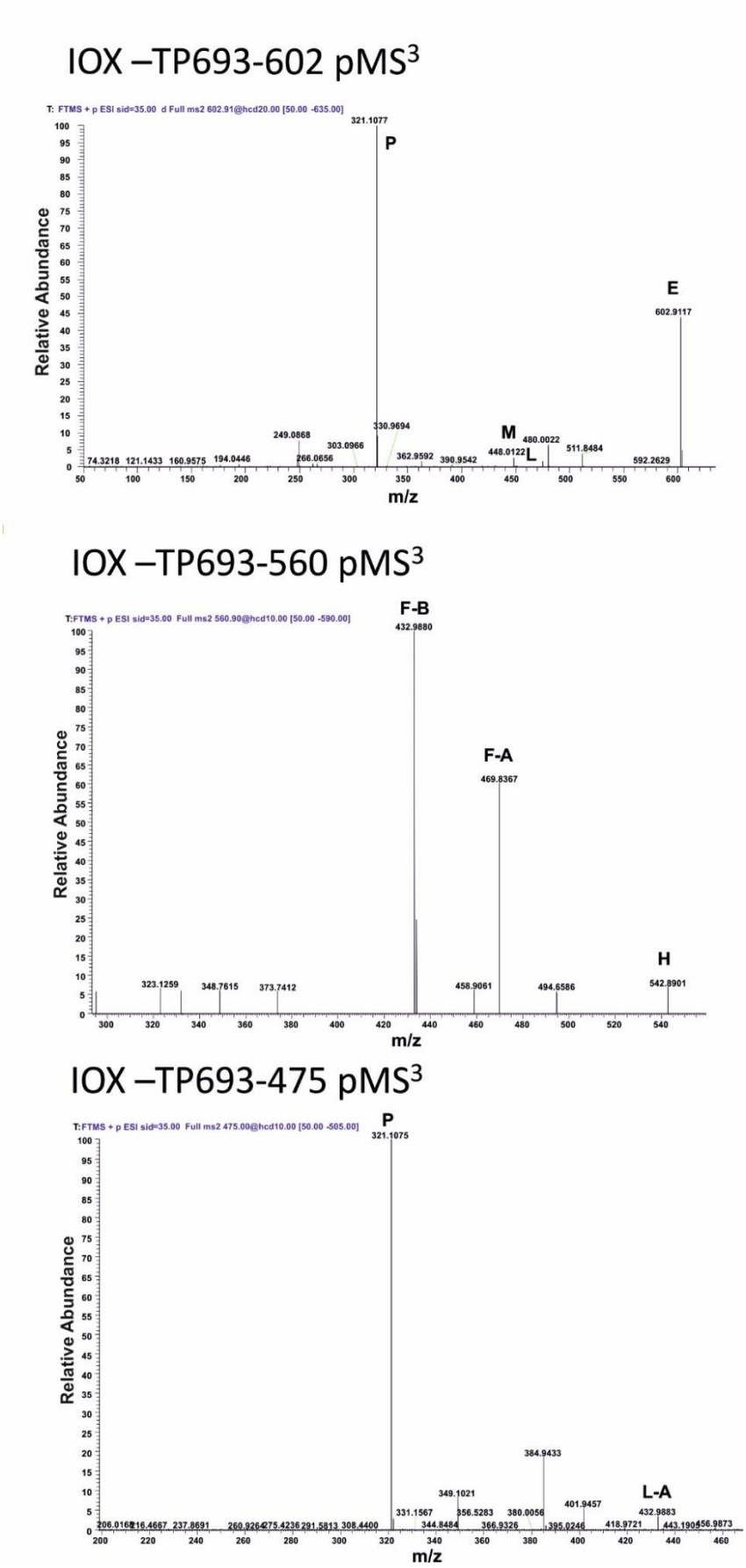

Figure SI-5.7-C. (HSQC)-NMR spectra of Iohexol –TP693 (IOX-TP693)

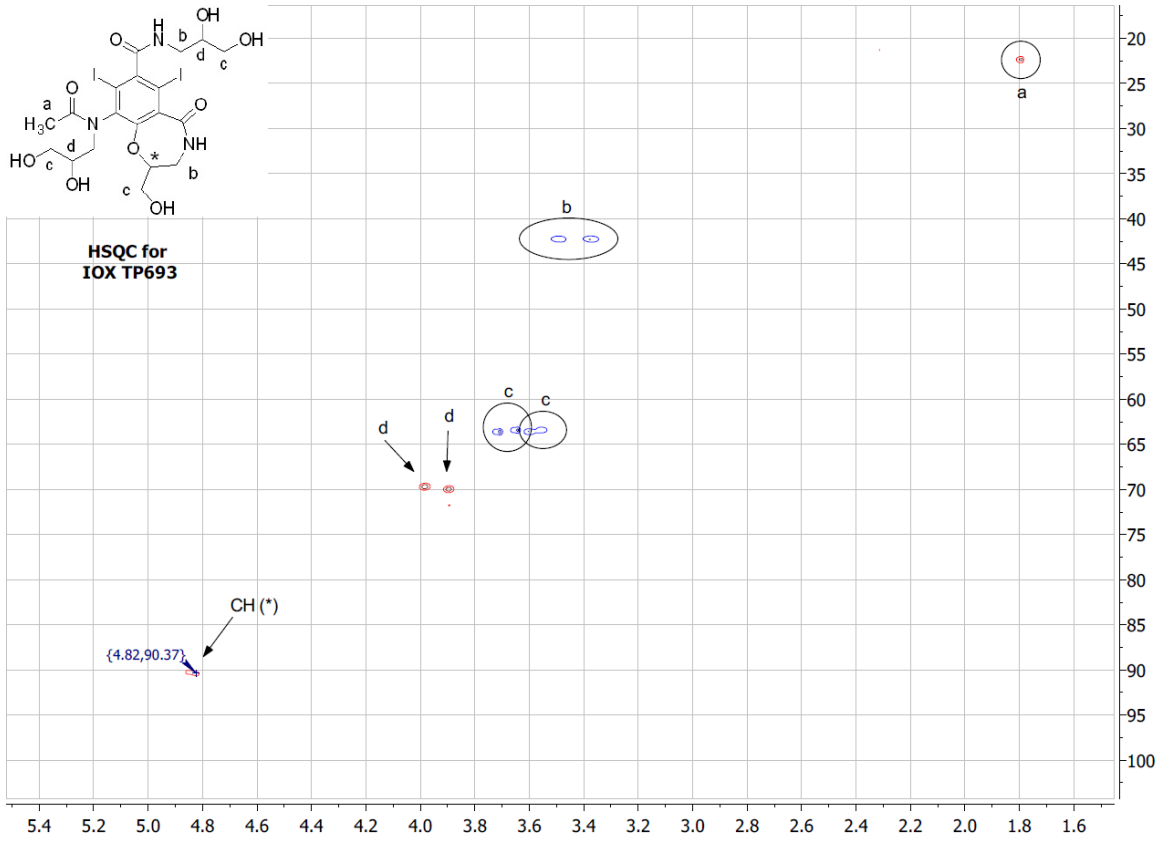

IOHEXOL TP695 A-B (IOX-TP695 A-B)

IOX-TP695A and B have the elemental composition that shows the deiodination of the molecule with the replacement by hydrogen. IOX-TP695-A and B were not possible to separate by semipreparative chromatography and their structures were elucidated only based on HRMS data (**Figure SI-5.8-A and –B**) Both TPs presented similar losses in the mass spectra compared to parent IOX, namely loss of water, acetone and m/z 91.0627 from the *identical* side chain. However, IOX-TP695-A has a diagnostic ion at m/z 562.9170 lacking in the MS^2 spectra of IOX-TP695-B. The pMS^3 experiments confirmed that this fragment comes from the m/z 653.9804 after the acetone is lost from the original TP structure. Formation of this fragment suggests loss of the similar side chain from the m/z 653.9804. This is only possible if one of the iodine atoms ortho to the similar chain (position **4** or **6**) is already cleaved. This would suggest that the IOX-TP695-A has the structure where one iodine is missing from the position **4** or **6** (**Table 2**.), Regardless of which of the two are cleaved from the IOX, they will only render one molecule due to symmetry.

Figure SI-5.8-A Fragmentation pattern of Iohexol –TP695 A-B (IOX-TP695-A-B)

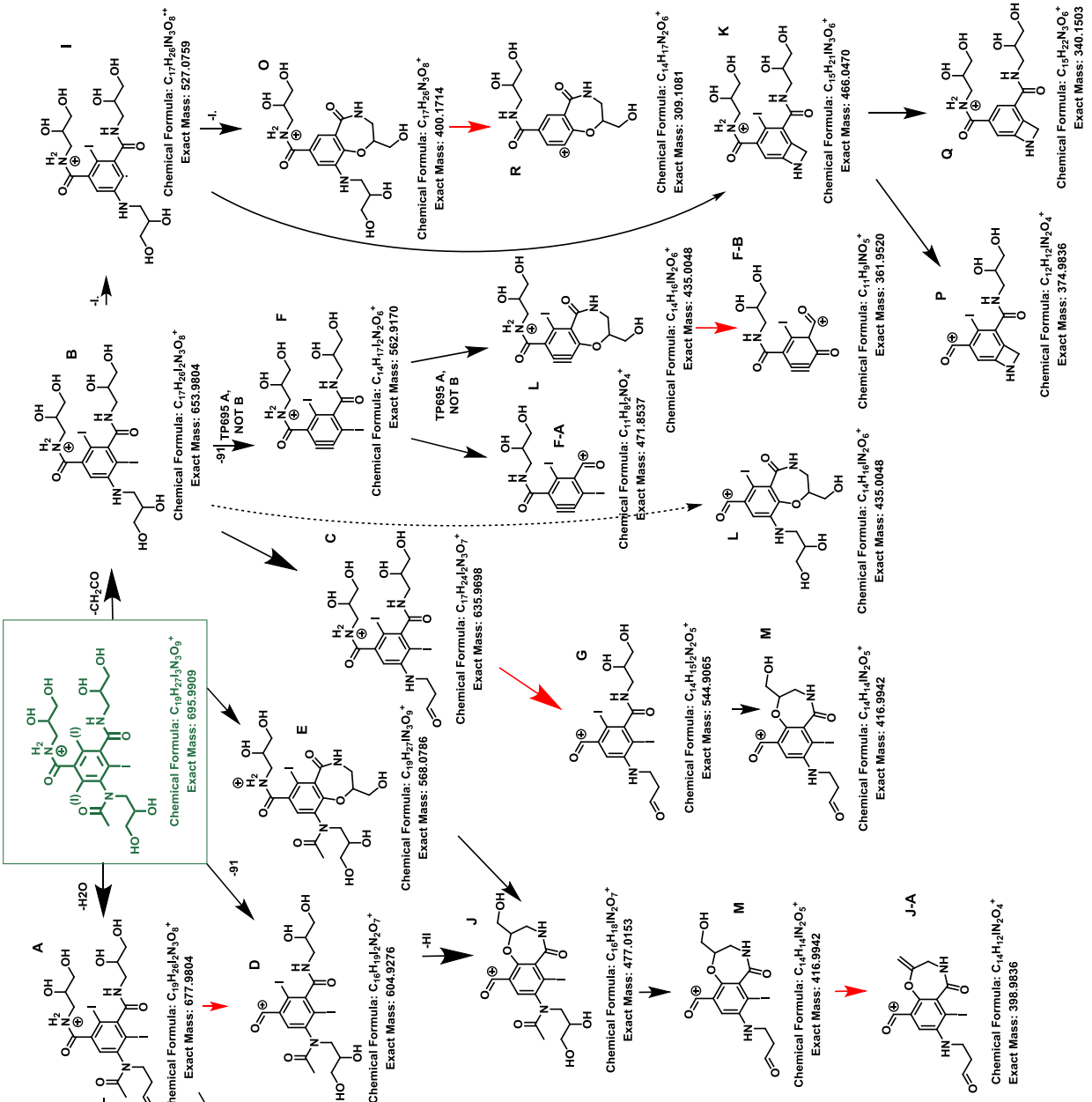

Figure SI-5.8-B MS² and pMS³ spectra of Iohexol –TP695 A-B (IOX-TP695-A-B)

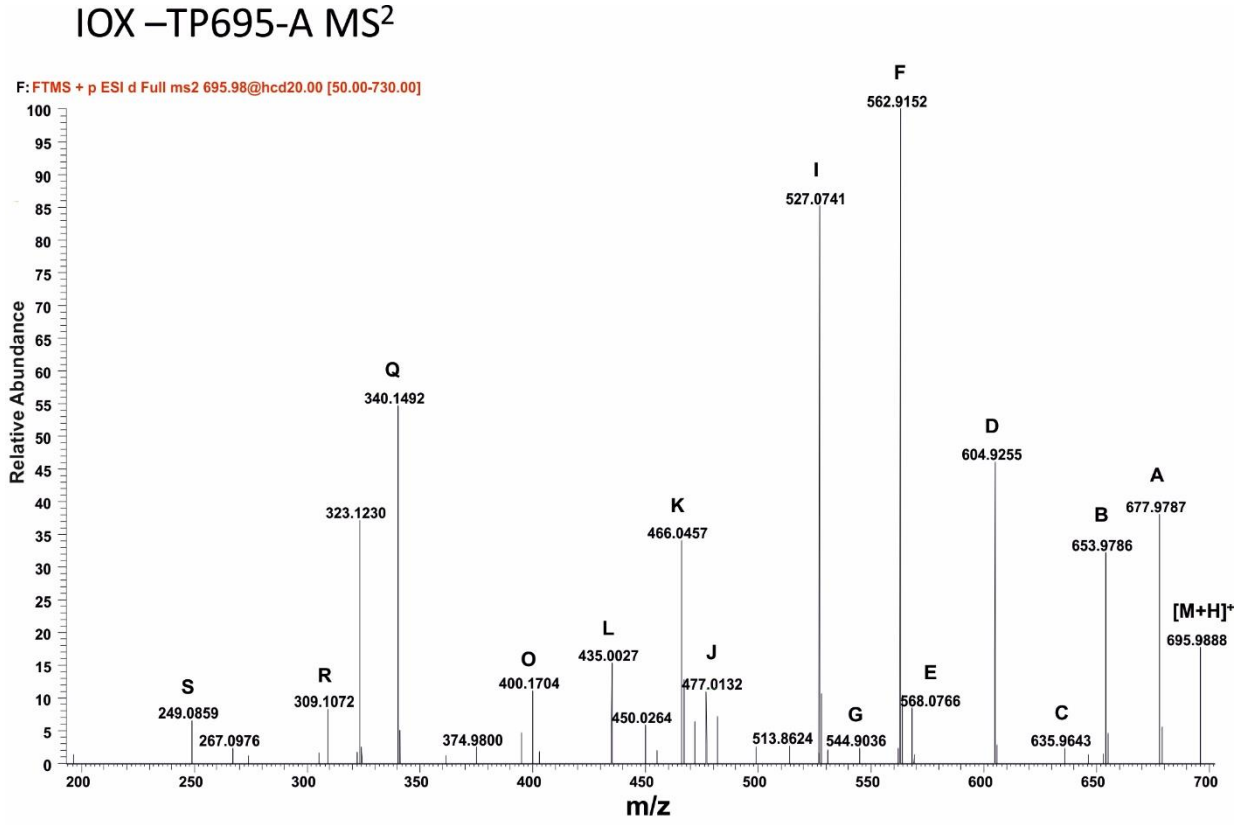

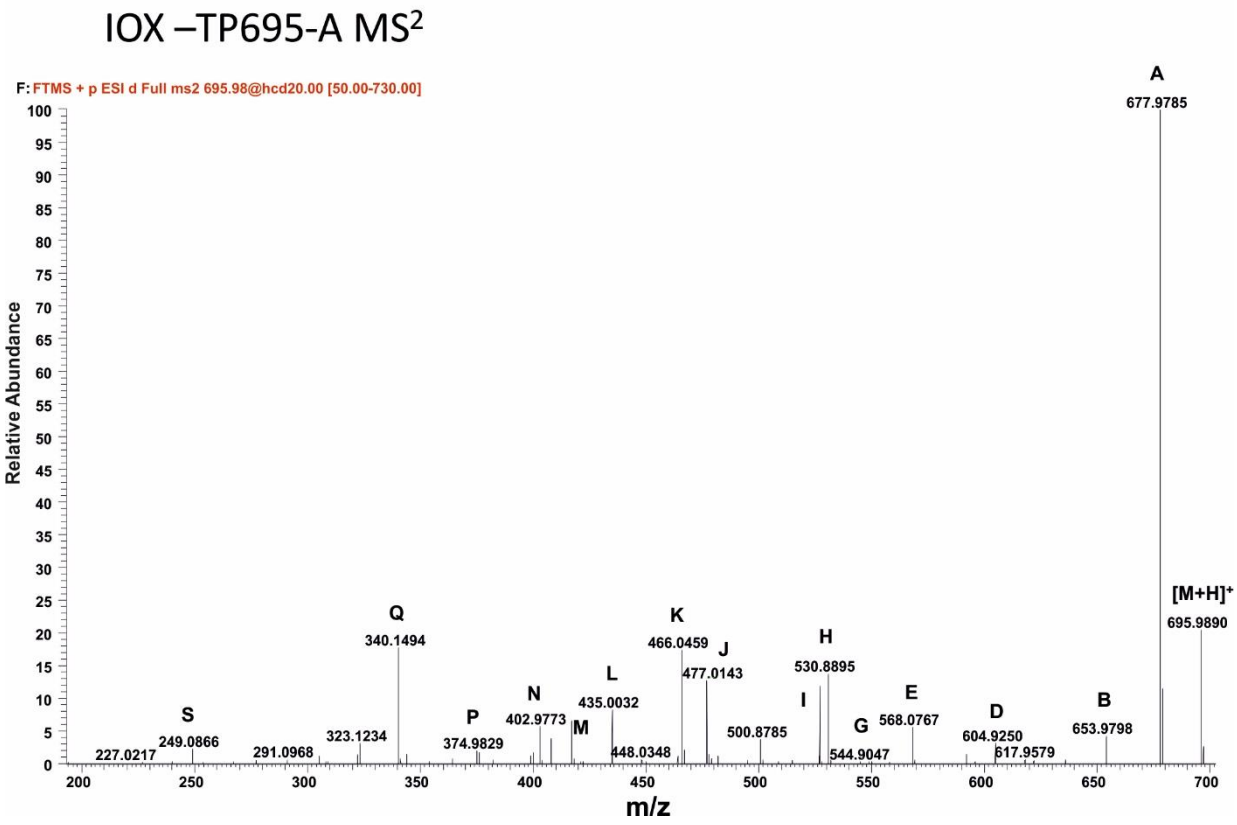

Figure SI-5.8-B MS² and pMS³ spectra of Iohexol –TP695 A-B (IOX-TP695-A-B) – *continued*

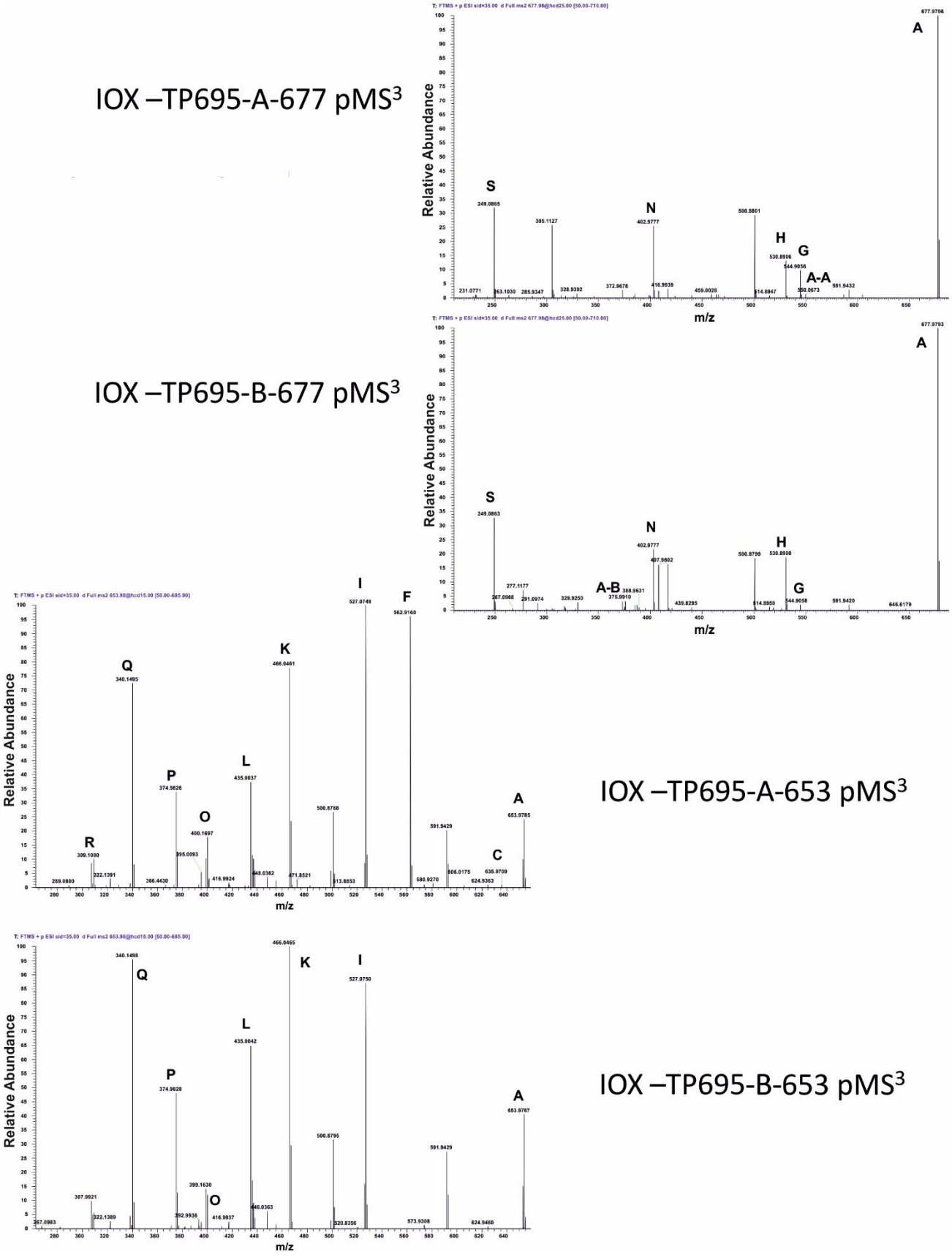

Figure SI-5.8-B MS^2 and pMS^3 spectra of Iohexol –TP695 A-B (IOX-TP695-A-B) – *continued*

IOX –TP695-A-604 pMS^3

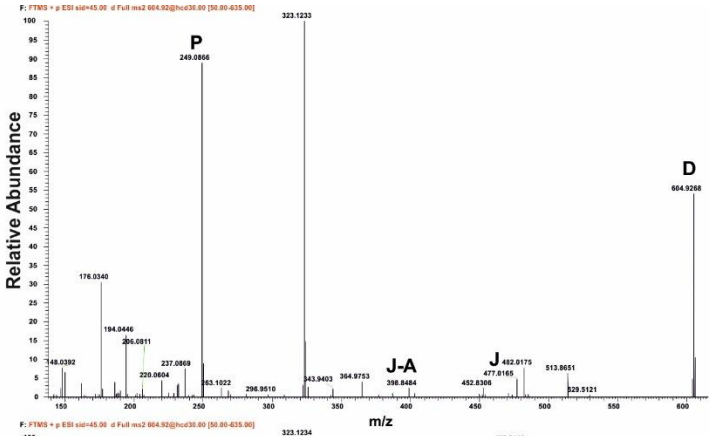

IOX –TP695-B-604 pMS^3

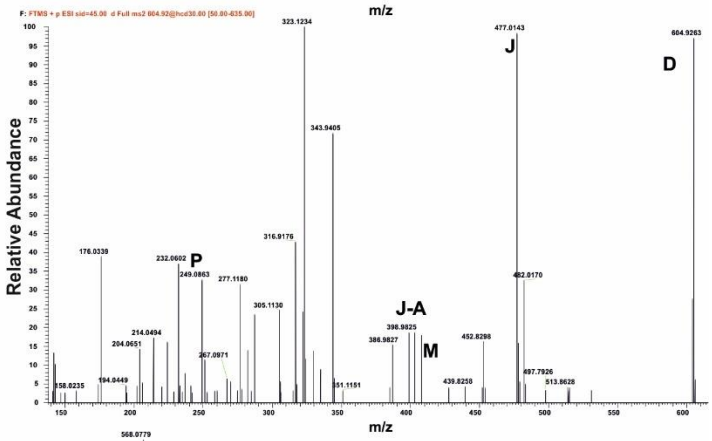

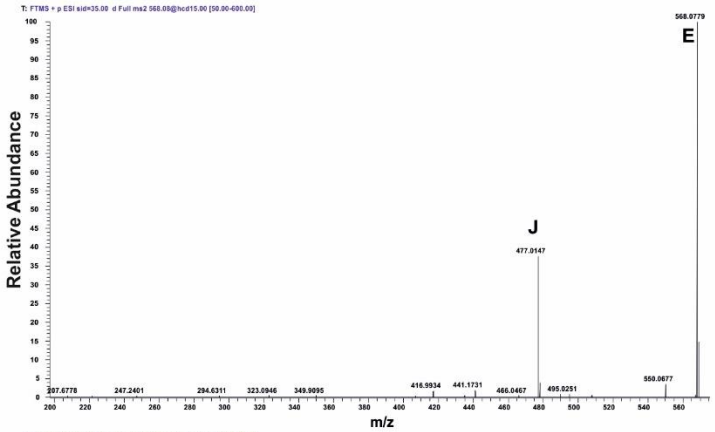

IOX –TP695-A-568 pMS^3

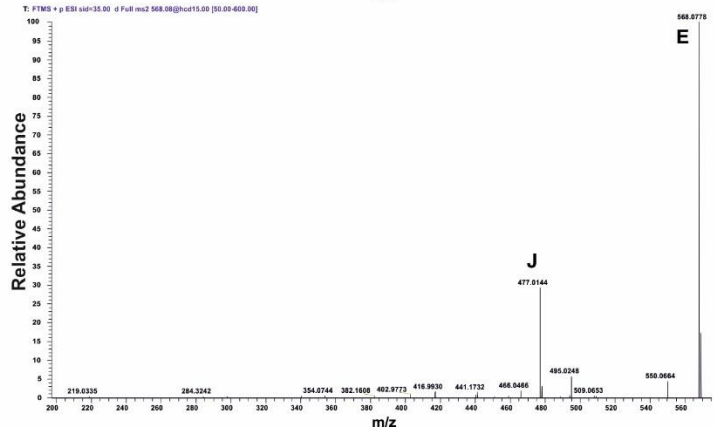

IOX –TP695-B-568 pMS^3

Figure SI-5.8-B MS² and pMS³ spectra of Iohexol –TP695 A-B (IOX-TP695-A-B) – *continued*

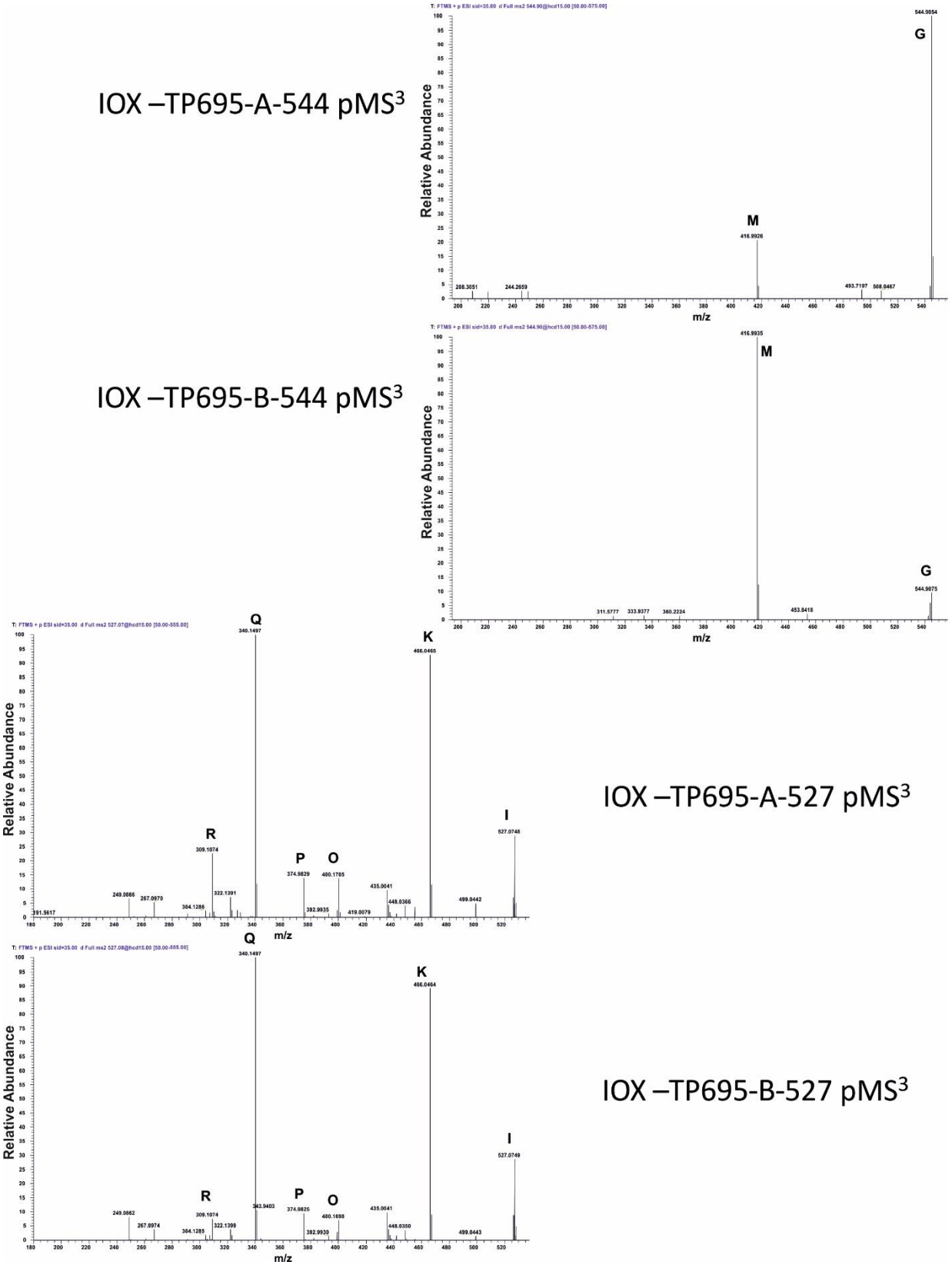

Figure SI-5.8-B MS² and pMS³ spectra of Iohexol –TP695 A-B (IOX-TP695-A-B) – *continued*

IOX –TP695-A-477 pMS³

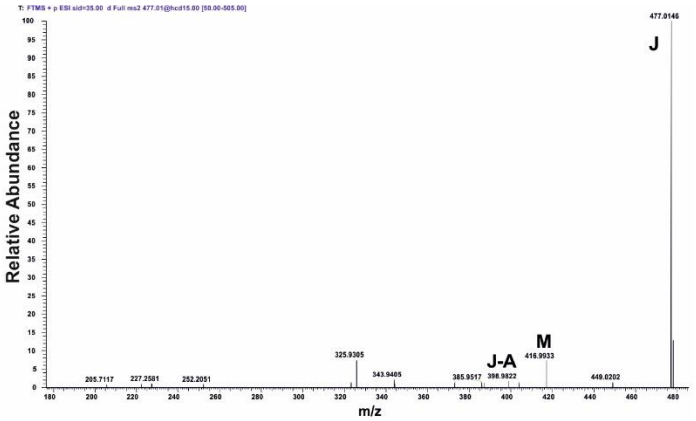

IOX –TP695-B-477 pMS³

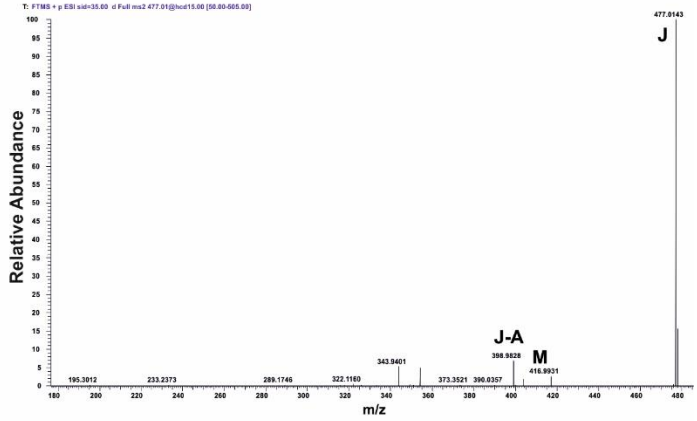

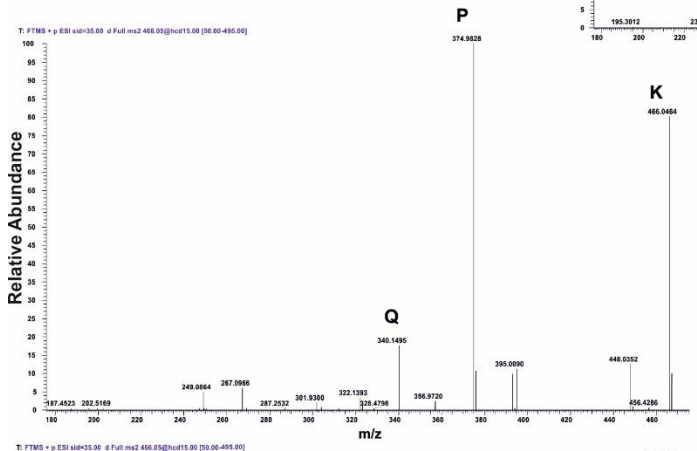

IOX –TP695-A-466 pMS³

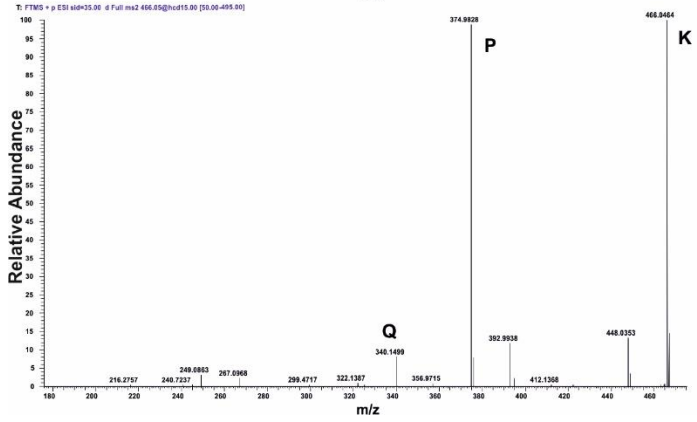

IOX –TP695-B-466 pMS³

Figure SI-5.8-B MS² and pMS³ spectra of Iohexol –TP695 A-B (IOX-TP695-A-B) – *continued*

IOX –TP695-A-562 pMS³

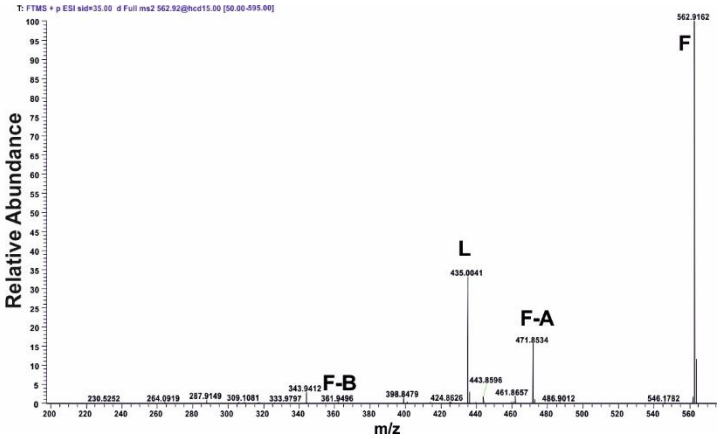

IOMEPROL (IMP)

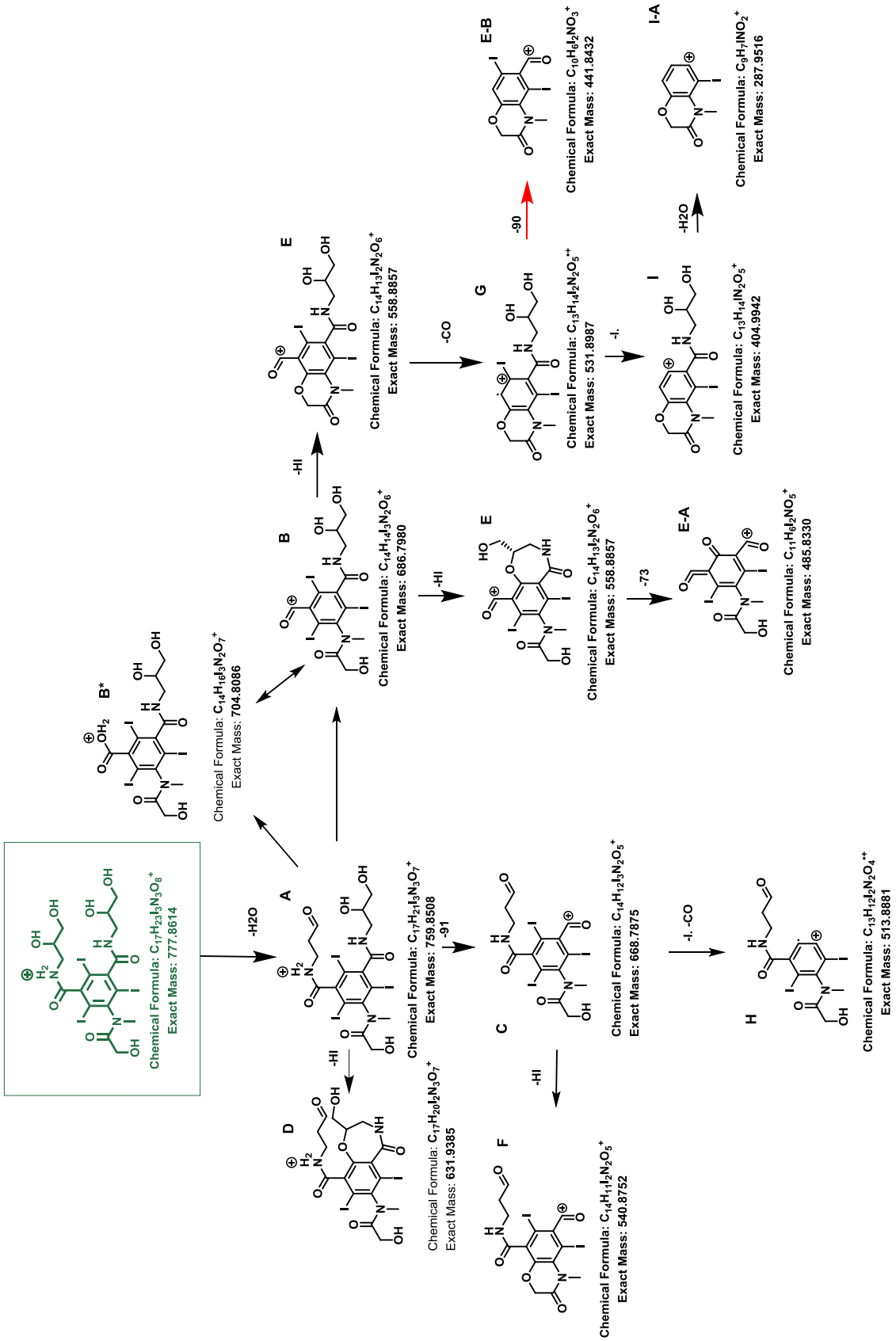

Figure SI-5.9-A. Fragmentation pattern of Iomeprol (IMP)

Figure SI-5.9-B. MS^2 and pMS^3 spectra of Iomeprol (IMP)

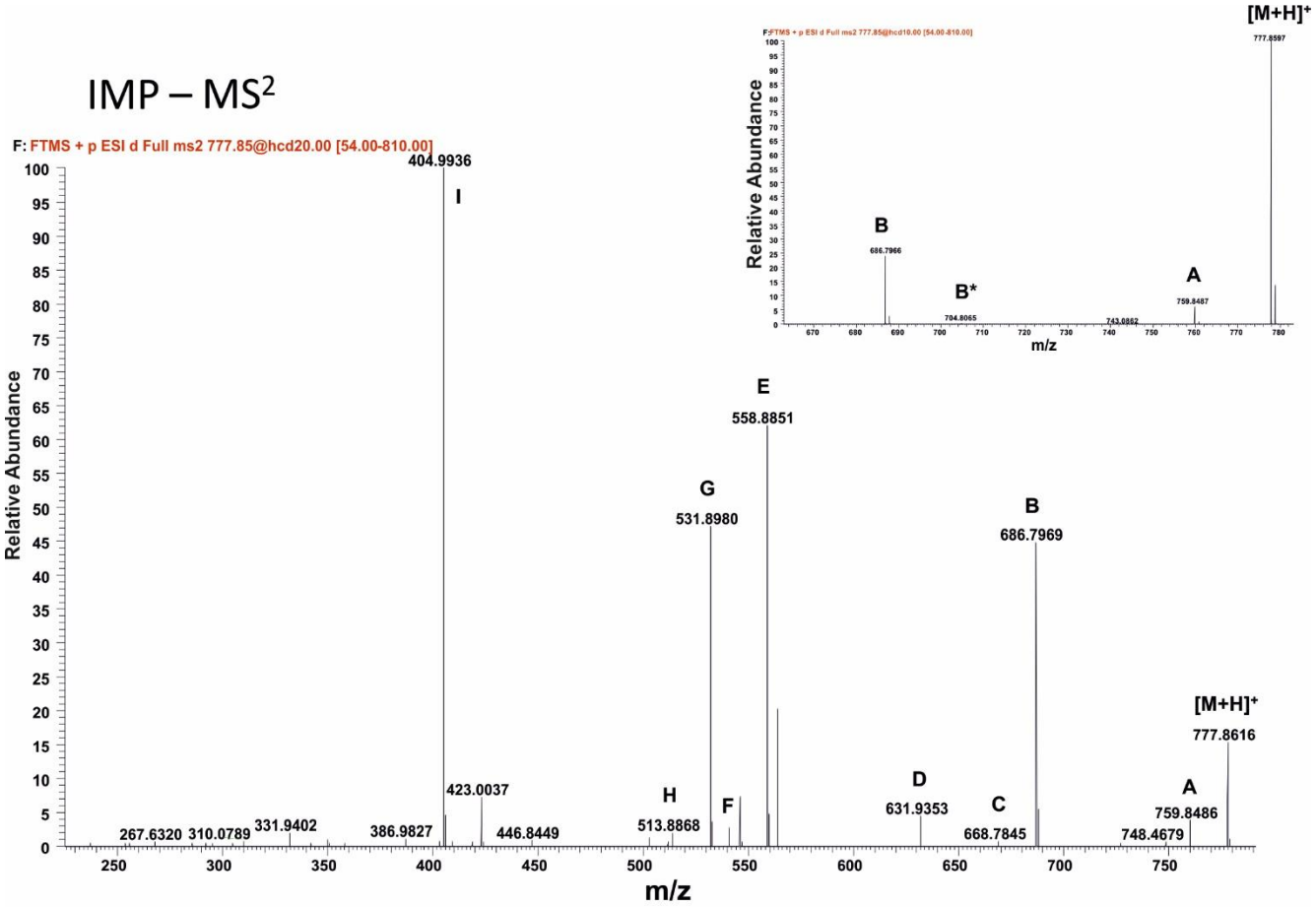

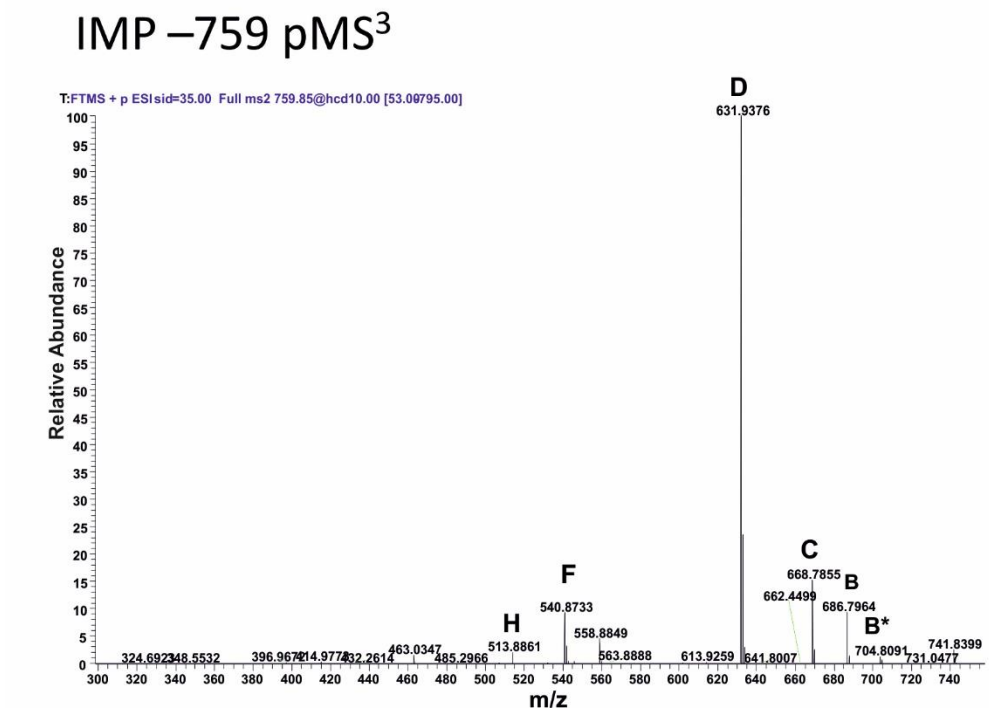

Figure SI-5.9-B. MS^2 and pMS^3 spectra of Iomeprol (IMP) – *continued*

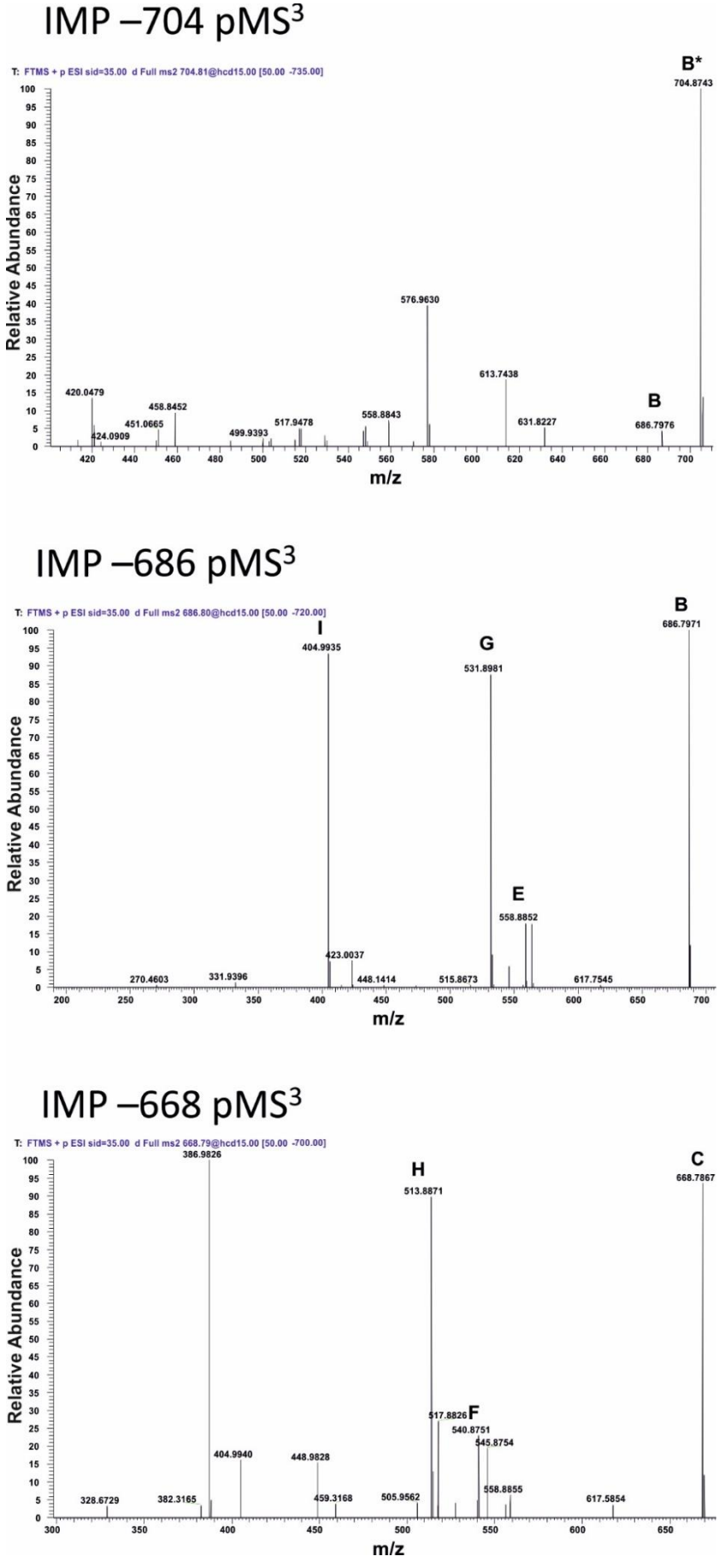

Figure SI-5.9-B. MS^2 and pMS^3 spectra of Iomeprol (IMP) – *continued*

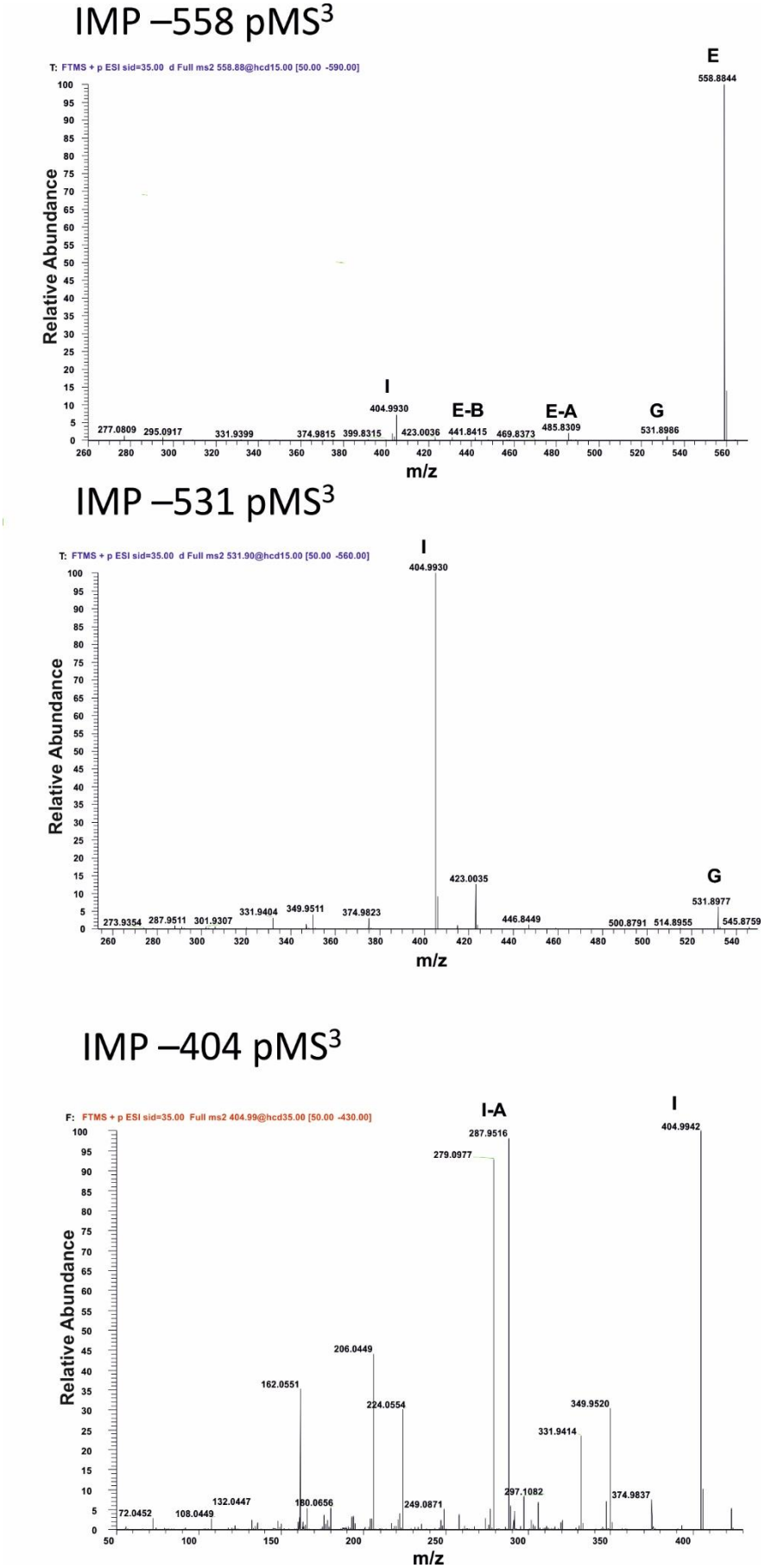

IOMEPROL TP651 A-B (IMP-TP651 A-B)

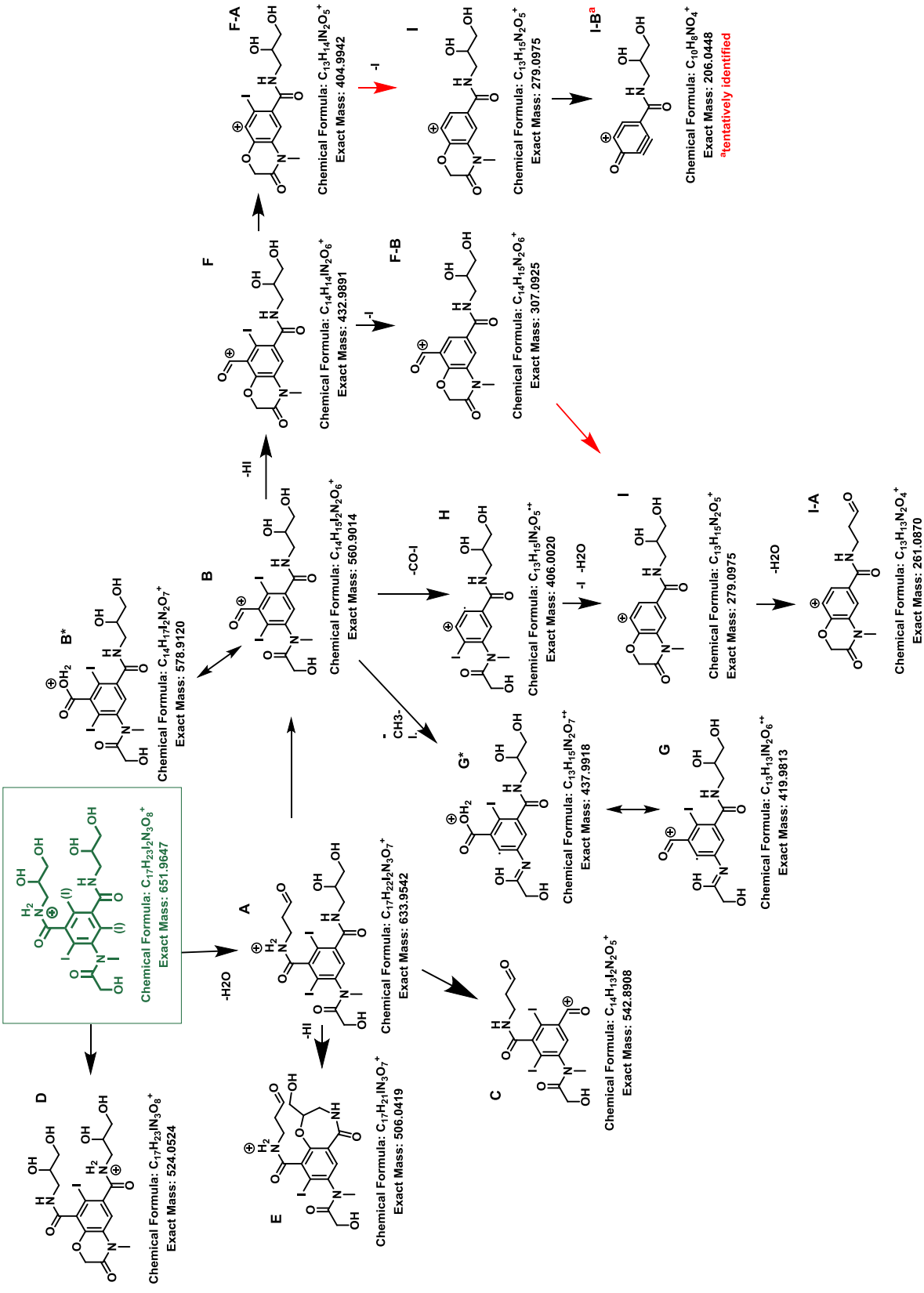

Figure SI-5.10-A. Fragmentation pattern of Iomeprol – TP651-A-B (IMP-TP651)

Figure SI-5.10-B. MS² and pMS³ spectra of Iomeprol – TP651-A-B (IMP-TP651)

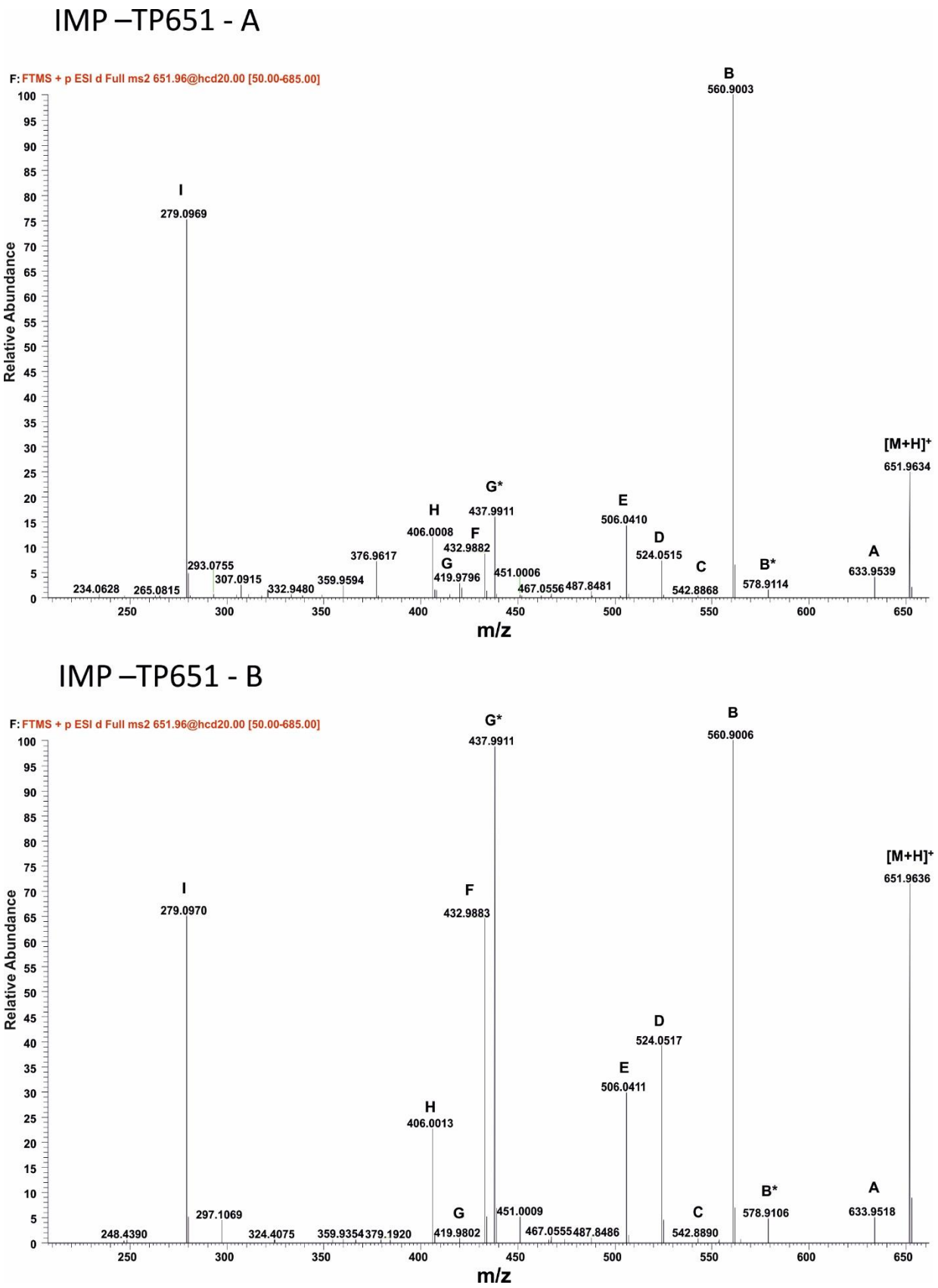

Figure SI-5.10-B. MS^2 and pMS^3 spectra of Iomeprol – TP651-A-B (IMP-TP651) – *continued*

IMP –TP651-B-633 pMS^3

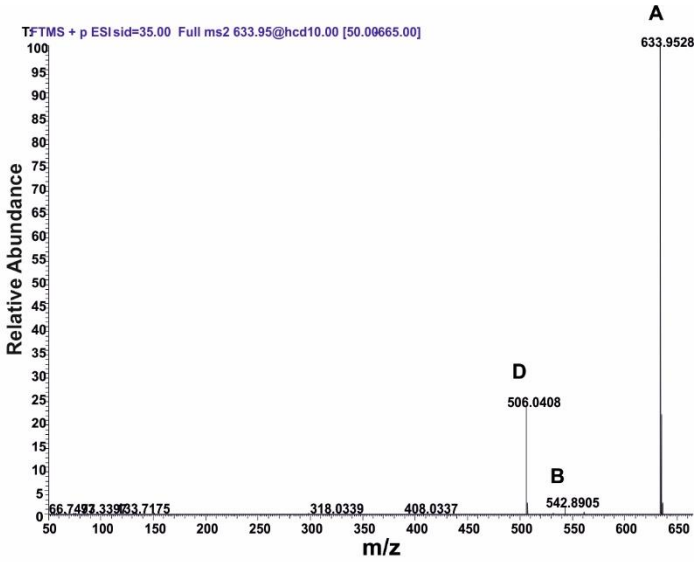

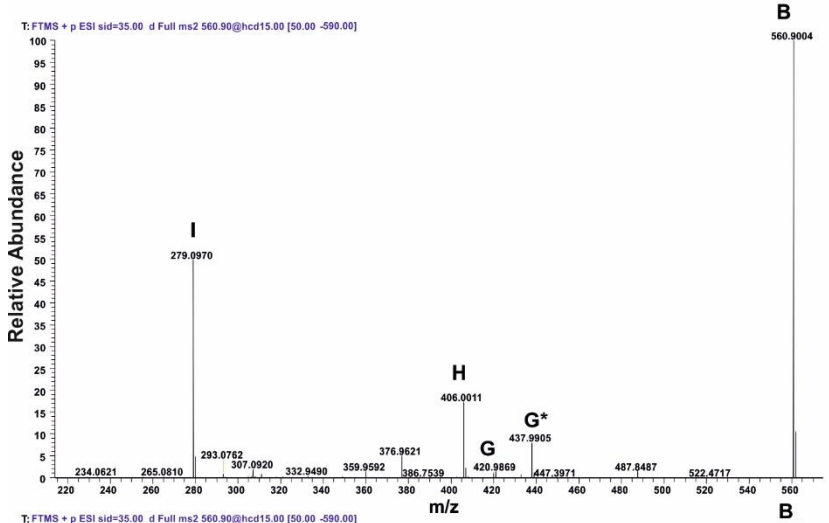

IMP –TP651-A-560 pMS^3

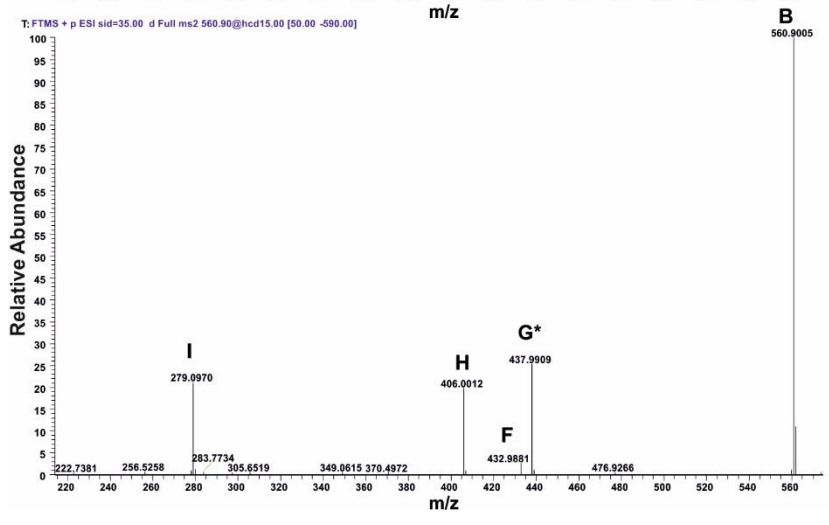

IMP –TP651-B-560 pMS^3

Figure SI-5.10-B. MS^2 and pMS^3 spectra of Iomeprol – TP651-A-B (IMP-TP651) – *continued*

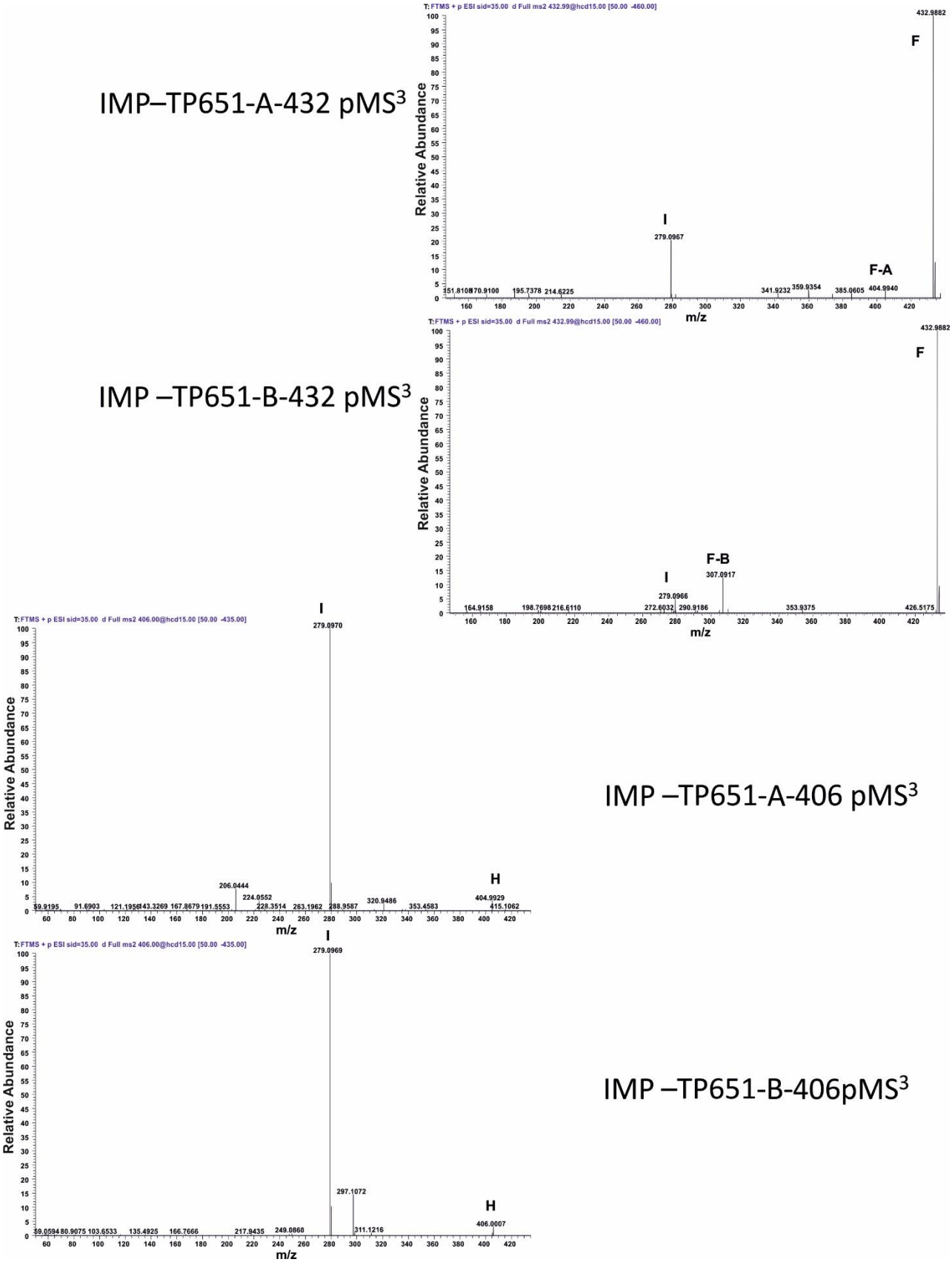

Figure SI-5.10-B. MS^2 and pMS^3 spectra of Iomeprol – TP651-A-B (IMP-TP651) – *continued*

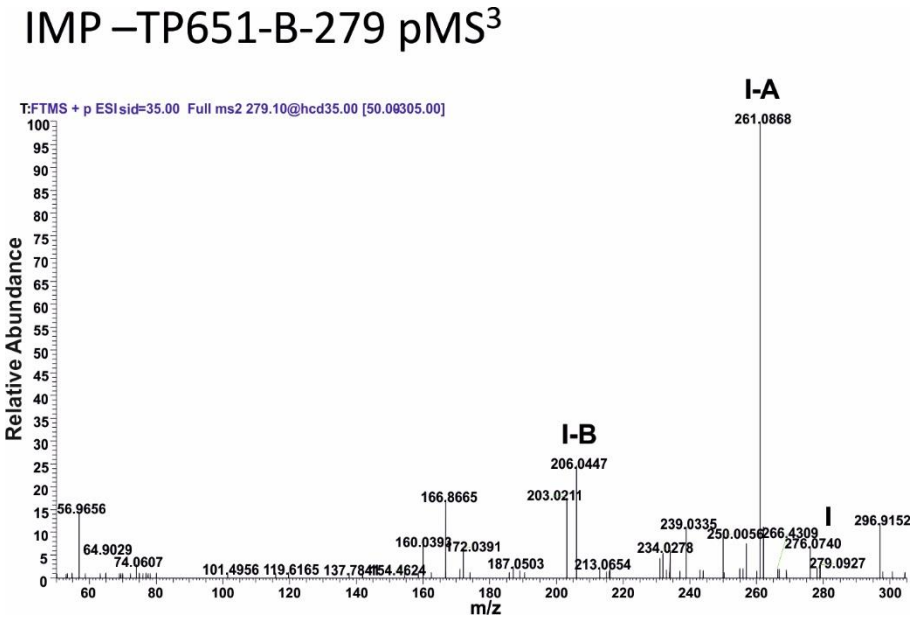

Figure SI-5.10-C. (HSQC)-NMR spectra of Iomeprol – TP651-B (IMP-TP651-B)

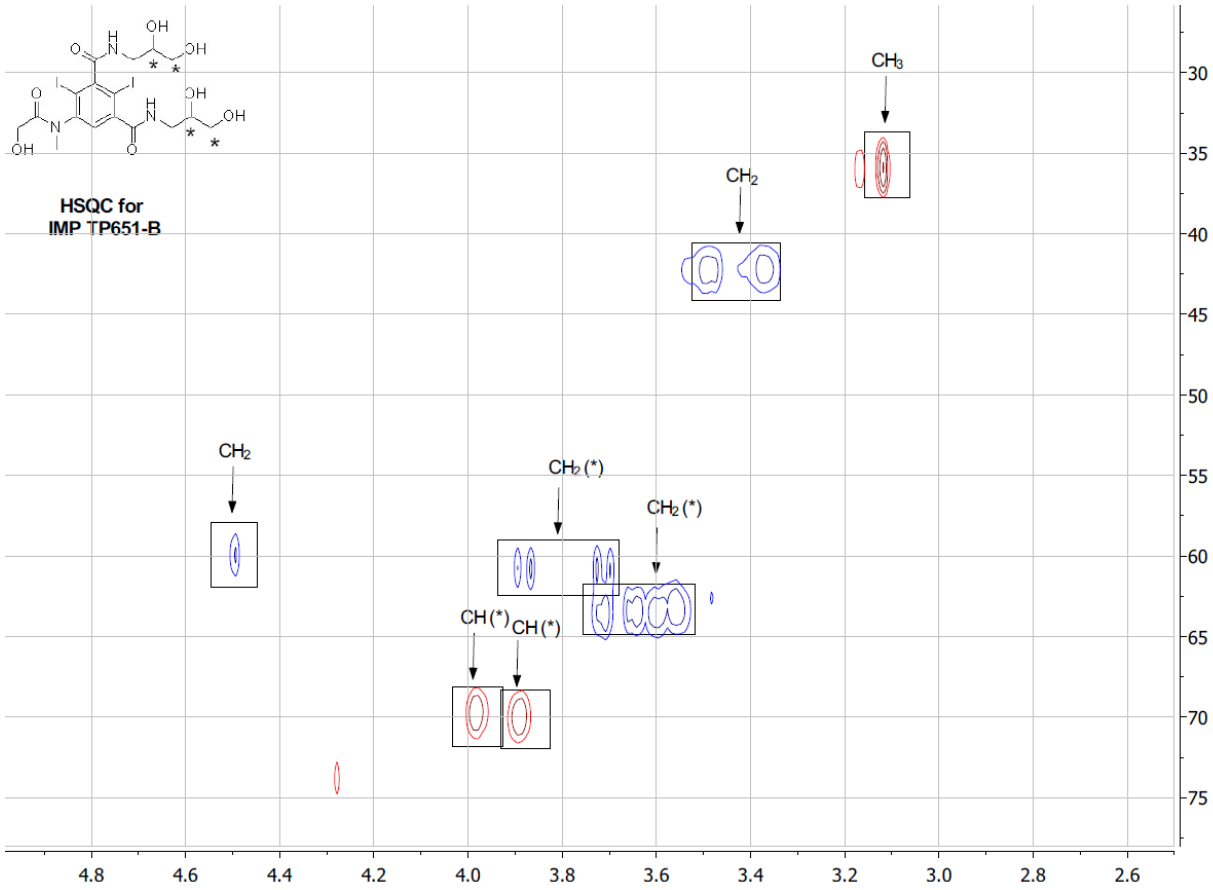

IOPAMIDOL (IPM)

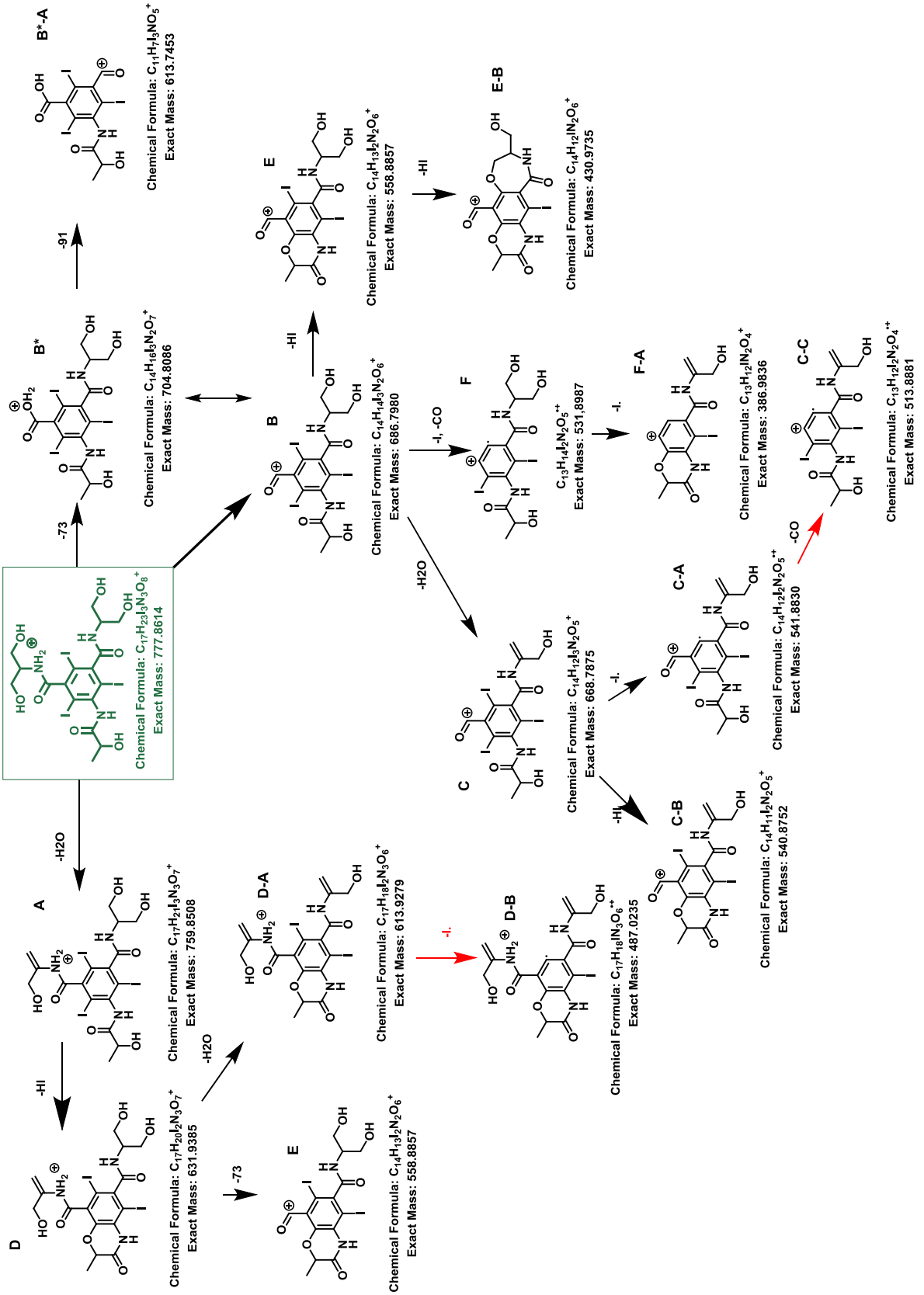

Figure SI-5.11-A. Fragmentation pattern of Iopamidol (IPM)

Figure SI-5.11-B. MS² and pMS³ spectra of Iopamidol (IPM)

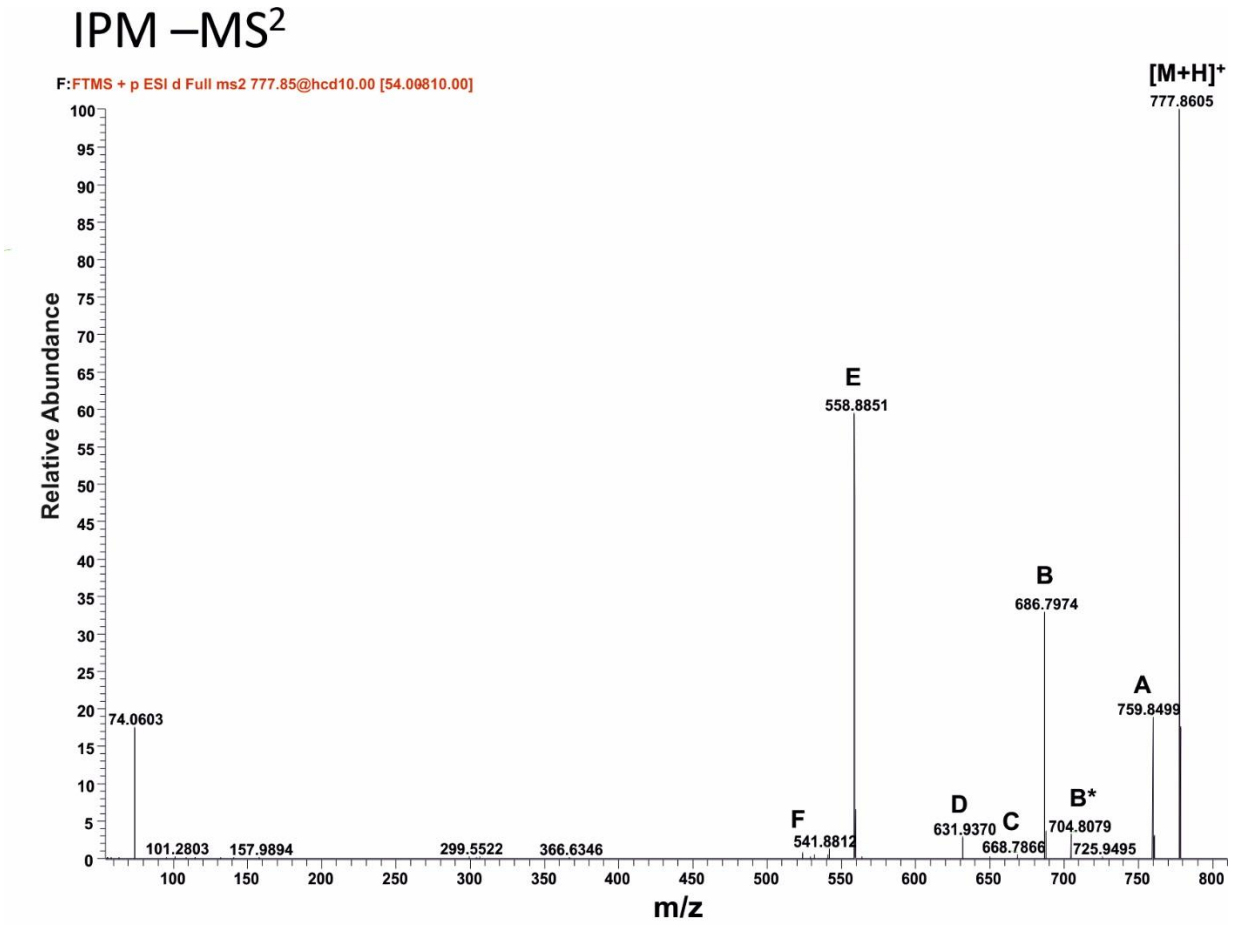

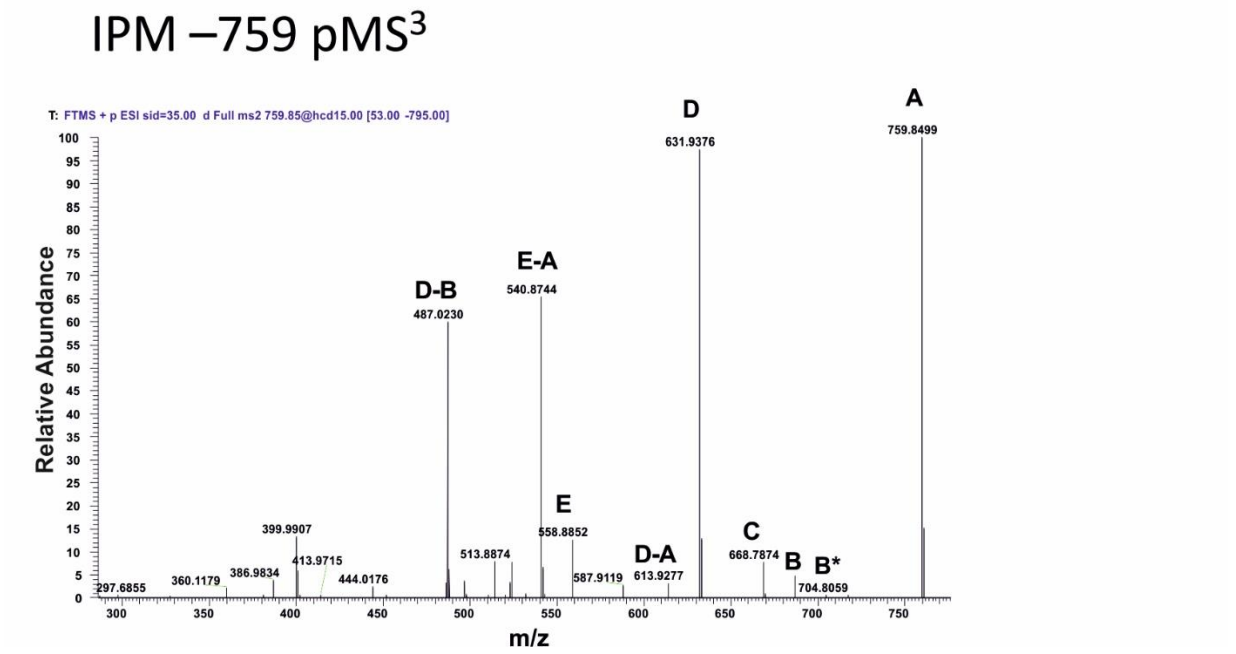

Figure SI-5.11-B. MS^2 and pMS^3 spectra of Iopamidol (IPM) – *continued*

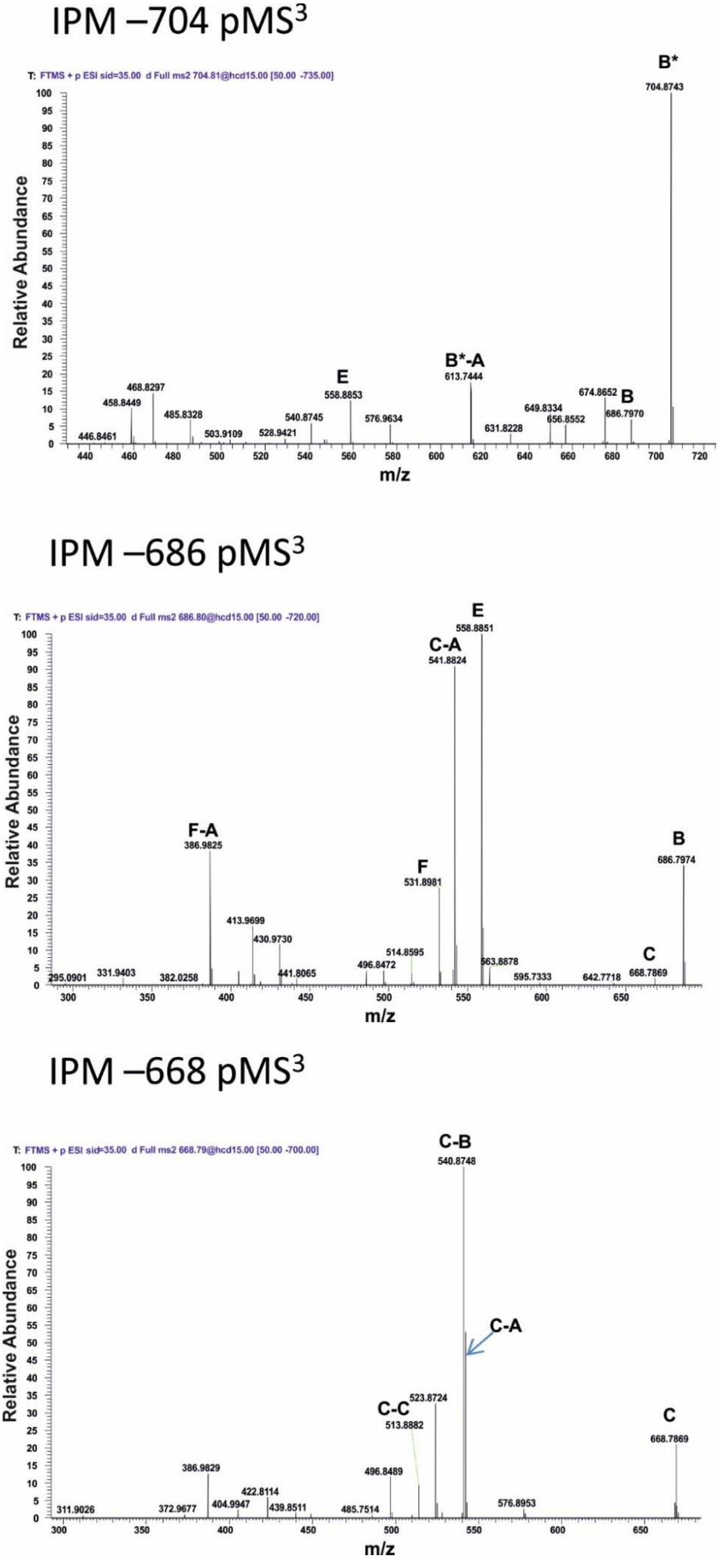

Figure SI-5.11-B. MS^2 and pMS^3 spectra of Iopamidol (IPM) – *continued*

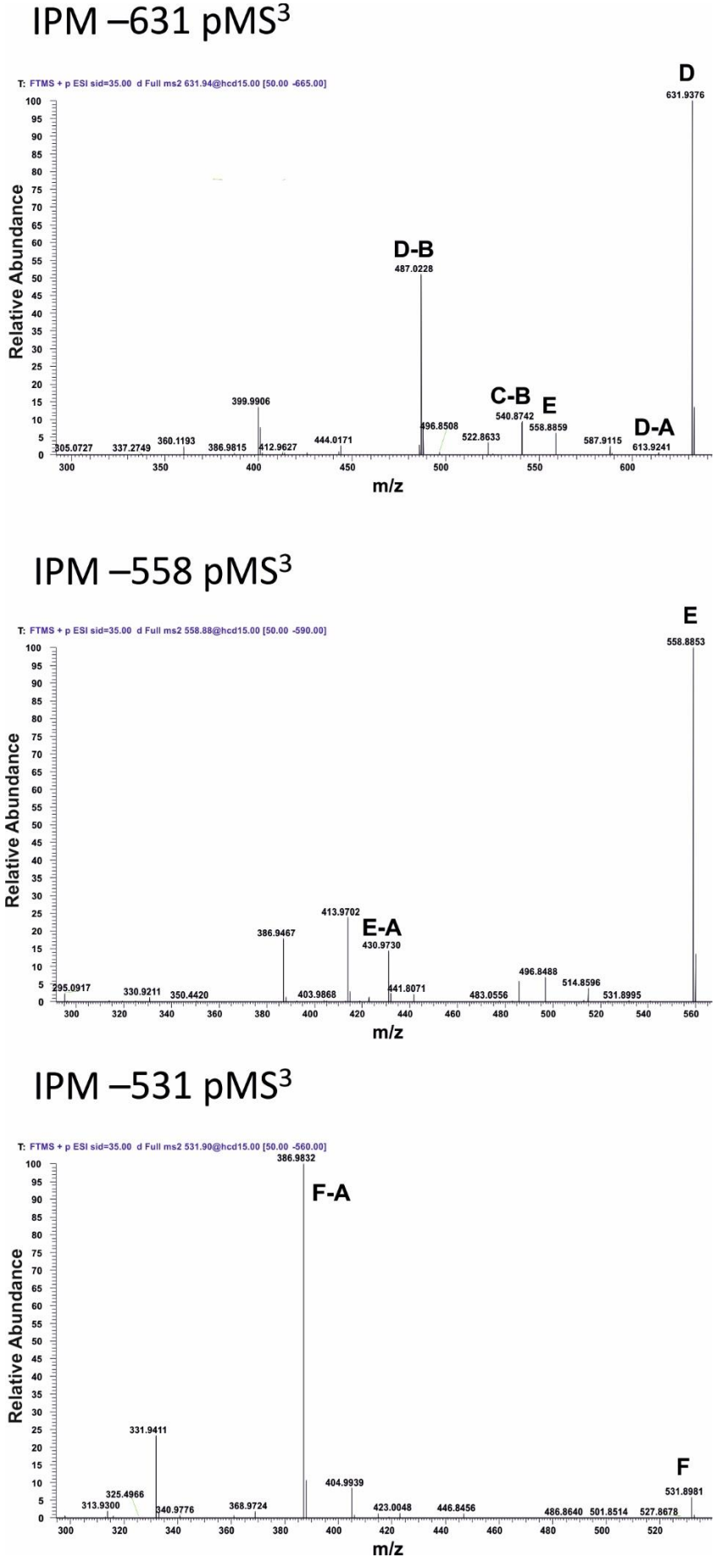

IOPAMIDOL TP667 (IPM-TP667)

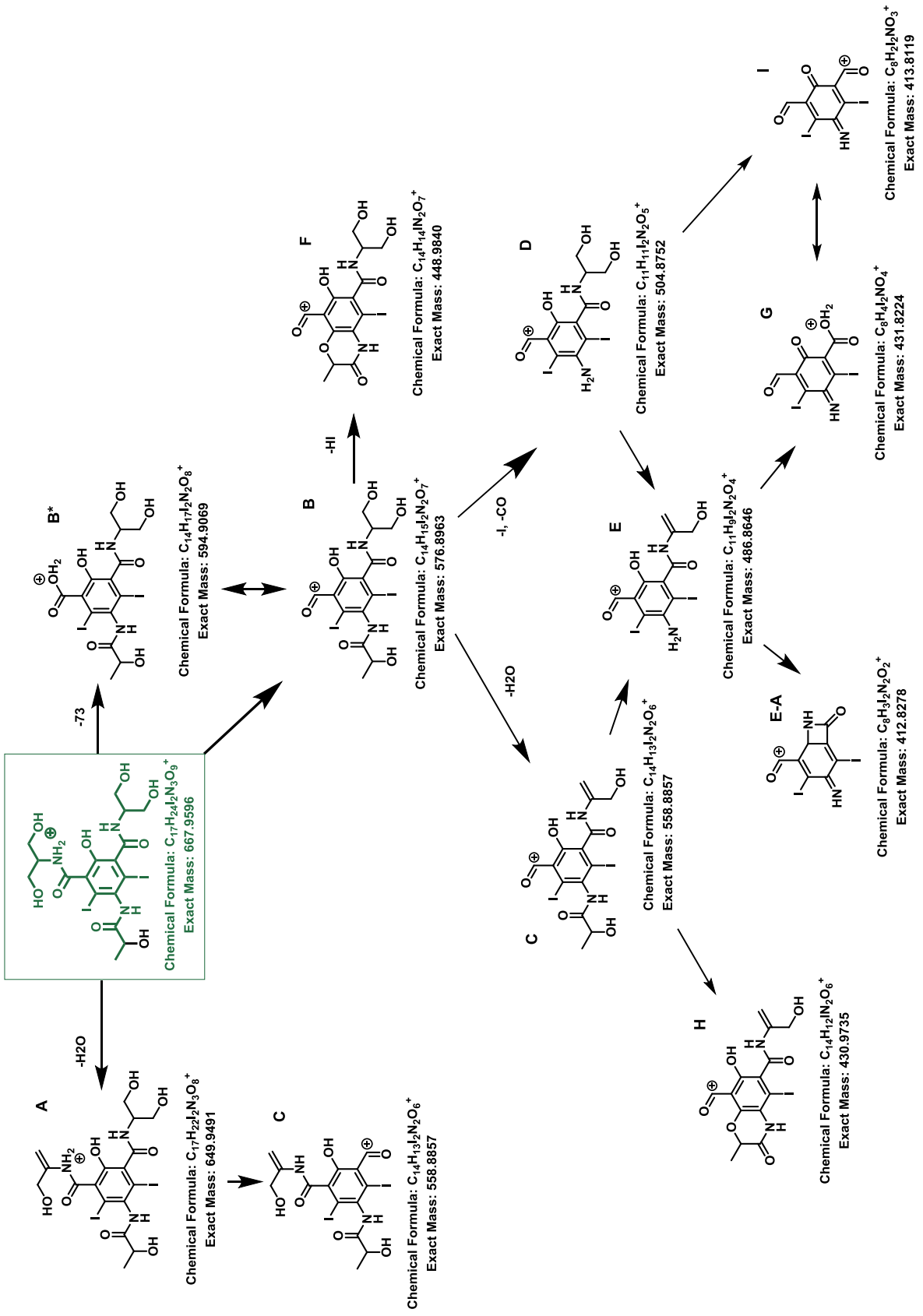

Figure SI-5.12-A. Fragmentation pattern of Iopamidol – TP667 (IPM-TP667)

Figure SI-5.12-B. MS² and pMS³ spectra of Iopamidol – TP667 (IPM-TP667)

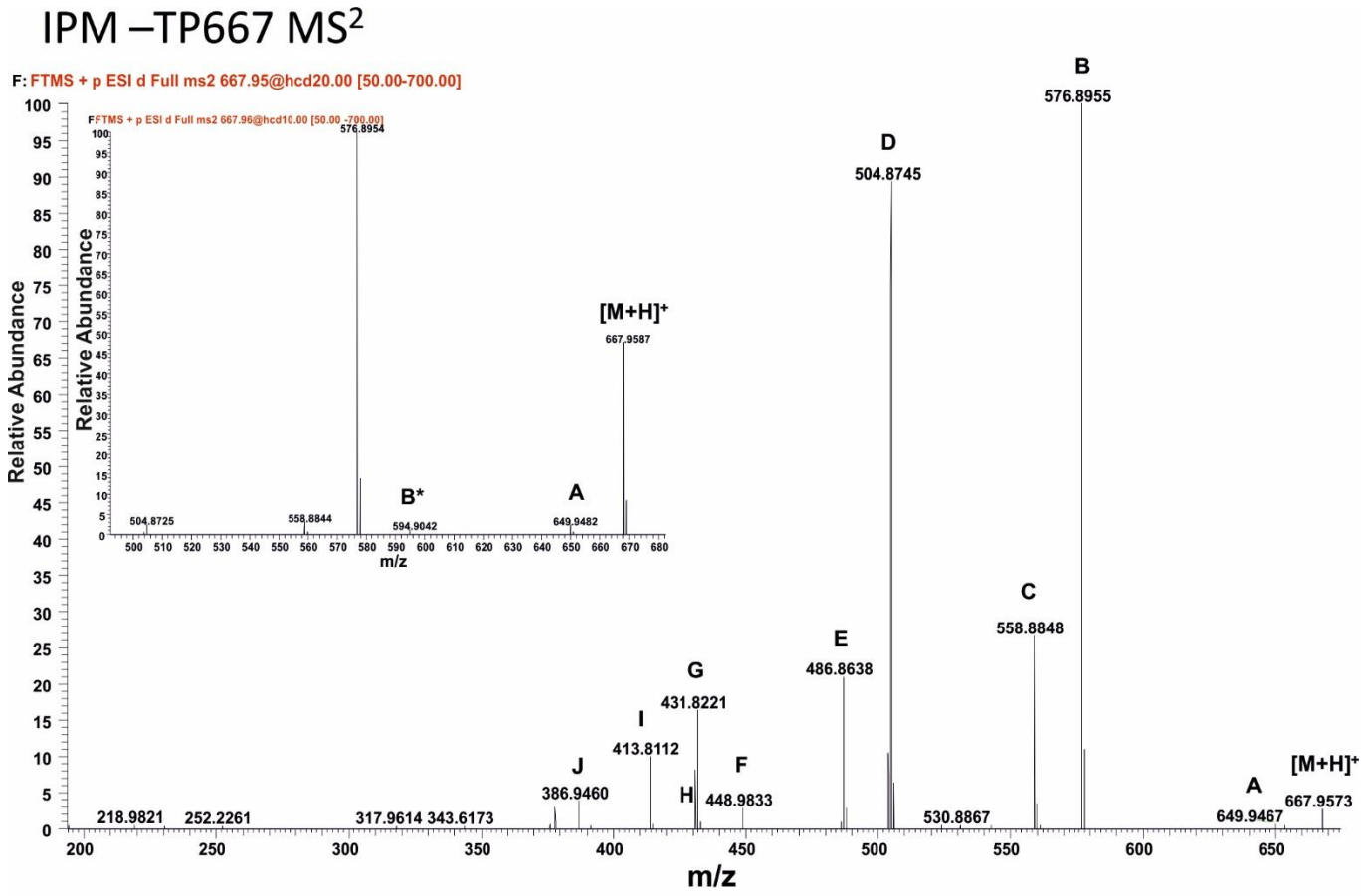

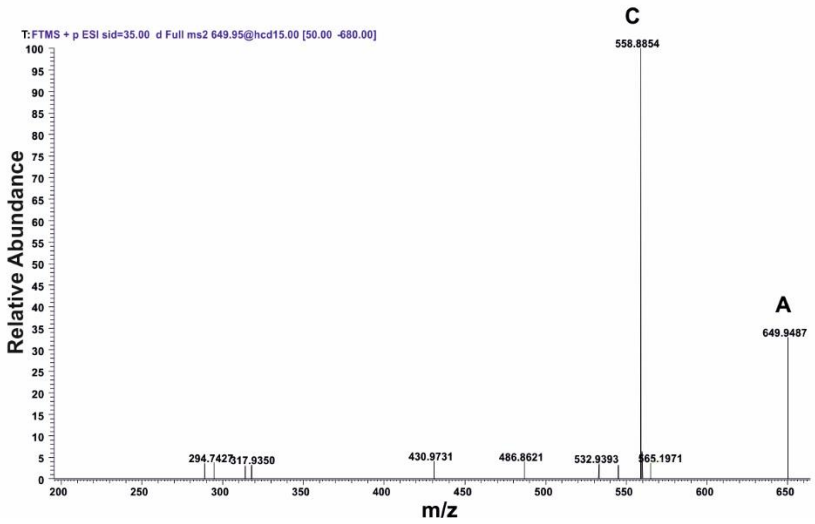

Figure SI-5.12-B. MS^2 and pMS^3 spectra of Iopamidol – TP667 (IPM-TP667) – *continued*

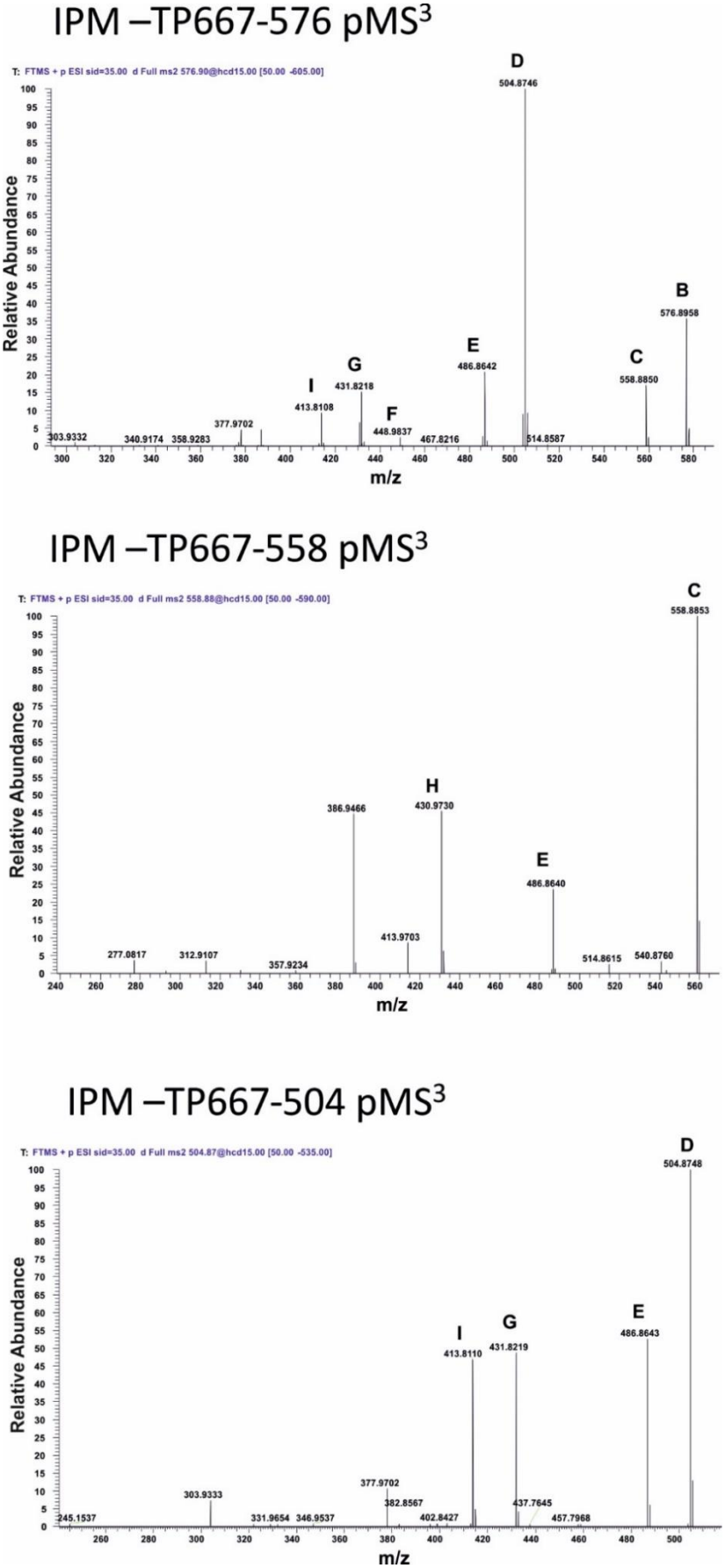

Figure SI-5.12-B. MS^2 and pMS^3 spectra of Iopamidol – TP667 (IPM-TP667) – *continued*

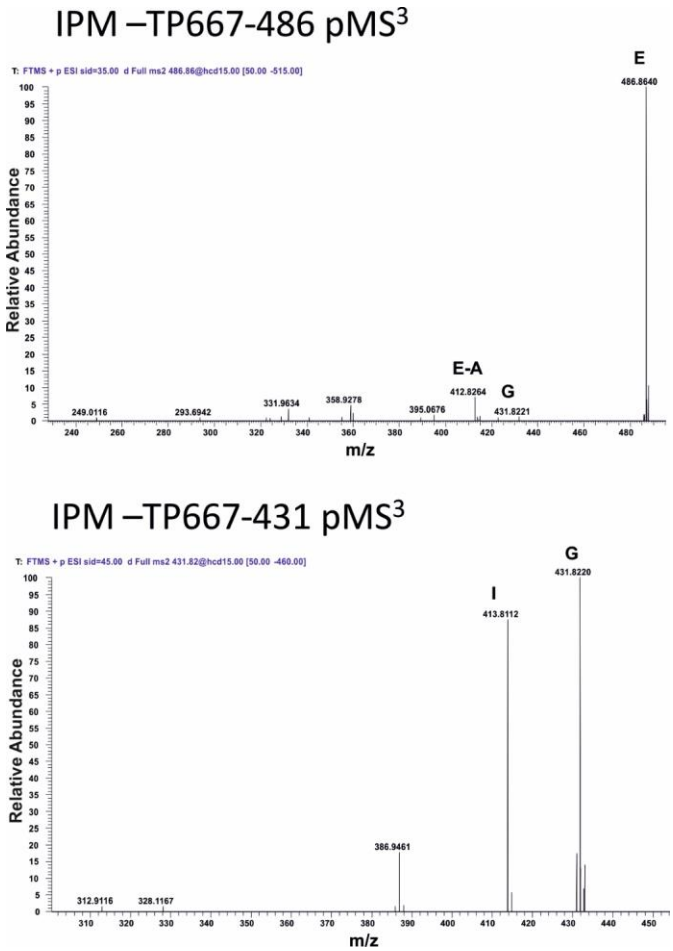

Figure SI-5.12-C. (HSQC)-NMR spectra of Iopamidol – TP667 (IPM-TP667)

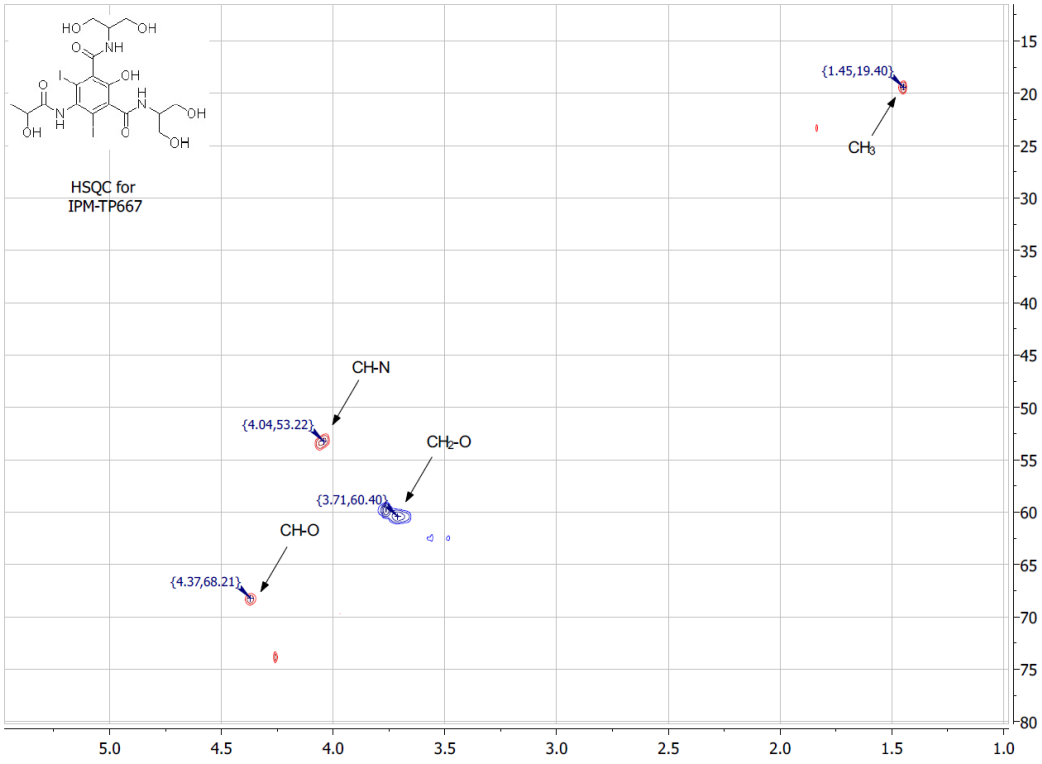

IOPAMIDOL- (IPM- d_3)

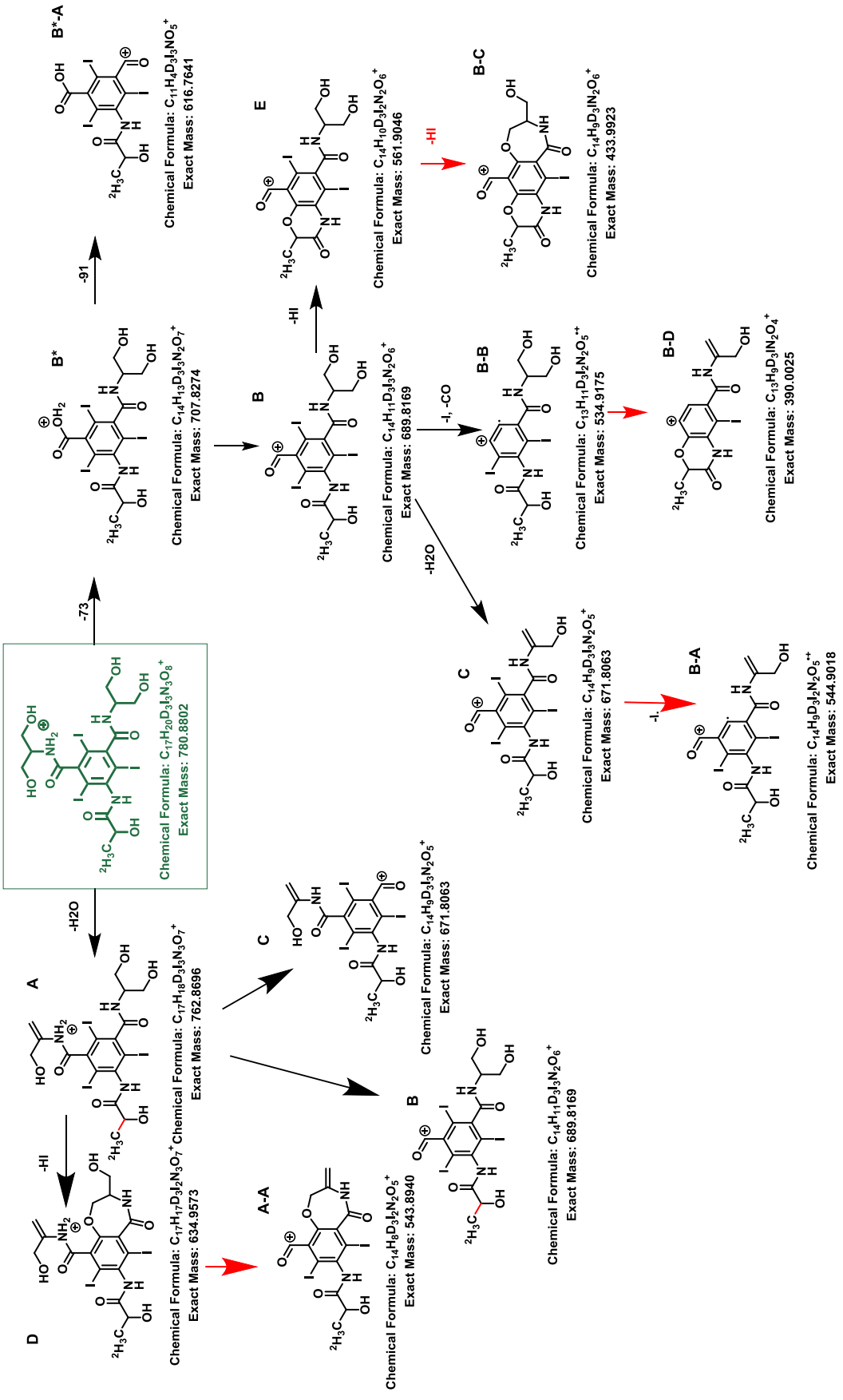

Figure SI-5.13-A. Fragmentation pattern of deuterated Iopamidol (IPM-d_3)

Figure SI-5.13-B. MS^2 and pMS^3 spectra of deuterated Iopamidol (IPM-d_3)

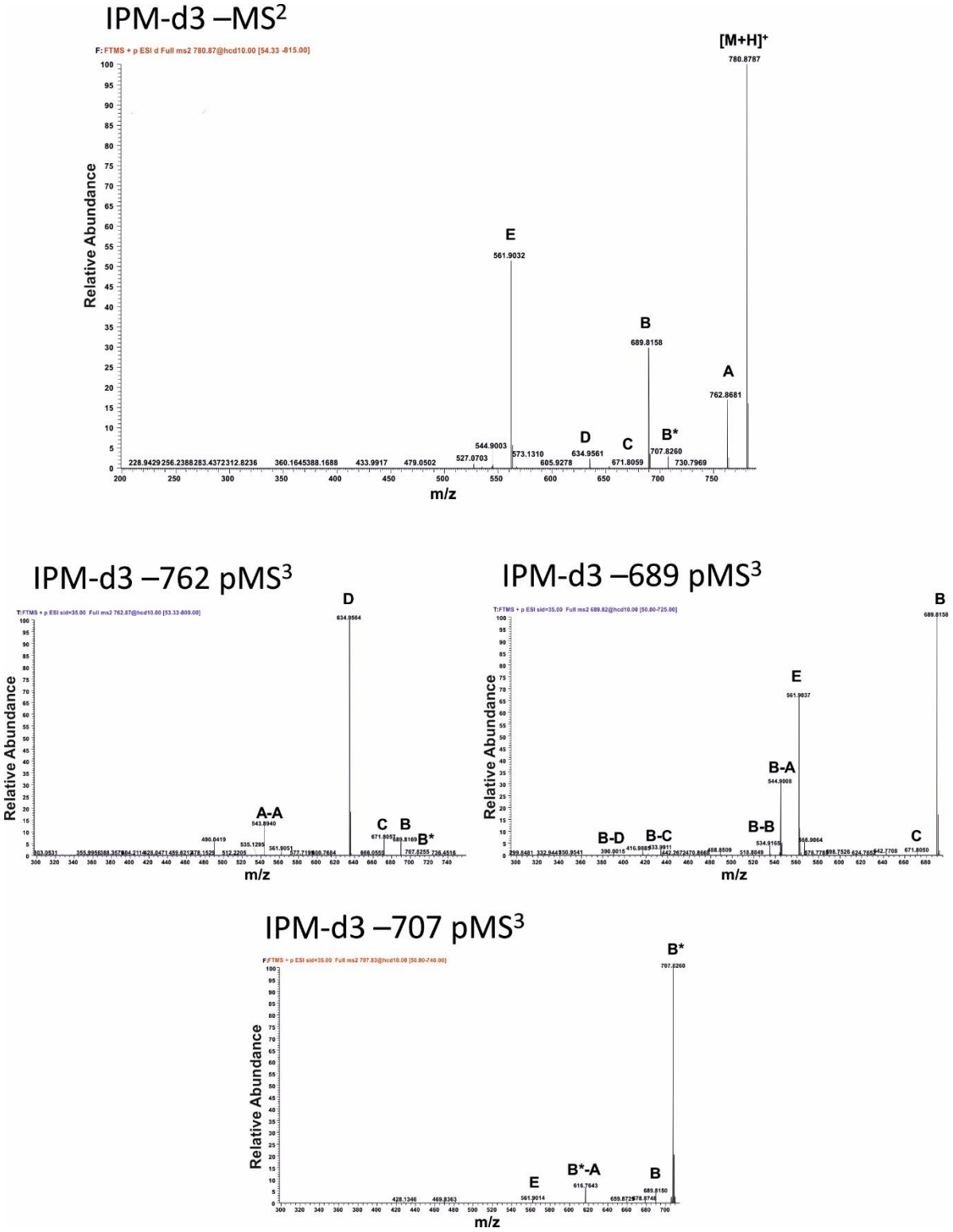

Table SI-3. Accurate mass measurements of protonated ICM photoproducts as determined by LC-QExactive-MS in MS/MS or pseudo MS³ modes

Nominal ion mass	Measured mass [m/z]	Mass error [ppm]	Elemental composition	Calculated mass [m/z]	DBE[a]
IODIXANOL					
$[M+H]^+$	1550.7198	-0.5	$C_{35}H_{45}N_6O_{15}I_6$	1550.7205	13.5
A 1532	1532.7068	-6.6	$C_{35}H_{43}N_6O_{14}I_6$	1532.7105	14.5
A-A 1514	1514.6959	-2.3	$C_{35}H_{41}N_6O_{13}I_6$	1514.6994	15.5
A-B 1490	1490.6949	-2.9	$C_{33}H_{41}N_6O_{13}I_6$	1490.6994	13.5
A-C 1404	1404.7909	-4.8	$C_{35}H_{42}N_5O_{14}I_5$	1404.7977	15.5
F 743	743.8552	-0.9	$C_{17}H_{21}N_3O_6I_3$	743.8559	7.5
G 652	652.7917	-1.2	$C_{14}H_{12}N_2O_4I_3$	652.7926	8.5
B 1508	1508.7080	-6.0	$C_{33}H_{43}N_6O_{14}I_6$	1508.7100	12.5
B-A 1490	1490.6854	-1.8	$C_{33}H_{41}N_6O_{13}I_6$	1490.6994	13.5
B-C 1417	1417.6362	0.6	$C_{30}H_{34}N_5O_{12}I_6$	1417.6467	13.5
E 803	803.8762	-1.0	$C_{19}H_{25}N_3O_8I_3$	803.8770	7.5
C 1459	1459.6545	-1.8	$C_{32}H_{36}N_5O_{13}I_6$	1459.6572	14.5
C-A 1441	1441.6451	-1.1	$C_{32}H_{34}N_5O_{12}I_6$	1441.6467	15.5
D 1399	1399.6334	-1.9	$C_{30}H_{32}N_5O_{11}I_6$	1399.6361	14.5
F 743	743.8544	-1.9	$C_{17}H_{21}N_3O_6I_3$	743.8559	7.5
D 1399	1399.6274	-1.9	$C_{30}H_{32}N_5O_{11}I_6$	1399.6361	14.5
D-A 1381	1381.6226	-2.0	$C_{30}H_{30}N_5O_{10}I_6$	1381.6255	15.5
D-B 1308	1308.5698	-2.1	$C_{27}H_{23}N_4O_9I_6$	1308.5728	15.5
G 652	652.7930	-1.2	$C_{14}H_{12}N_2O_4I_3$	652.7926	8.5
E 803	803.8784	1.7	$C_{19}H_{25}N_3O_8I_3$	803.8770	7.5
E-A 626	626.7773	0.6	$C_{12}H_{10}N_2O_4I_3$	626.7769	7.5
F 743	743.8548	-1.3	$C_{17}H_{21}N_3O_6I_3$	743.8559	7.5
G 652	652.7916	-1.3	$C_{14}H_{12}N_2O_4I_3$	652.7926	8.5
G-A 524	524.8798	-0.8	$C_{14}H_{11}N_2O_4I_2$	524.8803	9.5
G 652	652.7909	-1.8	$C_{14}H_{12}N_2O_4I_3$	652.7926	8.5
G-A 524	524.8791	-2.0	$C_{14}H_{11}N_2O_4I_2$	524.8803	9.5

Nominal ion mass	Measured mass [m/z]	Mass error [ppm]	Elemental composition	Calculated mass [m/z]	DBE[a]
TP IDX 747					
[M+H]+	747.8503	-0.6	$C_{16}H_{21}N_3O_7I_3$	747.8508	6.5
A 729	729.8398	-0.5	$C_{16}H_{19}N_3O_6I_3$	729.8402	7.5
B 674	674.7972	-1.2	$C_{13}H_{14}N_2O_6I_3$	674.7980	6.5
C 656	656.7858	-2.6	$C_{13}H_{12}N_2O_5I_3$	656.7875	7.5
D 638	638.7754	-2.3	$C_{13}H_{10}N_2O_4I_3$	638.7769	8.5
E 601	601.9267	-2.0	$C_{16}H_{18}N_3O_6I_2$	601.9279	8.5
F 528	528.8736	-3.0	$C_{13}H_{11}N_2O_5I_2$	528.8752	8.5
G 510	510.8636	-2.0	$C_{13}H_9N_2O_4I_2$	510.8646	9.5
B 674	674.7972	-1.2	$C_{13}H_{14}N_2O_6I_3$	674.7980	6.5
C 656	656.7865	-1.5	$C_{13}H_{12}N_2O_5I_3$	656.7875	7.5
B-A 583	583.7337	-1.7	$C_{10}H_5NO_4I_3$	583.7347	7.5
F 528	528.8747	-0.9	$C_{13}H_{11}N_2O_5I_2$	528.8752	8.5
B-B 455	455.8213	-2.4	$C_{10}H_4N_2O_4I_2$	455.8224	8.5
C 656	656.7869	-0.9	$C_{13}H_{12}N_2O_5I_3$	656.7875	7.5
D 638	638.7746	-3.6	$C_{13}H_{10}N_2O_4I_3$	638.7769	7.5
F 528	528.8744	-1.5	$C_{13}H_{11}N_2O_5I_2$	528.8752	8.5
D 638	638.7768	-0.2	$C_{13}H_{10}N_2O_4I_3$	638.7769	8.5
G 510	510.8643	-0.6	$C_{13}H_9N_2O_4I_2$	510.8646	9.5
E 601	601.9278	-0.2	$C_{16}H_{18}N_3O_6I_2$	601.9279	8.5
F 528	528.8741	-2.1	$C_{13}H_{11}N_2O_5I_2$	528.8752	8.5
G 510	510.8638	-1.6	$C_{13}H_9N_2O_4I_2$	510.8646	9.5
F 528	528.8750	-0.4	$C_{13}H_{11}N_2O_5I_2$	528.8752	8.5
G 510	510.8669	4.5	$C_{13}H_9N_2O_4I_2$	510.8646	9.5
F-A 426	426.8430	-1.2	$C_9H_5N_2O_2I_2$	426.8435	7.5
H 411	411.8319	-1.7	$C_9H_4NO_2I_2$	411.8326	7.5
F-B 355	355.8422	-1.7	$C_7H_4NI_2$	355.8428	5.5
F-C 299	299.9387	-1.0	$C_9H_5N_2O_2I$	299.9390	8.0
F-D 284	284.9276	-1.8	$C_9H_4NO_2I$	284.9281	8.0
G 510	510.8662	3.1	$C_{13}H_9N_2O_4I_2$	510.8646	9.5
H 501	501.8882	0.2	$C_{12}H_{12}N_2O_6I_2$	501.8881	7.0

Nominal ion mass	Measured mass [m/z]	Mass error [ppm]	Elemental composition	Calculated mass [m/z]	DBE[a]
I 411	411.8319	-1.7	$C_9H_4NO_2I_2$	411.8326	7.5
I-A 383	383.8371	-1.6	$C_8H_4NOI_2$	383.8377	6.5
I-B 355	355.8422	-1.7	$C_7H_4NI_2$	355.8428	5.5
J 374	374.9831	-1.4	$C_{12}H_{12}N_2O_4I$	374.9836	7.5
IOPROMIDE					
[M+H]+	791.8776	0.8	$C_{18}H_{25}N_3O_8I_3$	791.8770	6.5
A 773	773.8665	0.0	$C_{18}H_{23}N_3O_7I_3$	773.8665	7.5
C 686	686.7985	0.7	$C_{14}H_{14}N_2O_6I_3$	686.7980	7.5
A-A 668	668.7827	-7.2	$C_{14}H_{12}N_2O_5I_3$	668.7875	8.5
D 645	645.9527	-2.3	$C_{18}H_{22}N_3O_7I_2$	645.9542	8.5
F 558	558.8849	-1.4	$C_{14}H_{13}N_2O_6I_2$	558.8857	8.5
G 540	540.8727	-4.6	$C_{14}H_{11}N_2O_5I_2$	540.8752	9.5
I 527	527.8652	-4.2	$C_{13}H_{10}N_2O_5I_2$	527.8674	9.0
B* 718	718.8281	5.3	$C_{15}H_{18}N_2O_7I_3$	718.8243	6.5
B 700	700.8130	-1.0	$C_{15}H_{16}N_2O_6I_3$	700.8137	7.5
E 572	572.8988	-4.5	$C_{15}H_{15}N_2O_6I_3$	572.9014	8.5
B 700	700.8133	-0.6	$C_{15}H_{16}N_2O_6I_3$	700.8137	7.5
B-A* 577	577.9040	-0.2	$C_{14}H_{16}N_2O_7I_2$	577.9041	7.0
E 572	572.9005	-1.6	$C_{15}H_{15}N_2O_6I_3$	572.9014	8.5
B-A 559	559.8910	-4.6	$C_{13}H_{12}N_2O_6I_2$	559.8936	8.0
E-B 485	485.8323	-1.4	$C_{11}H_6NO_5I_2$	485.8330	8.5
K 413	413.9697	-2.4	$C_{14}H_{11}N_2O_5I$	413.9707	10.0
C 686	686.7974	-0.9	$C_{14}H_{14}N_2O_6I_3$	686.7980	7.5
C-A* 563	563.8876	-1.6	$C_{13}H_{14}N_2O_7I_2$	563.8885	7.0
F 558	558.8845	-2.1	$C_{14}H_{13}N_2O_6I_2$	558.8857	8.5
G 540	540.8744	-1.5	$C_{14}H_{11}N_2O_5I_2$	540.8752	9.5
I 527	527.8663	-2.1	$C_{13}H_{10}N_2O_5I_2$	527.8674	9.0
D 645	645.9551	1.4	$C_{18}H_{22}N_3O_7I_2$	645.9542	8.5
F 558	558.8855	-0.4	$C_{14}H_{13}N_2O_6I_2$	558.8857	8.5
G 540	540.8757	0.9	$C_{14}H_{11}N_2O_5I_2$	540.8752	9.5

Nominal ion mass	Measured mass [m/z]	Mass error [ppm]	Elemental composition	Calculated mass [m/z]	DBE[a]
E 572	572.9009	-0.9	$C_{15}H_{15}N_2O_6I_2$	572.9014	8.5
G 540	540.8730	-4.1	$C_{14}H_{11}N_2O_5I_2$	540.8752	9.5
E-A 516	516.8749	-0.6	$C_{12}H_{11}N_2O_5I_2$	516.8752	7.5
E-B* 503	503.8421	-2.8	$C_{11}H_8NO_6I_2$	503.8435	7.5
E-B 485	485.8325	-1.0	$C_{11}H_6NO_5I_2$	485.8330	8.5
J 444	444.9878	-2.9	$C_{15}H_{14}N_2O_6I$	444.9891	9.5
K 413	413.9695	-2.9	$C_{14}H_{11}N_2O_5I$	413.9707	10.0
F 558	558.8855	-0.4	$C_{14}H_{13}N_2O_6I_2$	558.8857	8.5
H 531	531.8980	-1.3	$C_{13}H_{14}N_2O_5I_2$	531.8987	7.0
F-A 526	526.8590	-0.9	$C_{13}H_9N_2O_5I_2$	526.8595	9.5
E-B* 503	503.8417	-3.6	$C_{11}H_8NO_6I_2$	503.8435	7.5
E-B 485	485.8322	-1.6	$C_{11}H_6NO_5I_2$	485.8330	8.5
E 430	430.9726	-2.1	$C_{14}H_{12}N_2O_6I$	430.9735	9.5
F-B 399	399.9543	-2.0	$C_{13}H_9N_2O_5I$	399.9551	10.0
G 540	540.8731	-3.9	$C_{14}H_{11}N_2O_5I_2$	540.8752	9.5
H 531	531.9016	-0.6	$C_{13}H_{14}N_2O_5I_2$	531.8987	7.0
H-A 404	404.9933	-2.2	$C_{13}H_{11}N_2O_5I$	404.9942	7.5
I 527	527.8674	-2.5	$C_{13}H_{10}N_2O_5I_2$	527.8687	9.0
J 444	444.9888	-0.7	$C_{15}H_{14}N_2O_6I$	444.9891	9.5
K 413	413.9702	-1.2	$C_{14}H_{11}N_2O_5I$	413.9707	10.0
TP IOP 665 A-C					
[M+H]+	665.9799	-0.8	$C_{18}H_{26}N_3O_8I_2$	665.9804	6.5
A 647	647.9691	-1.1	$C_{18}H_{24}N_3O_7I_2$	647.9698	7.5
C 560	560.8998	-2.9	$C_{14}H_{15}N_2O_6I_2$	560.9014	7.5
A-A 542	542.8914	1.1	$C_{14}H_{13}N_2O_5I_2$	542.8908	8.5
E 520	520.0561	-2.7	$C_{18}H_{23}N_3O_7I$	520.0575	8.5
B* 592	592.9275	-0.2	$C_{15}H_{19}N_2O_7I_2$	592.9276	6.5
B 574	574.9163	-1.2	$C_{15}H_{17}N_2O_6I_2$	574.9170	7.5
B 574	574.9180	1.7	$C_{15}H_{17}N_2O_6I_2$	574.9170	7.5
F 447	447.0038	-2.2	$C_{15}H_{16}N_2O_6I$	447.0048	8.5

Nominal ion mass	Measured mass [m/z]	Mass error [ppm]	Elemental composition	Calculated mass [m/z]	DBE[a]
B-A 433	433.9963	-1.4	$C_{14}H_{15}N_2O_6I$	433.9969	8.0
K 359	359.9367	1.1	$C_{11}H_7NO_5I$	359.9363	8.5
M 288	288.0741	0.0	$C_{14}H_{12}N_2O_5$	288.0741	10.0
C 560	560.9010	-0.7	$C_{14}H_{15}N_2O_6I_2$	560.9014	7.5
H* 437	437.9909	-2.1	$C_{14}H_{15}N_2O_6I$	437.9918	7.0
G 432	432.9882	-2.1	$C_{14}H_{14}N_2O_6I$	432.9891	8.5
H 419	419.9803	-2.4	$C_{13}H_{13}N_2O_6I$	419.9813	8.0
I 406	406.0011	-2.2	$C_{13}H_{15}N_2O_5I$	406.0020	7.0
J 401	401.9699	-2.0	$C_{13}H_{11}N_2O_5I$	401.9707	9.0
K 359	359.9358	-1.4	$C_{11}H_7NO_5I$	359.9363	8.5
N 279	279.0970	-1.8	$C_{13}H_{15}N_2O_5$	279.0975	7.5
D 538	538.0679	-0.4	$C_{18}H_{25}N_3O_8I$	538.0681	7.5
E 520	520.0571	-0.8	$C_{18}H_{23}N_3O_7I$	520.0575	8.5
E-A 502	502.0461	-1.8	$C_{18}H_{21}N_3O_6I$	502.0470	9.5
E-B 428	428.9931	-2.6	$C_{15}H_{14}N_2O_5I$	428.9942	9.5
F 447	447.0045	-0.7	$C_{15}H_{16}N_2O_6I$	447.0048	8.5
F-A 414	414.9781	-1.0	$C_{14}H_{12}N_2O_5I$	414.9785	9.5
F-B 390	390.9780	-1.3	$C_{12}H_{12}N_2O_5I$	390.9785	7.5
K* 377	377.9457	-3.2	$C_{11}H_9NO_6I$	377.9469	7.5
K 359	359.9367	1.1	$C_{11}H_7NO_5I$	359.9363	8.5
L 319	319.0916	-2.8	$C_{15}H_{15}N_2O_6$	319.0925	9.5
M 288	288.0735	-2.1	$C_{14}H_{12}N_2O_5$	288.0741	10.0
H* 437	437.9909	-2.1	$C_{14}H_{15}N_2O_6I$	437.9918	7.0
G 432	432.9887	-0.9	$C_{14}H_{14}N_2O_6I$	432.9891	8.5
G-A 400	406.1804	-3.5	$C_{13}H_{15}N_2O_5I$	400.9629	7.0
K 359	359.9359	-1.1	$C_{11}H_7NO_5I$	359.9363	8.5
G-B 305	305.0757	-3.6	$C_{14}H_{13}N_2O_6$	305.0768	9.5
G-C 274	274.0580	-1.5	$C_{13}H_{10}N_2O_5$	274.0584	10.0
H 419	419.9805	-1.9	$C_{13}H_{13}N_2O_6I$	419.9813	8.0
I 406	406.0034	3.4	$C_{13}H_{15}N_2O_5I$	406.0020	7.0
N 279	279.0968	-2.5	$C_{13}H_{15}N_2O_5$	279.0975	7.5

Nominal ion mass	Measured mass [m/z]	Mass error [ppm]	Elemental composition	Calculated mass [m/z]	DBE[a]
J 401	401.9699	-2.0	$C_{13}H_{11}N_2O_5I$	401.9707	9.0
K 359	359.9362	-0.3	$C_{11}H_7NO_5I$	359.9363	8.5
L 319	319.0920	-1.6	$C_{15}H_{15}N_2O_6$	319.0925	9.5
M 288	288.0738	-1.0	$C_{14}H_{12}N_2O_5$	288.0741	10.0
N 279	279.0975	0.0	$C_{13}H_{15}N_2O_5$	279.0975	7.5
TP IOP 651					
[M+H]+	651.9644	-0.5	$C_{17}H_{24}N_3O_8I_2$	651.9647	6.5
A 633	633.9539	-0.5	$C_{17}H_{22}N_3O_7I_2$	633.9542	7.5
B 560	560.9003	-2.0	$C_{14}H_{15}N_2O_6I_2$	560.9014	7.5
C 542	542.8903	-0.9	$C_{14}H_{13}N_2O_5I_2$	542.8908	8.5
E 506	506.0414	-1.0	$C_{17}H_{21}N_3O_7I$	506.0419	8.5
E-A 474	474.0153	-0.8	$C_{16}H_{17}N_3O_6I$	474.0157	9.5
F 432	432.9893	0.5	$C_{14}H_{14}N_2O_6I$	432.9891	8.5
E-B 414	414.9772	-3.1	$C_{14}H_{12}N_2O_5I$	414.9785	9.5
B* 578	578.9109	-1.9	$C_{14}H_{17}N_2O_7I_2$	578.9120	6.5
B 560	560.9015	0.2	$C_{14}H_{15}N_2O_6I_2$	560.9014	7.5
B 560	560.9012	-0.4	$C_{14}H_{15}N_2O_6I_2$	560.9014	7.5
G* 437	437.9908	-2.3	$C_{13}H_{15}N_2O_7I$	437.9918	7.0
F 432	432.9880	-2.5	$C_{14}H_{14}N_2O_6I$	432.9891	8.5
G 419	419.9800	-3.1	$C_{13}H_{13}N_2O_6I$	419.9813	8.0
H 406	406.0010	-2.5	$C_{13}H_{15}N_2O_5I$	406.0020	7.0
I 401	401.9696	-2.7	$C_{13}H_{11}N_2O_5I$	401.9707	9.0
J* 377	377.9452	-4.5	$C_{11}H_9NO_6I$	377.9469	7.5
J 359	359.9348	-4.2	$C_{11}H_7NO_5I$	359.9363	8.5
K 305	305.0774	2.0	$C_{14}H_{13}N_2O_6$	305.0768	9.5
L 279	279.0967	-2.9	$C_{13}H_{15}N_2O_5$	279.0975	7.5
M 274	274.0573	-4.0	$C_{13}H_{10}N_2O_5$	274.0584	10.0
C 542	542.8917	1.7	$C_{14}H_{13}N_2O_5I_2$	542.8908	8.5
C-A 414	414.9777	-1.9	$C_{14}H_{12}N_2O_5I$	414.9785	9.5
D 524	524.0524	0.0	$C_{17}H_{23}N_3O_8I$	524.0524	7.5

Nominal ion mass	Measured mass [m/z]	Mass error [ppm]	Elemental composition	Calculated mass [m/z]	DBE[a]
E 506	506.0423	0.8	$C_{17}H_{21}N_3O_7I$	506.0419	8.5
E-A 474	474.0158	0.2	$C_{16}H_{17}N_3O_6I$	474.0157	9.5
E-B 414	414.9779	-1.4	$C_{14}H_{12}N_2O_5I$	414.9785	9.5
G* 437	437.9914	-0.9	$C_{13}H_{15}N_2O_7I$	437.9918	7.0
F 432	432.9888	-0.7	$C_{14}H_{14}N_2O_6I$	432.9891	8.5
F-A 400	400.9623	-1.5	$C_{13}H_{10}N_2O_5I$	400.9629	9.5
J* 377	377.9461	-2.1	$C_{11}H_9NO_6I$	377.9469	7.5
J 359	359.9355	-2.2	$C_{11}H_7NO_5I$	359.9363	8.5
K 305	305.0763	-1.6	$C_{14}H_{13}N_2O_6$	305.0768	9.5
M 274	274.0579	-1.8	$C_{13}H_{10}N_2O_5$	274.0584	10.0
G 419	419.9805	-1.9	$C_{13}H_{13}N_2O_6I$	419.9813	8.0
H 406	406.0005	-3.7	$C_{13}H_{15}N_2O_5I$	406.0020	7.0
L 279	279.0969	-2.1	$C_{13}H_{15}N_2O_5$	279.0975	7.5
I 401	401.9703	-1.0	$C_{13}H_{11}N_2O_5I$	401.9707	9.0
J 359	359.9359	-1.1	$C_{11}H_7NO_5I$	359.9363	8.5
K 305	305.0764	-1.3	$C_{14}H_{13}N_2O_6$	305.0768	9.5
L 279	279.0975	0.0	$C_{13}H_{15}N_2O_5$	279.0975	7.5
M 274	274.0579	-1.8	$C_{13}H_{10}N_2O_5$	274.0584	10.0
IOHEXOL					
$[M+H]^+$	821.8861	-1.1	$C_{19}H_{27}N_3O_9I_3$	821.8870	6.5
A 803	803.8757	-1.6	$C_{19}H_{25}N_3O_8I_3$	803.8770	7.5
C 761	761.8715	6.6	$C_{17}H_{23}N_3O_7I_3$	761.8665	6.5
A-A 747	747.8497	-1.5	$C_{16}H_{21}N_3O_7I_3$	747.8508	6.5
D 730	730.8230	-1.8	$C_{16}H_{18}N_2O_7I_3$	730.8243	7.5
A-B 675	675.9646	-0.1	$C_{19}H_{24}N_3O_8I_2$	675.9647	8.5
E 656	656.7860	-2.3	$C_{13}H_{12}N_2O_5I_3$	656.7875	7.5
I 542	542.8927	3.5	$C_{14}H_{13}N_2O_5I_2$	542.8908	8.5
J 528	528.8736	-3.0	$C_{13}H_{11}N_2O_5I_2$	528.8752	8.5
B 779	779.8760	-1.3	$C_{17}H_{25}N_3O_8I_3$	779.8770	5.5
F 652	652.9708	-2.8	$C_{17}H_{25}N_3O_8I_2$	652.9726	6.0

Nominal ion mass	Measured mass [m/z]	Mass error [ppm]	Elemental composition	Calculated mass [m/z]	DBE[a]
H 560	560.9000	-2.5	$C_{14}H_{15}N_2O_6I_2$	560.9014	7.5
K 526	526.0668	-2.5	$C_{17}H_{25}N_3O_8I$	526.0681	6.5
F-A 399	399.1628	-2.0	$C_{17}H_{25}N_3O_8$	399.1636	7.0
C 761	761.8683	2.4	$C_{17}H_{23}N_3O_7I_3$	761.8665	6.5
C-A 670	670.8023	-1.2	$C_{14}H_{14}N_2O_5I_3$	670.8031	7.5
I 542	542.8902	-1.1	$C_{14}H_{13}N_2O_5I_2$	542.8908	8.5
D 730	730.8230	-1.8	$C_{16}H_{18}N_2O_7I_3$	730.8243	7.5
E 656	656.7860	-2.3	$C_{13}H_{12}N_2O_5I_3$	656.7875	7.5
G 602	602.9109	-1.8	$C_{16}H_{17}N_2O_7I_2$	602.9120	8.5
I 542	542.8908	0.0	$C_{14}H_{13}N_2O_5I_2$	542.8908	8.5
G-A 524	524.8795	-1.5	$C_{14}H_{13}N_2O_5I_2$	524.8803	9.5
E 656	656.7860	-2.3	$C_{13}H_{12}N_2O_5I_3$	656.7875	7.5
J 528	528.8746	-1.1	$C_{13}H_{11}N_2O_5I_2$	528.8752	8.5
L 501	501.8870	-2.2	$C_{12}H_{12}N_2O_4I_2$	501.8881	7.0
N 374	374.9829	-1.9	$C_{12}H_{12}N_2O_4I$	374.9836	7.5
F 652	652.9712	-2.1	$C_{17}H_{25}N_3O_8I_2$	652.9726	6.0
K 526	526.0678	-0.6	$C_{17}H_{25}N_3O_8I$	526.0681	6.5
F-A 399	399.1631	-1.3	$C_{17}H_{25}N_3O_8$	399.1636	7.0
G 602	602.9108	-2.0	$C_{16}H_{17}N_2O_7I_2$	602.9120	8.5
I 542	542.8892	-2.9	$C_{14}H_{13}N_2O_5I_2$	542.8908	8.5
G-A 524	524.8789	-2.7	$C_{14}H_{11}N_2O_4I_2$	524.8803	9.5
H 560	560.9006	-1.4	$C_{14}H_{15}N_2O_6I_2$	560.9014	7.5
H-A 487	487.8481	-1.0	$C_{11}H_8NO_5I_2$	487.8486	7.5
M 469	469.8380	-0.2	$C_{11}H_6NO_4I_2$	469.8381	8.5
H-B 413	413.8103	-3.9	$C_8H_2NO_3I_2$	413.8119	7.5
I 542	542.8900	-1.5	$C_{14}H_{13}N_2O_5I_2$	542.8908	8.5
J 528	528.8754	0.4	$C_{13}H_{11}N_2O_5I_2$	528.8752	8.5
K 526	526.0677	-0.8	$C_{17}H_{25}N_3O_8I$	526.0681	6.5
L 501	501.8866	-3.0	$C_{17}H_{25}N_3O_8I$	501.8881	6.5
M 469	469.8391	2.1	$C_{11}H_6NO_4I_2$	469.8381	8.5
N 374	374.9829	-1.9	$C_{12}H_{12}N_2O_4I$	374.9836	7.5

Nominal ion mass	Measured mass [m/z]	Mass error [ppm]	Elemental composition	Calculated mass [m/z]	DBE[a]
TP IOX 693					
[M+H]+	693.9748	-2.6	$C_{19}H_{26}N_3O_9I_2$	693.9766	7.5
A 675	675.9644	-0.4	$C_{19}H_{24}N_3O_8I_2$	675.9647	8.5
C 633	633.9529	-2.1	$C_{17}H_{22}N_3O_7I_2$	633.9542	7.5
G 548	548.0510	-2.6	$C_{19}H_{23}N_3O_8I$	548.0524	9.5
B 651	651.9645	-0.3	$C_{17}H_{24}N_3O_8I_2$	651.9647	6.5
C 633	633.9532	-1.6	$C_{17}H_{22}N_3O_7I_2$	633.9542	7.5
F 560	560.9008	-1.1	$C_{14}H_{15}N_2O_6I_2$	560.9014	7.5
H 542	542.8901	-1.3	$C_{14}H_{13}N_2O_5I_2$	542.8908	8.5
J 525	525.0598	-1.0	$C_{17}H_{24}N_3O_8I$	525.0603	7.0
K 500	500.8795	-1.6	$C_{12}H_{11}N_2O_4I_2$	500.8803	7.5
O 398	398.1551	-1.8	$C_{17}H_{24}N_3O_8$	398.1558	7.5
C 633	633.9538	-0.6	$C_{17}H_{22}N_3O_7I_2$	633.9542	7.5
H 542	542.8902	-1.1	$C_{14}H_{13}N_2O_5I_2$	542.8908	8.5
C-A 524	524.8802	-0.2	$C_{14}H_{11}N_2O_4I_2$	524.8803	9.5
K 500	500.8802	-0.2	$C_{12}H_{11}N_2O_4I_2$	500.8803	7.5
D 621	621.9537	-0.8	$C_{16}H_{22}N_3O_7I_2$	621.9542	6.5
D-A 603	603.9424	-2.0	$C_{16}H_{20}N_3O_6I_2$	603.9436	7.5
I 530	530.8906	-0.4	$C_{13}H_{13}N_2O_5I_2$	530.8908	7.5
N 402	402.9782	-0.7	$C_{13}H_{12}N_2O_5I$	402.9785	8.5
E 602	602.9117	-0.5	$C_{16}H_{17}N_2O_7I_2$	602.9120	8.5
L 474	474.9995	-0.4	$C_{16}H_{16}N_2O_7I$	474.9997	9.5
M 448	448.0122	-0.9	$C_{15}H_{17}N_2O_6I$	448.0126	8.0
P 321	321.1077	-1.2	$C_{15}H_{17}N_2O_6$	321.1081	8.5
F 560	560.9008	-1.1	$C_{14}H_{15}N_2O_6I_2$	560.9014	7.5
H 542	542.8901	-1.3	$C_{14}H_{13}N_2O_5I_2$	542.8908	8.5
F-A 469	469.8367	-3.0	$C_{11}H_6NO_4I_2$	469.8381	8.5
F-B 432	432.9880	-2.5	$C_{14}H_{14}N_2O_6I$	432.9891	8.5
G 548	548.0523	-0.2	$C_{19}H_{23}N_3O_8I$	548.0524	9.5
H 542	542.8897	-2.0	$C_{14}H_{13}N_2O_5I_2$	542.8908	8.5
I 530	530.8907	-0.2	$C_{13}H_{13}N_2O_5I_2$	530.8908	7.5

Nominal ion mass	Measured mass [m/z]	Mass error [ppm]	Elemental composition	Calculated mass [m/z]	DBE[a]
J 525	525.0598	-1.0	$C_{17}H_{24}N_3O_8I$	525.0603	7.0
K 500	500.8800	-0.6	$C_{12}H_{11}N_2O_4I_2$	500.8803	7.5
L 474	474.9993	-0.8	$C_{16}H_{16}N_2O_7I$	474.9997	9.5
I 432	432.9883	-1.8	$C_{14}H_{14}N_2O_6I$	432.9891	8.5
P 321	321.1077	-1.2	$C_{15}H_{17}N_2O_6$	321.1081	8.5
M 448	448.0124	-0.4	$C_{15}H_{17}N_2O_6I$	448.0126	8.0
N 402	402.9778	-1.7	$C_{13}H_{12}N_2O_5I$	402.9785	8.5
O 398	398.1552	-1.5	$C_{17}H_{24}N_3O_8$	398.1558	7.5
P 321	321.1078	-0.9	$C_{15}H_{17}N_2O_6$	321.1081	8.5
TP IOX 695 A-B					
[M+H]+	693.9888	-2.6	$C_{19}H_{28}N_3O_9I_2$	695.9909	6.5
A 677	677.9787	-2.5	$C_{19}H_{26}N_3O_8I_2$	677.9804	7.5
A-A 550	550.0673	-1.5	$C_{19}H_{25}N_3O_8I$	550.0681	8.5
G 544	544.9056	-1.7	$C_{14}H_{15}N_2O_5I_2$	544.9065	7.5
H 530	530.8906	-0.4	$C_{13}H_{13}N_2O_5I_2$	530.8908	7.5
N 402	402.9777	-2.0	$C_{13}H_{12}N_2O_5I$	402.9785	8.5
A-B 375	375.9910	-1.3	$C_{12}H_{13}N_2O_4I$	375.9915	7.0
S 249	249.0865	-2.0	$C_{12}H_{13}N_2O_8$	249.0870	7.5
B 653	653.9786	-2.8	$C_{17}H_{26}N_3O_8I_2$	653.9804	5.5
C 635	635.9709	1.7	$C_{17}H_{24}N_3O_7I_2$	635.9698	6.5
F 562	562.9160	-1.8	$C_{14}H_{17}N_2O_6I_2$	562.9170	6.5
I 527	527.0749	-1.9	$C_{17}H_{26}N_3O_8I$	527.0759	6.0
K 466	466.0461	-1.9	$C_{15}H_{21}N_3O_6I$	466.0470	6.5
L 435	435.0037	-2.5	$C_{14}H_{16}N_2O_6I$	435.0048	7.5
O 400	400.1697	-4.2	$C_{17}H_{26}N_3O_8$	400.1714	6.5
P 374	374.9826	-2.7	$C_{12}H_{12}N_2O_4I$	374.9836	7.5
Q 340	340.1495	-2.4	$C_{15}H_{22}N_3O_6$	340.1503	6.5
R 309	309.1080	-0.3	$C_{14}H_{17}N_2O_6$	309.1081	7.5
C 635	635.9643	-8.6	$C_{17}H_{24}N_3O_7I_2$	635.9698	6.5
D 604	604.9255	-3.5	$C_{16}H_{19}N_2O_7I_2$	604.9276	7.5

Nominal ion mass	Measured mass [m/z]	Mass error [ppm]	Elemental composition	Calculated mass [m/z]	DBE[a]
J 477	477.0165	2.5	$C_{16}H_{18}N_2O_7I$	477.0153	8.5
M 416	416.9915	-6.7	$C_{19}H_{26}N_3O_9I_2$	416.9943	8.5
J-A 398	398.9825	-2.8	$C_{14}H_{12}N_2O_4$	398.9836	9.5
S 249	249.0866	-1.6	$C_{12}H_{13}N_2O_8$	249.0870	7.5
E 568	568.0766	-3.5	$C_{19}H_{27}N_3O_9I$	568.0786	7.5
J 477	477.0147	-1.3	$C_{16}H_{18}N_2O_7I$	477.0153	8.5
F 562	562.9152	-3.2	$C_{14}H_{17}N_2O_6I_2$	562.9170	6.5
F-A 471	471.8534	-0.6	$C_{11}H_8NO_4I_2$	471.8537	7.5
L 435	435.0041	-1.6	$C_{14}H_{16}N_2O_6I$	435.0048	7.5
F-B 361	361.9496	-6.6	$C_{11}H_9NO_5I$	361.9520	7.5
G 544	544.9036	-5.3	$C_{14}H_{15}N_2O_5I_2$	544.9065	7.5
M 416	416.9926	-4.1	$C_{19}H_{26}N_3O_9I_2$	416.9943	8.5
H 530	530.8895	-2.4	$C_{13}H_{13}N_2O_5I_2$	530.8908	7.5
I 527	527.0741	-3.4	$C_{17}H_{26}N_3O_8I$	527.0759	6.0
K 466	466.0465	-1.1	$C_{15}H_{21}N_3O_6I$	466.0470	6.5
O 400	400.1705	-2.2	$C_{17}H_{26}N_3O_8$	400.1714	6.5
P 374	374.9829	-1.9	$C_{12}H_{12}N_2O_4I$	374.9836	7.5
Q 340	340.1497	-1.8	$C_{15}H_{22}N_3O_6$	340.1503	6.5
R 309	309.1074	-2.3	$C_{14}H_{17}N_2O_6$	309.1081	7.5
J 477	477.0132	-4.4	$C_{16}H_{18}N_2O_7I$	477.0153	8.5
M 416	416.9933	-2.4	$C_{19}H_{26}N_3O_9I_2$	416.9943	8.5
J-A 398	398.9822	-3.5	$C_{14}H_{12}N_2O_4$	398.9836	9.5
K 466	466.0457	-2.8	$C_{15}H_{21}N_3O_6I$	466.0470	6.5
P 374	374.9828	-2.1	$C_{12}H_{12}N_2O_4I$	374.9836	7.5
Q 340	340.1495	-2.4	$C_{15}H_{22}N_3O_6$	340.1503	6.5
L 435	435.0027	-4.8	$C_{14}H_{16}N_2O_6I$	435.0048	7.5
M 416	416.9939	-1.0	$C_{19}H_{26}N_3O_9I_2$	416.9943	8.5
N 402	402.9773	-3.0	$C_{13}H_{12}N_2O_5I$	402.9785	8.5
O 400	400.1704	-2.5	$C_{17}H_{26}N_3O_8$	400.1714	6.5
P 374	374.9800	-9.6	$C_{12}H_{12}N_2O_4I$	374.9836	7.5
Q 340	340.1492	-3.2	$C_{15}H_{22}N_3O_6$	340.1503	6.5

Nominal ion mass	Measured mass [m/z]	Mass error [ppm]	Elemental composition	Calculated mass [m/z]	DBE[a]
R 309	309.1072	-2.9	$C_{14}H_{17}N_2O_6$	309.1081	7.5
S 249	249.0859	-4.4	$C_{12}H_{13}N_2O_8$	249.0870	7.5
IOMEPROL					
$[M+H]^+$	777.8619	0.6	$C_{17}H_{23}N_3O_8I_3$	777.8614	6.5
A 759	759.8486	-2.9	$C_{17}H_{21}N_3O_7I_3$	759.8508	7.5
B* 704	704.8091	0.7	$C_{14}H_{16}N_2O_7I_3$	704.8086	6.5
B 686	686.7964	-2.3	$C_{14}H_{14}N_2O_6I_3$	686.7980	7.5
C 668	668.7855	-3.0	$C_{14}H_{12}N_2O_5I_3$	668.7875	8.5
D 631	631.9376	-1.4	$C_{17}H_{20}N_3O_7I_2$	631.9385	8.5
F 540	540.8733	-3.5	$C_{14}H_{11}N_2O_5I_2$	540.8752	9.5
H 513	513.8861	-3.9	$C_{13}H_{12}N_2O_4I_2$	513.8881	8.0
B* 704	704.8065	-3.0	$C_{14}H_{16}N_2O_7I_3$	704.8086	6.5
B 686	686.7976	-0.6	$C_{14}H_{14}N_2O_6I_3$	686.7980	7.5
B 686	686.7969	-1.6	$C_{14}H_{14}N_2O_6I_3$	686.7980	7.5
E 558	558.8852	-0.9	$C_{14}H_{13}N_2O_6I_2$	558.8857	8.5
G 531	531.8981	-1.1	$C_{13}H_{14}N_2O_5I_2$	531.8987	7.0
I 404	404.9935	-1.7	$C_{13}H_{14}N_2O_5I$	404.9942	7.5
C 668	668.7845	-4.5	$C_{14}H_{12}N_2O_5I_3$	668.7875	8.5
F 540	540.8751	-0.2	$C_{14}H_{11}N_2O_5I_2$	540.8752	9.5
H 513	513.8871	-1.9	$C_{13}H_{12}N_2O_4I_2$	513.8881	8.0
D 631	631.9353	-5.1	$C_{17}H_{20}N_3O_7I_2$	631.9385	8.5
E 558	558.8851	-1.1	$C_{14}H_{13}N_2O_6I_2$	558.8857	8.5
G 531	531.8986	-0.2	$C_{13}H_{14}N_2O_5I_2$	531.8987	7.0
E-A 485	485.8309	-4.3	$C_{11}H_6NO_5I_2$	485.8330	8.5
E-B 441	441.8415	-3.8	$C_{12}H_9N_2O_5I_2$	441.8432	7.5
I 404	404.9930	-3.0	$C_{13}H_{14}N_2O_5I$	404.9942	7.5
F 540	540.8733	-3.5	$C_{14}H_{11}N_2O_5I_2$	540.8752	9.5
G 531	531.8980	-1.3	$C_{13}H_{14}N_2O_5I_2$	531.8987	7.0
I 404	404.9930	-3.0	$C_{13}H_{14}N_2O_5I$	404.9942	7.5
H 513	513.8868	-2.5	$C_{13}H_{12}N_2O_4I_2$	513.8881	8.0

Nominal ion mass	Measured mass [m/z]	Mass error [ppm]	Elemental composition	Calculated mass [m/z]	DBE[a]
I 404	404.9936	-1.5	$C_{13}H_{14}N_2O_5I$	404.9942	7.5
I 287	287.9516	0.0	$C_9H_7NO_2I$	287.9516	6.5
TP IMP 651					
$[M+H]^+$	651.9634	-3.7	$C_{17}H_{24}N_3O_8I_2$	651.9658	6.5
A 633	633.9539	-0.5	$C_{17}H_{22}N_3O_7I_2$	633.9542	7.5
B 560	560.9011	1.2	$C_{14}H_{15}N_2O_6I_2$	560.9004	7.5
C 542	542.8905	-0.6	$C_{14}H_{13}N_2O_5I_2$	542.8908	8.5
D 506	506.0408	-2.2	$C_{17}H_{21}N_3O_7I$	506.0419	8.5
B* 578	578.9114	-0.9	$C_{14}H_{17}N_2O_7I_2$	578.9119	6.5
B 560	560.9003	-2.0	$C_{14}H_{15}N_2O_6I_2$	560.9014	7.5
G* 437	437.9905	-3.0	$C_{13}H_{15}N_2O_7I$	437.9918	7.0
G 419	419.9818	1.2	$C_{13}H_{13}N_2O_6I$	419.9813	8.0
H 406	406.0011	-2.2	$C_{13}H_{15}N_2O_5I$	406.0020	7.0
I 279	279.0970	-0.4	$C_{13}H_{15}N_2O_5$	279.0971	7.5
C 542	542.8890	-3.3	$C_{14}H_{13}N_2O_5I_2$	542.8908	8.5
D 524	524.0515	-1.7	$C_{17}H_{23}N_3O_8I$	524.0524	7.5
E 506	506.0410	-1.8	$C_{17}H_{21}N_3O_7I$	506.0419	8.5
G* 437	437.9911	-1.6	$C_{13}H_{15}N_2O_7I$	437.9918	7.0
F 432	432.9882	-2.1	$C_{14}H_{14}N_2O_6I$	432.9891	8.5
F-A 404	404.9940	-0.5	$C_{13}H_{14}N_2O_5I$	404.9942	7.5
F-B 307	307.0917	-2.6	$C_{14}H_{15}N_2O_6$	307.0925	8.5
I 279	279.0967	-1.4	$C_{13}H_{15}N_2O_5$	279.0971	7.5
G 419	419.9796	-4.0	$C_{13}H_{13}N_2O_6I$	419.9813	8.0
H 406	406.0008	-1.5	$C_{13}H_{15}N_2O_5I$	406.0014	7.0
I 279	279.0970	-1.8	$C_{13}H_{15}N_2O_5$	279.0975	7.5
I 279	279.0969	-0.7	$C_{13}H_{15}N_2O_5$	279.0971	7.5
I-A 261	261.0868	-0.8	$C_{13}H_{13}N_2O_4$	261.0870	8.5
I-B 206	206.0447	-0.5	$C_{10}H_8NO_4$	206.0448	7.5

Nominal ion mass	Measured mass [m/z]	Mass error [ppm]	Elemental composition	Calculated mass [m/z]	DBE[a]
IOPAMIDOL					
$[M+H]^+$	777.8605	-1.2	$C_{17}H_{24}N_3O_8I_3$	777.8614	6.5
A 759	759.8499	-1.2	$C_{17}H_{21}N_3O_7I_3$	759.8508	7.5
B* 704	704.8059	-3.8	$C_{14}H_{16}N_2O_7I_3$	704.8086	6.5
B 686	686.7970	-1.5	$C_{14}H_{14}N_2O_6I_3$	686.7980	7.5
C 668	668.7874	-0.1	$C_{14}H_{12}N_3O_5I_3$	668.7875	8.5
D 631	631.9376	-1.4	$C_{17}H_{20}N_3O_7I_2$	631.9385	8.5
D-A 613	613.9277	-0.3	$C_{17}H_{18}N_3O_6I_2$	613.9279	9.5
E 558	558.8852	-0.9	$C_{14}H_{13}N_2O_6I_2$	558.8857	8.5
E-A 540	540.8744	-1.5	$C_{14}H_{11}N_2O_5I_2$	540.8752	9.5
D-B 487	487.0230	-1.0	$C_{17}H_{18}N_3O_6I$	487.0235	10.0
B* 704	704.8079	-1.0	$C_{14}H_{16}N_2O_7I_3$	704.8086	6.5
B 686	686.7970	-1.5	$C_{14}H_{14}N_2O_6I_3$	686.7980	7.5
B*-A 613	613.7444	-1.5	$C_{11}H_7NO_5I_3$	613.7453	7.5
E 558	558.8853	-0.7	$C_{14}H_{13}N_2O_6I_2$	558.8857	8.5
B 686	686.7974	-0.9	$C_{14}H_{14}N_2O_6I_3$	686.7980	7.5
C 668	668.7869	-0.9	$C_{14}H_{12}N_3O_5I_3$	668.7875	8.5
E 558	558.8851	-1.1	$C_{14}H_{13}N_2O_6I_2$	558.8857	8.5
C-A 541	541.8824	-1.1	$C_{14}H_{12}N_2O_5I_2$	541.8830	9.0
F 531	531.8981	-1.1	$C_{13}H_{14}N_2O_5I_2$	531.8987	7.0
F-A 386	386.9825	-2.8	$C_{13}H_{12}N_2O_4I$	386.9836	8.5
C 668	668.7866	-1.3	$C_{14}H_{12}N_3O_5I_3$	668.7875	8.5
C-A 541	541.8821	-1.7	$C_{14}H_{12}N_2O_5I_2$	541.8830	9.0
C-B 540	540.8748	-0.7	$C_{14}H_{11}N_2O_5I_2$	540.8752	9.5
C-C 513	513.8882	0.2	$C_{13}H_{12}N_2O_4I_2$	513.8881	8.0
D 631	631.9370	-2.4	$C_{17}H_{20}N_3O_7I_2$	631.9385	8.5
D-A 613	613.9241	-6.2	$C_{17}H_{18}N_3O_6I_2$	613.9279	9.5
E 558	558.8859	0.4	$C_{14}H_{13}N_2O_6I_2$	558.8857	8.5
D-B 487	487.0228	-1.4	$C_{17}H_{18}N_3O_6I$	487.0235	10.0
E 558	558.8851	-1.1	$C_{14}H_{13}N_2O_6I_2$	558.8857	8.5
E-B 430	430.9730	-1.2	$C_{14}H_{12}N_2O_6I$	430.9735	9.5

Nominal ion mass	Measured mass [m/z]	Mass error [ppm]	Elemental composition	Calculated mass [m/z]	DBE[a]
F 541	541.8812	-3.3	$C_{14}H_{12}N_2O_5I_2$	541.8830	9.0
F-A 386	386.9832	-1.0	$C_{13}H_{12}N_2O_4I$	386.9836	8.5
IOPAMIDOL-d_3					
[M+H]+	780.8787	-1.8	$C_{17}H_{20}D_3N_3O_8I_3$	780.8802	6.5
A 762	762.8681	-1.9	$C_{17}H_{18}D_3N_3O_7I_3$	762.8696	7.5
B* 707	707.8255	-2.7	$C_{14}H_{13}D_3N_2O_7I_3$	707.8274	6.5
B 689	689.8169	0.1	$C_{14}H_{11}D_3N_2O_6I_3$	689.8169	7.5
C 671	671.8057	-0.8	$C_{14}H_9D_3N_2O_5I_3$	671.8063	8.5
D 634	634.9564	-1.4	$C_{17}H_{17}D_3N_3O_7I_2$	634.9573	8.5
A-A 543	543.8940	0.0	$C_{14}H_8D_3N_2O_5I_2$	543.8940	9.5
B *707	707.8260	-1.9	$C_{14}H_{13}D_3N_2O_7I_3$	707.8274	6.5
B 689	689.8150	-2.7	$C_{14}H_{11}D_3N_2O_6I_3$	689.8169	7.5
B-A 616	616.7643	0.4	$C_{11}H_4D_3NO_5I_3$	616.7641	7.5
E 561	561.9014	-5.5	$C_{14}H_{10}D_3N_2O_6I_2$	561.9046	8.5
B 689	689.8158	-1.5	$C_{14}H_{11}D_3N_2O_6I_3$	689.8169	7.5
C 671	671.8050	-1.9	$C_{14}H_9D_3N_2O_5I_3$	671.8063	8.5
E 561	561.9037	-1.4	$C_{14}H_{10}D_3N_2O_6I_2$	561.9046	8.5
B-A 544	544.9008	-1.8	$C_{14}H_9D_3N_2O_5I_2$	544.9018	9.0
B-B 534	534.9165	-1.7	$C_{13}H_{11}D_3N_2O_5I_2$	534.9175	7.0
B-C 433	433.9911	-2.6	$C_{14}H_9D_3N_2O_6I$	433.9923	9.5
B-D 390	390.0015	-2.3	$C_{13}H_9D_3N_2O_4I$	390.0025	8.5
C 671	671.8059	-0.5	$C_{14}H_9D_3N_2O_5I_3$	671.8063	8.5
D 634	634.9561	-1.9	$C_{17}H_{17}D_3N_3O_7I_2$	634.9573	8.5
E 561	561.9032	-2.4	$C_{14}H_{10}D_3N_2O_6I_2$	561.9046	8.5
TP IPM 667					
$[M+H]^+$	667.9573	-3.4	$C_{17}H_{24}N_3O_9I_2$	667.9596	6.5
A 649	649.9467	-3.7	$C_{17}H_{22}N_3O_8I_2$	649.9491	7.5
C 558	558.8854	-0.5	$C_{14}H_{13}N_2O_6I_2$	558.8857	8.5
B* 594	594.9042	-4.5	$C_{14}H_{17}N_2O_8I_2$	594.9069	6.5

Nominal ion mass	Measured mass [m/z]	Mass error [ppm]	Elemental composition	Calculated mass [m/z]	DBE[a]
B 576	576.8955	-1.4	$C_{14}H_{15}N_2O_7I_2$	576.8963	7.5
C 558	558.8850	-1.3	$C_{14}H_{13}N_2O_6I_2$	558.8857	8.5
D 504	504.8746	-2.2	$C_{11}H_{11}N_2O_5I_2$	504.8757	6.5
E 486	486.8642	-0.8	$C_{11}H_9N_2O_4I_2$	486.8646	7.5
F 448	448.9837	-0.7	$C_{14}H_{14}N_2O_7I$	448.9840	8.5
G 431	431.8218	-1.4	$C_8H_4NO_4I_2$	431.8224	6.5
I 413	413.8108	-2.7	$C_8H_2NO_3I_2$	413.8119	7.5
C 558	558.8848	-1.6	$C_{14}H_{13}N_2O_6I_2$	558.8857	8.5
E 486	486.8640	-1.2	$C_{11}H_9N_2O_4I_2$	486.8646	7.5
H 430	430.9730	-0.9	$C_{14}H_{12}N_2O_6I$	430.9734	9.5
D 504	504.8745	-2.4	$C_{11}H_{11}N_2O_5I_2$	504.8757	6.5
E 486	486.8643	-0.6	$C_{11}H_9N_2O_4I_2$	486.8646	7.5
G 431	431.8219	-1.2	$C_8H_4NO_4I_2$	431.8224	6.5
I 413	413.8110	-2.2	$C_8H_2NO_3I_2$	413.8119	7.5
E 486	486.8638	-1.6	$C_{11}H_9N_2O_4I_2$	486.8646	7.5
G 431	431.8221	-0.7	$C_8H_4NO_4I_2$	431.8224	6.5
E-A 412	412.8264	-3.4	$C_8H_3N_2O_2I_2$	412.8278	7.5
F 448	448.9833	-1.6	$C_{14}H_{14}N_2O_7I$	448.9840	8.5
G 431	431.8221	-0.7	$C_8H_4NO_4I_2$	431.8224	6.5
I 413	413.8112	-1.7	$C_8H_2NO_3I_2$	413.8119	7.5
H 430	430.9728	-1.6	$C_{14}H_{12}N_2O_6I$	430.9735	9.5
I 413	413.8112	-1.7	$C_8H_2NO_3I_2$	413.8119	7.5

[a] Double-bond equivalents.

Scheme SI-1. Possible deiodination IMP to TP 651–A and –B

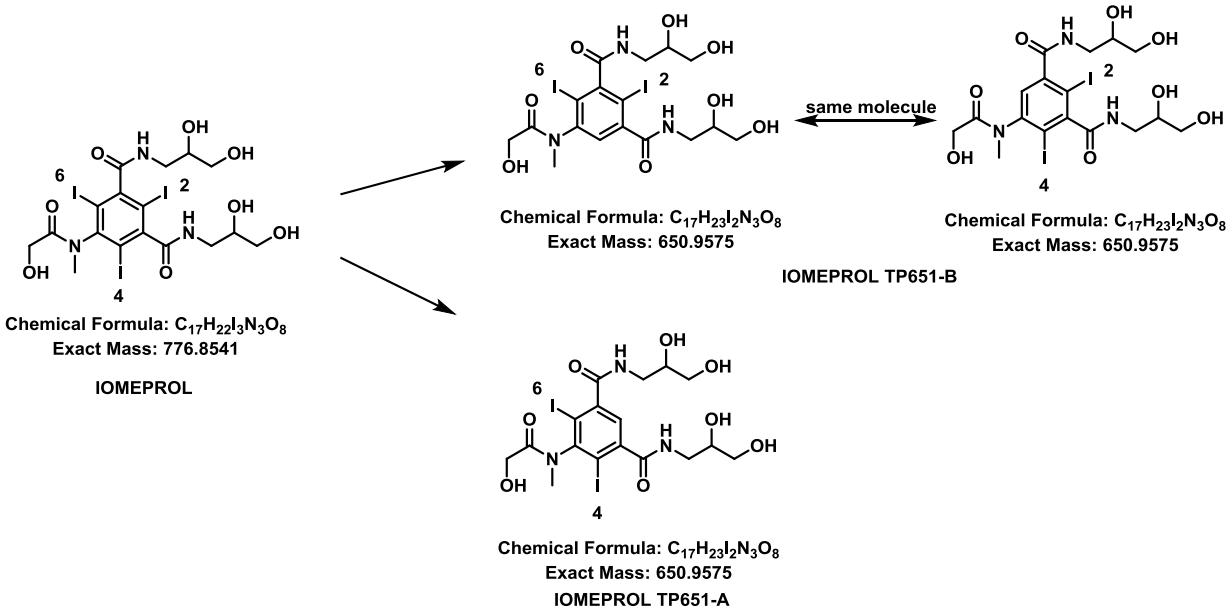

LC-HRMS method for determination of ICM and their prioritized TPs in surface waters

The surface waters extracts were reanalyzed for determination of the concentrations of ICM and their prioritized TPs with the following optimized method: with respect to the LC-MS screening method was modified as follows: 0 min (3 % A) - 1 min (3 % A) – 6 min (20 % A), - 7 min (95 % A) – 8 min (95 % A) – 8.5 min (3 % A) – 10 min (3 % A). As above, for other LC-HRMS methods, a data dependent MS^2 scan was used in combination with a full-scan but with a narrower scan window. Full scan data-acquisition was acquired over the mass range from 500 to 850 with an additional scan event m/z 1500-1600 m/z between 3.9 and 5.9 min to detect IDX. NCE tested for optimization were 10, 15, 20, 25, 30, 35, 40, 50 and 60. Final NCE used is given in the manuscript (**Table 2.**)

Recovery and Ion suppression measurements

For determining recoveries and ion suppression, a mixture of all 13 river water grab samples was used. The pH of the mixture was adjusted to 6.5 and then spiked with 250 ng of ICM standard mix (including deuterated standards) and TPs as in measured river water samples. All experiments were performed in triplicate. Recovery was calculated as the difference between the concentration after the SPE and the blank sample divided with spiked concentration.

Ion suppression was calculated as the difference between the area of the compound spiked at 100 ng after SPE and blank (raw river water SPE), divided by the area of 100 ng spiked in HPLC water.

Figure SI-6. Chromatograms of detected TPs in real surface waters (Besos-3)

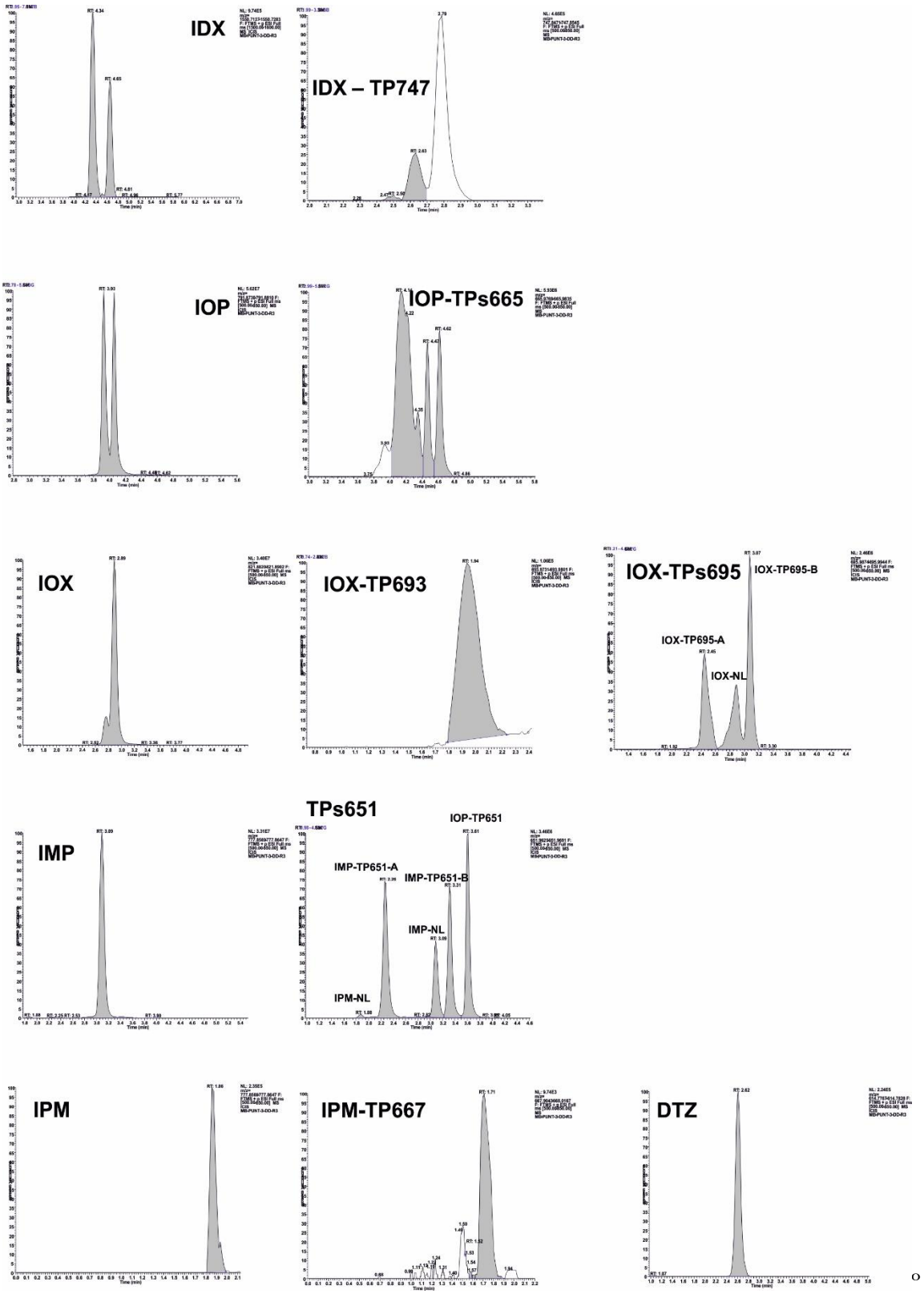

3.4. Discussion

3.4.1. Transformation products identified during degradation of zanamivir under simulated sunlight and advanced oxidation processes

As have been discussed in the previous sections, ZAN was reported not to metabolise in the human body, and, likewise, does not degrade during conventional WWTP treatment. For this reasons, a couple of studies tested the degradability of ZAN in wastewater using AOPs systems UV/TiO_2 (Woche et al. 2016) and ozonation (Fedorova et al. 2016).

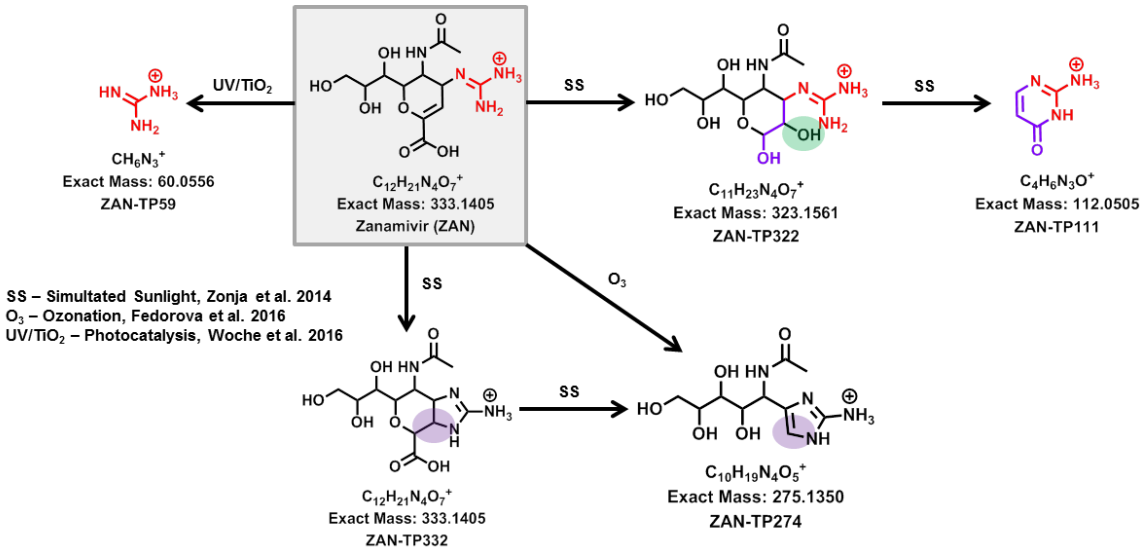

Figure 3.3. Phototransformation of Zanamivir as reported in the literature and this thesis.

In the paper presented in Article N°1, ZAN potential to degrade under simulated and natural sunlight was evaluated (Zonja et al. 2014b). Under the simulated sunlight, ZAN was transformed to four TPs (**Figure 3.3.**). They were identified as products of the following chemical reactions; i) Michael-type addition (TP 332); ii) decarboxylation followed by double bond epoxidation and subsequent hydration (TP 322); iii) series of successive decarboxylation and oxidation processes (TP 274) and iv) sequential reactions of oxidation of the hemiacetalic aldehyde to the corresponding carboxylic acid, followed by lactamization and final radical formation with subsequent side chain elimination (TP 111). In ozonation experiments (Fedorova et al. 2016), only one TP was detected – TP274 (**Figure 3.3**.) which is formed as a result of opening of the oxacyclohexane ring and cleavage of the $C_2H_2O_2$

group. This is one of the TPs identified as a result of photodegradation in this thesis. On the other hand, when ZAN was exposed to degradation with UV/TiO_2 (Woche et al. 2016), the only detected TP was guanidine (**Figure 3.3.**). However, this TP was not detected in Article N°1 (Zonja et al. 2014b), since to the m/z cut-off of the scan range used started at m/z 100 (TP-59 has m/z 60.0556).

3.4.2. Biological and photodegradation transformation pathways of iodinated contrast media and transformation products

As mentioned in the introduction section on ICM, their reaction pathways have been studied in at least a dozens of studies which mainly focused either on their: i) biodegradation in activated sludge or soil-water test systems, ii) removal with AOPs or ARPs, or iii) photodegradation under natural or simulated sunlight. While the biodegradation with activated sludge and removal using AO(R)Ps are engineered systems, photodegradation under natural sunlight is a natural process that can naturally attenuate the concentration of contaminants in, for example, surface water. Today the most ubiquitous WWTP process for treatment of domestic (urban) and industrial wastewater is an activated sludge process due to production of effluents that meet the required quality standards at relatively low cost. However, since the conventional WWTPs are not designed to remove contaminants (like pharmaceuticals), upgrading the conventional WWTPs with additional treatment is considered as a viable alternative to aid higher removal of more recalcitrant pharmaceuticals. Amongst other technologies like reverse osmosis or membrane bioreactors, AO(R)Ps could be used as a tertiary treatment in WWTPs. Due to high cost they are still not as common but several tertiary processes like ozonation, use of activated carbon or UV/H_2O_2 have been implemented in treatment of wastewater with success (Kovalova et al. 2013, Oller et al. 2011). As a result, transformation products of contaminants formed in secondary treatment with activated sludge are more frequent geographically and present higher load for receiving surface waters where they, together with their potential biological TPs, can be further degraded under solar light.

In order to properly characterise transformation pathways of a selected compound, reliable structural elucidation of TPs is essential. Most used strategy for identification of TPs is by studying its fragmentation pattern in comparison to the fragmentation pattern of its

parent compound. Although it is to be expected that the fragmentation pattern between the parent compound and the TP should be similar, this is not always straightforward. Even if the overall reaction type can be deduced by the difference in elemental composition, it is not as easy to pinpoint the exact position where the modification occurred. In Article N°2, a special attention was paid to structural elucidation of positional isomers, since several TPs were detected with an overall change in chemical composition which corresponded to the replacement of one iodine by hydrogen. In the case of iohexol (IOX), two deiodinated TPs (TP695-A and TP695-B) could form from dehalogenation of three iodines from the aromatic ring, considering the equivalence of positions **4** and **6** (*Figure SI-5.8-A, Article N°2, SI, p182.*). For the positions numbering on the ICM structure, please consult **Figure 3.2**. For structural elucidation of these two compounds it was necessary to rely on fragmentation patters since it was not possible to separate them using semipreparative LC. While both TPs exhibited similar losses in their fragmentation spectra (like the loss of water or acetone), one TP had a diagnostic ion at m/z 562.9170 which was missing from the spectra of its positional isomer (*Figure SI-5.8-A, B, Article N°2, SI, p182.-188.*). From the pMS^3 spectra recorded, it was evident that this fragment originated from the m/z 653.9804, suggesting loss of the *similar* chain which would only be possible if one of the iodine atoms ortho to the *similar* chain is already cleaved (*Figure SI-5.8-A, B, Article N°2, SI, p182-188*). This provided a diagnostic evidence that this TP (denominated IOX-TP-695-A) had a structure where one iodine is missing from the position **4** or **6**. Consequently, it was possible to identify these TPs with a *confidence level 2b* (probable structure by diagnostic evidence) from Schymanski guidelines (**Chapter 1.3.** and **Figure 1.3.**). Conversely, in the case of dehalogenation of iomeprol (IMP), again two TPs were detected as the result of dehalogenation of three iodines from the aromatic ring. But, these positional isomers did not exhibit any diagnostic fragments particular for either of TPs (*Figure SI-5.10-A, B, Article N°2, SI, p193.-197.*). The only noticeable differences were seen in the relative intensities of the majority of fragment ions. Even when the pMS^3 spectra performed on several fragments showed slight difference in fragmentation, it was not possible to distinguish these two compounds (*Figure SI-5.10-A, B, Article N°2, SI, p193.-197.*). Luckily, in this case it was possible to purify one TP with semipreparative-LC experiments. The NMR spectra that was run subsequently, showed an indication of the nonmagnetic equivalence of the hydroxybenzamido side chains and, confirmed the asymmetric nature of the isolated TP with elimination of the iodine from the

position **4** or **6** (*Figure SI-5.10-C, Article Nº2, SI, p197.*). This TP was denominated TP651-B and its structure was confirmed with the highest *confidence level 1* (confirmed structure with the authentic standard) from Schymanski guidelines (**Chapter 1.3.** and **Figure 1.3.**). Since it was not possible to isolate its counterpart TP651-A, its structure was inferred by the diagnostic evidence to form as a result of deiodination from the position **2.**, reaching the *confidence level 2b*.

Figure 3.4. shows the compilation of results from Article Nº2 and of several studies (Kormos et al. 2010, Kormos et al. 2009, Perez et al. 2009, Schulz et al. 2008, Zonja et al. 2015) that have addressed the formation of both biodegradation and phototransformation TPs of ICM. Main biotranformation pathways are shown in red. As reported, ICM are principally transformed via:

i) Biotransformation pathway B1: Oxidation of primary and/or secondary alcohol groups on either identical (ID) and similar (SM) side chains;

ii) Biotransformation pathway B2 Cleavage of N-C bond (one or both 3-hydroxyl propanoic acid and acetyl group) on either ID and SM side chains;

iii) Biotransformation pathway B3: Decarboxylation or decarboxylation followed by oxidation on either ID and SM side chains

Of course, both the combination of several B pathways and the same pathway on both ID side chains is possible and reported to occur. On the other hand, photodegradation pathways of the ICM investigated in this thesis and recorded are shown in purple in **Figure 3.4**. In our experimets, ICM were transformed to eleven photoTPs that have been detected in surface water in more than 50 % of the samples. These TPs were the result of:

i) Phototransformation pathway P1: N-demethylation on one of the ID side chains. This is a reaction specific only to IOP since it is the only ICM investigated with the methylated tertiary amide in the ID side chain.

ii) Phototransformation pathway P2: Deiodination of either iodine from the benzene ring.

iii) Phototransformation pathway P3: Oxidative deiodination (exchange of iodide with hydroxyl group)

iv) Phototransformation pathway P4: Intramolecular elimination (loss of iodide)

v) Phototransformation pathway P5: N-dealkylation of the hydroxylpropylene group. This is a reaction specific to IDX since it is the only investigated ICM here

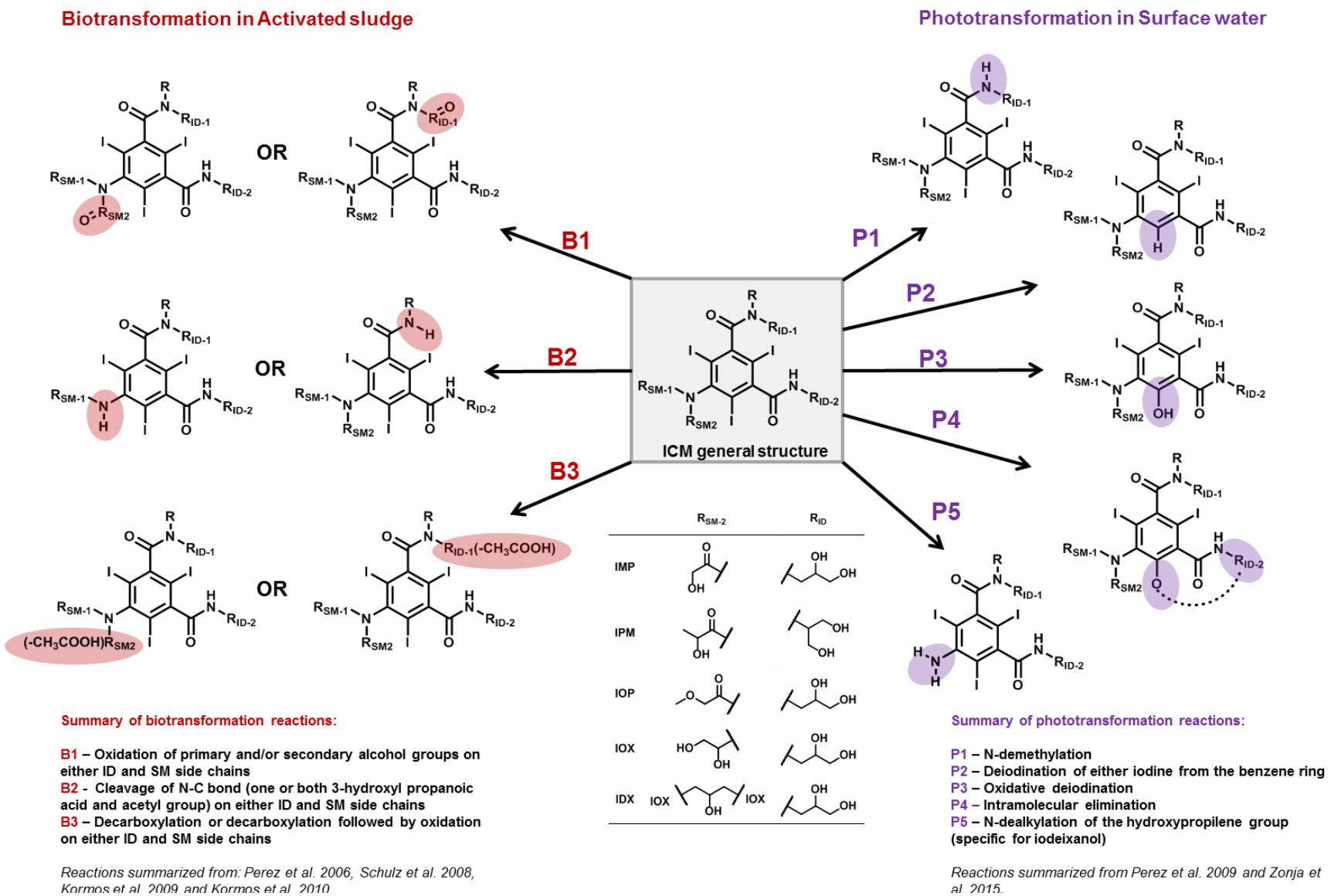

Figure 3.4. Biotransformation and phototransformation reactions of ICM as reported in the literature and this thesis.

that is a dimer molecule. In the case of IDX, two IOX molecules are connected over the hydroxylpropylene bridge.

Like in the case of biotransformation pathways, the combination of several P pathways and the same pathway on both ID side chains is possible.

The main difference between the two degradation pathways is that one exclusively relies on modification on one of the side chains (biotransformation pathway) while the other (phototransformation pathway) almost exclusively forms TPs as the result of loss of iodide (in our case all three P2, P3 and P4 include deiodination in the step). Overall, out of the eleven prioritised ICM TPs in surface water, ten could be attributed to these three phototransformation pathways. Only one TP detected did not lose iodide – iodixanol TP747 which was formed as the result of the P5 pathway (bond cleavage of the dimer iodixanol). Although it seems obvious that these reaction pathways are different since different mechanisms are involved in the TPs formation, there is a certain combined overlap between the bio- and phototransformation pathways. On one hand, we have biotransformation in biological wastewater treatment which is the result of catabolic activity of the micro-organisms and mediated by the enzymatic activity. Kormos et al. (Kormos et al. 2010) related the presence of enzymes like NAD(P)-dependent alcohol dehydrogenases, alcohol oxidases, peroxidases, monooxygenases with the pathway B1 or presence of monooxygenases and dehydrogenases responsible for the N-C bond cleavage (pathway B2). In case of the phototransformation the molecule is electronically excited once it absorbs light and this can result in transformation in case of a direct photolysis. In the indirect photolysis, transformation started with the absorption of light of a co-present species like dissolved organic matter and different reactive species can be generated like hydroxyl radicals (•OH) which are involved in the transformation of a molecule. Photodegradation in general proceeds via a more complex mechanism which translates to more diverse and higher number TPs. In the case reported here a total of 108 TPs have been detected for the six parent compound (18 on average). As was discussed previously, this was the reason to devote time to prioritisation rather than complete identification. Since the majority of the TPs formed in batch experiments were not identified it is not possible to compare similar pathways with the ones identified in this study. However, overlap in transformation pathways has been reported for ICM in other studies. Perez et al (Perez et al. 2009) identified phototransformation TPs TP464 and TP450 which were detected in our batch experiments.

They were the result of both deiodination and N-C cleavage (a combination of a B2 and P2 pathways). Similarly, Fabbri et al. (Fabbri et al. 2016) identified phototransformation TP of IOP-TP554 as a result of B1 and P2 pathway and IPM-photoTP706 which formed via B2 pathway. Likewise, biodegradation of DTZ under anaerobic conditions yielded deiodinated and deacetylated TPs (combination of B2 and P2 pathways) (Redeker et al. 2014). Knowledge on both pathways could be of interest in determining the transformation and removal rates of compounds. Basically, a compound which is initially degraded photochemically can later be degraded biotically with the mixture of the parent compounds and its TPs like in the case of Rastogi et al. (Rastogi et al. 2014). There a mixture of photoTPs formed after the degradation of DTZ under a UV light were biodegraded aerobically following OECD guidelines. This approach could be more effective in removal of ICM since the steric hindrance of the iodine atoms could be responsible why some enzymes are unable to degrade the ICM aromatic rings (Kormos et al. 2010, Kroutil et al. 2004).

3.4.3. Two different approaches for detection and identification of transformation products of zanamivir and iodinated contrast media under simulated and natural sunlight

The first approach used in this thesis, transformation products profiling in the case of photodegradation of ZAN in surface water, was a common approach used in many previously published studies (**Tables 1.1.** and **1.2.** in the introduction chapter). It consisted of initially choosing a compound to be degraded (in our case ZAN because of reasons explained in section *introduction to ZAN*). The following step which consists of detection and identification of TPs which were formed as a result of the process applied has often been referred in literature as non-target analysis (Gros et al. 2014, Gros et al. 2015, Negreira et al. 2015b). However, probably a more illustrative name for this approach would be a *bias* non-target analysis since the degradation process applied is already known, the initial concentrations of the spiked analytes are significantly higher than the matrix (typically > 1000 times), and there is a presumable structural similarity of the TPs to the parent compound. This makes it a much less exhaustive process of detection than a genuine non-target screening (automated) from a complex matrix when compounds detected are true unknowns (Schymanski et al. 2014b, van Leerdam et al. 2014). But, besides the terminology, in the case

of ZAN, an overall TPs profiling (or non-automated) approach was applied to evaluation of degradability of ZAN under natural and simulated sunlight. The term common is used to acknowledge that many authors have reported using it.

In our case the evaluation of degradability consisted of the following four steps:

i) Degradation of ZAN in surface water under simulated sunlight at high spiked concentration in order to facilitate TP identification

ii) Transformation products were detected and identified using LC-HRMS (LTQ-Orbitrap-Velos) and vendor software from Thermo Scientific

iii) For each of the TPs detected, a mechanistic pathway was proposed

iv) Kinetic studies were performed in order to evaluate the degradation at different initial concentrations of the parent, different light source (natural or simulated) or addition of different water constituents like humic acids or nitrates. For the kinetic studies, a separate method was created and applied using LC-MS/MS (TqD)

The final step of this workflow would be to screen real surface water samples for the presence of the parent compound and/or TPs. For this step, typically either a LRMS or HRMS method based on LC-MS/MS is created for quantification purposes, if the TPs are available as authentic standards, or parent validation parameters are used in order to determine (semi-)quantitative concentrations (Beel et al. 2013, Kaiser et al. 2014, Kormos et al. 2010, Kormos et al. 2009, Luft et al. 2014, Negreira et al. 2015a, Prasse et al. 2011, Wick et al. 2011).

The advantage of this approach is that it allows the complete characterisation of TPs of a compound, and, since the initial spiked concentration is usually very high, there are no problems in instrument sensitivity, so even many minor TPs can be detected, identified, and used to explain the overall transformation of the compound during the degradation process. However, since it is not up until the TPs have been identified and kinetics characterised that they are actually screened for in real environmental samples, the overall outcome of the study leaves uncertainty whether the applied transformation process is environmentally relevant. Although in the initial work of ZAN, its TPs were not screened in real environmental samples, this was performed retrospectively. ZAN and its TPs were searched for in the

surface water samples that were analysed in **Article Nº3**. In this case, a total of thirteen surface water samples were screened for the presence of ZAN and its TPs using suspect screening approach. The chromatographic and MS method details can be found in **Article Nº3** (Zonja et al. 2016b). In brief, the samples were run using an Acquity UPLC (Waters Milford, MA) which was coupled to a Q-Exactive-MS (Thermo Scientific, Bremen, Germany). The ionisation source was electrospray ionisation (ESI) which was operated in positive mode. For the chromatographic separation here, an Acquity-C_{18} column (150 × 2.1 mm, 1.7 μm) was used. For the detection, a data dependent scan was used with the resolution of 35,000 of both full MS and MS/MS and the scan range was from m/z 100 – 1000. The total run was 25 min. (At this point, there was a major difference in chromatographic retention between ZAN using Aquity BEH HILIC (Zonja et al. 2014b) and the Aquity-C_{18} column which was used to analyse the surface water samples (Zonja et al. 2016b) due to ZAN's high polarity.) However, in the screening method the exact mass of the ZAN and its TPs were searched for in the surface water samples as a starting point. The results showed that neither ZAN nor any of its TPs have been detected in any of the surface water samples analysed. Since neither exact m/z was detected in the retrospective analysis of surface water samples, no further attempts were made to improve the elution behaviour of the polar ZAN and its TPs.

In the case of ZAN, only four TPs have been detected in the laboratory degradation experiments. However, in the case of the six ICM, a total number of 108 TPs were detected. In order to focus attention only to environmentally relevant TPs, the approach for detection and identification of phototransformation products of ICM needed to be rethought by using more sophisticated approach which would include a prioritisation step. Basic concept behind the approach used here was the prioritisation of only TPs that are detected in the real-world samples (in our case, surface water). In principle, an additional step was introduced into the ZAN degradation scheme described earlier between the ii) and iii) point. This step consisted of screening of a large number of TPs from the suspect-screening list that was created based on detection of phototransformation of ICM at laboratory scale. In essence, initial screening of TPs from both batch reactors and surface water samples was performed using HRMS (QExactive-Orbitrap-MS). This was possible since the newly marketed HRMS instruments,

not only have superior mass accuracy, but also sensitivity which is comparable with the triple-quad instruments (Eichhorn et al. 2012b, Zonja et al. 2014a, Zonja et al. 2013).

Considering the approach used for the ICM, it is not strictly suspect nor non-target but rather a *hybrid* between the two approaches. Suspect screening approach typically relies on large lists of known environmental contaminants (and their related compounds like human metabolites or TPs) which are characterised by their exact mass and/or by spectral libraries (Krauss et al. 2010, Singer et al. 2016). On the other hand, for a truly non-target screening, detected chromatographic peaks are again matched to large lists of probable contaminants at the end, but the initial selection of the unknown peaks is typically intensity-based (Gago-Ferrero et al. 2015, Schymanski et al. 2014b). This approach does open possibilities to find compounds not contemplated in the suspect database. Approach reported in this thesis did use a suspect screening list (or database) of all detected TPs, but a non-target analysis of the photodegradation samples led to the creation of the suspected list. This type of an approach could be comparable with the one reported in Kern et al. (Kern et al. 2009) or Helbling et al. (Helbling et al. 2010b) where a computer-assisted prediction of possible TPs can lead to confirmation of actual TPs formed in a given system (biodegradation in activated sludge or analysis of surface water in their case). However, even if the TPs detected are not fully identified or separated, they can still be easily used for creation of both suspect lists and spectral databases since they are characterised by both different retention times and fragmentation patterns.

3.5. Conclusions

In this chapter two different approaches were used for the identification of TPs. TPs profiling approach was applied for the identification of phototransformation products of an antiviral ZAN in surface water. This was followed by using a suspect screening approach for prioritization and identification of photoTPs of ICM in surface waters.

Based on the results obtained, the following specific conclusions could be drawn:

~ In Article N°1, under environmentally relevant concentrations (20 μgL^{-1}), ZAN was degraded under artificial sunlight in surface water samples with the degradation half-life of 3.6 h. However, experiments under natural sunlight and the same initial concentration suggested that natural attenuation of ZAN in surface water would likely proceed with slow kinetics. In the latter case, after 18 days of exposure ZAN concentration was only reduced by approximately 30 %.

~ Under simulated sunlight in surface water and at initial concentration of 40 mgL^{-1}, ZAN was transformed to four detectable photoTPs which were tentatively identified by rationalising their fragmentation pattern which was recorded using LC-HRMS (LC-LTQ-Orbitrap-MS). Given that ZAN is a highly polar compound, the use of HILIC instead of a more common reversed-phased chromatography afforded not only better retention of ZAN but also the separation of an isobaric compound that was later denominated as TP-332.

~ Four photo-mechanisms were proposed in the photolysis experiments under artificial sunlight: i) Michael-type addition (TP 332); ii) decarboxylation followed by double bond epoxidation and subsequent hydration (TP 322); iii) series of successive decarboxylation and oxidation processes (TP 274) and iv) sequential reactions of oxidation of the hemiacetalic aldehyde to the corresponding carboxylic acid, followed by lactamization and final radical formation with subsequent side chain elimination (TP 111). Under the initial concentration of 20 μgL^{-1}, only TP111 was detected and its structure was confirmed with an authentic standard (isocytosine).

~ In Article N°2, six ICM at initial concentration of 1mgL^{-1} were shown to degrade in batch reactors which were filled with surface water. In batch reactors, a total of 108

TPs (18 TPs for each ICM) were detected in LC-HRMS (LC-QExactive-MS) data using the differential sample analysis software (SIEVE, Thermo Scientific) and manually.

~ The TPs were solely characterised with retention times and their exact masses. In the present work, an additional step based on detection frequencies of TPs in real samples was applied to prioritize TPs. Following a generic SPE method thirteen surface water samples were extracted for detection of 108 TPs generated from six ICM under simulated sunlight in batch reactors. Out of the 108 TPs, only eleven were detected in more than 50 % of the surface water samples.

~ Using semipreparative LC, it was possible to isolate only four TPs from the samples of the photolysis experiments, while three positional isomers of IOP-TP665 were isolated as a mixture. Their structures were elucidated by studying their HRMS fragmentation pattern. The structures of the isolated TPs were additionally corroborated with NMR analysis.

~ LC-HRMS based target method was developed and applied to determine the concentrations of both parent compounds and their TPs in surface water samples. Parent compounds were detected with median concentration of 110 ngL^{-1} while the TPs were detected with the median concentration of 8 ngL^{-1}.

Chapter 4. Lamotrigine and Related Compounds: Biotic and Abiotic Transformation in Wastewater

4.1. Occurrence, fate and transformation of lamotrigine in the aquatic environment

Lamotrigine (LMG) is an anticonvulsant which is used for treatment of seizure disorders like epilepsy (Beattie et al. 2012, Ohman et al. 2008, Saracino et al. 2007). It prevents the presynaptic release of the excitatory neurotransmitters by blocking voltage-activated sodium channels and, hence, shows an antiseizure effect (Beattie et al. 2012, Coulter 1997). Chemically, LMG is a phenyltriazine derivative which is slightly soluble in water. **Figure 4.1.** summarises some physico-chemical and pharmaco-kinetic properties of LMG.

It is a relatively new drug which was introduced in the early 1990s. According to the Spanish Agency of Medicines and Healthcare Products (Agencia Española de Medicamentos y productos Sanitarios – AEMPS), in Spain LMG was marketed in 1993. and the first doses prescribed were in 1994 (AEMPS). In the period from 1992. to 2006. (the most recently available data), LMG daily defined dose (DDD) per 1000 inhabitants per day had a steady increase, reaching in 2006. 0.73 DDD (**Figure 4.1.**) (AEMPS). In comparison with the two frequently prescribed anticonvulsants (carbamazepine and oxacarbamazepine), the usage of carbamazepine slightly decreased while both oxacarbamazepine and LMG showed similar usage which was approximately the same in 2006 (**Figure 4.1.**). Recently Stokes et al. (Stokes et al. 2014) found that lamotrigine induces cold sensitivity growth inhibition in the *Escherichia coli* bacterium. This suggests that lamotrigine might be used in future to help develop a novel mechanistic class of antibiotics. As a result, possible increase in its usage can be expected.

In the human body, LMG is extensively metabolized primarily by the action of uridine 5'-diphosphate–glucuronosyl transferases at the N-2 position of the 1,2,4-triazine ring (Beattie et al. 2012) yielding predominantly lamotrigine N2-glucuronide (LMG-N2-G). This metabolite was first isolated and characterized from human urine by Sinz and Remmel (Sinz and Remmel 1991). Other, minor metabolites reported are N5-glucuronide, N2-oxide, and

N2-methyl-LMG (Doig and Clare 1991, Lu and Uetrecht 2007, Ramsay et al. 1991, Sidhu et al. 2006) (**Figure 4.2.**).

A

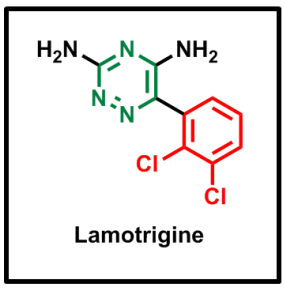

B

Physico-chemical and pharmaco-kinetic properties of Lamotrigine	
Names	Lamotrigine, Lamictin, Lamictal
MW	256.09 g/mol
Formula	$C_9H_7Cl_2N_5$
CAS	84057-84-1
Water solubility	170 mgL^{-1} (25°C)
logP	1.93
pKa (strongest acidic/basic)	14.98 / 5.87
Dosage	2 – 200 mg
Excretion	94 % excreted via urine, 2 % in feces (unchanges lamotrigine – 10 %)
Half life (healthy individuals)	25 ± 10 h
Metabolism	Hepatic via UGT1A4

C

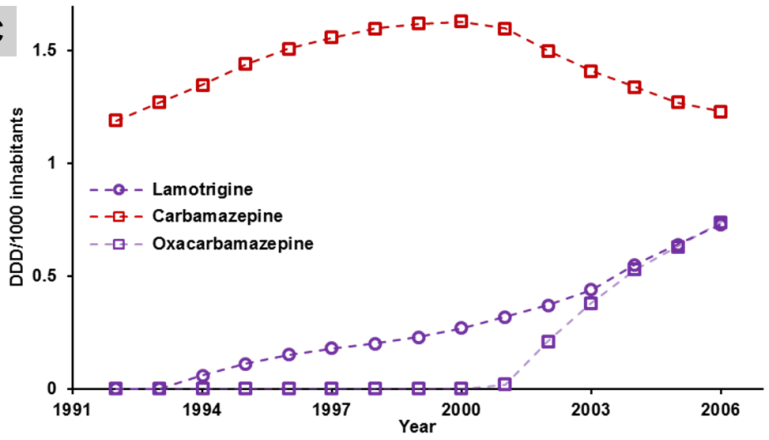

Figure 4.1. The structure of the anticonvulsant Lamotrigine (A), a phenyltriazine derivative of the dichlorobenzene. Phenyltriazine moiety is shown in green and the dichlorobenzene in red. The table (B) shows basic physicochemical and pharmaco-kinetic properties of Lamotrigine. The data shown here have been taken from: Chemaxon platform (Chemaxon 2016), PubChem (PubChem 2016), FDA (FDA 2016b) and DrugBank (DrugBank 2016). The graph in panel C shows the consumption data of lamotrigine in comparison to two other used anticonvulsants (carbamazepine and oxacarbamazepine). The data were taken from the webpage of the Spanish Agency of Medicines and Healthcare Products (Agencia Española de Medicamentos y productos Sanitarios – AEMPS) and the latest data available were up to the year 2006 (AEMPS).

Approximately 10 % of the dose is excreted intact via urine while LMG-N2-G accounts for 76 – 90 % of the initial administered dose (Cohen et al. 1987, Ramsay et al. 1991, Sidhu et al. 2006).

LMG and its major human metabolite LMG-N2-G were first detected in the aquatic environment in wastewater, surface, groundwater and drinking water by Ferrer and Thurman (Ferrer and Thurman 2010). LMG was detected in all four matrices with the mean concentrations range of 17 and 488 ngL^{-1} in drinking and wastewater, respectively. LMG-N2-G was not detected in the drinking water samples, but was quantified in the concentrations range of 17 and 209 ngL^{-1} in ground and wastewater, respectively. More surprising than the high concentrations of LMG was that its glucuronide survived the WWTP treatment making it a ground and surface water contaminant (Ferrer and Thurman 2010). From this point on, LMG and in some cases LMG-N2-G were readily included in multi-residue methods based on LC-MS/MS for screening and quantification of these micropollutants in environmental samples (Borova et al. 2014, Ferrer and Thurman 2012, Gurke et al. 2015a, Gurke et al. 2015b, Writer et al. 2013a, Writer et al. 2013b). In one of the subsequent studies by Ferrer and Thurman (Ferrer and Thurman 2012), in approximately 100 surface water samples analysed (all downstream of effluent discharge), LMG was detected in 97 % of the samples with the average concentration of 455 ngL^{-1}. LMG-N2-G was detected with 68 % frequency and average concentration of 95 ngL^{-1}.

As to the fate of LMG in surface water, Writer et al. (Writer et al. 2013a), studied the in-stream attenuation of neuro-active pharmaceuticals over the course of 5.4 km. The results showed that LMG was one of the most persistent compounds with a half-life of approximately 12 h (Writer et al. 2013a). In another study, other authors evaluated the direct photodegradation under simulated sunlight, and at neutral pH (Young et al. 2014), a degradation half-life of over 100 h suggested high resistance to solar degradation as well.

In general, little is known about the fate of LMG in WWTPs but from studies which analysed WWTP influent and effluent samples, it is clear that LMG is largely incompletely removed from the treatment plants (Ferrer and Thurman 2010, Gurke et al. 2015a). Since LMG is most likely poorly removed in biological secondary treatment in WWTPs, high concentrations of LMG in treated wastewater could be translated to high intake of this pharmaceutical by root crops when the agricultural fields are irrigated with post-biologically treated wastewater since LMG (together with carbamazepine and caffeine) was detected at

high concentrations in carrot roots and leaves (0.983 and 0.416 ngg^{-1}, respectively) (Goldstein et al. 2014, Malchi et al. 2014). Therefore, its degradation using advanced treatment processes was evaluated and reported as an alternative way to decrease its concentration in treated wastewater (Keen et al. 2014, Lester et al. 2014, Teixeira et al. 2016). However, when LMG was exposed to direct UV light, hydroxyl radicals or ozone it was seen that it is stable in these advanced treatments. But, LMG did react slightly with the OH radicals, at a much slower reaction rate compared to other micropollutants (Keen et al. 2014, Wols and Hofman-Caris 2012). As a result, little to no attenuation is expected in large-scale UV or ozone disinfection applications (Keen et al. 2014).

The previous paragraphs mainly reviewed what is known regarding the fate of LMG and the occurrence of both LMG and LMG-N2-G in environmental water samples. However, little is known about the fate of LMG-N2-G in both wastewater and surface water. Compared to the degradation behaviour of other glucuronide conjugates (D'Ascenzo et al. 2003, Gomes et al. 2009, Kumar et al. 2012, Lee et al. 2012), LMG-N2-G is also expected to undergo hydrolysis of the glycosidic bond and revert back to its parent LMG in WWTPs. This could also be the probable reaction occurring in the sewage-pipe where glucuronide hydrolysis could hinder the attenuation of pharmaceuticals from their discharge site (like hospital or household effluents). Negative removal rates in some cases could be either due to biotically-mediated hydrolysis of glucuronides, as the result of chemical hydrolysis dependent on pH in wastewater (Di Meo et al. 2013) or due to inadequate wastewater sampling (Brewer et al. 2012, Ort et al. 2010a, Ort et al. 2010b) . Overall, knowledge of the fate of glucuronides could be especially important for glucuronides like LMG-N2-G, which have been detected in wastewater, surface and groundwater at high ngL^{-1} concentrations.

4.2. Chapter objectives

Overall chapter objectives were to investigate the fate of the poorly studied anticonvulsant lamotrigine in wastewater treatment plants.

Here, mass balance studies were carried out in the laboratory batch reactors as well as in real raw and treated sewage samples from wastewater treatment plants in order to ensure that all relevant transformation products involved in the degradation pathways were qualified.

Owning to the negative or unknown removal of LMG in WWTPs and the detection of its human metabolite in the environmental water samples, this thesis aimed to investigate the fate of LMG and its principal human metabolite LMG-N2-G in WWTPs, relying on conventional biological treatment, by investigating both biotic and abiotic parameters and processes. Due to high wastewater and surface water concentrations of LMG and LMG-N2-G reported previously (Ferrer and Thurman 2010, 2012, Gurke et al. 2015a, Writer et al. 2013b), known simulated sunlight phototransformation products (Young et al. 2014), known human metabolites (Doig and Clare 1991, Lu and Uetrecht 2007, Ramsay et al. 1991, Sidhu et al. 2006), a suspect list was compiled including all reported related compounds.

In the **Article N°3** entitled ***Human Metabolite Lamotrigine-N2-glucuronide Is the Principal Source of Lamotrigine-Derived Compounds in Wastewater Treatment Plants and Surface Water***, and **Article N°4** entitled ***Abiotic Amidine and Guanidine hydrolysis of Lamotrigine-N2-Glucuronide and Related Compounds in Wastewater: The Role of pH and N2-substitution on Reaction Kinetics***; we investigated the degradation of LMG and LMG-N2-G in activated sludge, and in parallel, transformations of LMG and its metabolites and TPs in wastewater as a function of pH.

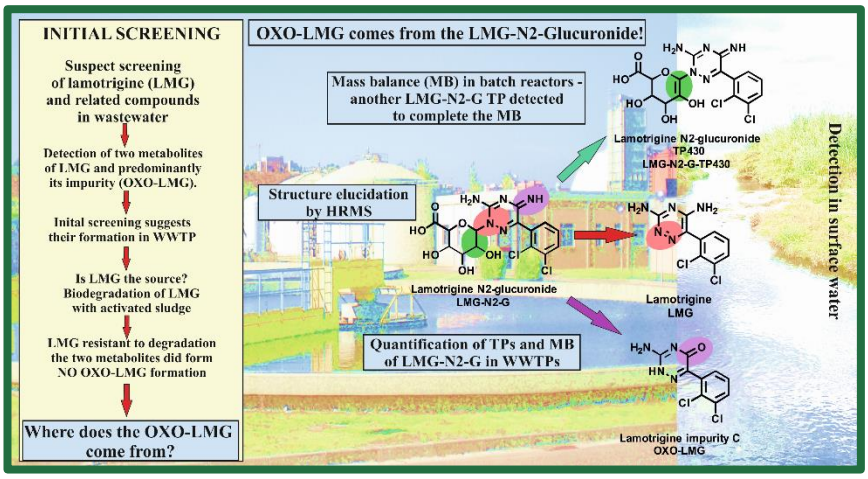

Article Nº3:

Zonja, B., Perez, S. and Barcelo, D.

Human Metabolite Lamotrigine-N(2)-glucuronide Is the Principal Source of Lamotrigine -Derived Compounds in Wastewater Treatment Plants and Surface Water.

(2016.) Environ Sci Technol 50(1), 154-164.

Environmental Science & Technology

Article

pubs.acs.org/est

Human Metabolite Lamotrigine-N^2-glucuronide Is the Principal Source of Lamotrigine-Derived Compounds in Wastewater Treatment Plants and Surface Water

Bozo Zonja,[†] Sandra Pérez,*[,†] and Damià Barceló[†,‡]

[†]Water and Soil Quality Research Group, Department of Environmental Chemistry, IDAEA-CSIC, c/Jordi Girona, 18-26, 08034 Barcelona, Spain

[‡]Catalan Institute of Water Research, Edifici H_2O, Parc Científic i Tecnològic de la Universitat de Girona, c/Emili Grahit, 101, E-17003 Girona, Spain

Supporting Information

ABSTRACT: Wastewater and surface water samples, extracted with four solid-phase extraction cartridges of different chemistries, were suspect-screened for the anticonvulsant lamotrigine (LMG), its metabolites, and related compounds. LMG, three human metabolites, and a LMG synthetic impurity (OXO-LMG) were detected. Preliminary results showed significantly higher concentrations of OXO-LMG in wastewater effluent, suggesting its formation in the wastewater treatment plants (WWTPs). However, biodegradation experiments with activated sludge demonstrated that LMG is resistant to degradation and that its human metabolite lamotrigine-N^2-glucuronide (LMG-N2-G) is the actual source of OXO-LMG in WWTPs. In batch reactors, LMG-N2-G was transformed, following pseudo-first-order kinetics to OXO-LMG and LMG, but kinetic experiments suggested an incomplete mass balance. A fragment ion search applied to batch-reactor and environmental samples revealed another transformation product (TP), formed by LMG-N2-G oxidation, which was identified by high-resolution mass spectrometry. Accounting for all TPs detected, a total mass balance at two concentration levels in batch reactors was closed at 86% and 102%, respectively. In three WWTPs, the total mass balance of LMG-N2-G ranged from 71 to 102%. Finally, LMG-N2-G and its TPs were detected in surface water samples with median concentration ranges of 23−139 ng L^{-1}. The results of this study suggest that glucuronides of pharmaceuticals might also be sources of yet undiscovered, but environmentally relevant, transformation products.

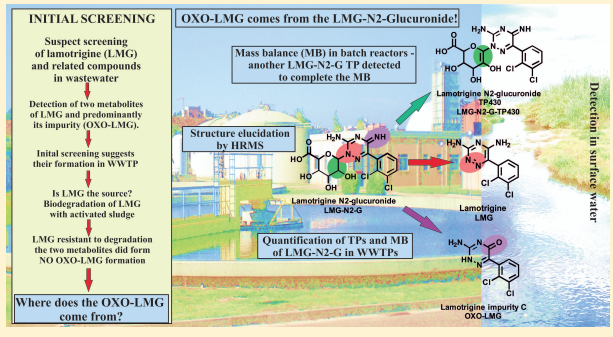

INTRODUCTION

Lamotrigine (LMG) is an anticonvulsant used in combination with carbamazepine for the treatment of epilepsy.[1,2] In the human body, LMG is extensively metabolized to yield predominantly lamotrigine-N^2-glucuronide (LMG-N2-G). In urine, it accounts for 76−90% of the dose, while approximately 10% is excreted intact.[3,4] Minor metabolites are the N^5-glucuronide, the N^2-oxide, and N^2-methyl-LMG.[3−6]

After excretion of LMG and its metabolites from the human body, they may enter the aquatic environment via wastewater treatment plants (WWTP). The first report of the presence of LMG and its major metabolite LMG-N2-G in the aquatic systems was published by Ferrer et al.[7] in 2010. Both compounds were found in relatively high concentrations (concentration range for LMG was from 17 to 488 ng L^{-1} and for LMG-N2-G was from not detected to 209 ng L^{-1}) and with high frequency in wastewater, surface water, and groundwater. The study confirmed that not only has LMG passed through the WWTP's treatments but its metabolite LMG-N2-G has also cleared. However, in a follow-up study that consisted of monitoring 24 Minnesota river and wastewater samples (effluent) for the occurrence of neuro-active pharmaceuticals, LMG-N2-G was found in only one wastewater effluent,[8] probably due to the high detection limit afforded by the MS instrument used (QToF-MS). As no authentic standard was available, the authors estimated the detection limit to be 100 ng L^{-1}.

The fate of LMG after biological treatment in WWTPs has been extensively investigated. Writer et al.[9] studied the in-stream attenuation of neuroactive pharmaceuticals over the course of 5.4 km, showing that LMG was, together with 10,11-dihydro-10,11-dihydroxycarbamazepine and carbamazepine, one of the most persistent compounds, with a half-life of approximately 12 h.[9] When lamotrigine was subjected to direct photodegradation under simulated sunlight,[10] at pH 7, a

Received: July 31, 2015
Revised: November 20, 2015
Accepted: November 25, 2015
Published: November 25, 2015

DOI: 10.1021/acs.est.5b03691
Environ. Sci. Technol. 2016, 50, 154−164

degradation half-life of over 100 h suggested high resistance to photodegradation as well. When lamotrigine was exposed to advanced treatment[11] by direct UV photolysis, hydroxyl radicals or ozone, similar conclusions were reached. Hence, no attenuation is expected in large-scale UV or ozone disinfection applications.[11] On the other hand, little is known about the fate of LMG in WWTPs apart from the observation that lamotrigine is incompletely removed during wastewater treatment.[7−10]

Against this background, we set out to investigate in more detail the fate of LMG in WWTPs relying on conventional biological treatment. As a first step, influent and effluent samples from municipal WWTPs were "suspect" screened for the presence of LMG and its known human metabolites and impurities. The same was performed with surface water samples with additional suspect analytes, reported phototransformation products (photoTPs). Using LMG as a standard, an initial estimation of their concentrations indicated incomplete mass balance of LMG-related compounds between untreated and treated sewage. This suggested a more complex degradation pathway of LMG, possibly involving its N^2-glucuronide. On the basis of previously reported hydrolysis of other glucuronide conjugates, (mostly estrogens), LMG-N2-G was expected to undergo the same reaction.[12−15] In order to elucidate the processes taking place during microbial degradation of LMG and LMG-N2-G, both compounds were assayed individually in batch experiments using activated sludge as the source of the microbial community. Any novel transformation product (TP) would then be considered for closing the mass balance of LMG and related compounds in batch reactors and WWTPs. All compounds were eventually determined in surface water samples. The step-by-step workflow of the paper is presented in Figure 1.

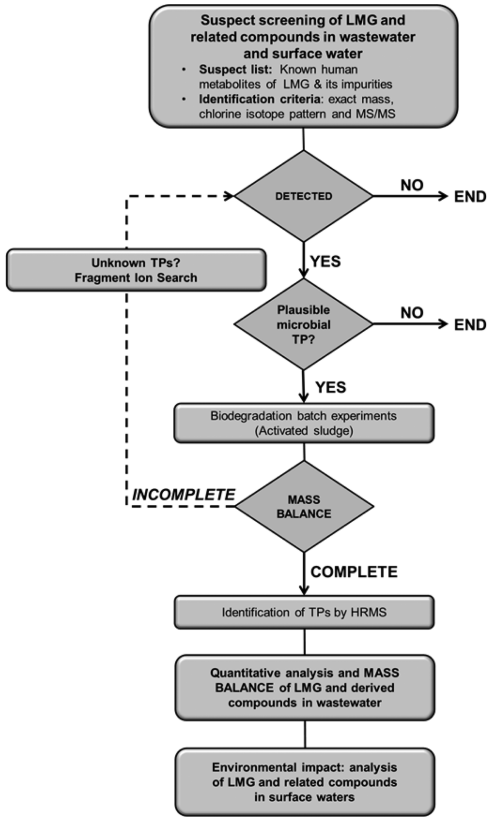

Figure 1. Workflow of the presented work.

EXPERIMENTAL SECTION

Chemicals and Standards. LMG, lamotrigine N^2-oxide (LMG-N2-oxide), 5-desamino-5-oxo-2,5-dihydrolamotrigine (OXO-LMG), and the internal standard, an isotopically labeled $^{13}C_3$-lamotrigine ($^{13}C_3$-LMG), were purchased from Toronto Research Chemicals (Toronto, Canada). LMG-N2-G (85%) was purchased from Santa Cruz Biotechnology. N^2-Methyl-lamotrigine (N2-Me-LMG) and an abiotic TP of LMG-N2-G (TP433-Amd) were chemically synthesized as previously reported[16] and explained by Zonja et al.[17] All solvents used (methanol, acetonitrile, and water) were purchased from Fisher Scientific (Geel, Belgium), except ethyl acetate, which was from Merck. Formic acid (98%−100%) was ACS grade and purchased from Sigma-Aldrich (Schnelldorf, Germany).

Solid-phase extraction (SPE) cartridges—Oasis HLB (500 mg) and MCX and MAX (both 200 mg)—were purchased from Waters (Waters, Milford, MA), and Bond Elut PPL cartridge (500 mg) was from Agilent Technologies (Waghaeusel-Wiesental, Germany). Calibration of the Q Exactive mass spectrometer was done with electrospray ionization (ESI) positive ion calibration solution from Thermo Scientific (Dresden, Germany).

Analysis of Wastewater. Wastewater (WW) samples were taken from four WWTPs discharging into the Besòs and Llobregat Rivers close to the city of Barcelona, Spain [more details on WWTPs can be found in the Supporting Information (SI)]. The sample treatment has been explained elsewhere.[18] In brief, the samples were filtered through 0.7 μm glass-fiber filters and spiked with 100 ng of the internal standard $^{13}C_3$-LMG. The samples were then frozen and stored at −20 °C until extraction. Following pH adjustment to 6.3−6.7, SPE was used to extract the samples: 600 mL of WWTP effluent and 400 mL of WWTP influent. To maximize the extraction efficiency, all four SPE cartridge types (in order HLB, PPL, MAX, and MCX) were connected in series. The cartridges were eluted separately, and the four extracts were combined, evaporated to dryness, and reconstituted in 400 μL of acetonitrile/water (3:97). Twenty microliters of the final extract was injected into the UPLC−Q Exactive-MS.

Screening of Wastewater Extracts and Retrospective Analysis of Surface Water Samples. In order to detect LMG, its human metabolites, and other related compounds, a screening method was applied using an Acquity UPLC (Waters Milford, MA) coupled to a Q Exactive-MS (Thermo Scientific, Bremen, Germany) equipped with heated-ESI (HESI) and operated in the positive ion mode. The chromatographic separation of the wastewater extracts was performed using an UPLC Acquity-C_{18} column (150 × 2.1 mm, 1.7 μm) preceded by a precolumn of the same packing material (5 × 2.1 mm, 1.7 μm).

Surface water grab samples, which had previously been monitored for the presence of X-ray contrast media agents and their photodegradates (Table SI-1, SI)[18] using the same sample extraction protocol as in the present study, were retrospectively screened for the LMG and related compounds.

Detailed information on chromatographic and MS conditions, as well as the parameters of the data-dependent acquisition, is provided in the SI (see "Screening method for wastewater samples and re-analyzed surface water samples"). Method validation and quantification parameters can be found in Table SI-8, provided in the SI.

DOI: 10.1021/acs.est.5b03691
Environ. Sci. Technol. 2016, 50, 154−164

Table 1. Overview of the Biodegradation Batch Experiments Performed

compd	spike concn	no. of reactors	sampling date and matrix	degradation time	type of experiment	Figure
LMG	5 μg L^{-1}	2 (1 + ^{13}1[a])	AS[b], May 2014	6 days	kinetics, mass balance	SI-2, -3
	50 μg L^{-1}	2 (1 + ^{13}1[a])	AS, May 2014	6 days	TP identification	–
	5 μg L^{-1}	1	WWeff[c], May 2014	6 days	abiotic control	SI-2
LMG-N2-G	5 μg L^{-1}	1	AS, May 2014	6 days	kinetics, mass balance	SI-6
	50 μg L^{-1}	1	AS, May 2014	6 days	TP identification	–
	0.5 μg L^{-1}	4 (2 + 2)	AS, Aug 2014 (I) + Nov 2014	8 h	kinetics, mass balance	2, 3A
	5 μg L^{-1}	4 (2 + 2)	AS, Aug 2014 (I) + Nov 2014	8 h	kinetics, mass balance	2, 3B
	5 μg L^{-1}	1	WWeff, Aug 2014 (I)	8 h	abiotic control	2
	0.5 μg L^{-1}	3	AS, Nov 2014	8 h	abiotic control	SI-9A
	5 μg L^{-1}	3	AS, Nov 2014	8 h	abiotic control	SI-9B
LMG	194[d] ± 13 ng L^{-1}	4	AS, Aug 2014 (II)	12 h	TP stability	SI-8A
OXO-LMG	55[d] ± 4 ng L^{-1}	4	AS, Aug 2014 (II)	12 h	TP stability	SI-8B
LMG-N2-G-TP430	17[d] ± 1 ng L^{-1}	4	AS, Aug 2014 (II)	12 h	TP stability	SI-8C
N2-Me-LMG	4.1[d] ± 0.3 ng L^{-1}	4	AS, Aug 2014 (II)	12 h	TP stability	SI-8D

[a] ^{13}1: one batch reactor, performed with labeled $^{13}C_3$-LMG; [b] AS: activated sludge. [c] WWeff: wastewater effluent. [d] Not spiked; experiment was performed with the background concentration in the AS.

Biodegradation Experiments. Mixed liquor was freshly collected from the aeration tanks of WWTP-5 located close to the city of Barcelona (Spain) with 4.5 g_{ss} L^{-1} of total suspended solids (TSS). Activated sludge was diluted to 0.9 g_{ss} L^{-1} with wastewater (WW) effluent grab samples in order to reduce the effect of sorption,[19] and 1 L was transferred to amber glass bottles. Summary of the batch reactors performed is given in Table 1. The batch reactors were spiked with LMG, $^{13}C_3$-LMG, and LMG-N2-G with a concentration at 50 μg L^{-1} for identification of TPs and with 0.5 and 5 μg L^{-1} for kinetic experiments and mass balance. Biologically inactive control batch reactors (5% formaldehyde) were run in parallel with the same substrate concentration for activated sludge taken in November 2014. Abiotic control for May and August 2014 (I) experiments was a wastewater effluent.[19] In the control reactors, the concentration profiles showed no relevant decline of the spiked test compound(s) (Figure 2 and Figure SI-9, SI).

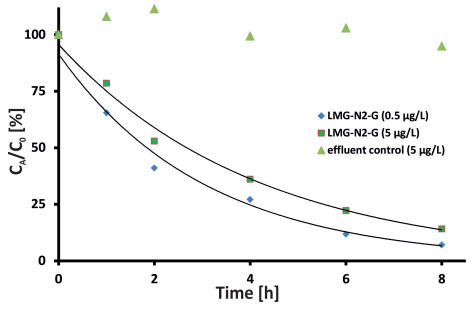

Figure 2. Degradation profile of LMG-N2-G in activated sludge with 0.9 g_{ss} L^{-1}. Each concentration profile corresponds to average concentrations of the four reactors loaded with sludge collected in Aug and Nov 2014 (see Table 1).

Over the course of all studies, the pH was maintained at 7.1 ± 0.3 using ammonium hydroxide or hydrochloric acid and checked twice daily (for biodegradation experiments in days) and after each sample was taken (for biodegradation in hours). The room temperature was 20−22 °C.

For every sampling point, 50 mL of the activated sludge mixture was taken, spiked with internal standard, and centrifuged. Then, the supernatant was taken and passed through an Oasis HLB cartridge, since all of the suspect analytes detected in wastewater samples were retained in this cartridge (Table SI-4, SI). The remainder of the extraction step was the same as performed in the analysis of real wastewater samples (see above).

Identification of Transformation Products with HRMS. Exact mass measurements of the parent compound and its biotransformation TPs obtained from the biodegradation samples were carried out in full-scan and product ion modes using a Q Exactive-MS (Thermo Scientific, Bremen, Germany) interfaced with an ACQUITY UPLC (Waters, Miliford, MA) system. Detailed information can be found in the SI.

RESULTS AND DISCUSSION

Preliminary Results of the Suspect Screening. The starting point of this work was a literature search for reported human metabolites of LMG and its relevant impurities in order to compile a list of LMG and related compounds (Table SI-2,[20] SI) for their subsequent screening in influent and effluent samples of WWTPs as well as in surface water samples. On the basis of the suspect list, their molecular ions $[^{35}M + H]^+$ and the $[^{37}M + H]^+$, which correspond to the ^{37}Cl isotope of suspect compounds in Table SI-2 (SI), were screened in WW and surface water extracts. They were extracted from the (+) ESI-HRMS chromatograms of samples from WWTPs and surface water with an isolation width of 5 ppm. At this point, authentic standards were not yet available and the mass spectra of the resulting peaks in the extracted ion chromatograms were examined for the presence of the highly characteristic isotope pattern of compounds bearing two chlorine atoms. Tentative detections were further rationalized by their relative retention times and MS^2 spectra. This approach provided strong hints for the presence of five suspect analytes in various influent, effluent, and surface water samples (Table SI-2, SI). Screening of the surface water samples showed the presence of the same compounds as in WW samples with none of the reported photodegradation products detected. Since other compounds from Table SI-2 (SI) were not detected, they were no longer considered as relevant for this study.

Results of the preliminary screening are reported in Table SI-3 with additional discussion in the SI. In brief, unexpectedly high concentrations of known LMG synthetic impurity (OXO-LMG) were found in effluent samples compared to the influent in two WWTPs. This suggested the formation of OXO-LMG in

DOI: 10.1021/acs.est.5b03691
Environ. Sci. Technol. 2016, 50, 154−164

WWTPs. Likewise, it can also be seen that the LMG concentration is increasing in WW effluent, most likely as a result of LMG-N2-G hydrolysis together with possible LMG degradation, which can result in formation of TPs. As a result of this initial screening, it was postulated that OXO-LMG together with N2-Me-LMG and N2-LMG-oxide (detected and shown in Table SI-3) are LMG TPs formed during aerobic sewage treatment in WWTPs.

LMG Biodegradation in Batch Reactors. In order to test this hypothesis, a set of lab-scale biodegradation experiments were performed using activated sludge from the activation tank of a municipal WWTP. As explained in the Experimental Section (Table 1), 1 L bioreactors set at 0.9 g_{ss} L^{-1} were spiked with LMG at 50 and 5 μg L^{-1} (background concentrations of analytes for all experiments reported in Table SI-5, SI) for the identification of TPs and for kinetic studies, respectively. Additional reactors were fortified with the same two concentrations of isotopically labeled $^{13}C_3$-LMG in order to gather evidence that supported the MS-derived identities of the TPs postulated in the degradation of unlabeled LMG. As can be seen in Figure SI-2 (SI), the degradation of LMG (5 μg L^{-1}) proceeded slowly with about 95% of the initial concentration still remaining after 6 days. On the basis of the exact mass data and the characteristic chlorine isotope pattern, two degradation products were readily spotted and tentatively identified as originating from the N-oxygenation (m/z 272.0100, LMG-N2-oxide) and N-methylation (m/z 270.308, N2-Me-LMG) of LMG (Figure SI-3, SI). The detection of the corresponding $^{13}C_3$-labeled TPs in the experiment performed with $^{13}C_3$-LMG confirmed the formation of these two species (Figures SI-4 and SI-5, SI). Analysis of wastewater extracts showed that both degradates from the batch reactors matched the retention times and MS^2 spectra of the compounds detected in real samples, thus supporting the validity of the laboratory experiments. In order to unequivocally confirm them as human metabolites, they were matched against the retention times and (+) ESI-MS product ion profiles of the commercially available standard (LMG-N2-oxide) and that synthesized by our group (N2-Me-LMG). As a result, this enabled their quantification in the samples from the biodegradation experiment and real samples.

However, in LMG batch reactors (Figure SI-3, SI), the concentration of OXO-LMG is minute and stable from the beginning of the experiment, where it was present due to the background concentration (Table SI-5, SI). What this experiment showed was that the compound detected in the WW samples does not form as a result of LMG biodegradation. A literature search suggested that LMG can be transformed to OXO-LMG only under harsh, basic hydrolysis conditions with prolonged heating under reflux,[21] an impossible reaction under environmental conditions. But since it was possible to obtain the commercially available standard of OXO-LMG, the compound was purchased and its retention time and spectra were compared with those of the compound found in wastewater samples (Figure 4b,c). This positively confirmed that the compound found in the WW samples was OXO-LMG. The next best plausible explanation seemed that this compound could be formed from LMG-N2-G due to its high concentration in the influent samples and its significant decrease in WWTP effluents (Table SI-3, SI).

Lamotrigine-N^2-glucuronide Biodegradation in Lab-Scale Reactors. Activated sludge from a biodegradation tank was again used and spiked with two concentrations of the LMG-N2-G, 5 and 50 μg L^{-1} (Table 1). Figure SI-6 (SI) shows the degradation of LMG-N2-G spiked at 5 μg L^{-1} over the course of 6 days. As can be seen from the figure, OXO-LMG did form as a result of LMG-N2-G degradation, not LMG. However, after 24 h, more than 90% of the LMG-N2-G was degraded. Due to this, biodegradation of LMG-N2-G was repeated for the 5 μg L^{-1} sample and joined with 0.5 μg L^{-1} over the course of 8 h (Table 1). The concentration at 0.5 μg L^{-1} was the lowest spiked concentration due to the high background of LMG in activated sludge, which was 284 μg L^{-1} for Aug 2014 (I) and 120 μg L^{-1} for Nov 2014 (Table SI-5, SI).

Transformation Kinetics of Lamotrigine-N2-glucuronide and Mass Balance. For the degradation of LMG-N2-G at both concentrations (0.5 and 5 μg L^{-1}), TSS of the activated sludge were normalized in all experiments to 0.9 g_{ss} L^{-1} to match the initial degradation experiments. Figure 2 shows the average degradation from four batch reactors (duplicate of AS taken in Aug 2014 (I) + duplicate of AS taken in Nov 2014) for both concentrations. The degradation of LMG-N2-G at both concentrations was exponential, and this decrease can be explained by pseudo-first-order kinetics. In the batch experiments, the calculated half-lives of LMG-N2-G were 2.0 ± 0.5 (R^2 = 0.9908) and 2.8 ± 0.8 (R^2 = 0.9931) h for 0.5 and 5 μg L^{-1} concentrations, respectively. The similar degradation rate of LMG-N2-G at 0.5 μg L^{-1} is also evidenced in the similar transformation rate constant (k_{biol}) of 0.4 ± 0.1 L g_{ss}^{-1} h^{-1} for 0.5 μg L^{-1} (for 5 μg L^{-1}, k_{biol} = 0.3 ± 0.1 L g_{ss}^{-1} h^{-1}).

Over the course of 8 h, the concentration of LMG-N2-G decreased by about 90% at both concentrations (0.5 and 5 μg L^{-1}). Concomitantly, LMG and OXO-LMG were formed with LMG accounting for approximately 60% of the degraded substrate in the last sample taken. At the end of the incubation, the percentage of OXO-LMG at the end of both experiments was between 2 and 5%. Figure SI-7 (SI) shows the LMG-N2-G mass balance at both concentrations (0.5 and 5 μg L^{-1}). At the end of the degradation study, the combined concentrations of LMG-N2-G, LMG and OXO-LMG amounted to 70% of the initial glucuronide concentration (0.5 μg L^{-1}) and 80% at 5 μg L^{-1}. This indicated the possibility that we were missing some transformations, since we were not able to close the mass balance of the LMG-N2-G in the batch reactors. For this, batch reactors and environmental sample extracts were checked for the presence of other TPs using a fragment ion search (FISh, Mass Frontier) and double-checked with SIEVE (Thermo Fisher). FISh was set to LMG fragment ion m/z 256.0156 as the LMG-N2-G fragment search. As a result, another compound at retention time (t_R) 5.72 min was found in the samples with the exact mass of m/z 430.0316 and elemental composition of $C_{15}H_{14}Cl_2N_5O_6$. Since it was not possible to obtain an authentic standard of the compound with m/z 430.0316 (named LMG-N2-G-TP430), its concentration was calculated on the basis of semiquantitative analysis by using LMG-N2-G as a reference standard. LMG-N2-G was used as a reference standard because of its proximity to m/z and the t_R of the TP. Likewise, the elemental composition of LMG-N2-G-TP430 suggested (this was later confirmed by structural elucidation) that this TP retained the 1,2,4-triazine-3,5-diamine moiety of the LMG-N2-G structure, which is expected to carry the positive charge when the molecule is ionized. In the batch reactors at the end of the incubation period of 8 h, the LMG-N2-G-TP430 concentration was about 20% compared to the initial concentration of LMG-N2-G (Figure 3). Adding the concentration of this TP into the mass balance calculation, it was possible to close the mass balance of the batch reactor at

DOI: 10.1021/acs.est.5b03691
Environ. Sci. Technol. 2016, 50, 154−164

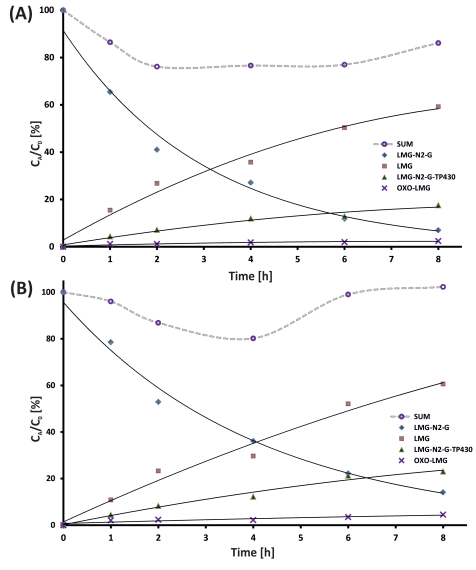

Figure 3. Average mass balance based on molar concentrations of four reactors with sludge taken in Aug 2014 (I) and Nov 2014 for (A) 0.5 μg L^{-1} and (B) 5 μg L^{-1} concentration of LMG N2-G degraded over the course of 8 h.

0.5 μg L^{-1} with 86% (Figure 3A) and batch reactor at 5 μg L^{-1} with 102% (Figure 3B). This would indicate an almost quantitative transformation of LMG-N2-G to three TPs—LMG, OXO-LMG, and LMG-N2-G-TP430—since no other formed TPs were detected. Once the LMG-N2-G-TP430 structure was elucidated, its presence was checked in the WW sample extracts, which is explained in the following sections.

It is likely that the transformations of LMG-N2-G were caused by enzymatic activity, since there was no apparent decrease of LMG-N2-G concentration in the abiotic control (Figure 2 and Figure SI-9, SI). Due to the high polarity of LMG-N2-G and its fast transformation rate, other parameters that would influence the concentration change of LMG-N2-G, like the effect of sorption on mass balance, can be expected to be negligible.

Following the results of LMG-N2-G degradation, the stability of TPs was also tested over the course of 12 h in activated sludge (TSS = 0.9 g_{ss} L^{-1}) (Figure SI-8, SI). Due to the high background concentration of these TPs (all but LMG-N2-oxide were detected) in activated sludge, the reactors were run with the background concentration reported in Table 1, and 194 ng L^{-1} of LMG (Figure SI-8A, SI) and 55 ng L^{-1} of OXO-LMG (Figure SI-8B, SI) were completely stable over 12 h (as similarly reported for LMG at higher concentration in Figure SI-2, SI). For 17 ng L^{-1} of LMG-N2-G-TP430 (Figure SI-8C, SI), a slight decrease was noticed, but this TP was more stable than its parent LMG-N2-G (Figure 2). The only LMG TP detected (N2-Me-LMG) at a concentration of 4.1 ng L^{-1} was likewise stable during the test (Figure SI-8D, SI).

Identification of TPs by UPLC–Q Exactive-MS. For the identification of TP LMG-N2-TP430, the MS^2 and pseudo-MS^3 (pMS^3) product ion spectra of the parent compounds LMG, LMG-N2-G, and TP430 were recorded to determine the plausible elemental compositions and structures of the fragment ions (see Table SI-6 for elemental compositions and Figure SI-10 for the fragmentation pathways and spectra in the SI).

In order to better understand the fragmentation of LMG-N2-G-TP430, the fragmentation patterns of both LMG and LMG-N2-G were studied. The absence of a readily cleavable bond in 1,2,4-triazine structure of LMG leads to generation of a complex fragmentation pattern producing many fragment ions in the midmass range (Figure 4A and Figure SI-10.1-A,B, SI). On the other hand, the aromaticity of the phenyl-1,2,4-triazine ring of LMG makes it a very stable molecule that requires higher collision energies to break [normalized collision energy (NCE) >50%]. In general, LMG undergoes reactions of gradual deamination of the 1,2,4-triazine ring followed by dechlorination, leaving the benzene moiety intact. This is in accordance with previous studies of LMG fragmentation.[7]

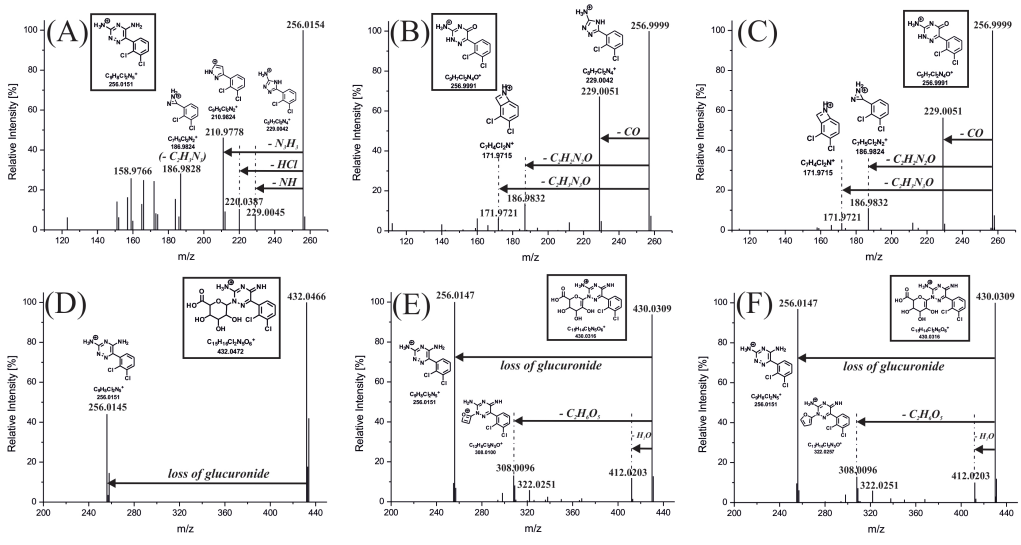

Figure 4. Fragmentation pattern of (A) LMG standard at NCE 70%, (B) OXO-LMG standard at NCE 40%, (C) OXO-LMG detected in the WW effluent samples at NCE 40%, (D) LMG-N2-G standard at NCE 10%, (E) LMG-N2-G-TP430 formed in biodegradation experiments at NCE 35%, and (F) LMG-N2-G-TP430 detected in WW effluent sample at NCE 35%.

DOI: 10.1021/acs.est.5b03691
Environ. Sci. Technol. 2016, 50, 154–164

Scheme 1. Proposed Transformation Pathways of LMG-N2-G in WWTP Activated Sludge[a]

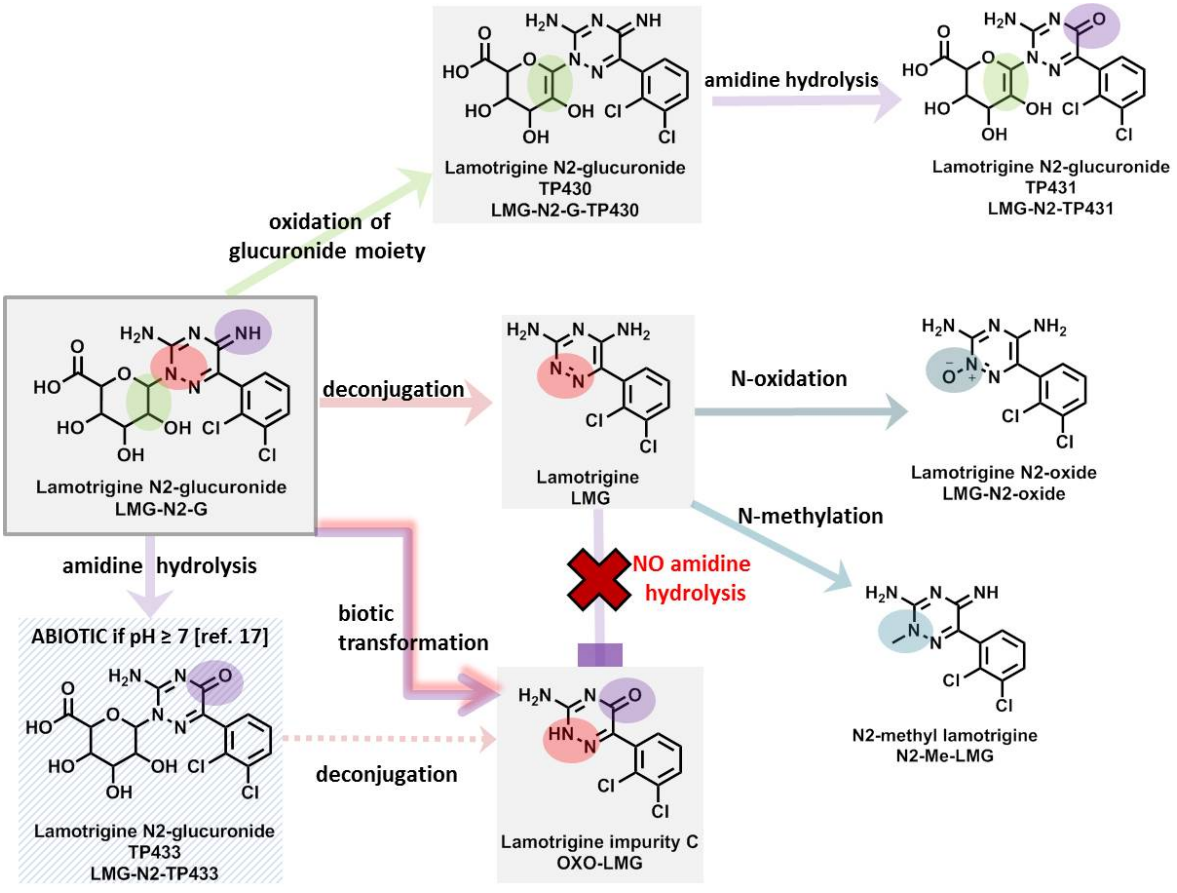

[a]LMG-N2-G principal TPs are presented with a gray background. Dashed lines represent possible reaction pathways suggested but not reported in this work.

LMG-N2-G breaks easily in the ESI source to yield its precursor drug (m/z 256.0151, LMG), which is characteristic for many glucuronides.[22] The same is seen, to a lesser extent, for LMG-N2-G-TP430. The MS^2 spectrum of LMG-N2-G (Figure 4D) likewise shows that the glycosidic bond cleaves easily,[7] yielding only one fragment with m/z 256.0151 (LMG) at low NCE of 10% (Figure 4D and Figure SI-10.2-A,B, SI). By increasing the NCE, only fragmentation of the fragment at m/z 256.0151 is seen.

LMG-N2-G-TP430, with m/z 430.0316, differs from LMG-N2-G (m/z 432.0472) by 2.0156 Da (Figure 4E), meaning that LMG-N2-G oxidized to form LMG-N2-G-TP430. The MS^2 of LMG-N2-G-TP430 shows that the compound breaks again to m/z 256.0151 as the most abundant fragment. The pMS^3 spectrum of the fragment m/z 256.0151 shows the same fragmentation pattern as the LMG standard (Figure SI-10.1-A,B, SI). This gives evidence that the LMG part of the LMG-N2-G-TP430 remains intact and that LMG is a building block of the TP430. However, LMG-N2-G-TP430 is more stable under applied NCE than LMG-N2-G, and at NCE 35%, parent ion is as abundant as m/z 256.0151. LMG-N2-G under NCE 35% breaks almost entirely to m/z 256.0151 and subsequent fragments. Moreover, what was also observed from the MS^2 spectrum of LMG-N2-G-TP430 is that the glucuronide moiety fragments while still attached to the LMG in LMG-N2-G-TP430. This would suggest higher stability through oxidation of the carbon attached with the glycosidic bond (C1) and C2 in the glucuronide moiety. In general, the fragmentation on LMG-N2-G-TP430 follows chain loss of water and gradual breakage of the glucuronide. A detailed fragmentation pattern scheme and spectra can be found in Figure SI-10.3-A,B (SI).

Transformation Reactions of LMG-N2-G. LMG-N2-G was degraded in activated sludge under aerobic conditions, forming three stable TPs (Scheme 1). Among the three TPs of LMG-N2-G, LMG is released by enzymatic hydrolysis of the glycosidic bond between the glucuronide and the aglycon, thereby constituting reversal of the reaction that leads to the formation of LMG-N2-G in the human liver (Scheme 1, red transformations). The hydrolytic pathway of glucuronides has been reported previously for a number of drug conjugates, in particular for estrogens.[12−15] As found in biodegradation reactors and shown in Scheme 1, LMG undergoes further transformation to LMG-N2-oxide and N2-Me-LMG, following slow kinetics (Figure SI-3, SI). These two TPs were also reported previously as human metabolites of LMG.[3−5]

The second transformation (Scheme 1, red/purple transformations) is the transformation of LMG-N2-G to OXO-LMG (m/z 256.9991). This TP is formed as a combination of two reactions. The first step is the hydrolysis of the amidine moiety on the LMG part of the LMG-N2-G molecule, followed by deconjugation of the glucuronide. The order of these reactions is evidenced in the biodegradation experiment of LMG and LMG-N2-G, where solely LMG is not undergoing amidine hydrolysis to form OXO-LMG. However, Zonja et al.[17]

DOI: 10.1021/acs.est.5b03691
Environ. Sci. Technol. 2016, 50, 154−164

Table 2. Concentrations (in nmol L^{-1}) of LMG-N2-G and Transformation Products in WWTPs

	WWTP 1		WWTP 2		WWTP 3	
	influent	effluent	influent	effluent	influent	effluent
Before the Degradation of LMG-N2-G						
LMG-N2-G (1)	7.623 ± 0.555	2.193 ± 0.165	0.525 ± 0.019	0.098 ± 0.006	0.103 ± 0.009	0.019 ± 0.001
$[^{37}Cl]/[^{35}Cl]$ (%)	62	59	66	68	63	61
LMG (2)	2.031 ± 0.114	4.897 ± 0.482	0.081 ± 0.027	0.378 ± 0.007	0.052 ± 0.012	0.072 ± 0.001
$[^{37}Cl]/[^{35}Cl]$ (%)	60	64	46	64	63	63
sum 1 + 2[a]	**9.654 (−27%)**	**7.090**	**0.606 (−21%)**	**0.476**	**0.155 (−41%)**	**0.091**
N2-Me-LMG (3)	nd[b]	0.074 ± 0.007	nd	0.004 ± 0.001	nd	<LOQ
$[^{37}Cl]/[^{35}Cl]$ (%)	–	60	–	50	–	52
LMG-N2-oxide (4)	nd	0.078 ± 0.003	nd	0.011 ± 0.001	nd	nd
$[^{37}Cl]/[^{35}Cl]$ (%)	–	63	–	42	–	–
sum 1−4	**9.654 (−25%)**	**7.242**	**0.606 (−19%)**	**0.491**	**0.155 (−41%)**	**0.091**
After the Degradation of LMG-N2-G						
OXO-LMG (5)	0.229 ± 0.047	1.204 ± 0.027	0.018 ± 0.006	0.094 ± 0.003	0.026 ± 0.001	0.031 ± 0.008
$[^{37}Cl]/[^{35}Cl]$ (%)	54	60	42	53	62	61
LMG-N2-G-TP433-Amd (6)	0.125 ± 0.024	nd	nd	nd	nd	nd
$[^{37}Cl]/[^{35}Cl]$ (%)	43	–	–	–	–	–
sum 1−6	**10.008 (−16%)**	**8.446**	**0.624 (−6%)**	**0.585**	**0.181 (−33%)**	**0.122**
LMG-N2-G-TP430 (7)[c]	nd	1.062 ± 0.182	nd	0.052 ± 0.001	0.002 ± 0.001	0.008 ± 0.005
$[^{37}Cl]/[^{35}Cl]$ (%)	–	62	–	60	50	65
SUM all (1−7)	**10.008 (−5%)**	**9.508**	**0.624 (+2%)**	**0.637**	**0.183 (−29%)**	**0.130**

[a]The numbers in parentheses represents the percentage of difference between influent and effluent with respect to mass balance. [b]nd = not detected. [c]LMG-N2-G-TP430 concentration was calculated using LMG-N2-G as a reference standard; hence, its concentration reported here is semiquantitative.

investigated the abiotic, pH- and N2-substituent-dependent behavior of LMG and related compounds and found that an abiotic TP of LMG-N2-G (in blue), LMG-N2-G-TP433-Amd, forms as a result of pH-dependent amidine hydrolysis of LMG-N2-G under neutral to basic conditions.[17] It is probable that LMG-N2-G-TP433-Amd can easily undergo glucuronide hydrolysis and form OXO-LMG, which would explain why it was not found in any of the batch reactors. Although no apparent decrease of LMG-N2-G concentration was noticed in abiotic batch reactors (Figure 2 and Figure SI-9, SI), LMG-N2-G-TP433-Amd was detected at up to 0.7% of the initial LMG-N2-G concentration, which is in accordance with experiments performed in Zonja et al.[17] Having this in mind, the formation of OXO-LMG from LMG-N2-G is the result of these two reactions (amidine hydrolysis and deconjugation) happening sequentially. This would suggest either initial abiotic amidine hydrolysis followed by deconjugation or direct enzymatic transformation. Direct guanidine hydrolysis (without other modification on the molecule) as a biotic transformation was reported for the antidiabetic drug metformin.[23]

Finally, the third TP formed from LMG-N2-G is LMG-N2-G-TP430 (Scheme 1, green transformations). An aerobic microbial metabolites predictor, the EAWAG-BBD pathway prediction system (EAWAG-BBD[24]), suggested that the most likely biotic transformation of the LMG-N2-G would be an oxidation of one of the secondary glucuronide alcohols (C2, C3, or C4) to its corresponding ketone (although with neutral aerobic likelihood). However, it is more likely that this bioTP arose from the oxidation of the glucuronide to the corresponding glycal. As expected from the chemistry of glycals,[25] water adds preferentially to the C1−C2 double bond to give the corresponding hydration product. This explains the higher stability of the TP430 in comparison with the parent glucuronide (LMG-N2-G), where the hydrolysis of the hemiaminal moiety renders lamotrigine and glucuronic acid. This TP forms a second phase LMG-N2-G-TP431 via amidine hydrolysis. However, since the LMG-N2-G-TP431-Amd was formed and detected only in experiments over the course of 6 days (Table 1), it was excluded from LMG-N2-G mass balance. Additional information on LMG-N2-G-TP431-Amd can be found in the SI (Figures SI-11 and -12).

Analysis of TPs in WWTPs. Once the TPs have been identified, a quantitative method was applied to analysis of 24 h composite wastewater samples from four conventional Catalan WWTPs. At this point, purchased standards were used for LMG, LMG-N2-G, LMG-N2-oxide, and OXO-LMG. N2-Me-LMG and LMG-N2-G-TP433-Amd were synthesized, and LMG-N2-G-TP430 was semiquantified using LMG-N2-G as a standard. LMG-N2-G-TP433-Amd, an abiotic degradation product, was included in order to better describe the mass load and transformation of all LMG-N2-G TPs, since it can be formed before it enters in the WWTPs[17] and further deconjugate during the treatment in WWTP to OXO-LMG (Scheme 1). LMG-N2-G-TP431 was left out of the mass balance, since it was not found in any of the real wastewater samples. Concentrations (in nmol L^{-1}) are reported in Table 2. LMG-N2-G was detected in all three WWTPs (one WWTP was omitted due to a procedural error, and its results with detailed information can be seen in Table SI-7, SI). Concentrations in the WWTP influent ranged from 0.103 nmol L^{-1} (44 ng L^{-1}) for WWTP 3 to 7.623 nmol L^{-1} (3295 ng L^{-1}) for WWTP 1. The concentration of LMG-N2-G was significantly reduced in the effluent in comparison to the influent (71−81%). The decrease of LMG-N2-G concentration was most likely caused by transformation, because its biotransformation TPs, OXO-LMG and LMG-N2-G-TP-430, were detected in the effluent of all WWTPs. The LMG-N2-G mass balance shows that if only deconjugation reaction was taken into account, 21−41% of the glucuronide concentration would have been unaccounted for, depending on the WWTP

DOI: 10.1021/acs.est.5b03691
Environ. Sci. Technol. 2016, 50, 154−164

Table 3. Mass Concentrations of LMG-N2-G, LMG, and their TPs in 13 Surface Water Samples[a]

	LMG-N2-G		LMG		N2-Me-LMG		LMG-N2-oxide		OXO-LMG		LMG-N2-G-TP430	
	ng L^{-1}	$[^{37}Cl]/[^{35}Cl]$ (%)	ng L^{-1}	$[^{37}Cl]/[^{35}Cl]$ (%)	ng L^{-1}	$[^{37}Cl]/[^{35}Cl]$ (%)	ng L^{-1}	$[^{37}Cl]/[^{35}Cl]$ (%)	ng L^{-1}	$[^{37}Cl]/[^{35}Cl]$ (%)	ng L^{-1}	$[^{37}Cl]/[^{35}Cl]$ (%)
Ll-1	22.6 ± 9.9	55	40.9 ± 22.4	62	<LOQ	63	nd	–	15.5 ± 6.5	61	22.6 ± 11.6	61
Ll-2	18.2 ± 1.6	59	40.6 ± 5.2	63	nd	–	<LOQ	64	11.5 ± 2.2	53	15.9 ± 5.2	68
Ll-3	27.6 ± 7.1	59	37.1 ± 0.6	62	<LOQ	54	<LOQ	64	10.2 ± 1.1	62	5.8 ± 1.5	63
Ll-4	43.7 ± 23.5	60	64.3 ± 3.7	63	0.6 ± 0.4	74	<LOQ	58	24.0 ± 7.4	61	9.9 ± 2.5	57
Ll-5	371 ± 99	61	1011 ± 218	61	16.3 ± 4.6	64	nd	–	247 ± 72	61	549 ± 137	58
Ll-6	94.4 ± 15.4	60	139 ± 9	63	1.3 ± 0.1	41	nd	–	41.8 ± 7.2	63	34.4 ± 6.4	61
Ll-7	55.0 ± 11.1	64	111 ± 2	62	nd	–	<LOQ	58	29.7 ± 5.4	64	13.2 ± 4.2	52
Bs-1	29.5 ± 1.3	60	237 ± 8	63	5.3 ± 0.2	64	<LOQ	52	57.4 ± 1.9	62	59.7 ± 2.0	59
Bs-2	6.4 ± 0.3	51	162 ± 4	64	4.0 ± 0.3	60	<LOQ	54	49.9 ± 0.6	60	24.6 ± 1.6	62
Bs-3	41.8 ± 1.9	63	234 ± 14	64	7.4 ± 0.5	63	<LOQ	55	60.0 ± 2.5	60	109 ± 2	61
Bs-4	24.9 ± 2.6	59	172 ± 25	61	0.8 ± 0.2	52	nd	–	93.1 ± 12	63	22.6 ± 3.6	61
Bs-5	10.4 ± 2.3	57	141 ± 27	58	1.2 ± 0.2	49	nd	–	74.5 ± 4.1	52	16.3 ± 1.8	65
Bs-6	6.0 ± 0.4	60	63.6 ± 7.1	64	0.5 ± 0.1	54	nd	–	24.6 ± 1.6	61	nd	–
mean	57.8		189		2.9		–		56.9		67.9	
median	27.6		139		0.8		–		41.8		22.6	

[a]nd = not detected, Ll = Llobregat River sampling point, Bs = Besos River sampling point. The standard deviation was calculated on the basis of three separate measurements. LMG-N2-G-TP430 concentration was calculated using LMG-N2-G as a reference standard; hence, its concentration reported here is semiquantitative.

DOI: 10.1021/acs.est.5b03691
Environ. Sci. Technol. 2016, 50, 154−164

(Table 2, sum 1 + 2). It was possible to account for up to 98% of all LMG-N2-G entering the WWTP with LMG TPs: N2-Me-LMG and LMG-N2-oxide (Table 2, sum 1−4), LMG-N2-G amidine hydrolysis TPs (Table 2, sum 1−6), and LMG-N2-G oxidation TP LMG-N2-G-TP430 (Table 2, sum 1−7).

N2-Me-LMG and LMG-N2-oxide were also taken into account when calculating mass balance, since they are human metabolites and also TPs of LMG. However, since the two TPs are minor human metabolites of LMG, they were not detected in any of the influent samples. On the other hand, due to the low transformation rate of LMG in biodegradation batch experiments (as seen in Figure SI-3, SI), where 95% of LMG remained after 6 days of degradation, they were only expected to negligibly influence the LMG-N2-G mass balance. They were found to alter the final mass balance up to 2%.

Out of the two amidine hydrolysis TPs, OXO-LMG was already found in WWTP influent, with its concentration increasing significantly at the WWTP effluent. The concentration ranged from 0.031 to 1.204 nmol L^{-1} (7.9−310 ng L^{-1}). As to the abiotic TP LMG-N2-G-TP433-Amd, it was only detected in WWTP influent. This is in accordance with the batch experiments where, even at the higher concentration of 5 μg L^{-1}, this abiotic TP was not detected. It is likely quickly transformed to OXO-LMG during secondary treatment, where this biotic reaction of deconjugation in the WWTPs competes with the abiotic pH-dependent amidine hydrolysis, yielding LMG-N2-G-TP433-Amd.[17] The rate of the latter reaction is increasing exponentially when increasing the pH from 7 to 9.[17] Since the pH of the samples analyzed here was around 8, the formation of OXO-LMG is also influenced by this parameter. Unlike the batch reactors at pH 7, where only 2−5% of OXO-LMG is detected after an incubation period of 8 h, higher rates in all WWTPs reported (8−14%) depend on pH change in every stage of wastewater treatment and hydraulic retention time.

The last LMG-N2-G TP detected was the LMG-N2-G-TP430. This compound was found only in WWTP 3 in the influent sample, which suggests that it could be possible that the biotransformation could begin before LMG-N2-G enters the WWTPs. A significant increase of this TP in the WWTP effluent finally closed the mass balance of LMG-N2-G with less than 5% deviation for WWTP 1 and 2 and less than 30% for WWTP 3. While in WWTP 1 and 2 the sum of molar concentrations of LMG-related compounds in the effluent almost equals those in the influent, in WWTP 3 only 71 mol % was explained by taking into consideration LMG, LMG-N2-G, and all of its identified TPs. This could be attributed to the variability of concentrations due to fluctuations in wastewater.[26−28] It has been reported that even having in mind the hydraulic retention time of the wastewater when sampling a WWTP, it is not the only factor to take into account for reliable calculation of removal rates.[29,30] For example, the study by Gurke et al.,[30] where flow-proportional, 24-h composite samples from the influent and effluent of the same WWTP were taken on 10 consecutive days, showed that lamotrigine had negative removal rates of −30 to −70%. But since LMG-N2-G was not monitored in that study, no explanation for the removal rates could be put forward. Although flow-proportional and consecutive composite sampling is advised in order to compare the loads at different points within the WWTP,[27] the WWTPs sampled in this study employed three different sampling modes: time (WWTP 1), flow (WWTP 2), and volume proportional (WWTP 3) (see details in the SI, "Sampling of wastewater"). Therefore, the mass balance studies of WWTP1 and WWTP 3 are of rather semiquantitative nature. However, they do show that the comprehensive examination of the transformation pathways for LMG-N2-G has led us to revise the prevailing concept that glucuronides will only revert back to the parent compound in the WWTPs. These results suggest that for some glucuronides the transformation reactions are not as straightforward as reported so far for other glucuronides (especially estrogens), where the only reaction observed was limited to deconjugation in the WWTPs.[12−15]

The susceptibility to undergo transformations other than deconjugation is deemed to be higher for quaternary N-glucuronides because of their unique chemical structure[31] when compared to other types of glucuronide conjugates, which are either ethers or esters.

Environmental Relevance: Retrospective Analysis and Occurrence of LMG and Derived Compounds in Surface Waters. Surface water grab samples (Table 3) were sampled along the two rivers where the analyzed WWTPs discharge treated wastewater. LMG-N2-G, LMG, and OXO-LMG were found in every sample analyzed. The concentration for LMG-N2-G ranged from 6 to 371 ng L^{-1}, with median concentration of 27.6 ng L^{-1}. LMG had significantly higher concentration in comparison with its metabolite LMG-N2-G, which is in accordance with the results from the WWTP (range 37.1−1011 ng L^{-1}, median 139 ng L^{-1}). The LMG TPs N2-Me-LMG and LMG-N2-oxide have been found in low ng L^{-1} concentrations with a median concentration for N2-Me-LMG of 0.8 ng L^{-1}. LMG-N2-oxide has only been detected in half of the samples analyzed with all concentrations below the limit of quantitation (LOQ). The LMG-N2-G TPs OXO-LMG and LMG-N2-G-TP430 have been found more frequently and with higher concentrations. As mentioned earlier, the concentration of LMG-N2-G-TP430 was calculated using LMG-N2-G as a reference standard and its concentration should be considered semiquantitative. LMG-N2-G-TP430 has been found roughly at the same concentration as LMG-N2-G with a median of 22 ng L^{-1} (range from nd to 549 ng L^{-1}) while the concentration of OXO-LMG was higher than that of the parent LMG-N2-G (median concentration 41.8 ng L^{-1}, range 10.2−247 ng L^{-1}). A slightly higher concentration of OXO-LMG when compared with LMG-N2-G and LMG-N2-G-TP430 could be due to further transformations of the parent LMG-N2-G. The average pH of the surface water samples analyzed was slightly basic (Table SI-1, SI), which would have a sufficiently high enough pH for the LMG-N2-G to undergo further amidine hydrolysis (a neutral−basic pH governed reaction for LMG-N2-G) in surface water to form LMG-N2-G-TP433-Amd.[17] In comparison with other glucuronides, like sulfamethoxazole *N*-glucuronide, which can undergo hydrolysis in surface water,[32] the LMG-N2-G-TP433-Amd could also undergo further hydrolysis and deconjugate to OXO-LMG.

■ ASSOCIATED CONTENT

Supporting Information

The Supporting Information is available free of charge on the ACS Publications website at DOI: 10.1021/acs.est.5b03691.

Additional experimental details, figures, and tables as noted in the text (Figures SI-1−SI-13 and Tables SI-1−SI-8) (PDF)

DOI: 10.1021/acs.est.5b03691
Environ. Sci. Technol. 2016, 50, 154−164

AUTHOR INFORMATION

Corresponding Author

*Phone: +34934006100; e-mail: spsqam@cid.csic.es.

Author Contributions

The manuscript was written through contributions of all authors. All authors have given approval to the final version of the manuscript

Notes

The authors declare no competing financial interest.

ACKNOWLEDGMENTS

B.Z. acknowledges the Marie Curie Actions ITN CSI:Environment PITN-GA-2010-264329 for the early stage researcher contract and funding. S.P. acknowledges the contract from the Ramon y Cajal Program of the Spanish Ministry of Economy and Competitiveness. This work has been financially supported by the SOLUTIONS project, which has received funding from the European Union's Seventh Framework Programme for research, technological development, and demonstration under grant agreement no. 60343, and Generalitat de Catalunya (Consolidated Research Groups "2014 SGR 418−Water and Soil Quality Unit" and 2014 SGR 291−ICRA). R. Chaler and D. Fanjul are acknowledged for the maintenance and help within the mass spectrometry unit at IDAEA-CSIC. The authors wish to thank A. Delgado for the helpful discussion regarding the manuscript and to WWTP staff for providing the samples.

REFERENCES

(1) Ohman, I.; Beck, O.; Vitols, S.; Tomson, T. Plasma concentrations of lamotrigine and its 2-N-glucuronide metabolite during pregnancy in women with epilepsy. *Epilepsia* **2008**, *49* (6), 1075−80.

(2) Saracino, M. A.; Bugamelli, F.; Conti, M.; Amore, M.; Raggi, M. A. Rapid HPLC analysis of the antiepileptic lamotrigine and its metabolites in human plasma. *J. Sep. Sci.* **2007**, *30* (14), 2249−55.

(3) Ramsay, R. E.; Pellock, J. M.; Garnett, W. R.; Sanchez, R. M.; Valakas, A. M.; Wargin, W. A.; Lai, A. A.; Hubbell, J.; Chern, W. H.; Allsup, T.; Otto, V. Pharmacokinetics and safety of lamotrigine (Lamictal®) in patients with epilepsy. *Epilepsy Res.* **1991**, *10* (2−3), 191−200.

(4) Sidhu, J.; Job, S.; Bullman, J.; Francis, E.; Abbott, R.; Ascher, J.; Theis, J. G. W. Pharmacokinetics and tolerability of lamotrigine and olanzapine coadministered to healthy subjects. *Br. J. Clin. Pharmacol.* **2006**, *61* (4), 420−426.

(5) Lu, W.; Uetrecht, J. P. Possible bioactivation pathways of lamotrigine. *Drug Metab. Dispos.* **2007**, *35* (7), 1050−6.

(6) Doig, M. V.; Clare, R. A. Use of thermospray liquid chromatography-mass spectrometry to aid in the identification of urinary metabolites of a novel antiepileptic drug, Lamotrigine. *Journal of Chromatography A* **1991**, *554* (1−2), 181−189.

(7) Ferrer, I.; Thurman, E. M. Identification of a New Antidepressant and its Glucuronide Metabolite in Water Samples Using Liquid Chromatography/Quadrupole Time-of-Flight Mass Spectrometry. *Anal. Chem.* **2010**, *82* (19), 8161−8168.

(8) Writer, J. H.; Ferrer, I.; Barber, L. B.; Thurman, E. M. Widespread occurrence of neuro-active pharmaceuticals and metabolites in 24 minnesota rivers and wastewaters. *Sci. Total Environ.* **2013**, *461−462*, 519−27.

(9) Writer, J. H.; Antweiler, R. C.; Ferrer, I.; Ryan, J. N.; Thurman, E. M. In-stream attenuation of neuro-active pharmaceuticals and their metabolites. *Environ. Sci. Technol.* **2013**, *47* (17), 9781−90.

(10) Young, R. B.; Chefetz, B.; Liu, A.; Desyaterik, Y.; Borch, T. Direct photodegradation of lamotrigine (an antiepileptic) in simulated sunlight−pH influenced rates and products. *Environ. Sci. Process Impacts* **2014**, *16* (4), 848−57.

(11) Keen, O. S.; Ferrer, I.; Michael Thurman, E.; Linden, K. G. Degradation pathways of lamotrigine under advanced treatment by direct UV photolysis, hydroxyl radicals, and ozone. *Chemosphere* **2014**, *117* (0), 316−323.

(12) Kumar, V.; Johnson, A. C.; Nakada, N.; Yamashita, N.; Tanaka, H. De-conjugation behavior of conjugated estrogens in the raw sewage, activated sludge and river water. *J. Hazard. Mater.* **2012**, *227−228*, 49−54.

(13) Lee, H. J.; Lee, E.; Yoon, S. H.; Chang, H. R.; Kim, K.; Kwon, J. H. Enzymatic and microbial transformation assays for the evaluation of the environmental fate of diclofenac and its metabolites. *Chemosphere* **2012**, *87* (8), 969−74.

(14) D'Ascenzo, G.; Di Corcia, A.; Gentili, A.; Mancini, R.; Mastropasqua, R.; Nazzari, M.; Samperi, R. Fate of natural estrogen conjugates in municipal sewage transport and treatment facilities. *Sci. Total Environ.* **2003**, *302* (1−3), 199−209.

(15) Gomes, R. L.; Scrimshaw, M. D.; Lester, J. N. Fate of Conjugated Natural and Synthetic Steroid Estrogens in Crude Sewage and Activated Sludge Batch Studies. *Environ. Sci. Technol.* **2009**, *43* (10), 3612−3618.

(16) Manning, C. O.; Wadsworth, A. H.; Fellows, I. Synthesis of stable isotopically labelled versions of Lamotrigine and its methylated metabolite. *J. Labelled Compd. Radiopharm.* **2002**, *45* (7), 611−618.

(17) Zonja, B.; Delgado, A.; Abad, J. L.; Pérez, S.; Barceló, D. Abiotic Amidine and Guanidine Hydrolysis of Lamotrigine-N2-glucuronide in wastewater: The Role of pH and N2-Substitution on Reaction Kinetics. Unpublished data, 2015.

(18) Zonja, B.; Delgado, A.; Pérez, S.; Barceló, D. LC-HRMS Suspect Screening for Detection-Based Prioritization of Iodinated Contrast Media Photodegradates in Surface Waters. *Environ. Sci. Technol.* **2015**, *49* (6), 3464−3472.

(19) Luft, A.; Wagner, M.; Ternes, T. A. Transformation of biocides irgarol and terbutryn in the biological wastewater treatment. *Environ. Sci. Technol.* **2014**, *48* (1), 244−54.

(20) Marvin was used for drawing, displaying, and characterizing chemical structures, substructures and reactions: *Marvin 6.1*, 2013; ChemAxon (http://www.chemaxon.com).

(21) Beattie, K.; Phadke, G.; Novakovic, J. Lamotrigine. *Profiles Drug Subst., Excipients, Relat. Methodol.* **2012**, *37*, 245−85.

(22) Yan, Z.; Caldwell, G. W.; Jones, W. J.; Masucci, J. A. Cone voltage induced in-source dissociation of glucuronides in electrospray and implications in biological analyses. *Rapid Commun. Mass Spectrom.* **2003**, *17* (13), 1433−42.

(23) Trautwein, C.; Kummerer, K. Incomplete aerobic degradation of the antidiabetic drug Metformin and identification of the bacterial dead-end transformation product Guanylurea. *Chemosphere* **2011**, *85* (5), 765−73.

(24) Gao, J.; Ellis, L. B. M.; Wackett, L. P. The University of Minnesota Biocatalysis/Biodegradation Database: Improving public access. *Nucleic Acids Res.* **2010**, *38*, D488−D491.

(25) Stone, B. A.; Svensson, B.; Collins, M. E.; Rastall, R. A. Polysaccharide Degradation. In *Glycoscience*; Fraser-Reid, B., Tatsuta, K., Thiem, J., Eds.; Springer: Berlin, 2008; pp 2325−2375.

(26) Brewer, A. J.; Ort, C.; Banta-Green, C. J.; Berset, J. D.; Field, J. A. Normalized diurnal and between-day trends in illicit and legal drug loads that account for changes in population. *Environ. Sci. Technol.* **2012**, *46* (15), 8305−8314.

(27) Ort, C.; Lawrence, M. G.; Rieckermann, J.; Joss, A. Sampling for pharmaceuticals and personal care products (PPCPs) and illicit drugs in wastewater systems: Are your conclusions valid? A critical review. *Environ. Sci. Technol.* **2010**, *44* (16), 6024−6035.

(28) Ort, C.; Lawrence, M. G.; Reungoat, J.; Mueller, J. F. Sampling for PPCPs in wastewater systems: Comparison of different sampling modes and optimization strategies. *Environ. Sci. Technol.* **2010**, *44* (16), 6289−6296.

(29) Majewsky, M.; Gallé, T.; Bayerle, M.; Goel, R.; Fischer, K.; Vanrolleghem, P. A. Xenobiotic removal efficiencies in wastewater

DOI: 10.1021/acs.est.5b03691
Environ. Sci. Technol. 2016, 50, 154−164

treatment plants: Residence time distributions as a guiding principle for sampling strategies. *Water Res.* **2011**, *45* (18), 6152−6162.
(30) Gurke, R.; Rößler, M.; Marx, C.; Diamond, S.; Schubert, S.; Oertel, R.; Fauler, J. Occurrence and removal of frequently prescribed pharmaceuticals and corresponding metabolites in wastewater of a sewage treatment plant. *Sci. Total Environ.* **2015**, *532*, 762−770.
(31) Kowalczyk, I.; Hawes, E. M.; McKay, G. Stability and enzymatic hydrolysis of quaternary ammonium-linked glucuronide metabolites of drugs with an aliphatic tertiary amine-implications for analysis. *J. Pharm. Biomed. Anal.* **2000**, *22* (5), 803−811.
(32) Radke, M.; Lauwigi, C.; Heinkele, G.; Mürdter, T. E.; Letzel, M. Fate of the Antibiotic Sulfamethoxazole and Its Two Major Human Metabolites in a Water Sediment Test. *Environ. Sci. Technol.* **2009**, *43* (9), 3135−3141.

DOI: 10.1021/acs.est.5b03691
Environ. Sci. Technol. 2016, 50, 154−164

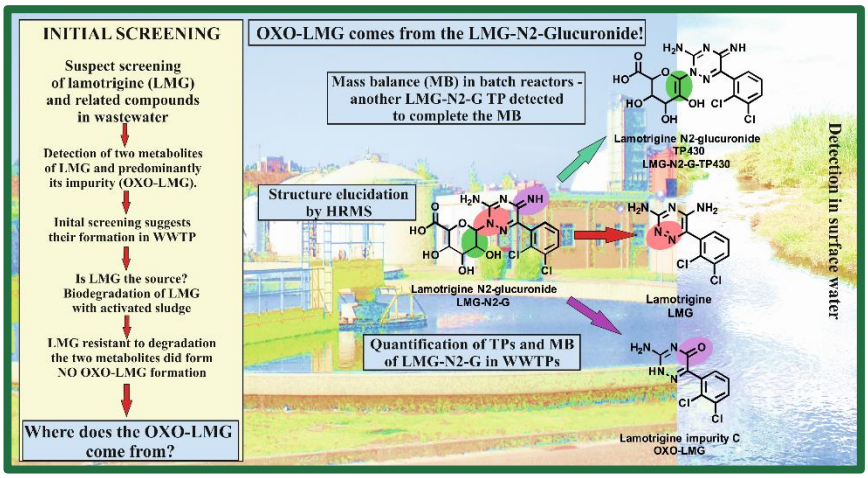

Article Nº3:

Zonja, B., Perez, S. and Barcelo, D.

Human Metabolite Lamotrigine-N(2)-glucuronide Is the Principal Source of Lamotrigine -Derived Compounds in Wastewater Treatment Plants and Surface Water.

(2016.) Environ Sci Technol 50(1), 154-164.

SUPPORTING INFORMATION

Total content: **Figures** – 13, and **Tables** – 8

Supporting information has been reformatted to match the style of the thesis.

Table of Contents

WWTPs

The five WWTPs (WWTP 1-5) are situated in the metropolitan area of the city of Barcelona. They are conventional WWTPs equipped with mechanical treatment (pre-treatment and primary clarifier), followed by activated sludge treatment with denitrification and nitrification, and phosphate removal. The parameters given correspond to hydraulic retention time (HRT), average daily flow and population equivalents (PE). They were as follows: WWTP - 1: HRT – 0.5 d, flow - 40,000 m^3d^{-1}, 165, 000 PE; WWTP - 2: HRT – 0.3 d, flow – 240,800 m^3d^{-1}, 1,142,000 PE; WWTP - 3: HRT – 0.3 d, flow – 50 000 m^3d^{-1}, 229,000 PE; WWTP - 4: HRT – 0.6 d, flow – 33,000 m^3d^{-1}, 220,000 PE; WWTP - 5: HRT – 0.32 d, flow -45,900 m^3d^{-1}, 198,000 PE.

Sampling of wastewater

Wastewater samples were provided by the staff of WWTPs involved in the study. All samples were 24-hour composite samples taken in period from November 2013 to January 2014. All samples were collected using automatic sampler but the sampling mode was different between the WWTPs sampled.

WWTP - 1 and WWTP - 4 use a time-proportional sampling mode. In the case of WWTP - 1 250 mL samples are collected every 15 minutes in 24 1-liter bottles. These are later combined and integrated to a single sample. WWTP - 4 uses likewise a time-proportional mode but with less frequent sample uptake – 250 ml are collected every hour over the course of 24 hours. Like in the case of WWTP - 1, samples are integrated after all the 24-h samples are collected. WWTP - 2 uses a flow-proportional sampling mode based on the official Catalan regulations.(Catalunya 2003) A total volume of 8 L is collected over the course of 24 hours with the following average distribution; 72 % from 11 a.m. to 22 p.m., 10 % from 11 p.m. to 2 a.m., 6 % from 3 a.m. to 6 a.m. and 12 % from 7 a.m. to 10 a.m. WWTP - 3 uses a volume-proportional sampling mode. In this case, a sample of approximately 100 mL is taken every 1000 m^3 of volume to reach 5 L daily collected wastewater.

Surface water samples

Surface water samples were taken as grab samples. They were located along the two rivers located near metropolitan area of the city of Barcelona. 7 samples were taken from Llobregat river and 6 samples from Besos river (**Figure SI-1**). Llobregat samples were marked LL-1-7 and Besos samples BS-1-6. Both Llobregat and Besos river receive discharge from the WWTP 1-4 analyzed. These surface water samples have been used previously for detection based detection of iodinated contrast media photodegradates and in this work were re-analyzed for suspect screening and quantification of lamotrigine and its derived compounds. **Table SI-1,** which shows physico-chemical properties and location of the surface water samples, is reproduced from previous published work by Zonja et al.(Zonja et al. 2015)

Figure SI-1. 13 sampling sites of Besos and Llobregat rivers.

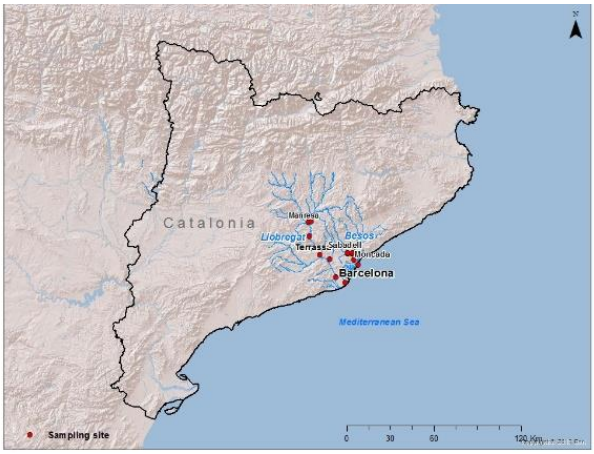

Table SI-1. Physico-chemical properties and location of the samples

SL	pH	T	O_2		σ	UTM coordinates		
		[ºC]	[mg/L]	[%]	[µS/cm]	Zone	X	Y
BS-1	8.3	16.1	8.30	86.2	1484	31	429192	4593550
BS-2	8.0	14.0	8.71	91.4	1165	31	429307	4593848
BS-3	8.3	13.5	9.25	96.2	838	31	432000	4593213
BS-4	8.1	15.3	9.10	95.4	1447	31	432651	4593766
BS-5	7.9	17.2	7.04	86.2	1388	31	433154	4589203
BS-6	7.8	16.8	6.33	80.5	35009	31	435804	4585677
LL-1	7.9	8.2	8.99	91.6	757	31	403881	4616871
LL-2	7.9	9.2	9.30	96.2	1087	31	405907	4617415
LL-3	7.8	7.9	9.04	92.8	1139	31	403792	4607459
LL-4	8.1	8.9	8.96	92.4	1220	31	410078	4594291
LL-5	8.1	14.2	8.72	90.4	1407	31	416614	4590452
LL-6	8.0	10.3	9.09	94.7	1395	31	420247	4577928
LL-7	7.3	12.1	*	*	6050	31	426109	4573894

BS - Besos river, LL – Llobregat river, SL - sampling location, T – temperature, σ – conductivity; * probe malfunctioned

Table SI-2. Suspect list comprised of lamotrigine and derived compounds (ChemAxon-Marvin 2016)

Name	Structure	SMILES	Type	Exact mass ^{35}Cl $[M+H]^+$	Exact mass ^{37}Cl $[M+H]^+$	Elemental composition	Log P	IUPAC name	Ref.
Lamotrigine (**LMG**)	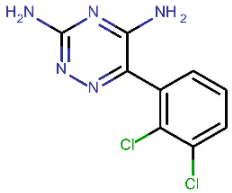	NC1=NN=C(C(N)=N1)C1=C(Cl)C(Cl)=CC=C1	Parent compound	256.0151	258.0122	$C_9H_7Cl_2N_5$	1.93	6-(2,3-dichlorophenyl)-1,2,4-triazine-3,5-diamine	
Lamotrigine N2-oxide (**LMG-N2-oxide**)	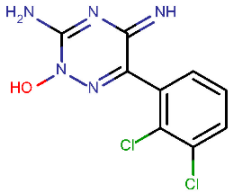	NC1=NC(=N)C(=NN1O)C1=C(Cl)C(Cl)=CC=C1	Minor human metabolite	272.0100	274.0071	$C_9H_7Cl_2N_5O$	1.76	3-amino-6-(2,3-dichlorophenyl)-5-imino-2,5-dihydro-1,2,4-triazin-2-ol	(Doig and Clare 1991, Lu and Uetrecht 2007)
N2-methyl-lamotrigine (**N2-Me-LMG**)	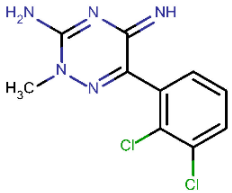	CN1N=C(C(=N)N=C1N)C1=C(Cl)C(Cl)=CC=C1	Minor human metabolite	270.0308	272.0278	$C_{10}H_9Cl_2N_5$	1.92	6-(2,3-dichlorophenyl)-5-imino-2-methyl-2,5-dihydro-1,2,4-triazin-3-amine	(Doig and Clare 1991, Lu and Uetrecht 2007)
Lamotrigine -N2-glucuronide (**LMG-N2-G**)	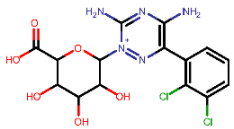	NC1=C(N=|N+|(C2OC(C(O)C(O)C2O)C(O)=O)C(N)=N1)C1=C(Cl)C(Cl)=CC=C1	Major human metabolite	432.0472	434.0443	$C_{15}H_{16}Cl_2N_5O_6$	-3.01	3,5-diamino-2-(6-carboxy-3,4,5-trihydroxyoxan-2-yl)-6-(2,3-dichlorophenyl)-1,2λ^5,4-triazin-2-ylium	(Doig and Clare 1991, Lu and Uetrecht 2007)

Name	Structure	SMILES	Type	Exact mass ^{35}Cl $[M+H]^+$	Exact mass ^{37}Cl $[M+H]^+$	Elemental composition	Log P	IUPAC name	Ref.
Lamotrigine -N5-glucuronide (**LMG-N5-G**)	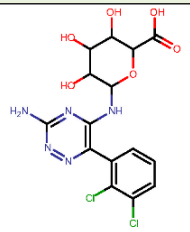	NC1=NC(NC2OC(C(O)C(O)C2O)C(O)=O)=C(N=N1)C1=C(Cl)C(Cl)=CC=C1	Minor human metabolite	432.0472	434.0443	$C_{15}H_{16}Cl_2N_5O_6$	-1.94	6-1-triazin-5-yl]amino-3,4,5-trihydroxyoxane-2-carboxylic acid	(Doig and Clare 1991, Lu and Uetrecht 2007)
Lamotrigine -impurity A (**OXO-LMG**)	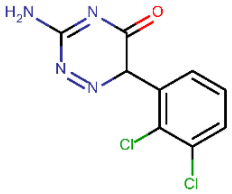	NC1=NC(=O)C(N=N1)C1=C(Cl)C(Cl)=CC=C1	USP Lamotrigine Related Compound C (impurity)	256.9991	258.9962	$C_9H_6Cl_2N_4O$	1.69	3-amino-6-(2,3-dichlorophenyl)-5,6-dihydro-1,2,4-triazin-5-one	(Srinivasulu et al. 2009)
Lamotrigine -impurity B (**diOXO-LMG**)	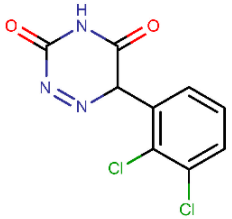	ClC1=CC=CC(C2N=NC(=O)NC2=O)=C1Cl	Lamotrigine Impurity D	257.9832	259.9802	$C_9H_5Cl_2N_3O_2$	2.01	6-(2,3-dichlorophenyl)-3,4,5,6-tetrahydro-1,2,4-triazine-3,5-dione	*(Hlaváč et al. 2003)
PhotoTP-1	Not identified	Not identified	PhotoTP@ pH7	259.0148	261.0118	*$C_9H_9Cl_2N_4O$*	-	-	(Young et al. 2014)
PhotoTP-2	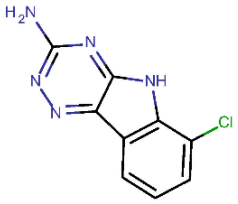	NC1=NN=C2C(NC3=C2C=CC=C3Cl)=N1	Photo-degradation product @pH7	219.0312	221.0282	$C_9H_6ClN_5$	1.39	6-chloro-5H-[1,2,4]triazino[5,6-b]indol-3-amine	(Young et al. 2014)

Name	Structure	SMILES	Type	Exact mass ^{35}Cl $[M+H]^+$	Exact mass ^{37}Cl $[M+H]^+$	Elemental composition	Log P	IUPAC name	Ref.
PhotoTP-3	Not identified	Not identified	PhotoTP@ pH7	256.0151	258.0122	$C_9H_7Cl_2N_5$	-	-	(Young et al. 2014)
N5-methyl-lamotrigine (**N5-Me-LMG**)	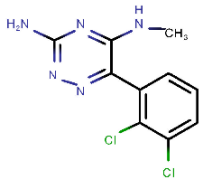	CNC1=NC(N)=NN=C1C1=C(Cl)C(Cl)=CC=C1	Lamotrigine impurity	270.0308	272.0278	$C_{10}H_9Cl_2N_5$	2.23	6-(2,3-dichlorophenyl)-N5-methyl-1,2,4-triazine-3,5-diamine	*
Chlorinated lamotrigine (**Cl-LMG**)	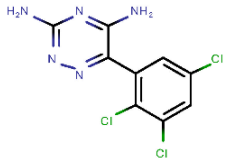	NC1=NN=C(C(N)=N1)C1=C(Cl)C(Cl)=CC(Cl)=C1	Pharmacopeia reported impurity	289.9762	291.9732	$C_9H_6Cl_3N_5$	2.53	6-(2,3,5-trichlorophenyl)-1,2,4-triazine-3,5-diamine	*

* Toronto Research Chemicals, http://www.trc-canada.com (accessed June 7th 2015)

Screening method for wastewater samples and re-analyzed surface water samples

Chromatographic conditions for the suspect screening were as follows:
The mobile phases used were: (A) acetonitrile with 0.1 % formic acid and (B) water (0.1 % formic acid). Elution was accomplished with the following solvent gradient: 0 min (3 % A) - 1 min (3 % A) – 17 min (95 % A), - 21 min (95 % A) – 21.5 min (3% A) and stabilized until 25 min. The flow rate was 300 µL min^{-1}, the column temperature was held at 40 ºC and the auto sampler was set to the temperature of 8 ºC.

For the MS screening method, Q-Orbitrap-MS was equipped with Electrospray ionization interface (ESI) which operated in the positive ion mode with the following settings: spray voltage +3.0 kV, heater temperature 250 ºC, and capillary temperature 350 ºC.

For the detection method, a data dependent scan was applied with the following parameters; Full scan and data dependant-MS^2 were both set to resolution of 35 000 [full width at half maximum (FWHM)], with the full scan range of m/z 100-1000. Quadrupole isolation window was set to m/z 2 and the normalized collision energy (NCE) to 35.

Suspect screening of WWTPs and surface water - preliminary results

Preliminary wastewater analysis

Results of wastewater which are shown in **Table SI-3** show that while N2-Me-LMG and LMG-N2-Oxide were only sporadically detected in effluents samples, LMG-N2-G was the most abundant LMG-related compound in influent samples followed by LMG. The predominance of the glucuronide with respect to the parent compound is in agreement with the reported excretion pattern in humans as summarized in the introduction.(Ramsay et al. 1991, Sidhu et al. 2006) Comparison of the levels of LMG and its related compounds in influent and effluent samples shows a substantial decrease in the concentration of the glucuronide, while LMG was measured at higher levels in the treated sewage. This observation would match the expectation of extensive deconjugation during biological WW treatment unmasking LMG. However, the two metabolites N2-Me-LMG and LMG-N2-Oxide (quantified using LMG as a standard), found at low concentrations in influent WWTP

1 and 4 seem to be formed in those WWTPs while there was no apparent change in concentration between influent and effluent of WWTPs 2 and 3. Also, high concentrations of the reported LMG impurity, OXO-LMG, were found in effluent samples of WWTP 1 and 2 at higher concentrations than in influent samples suggesting the possibility of its formation during biodegradation process in the secondary treatment of the WWTP.

Table SI-3. Screening for lamotrigine and related compounds in WWTPs and surface water.

The concentrations here presented are semi-quantitative and are based on using lamotrigine as a standard. This table was used solely; (i) to check whether the suspect compounds are present in the samples and (ii) to see, in very relative terms, if there is an increase or a decrease of these compounds between the influent and the effluent of WWTPs.

ngL^{-1}		**LMG-N2-G**	**LMG**	**N2-Me-LMG**	**N2-LMG-Oxide**	**OXO-LMG**
WWTP 1	***influent***	476	520	< 5	< 5	18
	effluent	137	1254	23	13	96
WWTP 2	***influent***	33	21	< 5	< 5	< 5
	effluent	6	97	< 5	< 5	8
WWTP 3	***influent***	6	13	< 5	< 5	< 5
	effluent	< 5	18	< 5	< 5	< 5
WWTP 4	***influent***	88	45	< 5	< 5	< 5
	effluent	37	325	7	< 5	15
Surface water**	***Ll- 1***	< 5	41	< 5	< 5	< 5
	Ll- 2	< 5	41	< 5	< 5	< 5
	Ll- 3	< 5	37	< 5	< 5	< 5
	Ll- 4	6	64	< 5	< 5	7
	Ll- 5	54	1011	18	< 5	77
	Ll- 6	14	139	< 5	< 5	13
	Ll- 7	8	111	< 5	< 5	9
	Bs- 1	< 5	237	6	< 5	18
	Bs- 2	< 5	162	< 5	< 5	15
	Bs- 3	6	234	8	< 5	18
	Bs- 4	< 5	172	< 5	< 5	29
	Bs- 5	< 5	141	< 5	< 5	23
	Bs- 6	< 5	64	< 5	< 5	7

*Concentration limit of quantification was set arbitrarily to 5 ngL^{-1} since at this point standards of other compounds were not available; **BS - Besos river, LL – Llobregat river

Activated sludge experiments

Before the biodegradation experiments, 50 mL of a mixture of WWTP-1 influent and effluent were extracted using the 4 cartridges. This was done in order to test whether it would be possible only to use one cartridge for biodegradation experiment. 50 mL was tested since this was the volume intended to be taken after each time-dependent sampling point in the batch reactors. For this purpose, the 50 mL were passed through the four cartridges which were connected in series. Each cartridge was eluted separately as in the analysis of wastewater; however, the extracts were not joined together. They were pre-concentrated to 200 μL and injected separately to LC-QExactive-Orbitrap-MS.

The results are given in the **Table SI-4**. As can be seen, all of the compounds tested were retained in the HLB cartridge and thus only HLB cartridge was used for all of the biodegradation batch experiments. The numbers in the **Table SI-4** do not represent real recovery since at this point only LMG was available. What the numbers represent is the percentage of area found in the extract of the four cartridges.

Table SI-4. Relative recovery of lamotrigine and derived compounds in activated sludge.

Matrix (volume)	Cartridge	LMG	LMG-N2-G	OXO-LMG	N2-Me-LMG	LMG-N2-oxide
Batch experiments (50 mL)	HLB [%]	100 ± 0	100 ± 0	100 ± 0	100 ± 0	100 ± 0
	PPL [%]	0	0	0	0	0
	MAX [%]	0	0	0	0	0
	MCX [%]	0	0	0	0	0

Biodegradation of lamotrigine, $^{13}C_3$-lamotrigine and lamotrigine N2-glucuronide - 6 days

Lamotrigine in Activated Sludge

Figure SI-2. Degradation of lamotrigine over the course of 6 days in activated sludge bioreactor at concentration 5 µgL^{-1}

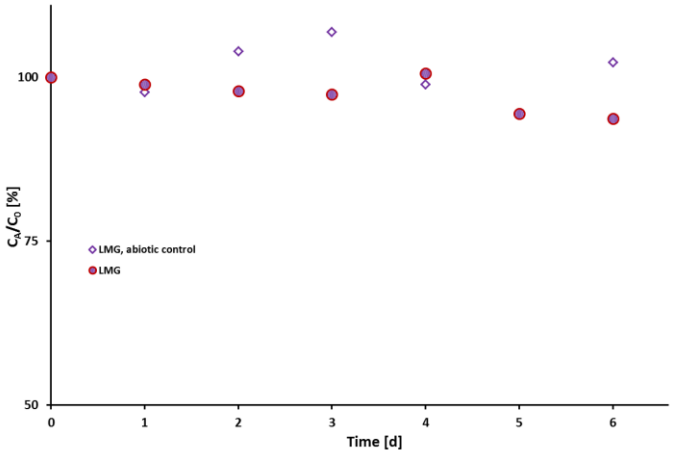

Figure SI-3. Mass balance for lamotrigine over the course of 6 days in activated sludge bioreactor at concentration of 5 µgL^{-1} showed as (A) logarithmic scale and (B) linear scale

Calculations were performed based on molar concentrations.

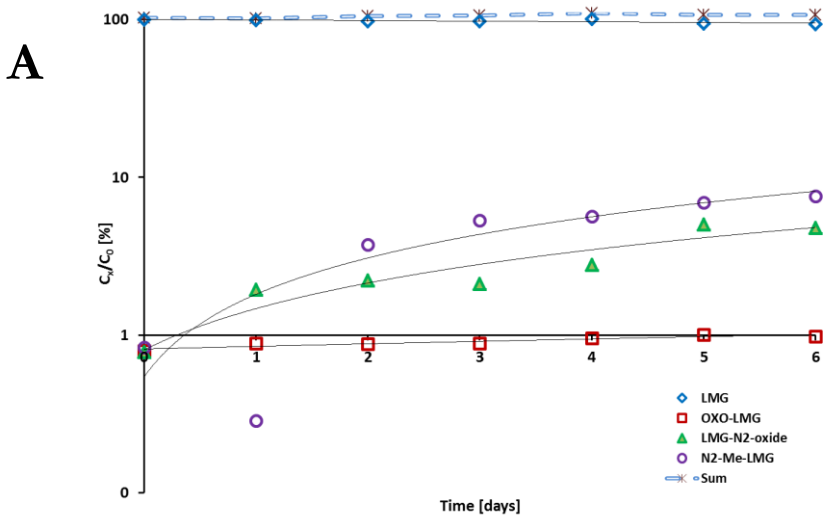

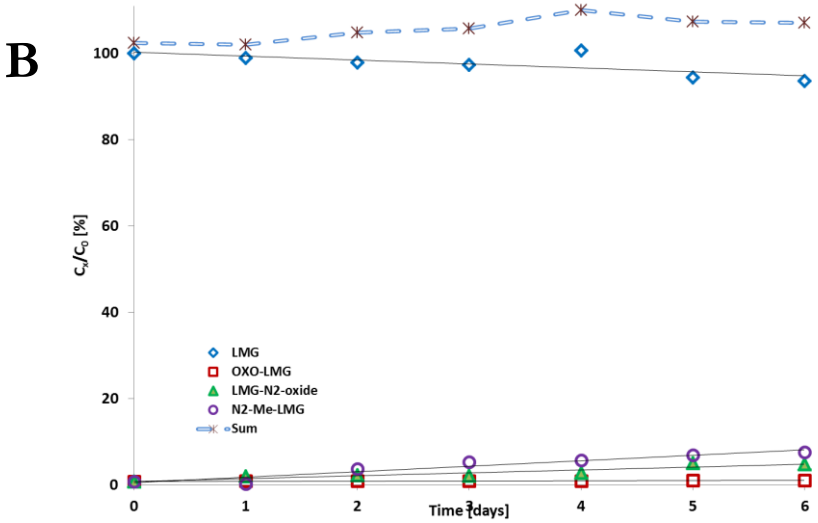

Lamotrigine-$^{13}C_3$ in Activated Sludge – TP identification

Lamotrigine – $^{13}C_3$, a labelled internal standard of lamotrigine was also degraded in activated sludge, where the concentration of 50 μgL^{-1} was used for identification purposes. As can be seen from the **Figures SI-4**. and **SI-5**, both **$^{13}C_3$-LMG-N2-oxide-** (SI-4) and **N2-Me-$^{13}C_3$-LMG** (SI-5) were formed. The chromatographic peaks of isotopically labelled compounds had a negative RT defect of 0.02 min while the $[M+H]^+$ of the parent ions deferred by 3.0101 of the exact mass. The same mass defect is seen in the high mass fragments before the phenyltriazine ring breaks (Figures SI-4 and 5; A' and B').

Figure SI-4. Detection of LMG-N2-oxide and $^{13}C_3$-LMG-N2-oxide in activated sludge degradation of LMG and $^{13}C_3$-LMG, respectively.

A shows the chromatogram and A' MS^2 spectrum at NCE 35 of LMG-N2-oxide. B and B' show the same for $^{13}C_3$-LMG-N2-oxide.

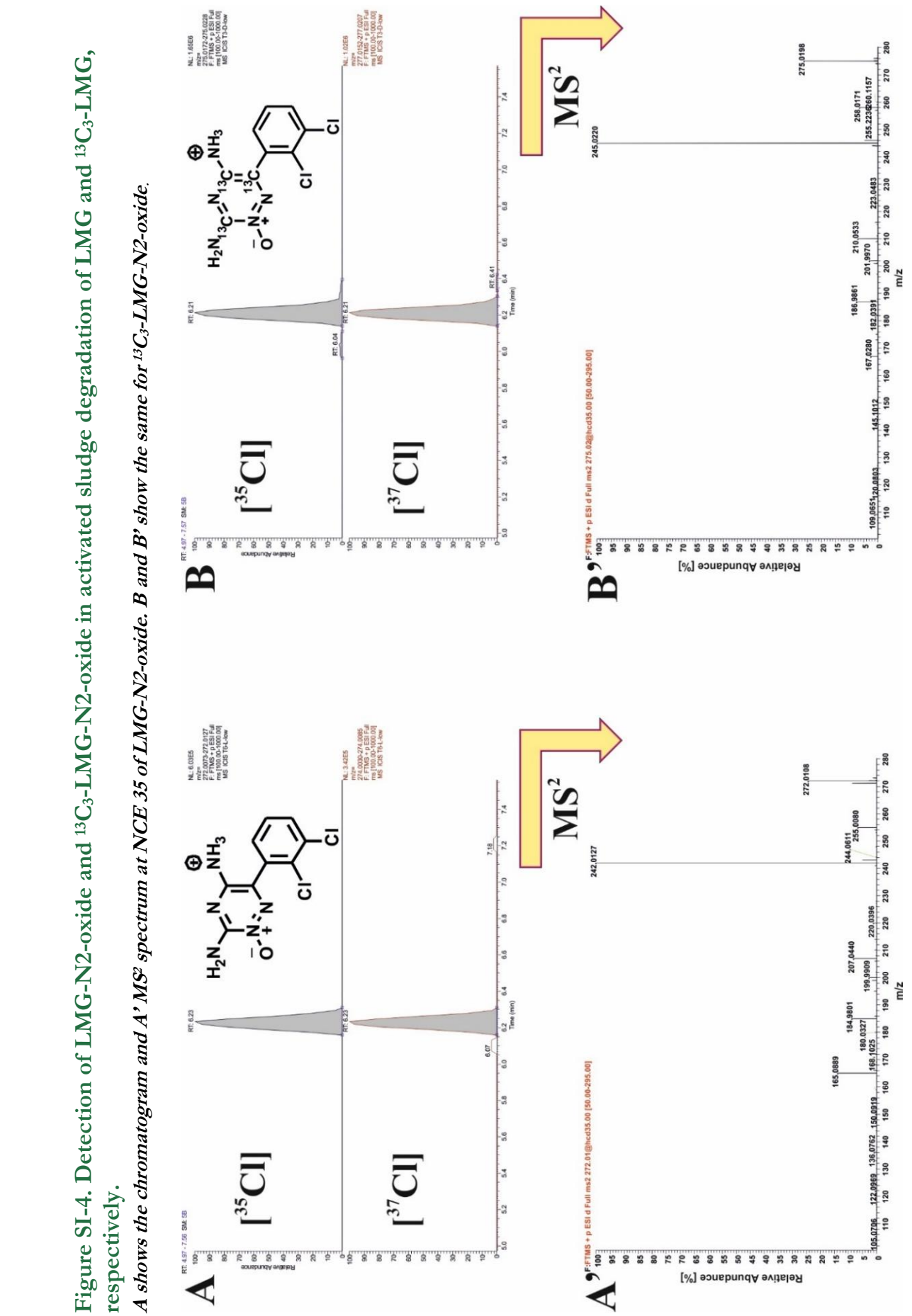

Figure SI-5. Detection of N2-Me-LMG and N2-Me-$^{13}C_3$-LMG in activated sludge degradation of LMG and $^{13}C_3$-LMG, respectively.

A shows the chromatogram and A' MS^2 spectrum at NCE 35 of N2-Me-LMG. B and B' show the same for N2-Me-$^{13}C_3$-LMG.

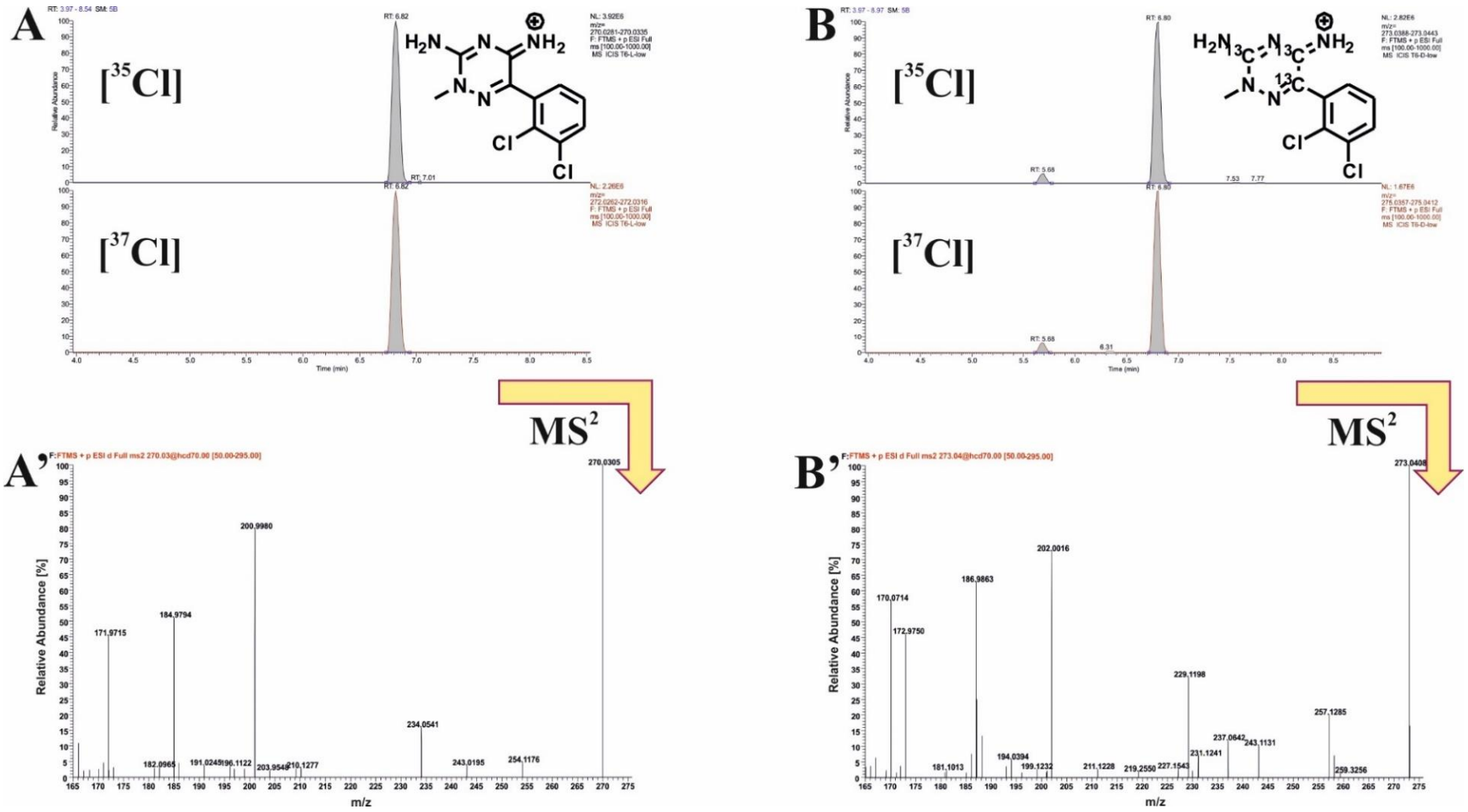

Lamotrigine N2-glucuronide in Activated Sludge

Figure SI-6. Mass balance for LMG-N2-G over the course of 6 days in activated sludge bioreactor at concentration of 5 µgL^{-1} showed as (A) linear scale and (B) logarithmic scale.

Calculations were performed based on molar concentrations.

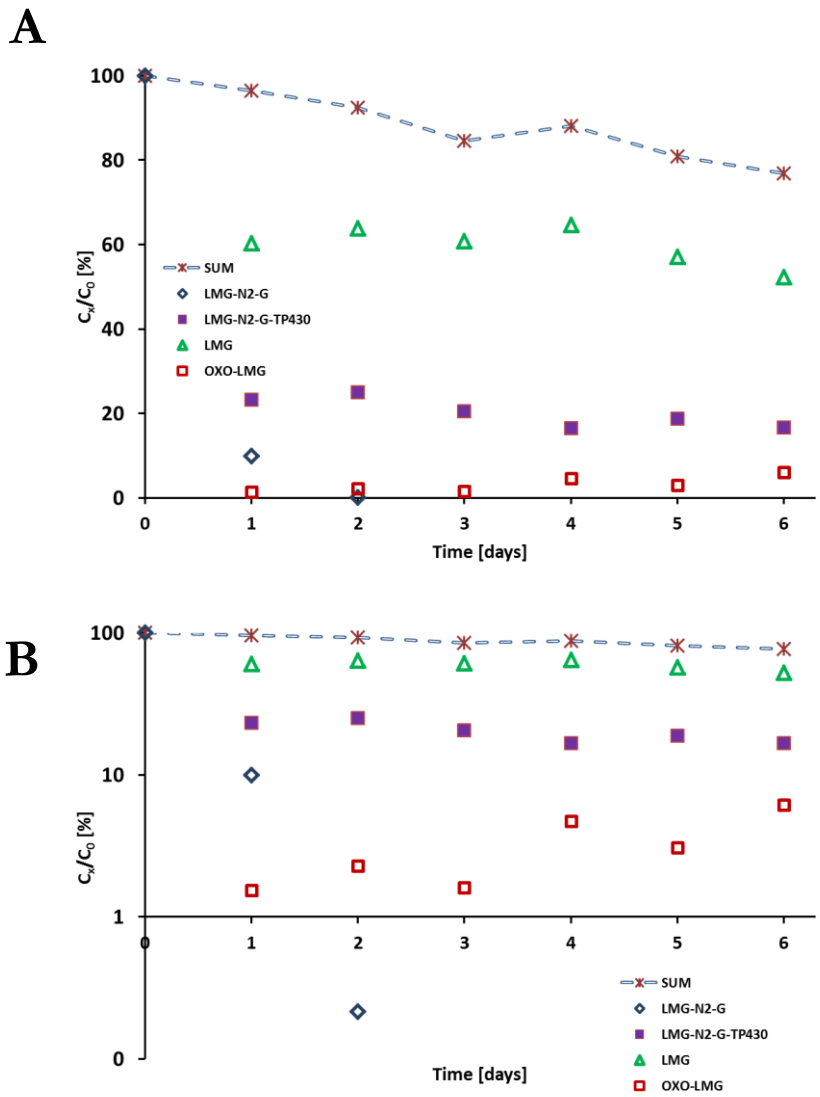

Biodegradation of lamotrigine N2-glucuronide - 8 hours

Background concentration in activated sludge for biodegradation experiments

Table SI-5. Background concentration of activated sludge.

Concentration ngL^{-1}	LMG	LMG-N2-G	OXO-LMG	N2-Me-LMG	LMG-N2-oxide	LMG-N2-G-TP430
May 2014	402	n.d.	33	15	7.3	7.0
August 2014 (I)	284	n.d.	100	9.6	n.d.	47
November 2014	120	n.d.	21	n.d.	n.d.	n.d.

n.d.- not detected

Mass balance of LMG-N2-G with its TPs LMG and OXO-LMG

Figure SI-7. Degradation of (A) 0.5 µgL^{-1} and (B) 5 µgL^{-1} of lamotrigine N2-glucuronide in activated sludge reactor over the course of 8 hours.

The graph shows the two LMG-N2-G TPs; LMG and OXO-LMG. Dashed line shows the mass balance as sum of the two TPs and LMG-N2-G. Points are given as average of 4 reactors (2 in Aug.(I) and 2 in Nov. 2014.) for the biotic degradation.

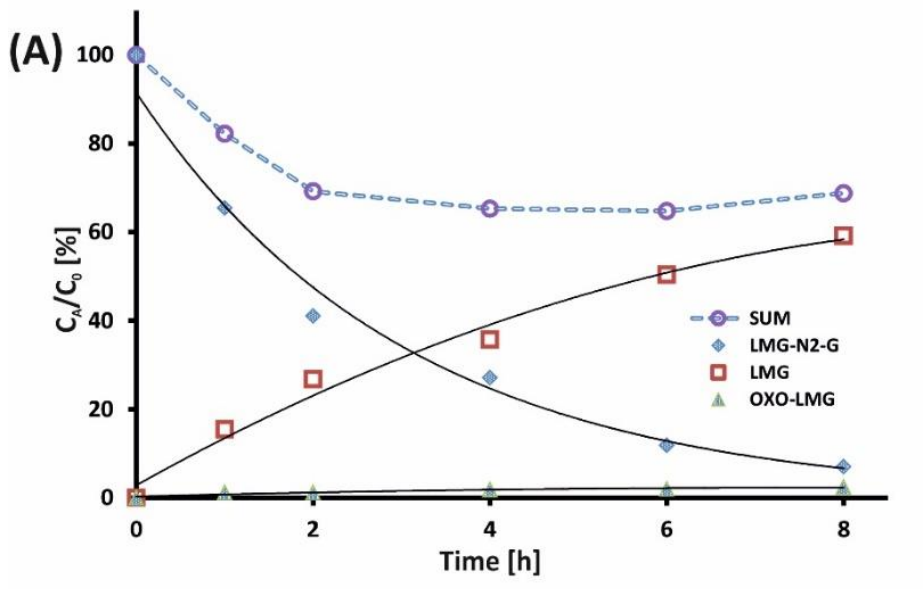

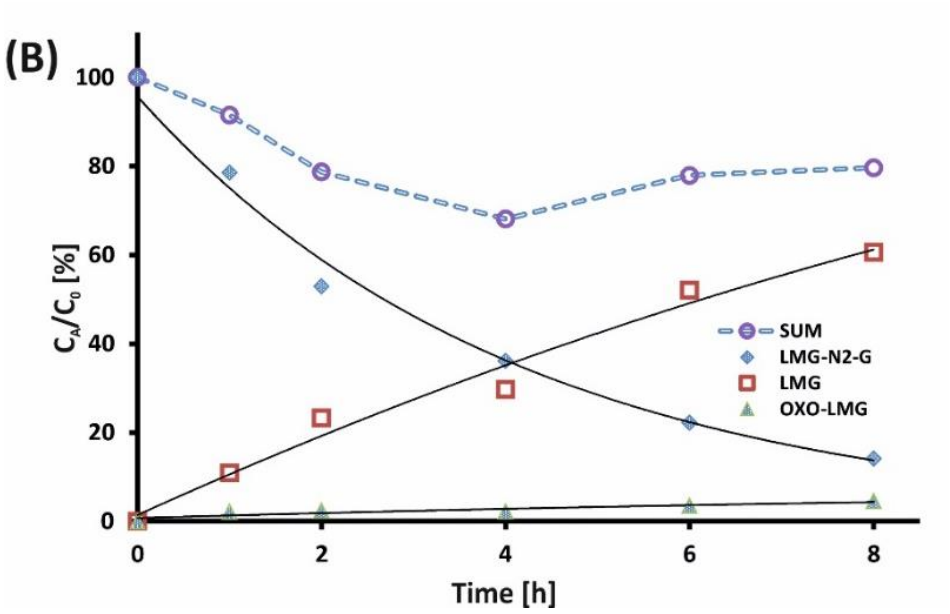

Stability of LMG-N2-G transformation products

For stability of transformation products of LMG-N2-G, activated sludge was taken in August 2014. (Aug.2014 (II)) from the same WWTP-5 plant and diluted to 0.9 g_{ss} with WW effluent. The reactors were not spiked and pH was adjusted to 7.0 ± 0.4. The degradation of diluted activated sludge was performed in four batch reactors (**Table 1**) and background concentration levels measured at T0 were considered as starting concentration. Four compounds were found to be present with the following concentrations: LMG (194 ± 13 ngL^{-1}), OXO – LMG (55 ± 4 ngL^{-1}), LMG-N2-G-TP430 (17 ± 1 ngL^{-1}) and N2-Me-LMG (4.1 ± 0.3 ngL^{-1}). LMG-N2-G and LMG-N2-oxide were not present in this activated sludge samples. Results of the TP stability are shown in **Figure SI-8**.

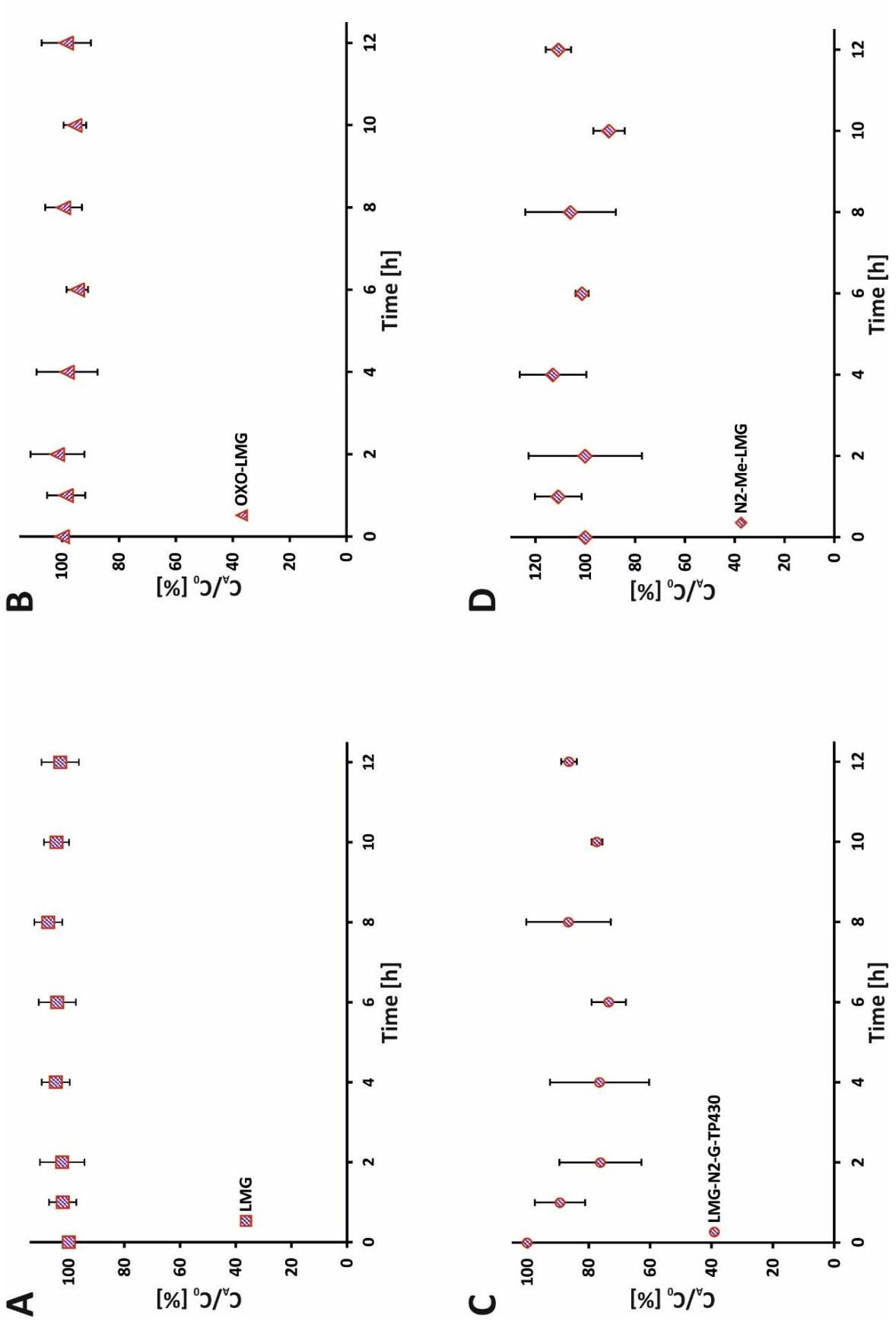

Figure SI-8. Stability of LMG-N2-G TPs: (A) 194 ngL^{-1} LMG; (B) 55 ngL^{-1} OXO-LMG; (C) 17 ngL^{-1} LMG-N2-G-TP430 and LMG TP (D) 4.1 ngL^{-1} N2-Me-LMG over the course of 12 hours

Abiotic experiments

Figure SI-9. Degradation of (A) 0.5 µgL^{-1} and (B) 5 µgL^{-1} lamotrigine N2-glucuronide in comparison with control reactors (activated sludge control).
Points are given as average of 4 reactors (Aug.(I) and Nov. 2014.) for the biotic degradation and as average of 3 reactors for the control reactors (Nov. 2014.).

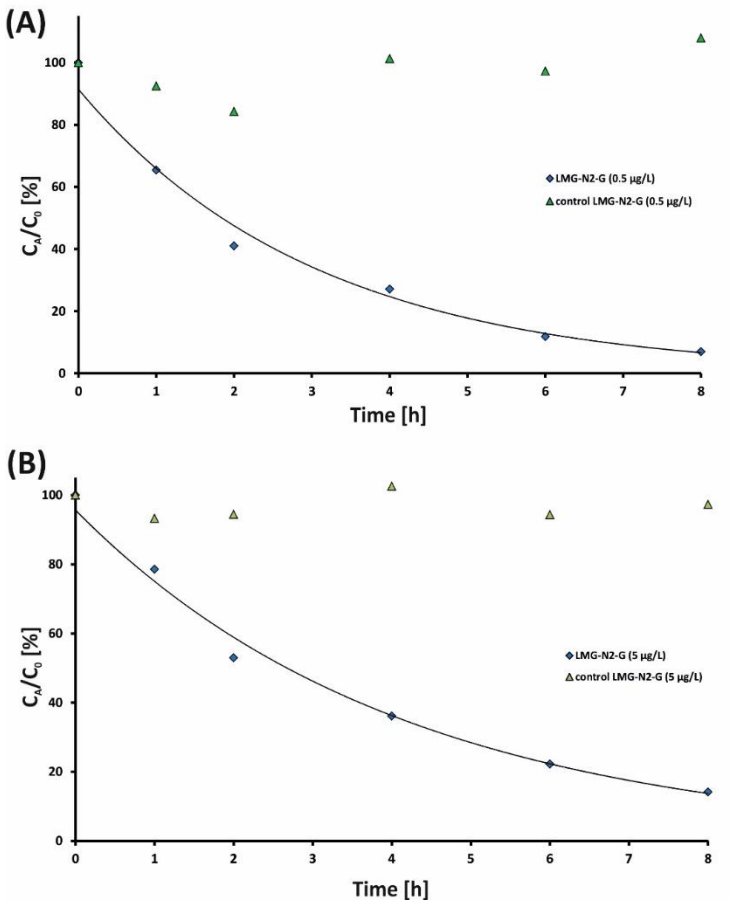

Identification of TPs using HRMS

The LC method used for identification was shortened to 10 minutes. The mobile phases employed were the same as before: (A) acetonitrile with 0.1 % formic acid and (B) water (0.1 % formic acid). Elution now had the following solvent gradient: 0 min (10 % A) - 1 min (10 % A) – 6 min (95 % A) - 7 min (95 % A) – 8 min (10 % A) and stabilized until 10 min. The flow rate was 300 µL min^{-1}, the column temperature was held at 40 °C and auto sampler temperature was set to 8 °C.

Electrospray ionization interface (ESI), as before, operated in the positive ion mode with the following settings: spray voltage +3.0 kV, heater temperature 250 ºC, and capillary temperature 350 ºC.

The Q-Exactive-MS method was set at a resolution of 140,000 for both scan mode and MS/MS experiments. The full scan was set to range of m/z 100 – 500. Isolation window was m/z 2 and inclusion list turned on and filled with the list of investigated masses. For pseudo-MS^3 (**pMS^3**) experiments *In-source ionization* was applied in order to produce the given m/z before breaking the ion in the HCD.

Figures of fragmentation pattern and MS spectra have been arranged in order that the fragmentation pattern and spectra have the same number i.e. **Figure SI-10** shows the fragmentation pattern (named: Figure SI-10.X-**A**., X = 1 - 4), MS^2 and pMS^3 spectra (named: Figure SI-10.X-**B**., X = 1 - 4) of a compound described.

Fragmentation patterns in **Figures SI-10.X-A, X= 1-4** are drawn with **black** and **red** arrows. **Black arrows** were drawn in cases where a given fragment has been seen in a pMS^3 spectrum of its direct predecessor. **Red arrows** were drawn all other cases and they represent the fragments which have been seen in the spectrum of its indirect predecessor.

Red arrows were used only in cases when it was not possible to do a pMS^3 experiment on a given mass and thus establish its direct predecessor.

Details on a specific MS^2 and pMS^3 performed can be found in the header of each spectrum. Example below is given for LMG for MS^2 and LMG-229 for pMS^3.

	Analyzer	Ionization	In-source	Experiment type	Selected mass	NCE	Mass range
LMG–MS^2	**FTMS**	**p ESI**	**-**	**Full ms2**	**256.01**	**@hcd 60**	**50-259**
LMG–229 pMS^3	**FTMS**	**p ESI**	**sid=35**	**Full ms2**	**229.01**	**@hcd 15**	**50-231**

NCEs (normalized collision energy) used throughout the experiments were 10, 15, 20, 35 and 60. Unless otherwise stated, the NCEs 15 and 20 were used with the ramp of 30%.

Accurate mass measurements of protonated LMG, LMG-N2-G and LMG-N2-G-TP430 as determined by LC-QExactive-MS in MS/MS or pseudo MS^3 modes can be found in **Table SI-6.**

LAMOTRIGINE (LMG)

Figure SI-10.1-A. Fragmentation pattern of Lamotrigine (LMG)

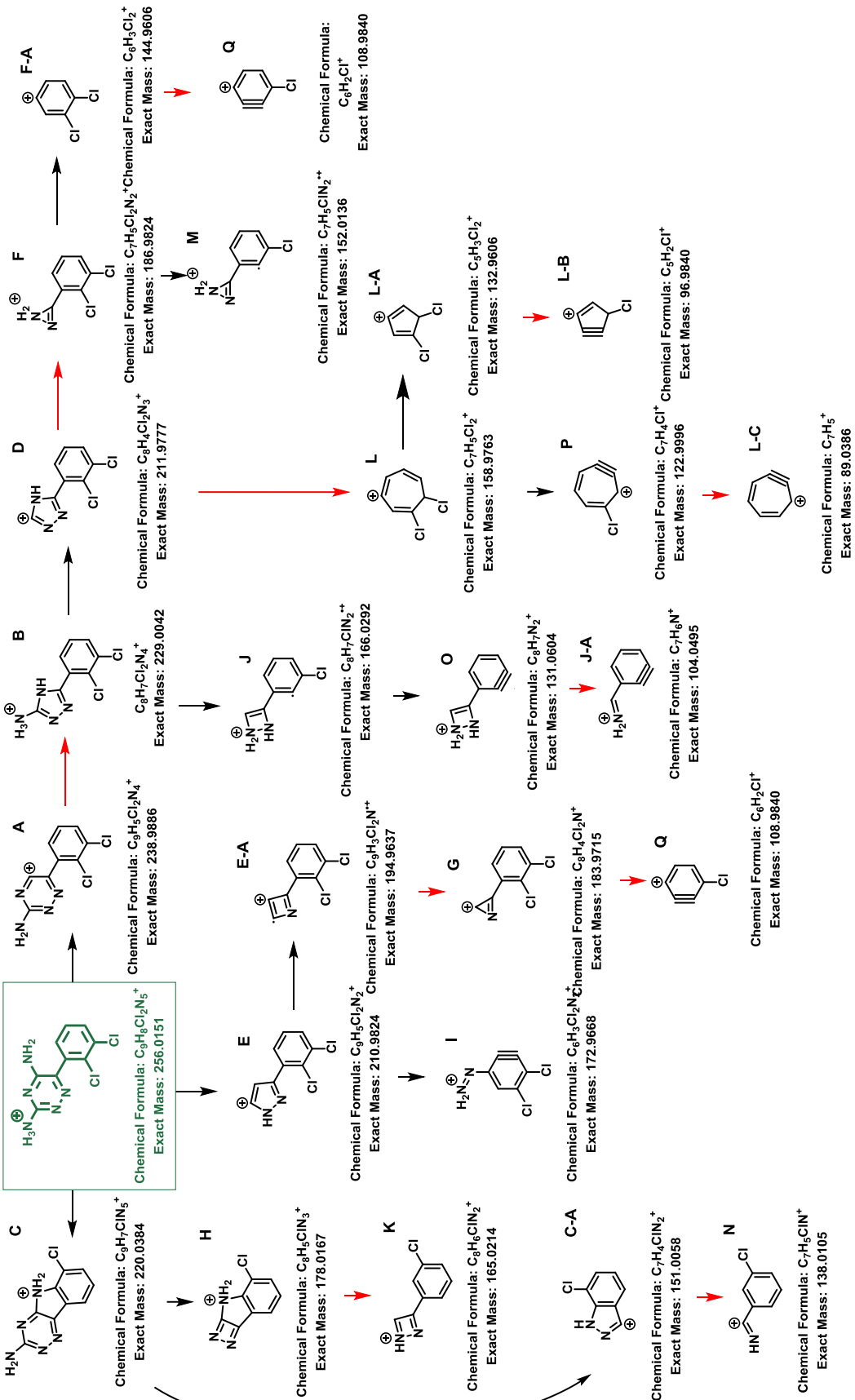

Figure SI-10.1-B. MS² and pMS³ spectra of Lamotrigine (LMG)

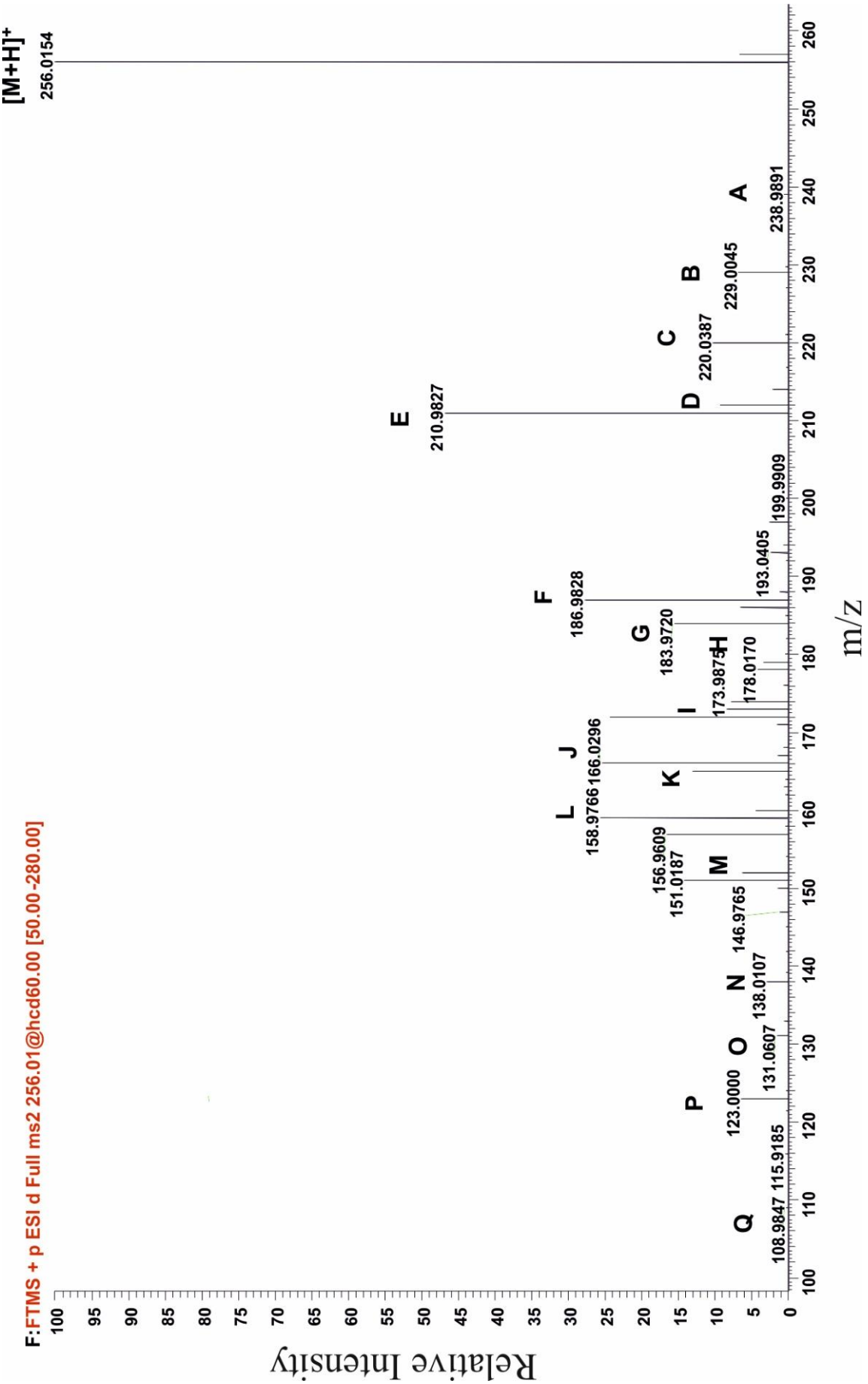

Figure SI-10.1-B. MS^2 and pMS^3 spectra of Lamotrigine (LMG) – *continued*

LMG – 229 pMS^3

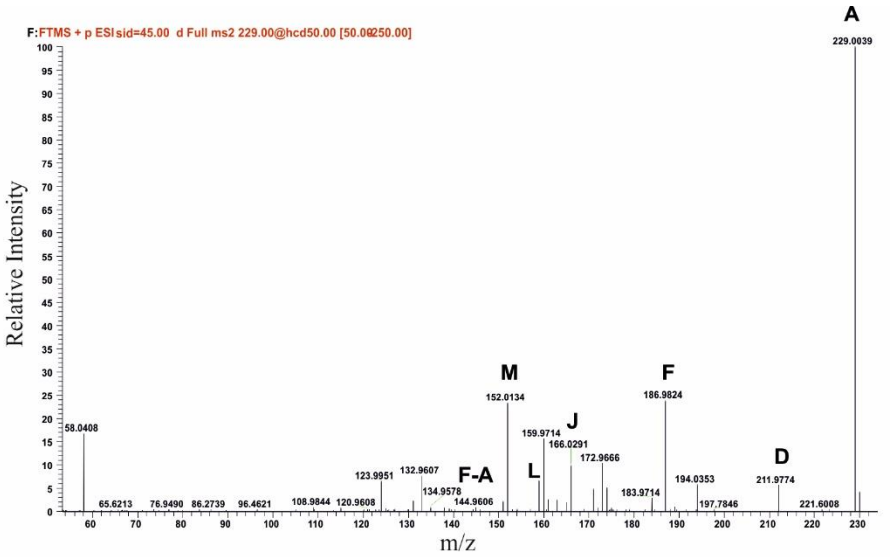

LMG – 220 pMS^3

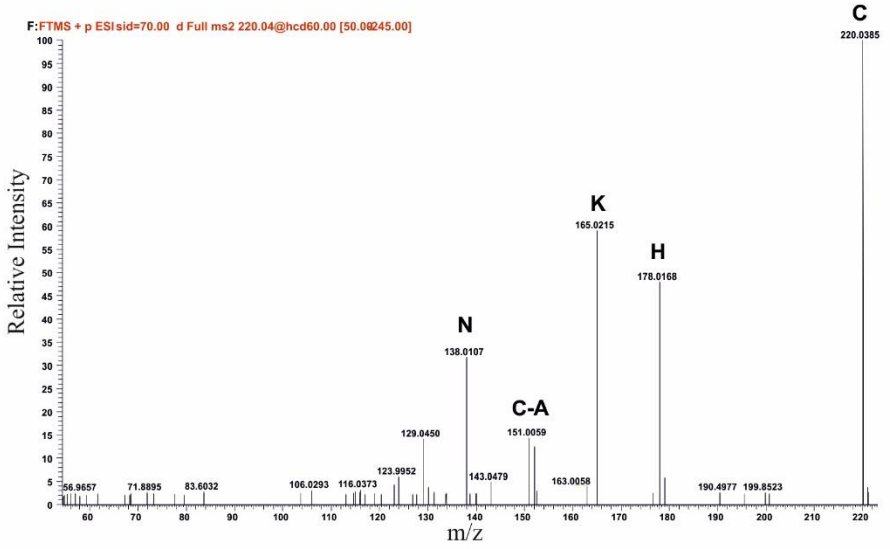

LMG – 210 pMS^3

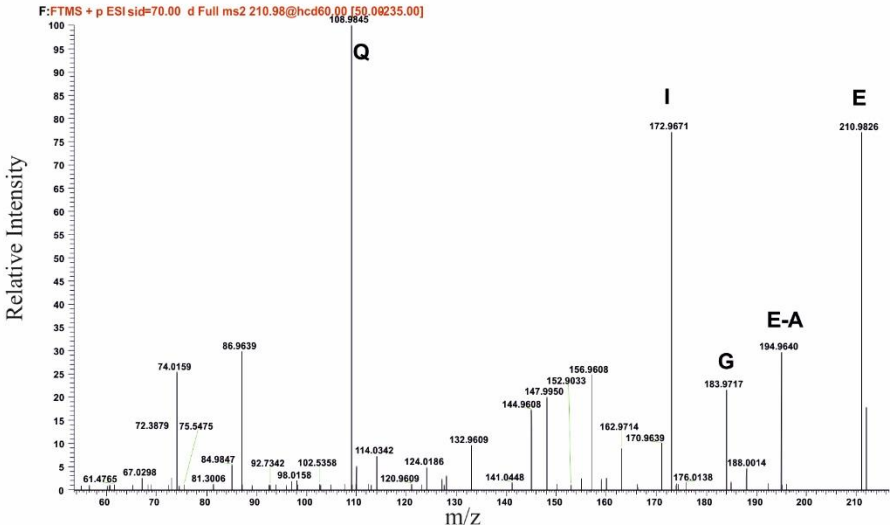

Figure SI-10.1-B. MS^2 and pMS^3 spectra of Lamotrigine (LMG) - *continued*

LMG – 186 pMS^3

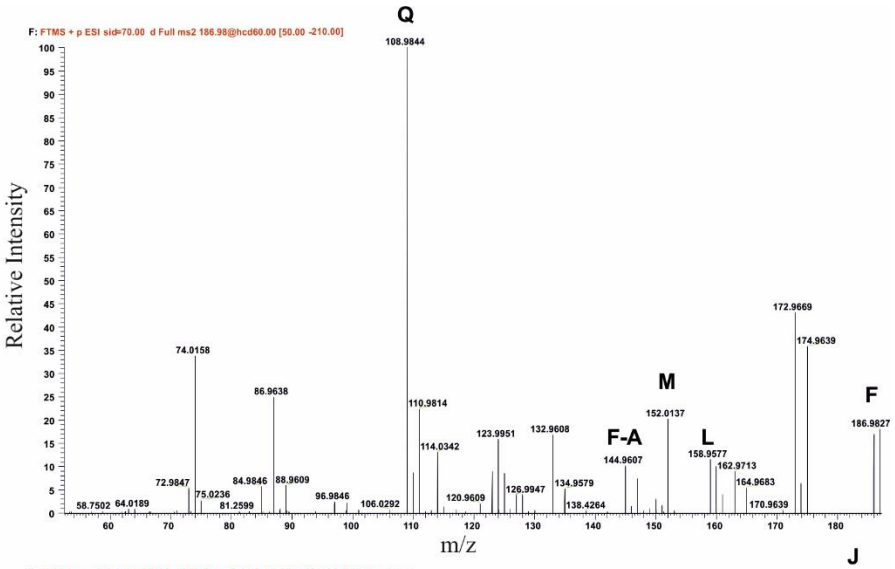

LMG – 166 pMS^3

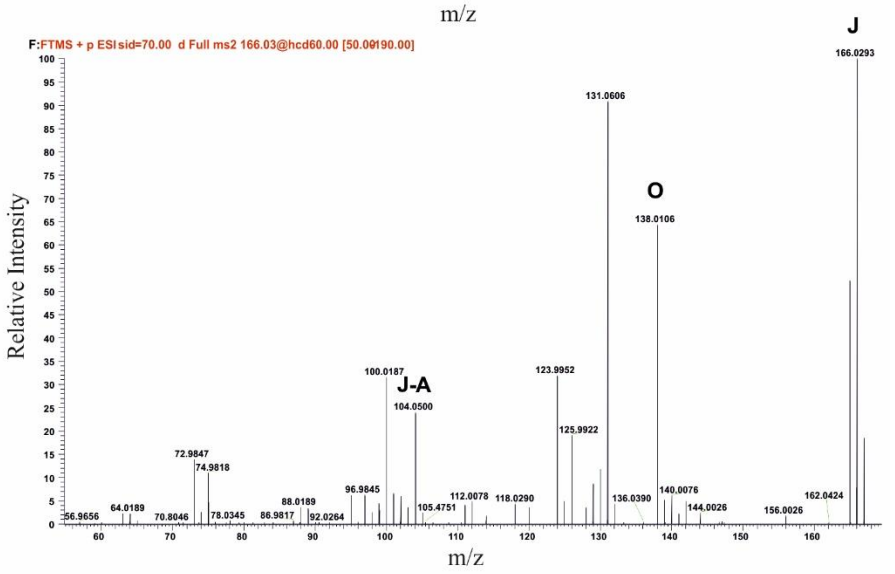

LMG – 158 pMS^3

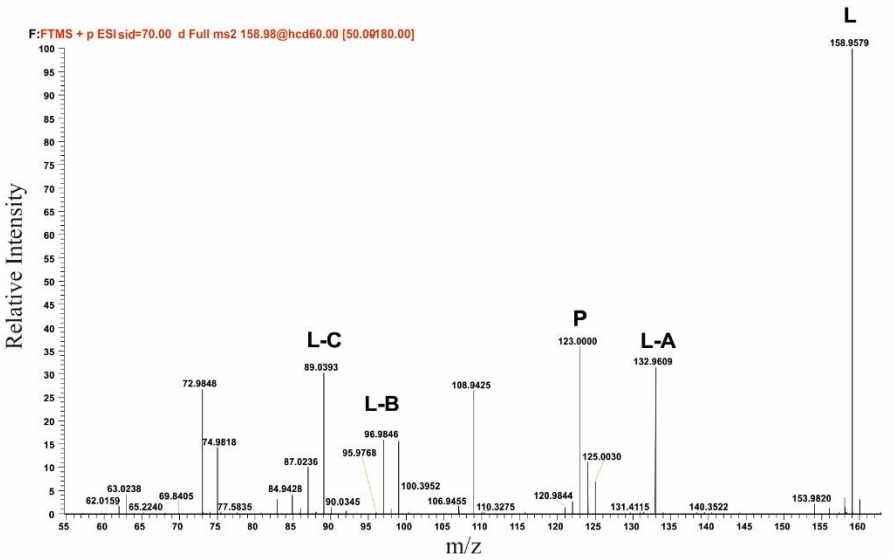

LAMOTRIGINE-N2-GLUCURONIDE (LMG-N2-G)

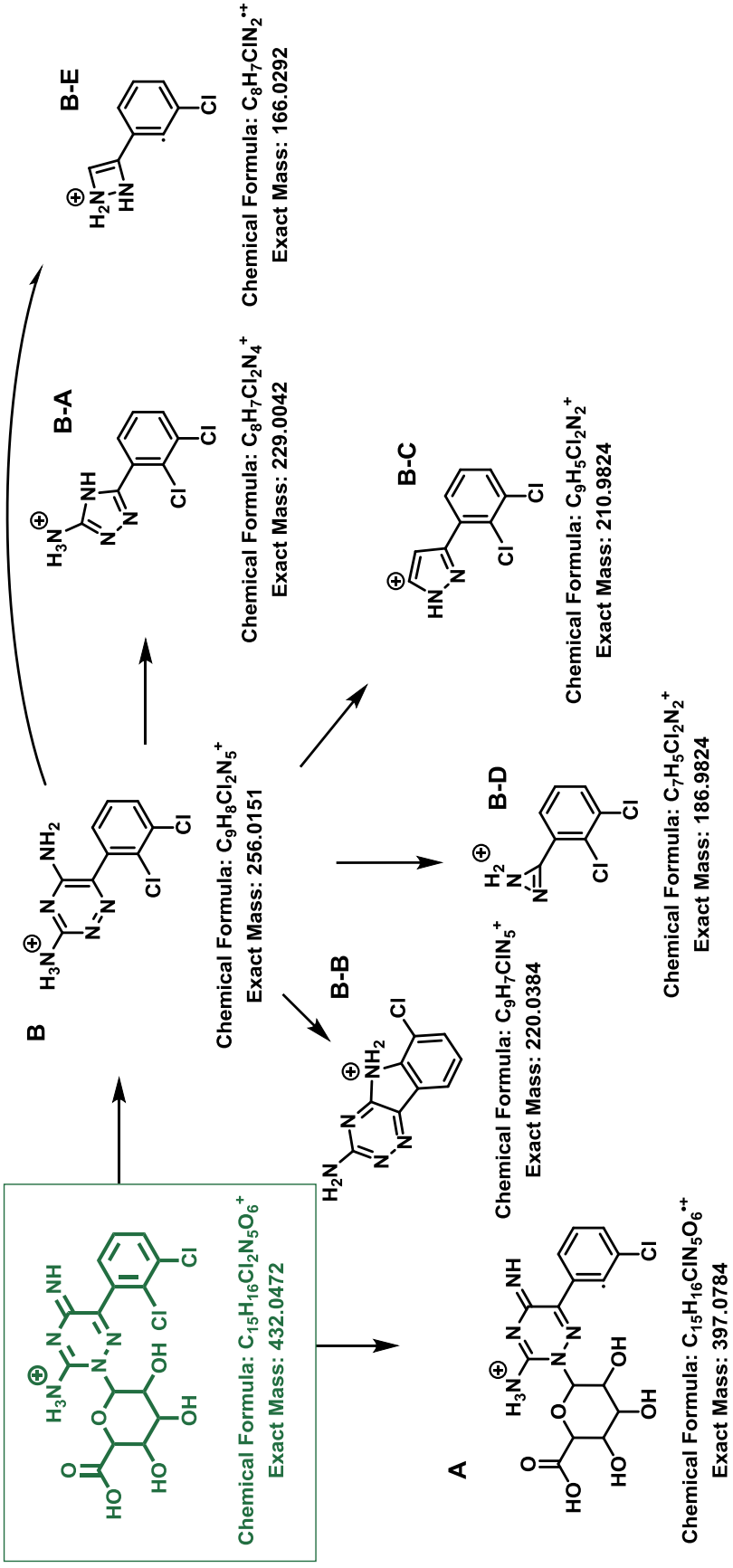

Figure SI-10.2-A. Fragmentation pattern of lamotrigine-N2-glucuronide (LMG-N2-G)

Figure SI-10.2-B. MS^2 and pMS^3 spectra of lamotrigine-N2-glucuronide (LMG-N2-G)

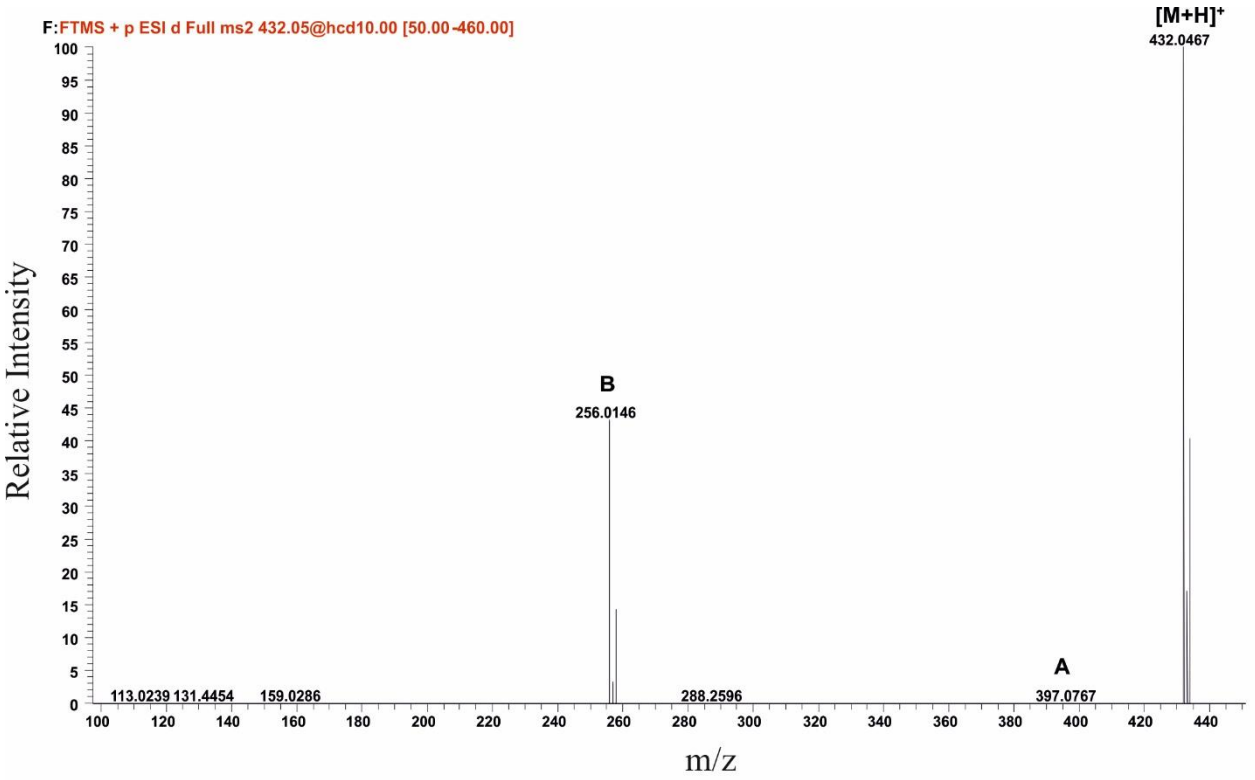

LMG-N2-G – LMG pMS^3

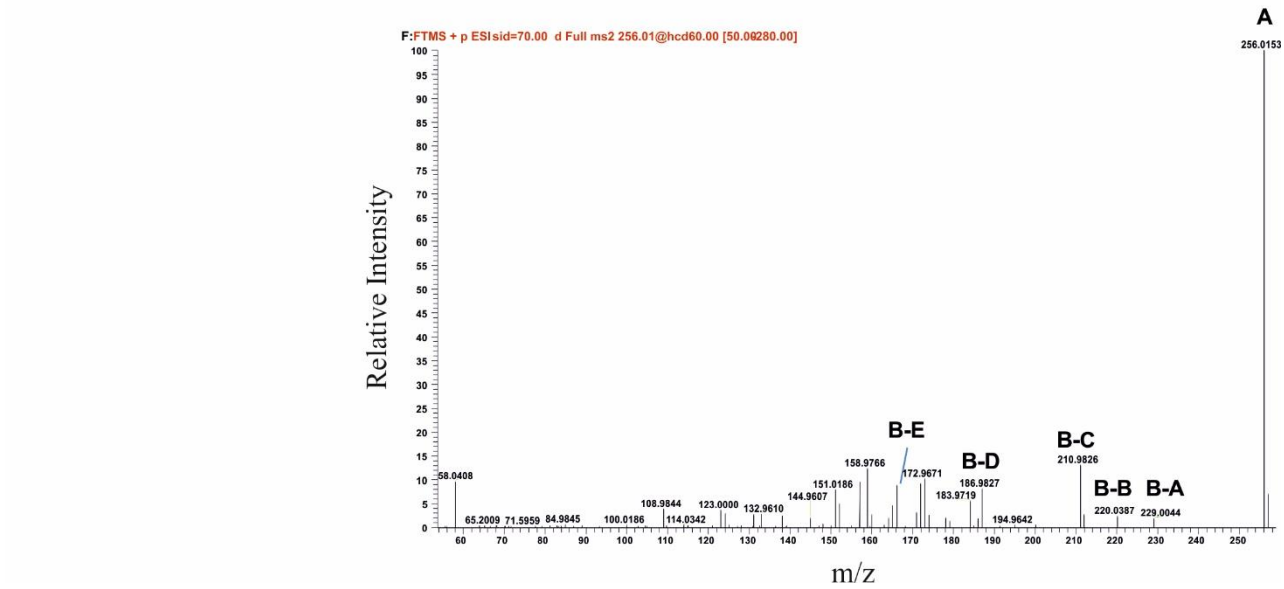

LAMOTRIGINE-N2-GLUCURONIDE TP430 (LMG-N2-G TP430)

Figure SI-10.3-A. Fragmentation pattern of lamotrigine-N2-glucuronide TP430 (LMG-N2-G-TP430)

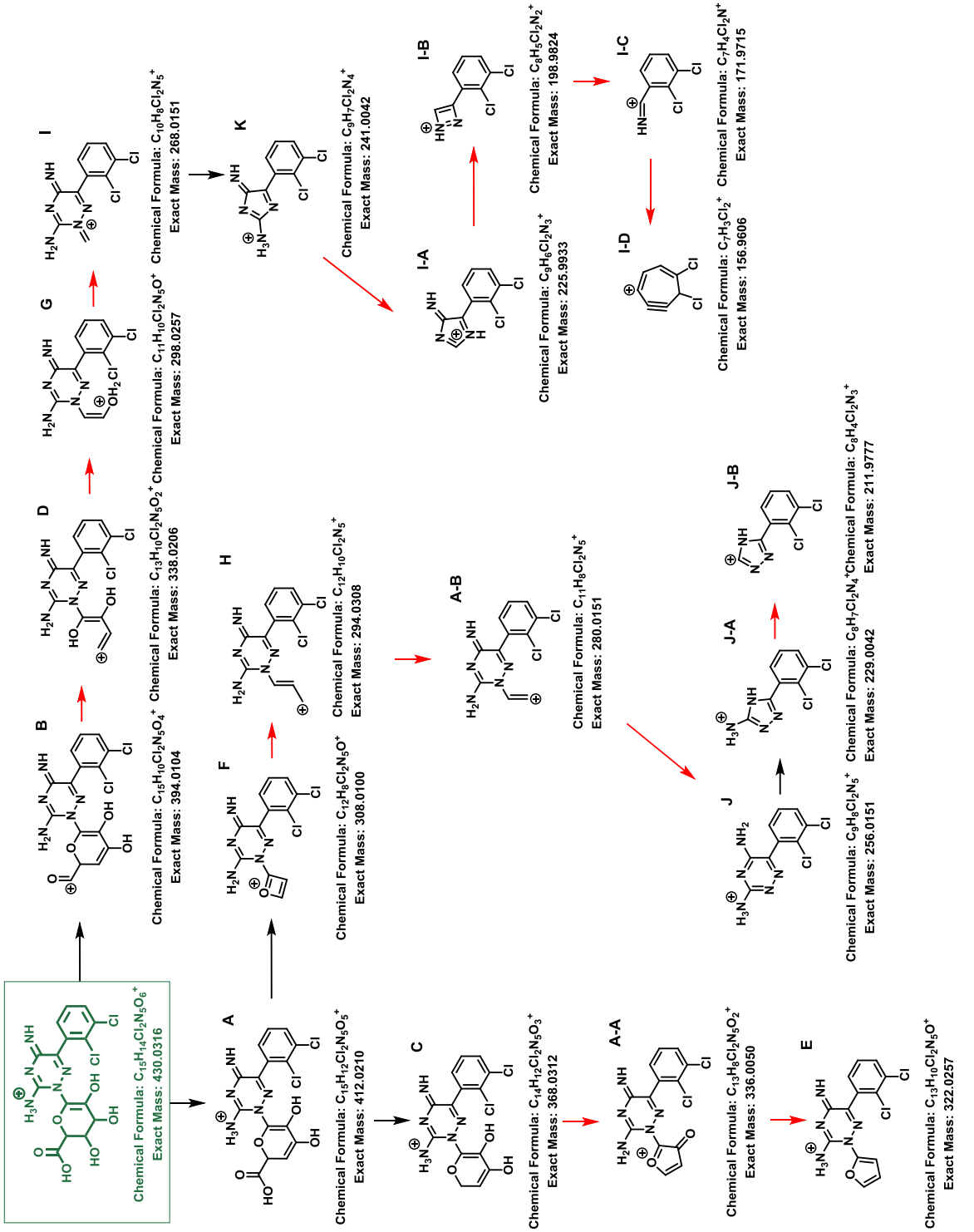

Figure SI-10.3-B. MS^2 and pMS^3 spectra of lamotrigine-N2-glucuronide TP430 (LMG-N2-G-TP430)

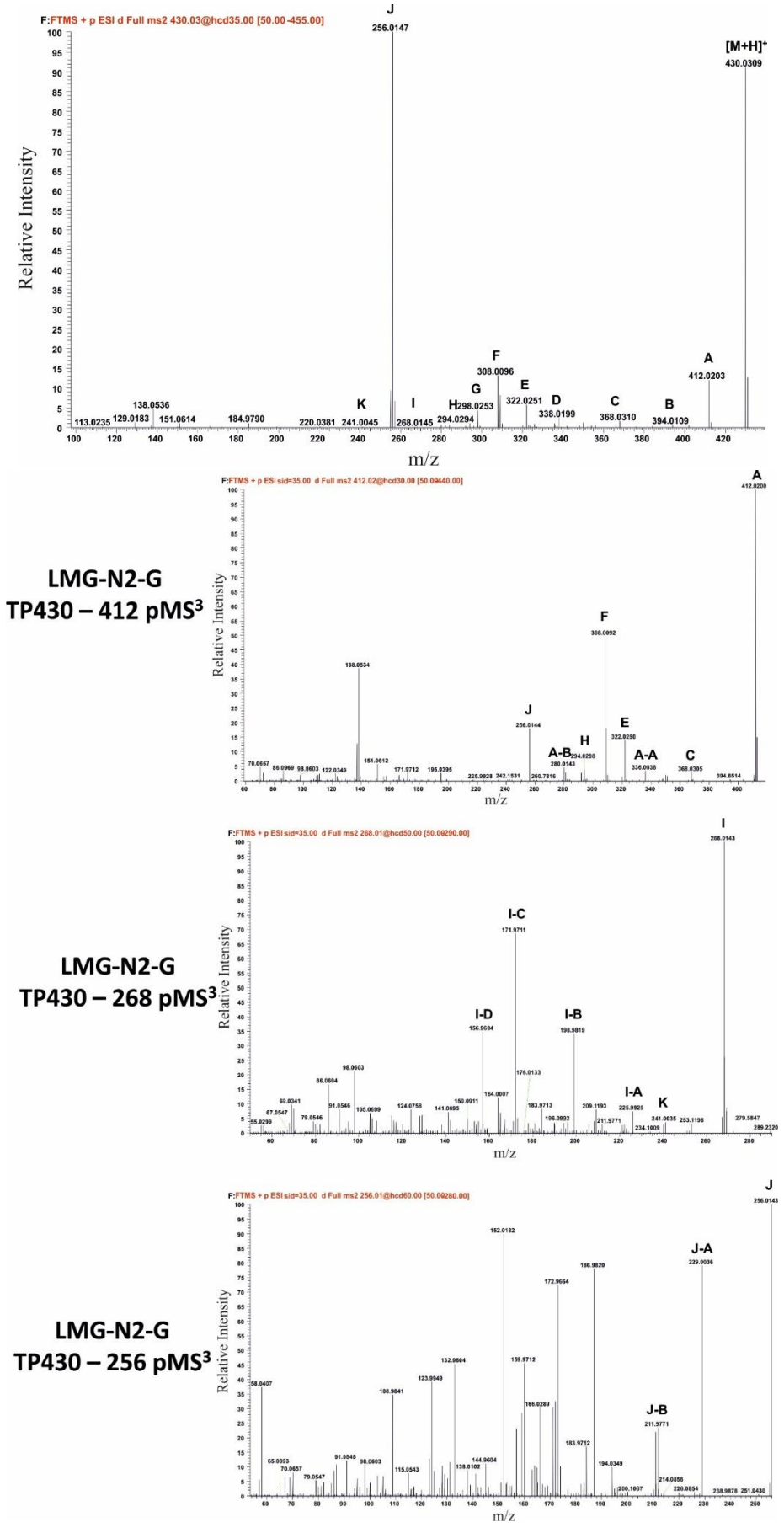

Table SI-6. Accurate mass measurements of protonated LMG, LMG-N2-G and LMG-N2-G-TP430 as determined by LC-QExactive-MS in MS/MS or pseudo MS^3 modes

Nominal ion mass	Measured mass [m/z]	Mass error [ppm]	Elemental composition	Calculated mass [m/z]	DBE[a]
Lamotrigine (LMG)					
$[M+H]^+$	256.0154	1.2	$C_9H_8Cl_2N_5$	256.0151	7.5
A 238	238.9891	2.1	$C_9H_5Cl_2N_4$	238.9886	8.5
B 229	229.0045	1.3	$C_8H_7Cl_2N_4$	229.0042	6.5
D 211	211.9774	-1.4	$C_8H_4Cl_2N_3$	211.9777	7.5
F 186	186.9824	0.0	$C_7H_5Cl_2N_2$	186.9824	5.5
J 166	166.0291	-0.6	$C_8H_7ClN_2$	166.0292	6.0
L 158	158.9760	-1.9	$C_7H_5Cl_2$	158.9763	4.5
M 152	152.0134	-1.3	$C_7H_5ClN_2$	152.0136	6.0
F-A 144	144.9606	0.0	$C_6H_3Cl_2$	144.9606	4.5
C 220	220.0387	1.4	$C_9H_7ClN_5$	220.0384	8.5
H 178	178.0168	0.6	$C_8H_5ClN_3$	178.0167	7.5
K 165	165.0215	0.6	$C_8H_6ClN_2$	165.0214	6.5
C-A 151	151.0059	1.0	$C_7H_4ClN_2$	150.0058	6.5
N 138	138.0107	1.4	C_7H_5ClN	138.0105	5.5
D 211	211.9775	-0.9	$C_8H_4Cl_2N_3$	211.9777	7.5
E 210	210.9827	1.4	$C_9H_5Cl_2N_2$	210.9824	7.5
E-A 194	194.9640	1.5	$C_9H_3Cl_2N$	194.9637	8.0
G 183	183.9717	1.1	$C_8H_4Cl_2N$	183.9715	6.5
I 172	172.9671	1.7	$C_6H_3Cl_2N_2$	172.9668	5.5
Q 108	108.9845	4.6	C_6H_2Cl	108.9840	5.5
F 186	186.9828	2.1	$C_7H_5Cl_2N_2$	186.9824	5.5
M 152	152.0137	0.7	$C_7H_5ClN_2$	152.0136	6.0
F-A 144	144.9607	0.7	$C_6H_3Cl_2$	144.9606	4.5
L-A 132	132.9608	1.5	$C_5H_3Cl_2$	132.9606	3.5
Q 108	108.9844	3.7	C_6H_2Cl	108.9840	5.5
G 183	183.9720	2.7	$C_8H_4Cl_2N$	183.9715	6.5
H 178	178.0170	1.7	$C_8H_5ClN_3$	178.0167	7.5
I 172	172.9665	-1.7	$C_6H_3Cl_2N_2$	172.9668	5.5

Nominal ion mass	Measured mass [m/z]	Mass error [ppm]	Elemental composition	Calculated mass [m/z]	DBE[a]
J 166	166.0296	2.4	$C_8H_7ClN_2$	166.0292	6.0
O 131	131.0606	1.5	$C_8H_7N_2$	131.0604	6.5
J-A 104	104.0500	4.8	C_7H_6N	104.0495	5.5
K 165	165.0211	-1.8	$C_8H_6ClN_2$	165.0214	6.5
L 158	158.9766	1.9	$C_7H_5Cl_2$	158.9763	4.5
L-A 132	132.9609	2.3	$C_5H_3Cl_2$	132.9606	3.5
P 122	123.0000	3.3	C_7H_4Cl	122.9996	5.5
L-B 96	96.9846	6.2	C_5H_2Cl	96.9840	4.5
L-C 89	89.0393	7.9	C_7H_5	89.0386	5.5
M 152	152.0132	-2.6	$C_7H_5ClN_2$	152.0136	6.0
N 138	138.0107	1.4	C_7H_5ClN	138.0105	5.5
O 131	131.0607	2.3	$C_8H_7N_2$	131.0604	6.5
P 123	123.0000	3.3	C_7H_4Cl	122.9996	5.5
Q 108	108.9847	6.4	C_6H_2Cl	108.9840	5.5
Lamotrigine-N2-glucuronide (LMG-N2-G)					
$[M+H]^+$	432.0467	-1.2	$C_{15}H_{16}Cl_2N_5O_6$	432.0472	9.5
A 397	397.0767	-4.3	$C_{15}H_{16}ClN_5O_6$	397.0784	10.0
B 256	256.0146	-2.0	$C_9H_8Cl_2N_5$	256.0151	7.5
B-A 229	229.0044	0.9	$C_8H_7Cl_2N_4$	229.0042	6.5
B-B 220	220.0387	1.4	$C_9H_7ClN_5$	220.0384	8.5
B-C 210	210.9826	0.9	$C_9H_5Cl_2N_2$	210.9824	7.5
B-D 186	186.9827	1.6	$C_7H_5Cl_2N_2$	186.9824	5.5
B-E 166	166.0288	-2.4	$C_8H_7ClN_2$	166.0292	6.0
Lamotrigine-N2-glucuronide TP430 (LMG-N2-G-TP430)					
[M+H]+	430.0318	0.5	$C_{15}H_{14}Cl_2N_5O_6$	430.0316	10.5
A 412	412.0203	-1.7	$C_{15}H_{12}Cl_2N_5O_5$	412.0210	11.5
C 368	368.0305	-1.9	$C_{14}H_{12}Cl_2N_5O_3$	368.0312	10.5
A-A 336	336.0038	-3.6	$C_{13}H_8Cl_2N_5O_2$	336.0050	11.5
E 322	322.0250	-2.2	$C_{13}H_{10}Cl_2N_5O$	322.0257	10.5

Nominal ion mass	Measured mass [m/z]	Mass error [ppm]	Elemental composition	Calculated mass [m/z]	DBE[a]
F 308	308.0092	-2.6	$C_{12}H_8Cl_2N_5O$	308.0100	10.5
H 294	294.0298	-3.4	$C_{12}H_{10}Cl_2N_5$	294.0308	9.5
A-B 280	280.0143	-2.9	$C_{11}H_8Cl_2N_5$	280.0151	9.5
J 256	256.0144	-2.7	$C_9H_8Cl_2N_5$	256.0151	7.5
B 394	394.0109	1.3	$C_{15}H_{10}Cl_2N_5O_4$	394.0104	12.5
C 368	368.0310	-0.5	$C_{14}H_{12}Cl_2N_5O_3$	368.0312	10.5
D 338	338.0199	-2.1	$C_{13}H_{10}Cl_2N_5O_2$	338.0206	10.5
E 322	322.0251	-1.9	$C_{13}H_{10}Cl_2N_5O$	322.0257	10.5
F 308	308.0096	-1.3	$C_{12}H_8Cl_2N_5O$	308.0100	10.5
G 298	298.0253	-1.3	$C_{11}H_{10}Cl_2N_5O$	298.0257	8.5
H 294	294.0294	-4.8	$C_{12}H_{10}Cl_2N_5$	294.0308	9.5
I 268	268.0145	-2.2	$C_{10}H_8Cl_2N_5$	268.0151	8.5
K 241	241.0035	-2.9	$C_9H_7Cl_2N_4$	241.0042	7.5
I-A 225	225.9925	-3.5	$C_9H_6Cl_2N_3$	225.9933	7.5
I-B 198	198.9819	-2.5	$C_8H_5Cl_2N_2$	198.9824	6.5
I-C 171	171.9711	-2.3	$C_7H_4Cl_2N$	171.9715	5.5
I-D 156	156.9604	-1.3	$C_7H_3Cl_2$	156.9606	5.5
J 256	256.0147	-1.6	$C_9H_8Cl_2N_5$	256.0151	7.5
J-A 229	229.0036	-2.7	$C_8H_7Cl_2N_4$	229.0042	6.5
J-B 211	211.9771	-2.7	$C_8H_4Cl_2N_3$	211.9777	7.5
K 241	241.0045	1.2	$C_9H_7Cl_2N_4$	241.0042	7.5

[a] Double-bond equivalents.

Transformation of LMG-N2-G-TP430 to LMG-N2-G-TP431-Amd

LMG-N2-G-TP431-Amd is a transformation product of LMG-N2-G-TP430 which is formed as a result of the amidine hydrolysis (purple transformation in the manuscript) of the LMG-N2-G-TP430. This TP was found at barely detectable concentrations in the experiments over the course of 8 hours of degradation of LMG-N2-G. This was the reason why it was not included in the mass balance of the LMG-N2-G. However, in the initial experiments where LMG-N2-G was degraded over the course of 6 days at concentrations of 50 and 5 μgL^{-1} (concentrations for identifications of TPs and kinetics, respectively), this compound was detected at higher concentrations. In the degradation experiments for identification purposes (50 μgL^{-1} concentration) its abundance was sufficient enough to perform the MS^2 experiments and to characterize the compound (**Figure SI-12**). In the **Figure SI-12** can be seen the fragmentation spectrum of the LMG-N2-G-TP431-Amd in comparison with the fragmentation spectrum of LMG-N2-G-TP430 (**Figure SI-11**). From the blue box spectra in the **Figure SI-11** it can be seen that while the LMG-N2-G-TP430 under NCE 35 fragments to its most abundant ion with m/z 256.0156 which is LMG. On the other hand, LMG-N2-G-TP431-Amd under the same NCE fragments to m/z 256.9991 which is the exact mass of OXO-LMG (**Figure SI-12)**. In the amplified spectra of both compounds it can be seen that the majority of other fragments forming (although with different intensities), are the same with the mass defect of 0.984.

As to reaction pattern, for LMG-N2-G, amidine hydrolysis TP was only detected as an abiotic transformation product which depended on the pH and was not detected in the biodegradation experiments. Furthermore, it was suggested that the reaction of amidine hydrolysis and decojugation happen simultaneously and that this could be the reason why LMG-N2-G-TP433-Amd was not detected in the batch experiments. Since the LMG-N2-G-TP431-Amd was formed in the same batch reactors (over the course of 6 days) where the pH was carefully monitored to be around 7, the source of this TP could be enzymatic transformation. Unlike in the case of LMG-N2-G-TP433-Amd, the deconjugation of LMG-N2-G-TP431-Amd to form OXO-LMG is far more difficult because of the higher stability of the corresponding glycal (similar to its parent compound LMG-N2-G-TP430).

Figure SI-11. MS² fragmentation of LMG-N2-G-TP430.

The difference with the spectrum in the blue box and the large spectra are the m/z range. The blue box spectrum has the m/z range from 100 – 435 and the enlarged spectrum has the m/z range from 260 - 435. Letters in the lower spectra correspond to the fragmentation pattern of LMG-N2-G-TP430 as depicted in the ***Figure SI-9.4.-A.***

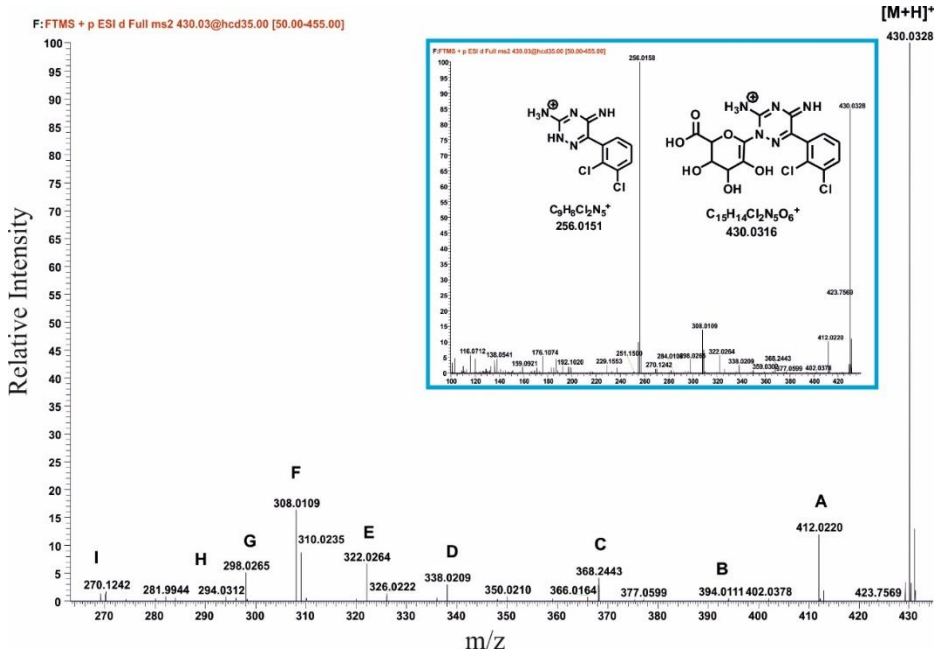

Figure SI-12. MS² fragmentation of LMG-N2-G-TP431-Amd.

The difference with the spectra in the blue box and the large spectra are the m/z range. The blue box spectrum has the m/z range from 100 – 435 and the enlarged spectrum has the m/z range from 260 - 435. Apostrophized letters in the lower spectra are put for comparison between the LMG-N2-G-TP430 and LMG-N2-G-TP431-Amd.

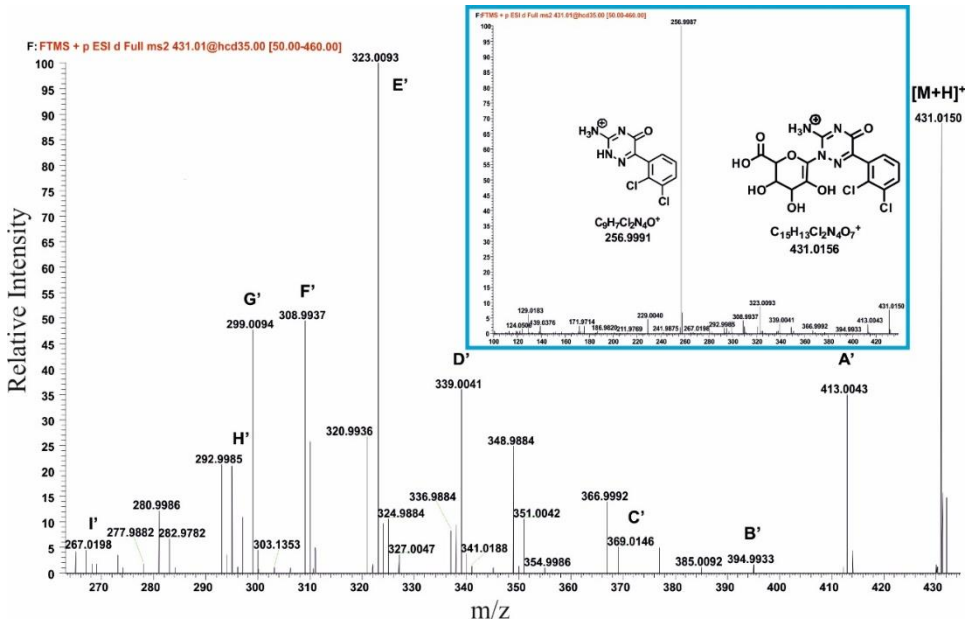

Determination of lamotrigine and derived compounds in wastewater and surface water

The wastewater and surface water samples already run were reanalysed using Xcalibur form Thermo Scientific since only scan filter was used for quantitation and determination (see LOQ section below).

As mentioned in the manuscript, for WWTP 4 (**Table SI-7**), a procedural error occurred and the internal standard was spiked approximately 1000 lower than the other wastewater samples which caused that in some cases it was below LOQ. Most likely due to this, the total LMG-N2-G mass balance was overestimated by 54 %.

Table SI-7. Concentration of LMG-N2-G and related compounds in the WWTP 4.

nmolL^{-1}	WWTP 4		
	influent		effluent
LMG-N2-G (1)	1.159 ± 0.066		0.498 ± 0.002
[^{37}Cl]/[^{35}Cl] [%]	64		62
LMG (2)	0.174 ± 0.006		1.270 ± 0.121
[^{37}Cl]/[^{35}Cl] [%]	60		64
SUM (1+2)	***1.333***	*(+32 %)*	***1.768***
N2-MeLMG (3)	< LOQ		0.024 ± 0.003
[^{37}Cl]/[^{35}Cl] [%]	-		62
LMG-N2-Oxide (4)	< LOQ		0.009 ± 0.000
[^{37}Cl]/[^{35}Cl] [%]	-		61
SUM (1-4)	***1.333***	*(+34%)*	***1.792***
OXO-LMG (5)	0.048 ± 0.002		0.180 ± 0.010
[^{37}Cl]/[^{35}Cl] [%]	62		62
LMG-N2-G-TP433-Amd (6)	0.012 ± 0.001		< LOQ
[^{37}Cl]/[^{35}Cl] [%]	54		-
SUM (1-6)	***1.393***	*(+42%)*	***1.972***
LMG-N2-G-TP430 (7)	n.d.		0.170 ± 0.008
[^{37}Cl]/[^{35}Cl] [%]	-		60
SUM all (1-7)	***1.393***	*(+54 %)*	***2.142***

Recovery measurements

For recovery calculations each matrix (WW influent, WW effluent and surface water) a mixture of samples was joined together. As in the screening method, 400 mL of WW influent, 600 mL of WW effluent and 800 mL of surface water were used for pre-concentration. The pH of the mixture was adjusted to 6.5 and then spiked with 200 ng of standards available (including $^{13}C_3$-LMG). All experiments were performed in triplicate. The extracts of different cartridges were eluted separately and analysed separately.

Recovery was calculated as the difference between the sum of concentrations from the four cartridges after the SPE and the blank sample divided with spiked concentration.

The results of the recovery experiments are shown in **Table SI-8**.

Since the four cartridges were analysed separately, the relative distribution of analytes between them is also reported. The arrows in the table report the order how the cartridges were connected.

As can be seen from the **Table SI-8**, recoveries in all matrices ranged from 68 % (for OXO-LMG in WW influent) to 134 % (for LMG-N2-oxide in WW effluent). What can also be noted is that almost all of the analytes were retained in the first cartridge to be connected in the series – HLB. The only exception to this was the extraction efficiency for LMG-N2-G in surface water samples where LMG-N2-G was distributed between the HLB and BondElute PPL with 72 – 28 % ratio. Since LMG-N2-G was completely extracted when less volume was preconcentrated (400 mL for WW influent and 600 mL for WW effluent), it is likely that the 800 mL of surface water caused saturation of the HLB cartridge. LMG-N2-G-TP433-Amd recovery was determined only in WW influent since this compound was not detected in any of the effluent or surface water samples.

LOQ measurements

Limit of quantification (LOQ) is also shown in the **Table SI-8**. For a compound to be identified a set of parameters must have been fulfilled and match the parent compound. The compound was determined if it matched retention time (+/- 0.2 min), exact mass accuracy

(<5 ppm) and relative chlorine isotope pattern which was calculated for every compound and sample. This value is given below each reported concentration. LOQ values were calculated as signal-to-noise ratio (S/N) higher than 10. <LOQ was reported for compounds where the identification rules applied but the S/N was lower than 10.

LOQs determined for all compounds were in the low ngL^{-1} ranges (**Table SI-8**) which afforded the quantification of all of the compounds in the majority of the samples investigated. The highest LOQ determined in all matrices was that of LMG. This was due to a high background noise detected of the m/z 256.0151. Similar to the recovery measurements, LOQ of LMG-N2-G-TP-433-Amd was only determined in the WW influent since this was the only matrix where this compound was detected. As for LMG-N2-G-TP430, LOQ used was the one of LMG-N2-G since it was not possible to obtain this compound as an authentic standard.

Table SI-8. Recoveries and LOQ of LMG and derived compounds in WW influent, WW effluent and surface water.

Arrows denote which was the order of SPE cartridges which were connected in series.

Matrix (volume)	Cartridge	LMG	LMG-N2-G	OXO-LMG	N2-Me-LMG	LMG-N2-oxide	LMG-N2-G TP430	LMG-N2-G TP433-Amd
WWTP influent (400 mL)[a]	Rec tot[b] [%]	104 ± 10[c]	100 ± 8	65 ± 8	85 ± 14	114 ± 9	N/A[e]	104 ± 7
	↓ HLB[d] [%]	99	100	100	100	100	100	95
	↓ PPL[d] [%]	0	0	0	0	0	0	5
	↓ MAX[d] [%]	1	0	0	0	0	0	0
	↓ MCX[d] [%]	0	0	0	0	0	0	0
LOQ [ngL^{-1}]		7.3	0.5	1.1	6.5	4.9	LMG-N2-G	1.0
WWTP effluent (600 mL)	Rec tot [%]	79 ± 10	96 ± 4	99 ± 1	105 ± 2	134 ± 2	N/A	N/A
	↓ HLB [%]	100	100	100	100	100	100	N/A
	↓ PPL [%]	0	0	0	0	0	0	N/A
	↓ MAX [%]	0	0	0	0	0	0	N/A
	↓ MCX [%]	0	0	0	0	0	0	N/A
LOQ [ngL^{-1}]		2.2	0.3	0.5	0.6	2.1	LMG-N2-G	N/A
Surface water (800 mL)	Rec tot [%]	100 ± 13	103 ± 3	118 ± 8	81 ± 5	78 ± 4	N/A	N/A
	↓ HLB [%]	100	72	100	100	100	100	N/A
	↓ PPL [%]	0	28	0	0	0	0	N/A
	↓ MAX [%]	0	0	0	0	0	0	N/A
	↓ MCX [%]	0	0	0	0	0	0	N/A
LOQ [ngL^{-1}]		1.5	0.2	0.2	0.3	1.2	LMG-N2-G	N/A
RT [min]		6.42	4.68	6.87	6.73	6.36	5.72	5.47

[a] preconcentration volume; [b] total recovery of a compound; [c] average of three measurements and standard deviation; [d] percentage of total recovery that was retained in the cartridge; [e] not analyzed

Figure SI-13. Representative chromatograms of detected TPs in influent (LMG-N2-TP433-Amd) and effluent samples (the rest)

Figure SI-13 shows the chromatograms of the (A) LMG, (B) N2-Me-LMG, (C) LMG-N2-oxide, (D) LMG-N2-G, (E) OXO-LMG, (F) LMG-N2-G-TP430 and (G) LMG-N2-G-TP433-Amd together with their corresponding ^{37}Cl isotope peak. For (B) N2-Me-LMG another peak that eluted later was detected with the same isobaric mass as LMG metabolite but without the corresponding ^{37}Cl isotope and was discarded from further analysis. For (C) LMG-N2-oxide again another peak was detected with the ^{35}Cl and ^{37}Cl isotope ration which indicated that the compound had two chlorine atoms. However, since this compound was detected in only one sample (one WW effluent sample) it was further used as a positive finding of a suspect analyte.

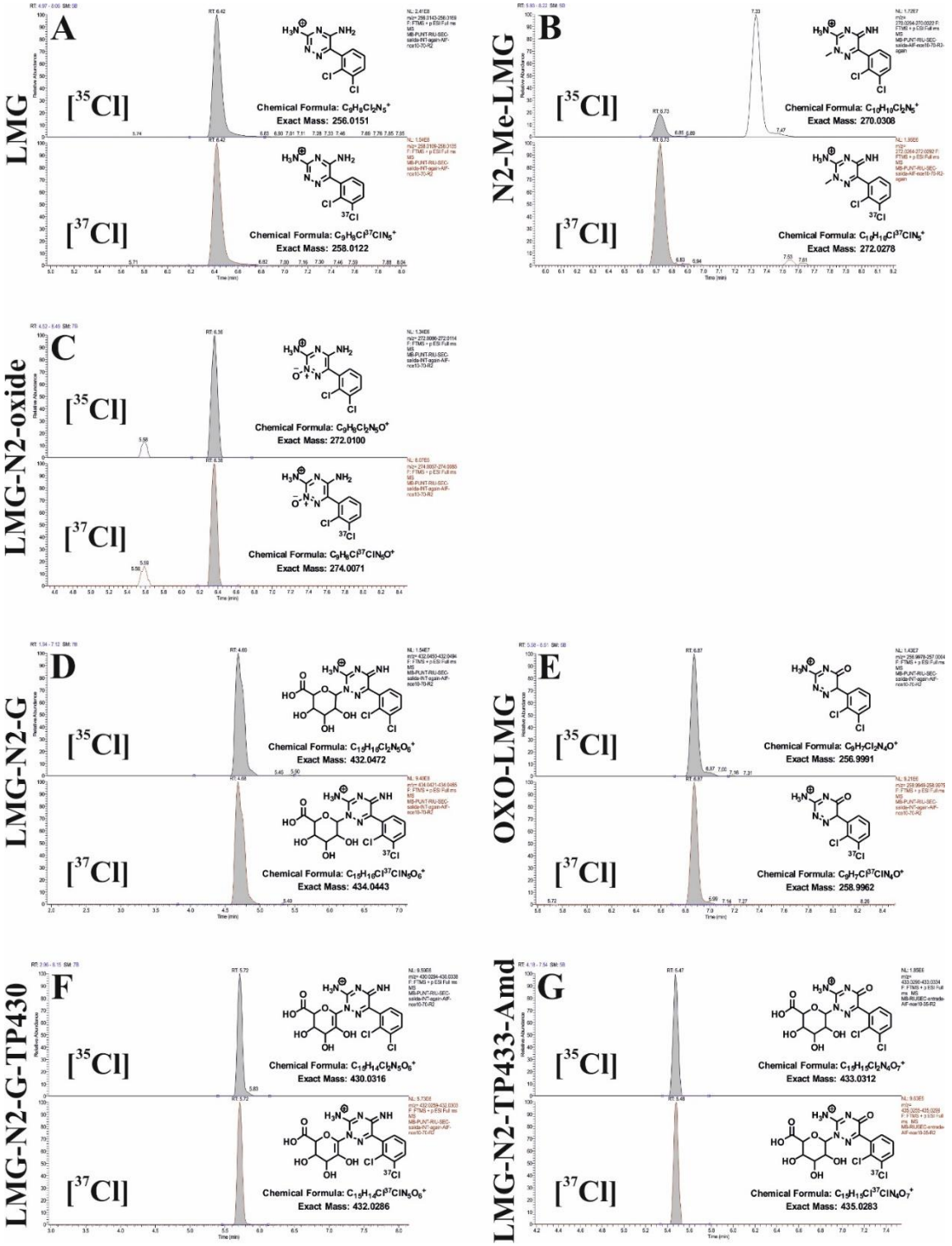

SI-Reference

1. Reglament dels serveis públics de sanejament (in catalan). *Diari Oficial de la Generalitat de Catalunya* **2003,** *130*, (3894), 11143-11158.

2. Zonja, B.; Delgado, A.; Pérez, S.; Barceló, D., LC-HRMS Suspect Screening for Detection-Based Prioritization of Iodinated Contrast Media Photodegradates in Surface Waters. *Environmental Science & Technology* **2015,** *49*, (6), 3464-3472.

3. Marvin was used for drawing, displaying and characterizing chemical structures, substructures and reactions, Marvin 6.1, 2013, ChemAxon (http://www.chemaxon.com).

4. Doig, M. V.; Clare, R. A., Use of thermospray liquid chromatography-mass spectrometry to aid in the identification of urinary metabolites of a novel antiepileptic drug, Lamotrigine. *Journal of Chromatography A* **1991,** *554*, (1-2), 181-189.

5. Lu, W.; Uetrecht, J. P., Possible bioactivation pathways of lamotrigine. *Drug Metab Dispos* **2007,** *35*, (7), 1050-6.

6. Srinivasulu, P.; Mukkanti, K.; Reguri, B. R.; Srinivas, K. S. V., Development of a Validated Stability Indicating LC Method for Lamotrigine. *Chromatographia* **2009,** *70*, (1-2), 271-276.

7. Hlaváč, J.; Buchtík, R.; Slouka, J.; Hradil, P.; Wiedermannová, I., Synthesis of oxo analogs of Lamotrigine and related compounds. *Arkivoc* **2003,** *2003*, (1), 22-28.

8. Young, R. B.; Chefetz, B.; Liu, A.; Desyaterik, Y.; Borch, T., Direct photodegradation of lamotrigine (an antiepileptic) in simulated sunlight--pH influenced rates and products. *Environ Sci Process Impacts* **2014,** *16*, (4), 848-57.

9. Ramsay, R. E.; Pellock, J. M.; Garnett, W. R.; Sanchez, R. M.; Valakas, A. M.; Wargin, W. A.; Lai, A. A.; Hubbell, J.; Chern, W. H.; Allsup, T.; Otto, V., Pharmacokinetics and safety of lamotrigine (Lamictal®) in patients with epilepsy. *Epilepsy Research* **1991,** *10*, (2–3), 191-200.

10. Sidhu, J.; Job, S.; Bullman, J.; Francis, E.; Abbott, R.; Ascher, J.; Theis, J. G. W., Pharmacokinetics and tolerability of lamotrigine and olanzapine coadministered to healthy subjects. *British Journal of Clinical Pharmacology* **2006,** *61*, (4), 420-426.

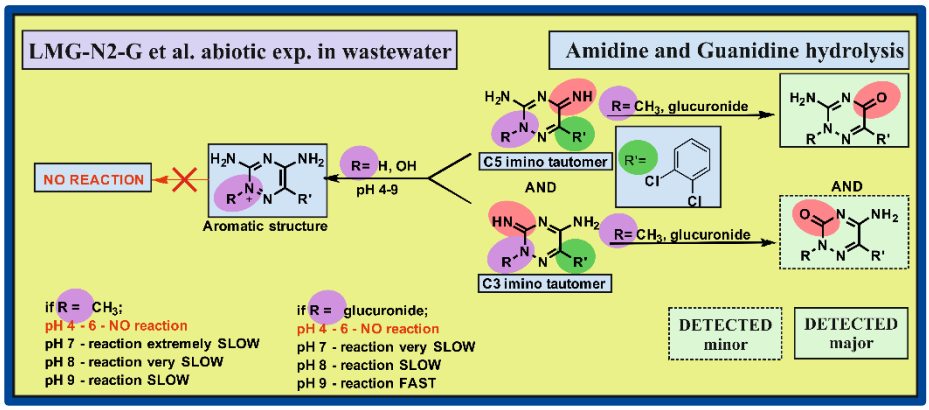

Article Nº4:

Zonja, B., Delgado, A., Abad, J.L., Pérez, S. and Barceló, D.

Abiotic amidine and guanidine hydrolysis of lamotrigine-N2-glucuronide and related compounds in wastewater: The role of pH and N2-substitution on reaction kinetics.

(2016.) Water Res 100, 466-475.

Water Research 100 (2016) 466–475

Contents lists available at ScienceDirect

Water Research

journal homepage: www.elsevier.com/locate/watres

Abiotic amidine and guanidine hydrolysis of lamotrigine-N2-glucuronide and related compounds in wastewater: The role of pH and N2-substitution on reaction kinetics

Bozo Zonja [a], Antonio Delgado [b, c], J. Luis Abad [c], Sandra Pérez [a, *], Damià Barceló [a, d]

[a] Water and Soil Quality Research Group, Department of Environmental Chemistry, IDAEA-CSIC, c/Jordi Girona, 18-26, 08034 Barcelona, Spain
[b] University of Barcelona (UB), Faculty of Pharmacy, Department of Pharmacology and Medicinal Chemistry, Avga. Joan XXIII s/n, E-08028 Barcelona, Spain
[c] Department of Biomedicinal Chemistry, Research Unit on BioActive Molecules (RUBAM), IQAC-CSIC, c/Jordi Girona, 18-26, 08034 Barcelona, Spain
[d] Catalan Institute of Water Research, c/Emili Grahit, 101, Edifici H_2O, Parc Científic i Tecnològic de la Universitat de Girona, E-17003 Girona, Spain

ARTICLE INFO

Article history:
Received 8 September 2015
Received in revised form
24 April 2016
Accepted 30 April 2016
Available online 3 May 2016

Keywords:
Lamotrigine-N2-glucuronide
pH stability
Wastewater
LC-HRMS
Amidine and guanidine hydrolysis
transformation products
Imino tautomers

ABSTRACT

The stability of lamotrigine (LMG) and its principal human metabolite, lamotrigine N2-glucuronide (LMG-N2-G), was studied as a function of pH (4–9). While LMG was stable across the entire pH range, under neutral-basic conditions, LMG-N2-G was converted to three transformation products (TPs) which were identified using high resolution mass spectrometry (HRMS). The MS fragmentation studies indicated that two TPs were the result of the hydrolysis of the amidine and guanidine moieties. The third TP detected was an intermediate in the guanidine hydrolysis reaction. In order to evaluate the transformation kinetics of the LMG-N2-G degradation, another set of pH-dependent experiments was carried out in hospital effluent, wastewater influent and effluent spiked at 20 and 200 nM after pH adjustment (pH 6.5, 7, 8, 8.5 and 9), demonstrating that, at higher pH, LMG-N2-G is degraded at higher rate. Later, the pH-dependent stability of related compounds with different nitrogen N2-substituents (N2-R) on the 1,2,4-triazine ring was studied. This revealed that because of different imino tautomer equilibrium LMG (N2-H) and LMG-N2-oxide ($^{+}$N2-O^{-}) were stable at all pHs but N2-methyl-LMG (N2-CH_3) as well as LMG-N2-G were susceptible to amidine and guanidine hydrolysis at basic pH. Finally, hospital effluent samples collected over the course of one week were monitored for their presence. LMG, LMG-N2-G and two of its TPs were detected with concentrations ranging between 0.01 and 1 μgL^{-1}.

1. Introduction

Lamotrigine N2-glucuronide (LMG-N2-G) is the principal human metabolite of the anticonvulsant lamotrigine (LMG) (Fig. 2) (Ohman et al., 2008; Saracino et al., 2007) with the LMG – LMG-N2-G ratio in urine of normal volunteers reported to be about 10: 90% (Ramsay et al., 1991). LMG-N2-G is formed by glucuronidation at the position N2 of the 1,2,4-triazine ring in the LMG structure. In general, these *N*-glucuronides are represented by the tautomer with a permanent positive charge on the N2 in addition to the negative charge of the carboxylate, making them zwitterions (Pagliara et al., 1997; Testa and Krämer, 2008), despite that other tautomeric forms are also possible. In a study of the stability of the aliphatic quaternary ammonium glucuronides of the drugs chlorpromazine, cyclizine, doxepin and clozapine under enzymatic reactions, they were shown to be resistant to hydrolysis (deconjugation) except after treatment with *β-glucuronidase* from *Escherichia coli* at pH 7.4 (Kowalczyk et al., 2000). In the same study, pH dependent experiments (in the pH range of 4–10) proved these glucuronides to be stable for a period of three months. However, glucuronides can undergo deconjugation at acidic pH with some reported exceptions like the acyl-glucuronide of mycophenolic acid (Di Meo et al., 2013). The glucuronide of mycophenolic acid remained stable for various hours at neutral pH but was deconjugated rapidly at basic pH.

The pH dependence or biotic stability of glucuronides could be environmentally relevant since it allows assessing the relevance of the transformation of the glucuronide back to the parent compound (Jelic et al., 2015). This is especially important for glucuronides like LMG-N2-G, which have been detected in wastewater,

* Corresponding author.
E-mail address: spsqam@cid.csic.es (S. Pérez).

http://dx.doi.org/10.1016/j.watres.2016.04.072
0043-1354/

surface and groundwater at high ngL^{-1} up to μgL^{-1} concentrations (Ferrer and Thurman, 2010; Writer et al., 2013a, 2013b; Zonja et al., 2016).

Jelic et al (Jelic et al., 2015). recently evaluated sewage-pipe attenuation of pharmaceuticals from their discharge site (hospital effluent) to the receiving wastewater treatment plant (WWTP) influent. They reported negative removal for some compounds (the glucuronide-forming sulfamethoxazole and irbesartan) suggesting that along the sewer system the glucuronides could undergo deconjugation and revert back to their parent compounds. However, their glucuronide metabolites were not monitored in that study. Up to date, little is known about the fate of glucuronides in the aquatic environment with the exception of conjugated steroid estrogens (D'Ascenzo et al., 2003; Gomes et al., 2009; Johnson and Williams, 2004; Kumar et al., 2012). Even in this case, the only reported reaction was the hydrolysis (deconjugation) reaction, by which the conjugated steroid estrogens reverted back to their respective parent compounds. This is generally accepted to be the major, if not the only metabolic pathway of the glucuronides. This was proven different for the biotic degradation of LMG-N2-G in activated sludge (Zonja et al., 2016). Biodegradation batch-experiments with activated sludge showed that LMG-N2-G is transformed into three stable TPs. The main reaction in the reactors was the hydrolysis of LMG-N2-G to LMG. But, two additional detected TPs originated from oxidation of the glucuronide moiety and of biotic amidine hydrolysis. The two latter TPs were detected in WWTPs and surface water at ng L^{-1} concentrations (Zonja et al., 2016).

Back in 1991, when LMG was still undergoing clinical trials, Sinz and Remmel (Sinz and Remmel, 1991) isolated and characterized the LMG-N2-G from human urine. In addition to the structure elucidation, they subjected the glucuronide to chemical and enzymatic hydrolysis. They observed that LMG-N2-G was transformed under basic conditions but the emerging peak in the chromatogram was not further characterized. The only information was that it eluted earlier than the parent compound and that it was completely degraded to presumably its transformation product (TP) after 5 h at room temperature and at pH 11. However, neither the mass nor the structure of the resulting TP was reported. It was deemed a product of a rearrangement reaction or degradation.

The objective of this study was to examine the stability and transformations of LMG-N2-G under different pH conditions. Based on the findings of Sinz and Remmel 1991 (Sinz and Remmel, 1991), a set of pH-dependent experiments were designed to detect and characterize other possible TPs. Degradations were explored in different types of wastewater (hospital effluent, WWTP influent and effluent) in order to establish mass balances of LMG-N2-G. Once they were identified using HRMS, stability of other LMG and LMG-N2-G related compounds (N2-methylated and N2-hydroxylated metabolites of LMG) were also studied at different pHs, to compare their degradation behavior. Since the related compounds had the same basic structure as LMG, deferring only by the substituent on the N-2 position, the reactivity of these molecules was explored and reported. Finally, hospital effluent samples were analyzed for their presence.

2. Materials and methods

2.1. Chemicals and standards

Lamotrigine (LMG), lamotrigine N2-oxide (LMG-N2-oxide), 5-desamino 5-oxo-2,5-dihydro lamotrigine (OXO-LMG) and internal standard lamotrigine-$^{13}C_3$ (LMG-$^{13}C_3$) were purchased from Toronto Research Chemicals (Toronto, Canada). Lamotrigine-N2-glucuronide (LMG-N2-G) was purchased from Santa Cruz Biotechnology (Dallas, Texas, USA). Lamotrigine N2-glucuronide TP433-Amd (LMG-N2-G-TP433-Amd) and N2-methyl lamotrigine (N2-Me-LMG) were synthesized, as explained in the following sections. All other organic and inorganic chemicals were of ACS reagent grade.

SPE cartridges Oasis HLB (500 mg), MCX and MAX (both 200 mg) were bought from Waters (Milford, MA, USA) and Bond Elut PPL (500 mg) from Agilent Technologies (Waghaeusel-Wiesental, Germany). Calibration of the Q-Exactive was done with ESI positive calibration solution from Thermo Scientific (Dresden, Germany).

2.2. Degradation in ultrapure water, hospital effluent, WWTP influent and effluent

Experiments for stability of compounds were adapted from OECD guidelines 111 (Hydrolysis as a function of pH) (OECD). Summary of the abiotic experiments performed can be found in Tables SI-1-7. Stock solutions of all compounds were prepared in methanol and stored at −20 °C prior to use. HPLC grade water used for ultrapure water (UPwater) experiment was from Baker (Deventer, The Netherlands). Hospital wastewater samples were collected from a general hospital and urban wastewater samples used were from a WWTP, both located in the municipality of the city of Barcelona (Table SI-4). All wastewater samples were filtered through 0.7 μm glass fiber filters. Samples at pH 8.5 were additionally filtered through 0.2 μm cellulose acetate filters (Whatman, Barcelona, Spain) (Table SI-1) in order to test the potential biotic activity in comparison with the samples filtered through 0.7 μm filters. The pH was directly set to the desired value using 50 mM of sterile acetate buffer (pH 4, 5 and 6), phosphate buffer (pH 7) and borate buffer (pH 8, 8.5 and 9). The buffered solutions were spiked with individual compound stock solutions in 1.5 mL amber glass vials to achieve final concentrations of 200 and 20 nM for LMG-N2-G and 400 nM for the other compounds. After the addition of the analytes, each vial was spiked with the internal standard solution (LMG-$^{13}C_3$) to achieve the concentration of 200 nM. Subsequently, each solution was shaken for 1 min and injected directly onto LC-QExactive-MS. Each vial was analyzed every three hours with the total degradation time from 27 to 42 h, depending on the experiment (Tables SI-1-7). The autosampler was set to room temperature (22 °C). The chromatographic separation was achieved using Acquity-BEH C_{18} column (100 × 2.1 mm, 1.7 μm) preceded by a pre-column of the same packing material (5 × 2.1 mm, 1.7 μm). The mobile phases for the chromatographic run were: (A) acetonitrile with 0.1% formic acid and (B) water (0.1% formic acid). The total chromatographic run was 7 min with a flow rate of 300 $\mu L\ min^{-1}$. The elution was accomplished with the following solvent gradient: 0 min (20% A) − 0.5 min (20% A) − 4 min (80% A), − 5 min (80% A) − 5.5 min (20% A) and stabilized until 7 min. The MS method used an electrospray ionization interface (ESI) which was operated in the positive ion mode with the following settings: spray voltage +3.0 kV, heater temperature 250 °C, and capillary temperature 350 °C. The MS acquisition method was a data dependent scan, programmed with the following parameters; full scan and data dependant-MS^2 were set to resolution of 70 000 [full width at half maximum (FWHM)], with the full scan range of m/z 100–600. In the data dependent scan the precursor ion isolation window was m/z 2.0 and the normalised collision energy (NCE) was 40 with a stepped NCE of 50%. The concentration of the compounds was determined by isotope-dilution method using LMG-$^{13}C_3$ as an internal standard for all compounds. For the exact number of replicates and the total duration of each experiment, please refer to Tables SI-1-7.

2.3. Detection and identification of TPs by HRMS

Exact mass measurements of all the compounds (OXO-LMG and LMG-N2-oxide, LMG-N2-G, N2-Me-LMG and their TPs) and their respective product ions were obtained using Q-Exactive-MS (Thermo Fischer, Bremen, Germany). Experiments were run in full-scan and product ion mode using positive ESI ionization. QExactive was interfaced with an ACQUITY UPLC system, Waters (USA). Peak deconvolution and extraction of the UPLC-chromatograms were performed using SIEVE (Thermo Fisher, Bremen, Germany) in the m/z range 100–600, m/z width of 5 ppm and intensity threshold of $1e^6$. The initial sample (T0) in every sample set was used as the control. *Detailed information on LC-MS parameters as well as fragmentation experiments can be found in SI.*

2.4. Synthesis of LMG-N2-G-TP433-Amd and N2-Me-LMG

Based on the results of the mass balance in UPwater, the major LMG-N2-G amidine hydrolysis TP, LMG-N2-G-TP433-Amd, was synthetized from LMG-N2-G. A volume of 10 mL of 0.1 M NaOH was spiked with 10 μL of a 1000 mgL^{-1} solution of LMG-N2-G and stirred with a magnetic stirrer at room temperature (Scheme 1.). The reaction was carried out in the dark and monitored by taking regular samples of the reaction mixture and checking the purity by running it on the UPLC-QExactive-MS. After 20 h, LMG-N2-G was completely converted into TP433-Amd.

N2-Me-LMG was synthesized with minor modifications according to the procedure described by Manning et al (Manning et al., 2002). In brief, LMG was treated with excess methyl iodide in acetone, followed by treatment with aqueous NH_3 and purification by flash chromatography using a gradient of MeOH in CH_2Cl_2. The resulting yield of the product was 93%. NMR experiments (1D and 2D NMR) were carried out on a 400 MHz Varian Mercury spectrometer (^1H NMR at 400 MHz and ^{13}C NMR at 100.6 MHz). More detailed information can be found in *SI*: *Synthesis and identification of N2-Me-LMG.*

2.5. Chlorination kinetic experiments

The reactivity of LMG-N2-G in the presence of 25 (for 200 nM concentration of LMG-N2-G) and 250 (for 20 nM) times molar excess of free chlorine in hospital wastewater was investigated as well. The procedure and UPLC-Q-Exactive-MS method were the same as explained for experiments without the addition of free chlorine (Section 2.2.). In the chlorination experiments, the free chlorine content was determined by reaction with *N,N*-diethyl-p-phenylenediamine using photometric detection.

2.6. Hospital effluent samples and analysis

Twenty-four hour – time proportional composite hospital effluent samples (integration of 144 × 50-mL subsamples collected every 10 min) were taken daily, over the course of one week from one large hospital in Barcelona, Spain. A detailed description of hospital effluent samples can be found in Negreira et al. (Negreira et al., 2014). After collection, each sample was transported under chilled conditions to the laboratory and the pH of the samples was measured (8.65–8.90).

Extraction and LC-HRMS method were adopted from a 4-cartridge method (Oasis HLB, Bond Elut PPL, Oasis MAX and MCX) reported in Zonja et al (Zonja et al., 2015). with minor adjustments for hospital effluents. Samples were spiked with 300 ng of internal standard (LMG- $^{13}C_3$) and adjusted to pH 6.5–6.8. Sample (100 mL) was enriched using solid-phase extraction (SPE). After elution, extracts were dissolved in 400 μL of the initial mobile phase conditions (acetonitrile/water – 3:97). 20 μL of the final extract were injected into the UPLC-QExactive-MS and LC-HRMS method was the same as used for suspect screening in Zonja et al. (Zonja et al., 2016).

3. Results and discussion

3.1. Transformation kinetics and mass balance of LMG-N2-G in UPwater

Based on previous findings where LMG-N2-G was transformed at high basic pH (Sinz and Remmel, 1991), the stability of the LMG-N2-G was initially tested in pure water in the pH range of 4–9, thus covering environmentally relevant pH range. As shown in Fig. SI-2, over the course of 42 h, LMG-N2-G was stable at pH 4–6 (in accordance with results of Sinz and Remmel (Sinz and Remmel, 1991)), while very minor degradation is observed at pH 7. A fast degradation occurred at pH 8 ($t_{1/2}$ = 56.4 h, R = 0.9503) and was faster at pH 9, with a degradation half-life of 18.0 h (R = 0.9946). As a result of peak deconvolution and extraction using SIEVE, three novel LMG-N2-G related peaks were detected. Two of them had a molecular ion of m/z 433.0308 (TP-433-1 – RT 1.48 and TP433-2 - RT 1.67 min) while the third peak detected had m/z 450.0560 (TP450 – RT 1.12 min). LMG as the product of potential hydrolysis of the glycosidic bond was not detected in any of the samples. In Fig. 1, the formation of the detected compounds at pH 8 and pH 9 is plotted (normalized to the initial concentration of the LMG-N2-G) against degradation time and using LMG-N2-G as a reference standard for the quantification of the novel TPs (Fig. 1). The disappearance of LMG-N2-G is attributed to its transformation to one predominant TP (calculated with the semi-quantitative approach), TP433-2 (RT 1.67 min). At pH 9, the TP433-2 reached 43% of initial LMG-N2-G concentration. The other two compounds, TP433-1 and TP450 after 27 h (shown in Fig. 1A) reached 2 and 0.2%, respectively. As for the degradation of LMG-N2-G at pH 8 (Fig. 1B), after 27 h the concentration of LMG-N2-G-TP433-2 reached 17% of the initial LMG-N2-G concentration while LMG-N2-G-TP433-1 built

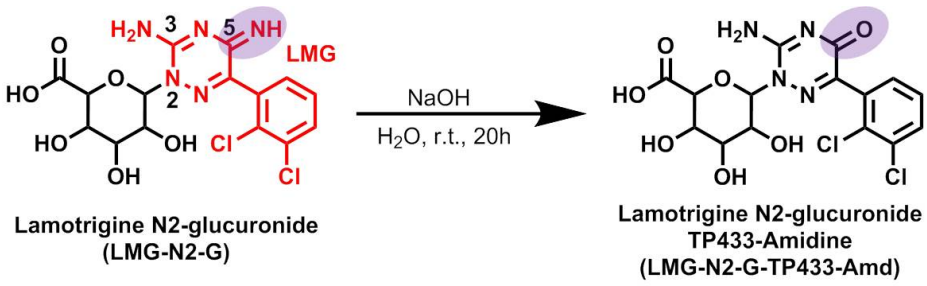

Scheme 1. Synthesis of LMG-N2-G-TP433-Amd from LMG-N2-G.

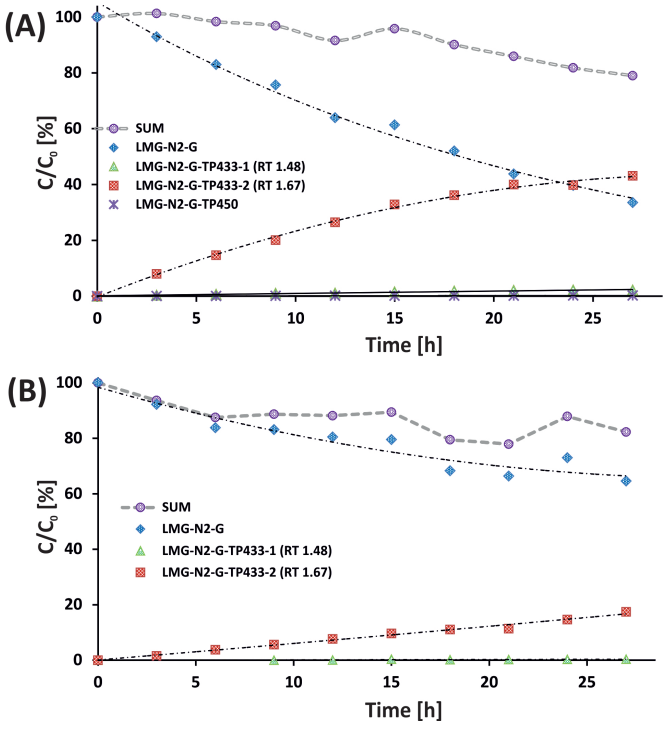

Fig. 1. Degradation profiles of LMG-N2-G in molar concentrations for degradation study of 200 nM of LMG-N2-G in ultra-pure water at A) pH 9 and B) pH 8.

up to 0.3%. The third TP, TP450, was not detected in the samples adjusted to pH 8.

Since none of these TPs could be purchased as standards, TP433-2 was synthetized as described in the experimental section. For the synthesis, strong basic conditions were used (0.1 M NaOH). After 20 h, less than 0.1% of LMG-N2-G was detected. Likewise, TPs 433-1 and TP450 were not detected. Since the peak deconvolution of the chromatograms (in both positive and negative ionization mode) of the synthesis product (using SIEVE, Thermo Scientific) did not reveal formation of any other TP, the conversion of LMG-N2-G to LMG-N2-G-TP433-2 was deemed quantitative and therefore the product was used as a standard.

3.2. Identification of TPs by HRMS

Detailed information of fragmentation experiments can be found in supporting information section on fragmentation.

For the identification of the transformation products, the (+) ESI MS^2 and in-source fragmentation followed by MS^2 (pseudo-MS^3 - pMS^3) product ion spectra of the parent compounds LMG-N2-G and TPs were recorded to determine plausible elemental compositions and the most likely structures of the fragment ions (see Table SI-8 for elemental compositions and Figs. SI-4 for the fragmentation pathways and spectra).

A summary of the detected abiotic transformations of LMG-N2-G and the nomenclature of the formed TPs are presented in Fig. 2. The fragmentation patterns are shown in Fig. 3. The fragments in Fig. 3 are labeled with theoretical masses for easier comparison between different compounds. Measured masses with the associated error can be found in Table SI-8 and Figs. SI-4.

The fragmentation pattern of parent LMG-N2-G (Fig. 3A and Fig. SI-4.1) has been reported previously (Ferrer and Thurman, 2010; Zonja et al., 2016). In brief, under positive ESI ionization LMG-N2-G readily loses the glucuronide moiety in the ion source to form LMG fragment ion (m/z 256.0151), a characteristic feature of many glucuronides (Yan et al., 2003). Expectedly, this fragment ion is also the most abundant one in the MS^2 spectrum of LMG-N2-G (at normalized collision energy (NCE) of 20 ± 50%) and it is practically the only fragment observed. At higher collision energies, more fragments are detected as a result of further fragmentation of the LMG fragment (m/z 256.0151) (Ferrer and Thurman, 2010; Zonja et al., 2016). A principal abiotic TP of LMG-N2-G was detected with the m/z 433.0312 and RT 1.67 min, together with another isobaric compound, which eluted earlier (RT 1.48 min). They both showed that the M + H mass (at NCE 20± 50%) favorably fragmented to only one fragment with the m/z 256.9991, which suggests that the initial molecule underwent modification on the phenyltriazine part of the molecule rather than the glucuronide moiety. If glucuronide modification had taken place, it would have been possible to detect the fragment m/z 256.0151 (the LMG moiety). However, fragment seen in the MS^2 spectra of the TPs433 (m/z 256.9991) defers from the mass of LMG by 0.9840 Da which indicated that one nitrogen was exchanged by oxygen. This suggested that the TPs formed were the result of amidine (LMG-N2-G TP433-Amd) and guanidine (LMG-N2-G TP433-Amd) hydrolysis of the 1,2,4-triazine ring (Fig. 2). In order to identify the above TP433 structures, a pMS^3 of the fragment m/z 256.9991 was studied together with the MS^2 and pMS^3 of a compound 5-desamino-5-oxo-2,5-dihydro lamotrigine (OXO-LMG). This was possible since OXO-LMG; an amidine-hydrolysis derivative, is a commercially available standard and a synthetic impurity of LMG. OXO-LMG (Fig. 3B and SI-4.3) fragments with the series of cleavages from the 1,2,4-triazine ring, while the dichlorophenyl moiety undergoes gradual dechlorination until the complete cleavage of the 1,2,4-triazine ring. The OXO-LMG initially fragments to its most abundant fragment m/z 229.0042 ($C_8H_7Cl_2N_4^+$), which is the result of the net loss of carbonyl (- 27.9949 − CO). The pMS^3 spectrum of this fragment (m/z 229.0042) shows subsequent loss of ammonia (- 17.0265, NH_3) to form m/z 211.9777, a step which precedes a gradual deamination and, in parallel, the triazine ring reduction ($C_8H_4Cl_2N_3^+$, $C_7H_5Cl_2N_2^+$, $C_8H_4Cl_2N^+$).

Comparison of MS^2 spectrum of OXO-LMG (m/z 256.9991) with pMS^3 spectra of the fragment ion m/z 256.9991 formed by the two TPs433 detected (Fig. 3D and F) shows that the TP433 at RT 1.67 min matches the OXO-LMG fragmentation pattern (Fig. 3B). This confirmed the OXO-LMG (an amidine hydrolysis derivative) is the building-block of this TP (RT 1.67 min). Hence this compound was named LMG-N2-G-TP433-Amd (Fig. 2.). The structure of the other TP-433 detected (RT 1.48) was inferred by method of elimination and was named LMG-N2-G-TP433-Gnd (Fig. 2.). This structure was further rationalized analyzing the pMS^3 spectra of its main fragment m/z 256.9991 which showed not only different intensity distribution but also different fragments. Two diagnostic fragments were identified in the spectrum. The first one, with m/z 221.0225 ($C_9H_6ClN_4O^+$), is the result of the loss of hydrochloric acid (- 35.9766) followed by ring closure via the amine at position **5**. The formation of this fragment was also reported in the fragmentation of LMG (Zonja et al., 2016). However, in OXO-LMG its formation is inhibited as a result of the replacement of the amino group by an oxygen atom; hence, only a radical dechlorination is seen (m/z 194.0354; $C_8H_7ClN_4^{\cdot+}$) (Fig. SI-4.2-B). The second diagnostic fragment 229.9882 ($C_8H_6Cl_2N_3O^+$) has a counterpart in the MS^2 of OXO-LMG (m/z 229.0042; $C_8H_7Cl_2N_4^+$). While the OXO-LMG loses carbonyl from position **5**, LMG-N2-G-TP433-Gnd fragment loses methylamine from the same position of the 1,2,4-triazine moiety, forming the m/z 229.9882. Unlike the fragment ion of OXO-LMG at m/z 229.0042, this fragment had retained the oxygen in its structure (not the nitrogen), which explains the mass difference of 0.984 Da between the two fragments.

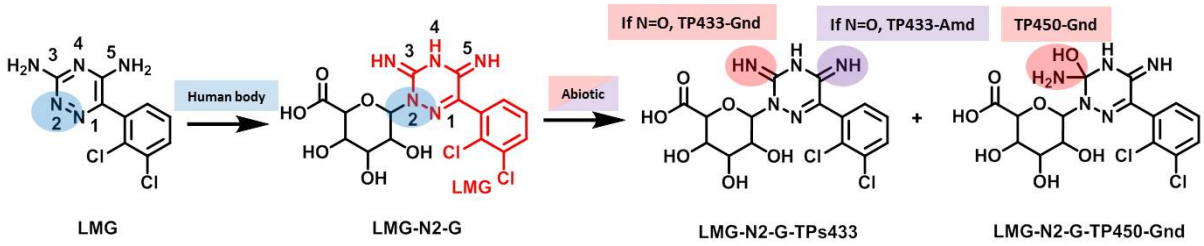

Fig. 2. LMG metabolism in the human body by UDP-glucuronosyltransferase to LMG-N2-G and three LMG-N2-G TPs as a result of amidine (LMG-N2-G-TP433-Amd) and guanidine hydrolysis (LMG-N2-G-TP433-Gnd and LMG-N2-G-TP450-Gnd).

Finally, a third TP was detected with m/z 450.0578 and RT 1.12 min. This m/z defers by one hydroxyl group (+17.0266; OH) from LMG-N2-G-TPs433. The MS^2 (Fig. 3-G) of m/z 450.0578 showed that this compound breaks principally to m/z 433.0312 (loss of ammonia), m/z 407.0520 (loss of CHNO from position 3 of the triazine ring) and m/z 256.9991 (loss of the glucuronide moiety and ammonia). These fragment ions suggest the hydroxylation of the amidine or the guanidine moieties, which would make them a stable reaction intermediate in the process of amidine or guanidine hydrolysis. In order to unambiguously assign the structure of TP450, the pMS^3 of m/z 256.9991 was studied, since the pMS^3 of m/z 433.0312 principally produced the ion at m/z 256.9991, a fragment that could be either amidine or the guanidine derivative (Fig. SI-4.4). From the Fig. 3-H, it can be seen that the m/z 256.9991 fragments identically as the fragment with the same m/z in LMG-N2-G-TP433-Gnd spectrum (Fig. 3-F). This would confirm that this is an intermediate in the formation of LMG-N2-G-TP433-Gnd and was named LMG-N2-G-TP450-Gnd.

3.3. Transformation kinetics of lamotrigine-N2 glucuronide in wastewater

In order to examine the kinetics of the LMG-N2-G degradation, another set of pH-based experiments was performed (at pH 6.5, 7, 8, 8.5 and 9) over the course of 36 h in hospital effluent (HOSeff), wastewater influent (WWinf) and effluent (WWeff) at LMG-N2-G concentrations of 20 and 200 nM. For a detailed list of all the experiments performed, please refer to Table SI-1. Since the internal standard (LMG-$^{13}C_3$) was added to the solution at the beginning of the experiment, its chemical stability was tested in HOSww and WWinf at pHs 8 and 9. As can be seen in Fig. SI-5, no degradation was observed. The results of the degradation of LMG-N2-G at pH 9 are shown in Fig. 4 (refer to Fig. SI-7, SI-8, SI-10 and SI-11 for the graphs obtained at other pH values). The degradation of LMG-N2-G in all three waste matrices as well as in pure water followed pseudo-first order kinetics (Fig. 4). As shown below (Section 3.4.), the disappearance of LMG-N2-G is mainly caused by transformation. In all wastewater matrices spiked with LMG-N2-G at a concentration of 200 nM, its half-life was calculated to be between 12.3 and 19.6 h ($R^2_{200nM,wastewater-pH9}$ = 0.985–0.998); in pure water the degradation proceeded at a similar rate ($t_{1/2}$ = 18 h). The degradation of LMG-N2-G in HOSeff and WWinf at a concentration of 20 nM is shown in Fig. 5 and SI-16 indicating concentration-independent degradation rate constants (half-lives ranging from 15.1 to 17.1 h). At a concentration of 200 nM, the degradation was slower at pH 8.5 as compared to that at pH 9 ((30.1–54.1 h vs 12.3–19.6); Fig. SI-15)). At pH 8 (Fig. SI-7) the degradation rate was lower than at pH 8.5 and 9, evidenced in lower degradation constants which were in range of 0.007–0.011 h^{-1} ($R^2_{200nM-wastewater-pH8}$ = 0.828–0.920). However, the slope of the regression line for the degradation of LMG-N2-G at pH 8 in hospital effluent was not significantly different from zero ($R^2_{HOS-pH8}$ = 0.3959). At pH 8 and concentration of 20 mM (Fig. SI-16), the degradation rate were between 0.016 and 0.022 ($R^2_{20nM-wastewater-pH8}$ = 0.735–0.909). At pH 7 there was practically no noticeable decrease in the concentration of LMG-N2-G in all three matrices and again the slope of the regression line for all three matrices were not significantly different from zero ($R^2_{200nM-wastewater-pH7}$ = 0.032–0.545). Like in the UPwater experiments, in all samples collected from the degradation experiments the biotic TPs of LMG-N2-G were monitored as reported in Zonja et al. (Zonja et al., 2016), but none of them was detected over the course of the incubation time of 36 h. Moreover, no differences in degradation rates of LMG-N2-G (200 nM, pH 8.5) were observed irrespective of the pore size (0.7 vs. 0.2 μm) of the filters used for filtering different wastewater sample before degradation (Fig. SI-11). On the other hand, while the concentration of LMG-N2-G in the experiment at pH 8.5 (filtered through 0.2 μm) decreases, there is no degradation in the experiment at pH 6.5 with the same sample filtered through 0.7 μm (Fig. SI-10 and SI-15). This proves the pH to be the relevant parameter governing the transformation of LMG-N2-G.

3.4. Mass balance in wastewater

At pH 9, the initial LMG-N2-G concentration of 200 nM decreased by 75–88% in wastewater, over the course of 36 h (Fig. 5A and C). At concentration of 20 nM, LMG-N2-G decreased by 77–78% (Fig. 5B and D). The decrease of the LMG-N2-G at both concentrations resulted in the formation of TP433-Amd. TP433-Amd in 200 nM experiment was formed up to 73% in WWinf (Figs. 5 and 6). In the same experiments, LMG-N2-G-TP433-Gnd formed up to 2.6% in WWeff. In 20 nM experiments, TP433-Amd was formed up to 66%, but the TP433-Gnd was not detected most likely due to very low initial concentration of LMG-N2-G. Mass balances plotted in Fig. 5 indicate an almost quantitative transformation to TP433-Amd (mass balance closed between 81 and 93%) and, to a much lesser extent to TP433-Gnd for the 200 nM experiments. TP450-Gnd was also detected at trace levels in the experiments at pH 9 (0.1–0.5% of initial LMG-N2-G concentration). Lowering the pH of the spiked matrices to 8 and 7 reduced the formation rates of LMG-N2-G-TP433-Amd and LMG-N2-G-TP433-Gnd (Fig. 6, SI-7). The mass balances at the end of the incubation time (pH 8) were between 90 and 108%. In wastewater adjusted to pH 7, the transformation rate of LMG-N2-G (Fig. SI-8) was slower and resulted in the formation of LMG-N2-G-TP433-Amd of up to 10% with the mass balance at the end of the 36 h closed between 90% and 101%.

Fig. 6 shows the formation rate of TP433-Amd in wastewater and the three pHs. During the 36 h period of incubation, formation of TP433-Amd at pH 9 was exponential, while at pH 8 and pH 7 the formation was less pronounce (in accordance with the disappearance rate of LMG-N2-G shown in Fig. SI-6). The pKa of the amidine = NH conjugated acid in C5-imino tautomer of LMG-N2-G

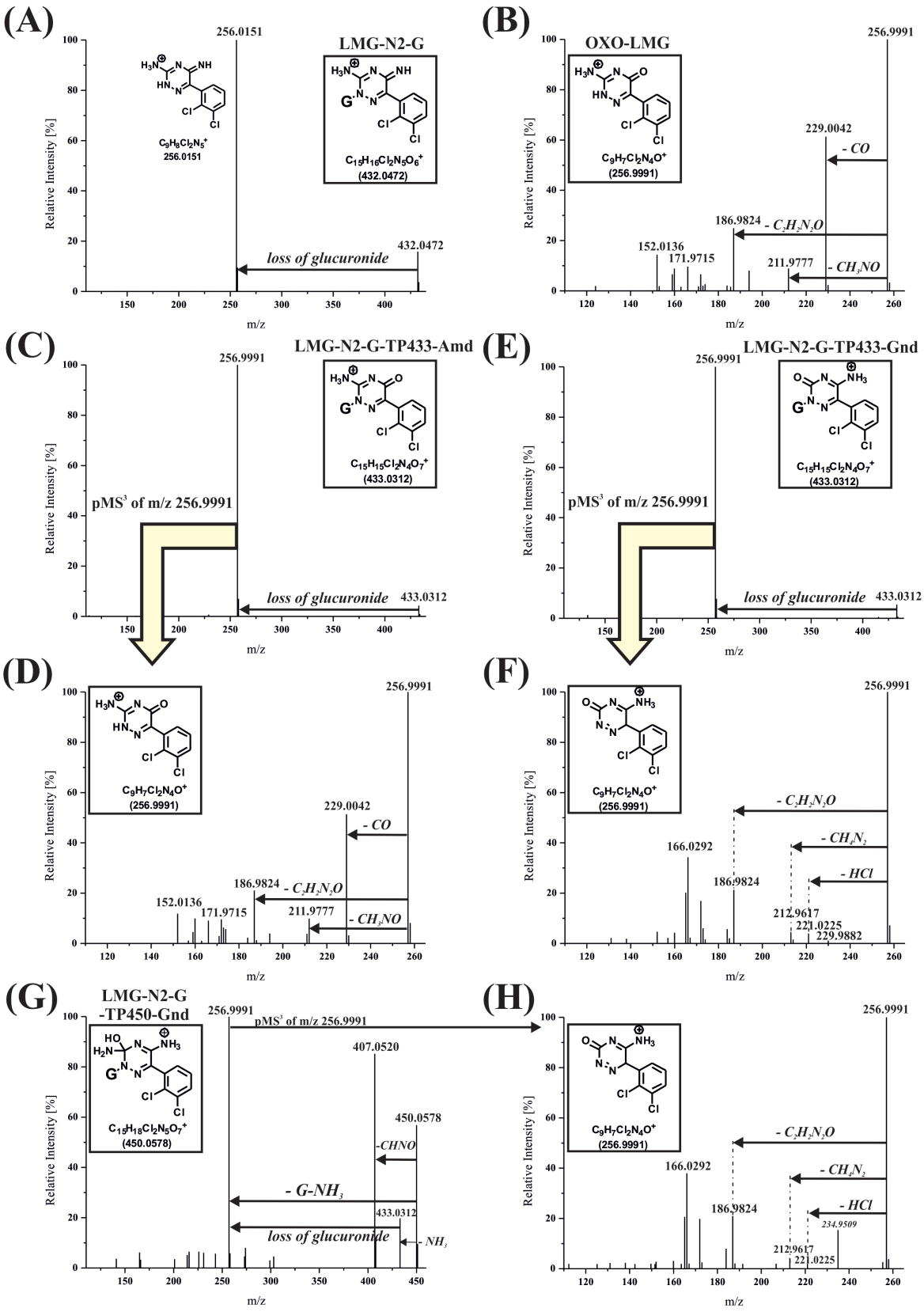

Fig. 3. Fragmentation of: (A) LMG-N2-G at NCE 20 ± 50%, (B) OXO-LMG at NCE 40 ± 50%, (C) LMG-N2-G-TP433-Amd at NCE 20 ± 50%, (D) pMS^3 of LMG-N2-G-TP433-Amd fragment with m/z 256.9991 at NCE 40 ± 50%, (E) LMG-N2-G-TP433-Gnd at NCE 20 ± 50%, (F) pMS^3 of LMG-N2-G-TP433-Gnd fragment with m/z 256.9991, at NCE 40 ± 50%, (G) LMG-N2-G-TP450-Gnd at NCE 20 ± 50%, (H) pMS^3 of LMG-N2-G-TP450-Gnd fragment with m/z 256.9991 at NCE 40 ± 50%.

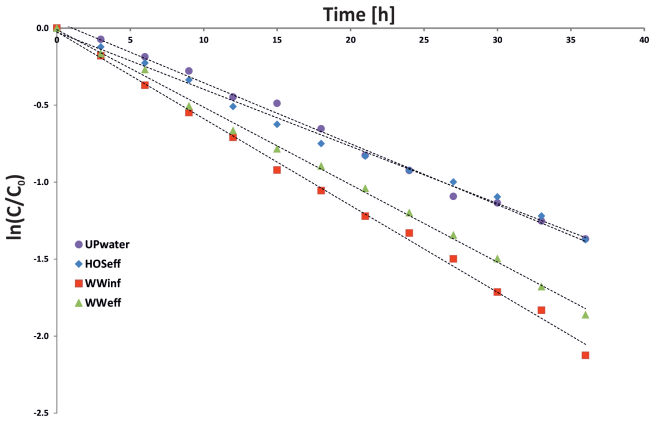

Fig. 4. Degradation of LMG-N2-G at 200 nM and pH9 in hospital effluent, WWTP wastewater and UPwater.

was calculated to be −1.11 (Marvin, 2013, ChemAxon). This indicates that the amidine = NH is present in its neutral form across the pH range tested (4–9). Having this in mind, it is likely that the variation in OH- concentration with the pH is capital for the observed reaction kinetics. The formation rate of TP-433-Amd in wastewater samples was similar at both pH 8 and 7, but was quite different at pH 9. In HOSeff, 50% formation of TP433-Amd took place after approximately 27 h, while in WWinf the TP433-Amd reached 50% formation after 18 h. In WWeff, a 50% formation was reached after 21 h. In hospital effluents, the presence of excess chlorine could result in formation of a transient N chloroimine, arising from reaction of the major imine tautomer with hypochlorite (Volmajer et al., 2003). Assuming that the resonance electron donating effect of the chlorine ion pairs in the N chloroimine, they could cause lower hydrolysis rates. In our case, initial experiments with 25 times molar excess of free chlorine showed that it had an inhibitory effect on the formation of TP433-Amd (Figs. SI-12 and SI-13). However, subsequent experiments with the same free chlorine concentration but lower concentration of LMG-N2-G (20 nM, Fig. SI-16) and free chlorine experiments in HOSeff and WWinf at pH 8.5 and 200 nM concentration (Figs. SI-14 and SI-15) showed that it had little to no effect on the degradation of LMG-N2-G. Further discussion and results can be found in SI section: *Chlorination of LMG-N2-G.*

3.5. Amidine/guanidine hydrolysis reactions and dependence on N2 substituent

The hydrolysis of imines, amidines and guanidines is a common transformation process in (environmental) chemistry under both abiotic and biotic conditions. The metabolic conversion of the guanidine moiety of arginine to form citrulline by peptidylarganine deaminases (PADs) (György et al., 2006), the biodegradation of metformin to guanylurea (Trautwein and Kummerer, 2011) or the hydrolysis of the imine TP, resulting from oxidation of sertraline (Shen et al., 2011), to the corresponding ketone are illustrative examples. On the other hand, it is also known that the rate of hydrolysis of the carbon-nitrogen double bond strongly depends on the pH, since either acidic or basic conditions are required for efficient transformations to the corresponding carbonyl group (Lewis and Wolfenden, 2014).

In order to test the influence of the nitrogen N2-substituents in the 1,2,4-triazine ring, three LMG-N2-G analogues were also degraded at different pHs (Table SI-1); LMG (N2-H), N2-methyl-LMG (N2-CH_3) and LMG-N2-oxide ($^{+}$N2-O^{-}). *Detailed information on LMG hydrolysis* (Figs. SI-1), *N2-Me-LMG* (Figs. SI-18 – SI-26) *and LMG-N2-oxide* (Figs. SI-27 *and* SI-28) *can be found in the Supporting Information.*

Although there are three possible amino-imino tautomeric

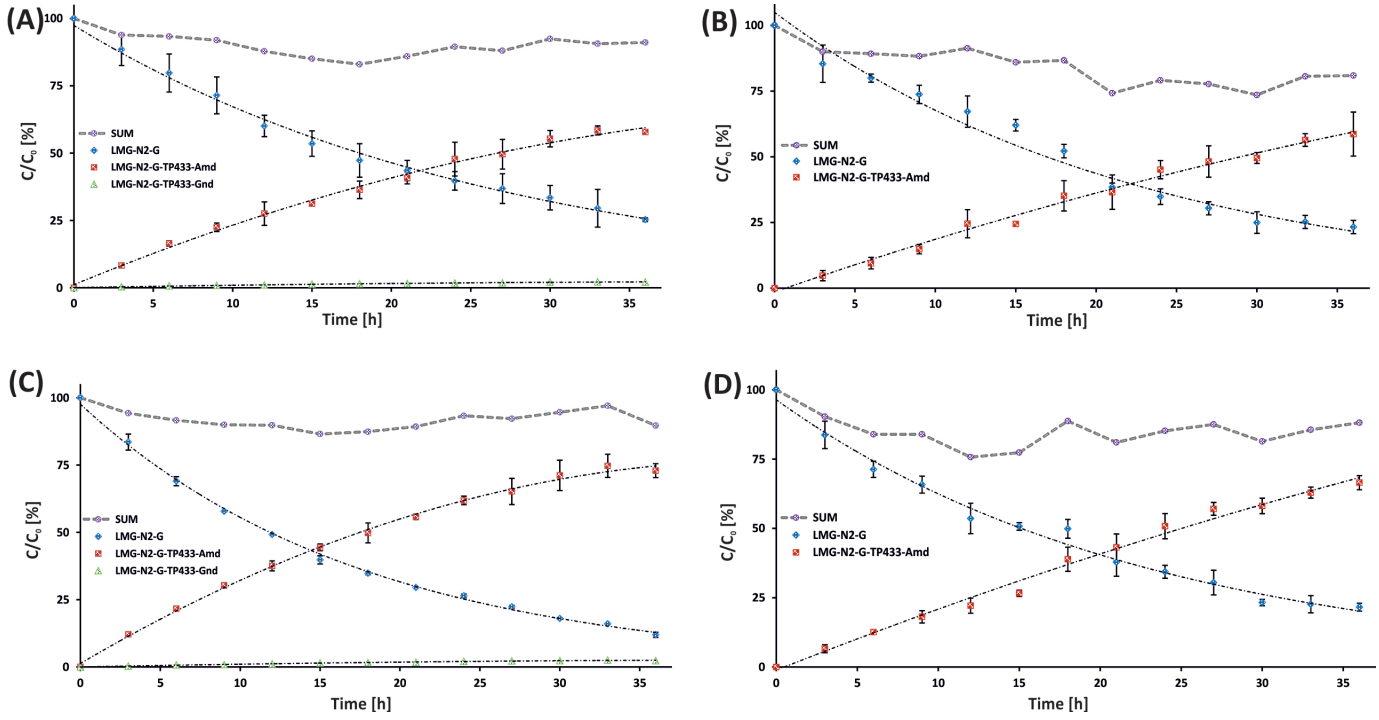

Fig. 5. Mass balance based on molar concentrations of LMG-N2-G at pH 9: (A)200 nM in hospital effluent, (B)20 nM in hospital effluent, (C)200 nM in WWTP influent and (D)20 nM in WWTP influent.

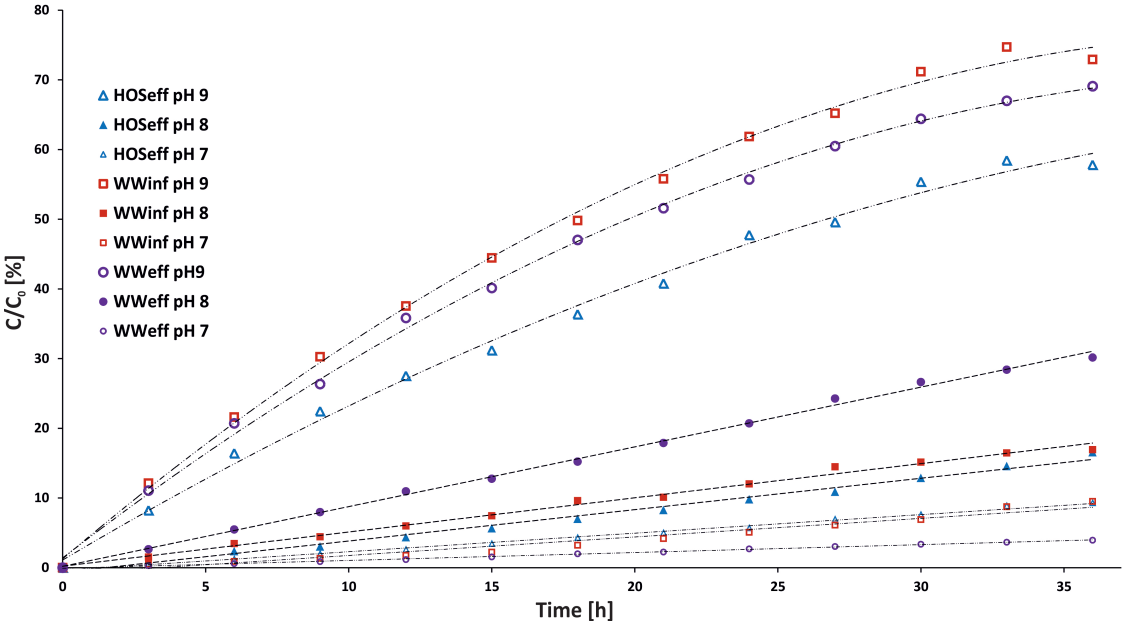

Fig. 6. Formation of LMG-N2-G-TP433-Amd in hospital effluent (HOSeff), WW influent (WWinf) and WW effluent (WWeff) at three different pHs (7, 8 and 9). Calculations were performed based on molar concentrations and normalized to initial concentration (200 nM) of LMG- N2-G.

equilibria in the LMG structure, none of the resulting imino tautomers appears favored over the highly stable aromatic diaminotriazine structure (Alkorta et al., 2014; Testa and Krämer, 2008). This can explain why no OXO-LMG TPs, resulting from imine hydrolysis, have been observed in our experiments (Figs. SI-1 and SI-30). The same holds true for the corresponding LMG-N2-oxide, which was unreactive at the studied pH range of 4–9 (Fig. SI-27 and SI-30). However, a different tautomeric equilibrium seems to be present in N2-Me-LMG and LMG-N2-G (Fig. SI-29). In both cases, the C5-imino tautomers are the major ones, as evidenced by their hydrolysis, albeit at different rates, to the corresponding C5-(OXO)-LMG TPs at pH 9 (amidine hydrolysis, see Scheme 2). The quinonimine-like nature of the above C5-imino tautomers can account for their higher stability in comparison with the alternative C3-imino tautomers, which ultimately lead to the C3-(OXO)-LMG TPs as minor products (guanidine hydrolysis, see Scheme 2). This would confirm that LMG-N2-G is, in fact, a tertiary *N*-glucuronide (a deprotonated version of a quaternary *N*-glucuronide (Testa and Krämer, 2008)) with the prevalent C5-imino tautomer. Interestingly, the detected LMG-N2-G-TP450-Gnd (see Fig. 3 and Scheme 2) and N2-Me-LMG-TP288-Gnd (Fig. SI-22.2) are in agreement with the corresponding tetrahedral intermediates arising from hydroxide addition to the C3-imino tautomer in what seems to be the slow step of the overall transformation leading to the minor C3-(OXO)-LMG TPs. By contrast, the equivalent tetrahedral adducts resulting from hydroxide addition to the C5-imino tautomers have not been detected.

3.6. Hospital effluent analysis and environmental impact

Hospital effluent samples were screened for LMG-N2-G and its abiotic TPs. The results of the screening can be found in Fig. 7 and SI-17 and method parameters in Table SI-10. LMG-N2-G was detected in every sample with the median concentration 389 ngL^{-1} (range 155–1741 ng L^{-1}) and the LMG-N2-G-TP433-Amd was detected in every sample and with the median concentration of 134 ngL^{-1} (range 5.4–357 ng L^{-1}). The second abiotic TP, LMG-N2-G-TP433-Gnd was detected in only two samples with low ngL^{-1} concentrations of 17 and 5.4. Similar levels of concentrations as the LMG-N2-G-TP433-Amd have been found for LMG, with the median concentration of 128 ngL^{-1} (range 13–260 ng L^{-1}) The presence of LMG in the hospital effluent can be linked to both excretion via human metabolism (approximately 15% of LMG is excreted unchanged) and to the presence of enzymes like *β-glucuronidase*, which can cause LMG-N2-G to deconjugate and form LMG. Indication of biotic/enzymatic activity is also revealed by the presence of OXO-LMG, a biotic metabolite of LMG-N2-G found to form in WWTPs (Zonja et al., 2016). This biotic TP was found at concentrations about 10 times lower than those of LMG-N2-G-TP433-Amd and LMG, with the median concentration of 13 ngL^{-1} (range 2.2–75 ng L^{-1}).

Keeping in mind that LMG-N2-G forms LMG-N2-G-TPs433 under neutral-basic pH, the pH range of the samples (8.65–8.90), and the fact that the samples were collected over 24 h, further hydrolysis of LMG-N2-G to form TPs433 in the autosampler is likely. This is supported by the fact that the TPs433 haven't been reported as human metabolites of LMG (Ohman et al., 2008; Saracino et al., 2007). However, they do add information about the total LMG-N2-G load to the wastewater and both concentrations (LMG-N2-G and TP-433-Amd) should be taken into account especially with integrated sampling in order to disregard possible underestimation of the LMG-N2-G concentration due to hydrolysis.

In Zonja et al.(Zonja et al., 2016), we reported the degradation of LMG-N2-G in activated sludge at pH 7. Over the course of 8 h, LMG-N2-G degraded by approximately 90%. This was followed by the appearance of up to 5% of OXO-LMG while LMG-N2-G-TP433-Amd was not detected. This was most likely due to the low formation rate of TP433-Amd at pH 7 (Fig. 6) and the hydrolysis of TP433-Amd to OXO-LMG (Zonja et al., 2016). The hydrolysis rate of TP433-Amd could be similar to the hydrolysis rate of LMG-N2-G to form LMG (LMG-N2-G transformation rate constant (k_{biol}) was calculated to be 0.3 L g_{ss}^{-1} h^{-1} for an initial LMG-N2-G concentration of 5 μg L^{-1}). Here, at pH 7, TP433-Amd was formed approximately up to 1% after 8 h for the initial concentration of 200 nM of LMG-N2-G. For a similar initial concentration of LMG-N2-G (12 nM in biotic experiments and 20 nM in abiotic experiments), the calculated half-life of

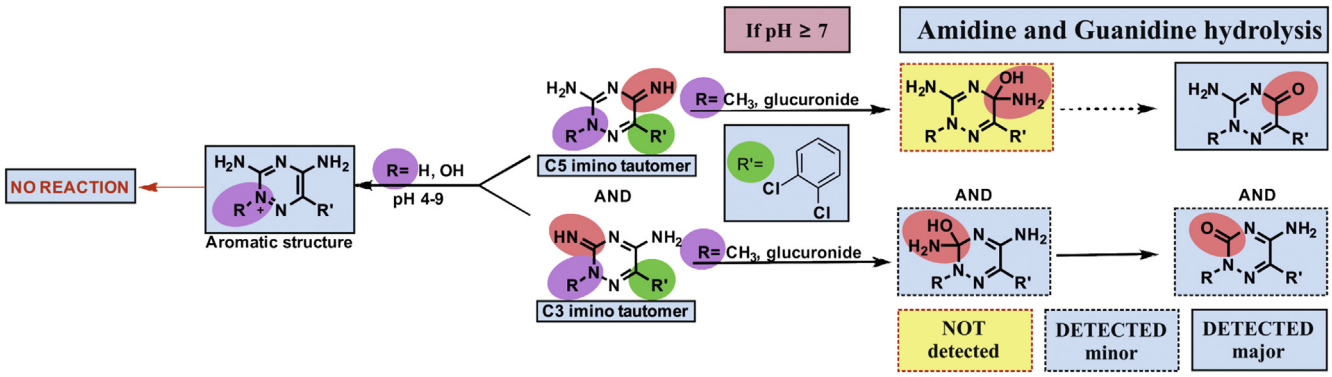

Scheme 2. Summary of abiotic reactions of LMG-N2-G and related compounds that occur in the pH range 4–9.

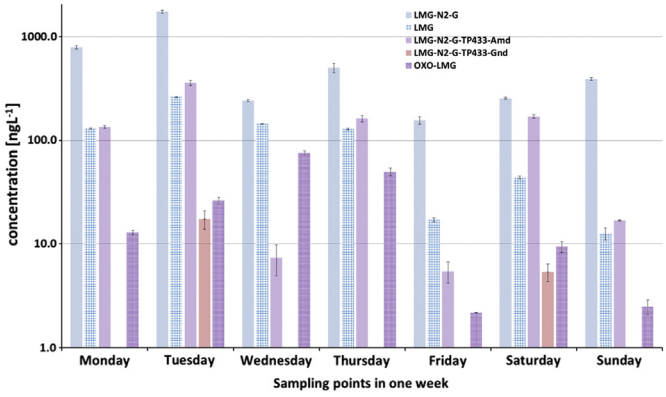

Fig. 7. Concentrations of LMG-N2-G and its abiotic TPs LMG-N2-G-TP433-Amd and -Gnd, and biotic TP – OXO-LMG in 24 h composite hospital effluents monitored over the course of one week.

LMG-N2-G in biotic reactors was much shorter than, for example, that of the abiotic degradation in wastewater at pH 9 (2.8 ± 0.8 h vs. 16.0 ± 1.0 h). Considering these results, both abiotic and biotic reaction pathways can be expected to compete in the degradation/transformation of LMG-N2-G in the environment. However, in abiotic experiments at lower pH, the differences in degradation rates are even more pronounced. This suggests that in WWTPs the LMG-N2-G degradation would preferentially proceed through a biotic pathway. On the other hand, in surface water samples, both abiotic and biotic pathways could occur. The rate of biotic degradation will depend on the concentration of biomass while the abiotic route is largely dependent on the pH of the surface water. Likewise, a combination of the two processes (abiotic and biotic) could additionally yield OXO-LMG (Zonja et al., 2016).

4. Conclusions

In this paper, the reaction pathways of LMG-N2-G under different pHs (pH 4–9) were investigated in both UPwater and environmental samples (HOSeff, WWinf, WWeff – for pH 6.5–9). In addition, related compounds to LMG-N2-G; LMG, N2-Me-LMG and LMG-N2-oxide, with different substituents on the N2, were also investigated for amidine/guanidine hydrolysis reactions. From the results obtained, the following conclusions were drawn:

* LMG-N2-G was degraded under environmentally relevant neutral-basic conditions (pH 7- pH 9) and it was completely stable under acidic pH. At basic pH, LMG-N2-G was transformed primarily, via amidine hydrolysis, into LMG-N2-G-TP433-Amd with two minor TPs related to guanidine hydrolysis (LMG-N2-G-TP433-Gnd and LMG-N2-G-TP450-Gnd).
* Degradation at different pH and in different matrices (HOSeff, WWinf, WWeff) showed different kinetics and the reaction rate was increased exponentially at pH 9 with exponential increase of LMG-N2-G-TP433-Amd concentration.
* The structure of LMG-N2-G should be drawn as a deprotonated C5-imino tautomer.
* The amidine/guanidine hydrolysis of LMG and LMG-N2-oxide is not possible since the formation of the imine tautomer is not favored over the highly stable aromatic diaminotriazine tautomer. In contrast, the existence of different tautomeric equilibria in LMG-N2-G and N2-Me-LMG favors imine formation, making possible the hydrolysis of the amidine and guanidine moieties.
* Since LMG is extensively metabolized by glucuronidation in the human body (>85%), high environmental concentrations of LMG could be reduced by increasing the pH of the wastewaters containing LMG-N2-G, forcing the formation of TP433-Amd. However, this would likely yield OXO-LMG by deconjugation in WWTPs.

Acknowledgment

B. Zonja acknowledges the Marie Curie Actions ITN CSI:Environment PITN-GA-2010-264329 for the early-stage researcher contract and funding. S. Perez acknowledges the contract from the Ramon y Cajal Program of the Spanish Ministry of Economy and Competitiveness. This work has been financially supported by the SOLUTIONS project which has received funding from the European Union's Seventh Framework Programme for research, technological development and demonstration under grant agreement no. 60343, Generalitat de Catalunya (Consolidated Research Groups "2014 SGR 418 – Water and Soil Quality Unit" and 2014 SGR 291 – ICRA). R. Chaler and D. Fanjul are acknowledged for the maintenance and help within the Mass spectrometry unit at IDAEA-CSIC. The authors would like to thank J. Lopez for helpful discussion regarding the manuscript and to anonymous reviewers for their valuable comments which helped improve significantly the earlier version of the manuscript.

Appendix A. Supplementary data

Supplementary data related to this article can be found at http://dx.doi.org/10.1016/j.watres.2016.04.072.

References

Alkorta, I., Elguero, J., Font, A., Galcera, J., Mata, I., Molins, E., Virgili, A., 2014. An experimental and theoretical study of the structure of Lamotrigine in its neutral and protonated forms: evidence of Lamotrigine enantiomers. Tetrahedron 70 (17), 2784–2795.

D'Ascenzo, G., Di Corcia, A., Gentili, A., Mancini, R., Mastropasqua, R., Nazzari, M., Samperi, R., 2003. Fate of natural estrogen conjugates in municipal sewage transport and treatment facilities. Sci. Total Environ. 302 (1–3), 199–209.

Di Meo, F., Steel, M., Nicolas, P., Marquet, P., Duroux, J.-L., Trouillas, P., 2013. Acyl-glucuronide in alkaline conditions: migration vs. hydrolysis. J. Mol. Model. 19 (6), 2423–2432.

Ferrer, I., Thurman, E.M., 2010. Identification of a new antidepressant and its glucuronide metabolite in water samples using liquid chromatography/quadrupole time-of-flight mass spectrometry. Anal. Chem. 82 (19), 8161–8168.

Gomes, R.L., Scrimshaw, M.D., Lester, J.N., 2009. Fate of conjugated natural and synthetic steroid estrogens in crude sewage and activated sludge batch studies. Environ. Sci. Technol. 43 (10), 3612–3618.

György, B., Tóth, E., Tarcsa, E., Falus, A., Buzás, E.I., 2006. Citrullination: a post-translational modification in health and disease. Int. J. Biochem. Cell Biol. 38 (10), 1662–1677.

Jelic, A., Rodriguez-Mozaz, S., Barcelo, D., Gutierrez, O., 2015. Impact of in-sewer transformation on 43 pharmaceuticals in a pressurized sewer under anaerobic conditions. Water Res. 68, 98–108.

Johnson, A.C., Williams, R.J., 2004. A model to estimate influent and effluent concentrations of estradiol, estrone, and ethinylestradiol at sewage treatment works. Environ. Sci. Technol. 38 (13), 3649–3658.

Kowalczyk, I., Hawes, E.M., McKay, G., 2000. Stability and enzymatic hydrolysis of quaternary ammonium-linked glucuronide metabolites of drugs with an aliphatic tertiary amine-implications for analysis. J. Pharm. Biomed. Anal. 22 (5), 803–811.

Kumar, V., Johnson, A.C., Nakada, N., Yamashita, N., Tanaka, H., 2012. De-conjugation behavior of conjugated estrogens in the raw sewage, activated sludge and river water. J. Hazard Mater 227–228, 49–54.

Lewis, C.A., Wolfenden, R., 2014. The nonenzymatic decomposition of guanidines and amidines. J. Am. Chem. Soc. 136 (1), 130–136.

Manning, C.O., Wadsworth, A.H., Fellows, I., 2002. Synthesis of stable isotopically labelled versions of Lamotrigine and its methylated metabolite. J. Label. Compd. Radiopharm. 45 (7), 611–618.

Marvin Was Used for Drawing, Displaying and Characterizing Chemical Structures, Substructures and Reactions, Marvin 6.1, 2013. ChemAxon. http://www.chemaxon.com.

Negreira, N., de Alda, M.L., Barceló, D., 2014. Cytostatic drugs and metabolites in municipal and hospital wastewaters in Spain: filtration, occurrence, and environmental risk. Sci. Total Environ. 497, 68–77.

OECD Test No. 111: Hydrolysis as a Function of pH, OECD Publishing.

Ohman, I., Beck, O., Vitols, S., Tomson, T., 2008. Plasma concentrations of lamotrigine and its 2-N-glucuronide metabolite during pregnancy in women with epilepsy. Epilepsia 49 (6), 1075–1080.

Pagliara, A., Carrupt, P.A., Caron, G., Gaillard, P., Testa, B., 1997. Lipophilicity profiles of ampholytes. Chem. Rev. 97 (8), 3385–3400.

Ramsay, R.E., Pellock, J.M., Garnett, W.R., Sanchez, R.M., Valakas, A.M., Wargin, W.A., Lai, A.A., Hubbell, J., Chern, W.H., Allsup, T., Otto, V., 1991. Pharmacokinetics and safety of lamotrigine (Lamictal®) in patients with epilepsy. Epilepsy Res. 10 (2–3), 191–200.

Saracino, M.A., Bugamelli, F., Conti, M., Amore, M., Raggi, M.A., 2007. Rapid HPLC analysis of the antiepileptic lamotrigine and its metabolites in human plasma. J. Sep. Sci. 30 (14), 2249–2255.

Shen, L.Q., Beach, E.S., Xiang, Y., Tshudy, D.J., Khanina, N., Horwitz, C.P., Bier, M.E., Collins, T.J., 2011. Rapid, biomimetic degradation in water of the persistent drug sertraline by TAML catalysts and hydrogen peroxide. Environ. Sci. Technol. 45 (18), 7882–7887.

Sinz, M.W., Remmel, R.P., 1991. Isolation and characterization of a novel quaternary ammonium-linked glucuronide of lamotrigine. Drug Metabol. Dispos. 19 (1), 149–153.

Testa, B., Krämer, S.D., 2008. The biochemistry of drug metabolism – an introduction: part 4. Reactions of conjugation and their enzymes. Chem. Biodivers. 5 (11), 2171–2336.

Trautwein, C., Kummerer, K., 2011. Incomplete aerobic degradation of the antidiabetic drug Metformin and identification of the bacterial dead-end transformation product Guanylurea. Chemosphere 85 (5), 765–773.

Volmajer, J., Toplak, R., Bittner, S., Leban, I., Le Marechal, A.M., 2003. Novel N-chlorinated derivatives of 2H-1-benzopyran-2-imines. Tetrahedron Lett. 44 (11), 2363–2366.

Writer, J.H., Antweiler, R.C., Ferrer, I., Ryan, J.N., Thurman, E.M., 2013a. In-stream attenuation of neuro-active pharmaceuticals and their metabolites. Environ. Sci. Technol. 47 (17), 9781–9790.

Writer, J.H., Ferrer, I., Barber, L.B., Thurman, E.M., 2013b. Widespread occurrence of neuro-active pharmaceuticals and metabolites in 24 Minnesota rivers and wastewaters. Sci. Total Environ. 461–462, 519–527.

Yan, Z., Caldwell, G.W., Jones, W.J., Masucci, J.A., 2003. Cone voltage induced in-source dissociation of glucuronides in electrospray and implications in biological analyses. Rapid Commun. Mass Spectrom. 17 (13), 1433–1442.

Zonja, B., Delgado, A., Perez, S., Barcelo, D., 2015. LC-HRMS suspect screening for detection-based prioritization of iodinated contrast media photodegradates in surface waters. Environ. Sci. Technol. 49 (6), 3464–3472.

Zonja, B., Perez, S., Barcelo, D., 2016. Human metabolite lamotrigine-N(2)-glucuronide is the principal source of lamotrigine-derived compounds in wastewater treatment plants and surface water. Environ. Sci. Technol. 50 (1), 154–164.

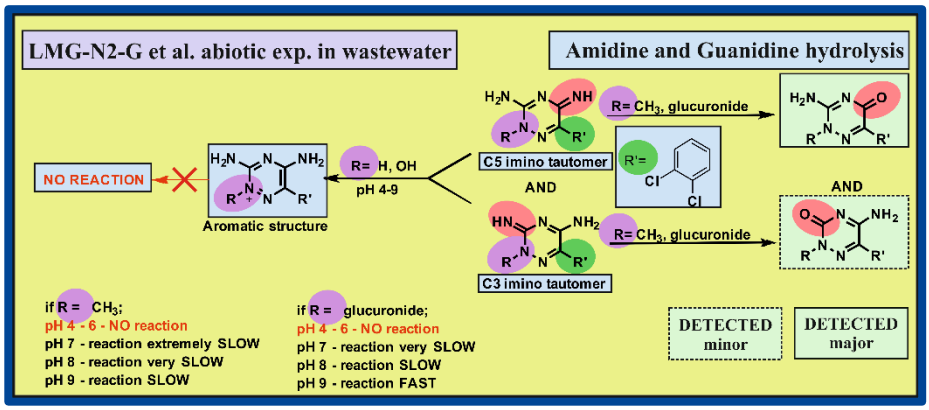

Article Nº4:

Zonja, B., Delgado, A., Abad, J.L., Pérez, S. and Barceló, D.

Abiotic amidine and guanidine hydrolysis of lamotrigine-N2-glucuronide and related compounds in wastewater: The role of pH and N2-substitution on reaction kinetics.

(2016.) Water Res 100, 466-475.

SUPPORTING INFORMATION

Total content: **Figures** – 30, and **Tables** – 12

Supporting information has been reformatted to match the style of the thesis.

Table of Contents

Summaries of the Experiments Performed

Table SI-1. Summary of abiotic experiments performed for LMG-N2-G.

pH	LMG-N2-G						
	Matrix	n	T [h]	k [h^{-1}]	$t_{½}$ [h]	R^2	*Figure*
4	UPW	1	42		No Degradation		*SI-2*
5	UPW	1	42		No Degradation		*SI-2*
6	UPW	1	42		No Degradation		*SI-2*
6.5	HOSeff	3	36		No Degradation		*SI-11, SI-16-A*
	WWinf	3	36		No Degradation		*SI-11, SI-16-B*
7	UPW	1	42	-	-	0.410	*SI-2*
	HOSeff	2	36	-	-	0.228; 0.432	*7, SI-7-A, SI-9-A*
	WWinf	2	36	-	-	0.243; 0.545	*7, SI-7-B, SI-9-B*
	WWeff	2	36	-	-	< 0.1; < 0.1	*7, SI-7-C, SI-9-C*
8	UPW	1	42	0.012	56.4	0.950	*1-A, SI-2*
	HOSeff	2	36	-	-	0.454; 0.536	*7, SI-7-A, SI-8-A*
	WWinf	2	36	0.007; 0.008	106.2; 92.9	0.828; 0.864	*7, SI-7-B, SI-8-B*
	WWeff	2	36	0.011; 0.012	61.6; 59.3	0.887; 0.920	*7, SI-7-C, SI-8-C*
	HOSeff-Cl	3	36	-	-	< 0.1; < 0.1	*SI-14-A*
	$HOSeff_{20}$	3	36	0.017 – 0.022	31.5 – 39.4	0.834 – 0.882	*SI-12, SI-17*
	$WWinf_{20}$	3	36	0.016 – 0.021	33.1 – 43.6	0.735 - 0.909	*SI-12, SI-17*
8.5	HOSeff	3	36	0.013 – 0.015	45.5 – 54.1	0.876 – 0.926	*SI-15-A, SI-16-A*
	HOSeff-Cl	3	36	0.015 – 0.016	42.9 – 46.1	0.921 – 0.958	*SI-15-B, SI-16-A*
	WWinf	3	36	0.021 – 0.023	30.1 – 32.9	0.955 – 0.968	*SI-15-C, SI-16-B*
	WWinf-Cl	3	36	0.021 – 0.023	29.9 – 33.3	0.974 – 0.980	*SI-15-D, SI-16-B*
	HOSeff –1	2	27	0.014; 0.016	50.0; 44.1	0.912; 0.939	*SI-10-A*
	HOSeff –1 (0.2 µm)	2	27	0.015; 0.019	47.6; 37.4	0.944; 0.985	*SI-10-A*
	HOSeff –2	2	27	0.016; 0.017	42.0; 39.8	0.913; 0.972	*SI-10-B*
	HOSeff –2 (0.2 µm)	2	27	0.017; 0.017	39.9; 41.9	0.970; 0.956	*SI-10-B*
	WWinf –1	2	27	0.017; 0.020	40.1; 34.9	0.953; 0.973	*SI-10-C*
	WWinf –1 (0.2 µm)	2	27	0.017; 0.020	39.8; 35.1	0.971; 0.985	*SI-10-C*
	WWinf –2	2	27	0.014; 0.016	48.5; 43.1	0.889; 0.949	*SI-10-D*
	WWinf –2 (0.2 µm)	2	27	0.014; 0.018	50.2; 38.8	0.936; 0.977	*SI-10-D*
9	UPW	1	42	0.040	18.0	0.995	*1-B, SI-2*
	HOSeff	2	36	0.035; 0.039	19.6; 17.7	0.991; 0.985	*5, 6, SI-7-A*
	WWinf	2	36	0.056; 0.056	12.3; 12.3	0.994; 0.998	*5, 6, SI-7-B*
	WWeff	2	36	0.048; 0.052	14.3; 13.2	0.997; 0.994	*5, 6, SI-7-C*
	HOSeff – 12h	3	12	0.037 – 0.045	-	0.985 – 0.991	*SI-13, SI-14-B*
	HOSeff-Cl – 12h	3	12	0.017 – 0.020	-	0.905 – 0.967	*SI-13, SI-14-B*
	$HOSeff_{20}$	3	36	0.042 – 0.046	15.1 – 16.7	0.957 – 0.983	*SI-17-A*
	$WWinf_{20}$	3	36	0.041 – 0.046	15.2 – 17.1	0.971 – 0.993	*SI-17-B*
	$HOSeff_{20}$-Cl	3	36	0.039 – 0.041	16.6 – 17.6	0.943 – 0.967	*SI-17-A*
	$WWinf_{20}$-Cl	3	36	0.041 – 0.043	16.2 – 17.1	0.971 – 0.993	*SI-17-B*

Abbreviations used: **UPW** – ultrapure water; **HOSeff** – hospital effluent; **WWinf** – WWTP influent water; **WWeff** – WWTP effluent water; **HOSeff – Cl** – experiments with 25 x excess of chlorine compared to the compound concentration; **XX_{20}** – experiments performed with the concentration of 20 nM; **0.2 µm** – the samples were additionally filtered with 0.2 µm before degradation; **n** – number of replicates; **T** – total degradation time; **k** – degradation constant calculated from slope (range is given for n= 3, and individual values for n= 2 or 1); **$t_{½}$** - degradation half-life (range is given for n= 3, and individual values for n= 2 or 1); **R^2** - coefficient of determination for linear regression; **Figure** – denotes the name of the figure where the corresponding degradation can be found

Table SI-2. Summary of abiotic experiments performed for LMG.

pH	LMG						
	Matrix	n	T [h]	k [h^{-1}]	$t_{½}$ [h]	R^2	*Figure*
5	UPW	1	42	No Degradation			*SI-1*
7	UPW	1	42	No Degradation			*SI-1*
9	UPW	1	42	No Degradation			*SI-1*

Abbreviations used: **UPW** – ultrapure water; n – number of replicates; **T** – total degradation time; **k** – degradation constant calculated from slope; **$t_{½}$** - degradation half-life; **R^2** - coefficient of determination for linear regression; **Figure** – denotes the name of the figure where the corresponding degradation can be found

Table SI-3. Summary of abiotic experiments performed for LMG-$^{13}C_3$.

pH	LMG-$^{13}C_3$						
	Matrix	n	T [h]	k [h^{-1}]	$t_{½}$ [h]	R^2	*Figure*
8	HOSeff	3	36	No Degradation			*SI-6-A*
	WWinf	3	36	No Degradation			*SI-6-B*
9	HOSeff	3	36	No Degradation			*SI-6-C*
	WWinf	3	36	No Degradation			*SI-6-D*
	HOSeff-Cl	3	36	No Degradation			*SI-6-E*
	WWinf-Cl	3	36	No Degradation			*SI-6-F*

Abbreviations used: **HOSeff** – hospital effluent; **WWinf** – WWTP influent water; **HOSeff – Cl** – experiments with 25 x excess of chlorine compared to the compound concentration; **n** – number of replicates; **T** – total degradation time; **k** – degradation constant calculated from; **$t_{½}$** - degradation half-life; **R^2** - coefficient of determination for linear regression; **Figure** – denotes the name of the figure where the corresponding degradation can be found

Table SI-4. Summary of abiotic experiments performed for LMG-N2-G-TP433-Amd.

pH	LMG-N2-G-TP433-Amd						
	Matrix	n	T [h]	k [h^{-1}]	$t_{½}$ [h]	R^2	*Figure*
4	UPW	1	39	No Degradation			*SI-3*
5	UPW	1	39	No Degradation			*SI-3*
6	UPW	1	39	No Degradation			*SI-3*
7	UPW	1	39	No Degradation			*SI-3*

Abbreviations used: **UPW** – ultrapure water; **n** – number of replicates; **T** – total degradation time; **k** – degradation constant calculated from slope; **$t_{½}$** - degradation half-life; **R^2** - coefficient of determination for linear regression; **Figure** – denotes the name of the figure where the corresponding degradation can be found

Table SI-5. Summary of abiotic experiments performed for N2-Me-LMG.

pH	LMG-N2-G						
	Matrix	n	T [h]	k [h^{-1}]	$t_{½}$ [h]	R^2	*Figure*
4	UPW	1	42	No Degradation			*SI-18*
5	UPW	1	42	No Degradation			*SI-18*
6	UPW	1	42	No Degradation			*SI-18*
7	UPW	1	42	No apparent decrease in concentration			*SI-18*
	HOSeff	1	36	No apparent decrease in concentration			*SI-23-A, SI-24*
	WWinf	1	36	No apparent decrease in concentration			*SI-23-B, SI-24*
	WWeff	1	36	No apparent decrease in concentration			*SI-23-C, SI-24*
8	UPW	1	42	-	-	0.701	*SI-18*
	HOSeff	1	36	-	-	0.501	*SI-23-A, SI-24*
	WWinf	1	36	-	-	0.385	*SI-23-B, SI-24*
	WWeff	1	36	-	-	< 0.1	*SI-23-C, SI-24*
8.5	HOSeff	3	36	-	-	< 0.1 – 0.339	*SI-26-A*
	HOSeff-Cl	3	36	-	-	< 0.1 – 0.235	*SI-26-B*
	WWinf	3	36	-	-	0.124 – 0.450	*SI-26-C*
	WWinf-Cl	3	36	-	-	0.283 – 0.471	*SI-26-D*
	HOSeff –1	2	27	-	-	0.337; 0.302	*SI-25-A*
	HOSeff –1 (0.2 µm)	2	27	-	-	0.302; 0.337	*SI-25-A*
	HOSeff –2	2	27	-	-	< 0.1; 0.261	*SI-25-B*
	HOSeff –2 (0.2 µm)	2	27	-	-	< 0.1; < 0.1	*SI-25-B*
	WWinf –1	2	27	-	-	< 0.1; < 0.1	*SI-25-C*
	WWinf –1 (0.2 µm)	2	27	-	-	< 0.1; < 0.1	*SI-25-C*
	WWinf –2	2	27	-	-	0.164; 0.323	*SI-25-D*
	WWinf –2 (0.2 µm)	2	27	-	-	< 0.1; < 0.1	*SI-25-D*
9	UPW	1	42	-	-	< 0.1	*SI-19*
	HOSeff	1	36	-	-	0.286	*SI-23-A, SI-24*
	WWinf	1	36	-	-	0.132	*SI-23-B, SI-24*
	WWeff	1	36	-	-	0.145	*SI-23-C, SI-24*

Abbreviations used: **UPW** – ultrapure water; **HOSeff** – hospital effluent; **WWinf** – WWTP influent water; **WWeff** – WWTP effluent water; **HOSeff – Cl** – experiments with 25 x excess of chlorine compared to the compound concentration; **0.2 µm** – the samples were additionally filtered with 0.2 µm before degradation; **n** – number of replicates; **T** – total degradation time; **k** – degradation constant calculated from slope; **$t_{½}$** - degradation half-life; **R^2** - coefficient of determination for linear regression; **Figure** – denotes the name of the figure where the corresponding degradation can be found

Table SI-6. Summary of abiotic experiments performed for N2-Me-LMG-TP271-Amd.

pH	N2-Me-LMG-TP271-Amd						
	Matrix	n	T [h]	k [h^{-1}]	$t_{½}$ [h]	R^2	*Figure*
4	UPW	1	39	No Degradation			*SI-20*
5	UPW	1	39	No Degradation			*SI-20*
6	UPW	1	39	No Degradation			*SI-20*
7	UPW	1	39	No Degradation			*SI-20*

Abbreviations used: **UPW** – ultrapure water; **n** – number of replicates; **T** – total degradation time; **k** – degradation constant calculated from slope; **$t_{½}$** - degradation half-life; **R^2** - coefficient of determination for linear regression; **Figure** – denotes the name of the figure where the corresponding degradation can be found

Table SI-7. Summary of abiotic experiments performed for LMG-N2-oxide.

pH	LMG-N2-oxide						
	Matrix	n	T [h]	k [h^{-1}]	$t_{½}$ [h]	R^2	*Figure*
5	UPW	1	42	No Degradation			*SI-27*
7	UPW	1	42	No Degradation			*SI-27*
9	UPW	1	42	No Degradation			*SI-27*

Abbreviations used: **UPW** – ultrapure water; **n** – number of replicates; **T** – total degradation time; **k** – degradation constant calculated from slope; **$t_{½}$** - degradation half-life; **R^2** - coefficient of determination for linear regression; **Figure** – denotes the name of the figure where the corresponding degradation can be found

I. LAMOTRIGINE (LMG)

pH EXPERIMENTS - degradations in UPW @pH 5, 7 and 9

Figure SI-1. Degradation of 400 nM of LMG in UPW at pH 5, 7 and 9 over the course of 42 hours.

The point on the graph corresponds to the average measurement of the three pHs with the error bars representing deviation.

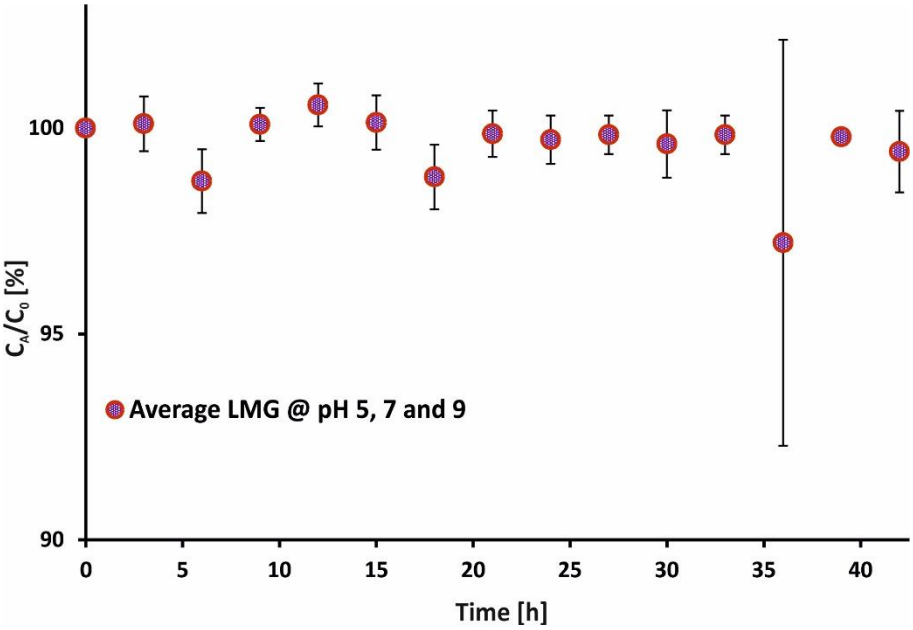

II. LAMOTRIGINE-N2-GLUCURONIDE (LMG-N2-G)

pH EXPERIMENTS - degradations in UPW @pH 4 – 9

Figure SI-2. Degradation of 200 nM of LMG-N2-G in UPW at pH 4 - 9 over the course of 42 hours.

The point on the graph corresponds to the average measurement of the three pHs with the error bars representing deviation.

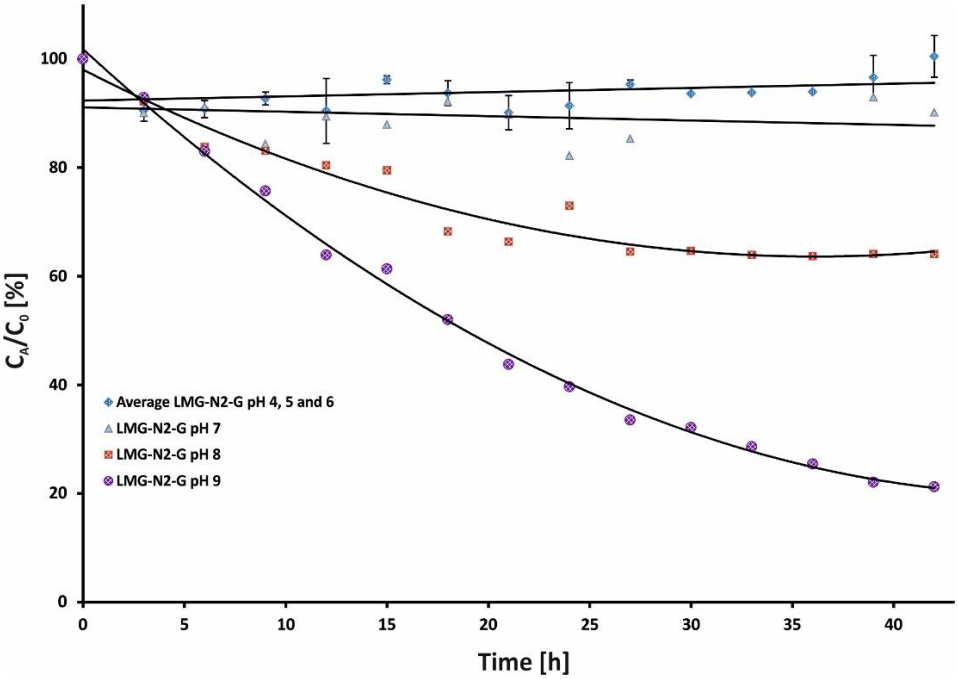

Figure SI-3. Stability of 200 nM of LMG-N2-G-TP433-Amd in UPW at pH 4 - 7 over the course of 39 hours.

The point on the graph corresponds to the average measurement of the three pHs with the error bars representing deviation

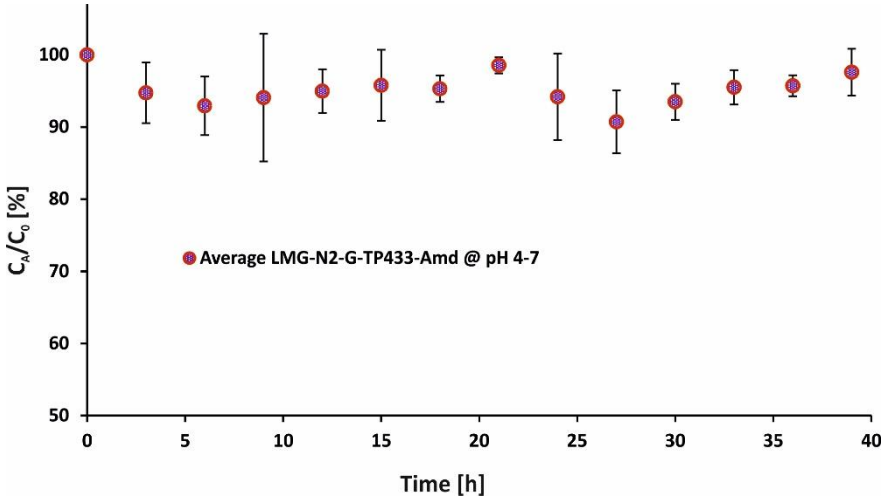

Identification of LMG-N2-G TPs with HRMS

For identification of the parent compounds and their transformation products, the following method was used; Electrospray ionization interface (ESI) was operated in the positive ion mode with the following settings: spray voltage +3.0 kV, heater temperature 250 ºC, and capillary temperature 350 ºC.

For the chromatographic method mobile phases used were: (A) acetonitrile with 0.1 % formic acid and (B) water (0.1 % formic acid). The method had the following gradient: 0 min (10 % A) - 1 min (10 % A) – 6 min (95 % A) - 7 min (95 % A) – 8 min (10 % A) and stabilized until 10 min. Flow rate was 300 µL min^{-1} and the column temperature was held at 40 ºC.

As to HRMS method, a data dependent scan was applied with the following parameters; Full scan and data dependant-MS^2 were set to resolution of 70,000, with the full scan range of depending on the compound identified (general range m/z 100-600). Quadrupole Isolation window was m/z 2 and inclusion list turned on and filled with the list of investigated masses. For pseudo- MS^3 (pMS^3) experiments *In-source ionization* was applied in order to produce the given m/z before breaking the ion in the HCD.

Figure SI-4 (LMG-N2-G and TPs), **SI-22** (N2-Me-LMG and TPs) and **SI-18** (LMG-N2-oxide) show the fragmentation pattern (named for example: Figure SI-4.X-**A**., X = 1 - 4), MS^2 and pMS^3 spectra (named: Figure SI-4.X-**B**., X = 2 - 4).

Fragmentation pattern in **Figure SI-4. X-A**, X= 1-4; **Figure SI-22. X-A**, X= 1-3 and **Figure SI-28. 1-A** is drawn, in general, with **black** and **red** arrows in which the **black** stands that a certain fragment has been seen in a pMS^3 spectrum of its direct predecessor and the **red** arrow states that the fragment was seen in the spectrum of its indirect predecessor. **Red** arrow was used only in cases when it was not possible to do a pMS^3 experiment on a given mass.

Details on a specific MS^2 and pMS^3 performed can be found in the header of each spectrum. Example below is given for OXO-LMG – MS^2 and OXO-LMG – 229 pMS^3.

	Analyzer	Ionization	In-source	Experiment type	Selected mass	NCE	Mass range
OXO – LMG –MS^2	**FTMS**	**p ESI**	**-**	**Full ms2**	**257.00**	**@hcd 35**	**50.00-280.00**
OXO-LMG – 229 pMS^3	**FTMS**	**p ESI**	**sid=45**	**Full ms2**	**229.00**	**@hcd 50**	**50.00-250.00**

NCE (normalized collision energy) used throughout the experiments were 10, 15, 20 and 35. Unless otherwise stated, the NCEs 15 and 20 were used with the ramp of 50%.

Accurate mass measurements of protonated parent compounds and TPs as determined by LC-QExactive-MS in MS/MS or pseudo MS^3 modes for **LMG-N2-G TPs** can be found in **Table SI-8**, for **N2-Me-LMG** in **Table SI-11** and **LMG-N2-oxide** in **Table SI-12.**

Fragmentation pattern of LMG-N2-G shown in **Figure 4.1-A** has been reported previously (Ferrer and Thurman 2010, Zonja et al. 2016b) and was drawn here only to aid comparison of fragmentation between the LMG-N2-G and its abiotic transformation products (LMG-N2-G-TP433-Amd, LMG-N2-G-TP433-Gnd and LMG-N2-G-TP450-Gnd). Original MS^2 and pMS^3 spectra, as well as accurate mass measurements of protonated LMG-N2-G can be found in Zonja et al.(Zonja et al. 2016b).

LAMOTRIGINE-N2-GLUCURONIDE (LMG-N2-G)

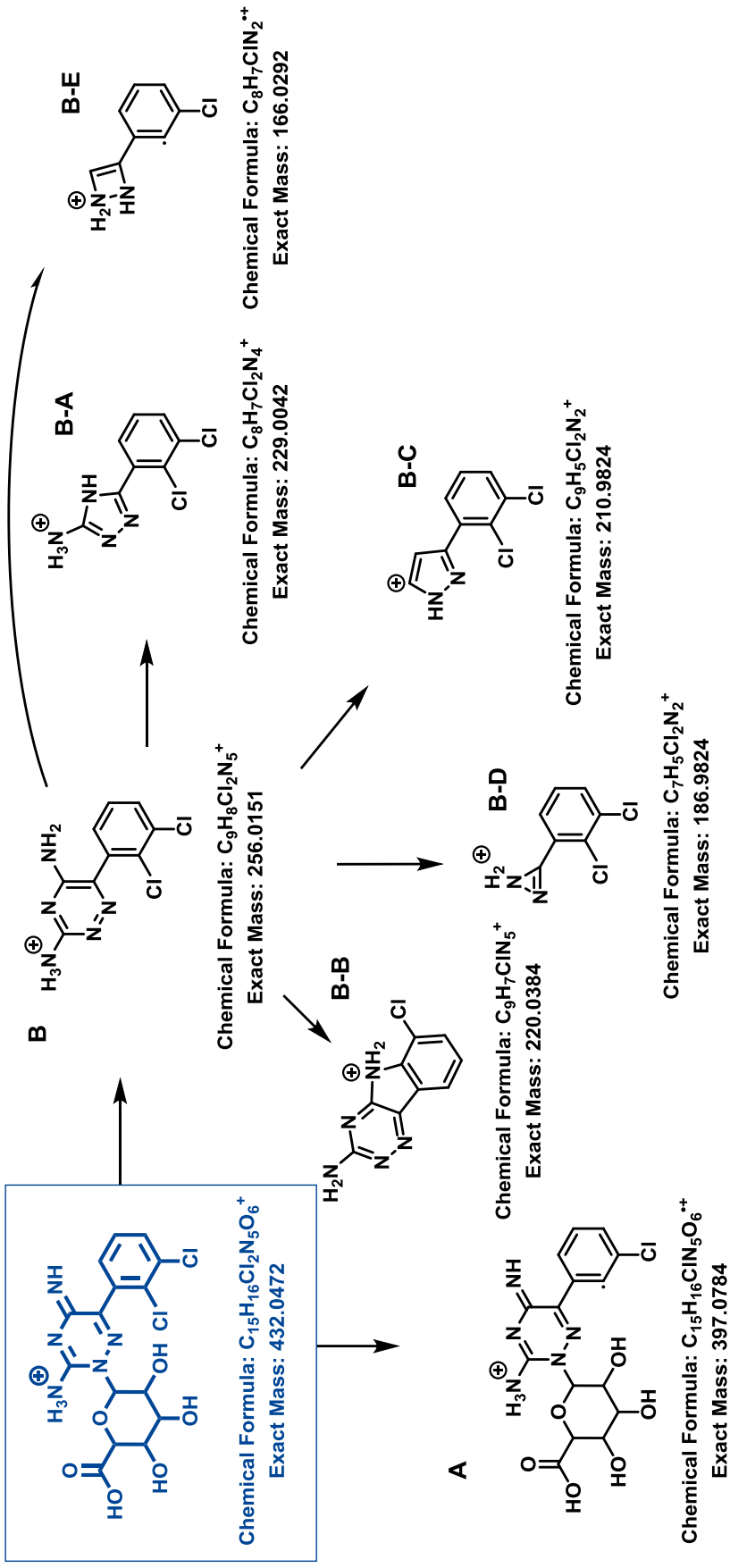

Figure SI-4.1-A. Fragmentation pattern of LMG-N2-G

LAMOTRIGINE-N2-GLUCURONIDE TP433 amidine and guanidine (LMG-N2-G-TP433 - Amd and Gnd)

Figure SI-4.2-A. Fragmentation pattern LMG-N2-G-TP433 – Amd and Gnd

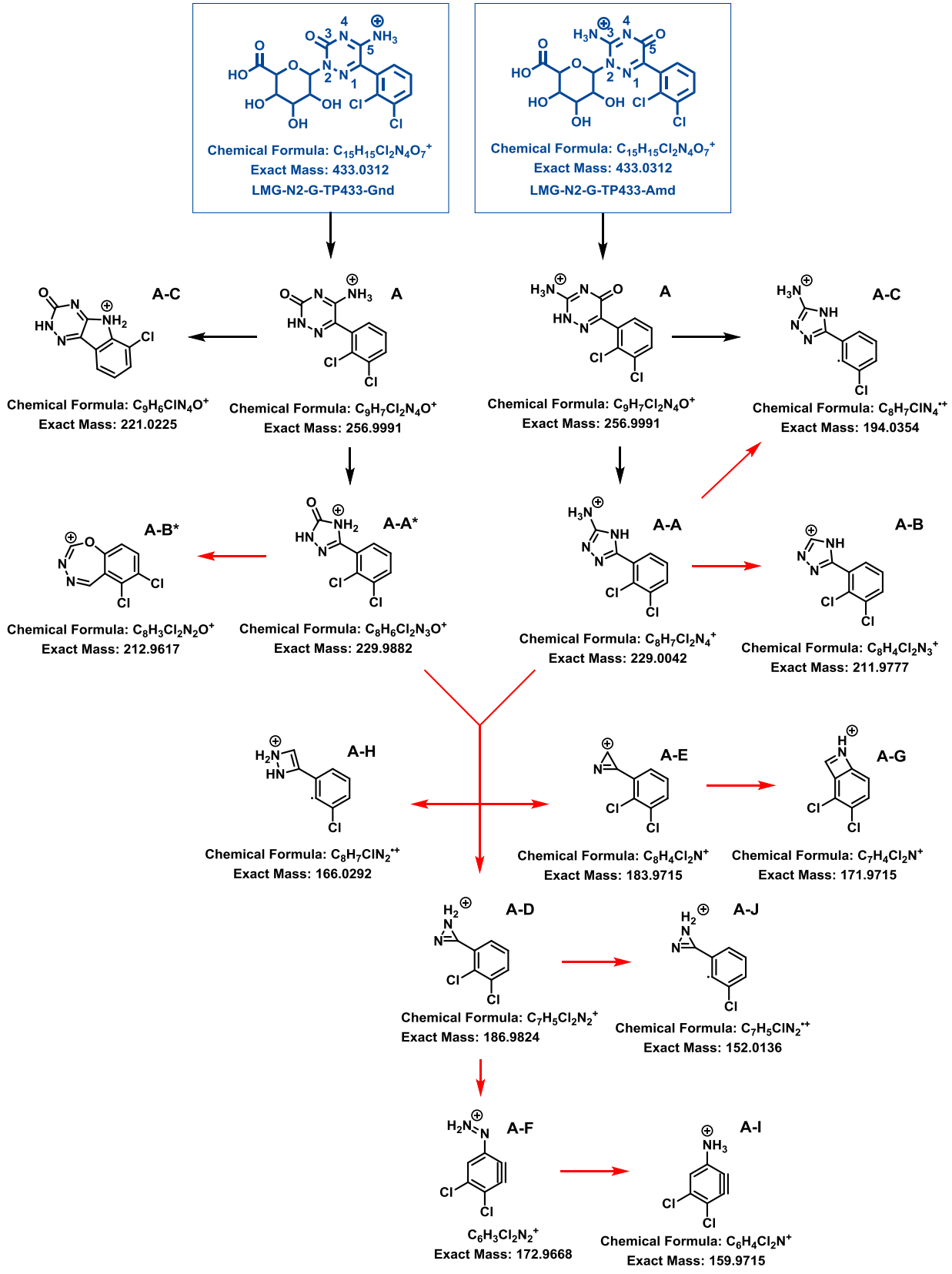

Figure SI-4.2-B. MS² and pMS³ spectra of LMG-N2-G-TP433 - Amd and Gnd

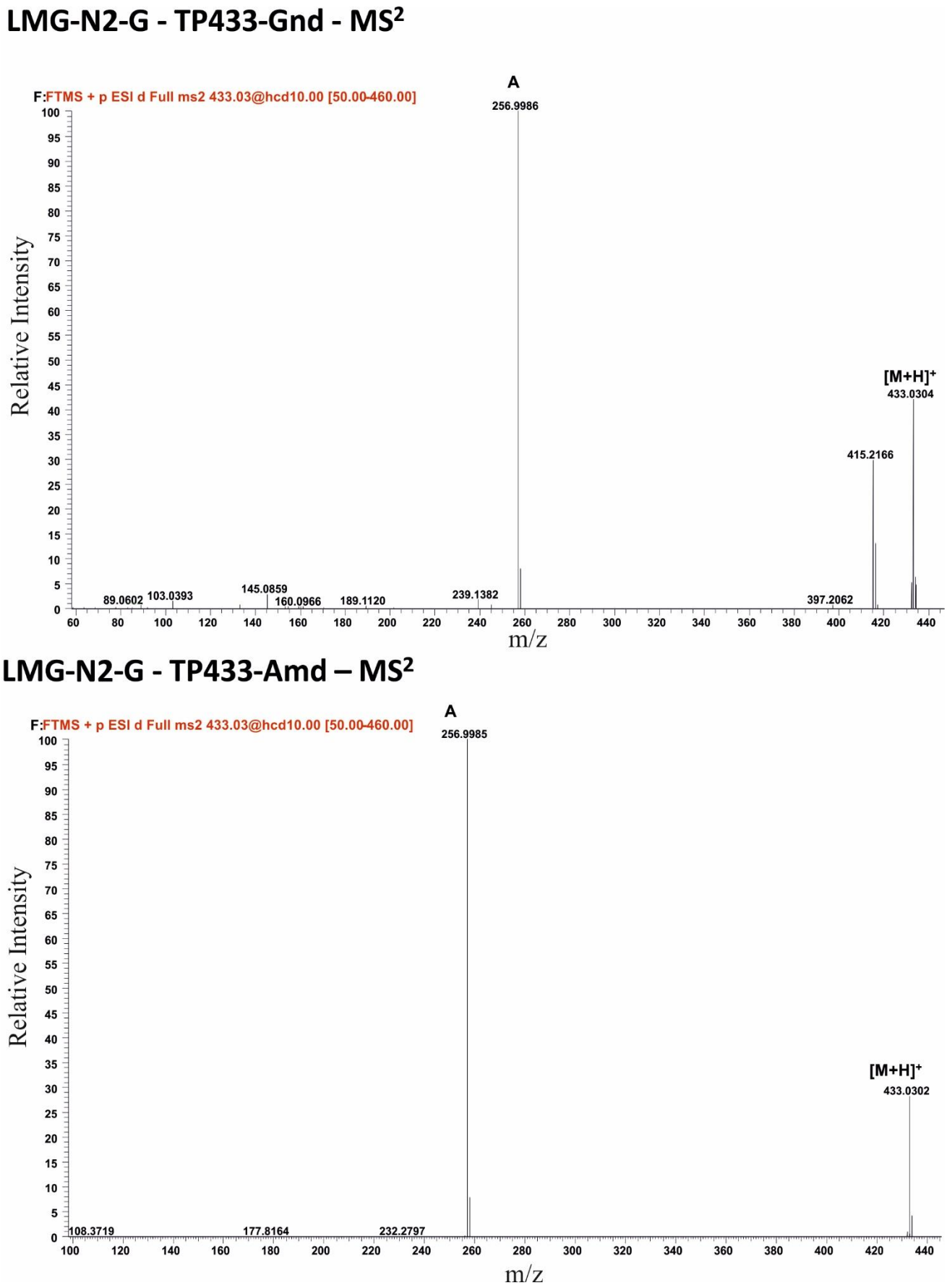

Figure SI-4.2-B. MS^2 and pMS^3 spectra of LMG-N2-G-TP433 - Amd and Gnd - *continued*

LMG-N2-G-TP433-Gnd – 257 pMS^3

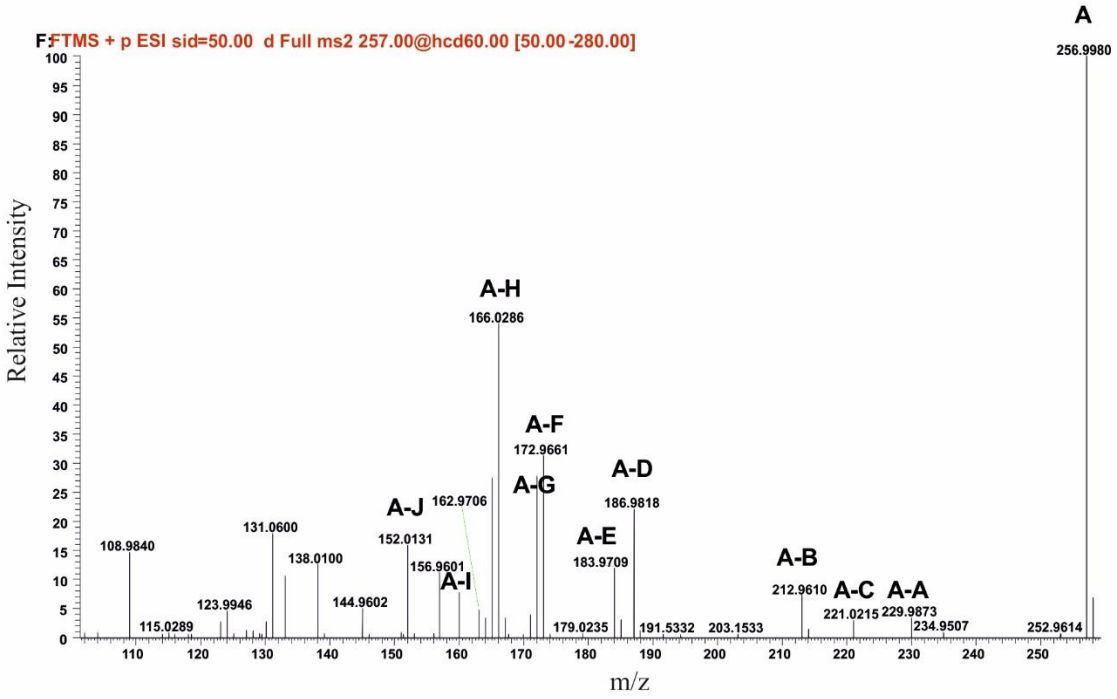

LMG-N2-G - TP433-Amd – 257 pMS^3

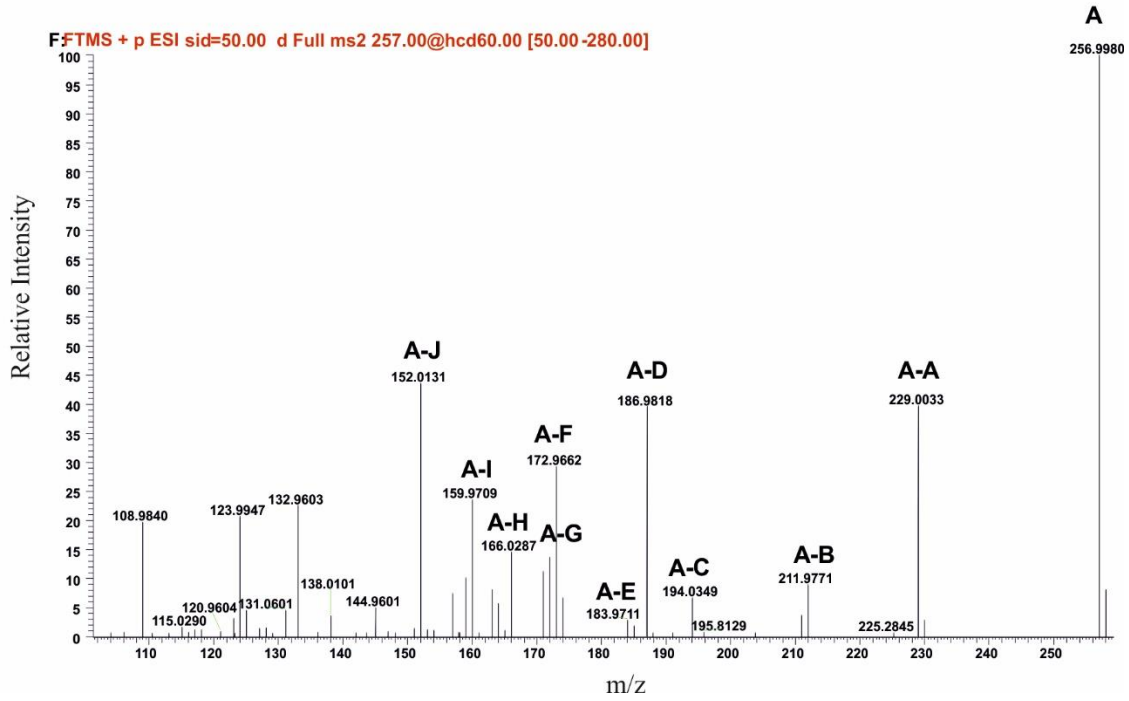

LAMOTRIGINE-N2-GLUCURONIDE TP257 (OXO-LMG)

Figure SI-4.3-A. Fragmentation pattern of OXO-LMG

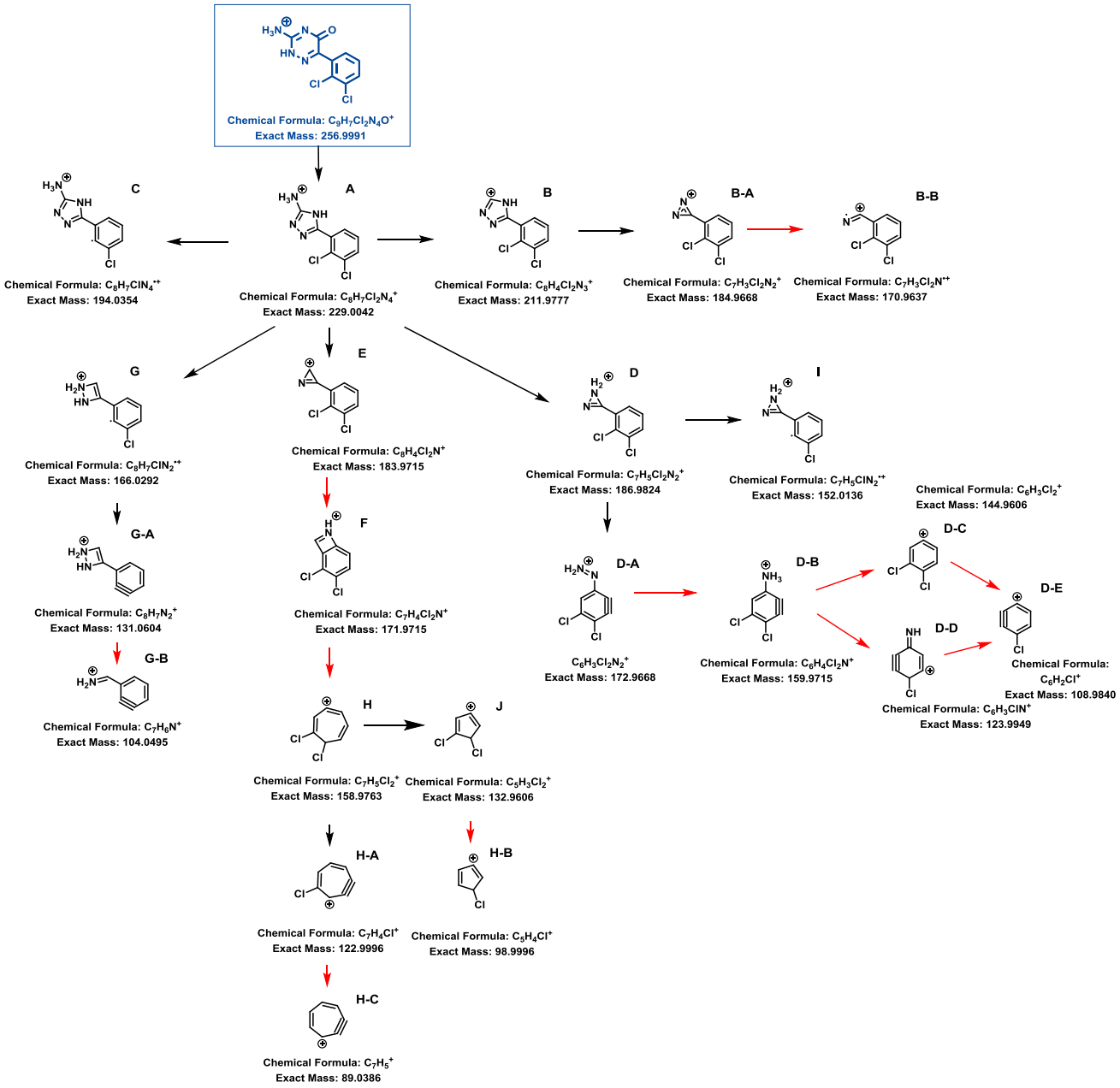

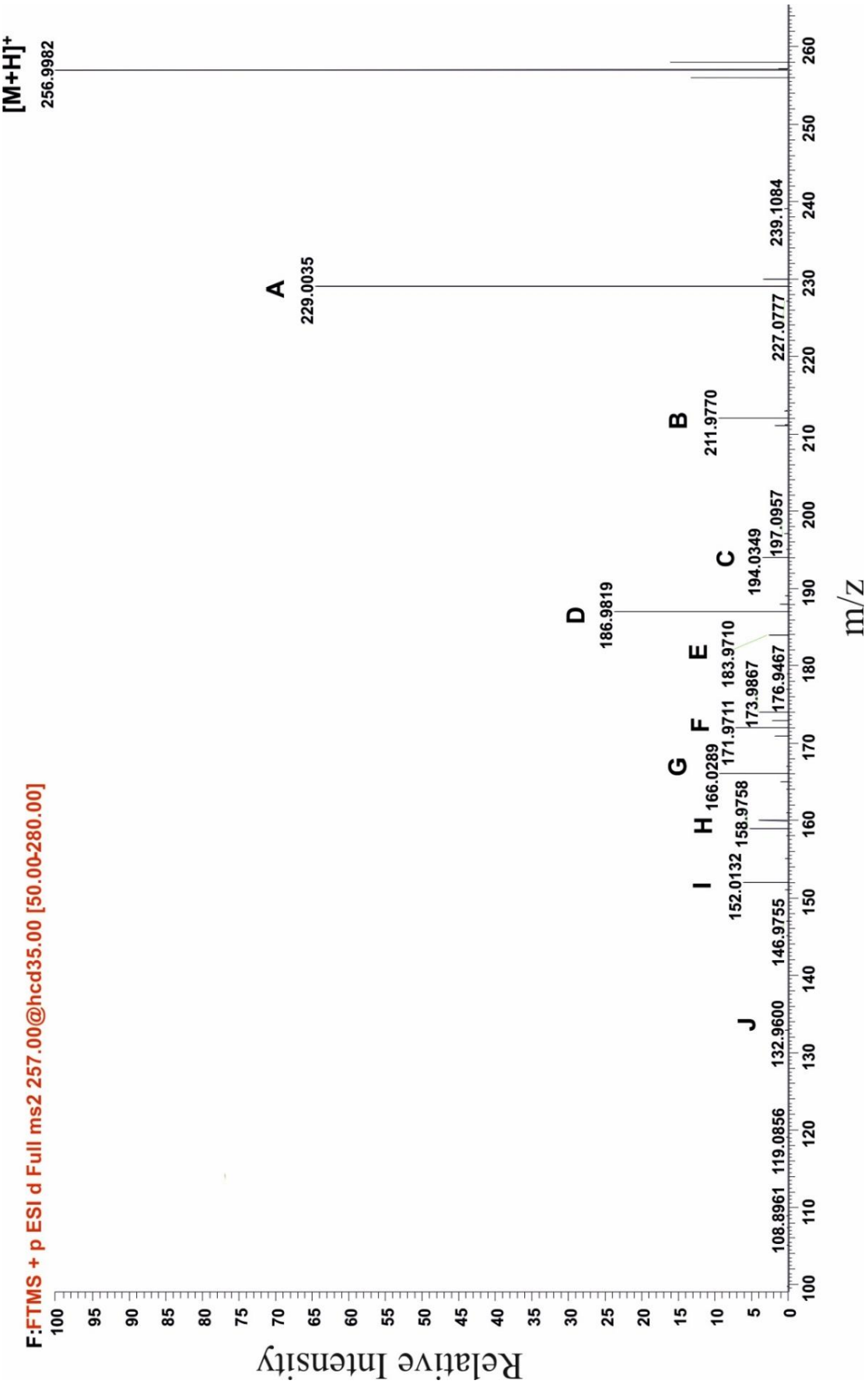

Figure SI-4.3-B. MS² and pMS³ spectra of OXO-LMG

Figure SI-4.3-B. MS^2 and pMS^3 spectra of OXO-LMG – *continued*

OXO-LMG – 229 pMS^3

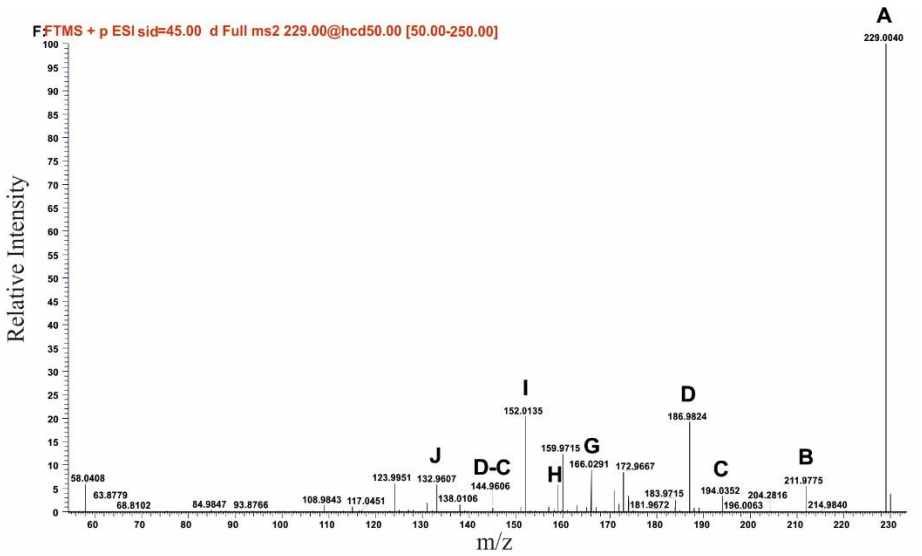

OXO-LMG – 211 pMS^3

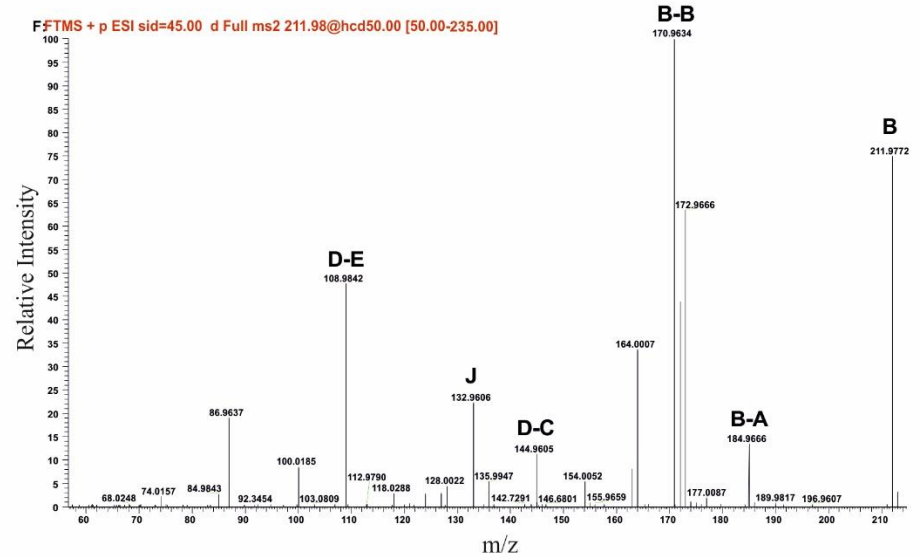

OXO-LMG – 186 pMS^3

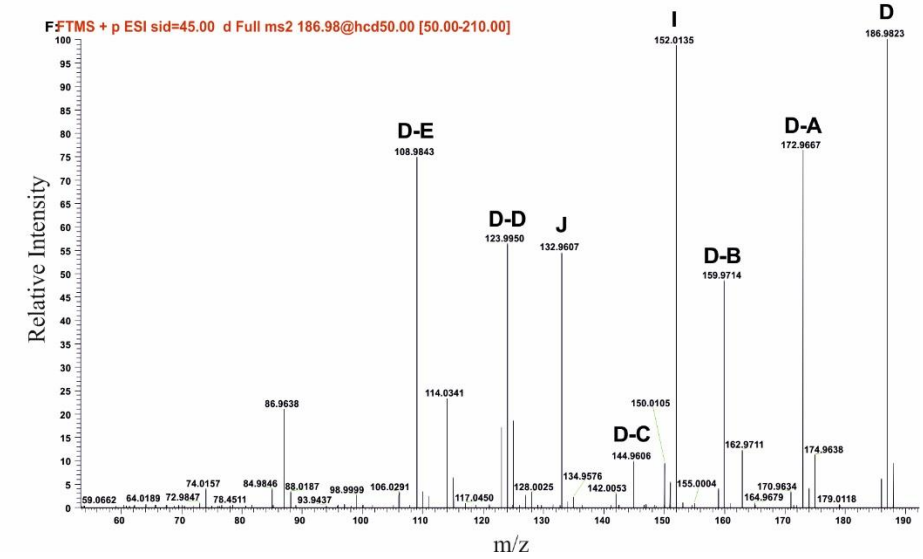

Figure SI-4.3-B. MS^2 and pMS^3 spectra of OXO-LMG – *continued*

OXO-LMG – 166 pMS^3

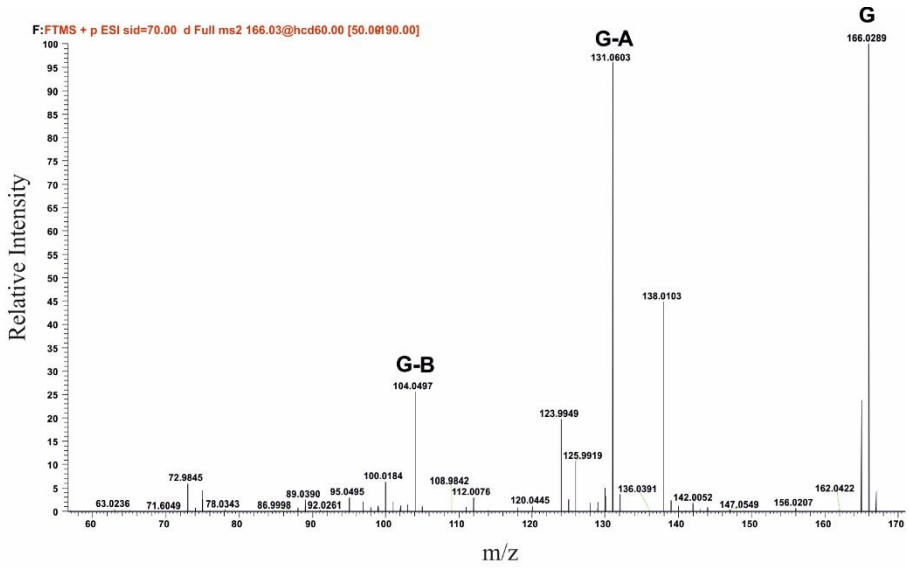

OXO-LMG – 158 pMS^3

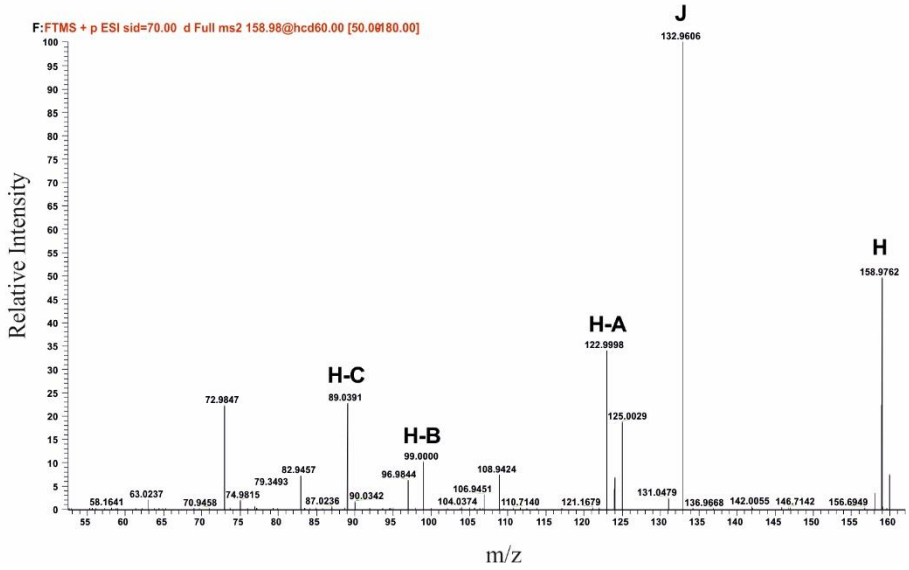

LAMOTRIGINE-N2-GLUCURONIDE TP450 - guanidine (LMG-N2-G-TP450-Gnd)

Figure SI-4.4-A. Fragmentation pattern of LMG-N2-G-TP450-Gnd

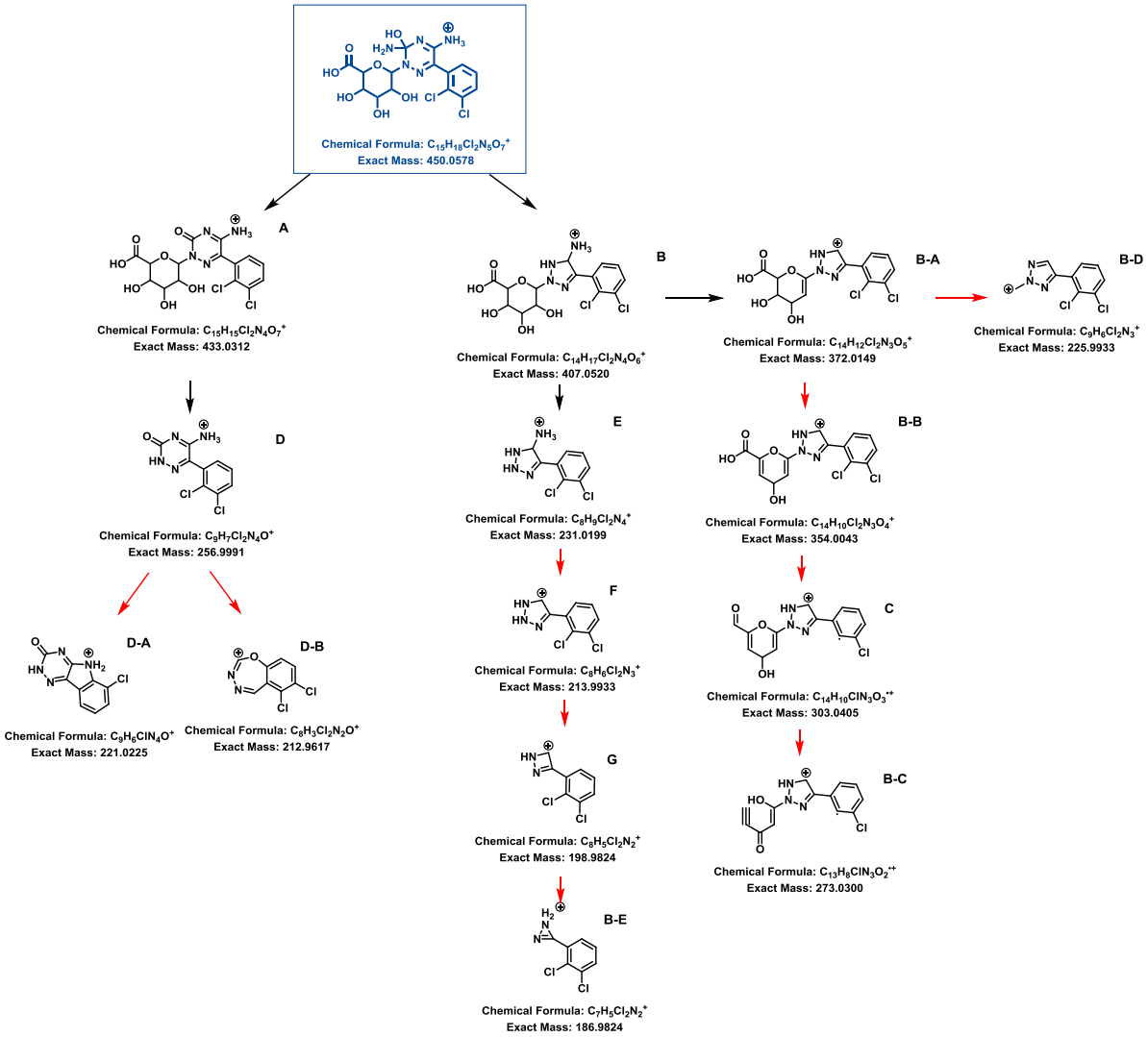

Figure SI-4.4-B. MS² and pMS³ spectra of LMG-N2-G-TP450-Gnd

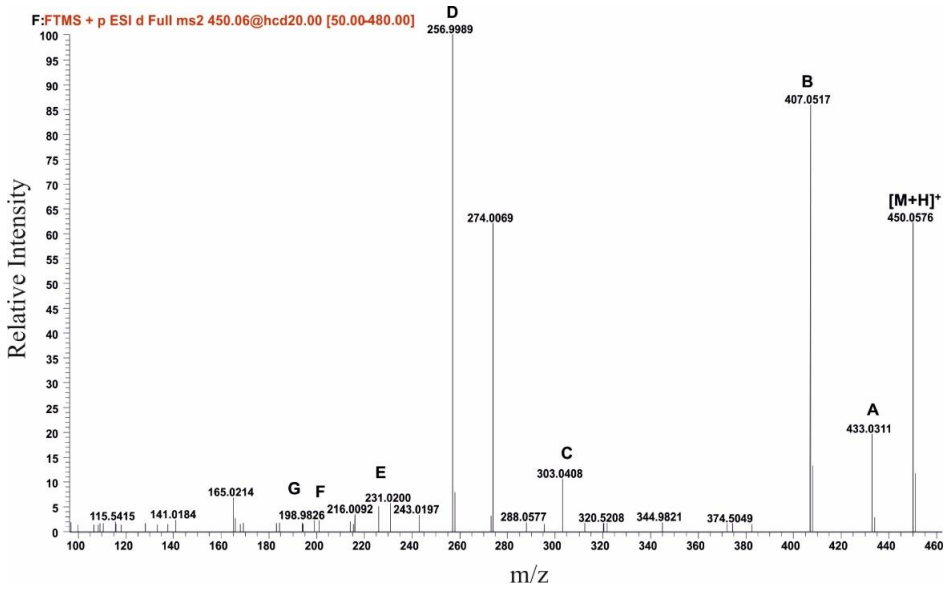

Figure SI-4.4-B. MS^2 and pMS^3 spectra of LMG-N2-G-TP450-Gnd - *continued*

LMG-N2-G
TP450 – 433 pMS^3

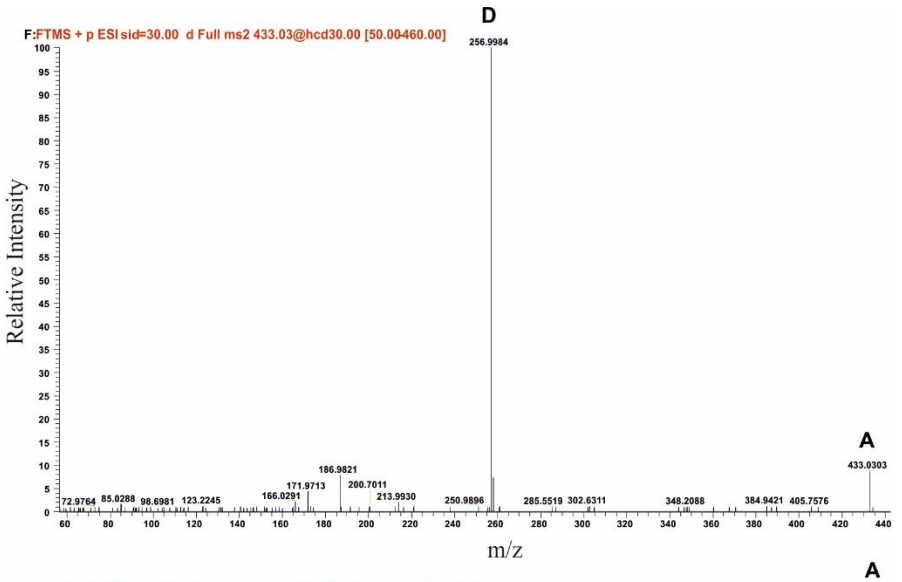

LMG-N2-G
TP450 – 407 pMS^3

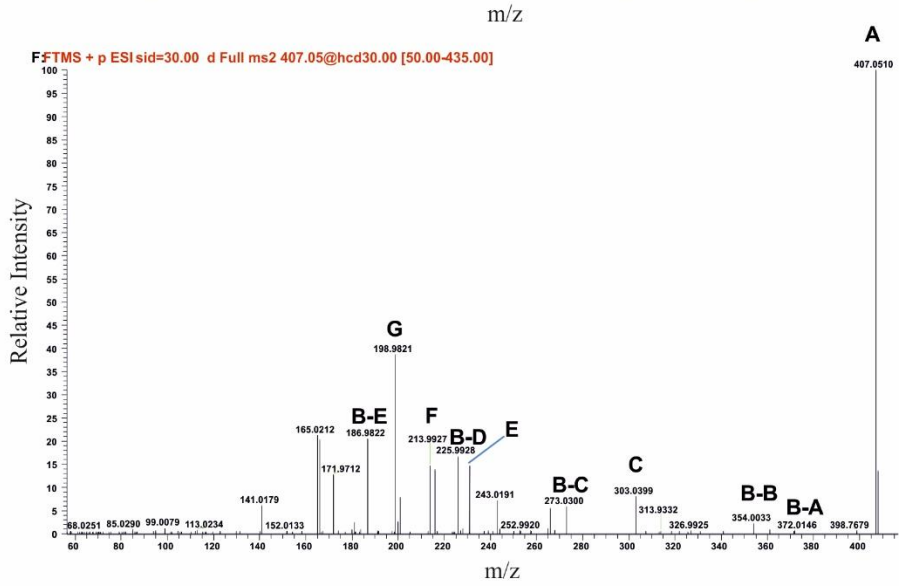

LMG-N2-G
TP450 – 257 pMS^3

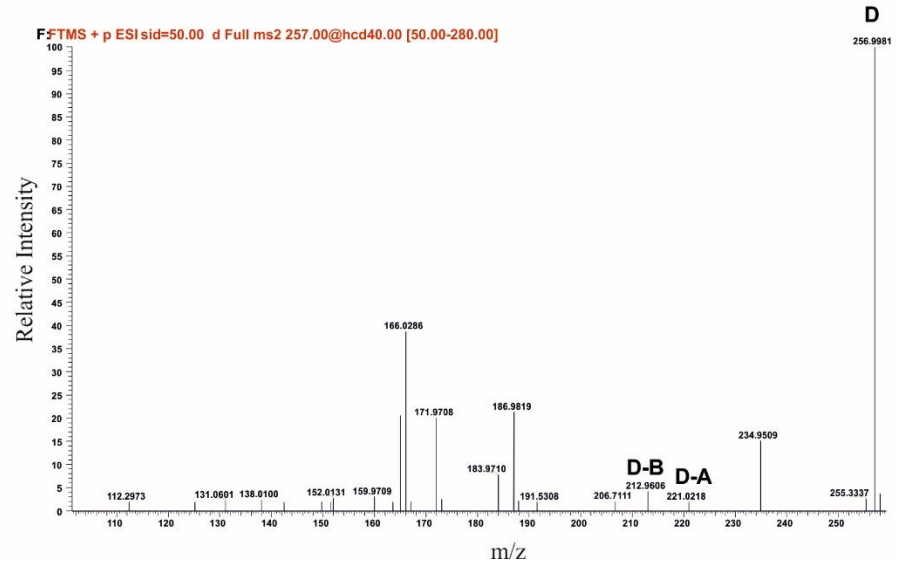

Table SI-8. Accurate mass measurements of protonated LMG-N2-G and transformation products as determined by LC-QExactive-MS in MS/MS or pseudo MS^3 modes

Nominal ion mass	Measured mass [m/z]	Mass error [ppm]	Elemental composition	Calculated mass [m/z]	DBE[a]
LMG-N2-G-TP433-Amd					
[M+H]+	433.0311	-0.2	$C_{15}H_{15}Cl_2N_4O_7$	433.0312	9.5
A 257	256.9985	-2.3	$C_9H_7Cl_2N_4O$	256.9991	7.5
A-A 229	229.0033	-3.9	$C_8H_7Cl_2N_4$	229.0042	6.5
A-B 211	211.9771	-2.8	$C_8H_4Cl_2N_3$	211.9777	7.5
A-C 194	194.0349	-2.6	$C_8H_7ClN_4$	194.0354	7.0
A-D 186	186.9818	-3.2	$C_7H_5Cl_2N_2$	186.9824	5.5
A-E 186	183.9711	-2.2	$C_8H_4Cl_2N$	183.9715	6.5
A-F 172	172.9662	-3.5	$C_8H_7ClN_2$	172.9668	5.5
A-G 171	171.9709	-3.5	$C_7H_4Cl_2N$	171.9715	5.5
A-H 166	166.0287	-3.0	$C_8H_7Cl_2N_2$	166.0292	6.0
A-I 159	159.9709	-3.8	$C_6H_4Cl_2N$	159.9715	4.5
A-J 152	152.0131	-3.3	$C_7H_5ClN_2$	152.0136	6.0
LMG-N2-G-TP433-Gnd					
[M+H]+	433.0311	-0.2	$C_{15}H_{15}Cl_2N_4O_7$	433.0312	9.5
A 257	256.9985	-2.3	$C_9H_7Cl_2N_4O$	256.9991	7.5
A-A 229	229.9873	-3.9	$C_8H_6Cl_2N_3O$	229.9882	6.5
A-B 221	221.0215	-4.5	$C_9H_6ClN_4O$	221.0225	8.5
A-C 212	212.9610	-3.3	$C_8H_3Cl_2N_2O$	212.9617	7.5
A-D 186	186.9818	-3.2	$C_7H_5Cl_2N_2$	186.9824	5.5
A-E 183	183.9709	-3.3	$C_8H_4Cl_2N$	183.9715	6.5
A-F 172	172.9661	-4.0	$C_8H_7ClN_2$	172.9668	5.5
A-G 171	171.9709	-3.5	$C_7H_4Cl_2N$	171.9715	5.5
A-H 166	166.0286	-3.6	$C_8H_7Cl_2N_2$	166.0292	6.0
A-I 159	159.9709	-3.8	$C_6H_4Cl_2N$	159.9715	4.5
A-J 152	152.0131	-3.3	$C_7H_5ClN_2$	152.0136	6.0

Nominal ion mass	Measured mass [m/z]	Mass error [ppm]	Elemental composition	Calculated mass [m/z]	DBE[a]
OXO-LMG					
$[M+H]^+$	256.9985	-2.3	$C_9H_7Cl_2N_4O$	256.9991	7.5
A 229	229.0035	-3.1	$C_8H_7Cl_2N_4$	229.0042	6.5
B 211	211.9775	-0.9	$C_8H_4Cl_2N_3$	211.9777	7.5
C 194	194.0352	-1.0	$C_8H_7ClN_4$	194.0354	7.0
D 186	186.9824	0.0	$C_7H_5Cl_2N_2$	186.9824	5.5
G 166	166.0291	-0.6	$C_8H_7ClN_2$	166.0292	6.0
H 158	158.9762	-0.6	$C_7H_5Cl_2$	158.9763	4.5
I 152	152.0135	-0.7	$C_7H_5ClN_2$	152.0136	6.0
D-C 144	144.9606	0.0	$C_6H_3Cl_2$	144.9606	4.5
J 132	132.9607	0.8	$C_5H_3Cl_2$	132.9606	3.5
B 211	211.9770	-3.3	$C_8H_4Cl_2N_3$	211.9777	7.5
B-A 184	184.9666	-1.1	$C_7H_3Cl_2N_2$	184.9668	6.5
B-B 170	170.9634	-1.8	$C_7H_3Cl_2N$	170.9637	6.0
D-C 144	144.9605	-0.7	$C_6H_3Cl_2$	144.9606	4.5
J 132	132.9606	0.0	$C_5H_3Cl_2$	132.9606	3.5
D-E 108	108.9842	1.8	C_6H_3Cl	108.9840	5.5
C 194	194.0349	-2.6	$C_8H_7ClN_4$	194.0354	7.0
D 186	186.9819	-2.7	$C_7H_5Cl_2N_2$	186.9824	5.5
D-A 172	172.9667	-0.6	$C_6H_3Cl_2N_2$	172.9668	5.5
D-B 159	159.9714	-0.6	$C_6H_4Cl_2N$	159.9715	4.5
I 152	152.0135	-0.7	$C_7H_5ClN_2$	152.0136	6.0
D-C 144	144.9606	0.0	$C_6H_3Cl_2$	144.9606	4.5
J 132	132.9607	-1.5	$C_5H_3Cl_2$	132.9609	3.5
D-D 123	123.9950	0.8	C_6H_3ClN	123.9949	5.5
D-E 108	108.9843	2.8	C_6H_2Cl	108.9840	5.5
E 183	183.9710	-2.7	$C_8H_4Cl_2N$	183.9715	6.5
F 171	171.9711	-2.3	$C_7H_4Cl_2N$	171.9715	5.5
G 166	166.0289	-1.8	$C_8H_7ClN_2$	166.0292	6.0
G-A 131	131.0603	-0.8	$C_8H_7N_2$	131.0604	6.5
G-B 104	104.0497	1.9	C_7H_6N	104.0495	5.5

Nominal ion mass	Measured mass [m/z]	Mass error [ppm]	Elemental composition	Calculated mass [m/z]	DBE[a]
H 158	158.9758	-3.1	$C_7H_5Cl_2$	158.9763	4.5
J 132	132.9606	0.0	$C_5H_3Cl_2$	132.9606	3.5
H-A 122	122.9998	1.6	C_7H_4Cl	122.9996	5.5
H-B 99	99.0000	4.1	C_5H_4Cl	98.9996	3.5
H-C 89	89.0391	5.6	C_7H_5	89.0386	5.5
I 152	152.0132	-2.6	$C_7H_5ClN_2$	152.0136	6.0
J 132	132.9600	-4.5	$C_5H_3Cl_2$	132.9606	3.5
LMG-N2-G-TP450-Gnd					
[M+H]+	450.0576	-0.4	$C_{15}H_{18}Cl_2N_5O_7$	450.0578	8.5
A 433	433.0311	-0.2	$C_{15}H_{15}Cl_2N_4O_7$	433.0312	9.5
D 257	256.9984	-2.7	$C_9H_7Cl_2N_4O$	256.9991	7.5
B 407	407.0517	-0.7	$C_{15}H_{17}Cl_2N_4O_7$	407.0520	7.5
B-A 372	372.0146	-0.8	$C_{14}H_{12}Cl_2N_3O_5$	372.0149	9.5
B-B 354	354.0033	-2.8	$C_{14}H_{10}Cl_2N_3O_4$	354.0043	10.5
C 303	303.0399	-2.0	$C_{14}H_{10}ClN_3O_3$	303.0405	11.0
B-C 273	273.0300	0.0	$C_{13}H_8ClN_3O_2$	273.0300	11.0
E 231	231.0193	-2.6	$C_8H_9Cl_2N_4$	231.0199	5.5
B-D 225	225.9928	-2.2	$C_9H_6Cl_2N_3$	225.9933	7.5
F 213	213.9927	-2.8	$C_8H_6Cl_2N_3$	213.9933	6.5
G 198	198.9821	-1.5	$C_8H_5Cl_2N_2$	198.9824	6.5
B-E 186	186.9822	-1.1	$C_7H_5Cl_2N_2$	186.9824	5.5
C 303	303.0408	1.0	$C_{14}H_{10}ClN_3O_3$	303.0405	11.0
D 257	256.9989	-0.8	$C_9H_7Cl_2N_4O$	256.9991	7.5
D-A 221	221.0218	-3.2	$C_9H_6ClN_4O$	221.0225	8.5
D-B 212	212.9606	-5.2	$C_8H_3Cl_2N_2O$	212.9617	7.5
E 231	231.0200	0.4	$C_8H_9Cl_2N_4$	231.0199	5.5
F 213	213.9933	0.0	$C_8H_6Cl_2N_3$	213.9933	6.5
G 198	198.9826	1.0	$C_8H_5Cl_2N_2$	198.9824	6.5

[a] Double-bond equivalents

pH EXPERIMENTS - degradations in hospital effluent and WW influent and effluent @pH 7 - 9

Table SI-9. Physico-chemical properties of the samples used as matrix

	pH	Dissolved oxygen [mgL^{-1}]	Conductivity [µScm^{-2}]	Free chlorine [mgL^{-1}]
HOS effluent	9.09	5.40	470	0.09
WW influent	8.55	5.83	960	not detected
WW effluent	8.32	7.14	1710	not detected

Figure SI-5. Stability of the internal standard LMG-$^{13}C_3$ in (A) HOSeff (pH 8), (B) WWinf (pH 8), (C) HOSeff (pH 9), (D) WWinf (pH 9), (E) HOSeff (pH 9 and free chlorine) and (F) WWinf (pH9 and free chlorine) over the course of 36 hours

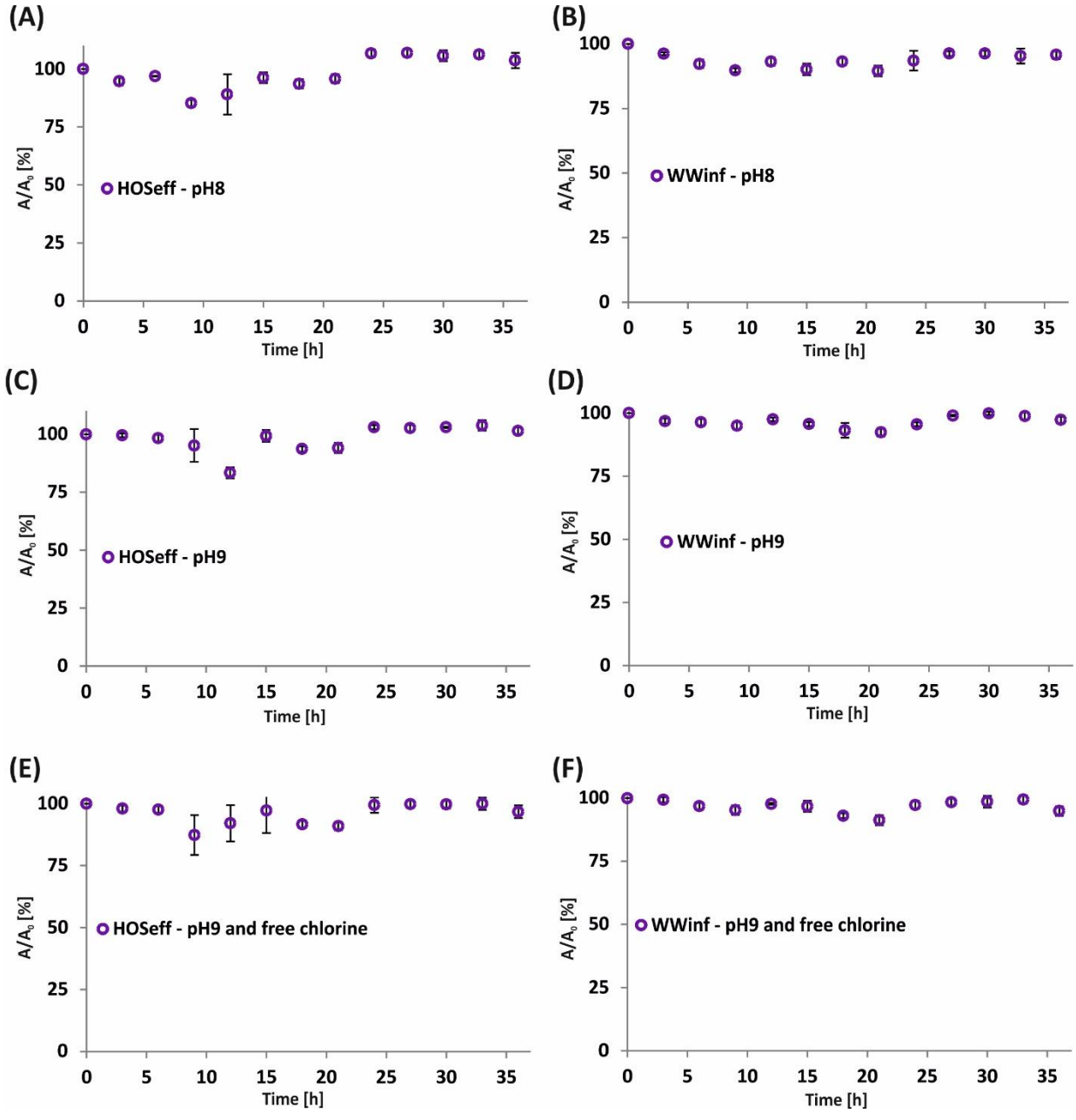

Figure SI-6. Degradation of 200 nM of LMG-N2-G in: HOSeff (A), WWinf (B) and WWeff (C) at pHs 7- 9 over the course of 36 hours.

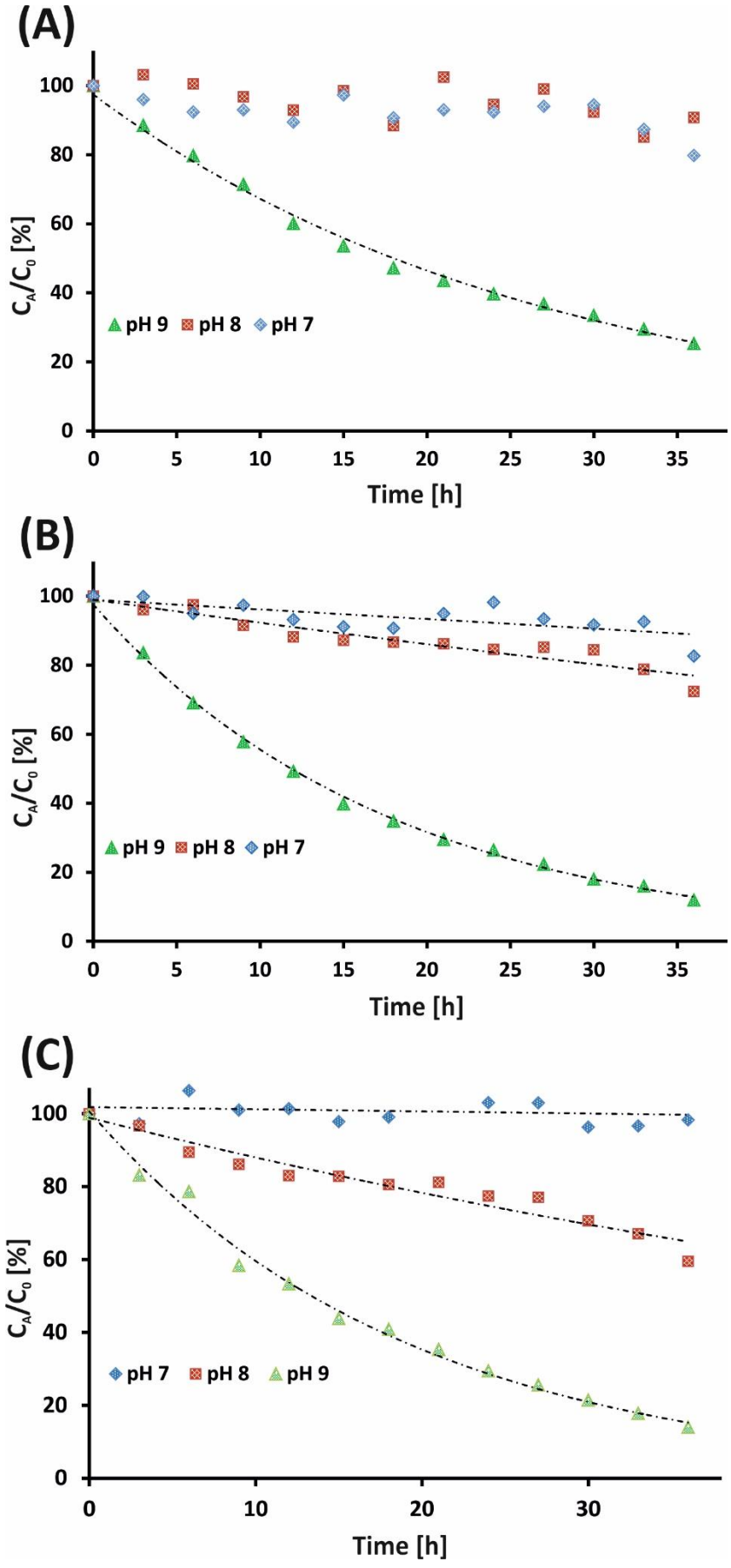

Figure SI-7. Mass balance based on molar concentrations in logarithmic scale for degradation of 200 nM of LMG-N2-G at pH 8 for HOSeff(A), WWinf (B) and WWeff (C) over the course of 36 hours

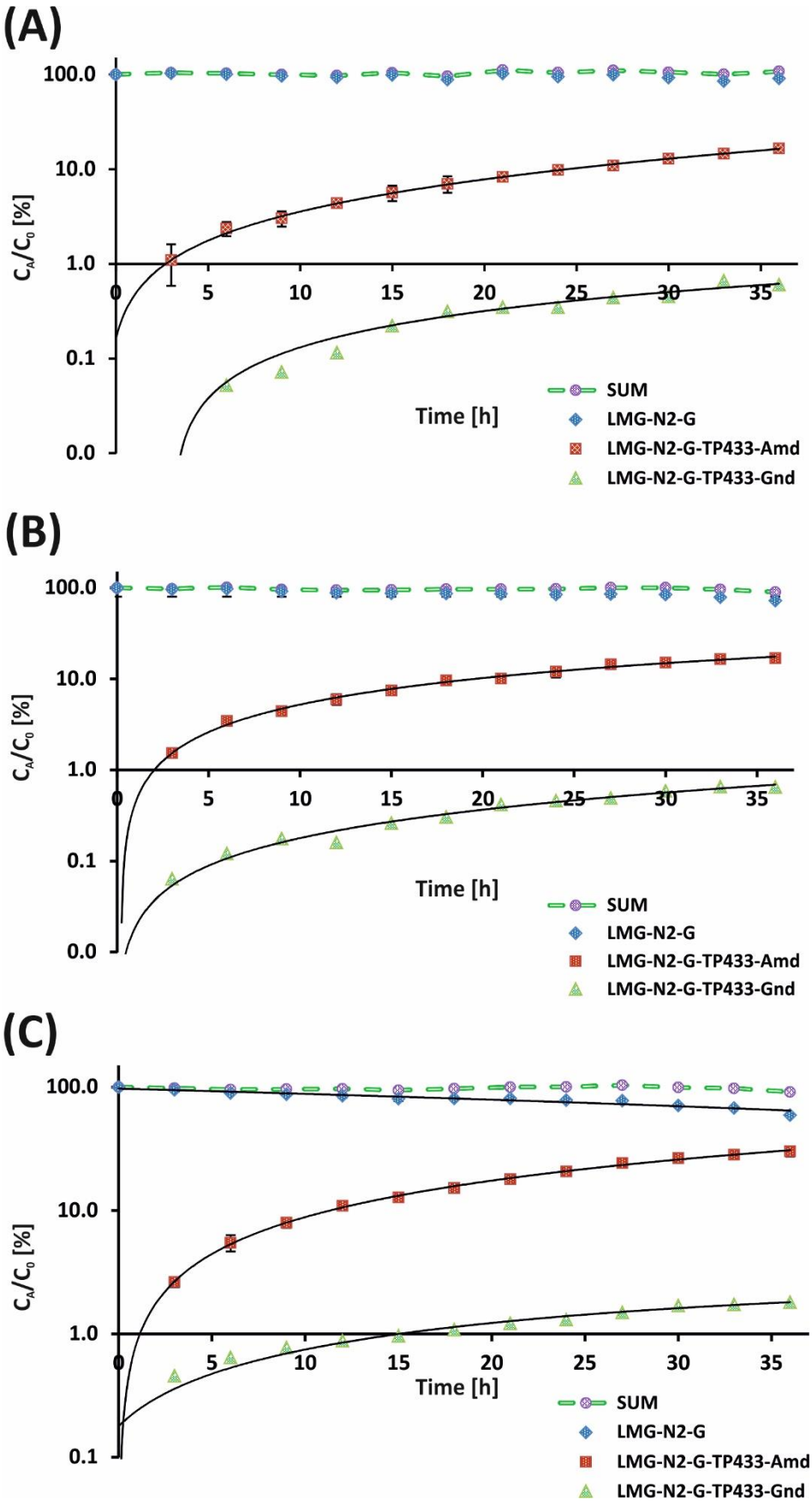

Figure SI-8. Mass balance based on molar concentrations in logarithmic scale for degradation of 200 nM of LMG-N2-G at pH 7 for HOSeff (A), WWinf (B) and WWeff (C) over the course of 36 hours

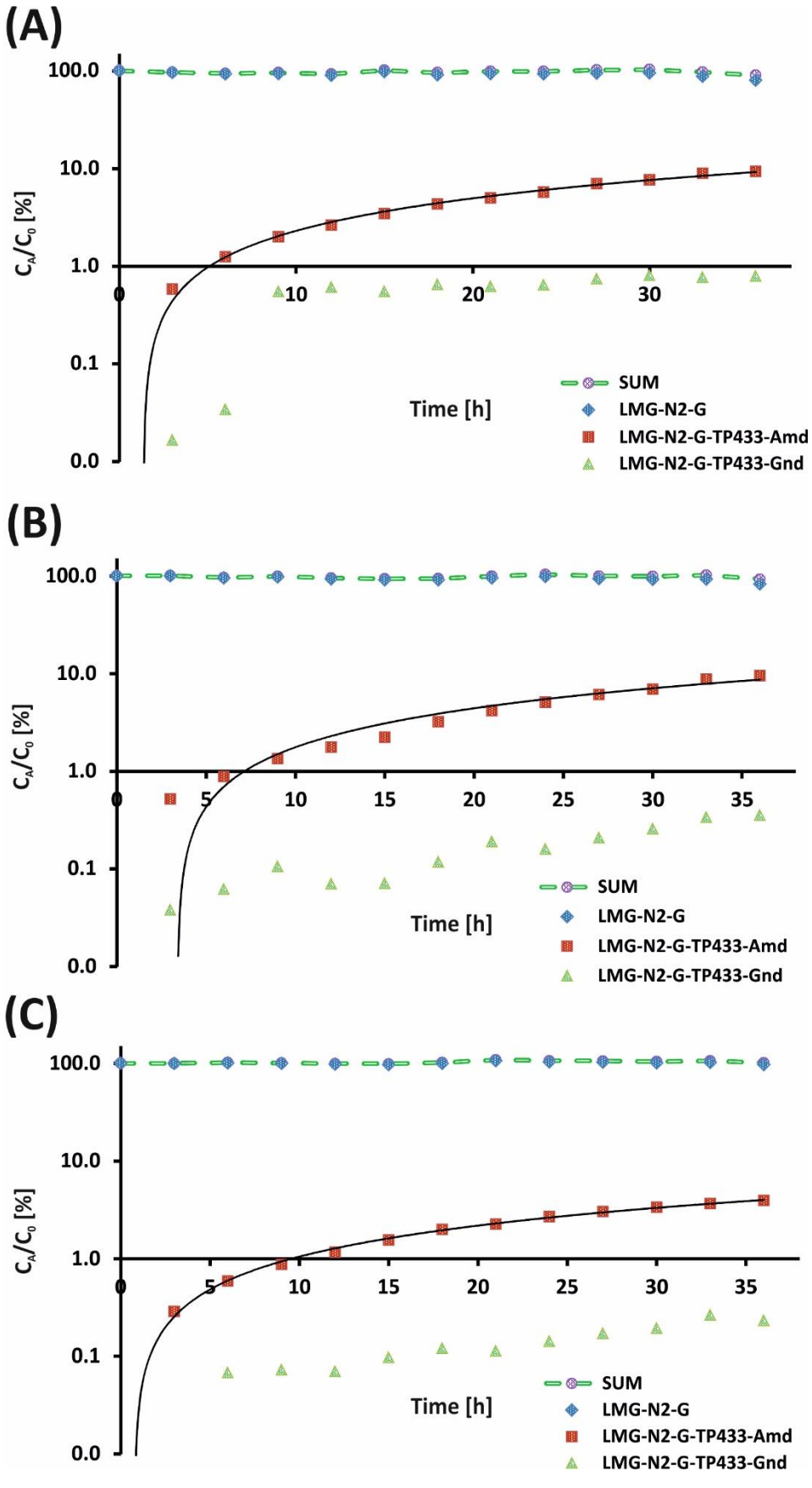

Figure SI-9. Mass balance based on molar concentrations for degradation of 200 nM of LMG-N2-G at pH 9 in WWeff. *Total degradation time was 36 hours.*

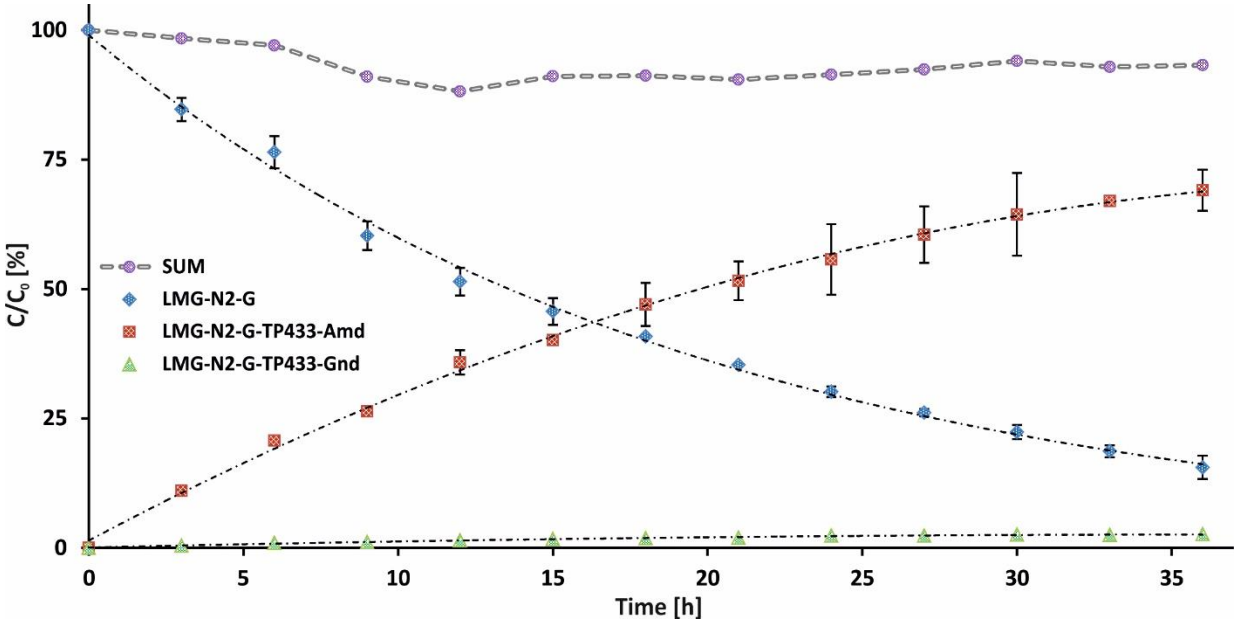

Figure SI-10. Degradation of 200 nM of LMG-N2-G at pH 6.5 filtered through 0.7 µm in HOSeff (A) and WWinf (B). *Total degradation time was 36 hours.*

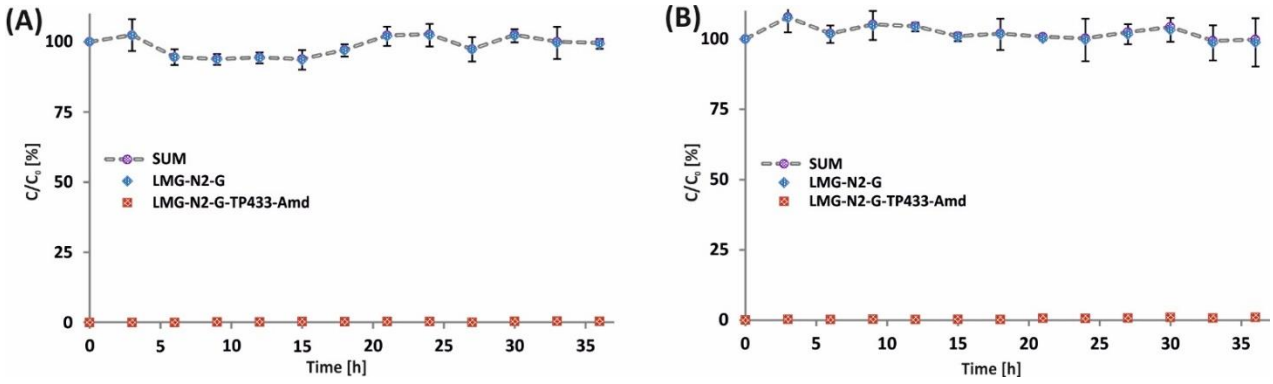

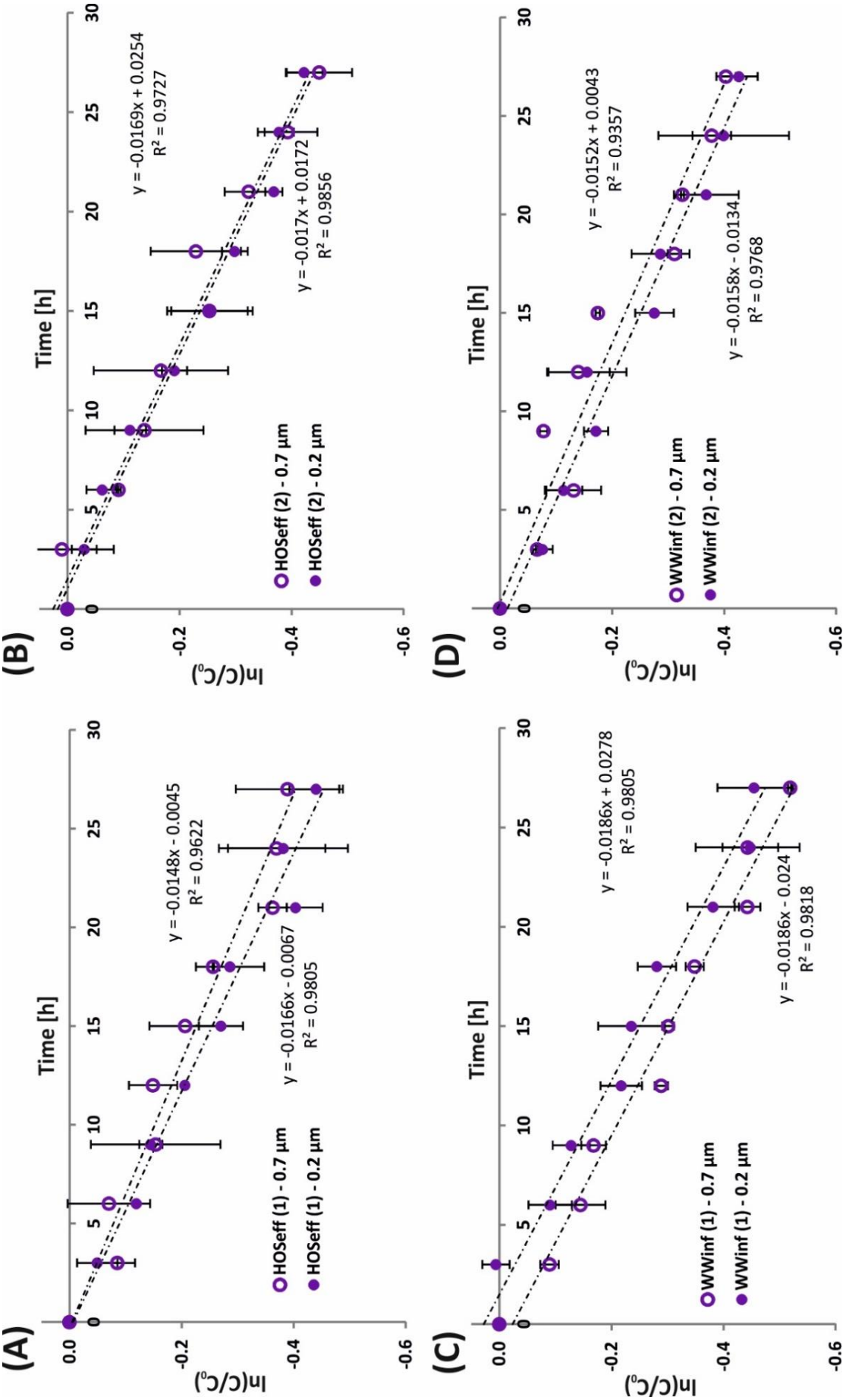

Figure SI-11. Degradation of 200 nM of LMG-N2-G at pH 8.5, filtered through 0.7 and 0.2 µm in two different HOSeff samples (A and B) and in two different WWinf samples (C and D). *Total degradation time was 27 hours.*

CHLORINATION of LMG-N2-G in hospital effluents and wastewater influent @ pH 8, 8.5 and 9

The same degradation experiment of LMG-N2-G reported earlier in HOSeff was repeated with the addition of 25 times molar excess of free chlorine. The concentration again was 200 nM and the degradation was performed in triplicate over the course of 12 hours. Degradation is for pH 9 is shown in **Figures SI-12** and **SI-13-B** and for pH 8 in **Figure SI-13-A**. The results initially suggest that one of the possible inhibitors of amidine hydrolysis of LMG-N2-G in hospital effluents could be the presence of free chlorine, since its addition had an inhibitory effect in our experiments. This was evidenced in the different degradation constants observed. Thus, for degradation at pH 9 (without free chlorine), $k_{HOS\ (12h)}$ = 0.041 ± 0.005 h^{-1} (R^2_{HOS} = 0.9902), whereas for degradation in the presence of 25 times molar concentration of free chlorine, $k_{HOS\text{-}Cl\ (12h)}$ = 0.018 ± 0.001 h^{-1} ($R^2_{HOS\text{-}Cl}$ = 0.9402). It was postulated that one reason for the slow amidine hydrolysis rate observed for LMG-N2-G in the presence of excess chlorine could be explained by assuming the formation of a transient *N*-chloroimine, arising from reaction of the major imine tautomer with hypochlorite. The formation of *N*-chloroimines from imines and hypochlorite is well-known in the literature (Volmajer et al. 2003). In our case, the resonance electron donating effect of the chlorine lone pairs in the *N*-chloroimine would account for the observed lower hydrolysis rates observed for the degradation of LMG-N2-G at pH 9. However, in subsequent experiments of degradation of LMG-N2-G in the presence of free chlorine over 36 hours, this effect is not seen. In **Figure SI-16** and **SI-17**, 200 nM of LMG-N2-G was degraded both HOSeff and WWinf at pH 8.5 the degradation constants almost the same. For HOSeff they were $k_{HOS\ (36h)}$ = 0.014 ± 0.001 h^{-1} (R^2_{HOS} = 0.9770) vs. $k_{HOS\text{-}Cl\ (36h)}$ = 0.016 ± 0.001 h^{-1} ($R^2_{HOS\text{-}Cl}$ = 0.9726) and WWinf they were $k_{inf\ (36h)}$ = 0.022 ± 0.001 h^{-1} (R^2_{inf} = 0.9761) vs. $k_{inf\text{-}Cl\ (36h)}$ = 0.022 ± 0.001 h^{-1} ($R^2_{inf\text{-}Cl}$ = 0.9898). Likewise, the degradation of 20 nM of LMG-N2-G at pH 9 in the presence of 250 times molar excess compared to concentration of LMG-N2-G (**Figure SI-18**), similar results are obtained. In HOSeff they were $k_{HOS\ (36h)}$ = 0.044 ± 0.002 h^{-1} (R^2_{HOS} = 0.9766) vs. $k_{HOS\text{-}Cl\ (36h)}$ = 0.041 ± 0.001 h^{-1} ($R^2_{HOS\text{-}Cl}$ = 0.9727) and WWinf they were $k_{inf\ (36h)}$ = 0.044 ± 0.003 h^{-1} (R^2_{inf} = 0.9863) vs. $k_{inf\text{-}Cl\ (36h)}$ = 0.042 ± 0.001 h^{-1} ($R^2_{inf\text{-}Cl}$ = 0.9944).

Figure SI-12. Comparison of degradation of 200 nM LMG-N2-G and formation of LMG-N2-G-TP433-Amd with and without addition of 25 times molar excess of free chlorine in HOSeff buffered at pH 9

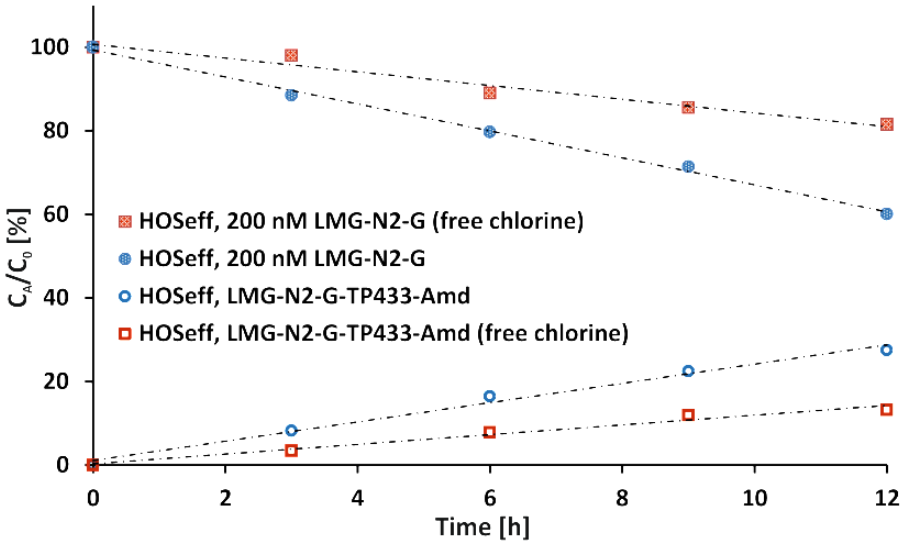

Figure SI-13. Mass balance of 200 nM of LMG-N2-G in HOSeff at (A) pH 8 and (B) pH 9, over the course of 12 hours with the free chlorine molar excess of 25 times.

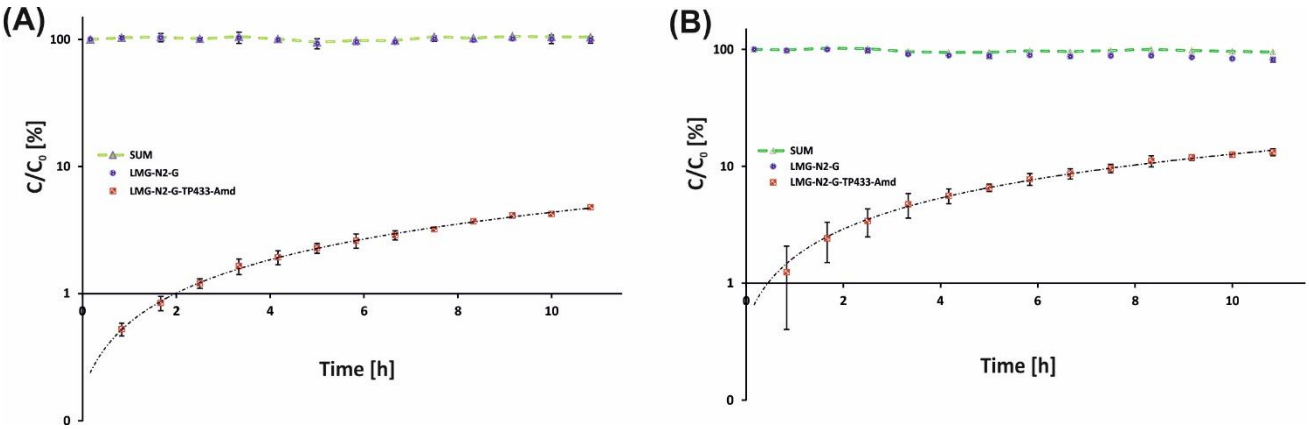

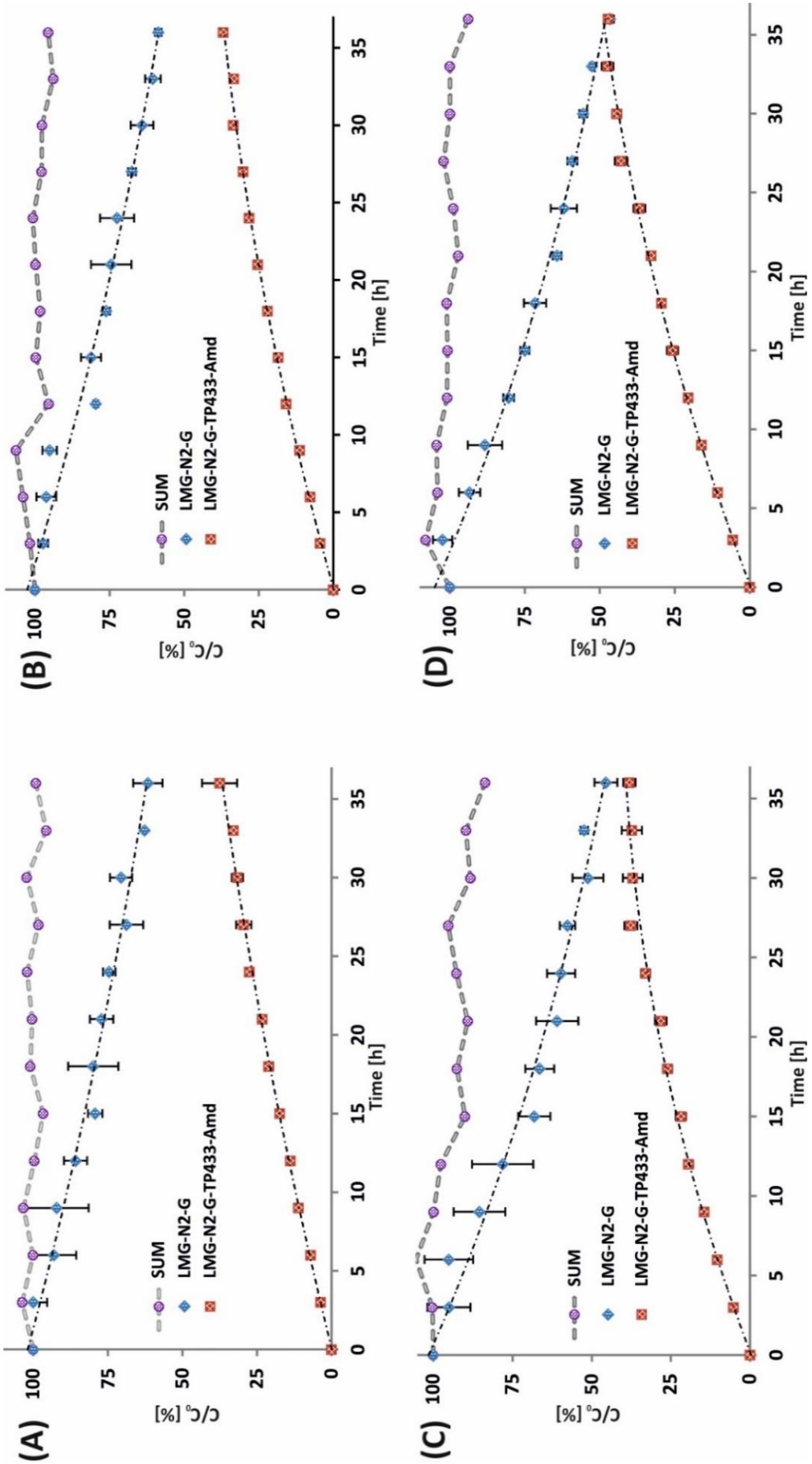

Figure SI-14. Mass balance of 200 nM of LMG-N2-G in HOSeff and WWinf at pH 8.5 with the free chlorine molar excess of 25 times. *(A) HOSeff , (B) HOSeff-free chlorine, (C) WWinf, (D) WWinf-free chlorine. Total degradation time was 36 hours.*

Figure SI-15. Degradation of 200 nM of LMG-N2-G at pH 8.5 with and without 25 molar excess of free chlorine (both filtered through 0.2 µm) and at pH 6.5 (filtered through 0.2 µm) in HOSeff (A) and WWinf (B). *Total degradation time was 36 hours.*

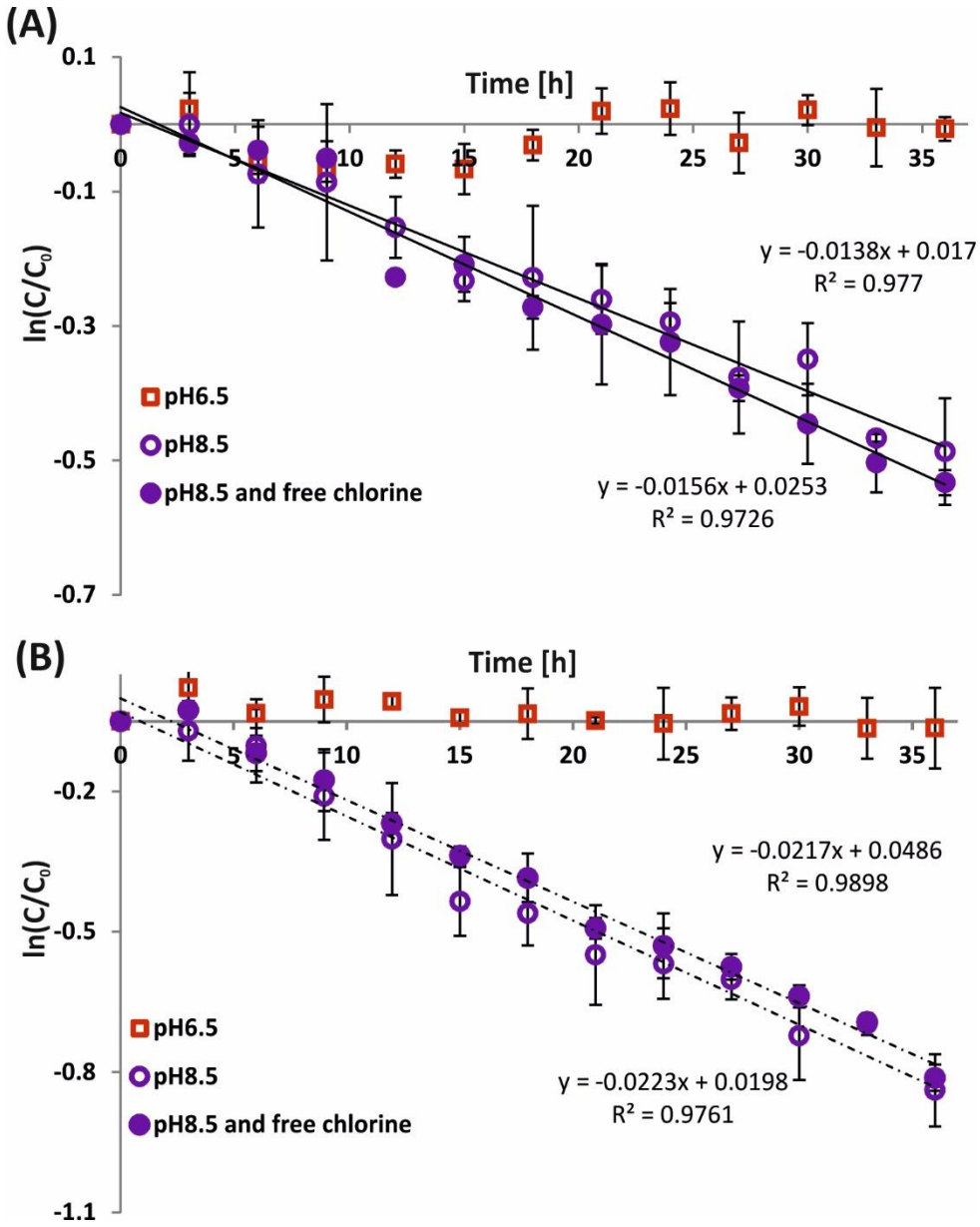

Figure SI-16. Degradation of 20 nM of LMG-N2-G at pH 9 with and without 250 molar excess of free chlorine and at pH 8 in HOSeff (A) and WWinf (B) (both filtered through 0.7 µm). *Total degradation time was 36 hours.*

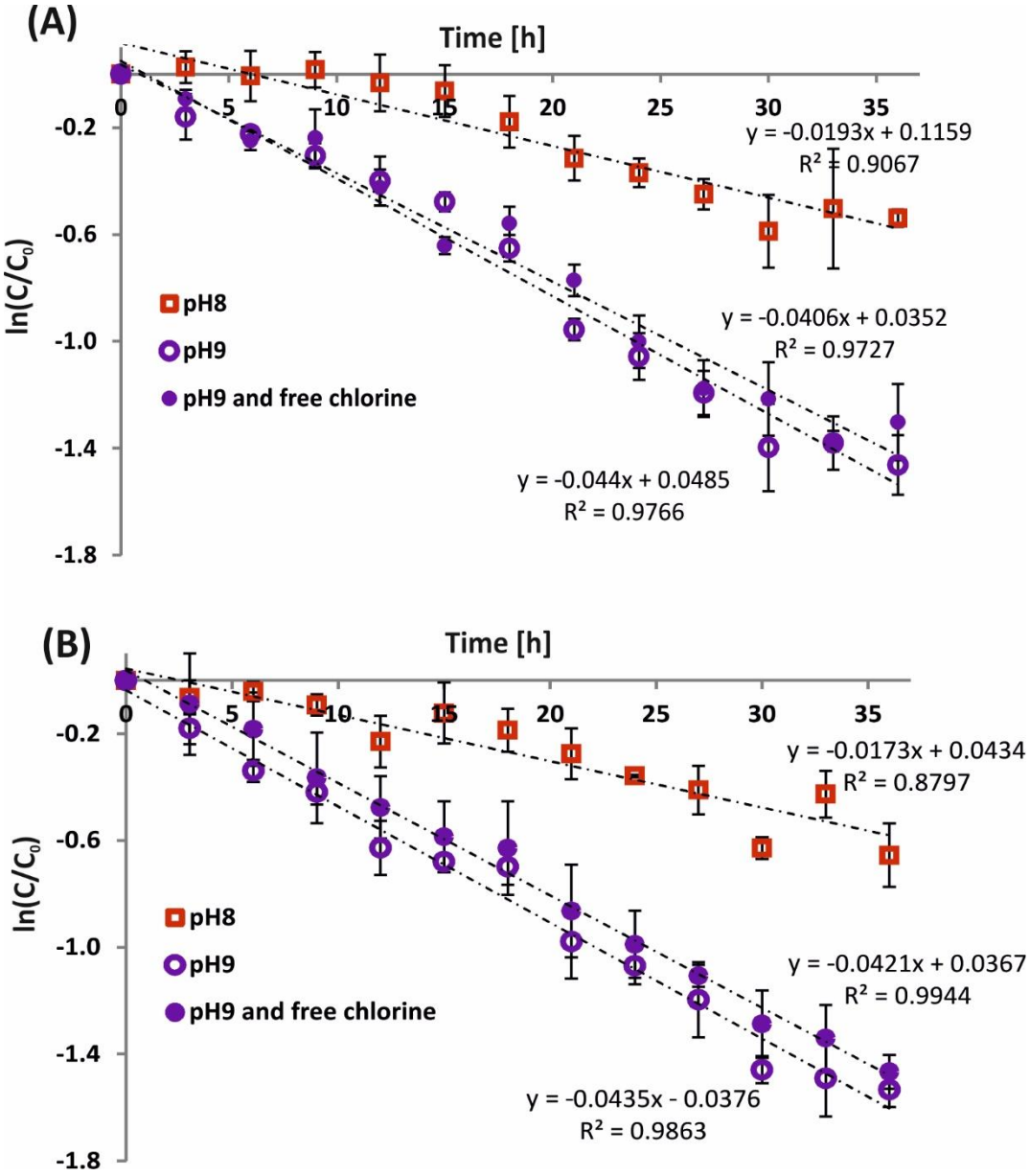

Determination of lamotrigine and its TPs in hospital wastewater

Method, recovery measurements and LOQ

Solid phase extraction (SPE), multiple generic cartridge method and LC-QExactive-MS analysis explained in Zonja et al.(Zonja et al. 2015, Zonja et al. 2016b) were applied here for the analysis of hospital effluents. For the SPE, all cartridges were conditioned using 5 mL of ethyl acetate – methanol (1:1) and 5 mL of water. Once the 100 mL of the sample (spiked with internal standard LMG-$^{13}C_3$) passed through the cartridges at flow rate of 10 mL min^{-1}, each cartridge was eluted separately. The elution of Oasis HLB and Bond Elute PPL cartridges was performed using 3x3 mL of ethyl acetate – methanol (1:1). The elution of the MAX and MCX cartridges was performed using first 3 mL of ethyl acetate – methanol (1:1), followed by 2x3 mL of 2 % formic acid in methanol for MAX and 5 % of ammonia in methanol for MCX. After the elution of all cartridges, all extracts were combined, evaporated using nitrogen and re-dissolved in 400 µL of mobile phase. Finally, a 20 µL aliquot was injected into LC-QExactive-MS.

The LC-QExactive-MS method was the same as in Zonja et al.(Zonja et al. 2016b) The chromatographic separation was achieved using Acquity-BEH C18 column (150 × 2.1 mm, 1.7 µm) preceded by a pre-column of the same packing material (5 × 2.1 mm, 1.7 µm). Mobile phases used were acetonitrile and water, both acidified with 0.1 % formic acid. Flow was set at 0.3 $mLmin^{-1}$, the column temperature was maintained at 40°C, and the total run was 25 min. For the detection method, a data dependent scan was used with the following parameters: resolution of 35 000 in both full scan and data-dependent MS^2, full scan range of m/z 100 – 1000 and normalised collision energy (NCE) of 35.

For recovery and LOQ determination (**Table SI-10**), non-integrate hospital effluent samples were used due to the high concentration of LMG-N2-G and other compounds in the samples analysed. The pH of the mixture was adjusted to 6.5 and then spiked with 250 ng of standard mix. All experiments were performed in triplicate following the procedure for analysis of hospital effluent samples.

Recovery was calculated as the difference between the concentration after the SPE and the blank sample divided with spiked concentration.

The compound was determined if it matched retention time of the standard (+/- 0.2 min), exact mass accuracy (<5 ppm) and relative chlorine isotope pattern which was calculated for every compound and sample.

LOQ values were calculated as signal-to-noise ratio (S/N) higher than 10. <LOQ was reported for compounds where the identification rules applied but the S/N was lower than 10.

Results of Hospital effluent samples

Table SI-10. Results of the 24 hour integrate hospital effluent samples.

ngL^{-1}	LMG-N2-G	LMG-N2-G TP433-Amd	LMG-N2-G TP433-Gnd	LMG	OXO-LMG
Monday	790	134	n.d.	130	13
Tuesday	1741	357	17	260	26
Wednesday	241	7.4	n.d.	143	75
Thursday	499	162	n.d.	128	50
Friday	155	5.4	n.d.	17	2.2
Saturday	253	169	5.4	44	9.4
Sunday	389	17	n.d.	13	2.5
Recovery [%]	116 ± 15	109 ± 4	TP433-Amd	106 ± 9	119 ± 9
LOQ [ngL^{-1}]	1.0	2.1	TP433-Amd	12	1.5
RT [min]	4.68	5.55	5.14	6.31	6.85

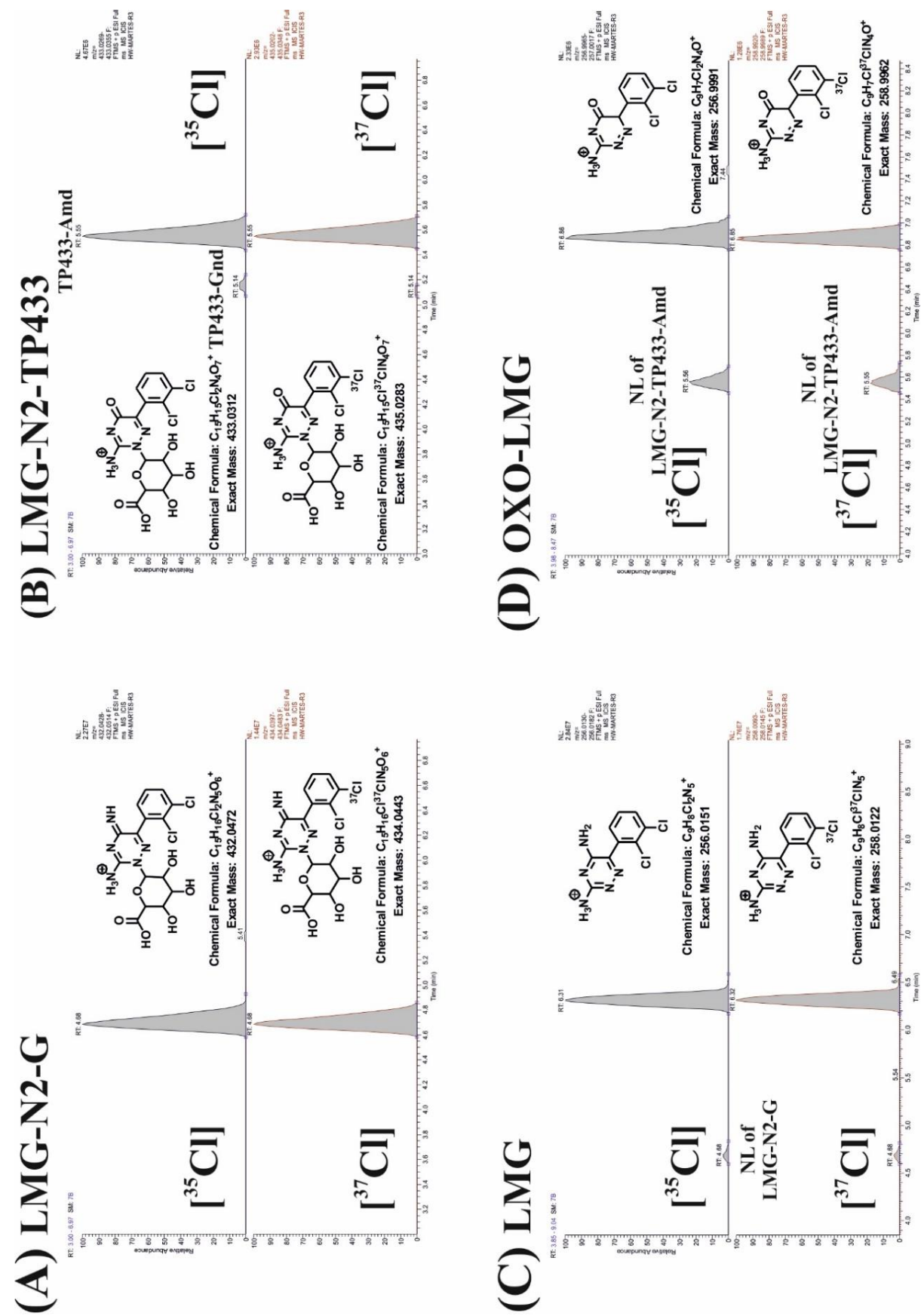

Figure SI-17. Chromatograms of LMG-N2-G TPs quantified in hospital wastewater

III. N2-METHYL-LAMOTRIGINE (N2-Me-LMG)

pH EXPERIMENTS - degradations in UPW @pH 4 – 9

Results of the stability of N2-Me-LMG in pure water at pH 4-8 are shown in **Figure SI-18**. As can be seen from the figure, over the course of 42 hours no apparent change of concentration of N2-Me-LMG is seen for pH 4-7. On the other hand, at pH 8, a slight decrease can be seen. A slightly more rapid degradation occurs at pH 9 (**Figure SI-19**). Once the peak deconvolution and extraction was performed with SIEVE (Thermo Fisher, Bremen, Germany) for the experiment at pH 9, three different peaks were detected. Two had the m/z 271.0148 (RT 2.57 and 2.73 min) and one had the m/z 288.0413 (RT 2.04 min). The formation of the detected compounds for pH 9 was plotted (normalized to the initial concentration of the N2-Me-LMG) against degradation time and using N2-Me-LMG as a reference standard (**Figure SI-19**). Disappearance of N2-Me-LMG is principally caused by transformation to N2-Me-LMG-TP271-Amd, N2-Me-LMG-TP271-Gnd and N2-Me-LMG-TP288-Gmd. At the end of degradation, passed the 42 h and at pH 9, N2-Me-LMG-TP271-Amd reached 5.9 %, N2-Me-LMG-TP271-Gnd 1.6 % and N2-Me-LMG-TP288-Gmd 0.3 % of the initial N2-Me-LMG concentration. Stability of N2-Me-LMG-TP271-Amd was assessed from a mixture at pHs 4-7 with no significant decrease in concentration which could suggest a reversible reaction (**Figure SI-20**).

Figure SI-18. Degradation of 400 nM of N2-Me-LMG in UPW at pH 4-8 over the course of 42 hours.

The point on the graph corresponds to the average measurement of the three pHs with the error bars representing deviation

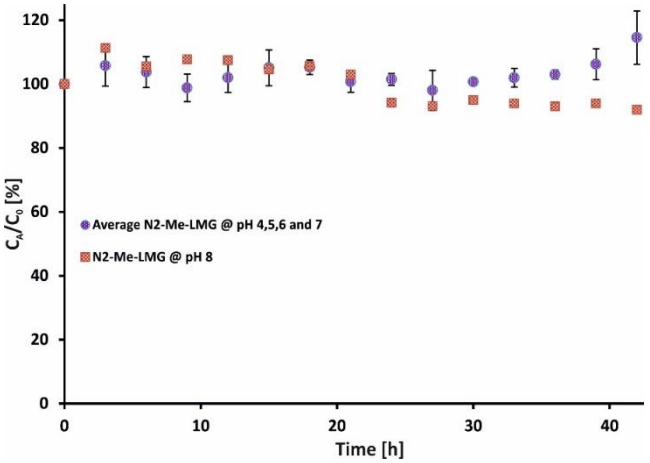

Figure SI-19. Degradation of 400 nM of N2-Me-LMG and mass balance in UPW at pH 9 over the course of 42 hours.

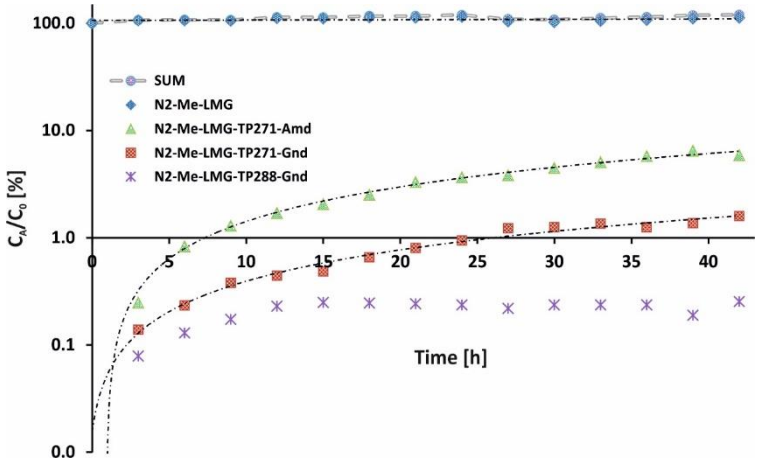

Figure SI-20. Stability of approximately 400 nM of N2-Me-LMG in UPW at pH 4-7 over the course of 39 hours.

The point on the graph corresponds to the average measurement of the three pHs with the error bars representing deviation

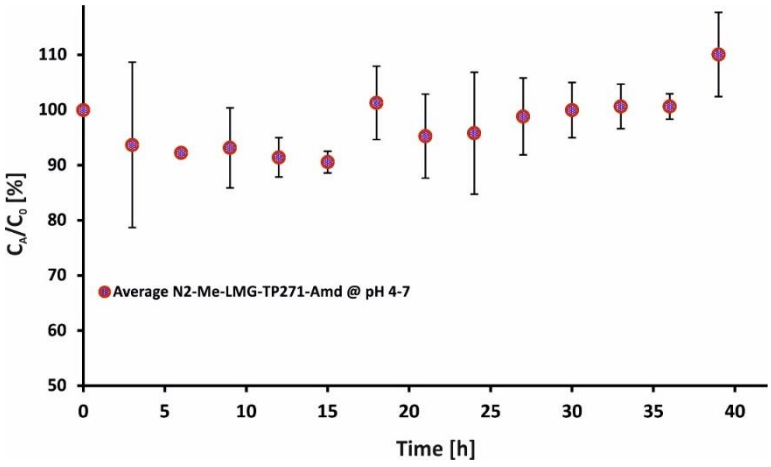

Synthesis of N2-Me-LMG and identification via NMR

N2-Me-LMG was synthesized with minor modifications according the procedure described by Manning et al.(Manning et al. 2002) as mentioned in the manuscript text.

Thus, lamotrigine obtained from a commercial drug source (GSK, Brentford, Middlesex, United Kingdom) was purified by flash chromatography (SiO_2: residue 40:1) performing a stepwise gradient of MeOH in CH_2Cl_2 from 0 to 10 %. This pure compound (129 mg, 0.5 mmol) was treated with an excess of methyl iodide (4 equivalent) in acetone (20 mL) for 24 h, concentrated to dryness and digested with concentrated aq. NH_3 (2 mL) for 4 h. The resulting reaction mixture was directly sown in a flash chromatography column (of SiO_2, 15 g) and the expected methyl derivative of the lamotrigine purified using a stepwise gradient of MeOH in CH_2Cl_2 from 0 to 16 % to afford 128 mg of the wanted product (93 % yield).

The NMR spectra are shown in **Figure SI-21** which include ^1H, DQCOSY, ^{13}C, DEPT (CH/CH_3 UP; CH_2 DOWN; C ANTIPHASE), DEPT (CH UP & C ANTIPHASE) and HSQC spectra.

Chemical shifts are expressed in ppm and constant couplings (J) are expressed in Hertz (Hz). CD_3OD chemical shifts have been used as internal references. When splitting patters could not be interpreted or correctly visualized, they are described as multiplet (m).

^{1}H NMR (400 MHz, CD_3OD): 7.77 (dd, J_1= 6.5 Hz, J_2=3 Hz, 1H), 7.55-7.47 (m, 2H), 3.86 (s, 3H);

^{13}C NMR (100 MHz, CD_3OD): 157.4 (C), 156.0 (C), 140.3 (C), 134.8 (C), 133.9 (CH), 133.1 (C), 133.0 (C), 131.3 (CH), 129.9 (CH), 43.2 (CH_3).

Figure SI-21. Nuclear Magnetic Resonance spectra used for identification of N2-Me-LMG; (A) ^{1}H NMR; (B) DQCOSY; (C) ^{13}C NMR; (D) DEPT (CH/CH_3 UP; CH_2 DOWN; C ANTIPHASE); (E) DEPT (CH UP & C ANTIPHASE); (F) HSQC.

(A) ^{1}H NMR

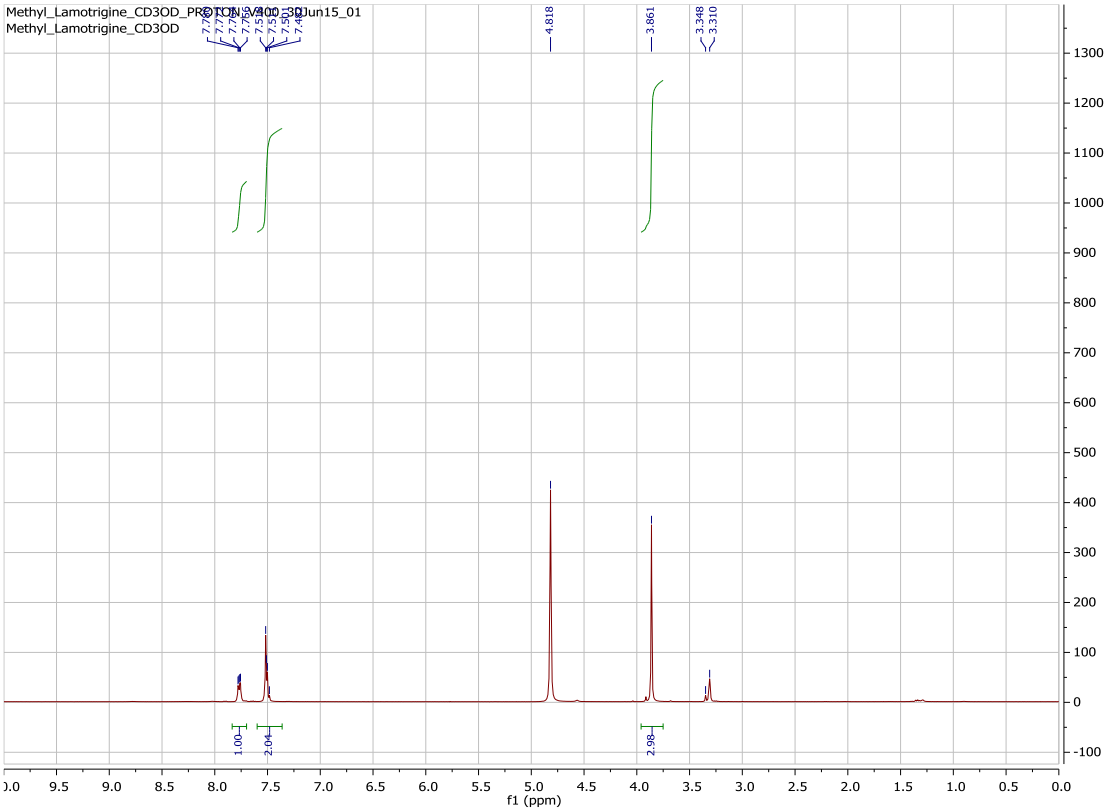

(B) DQCOSY

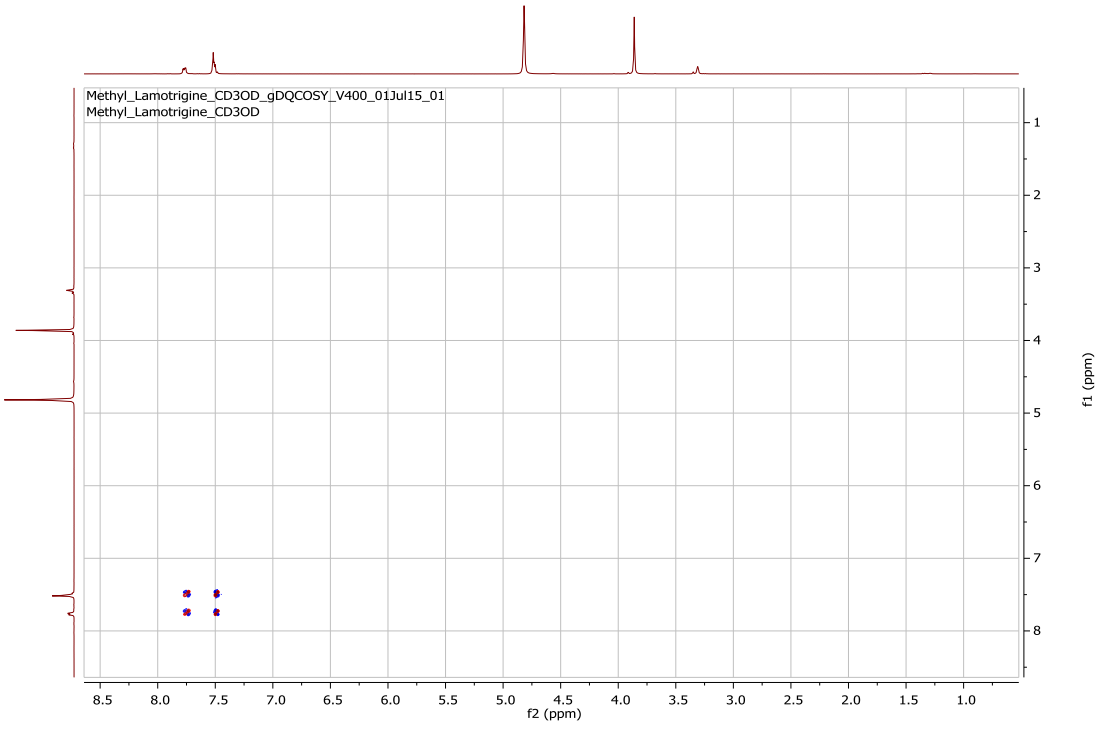

(C) ^{13}C NMR

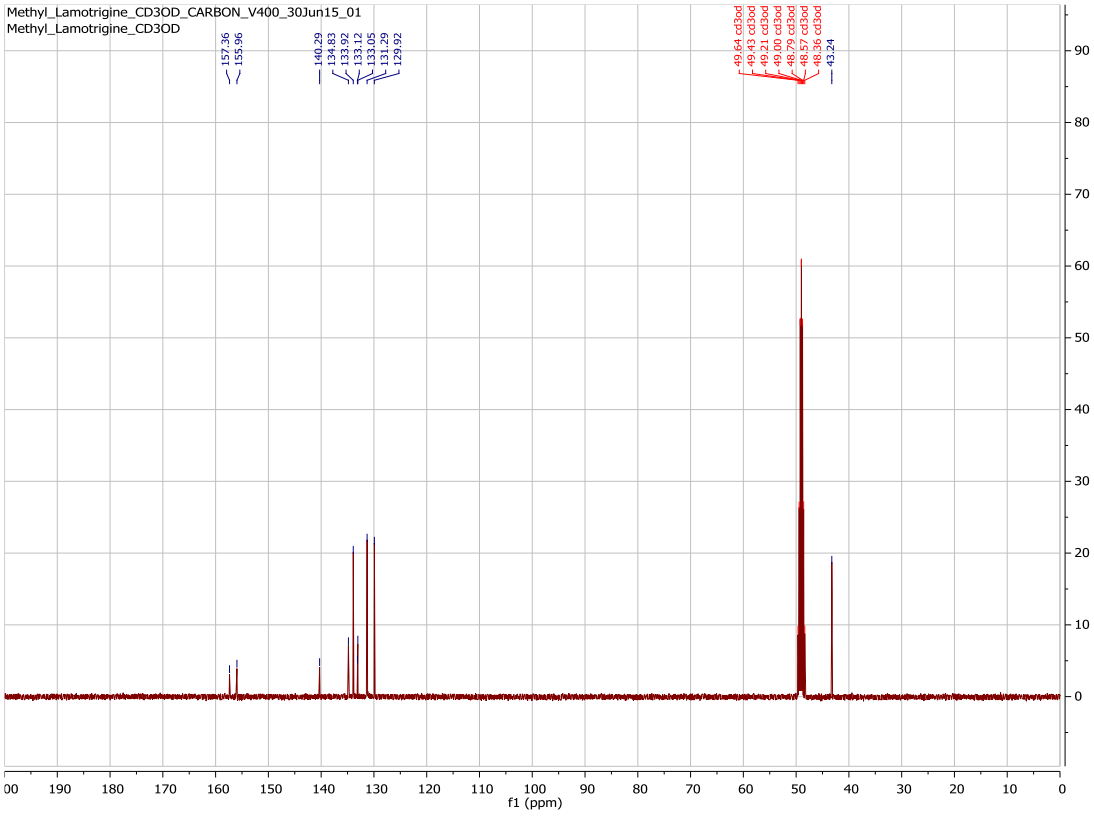

(D) DEPT (CH/CH$_3$ UP; CH$_2$ DOWN; C ANTIPHASE)

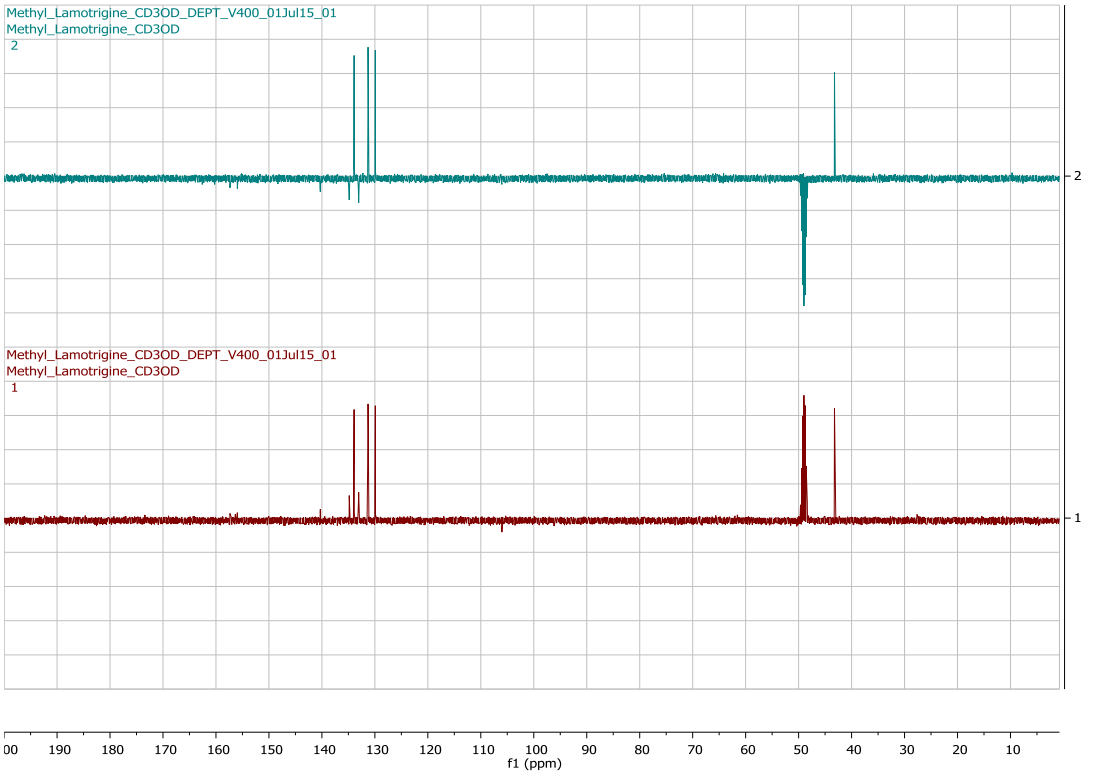

(E) DEPT (CH UP & C ANTIPHASE)

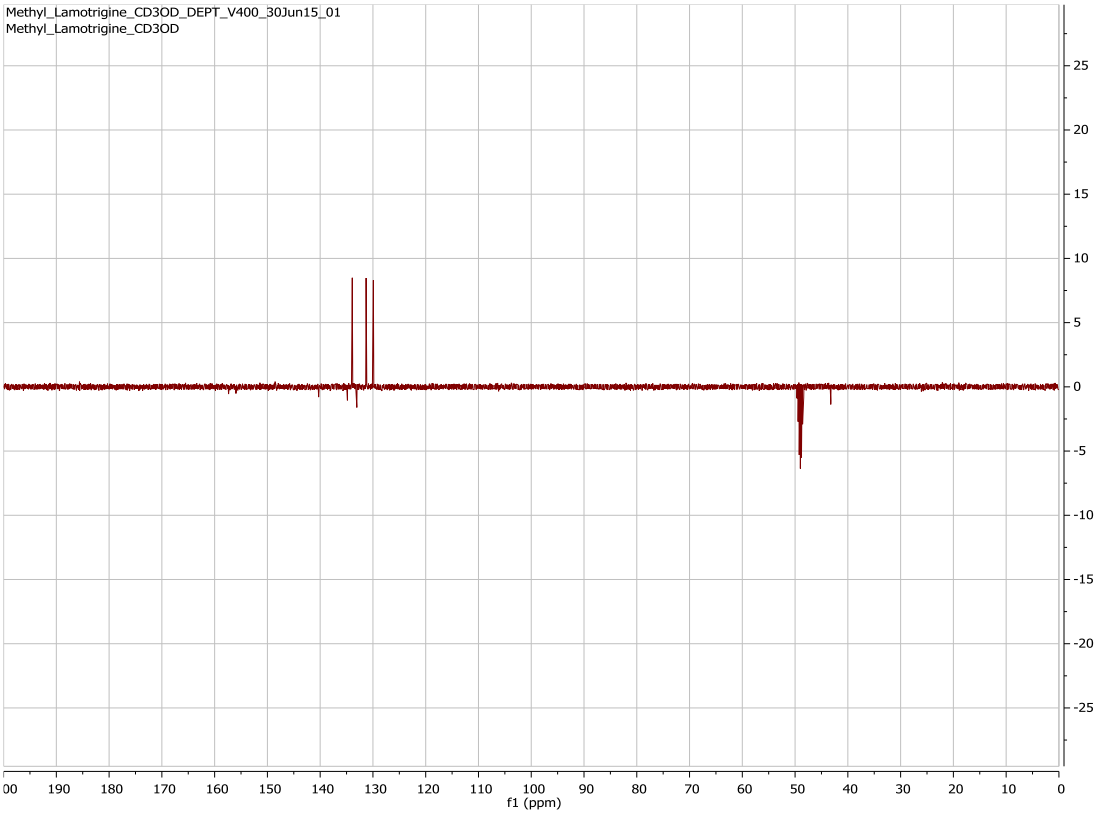

(F) HSQC

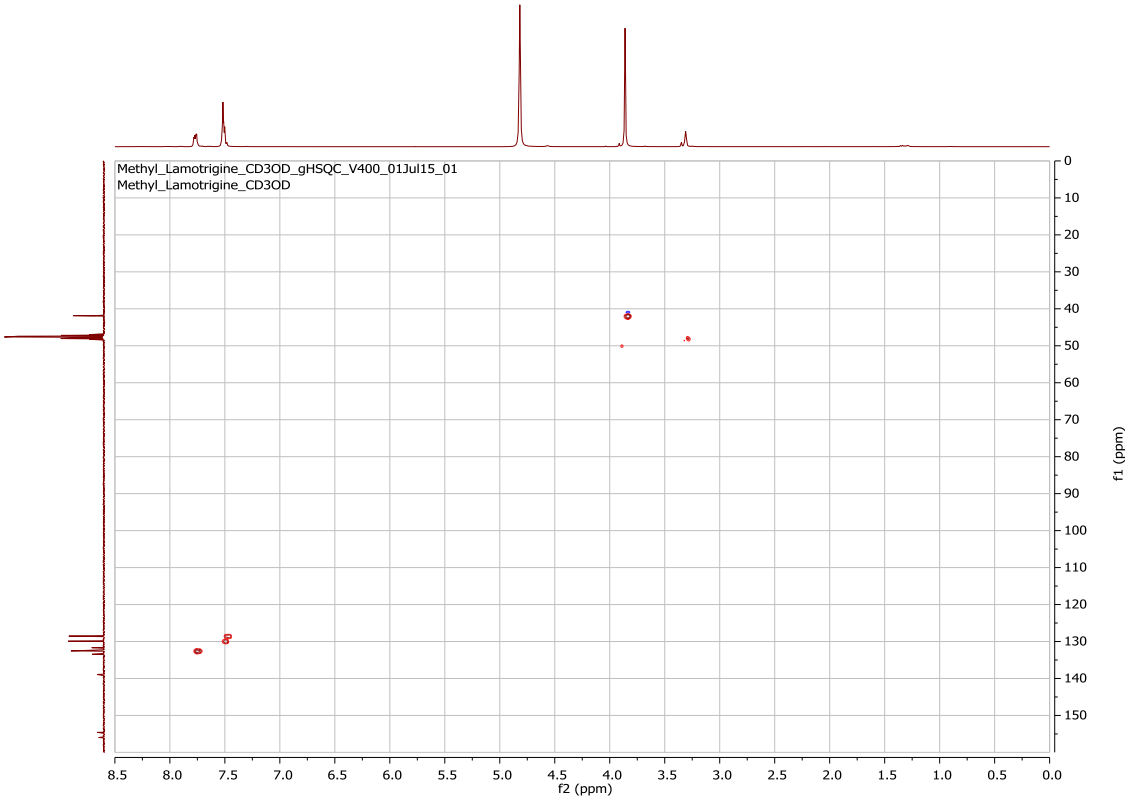

Identification of N2-Me-LMG and TPs with HRMS

Similarly, as for LMG-N2-G TPs, TPs of N2-Me-LMG were also studied using LC-QExactive-MS. For the identification of transformation products, the MS^2 and pseudo-MS^3 (pMS^3) product ion spectra of the parent compounds N2-Me-LMG and TPs were recorded to determine the plausible elemental compositions and structures of the fragment ions (see **Table SI-11** for elemental compositions and **Figures SI-22** for the fragmentation pathways and spectra). Method used and general observations on the fragmentation pattern and spectra recorder can be found in supporting information section "*Identification of LMG-N2-G TPs with the combination of MS*" on the page SI-8.

The same as with LMG-N2-G, N2-Me-LMG was transformed into three TPs. Two of them were the result of amidine and guanidine hydrolysis, N2-Me-LMG-TP271-Amd (RT 3.81 min) and N2-Me-LMG-TP271-Gnd (RT 4.01 min), respectively. The third TP was an intermediary product of guanidine hydrolysis, N2-Me-LMG-TP288-Gnd (RT 3.24 min).

N2-Me-LMG, parent to these three compounds, eluted at RT 3.55 and had the m/z 270.0308 with elemental composition $C_{10}H_{10}Cl_2N_5^+$. The MS^2 spectrum (**Figure SI-22.1**) of N2-Me-LMG shows similar fragmentation as LMG and OXO-LMG with initial deamination from the position **3** of the molecule of 1,2,4-triazine moiety. Subsequently, the parent molecule also loses methylamine (- 27.0109) from position **5** of 1,2,4-triazine moiety to yield m/z 243.0199 ($C_9H_9Cl_2N_4^+$). Loss from position **5** was also seen in the LMG as well as OXO-LMG to yield m/z 229.0042, a demethylated form of N2-Me-LMG fragment m/z 243.0199. The pMS^3 spectrum of this fragment shows subsequent deamination together with ring reduction, a pattern already seen in the analysis of OXO-LMG and LMG-N2-G-TPs433 and described in the main text of the manuscript. Another fragment, diagnostic to the position of methyl is the m/z 234.0541 ($C_{10}H_9ClN_5^+$). This fragment is formed as a result of loss of hydrochloric acid (- 35.9766) followed by ring closure via amine in the position **5**. If the methylation had occurred in the position N5, no ring closure would be expected to occur (similar to the formation of fragment m/z 194.0354 in the pMS^3 spectrum of m/z 256.9991 for LMG-N2-G-TP433-Amd).

As can be seen from **Figure SI-22.3-A** and **B**, MS^2 spectra of both N2-Me-LMG TPs with the m/z 271.0148 when compared show the significant difference as to how these two compounds fragment. Both spectra are comparable with the pMS^3 fragmentation of m/z 256.9991 in the molecules of LMG-N2-G-TPs433 (Figure SI-4) which served as basis for elucidation whether the product is a result of amandine or guanidine hydrolysis of N2-Me-LMG. As to identification of N2-Me-LMG-TP271-Amd, a diagnostic fragment m/z 243.0199 was identified. This fragment was

the result of a loss of carbonyl and gradual deamination (together with losses of N2-methyl, specific for this compound only), as in the MS^2 spectrum of OXO-LMG and pMS^3 spectrum of *m/z* 256.9991 from LMG-N2-G-TP433-Amd. On the other hand, N2-Me-LMG-TP271-Gnd had similar fragmentation as *m/z* 256.9991 in the LMG-N2-G-TP433-Gnd. Again, two diagnostic fragments were identified in the spectrum. The first one is the fragment *m/z* 235.0981 with elemental composition $C_{10}H_8ClN_4O^+$ (its counterpart in TP433-Gnd is *m/z* 221.0225 ($C_9H_6ClN_4O^+$)) which is the result of loss of hydrochloric acid (- 35.9766) followed by ring closure via amine in the position **5**. Similar as in OXO-LMG, in N2-Me-LMG-TP271-Amd this fragment is not found since it inhibited by the replacement of the amino group by oxygen where only radical dechlorination is seen (*m/z* 208.0510; $C_9H_9ClN_4^{\cdot+}$ - TP433-Gnd counterpart *m/z* 194.0354; $C_8H_7ClN_4^{\cdot+}$). The second diagnostic fragment in the MS^2 spectrum of *m/z* 271.0148-Gnd is the fragment with the *m/z* 244.0039 ($C_9H_8Cl_2N_3O^+$) which has a counterpart in the MS^2 of *m/z* 271.0148-Amd (*m/z* 243.0199; $C_9H_9Cl_2N_4^+$). Comparison of the two shows that there is a mass difference of 0.984 (the same as in pMS3 spectra of *m/z* 256.9991-Amd and *m/z* 256.9991-Gnd of LMG-N2-G-TPs433). While the N2-Me-LMG-TP271-Amd loses carbonyl from position **5,** N2-Me-LMG-TP271-Gnd loses methylamine from the same position of the 1,2,4-triazine moiety forming the fragment *m/z* 244.0039 had retained the oxygen (as opposed to N2-Me-LMG-TP271-Amd fragment *m/z* 243.0199; $C_9H_9Cl_2N_4^+$). Finally, as in the degradation of LMG-N2-G, apart from Amd and Gnd hydrolysis products, another N2-Me-LMG-TP was detected with the *m/z* 288.0413. This *m/z* defers by one hydroxyl group (+ 17.0266; OH) from N2-Me-LMG. MS^2 (**Figure SI-22.2**) of *m/z* 288.0413 showed that this compound fragments principally to *m/z* 271.0148 (loss of ammonia), *m/z* 245.0355 (loss of HNCO). This is followed by subsequent gradual deamination to form *m/z* 228.0090 ($C_9H_8Cl_2N_3^+$) and 200.9981 ($C_8H_7Cl_2N_2^+$). These fragments again suggest hydroxylation of amidine or guanidine moiety which would make it an intermediary product in the process of amidine or guanidine hydrolysis. In order to verify which of the two possible TPs the TP288 was, its spectra were compared to the ones of N2-Me-LMG-TP271-Amd and Gnd. As can be seen from the **Figure SI-22.2-B**, MS2 spectrum of *m/z* 288.0413 fragmented to a diagnostic fragment *m/z* 228.0090 ($C_9H_8Cl_2N_3^+$) which was the result of loss of double loss of ammonia and the loss of carbonyl. If it had been for the molecule to be a product of an amidine hydrolysis this fragment should have been 227.9964 ($C_8H_6Cl_2N_4^{\cdot+}$). This would make this TP with *m/z* 288.0413 N2-Me-LMG-TP288-Gnd an intermediary in the formation of N2-Me-LMG-TP271-Gnd.

N2-METHYL-LAMOTRIGINE (N2-Me-LMG)

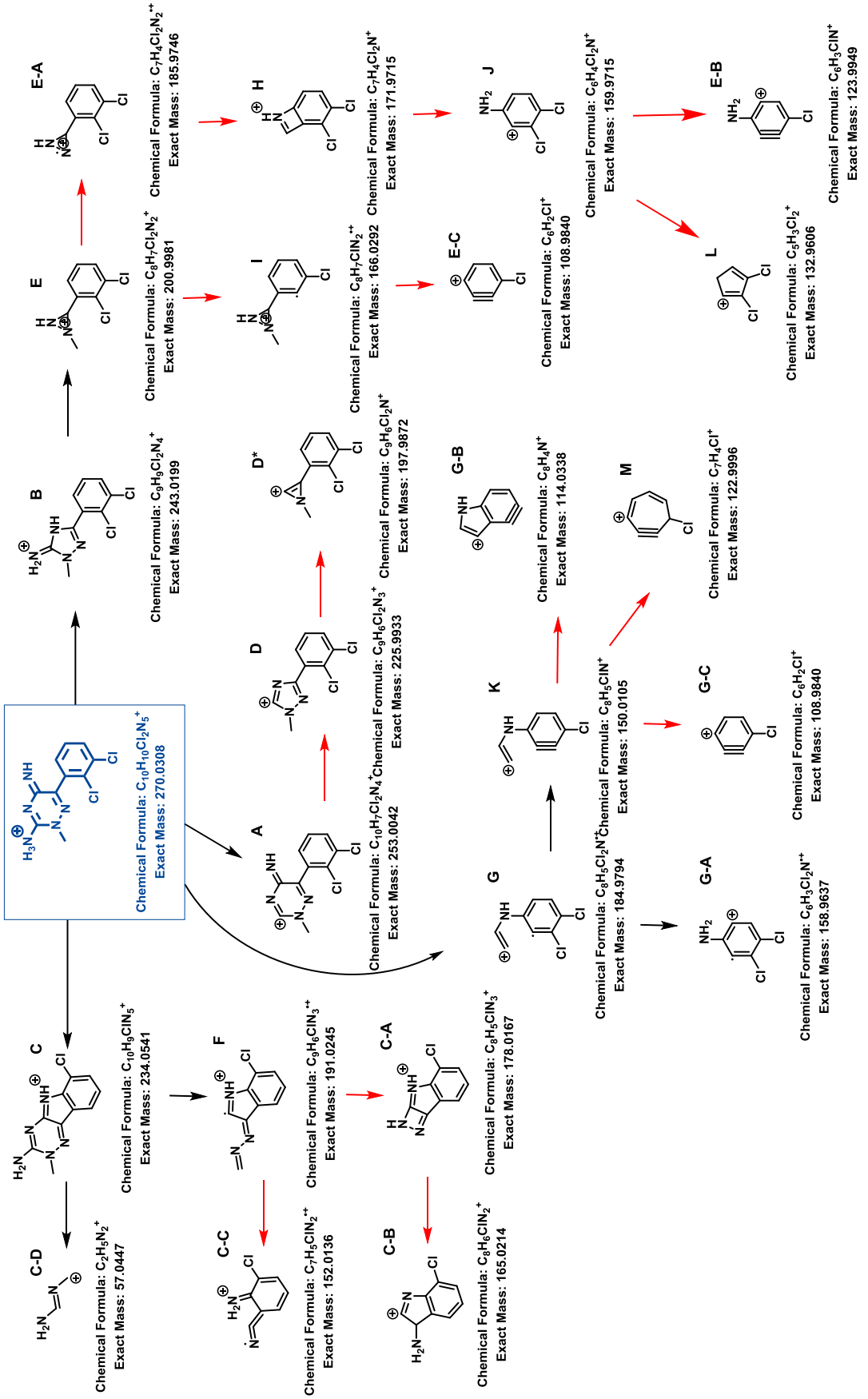

Figure SI-22.1-A. Fragmentation pattern of N2-Me-LMG

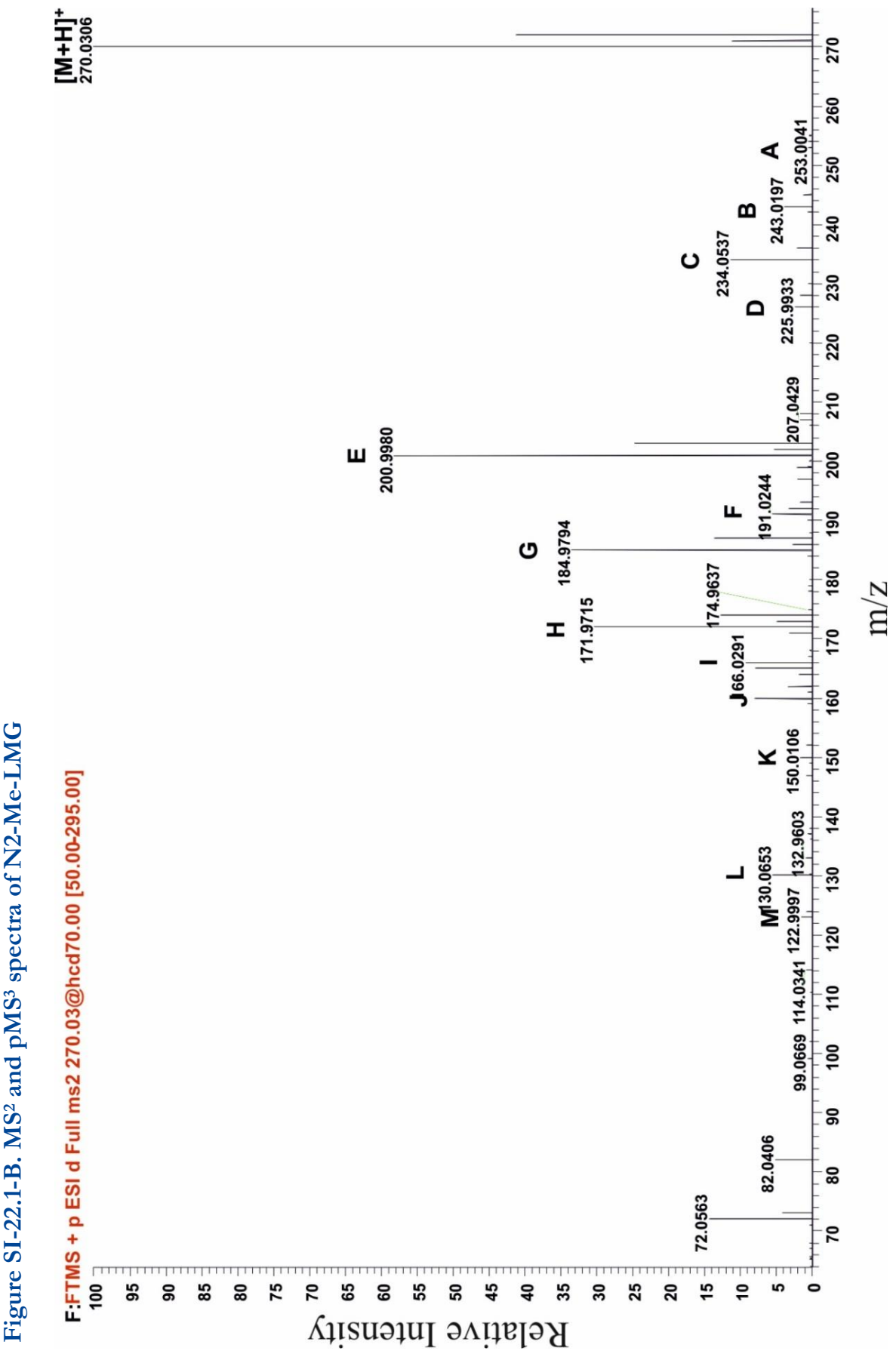

Figure SI-22.1-B. MS^2 and pMS^3 spectra of N2-Me-LMG

Figure SI-22.1-B. MS^2 and pMS^3 spectra of N2-Me-LMG – *continued*

N2-Me-LMG – 243 pMS^3

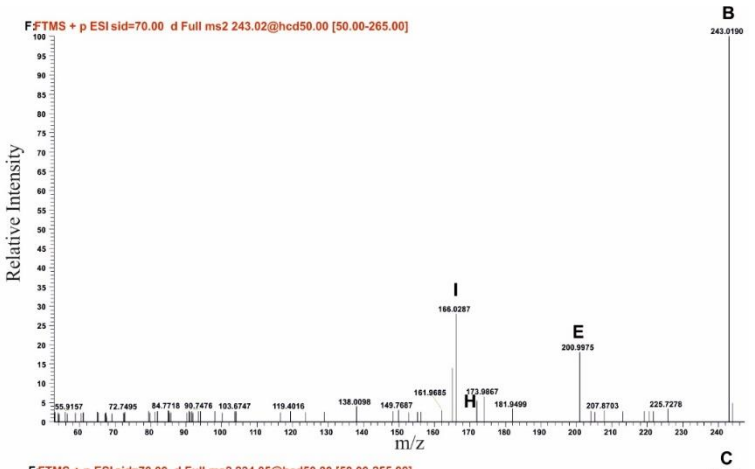

N2-Me-LMG – 234 pMS^3

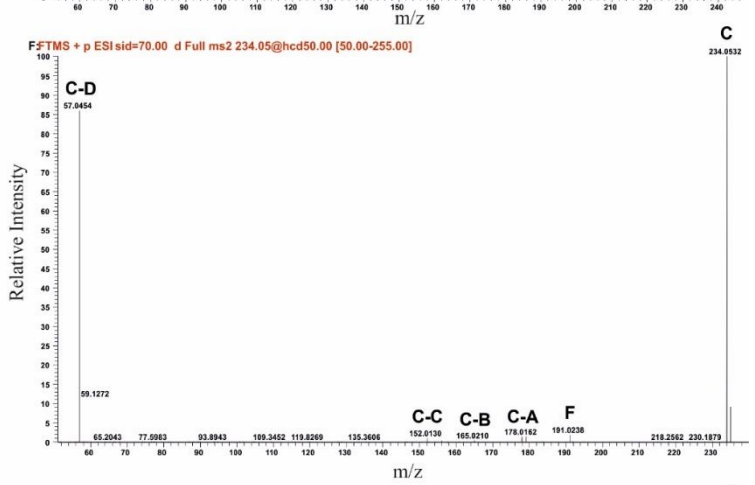

N2-Me-LMG – 200 pMS^3

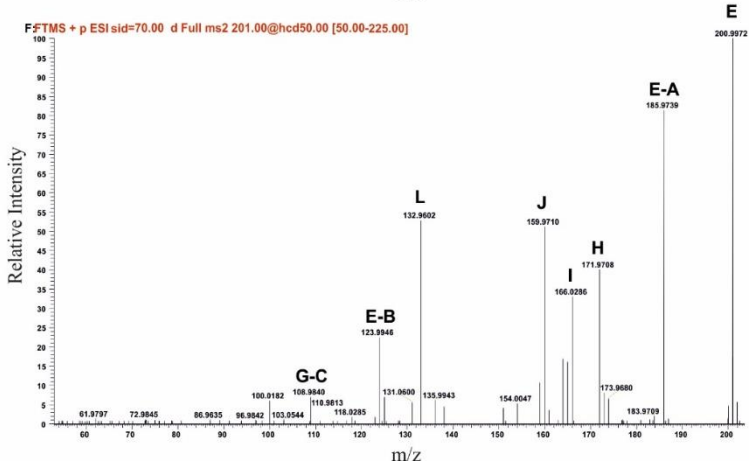

N2-Me-LMG – 184 pMS^3

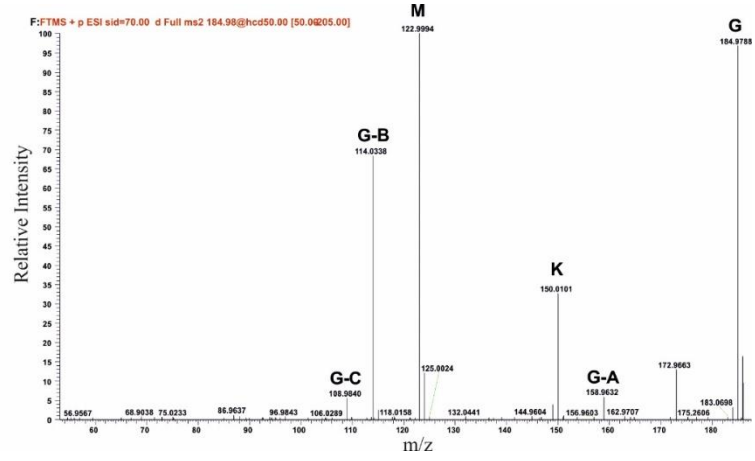

N2-METHYL LAMOTRIGINE-TP288-guanidine (N2-Me-LMG -TP288-Gnd)

Figure SI-22.2-A. Fragmentation pattern of N2-Me-LMG-TP288-Gnd

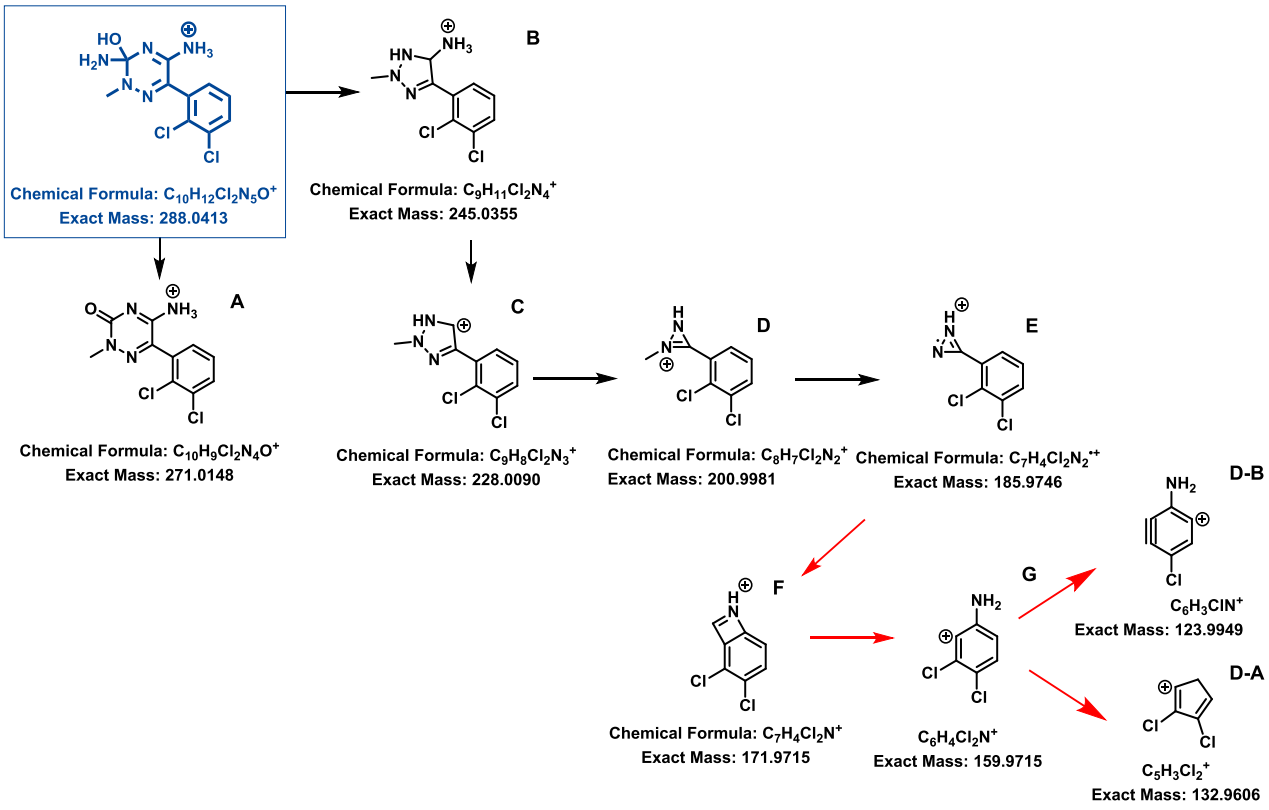

Figure SI-22.2-B. MS^2 and pMS^3 spectra of N2-Me-LMG-TP288-Gnd

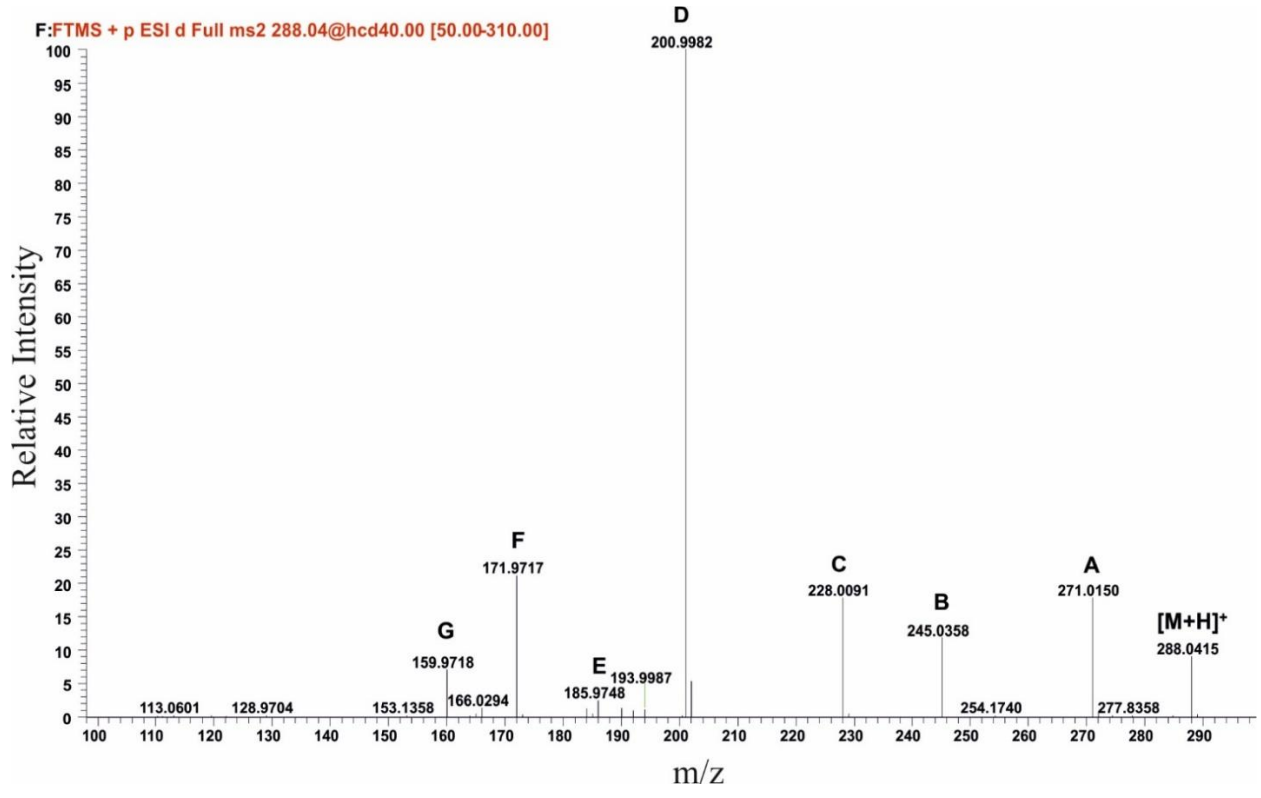

Figure SI-22.2-B. MS^2 and pMS^3 spectra of N2-Me-LMG-TP288-Gnd – *continued*

N2-Me-LMG
TP288 – 245 pMS^3

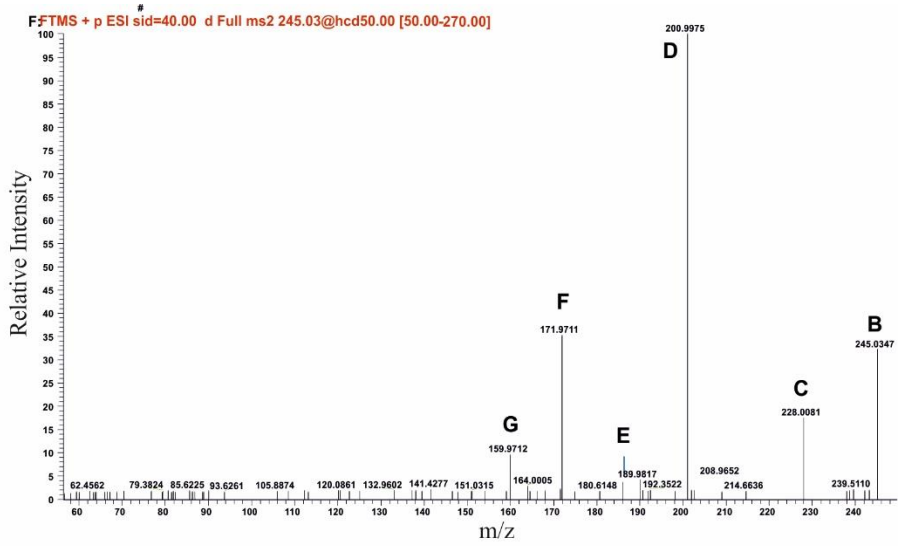

N2-Me-LMG
TP288 – 228 pMS^3

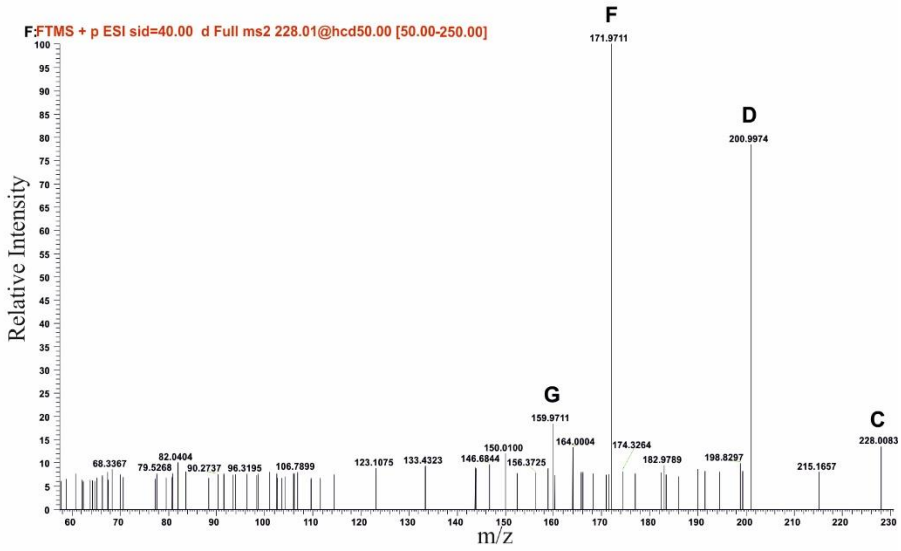

N2-Me-LMG
TP288 – 200 pMS^3

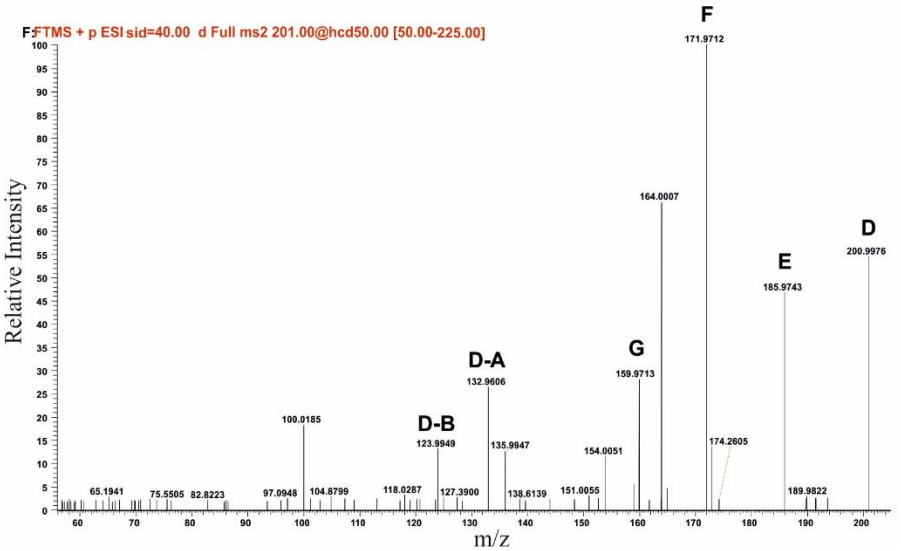

N2-METHYL LAMOTRIGINE TP271 amidine and guanidine (N2-Me-LMG-TP271-Amd and Gnd)

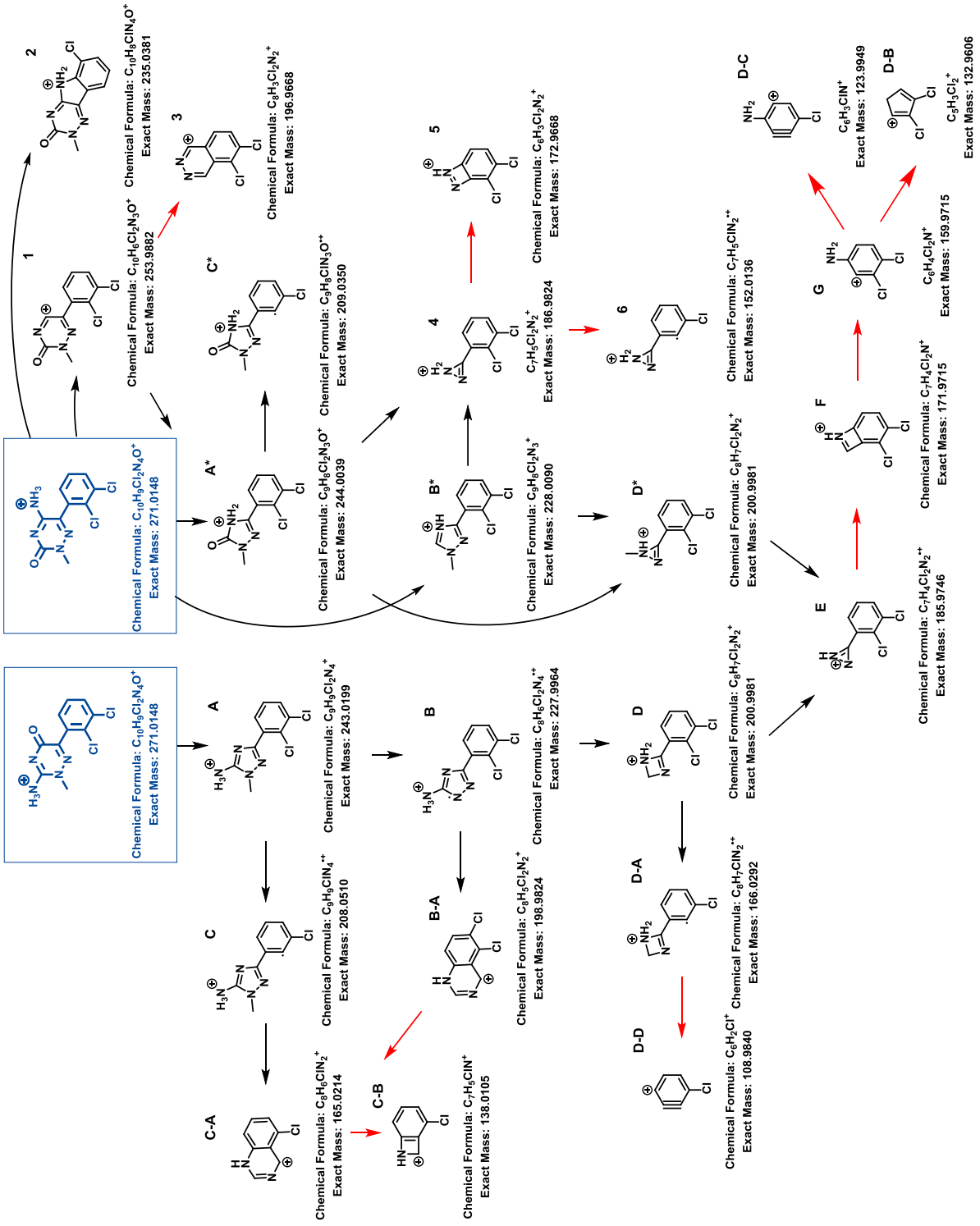

Figure SI-22.3-A. Fragmentation pattern of N2-Me-LMG-TP271 - Amd and Gnd

Figure SI-22.3-B. MS^2 and pMS^3 spectra of N2-Me-LMG-TP271-Amd and Gnd

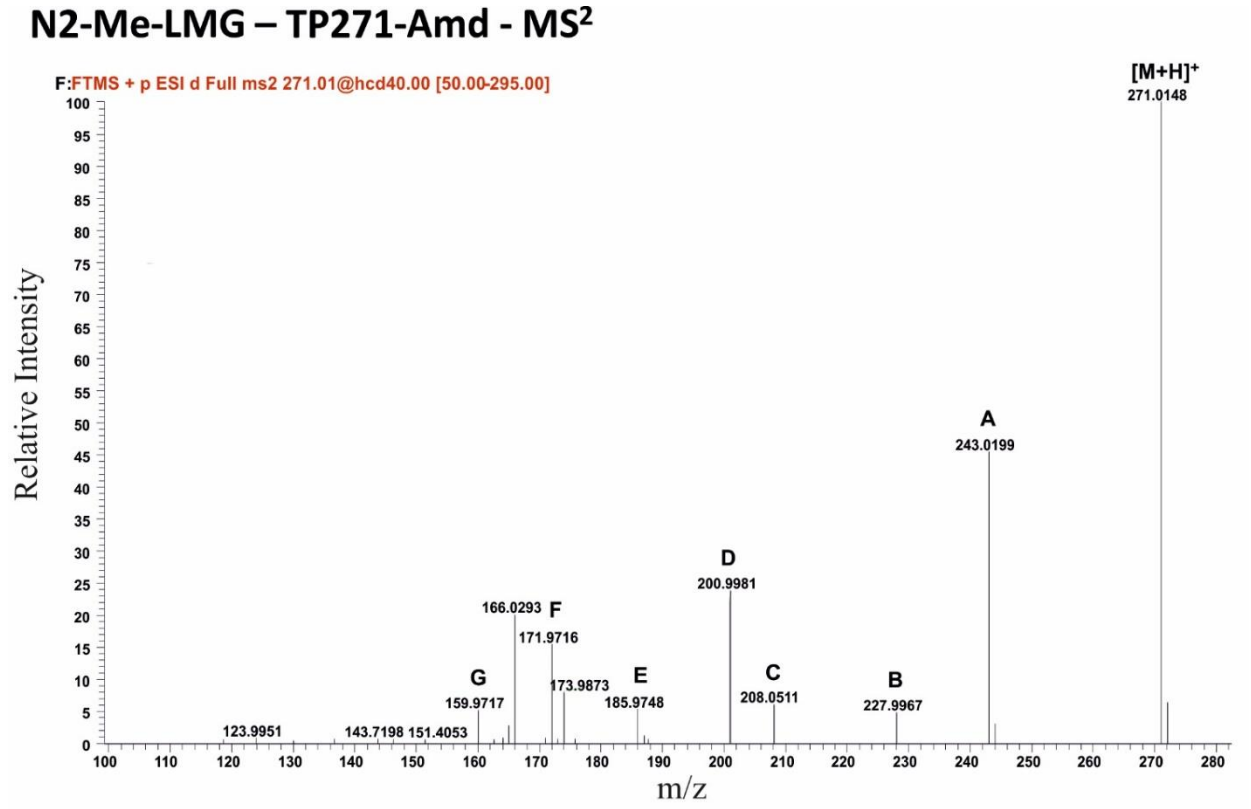

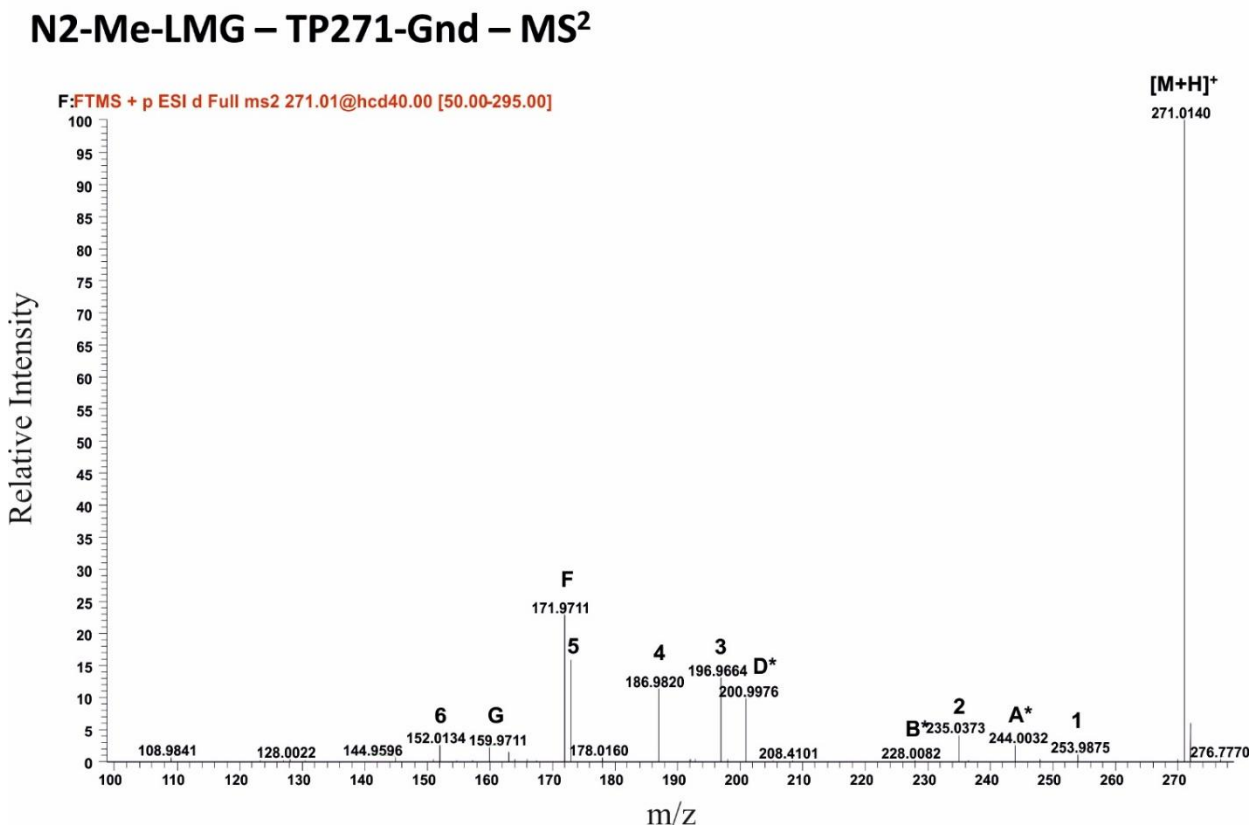

Figure SI-22.3-B. MS^2 and pMS^3 spectra of N2-Me-LMG-TP271-Amd and Gnd – *continued*

N2-Me-LMG
TP271-Amd – 243 pMS^3

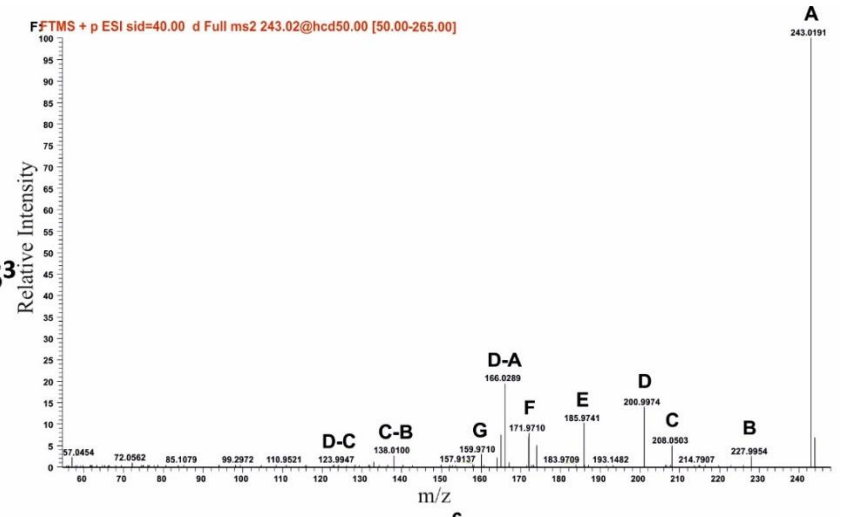

N2-Me-LMG
TP271-Gnd – 243 pMS^3

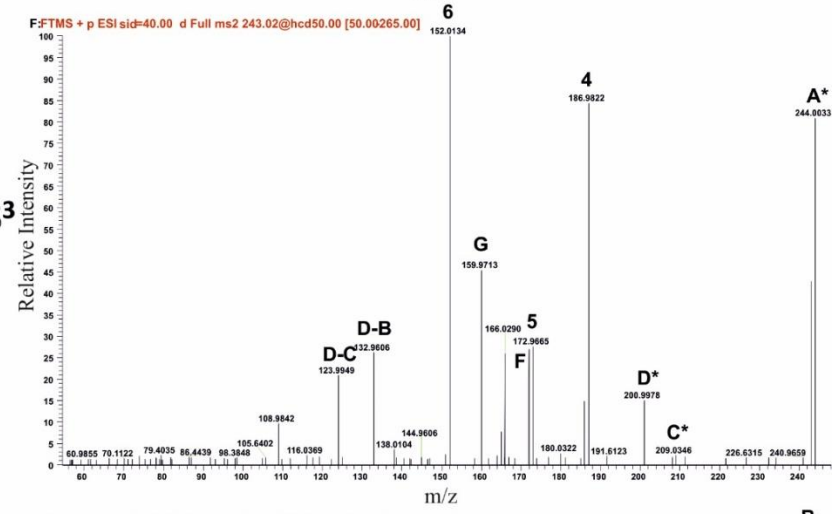

N2-Me-LMG
TP271-Amd – 227 pMS^3

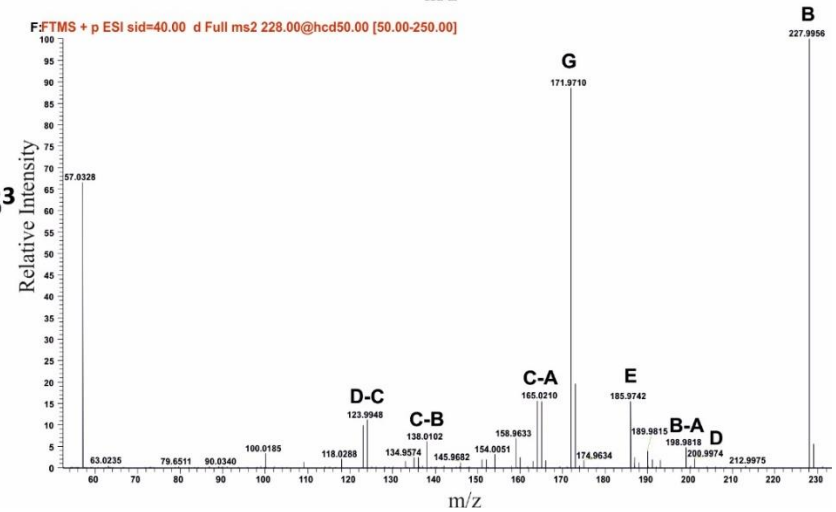

Figure SI-22.3-B. MS^2 and pMS^3 spectra of N2-Me-LMG-TP271-Amd and Gnd – *continued*

N2-Me-LMG
TP271 -Gnd– 228 pMS^3

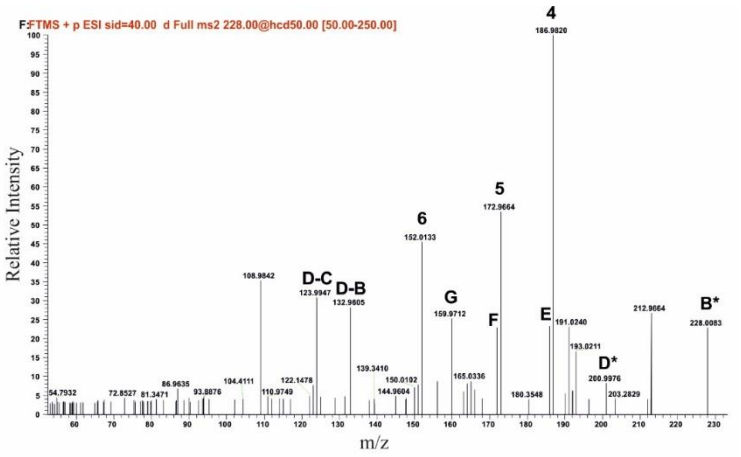

N2-Me-LMG
TP271-Amd – 200 pMS^3

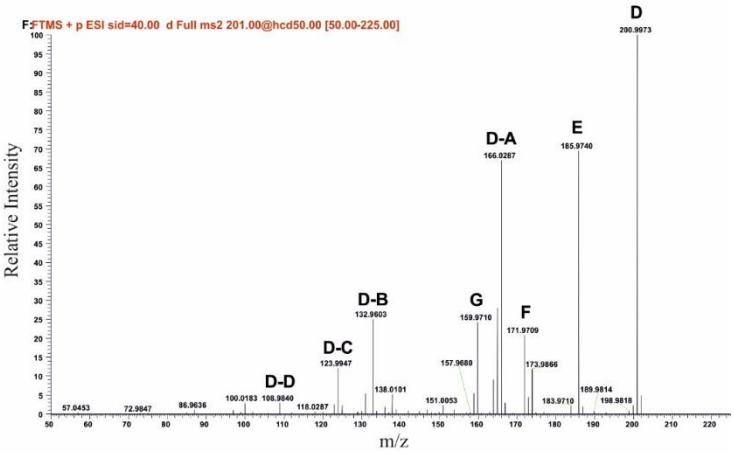

N2-Me-LMG
TP271-Gnd – 200 pMS^3

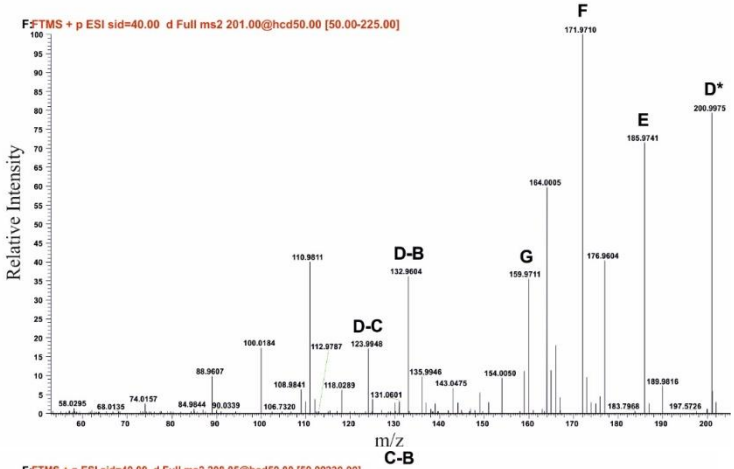

N2-Me-LMG
TP271-Amd – 208 pMS^3

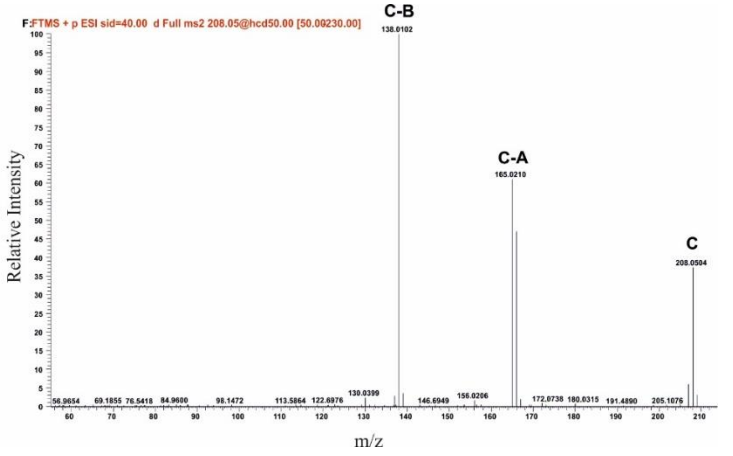

Table SI-11. Accurate mass measurements of protonated N2-Me-LMG and transformation products as determined by LC-QExactive-MS in MS/MS or pseudo MS^3 modes

Nominal ion mass	Measured mass [m/z]	Mass error [ppm]	Elemental composition	Calculated mass [m/z]	DBE[a]
N2-Me-LMG					
[M+H]+	270.0306	-0.7	$C_{10}H_{10}Cl_2N_5$	270.0308	7.5
A 253	253.0041	-0.4	$C_{10}H_7Cl_2N_4$	253.0042	8.5
B 243	243.0197	-0.8	$C_9H_9Cl_2N_4$	243.0199	6.5
E 200	200.9975	-3.0	$C_8H_7Cl_2N_2$	200.9981	5.5
H 171	171.9710	-2.9	$C_7H_4Cl_2N$	171.9715	5.5
I 166	166.0287	-3.0	$C_8H_7ClN_2$	166.0292	6.0
C 234	234.0537	-1.7	$C_{10}H_9ClN_5$	234.0541	8.5
F 191	191.0238	-3.7	$C_9H_6ClN_3$	191.0245	8.0
C-A 178	178.0162	-2.8	$C_8H_5ClN_3$	178.0167	7.5
C-B 165	165.0210	-2.4	$C_8H_6ClN_2$	165.0214	6.5
C-C 152	152.0130	-3.9	$C_7H_5ClN_2$	152.0136	6.0
C-D 57	57.0454	12.3	$C_2H_5N_2$	57.0447	1.5
D 225	225.9933	0.0	$C_9H_6Cl_2N_3$	225.9933	7.5
E 200	200.9980	-0.5	$C_8H_7Cl_2N_2$	200.9981	5.5
E-A 185	185.9739	-3.8	$C_7H_4Cl_2N_2$	185.9746	6.0
H 171	171.9708	-4.1	$C_7H_4Cl_2N$	171.9715	5.5
I 166	166.0286	-3.6	$C_8H_7ClN_2$	166.0292	6.0
J 159	159.9710	-3.1	$C_6H_4Cl_2N$	159.9715	4.5
L 132	132.9602	-3.0	$C_5H_3Cl_2$	132.9606	3.5
E-B 123	123.9946	-2.4	C_6H_3ClN	123.9949	5.5
G-C 108	108.9840	0.0	C_6H_2Cl	108.9840	5.5
F 191	191.0244	-0.5	$C_9H_6ClN_3$	191.0245	8.0
G 184	184.9794	0.0	$C_8H_5Cl_2N$	184.9794	6.0
G-A 158	158.9632	-3.1	$C_6H_3Cl_2N$	158.9637	5.0
K 150	150.0101	-2.7	C_8H_5ClN	150.0105	6.5
M 122	122.9994	-1.6	C_7H_4Cl	122.9996	5.5
G-B 114	114.0338	0.0	C_8H_4N	114.0338	7.5
G-C 108	108.9840	0.0	C_6H_2Cl	108.9840	5.5

Nominal ion mass	Measured mass [m/z]	Mass error [ppm]	Elemental composition	Calculated mass [m/z]	DBE[a]
H 171	171.9715	0.0	$C_7H_4Cl_2N$	171.9715	5.5
I 166	166.0291	-0.6	$C_8H_7ClN_2$	166.0292	6.0
J 159	159.9709	-3.8	$C_6H_4Cl_2N$	159.9715	4.5
K 150	150.0106	0.7	C_8H_5ClN	150.0105	6.5
L 132	132.9603	-2.3	$C_5H_3Cl_2$	132.9606	3.5
M 122	122.9997	0.8	C_7H_4Cl	122.9996	5.5
N2-Me-LMG - TP288-Gnd					
$[M+H]^+$	288.0415	0.7	$C_{10}H_{12}Cl_2N_5O$	288.0413	6.5
A 271	271.0150	0.7	$C_{10}H_9Cl_2N_4O$	271.0148	7.5
B 245	245.0358	1.2	$C_9H_{11}Cl_2N_4$	245.0355	5.5
C 228	228.0081	-3.9	$C_9H_8Cl_2N_3$	228.0090	6.5
D 200	200.9975	-3.0	$C_8H_7Cl_2N_2$	200.9981	5.5
E 185	185.9740	-3.2	$C_7H_4Cl_2N_2$	185.9746	6.0
F 171	171.9711	-2.3	$C_7H_4Cl_2N$	171.9715	5.5
G 159	159.9712	-1.9	$C_6H_4Cl_2O$	159.9715	4.5
C 228	228.0091	0.4	$C_9H_8Cl_2N_3$	228.0090	6.5
D 200	200.9974	-3.5	$C_8H_7Cl_2N_2$	200.9981	5.5
F 171	171.9711	-2.3	$C_7H_4Cl_2N$	171.9715	5.5
G 159	159.9711	-2.5	$C_6H_4Cl_2O$	159.9715	4.5
D 200	200.9982	0.5	$C_8H_7Cl_2N_2$	200.9981	5.5
E 185	185.9743	-1.6	$C_7H_4Cl_2N_2$	185.9746	6.0
F 171	171.9712	-1.7	$C_7H_4Cl_2N$	171.9715	5.5
G 159	159.9713	-1.3	$C_6H_4Cl_2O$	159.9715	4.5
D-A 132	132.9606	0.0	$C_5H_3Cl_2$	132.9606	3.5
D-B 123	123.9949	0.0	C_6H_3ClN	123.9949	5.5
E 185	185.9748	1.1	$C_7H_4Cl_2N_2$	185.9746	6.0
F 171	171.9717	1.2	$C_7H_4Cl_2N$	171.9715	5.5
G 159	159.9718	1.9	$C_6H_4Cl_2O$	159.9715	4.5

Nominal ion mass	Measured mass [m/z]	Mass error [ppm]	Elemental composition	Calculated mass [m/z]	DBE[a]
N2-Me-LMG - TP271-Amd					
$[M+H]^+$	271.0148	0.0	$C_{10}H_9Cl_2N_4O$	271.0148	7.5
A 243	243.0199	0.0	$C_9H_9Cl_2N_4$	243.0199	6.5
B 227	227.9954	-4.4	$C_8H_6Cl_2N_4$	227.9964	7.0
C 208	208.0503	-3.4	$C_9H_9ClN_4$	208.0510	7.0
D 200	200.9974	-3.5	$C_8H_7Cl_2N_2$	200.9981	5.5
E 185	185.9741	-2.7	$C_7H_4Cl_2N_2$	185.9746	6.0
F 171	171.9710	-2.9	$C_7H_4Cl_2N$	171.9715	5.5
D-A 166	166.0289	-1.8	$C_8H_7ClN_2$	166.0292	6.0
G 159	159.9710	-3.1	$C_6H_4Cl_2N$	159.9715	4.5
C-B 138	138.0100	-3.6	C_7H_5ClN	138.0105	5.5
D-C 123	123.9947	-1.6	C_6H_3ClN	123.9949	5.5
B 227	227.9967	1.3	$C_8H_6Cl_2N_4$	227.9964	7.0
D 200	200.9974	-3.5	$C_8H_7Cl_2N_2$	200.9981	5.5
B-A 198	198.9818	-3.0	$C_8H_5Cl_2N_2$	198.9824	6.5
E 185	185.9742	-2.2	$C_7H_4Cl_2N_2$	185.9746	6.0
G 171	171.9710	-2.9	$C_7H_4Cl_2N$	171.9715	5.5
C-A 165	165.0210	-2.4	$C_8H_9ClN_2$	165.0214	6.5
C-B 138	138.0102	-2.2	C_7H_5ClN	138.0105	5.5
D-C 123	123.9947	-1.6	C_6H_3ClN	123.9949	5.5
C 208	208.0511	0.5	$C_9H_9ClN_4$	208.0510	7.0
C-A 165	165.0210	-2.4	$C_8H_9ClN_2$	165.0214	6.5
C-B 138	138.0102	-2.2	C_7H_5ClN	138.0105	5.5
D 200	200.9981	0.0	$C_8H_7Cl_2N_2$	200.9981	5.5
E 185	185.9740	-3.2	$C_7H_4Cl_2N_2$	185.9746	6.0
F 171	171.9709	-3.5	$C_7H_4Cl_2N$	171.9715	5.5
D-A 166	166.0287	-3.0	$C_8H_7ClN_2$	166.0292	6.0
G 159	159.9710	-3.1	$C_6H_4Cl_2N$	159.9715	4.5
D-B 132	132.9603	-2.3	$C_5H_3Cl_2$	132.9606	3.5
D-C 123	123.9947	-1.6	C_6H_3ClN	123.9949	5.5
D-D 108	108.9740	-91.8	C_6H_2Cl	108.9840	5.5

Nominal ion mass	Measured mass [m/z]	Mass error [ppm]	Elemental composition	Calculated mass [m/z]	DBE[a]
E 185	185.9748	1.1	$C_7H_4Cl_2N_2$	185.9746	6.0
F 171	171.9716	0.6	$C_7H_4Cl_2N$	171.9715	5.5
G 159	159.9717	1.3	$C_6H_4Cl_2N$	159.9715	4.5
N2-Me-LMG - TP271-Gnd					
$[M+H]^+$	271.0140	-3.0	$C_{10}H_9Cl_2N_4O$	271.0148	7.5
1-253	253.9875	-2.8	$C_{10}H_6Cl_2N_3O$	253.9882	8.5
A* 244	244.0032	-2.9	$C_9H_8Cl_2N_3O$	244.0039	6.5
C* 209	209.0346	-1.9	$C_9H_8ClN_3O$	209.0350	7.0
D* 200	200.9978	-1.5	$C_8H_7Cl_2N_2$	200.9981	5.5
4 186	186.9822	-1.1	$C_7H_5Cl_2N_2$	186.9824	5.5
5 172	172.9665	-1.7	$C_6H_3Cl_2N_2$	172.9668	5.5
F 171	171.9710	-2.9	$C_7H_4Cl_2N$	171.9715	5.5
G 159	159.9713	-1.3	$C_6H_4Cl_2N$	159.9715	4.5
6 152	152.0134	-1.3	$C_7H_5ClN_2$	152.0136	6.0
D-B 132	132.9606	0.0	$C_5H_3Cl_2$	132.9606	3.5
D-C 123	123.9949	0.0	C_6H_3ClN	123.9949	5.5
2-235	235.0373	-3.4	$C_{10}H_8ClN_4O$	235.0381	8.5
B* 228	228.0082	-3.5	$C_9H_8Cl_2N_3$	228.0090	6.5
D* 200	200.9976	-2.5	$C_8H_7Cl_2N_2$	200.9981	5.5
4 186	186.9820	-2.1	$C_7H_5Cl_2N_2$	186.9824	5.5
E 185	185.9743	-1.6	$C_7H_4Cl_2N_2$	185.9746	6.0
5 172	172.9664	-2.3	$C_6H_3Cl_2N_2$	172.9668	5.5
F 171	171.9710	-2.9	$C_7H_4Cl_2N$	171.9715	5.5
G 159	159.9712	-1.9	$C_6H_4Cl_2N$	159.9715	4.5
6 152	152.0133	-2.0	$C_7H_5ClN_2$	152.0136	6.0
D-B 132	132.9605	-0.8	$C_5H_3Cl_2$	132.9606	3.5
D-C 123	123.9947	-1.6	C_6H_3ClN	123.9949	5.5
D* 200	200.9976	-2.5	$C_8H_7Cl_2N_2$	200.9981	5.5
E 185	185.9741	-2.7	$C_7H_4Cl_2N_2$	185.9746	6.0
F 171	171.9710	-2.9	$C_7H_4Cl_2N$	171.9715	5.5

Nominal ion mass	Measured mass [m/z]	Mass error [ppm]	Elemental composition	Calculated mass [m/z]	DBE[a]
G 159	159.9711	-2.5	$C_6H_4Cl_2N$	159.9715	4.5
D-B 132	132.9604	-1.5	$C_5H_3Cl_2$	132.9606	3.5
D-C 123	123.9948	-0.8	C_6H_3ClN	123.9949	5.5
3-196	196.9664	-2.0	$C_8H_3Cl_2N_2$	196.9668	7.5
4-186	186.9820	-2.1	$C_7H_5Cl_2N_2$	186.9824	5.5
5-172	172.9664	-2.3	$C_6H_3Cl_2N_2$	172.9668	5.5
F 171	171.9711	-2.3	$C_7H_4Cl_2N$	171.9715	5.5
G 159	159.9711	-2.5	$C_6H_4Cl_2N$	159.9715	4.5
6-152	152.0134	-1.3	$C_7H_5ClN_2$	152.0136	6.0

[a] Double-bond equivalents.

pH EXPERIMENTS - degradations in hospital effluent and WW influent and effluent @pH 7 – 9

The same experiments as for LMG-N2-G in hospital effluent and wastewater influent and effluent over the course of 36 hours at pH 7, 8 and 9 were performed for N2-Me-LMG as well (**Figure SI-23**). In general, formation of transformation products of N2-Me-LMG was much slower than compared with LMG-N2-G (**Figure SI-23**). After 36 hours of degradation at pH 9, only up to 3.5 % of N2-Me-LMG-TP271-Amd was formed (compared to 58 % formation of LMG-N2-G-TP433-Amd). Similar results are seen for other matrices as well. In WWinf, N2-Me-LMG-TP271-Amd was formed up to 4.0 % (LMG-N2-G-TP433-Amd – 73 %) and in WWeff up to 3.2 % (LMG-N2-G-TP433-Amd – 69 %). Unlike difference in the formation of LMG-N2-G-TP433-Amd in different matrix, no difference was seen for N2-Me-LMG-TP271-Amd. On the other hand, like in the LMG-N2-G transformation, pH affected the formation of N2-Me-LMG-TP271-Amd. Lowering the pH of the solution to pH 8 and pH 7 affected the formation rate of N2-Me-LMG-TP271-Amd by partially inhibiting the transformation (**Figure SI-23**). At the end of the experiment at pH 8, N2-Me-LMG-TP271-Amd was formed up to 0.7 % in HOSeff, 0.8 % in WWinf and 0.6 % in WWeff. The formation was even lower at pH 7 which was around 0.2 % for all three matrices.

N2-Me-LMG-TP271-Gnd was detected in all matrices studied but only in experiments at pH 9 (**Figure SI-24**). After the 36 hours of degradation, N2-Me-LMG-TP271-Gnd was detected at around 0.8% of initial concentration of N2-Me-LMG.

N2-Me-LMG concentration of 400 nM was degraded at pH 8.5 in two different hospital effluent samples and two different WWTP influent samples over the course of 27 hours (**Figure SI-25**). In all four cases, the degradation was performed with and without additional filtration through 0.2 μm filters. As can be seen from both HOSeff samples (**Figure SI-25-A** and **B**) and WWinf (**Figure SI-25-C** and **D**), there was very little degradation in general of N2-Me-LMG over the 27 hours. Likewise, there was almost no difference in degradation between the same sample filtered either through 0.7 or 0.2 μm filters. When the 400 nM concentration of N2-Me-LMG was exposed in wastewater and 25 molar excess of free chlorine, no difference in degradation was observed. In **Figure SI-26**, 200 nM of N2-Me-LMG was degraded in both HOSeff (**Figure SI-26-A** and **B**) and WWinf (**Figure SI-26-C** and **D**) at pH 8.5 but was practically no decrease in the concentration of N2-Me and the slope of the regression line for all three matrices were not significantly different from zero.

Figure SI-23. Formation over the course of 36 hours of N2-Me-LMG-TP271-Amd in (A) HOSeff, (B) WWinf and (C) WWeff

buffered at pH 7-9 with the initial starting concentration of parent N2-Me-LMG of 400 nM.

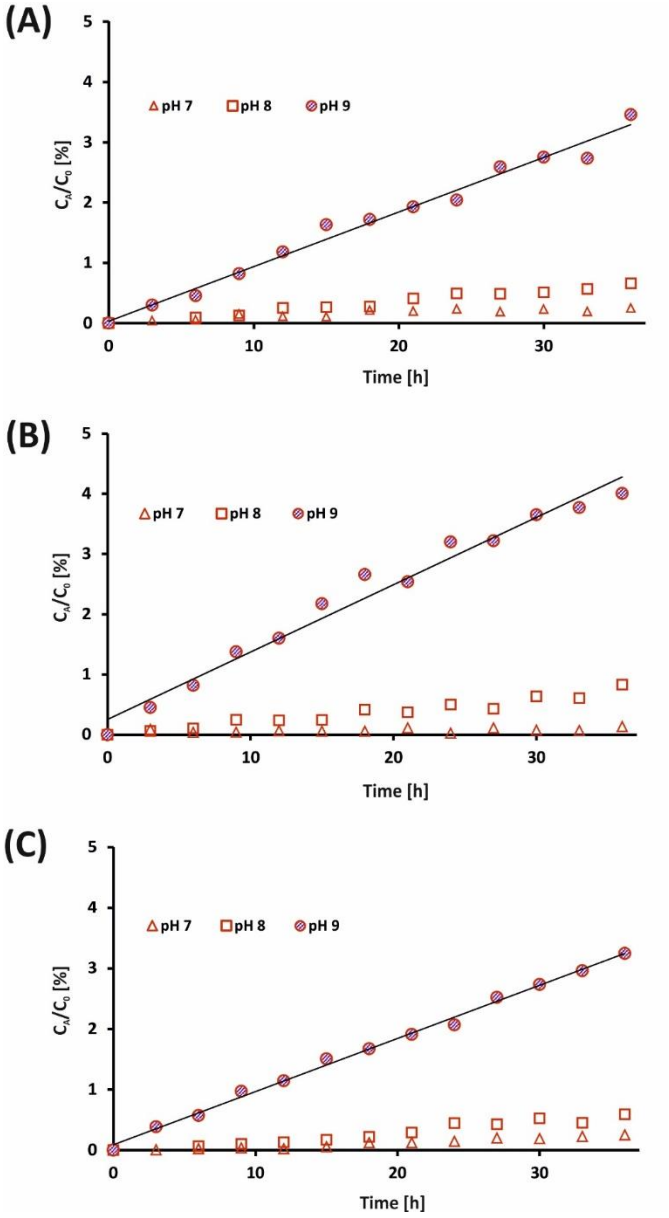

Figure SI-24. Formation over the course of 36 hours of N2-Me-LMG-TP271-Gnd at pH 9 in HOSeff, WWinf and WWeff

with the initial starting concentration of parent N2-Me-LMG of 400 nM.

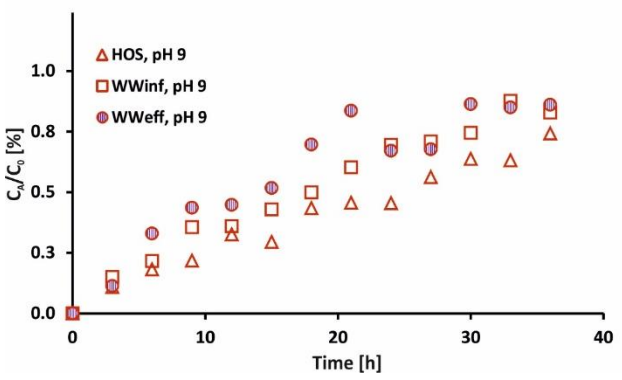

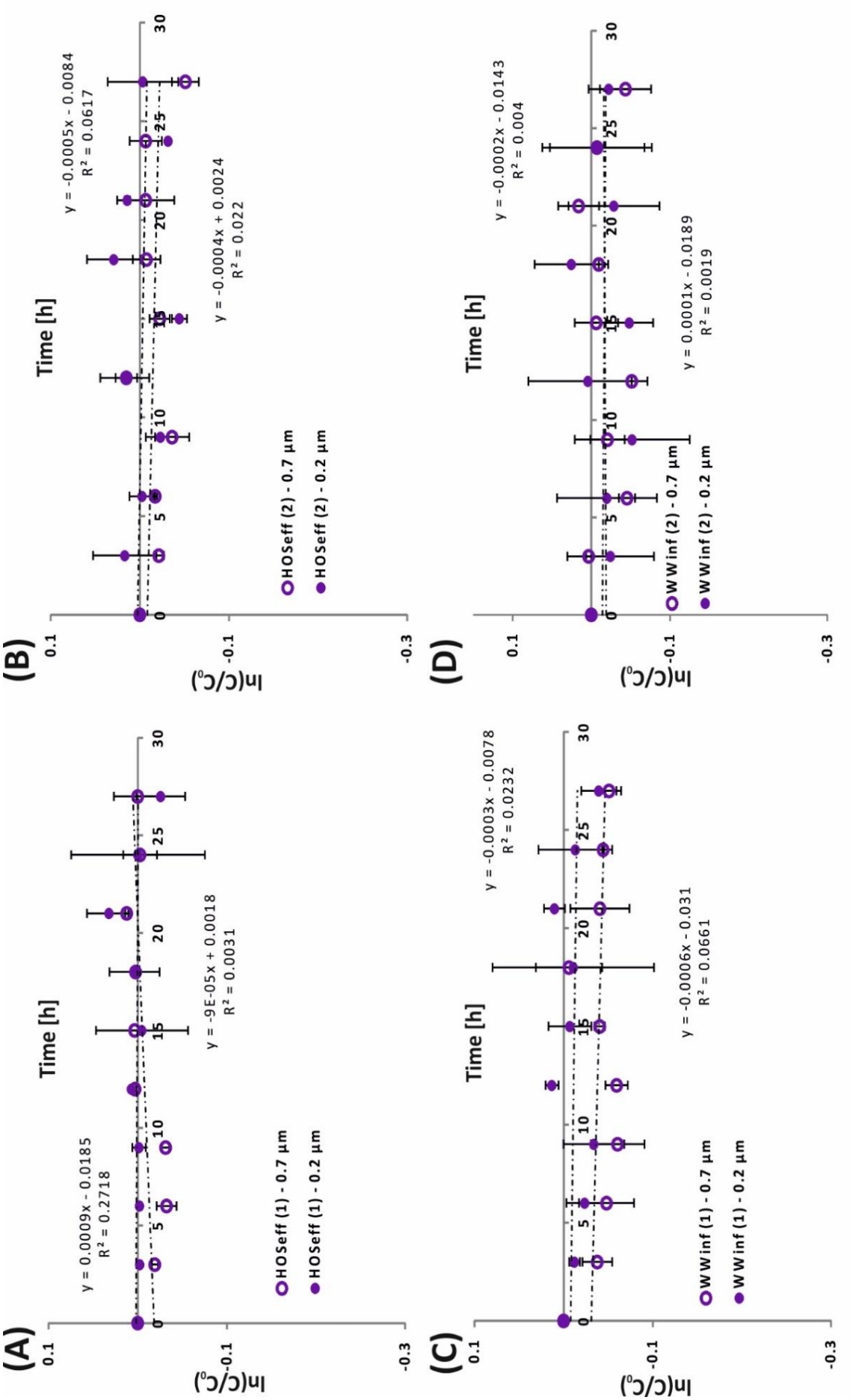

Figure SI-25. Degradation of 400 nM of N2-Me-LMG at pH 8.5, filtered through 0.7 and 0.2 µm in two different HOSeff samples (A and B) and in two different WWinf samples (C and D). *Total degradation time was 27 hours.*

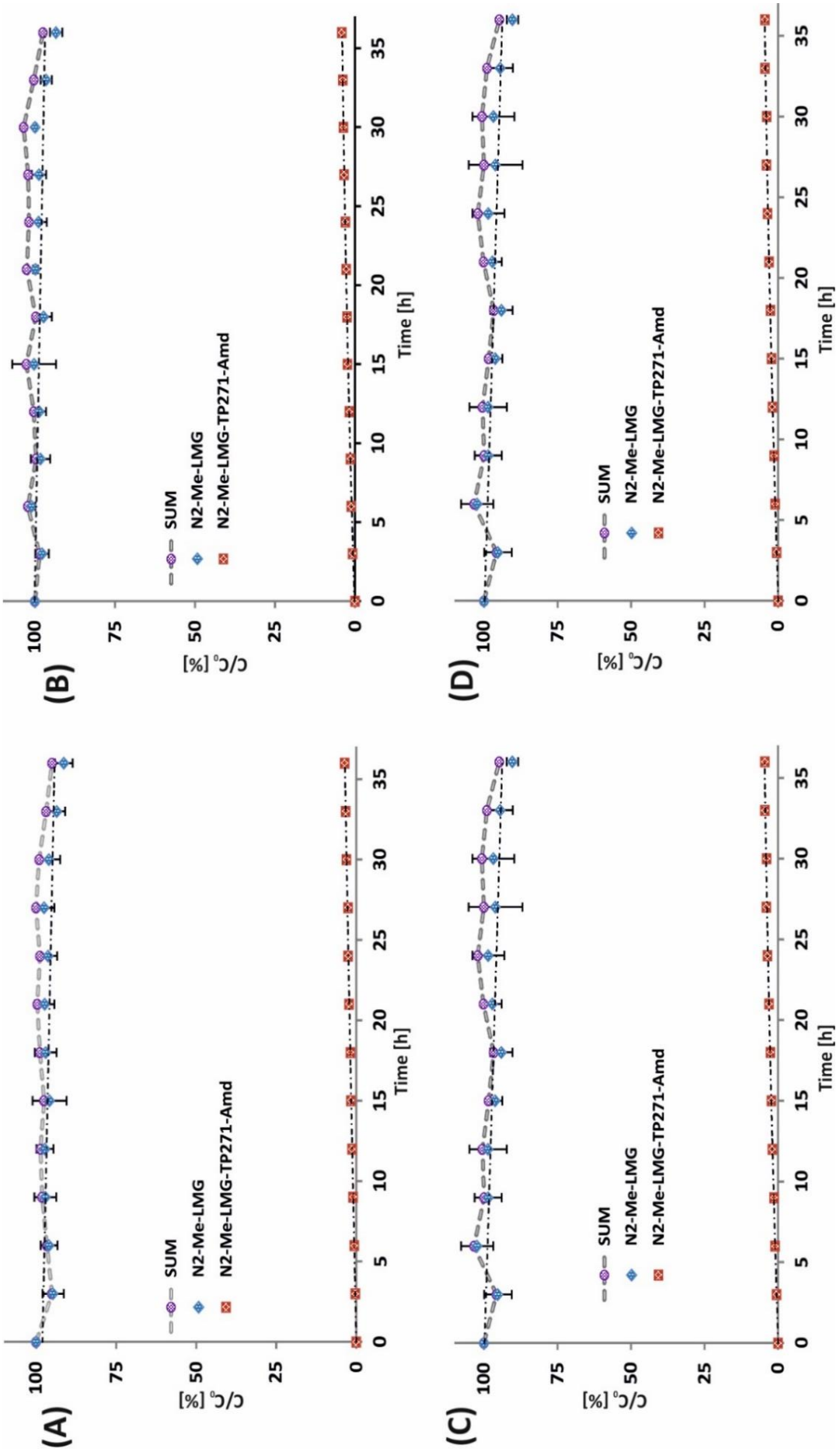

Figure SI-26. Mass balance of 400 nM of N2-Me-LMG in HOSeff and WWinf at pH 8.5 with the free chlorine molar excess of 25 times. *(A) HOSeff , (B) HOSeff-free chlorine, (C) WWinf, (D) WWinf-free chlorine. Total degradation time was 36 hours.*

IV. LAMOTRIGINE – N2-OXIDE (LMG-N2-oxide)

pH EXPERIMENTS - degradations in UPW @ pH 5, 7 and 9

Figure SI-27. Degradation of 400 nM of LMG-N2-oxide in UPW at pH 5, 7 and 9 over the course of 42 hours.

The point on the graph corresponds to the average measurement of the three pHs with the error bars representing deviation.

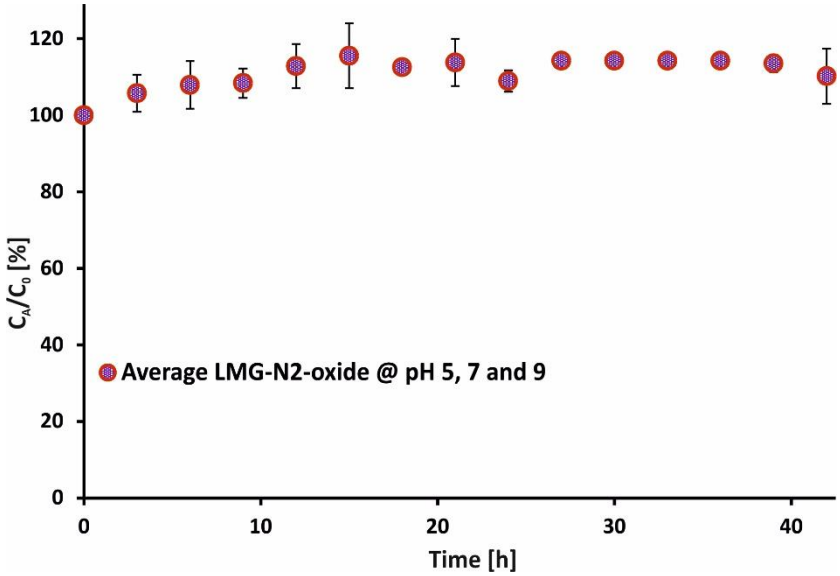

LAMOTRIGINE N2-OXIDE (LMG-N2-oxide)

Figure SI-28-A. Fragmentation pattern of LMG-N2-oxide

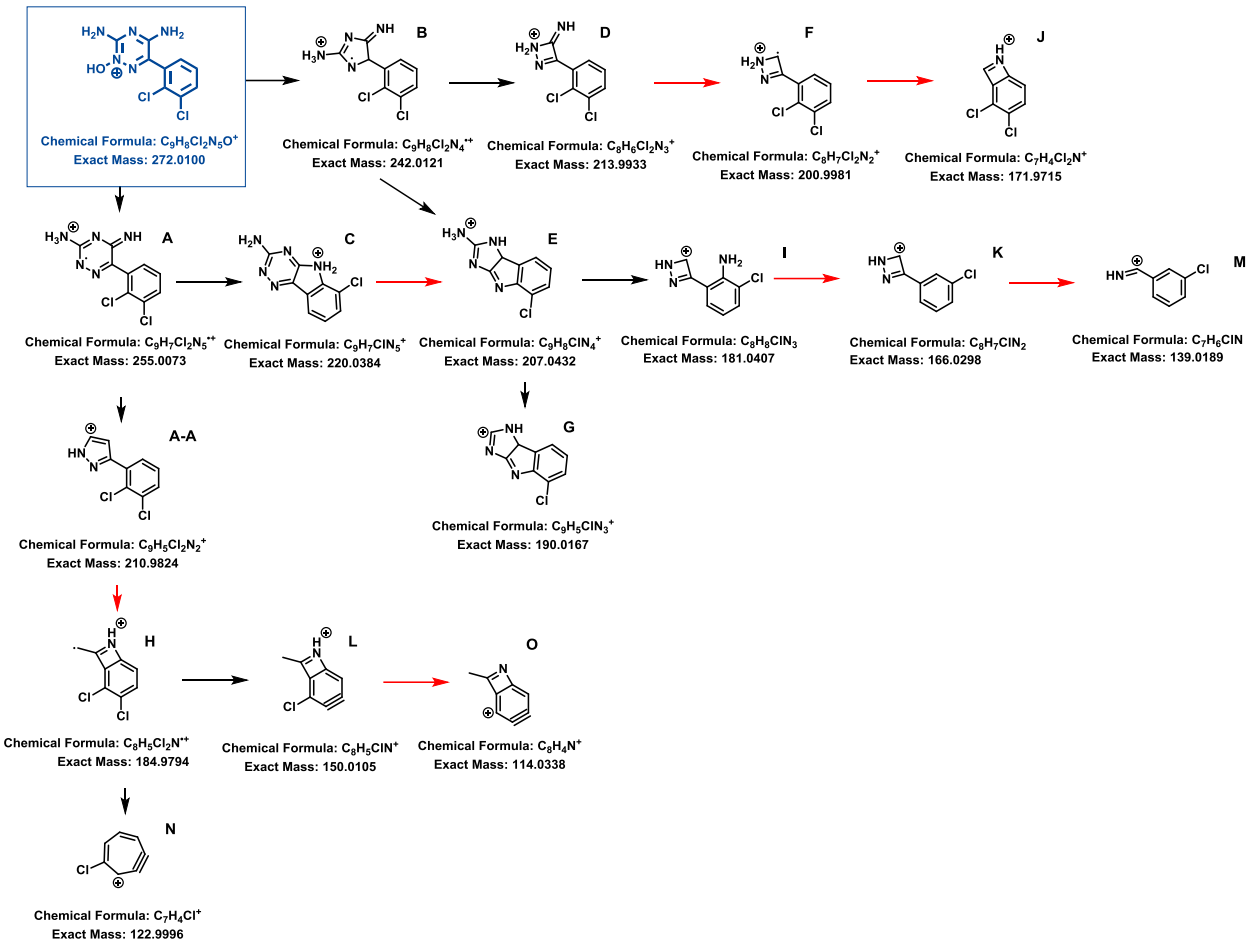

Figure SI-28-B. MS^2 and pMS^3 spectra of LMG-N2-oxide

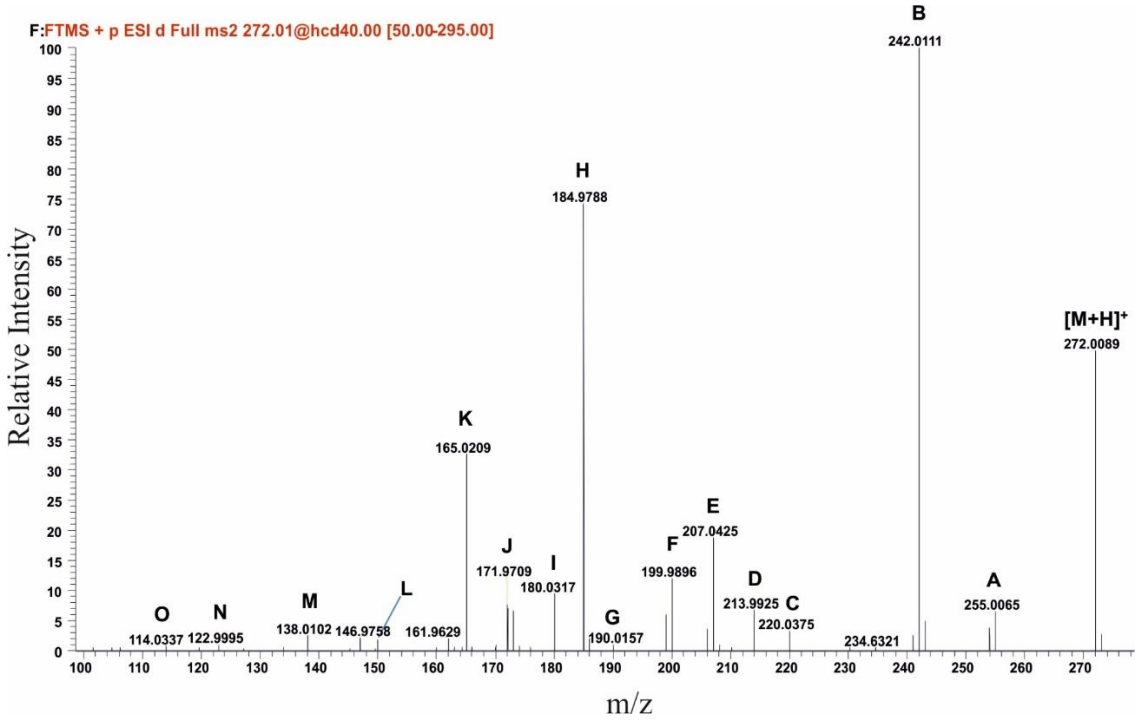

Figure SI-28-B. MS^2 and pMS^3 spectra of LMG-N2-oxide – *continued*

LMG-N2-oxide – 255 pMS^3

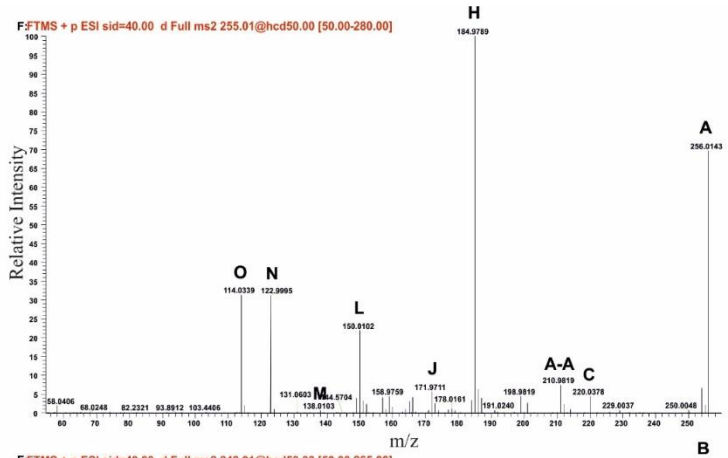

LMG-N2-oxide – 242 pMS^3

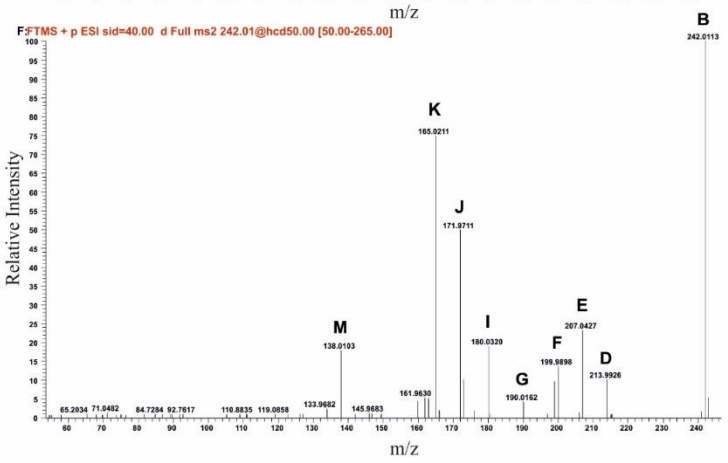

LMG-N2-oxide – 207 pMS^3

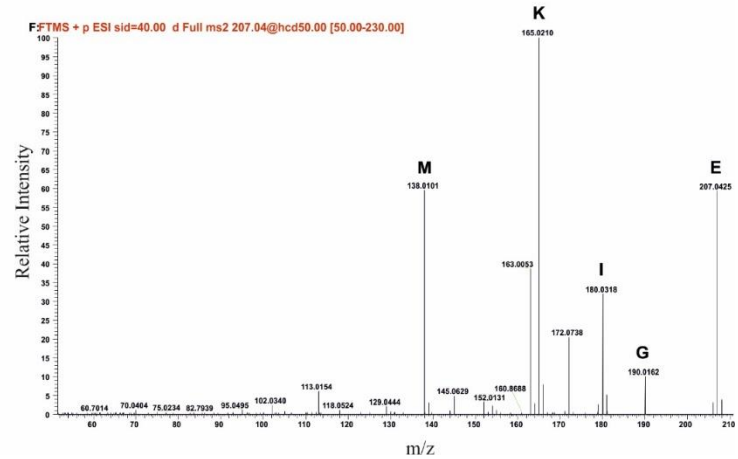

N2-Me-LMG – 184 pMS^3

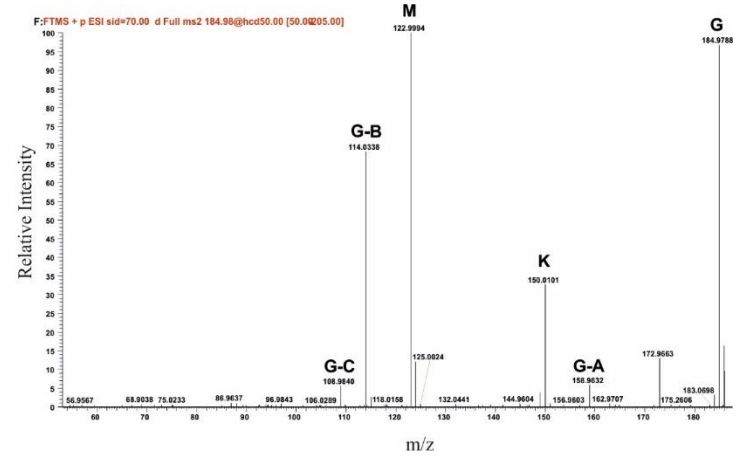

Table SI-12. Accurate mass measurements of protonated LMG-N2-oxide as determined by LC-QExactive-MS in MS/MS or pseudo MS³ modes

Nominal ion mass	Measured mass [m/z]	Mass error [ppm]	Elemental composition	Calculated mass [m/z]	DBE[a]
LMG-N2-oxide					
$[M+H]^+$	272.0089	-4.0	$C_9H_8Cl_2N_5O$	272.0100	7.5
A 255	255.0065	-3.1	$C_9H_7Cl_2N_5$	255.0073	8.0
C 220	220.0378	-2.7	$C_9H_7ClN_5$	220.0384	8.5
A-A 210	210.9819	-2.4	$C_9H_5Cl_2N_2$	210.9824	7.5
H 184	184.9789	-2.7	$C_8H_5Cl_2N$	184.9794	6.0
J 171	171.9711	-2.3	$C_7H_4Cl_2N$	171.9715	5.5
L 150	150.0102	-2.0	C_8H_5ClN	150.0105	6.5
M 138	138.0103	-1.4	C_7H_5ClN	138.0105	5.5
N 122	122.9995	-0.8	C_7H_4Cl	122.9996	5.5
O 114	114.0339	0.9	C_8H_4N	114.0338	7.5
B 242	242.0111	-4.1	$C_9H_8Cl_2N_4$	242.0121	7.0
D 213	213.9926	-3.3	$C_8H_6Cl_2N_3$	213.9933	6.5
E 207	207.0427	-2.4	$C_9H_8ClN_4$	207.0432	7.5
F 199	199.9898	-2.5	$C_8H_6Cl_2N_2$	199.9903	6.0
G 190	190.0162	-2.6	$C_9H_5ClN_3$	190.0167	8.5
I 180	180.0320	-1.7	$C_8H_7ClN_3$	180.0323	6.5
J 171	171.9711	-2.3	$C_7H_4Cl_2N$	171.9715	5.5
K 165	165.0211	-1.8	$C_8H_6ClN_2$	165.0214	6.5
M 138	138.0103	-1.4	C_7H_5ClN	138.0105	5.5
C 220	220.0375	-4.1	$C_9H_7ClN_5$	220.0384	8.5
D 213	213.9925	-3.7	$C_8H_6Cl_2N_3$	213.9933	6.5
E 207	207.0425	-3.4	$C_9H_8ClN_4$	207.0432	7.5
G 190	190.0162	-2.6	$C_9H_5ClN_3$	190.0167	8.5
I 180	180.0318	-2.8	$C_8H_7ClN_3$	180.0323	6.5
K 165	165.0210	-2.4	$C_8H_6ClN_2$	165.0214	6.5
M 138	138.0101	-2.9	C_7H_5ClN	138.0105	5.5
F 199	199.9896	-3.5	$C_8H_6Cl_2N_2$	199.9903	6.0
G 190	190.0157	-5.3	$C_9H_5ClN_3$	190.0167	8.5
H 184	184.9788	-3.2	$C_8H_5Cl_2N$	184.9794	6.0

Nominal ion mass	Measured mass [m/z]	Mass error [ppm]	Elemental composition	Calculated mass [m/z]	DBE[a]
L 150	150.0101	-2.7	C_8H_5ClN	150.0105	6.5
N 122	122.9995	-0.8	C_7H_4Cl	122.9996	5.5
O 114	114.0338	0.0	C_8H_4N	114.0338	7.5
I 180	180.0317	-3.3	$C_8H_7ClN_3$	180.0323	6.5
J 171	171.9709	-3.5	$C_7H_4Cl_2N$	171.9715	5.5
K 165	165.0209	-3.0	$C_8H_6ClN_2$	165.0214	6.5
L 150	150.0115	6.7	C_8H_5ClN	150.0105	6.5
M 138	138.0102	-2.2	C_7H_5ClN	138.0105	5.5
N 122	122.9995	-0.8	C_7H_4Cl	122.9996	5.5
O 114	114.0337	-0.9	C_8H_4N	114.0338	7.5

[a] Double-bond equivalents.

Amidine/Guandidine hydrolysis reactions and dependence on N2 substituent at different pHs

Figure SI-29. Tautomers of (A) N2-Me-LMG and (B) LMG-N2-G

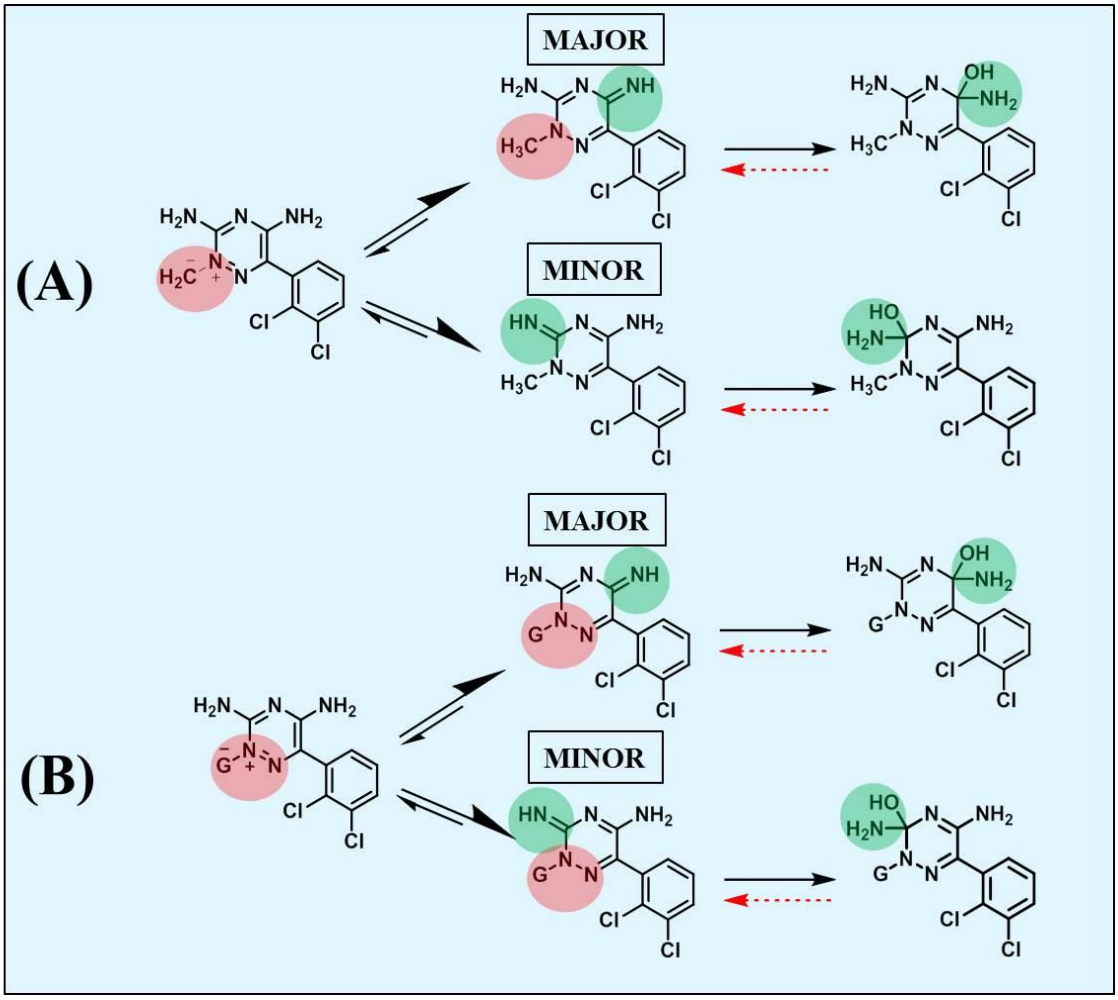

Figure SI-30. Tautomers of (A) LMG and (B) LMG-N2-oxide

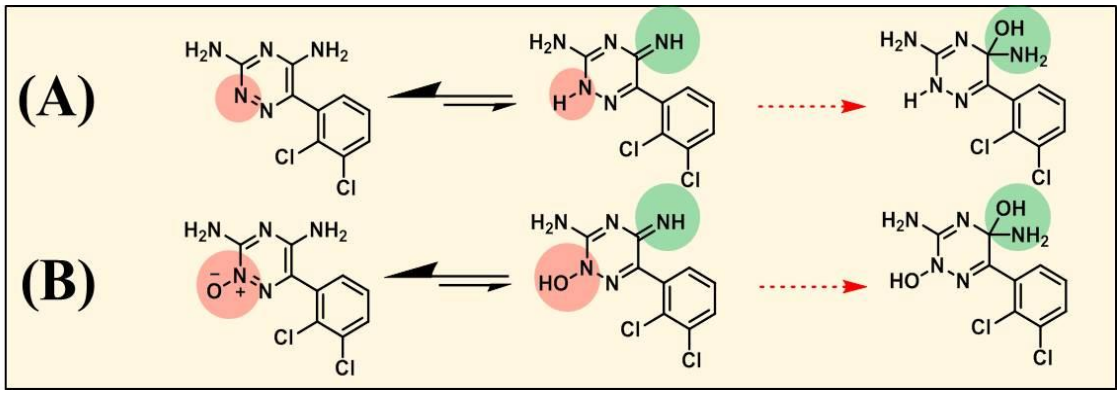

SI-References

Ferrer, I. and Thurman, E.M. (2010) Identification of a New Antidepressant and its Glucuronide Metabolite in Water Samples Using Liquid Chromatography/Quadrupole Time-of-Flight Mass Spectrometry. Analytical Chemistry 82(19), 8161-8168.

Manning, C.O., Wadsworth, A.H. and Fellows, I. (2002) Synthesis of stable isotopically labelled versions of Lamotrigine and its methylated metabolite. Journal of Labelled Compounds and Radiopharmaceuticals 45(7), 611-618.

Volmajer, J., Toplak, R., Bittner, S., Leban, I. and Le Marechal, A.M. (2003) Novel N-chlorinated derivatives of 2H-1-benzopyran-2-imines. Tetrahedron Letters 44(11), 2363-2366.

Zonja, B., Delgado, A., Perez, S. and Barcelo, D. (2015) LC-HRMS suspect screening for detection-based prioritization of iodinated contrast media photodegradates in surface waters. Environ Sci Technol 49(6), 3464-3472.

Zonja, B., Perez, S. and Barcelo, D. (2016) Human Metabolite Lamotrigine-N(2)-glucuronide Is the Principal Source of Lamotrigine-Derived Compounds in Wastewater Treatment Plants and Surface Water. Environ Sci Technol 50(1), 154-164.

4.3. Discussion

4.3.1. Abiotic vs. Biotic processes and their influence on the fate of lamotrigine and lamotrigine-N2-glucuronide

Figure 4.2. summarises all known transformation reactions of both LMG and its main human metabolite LMG-N2-G that could possibly yield environmentally relevant TPs. While the red (human metabolites), yellow (phototransformation products) and purple (pharmaceutical impurities) compounds (pathways) have been collected from literature, green (biotransformation products) and blue (chemical hydrolysis products) pathways drawn shown are the results obtained in this thesis and published in Articles N°3 and N°4.

As can be seen from **Figure 4.2.** LMG can principally be transformed either via i) human metabolism (red pathway), ii) biotransformation in activated sludge under aerobic conditions (green pathway) and iii) phototransformation under simulated sunlight and neutral pH (yellow pathway). Purple arrows do not necessarily indicate transformation to those compounds but they are listed as impurities that are known to be present in the LMG pharmaceutical tablets (Beattie et al. 2012). Human metabolism of LMG is mainly hepatic and metabolic reactions involve both phase I and phase II (conjugation) metabolism. Four metabolites have been identified for LMG; the N-oxidation and N-methylation as phase I metabolites and N2- and N5- glucuronidation as phase II metabolites. Out of the four identified metabolites, N2-glucuronide is the major one, accounting for around 80 % of administered dose (Doig and Clare 1991, Lu and Uetrecht 2007, Ramsay et al. 1991, Sidhu et al. 2006). As can be seen from **Figure 4.2.** (red/green pathway), LMG phase I metabolites are also formed in biodegradation batch reactors with activated sludge. Expectedly, this shows the overlap of reactions between human metabolism and activated sludge reactions. This correlation was previously reported for several pharmaceuticals like diclofenac (Pérez and Barceló 2008), acyclovir (Prasse et al. 2011) or metoprolol (Rubirola et al. 2014). Once the LMG and its metabolites are excreted from the human body they enter the sewage system. This leads them most likely to an urban WWTP where they are further degraded (green reactions). As mentioned earlier, in WWTPs biodegradation reactors with activated sludge LMG will be transformed, following slow kinetics, to two TPs (the same as the two human metabolites); N2-oxide and N-2 methyl. However, the prevalent reaction taking place will be the deconjugation of its major metabolite LMG-N2-G to the original active pharmaceutical ingredient (API) lamotrigine.

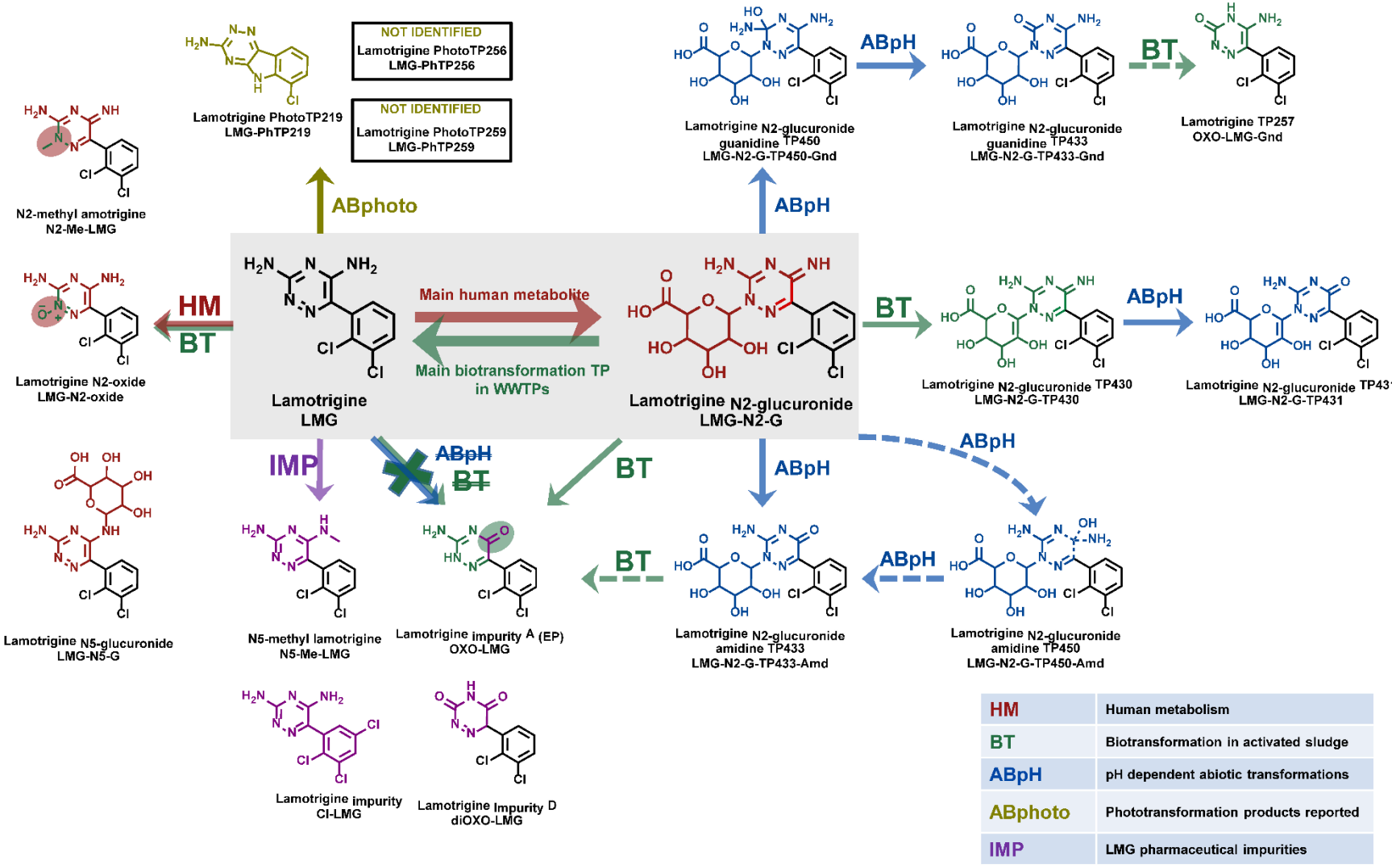

Figure 4.2. Transformation pathways of lamotrigine and its human metabolite, lamotrigine N2-glucuronide. Transformations types include human metabolism (HM) shown as red transformations, biological transformations in activated sludge (BT) shown as green transformations, pH dependent abiotic transformations (ABpH) shown as blue transformations, and phototransformation (ABphoto) shown as dark yellow transformations. Purple transformations indicate known LMG impurities (IMP)IM that are present in the LMG tablets.

Although it has been suggested that some glucuronides could revert back to the parent compound even before they enter the WWTP system (Jelic et al. 2015), the WWTP secondary treatment using activated sludge is most likely dominant in the formation of biotransformation TPs.

However, in the first paper on degradation of LMG (Article N°3), several bioTPs have been detected in the WWTP influent suggesting that LMG-N2-G already initiated transformation in the sewage system (Zonja et al. 2016b). Apart from the hydrolysis reaction of LMG-N2-G to the parent compound, LMG-N2-G was found to transform to other two TPs (green pathway). The first one is the result of the oxidation of the glucuronide moiety (TP-430) and the second one to the deconjugated amidine hydrolysis derivative (OXO-LMG). The metabolic logic behind the formation of the TP-430 was rather straightforward and was identified as oxidation of the glucuronide to glycal, alas not being able to confirm the exact structure of the compound with an authentic standard. For the TP-430, EAWAG-BBD pathway prediction system (Gao et al. 2010) suggested a reaction of oxidation of an alcohol to ketone. However, as for the OXO-LMG, initial explanation of the formation of this compound needed to be revaluated when it was discovered that OXO-LMG did not form from LMG in activated sludge batch reactors. It was later confirmed that the LMG-N2-G was source of the OXO-LMG once LMG-N2-G was biodegraded in batch reactors filled with activated sludge. Here the reaction pathway of the LMG-N2-G is more complex due to competing reactions reported in the article on the chemical hydrolysis of the amidine and guanidine groups in the LMG-N2-G structure (blue pathway) (Zonja et al. 2016a). As indicated by the blue pathway in the **Figure 4.2.**, besides biodegradation, LMG-N2-G is prone to selective hydrolysis of its amidine and guanidine moieties (to TPs433). This reaction pathway was found to be pH dependent and preferentially occurred at the amidine moiety of the LMG-N2-G.

In summary, LMG-N2-G will undergo abiotic hydrolysis in the neutral to basic pH range (here tested: pH 7 – pH 9). As the result, the fate of LMG-N2-G in wastewater system, and likely surface water, will be governed not only by biological reactions, but also by the pH of the medium. In essence, both degradation pathways should be taken into account for the interpretation of the removal or attenuation of LMG-N2-G in the aquatic environment, since both pathways are probable. However, it has been demonstrated in this thesis that the degradation kinetics of biologically mediated transformation is much faster than the abiotic

one. Therefore, in the WWTPs LMG-N2-G should be predominantly transformed by the pathway indicated in green arrows (**Figure 4.2.**). On the other hand, in an environment with lower biotic activity (like surface water), both pathways could be equally dominant. For the abiotic hydrolysis of the amidine and guanidine moieties to take place, LMG-N2-G has to be transformed to a TP433 (most likely via TP450) at neutral-basic pH. Then the biotic hydrolysis of the glucuronide moiety could release OXO-LMG. In this thesis, the formation of both TP433-Amd and its subsequent hydrolysis to OXO-LMG was not demonstrated nor observed in biotic batch reactors (Article N°3), most likely due to faster biological degradation. However, the formation of the abiotic amidine TP from biotic LMG-N2-G-TP430 was confirmed. As mentioned before, the initial oxidation of the LMG-N2-G rendered a stable TP430 which was able to further on transform to amidine hydrolysis TP431 because of its higher stability towards biodegradation. This TP431 was detected only in the batch experiments spiked at higher initial concentration of 50 μgL^{-1}. The alternative abiotic transformation pathway of LMG-N2-G (the guanidine hydrolysis) is shown in blue pathway. Since the guanidine hydrolysis is a minor pathway as compared to amidine hydrolysis, the former pathway is environmentally less relevant. As a result, detection of the OXO-LMG-Gnd in wastewater or surface water is unlikely.

As for the phototransformation relevance of these LMG-related compounds, yet no information exists on their degradability and TP formation. Only LMG photodegradation pathways have been reported by Young et al. (Young et al. 2014) using simulated sunlight (yellow pathway, **Figure 4.2.**). However, in that study LMG was shown to be resistant to photodegradation (half-life higher than 100 h). In this thesis, some of the photoTPs reported by Young et al (Young et al. 2014) (the ones formed at pH 7) were initially screened using LC-HRMS in the surface water samples but none of them were detected in any of the samples analysed. The failure to detect photoTPs in surface water is in accordance with the photo-stability postulated by Young et al. (Young et al. 2014).

Same as with the characterisation of ICM pathways reported in this thesis (Article N°2), accurate structural elucidation of TPs of LMG and LMG-N2-G led to discovery of the proposed pathways described above and presented in **Figure 4.2.** Moreover, pMS^3 fragmentation pattern interpretations proved to be an indispensable tool for reliable identification of the TPs detected. This was especially important for the many glucuronide moiety-bearing TPs. Glucuronides in general break easily, even in the ESI source, yielding a

clean MS^2 spectra with almost exclusively one fragment which corresponds to the unconjugated parent compound (for example, LMG-N2-G → LMG). Here, pMS^3 fragmentation was particularly crucial for the identification of the two abiotic TPs of LMG-N2-G with the same exact mass (TPs433). Both of these TPs (TP433-Amd and TP433-Gnd) have exactly the same MS^2 spectra showing only m/z 256.9991 (OXO-LMG) fragment which could either be OXO-LMG-Amd or OXO-LMG-Gnd (**Figure 4.2**. and *Figure SI-4.2, Article Nº4, SI, p331.*). However, comparison of the pMS^3 spectra of these fragments (*Figure 3 B, D and F, Article Nº4, p310.*) with the MS^2 spectra of OXO-LMG (OXO-LMG was available as an authentic standard), it was possible to unequivocally distinguish between the Amd or Gnd structure and, thus, the TPs, advancing their identification from tentative candidates (confidence level 3) to a *confidence level 2b* (probable structure by diagnostic evidence) from Schymanski guidelines (**Chapter 1.3.** and **Figure 1.3.**). As for the biotic TP430, although it wasn't possible to determine with absolute certainty the exact position where the oxidation occurred (**Figure 4.2.**), due to the pMS^3 spectra of its fragment m/z 256.0151 (LMG), it was possible to deduce that the oxidation occurred on the glucuronide moiety, not the LMG-part of the TP430 since its fragmentation matched with the one of the LMG standard (*Figure SI 11 and 12, Article Nº3, p297.*).

The LMG biodegradation TPs (green pathway, **Figure 4.2.**) that were identified are the same as the ones formed by human metabolism (red pathway, **Figure 4.2.**), and it was possible to obtain both authentic standards (LMG-N2-oxide was purchased and N2-Me-LMG was custom synthetized). Therefore, both compounds were confirmed with the *confidence level 1*. However, in order to exclude false positive results due to possible presence of these human metabolites in the activated sludge that served as the matrix, LMG isotopically labelled standard ($^{13}C_3$-LMG) was degraded as well. The results of this batch experiment gave an opportunity to double check that indeed both compounds formed in the batch reactors since their isotopically labelled analogues were detected as well (*Figure SI 4 and 5, Article Nº3, p277.-278.*). Although this confirmation was not used strictly for the precise structural identification of the TPs in this thesis (due to the availability of the genuine standards), still it demonstrates an additional strategy that can be used for elucidation of TPs.

4.3.2. Pharmaceutical impurities of lamotrigine and environmental relevance

The two papers dealing with the degradation of LMG and related compounds presented in this thesis were triggered by screening for potential pharmaceutical impurities of LMG. Initially, we wanted to check whether some pharmaceutical impurities could be environmentally relevant. List of selected impurities of LMG that were screened in wastewater and surface water samples are shown in **Figure 4.2.** as purple "pathway". One of those impurities drawn, OXO-LMG (OXO-LMG is named in European Pharmacopeia as Lamotrigine Imputiy A, and in the United States pharmacopeia (USP) as C) was detected in real-world samples, but, as can be seen in the two papers on degradation of LMG included here, the presence of OXO-LMG in the environmental samples was explained via transformation reactions of the metabolite LMG-N2-G. In order to test whether some of the pharmaceutical impurities shown in **Figure 4.2.** are present in the tablet itself, we extracted and analysed one tablet containing 25 mg of LMG. This tablet is sold under the name of Lamictal® by GlaxoSmithKline. The tablet was crushed to powder and the extraction was performed with methanol (MeOH) and ultrasonic bath (15 mL of MeOH in a 15 min cycle). The mixture containing the MeOH and the tablet was later centrifuged and the supernatant collected. An aliquot of the supernatant was collected, diluted with water and injected into LC-HRMS with the screening method reported in Article N° 3 (Zonja et al. 2016b). The results of the analysis can be seen in the **Figure 4.3.** In the

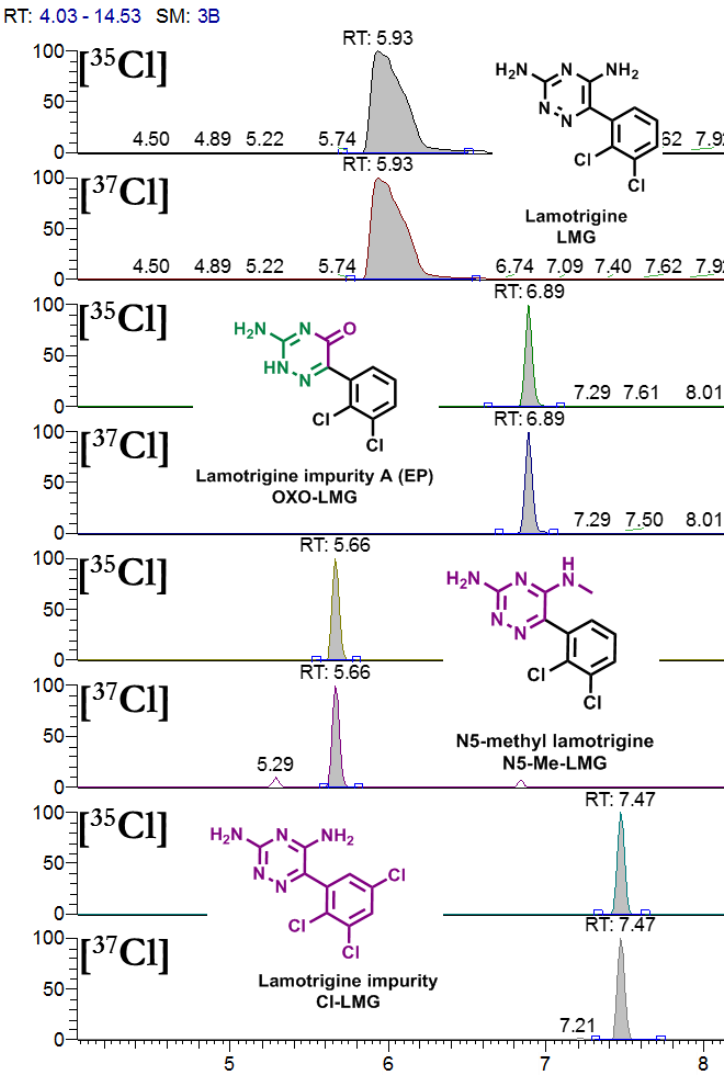

Figure 4.3 LMG and its impurities detected in the lamotrigine tablet. For every compound detected, both ^{35}Cl and ^{37}Cl isotopic $[M+H]^+$ are shown.

LMG tablet analysed, three impurities have been detected; Cl-LMG, N5-Me-LMG and OXO-LMG. Although no standards were available to quantify the first two detected impurities, their intensities are much lower than that of the OXO-LMG: As defined by the USP, the concentration of the OXO-LMG should not be more than (NMT) 0.5 % (USP 2016) and in the tablet analysed here, the relative concentration was a bit lower. This in turn means that while the final results did not go in favour that pharmaceutical impurities could be detected in the wastewater and surface water samples, the presence of OXO-LMG already in the WWTP influent samples (Article N°3) (Zonja et al. 2016b), and even in the hospital effluent samples (Article N°4) (Zonja et al. 2016) could indicate that the final concentration of the compound, in very small part only, is enhanced by the presence of the impurity in the tablet itself.

4.3.3. Quantification in high resolution mass spectrometry using chlorine isotopic pattern

In the two articles included in this chapter, LMG-related compounds were quantified in hospital, wastewater and surface water samples taking advantage of the characteristic isotopic pattern of the molecular ions, all of which contain two chlorine atoms (**Figure 4.4.**). In quantitative HRMS, there are several approaches with the two most prevalent i) the use of only the full scan MS data and ii) full scan MS data in combination with MS^2 i.e. full MS for the precursor and one fragment (MS^2). However, only the latter fulfils the requirements of the European Commission Decision 2002/657/EC which defines the criteria for using MS in

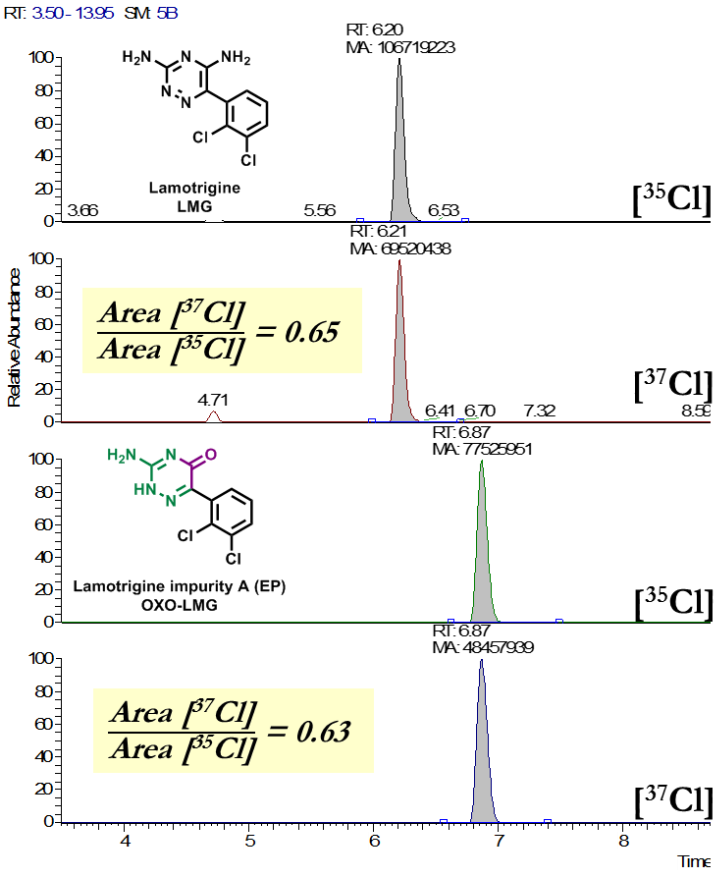

Figure 4.4. Chlorine isotopic ratio in the molecular ions used for quantification, here shown for LMG and OXO-LMG.

the analysis of organic compounds. When applying HRMS only the latter of the two quantification approaches can achieve the minimum numbers of identification points of 4.5 identification points (IP) (2 for the precursor and 2.5 for one fragment). Here, an alternative quantification method was used which afforded a comparable level of identification as the precursor ion/ fragment ion approach. It consisted of measuring the intensities of both m/z of the $[^{35}Cl\text{-}M+H]^+$ and m/z of the $[^{37}Cl\text{-}M+H]^+$ of all the analytes. The criteria for positive compound identification were set as follows i) retention time tolerance of +/- 0.2 min; ii) exact mass accuracy (<5 ppm) and; iii) relative chlorine isotope pattern tolerance with the theoretical ration of $^{35}Cl/^{37}Cl$. The advantage of using $[^{37}Cl\text{-}M+H]^+$ intensity over the fragmentation resides in the fact that the maximum sensitivity is achieved because of the high relative abundance of the ^{37}Cl isotope in the molecular ion cluster. Since LMG and all its related compounds detected here have two chlorine atoms, this amounts to ~63 % of the precursor ion intensity. This in terms results into much improved limits of detection. Isotopic pattern of other elements like bromine or compounds with several chlorine atoms would make it even more beneficial. On the other hand, the use of the ^{13}C isotope is less appealing since it only accounts approximately 1 % per carbon present in the molecule. In this case, a more appropriate option would be a use of fragment ion approach which was used here for quantification of ICM in surface water samples (Article N°2) (Zonja et al. 2015). But in special cases when a compound does not fragment no matter the collision energy applied (i.e. fullerene), then a isotopic ratio approach using ^{13}C could be the only option for HRMS confirmation of an analyte (Emke et al. 2015).

4.4. Conclusions

In this chapter, a combination of suspect and TPs profiling approach was explored for the detection of TPs of LMG and its main human metabolite lamotrigine N2-G formed in both aerated activated sludge batch reactors and pH-dependent hydrolysis.

Based on the results obtained, the following specific conclusions could be drawn:

~ In Article Nº3, a suspect screening approach was applied to wastewater and surface water samples using a suspect list containing the exact masses of LMG and its known human metabolites, phototransformation products, and its pharmaceutical impurities. Out of twelve suspect analytes from the list, five were detected in the analyzed samples. Among the suspect analytes detected, LMG synthetic impurity (OXO-LMG) was detected at relative higher concentrations in WWTP effluent samples, suggesting its formation as the result of the LMG biotransformation in the secondary treatment of WWTP.

~ In order to evaluate the origin of OXO-LMG, biodegradation batch reactors amended with mixed liquor from WWTPs were performed. LMG was resistant to biodegradation and it only formed two TPs as the result of N-methylation and N-oxidation (same as human metabolism), but OXO-LMG was not detected. But, when the human metabolite of LMG, LMG-N2-G, was degraded in the same batch setup, it was demonstrated that this compound was the source of OXO-LMG in wastewater. In this batch reactors, LMG-N2-G was transformed to three stable TPs following pseudo-first order kinetics; i) LMG as the result of common glucuronide hydrolysis, ii) OXO-LMG via amidine hydrolysis and iii) LMG-N2-G-TP430 as the result of oxidation of the glucuronide moiety to a corresponding glycal. Two of the TPs (LMG and OXO-LMG) were confirmed with an authentic standard. With the three LMG-N2-G TPs identified (LMG, OXO-LMG and LMG-N2-G-TP430), its mass balance in batch reactors with the initial concentration of 0.5 and 5 μg/L was closed at 86 and 102 %, respectively.

~ In order to also evaluate the possible abiotic route of OXO-LMG formation in wastewater, in Article Nº4, LMG-N2-G reaction pathways were explored at the pH

range of 4 – 9. This resulted in the finding that LMG-N2-G amidine and guanidine moieties underwent hydrolysis under neutral to basic pH (pH 7 – 9). In this pH range, LMG-N2-G was transformed to three stable TPs, TP433-Amd, TP433-Gnd and TP450-Gnd. Kinetic experiments with 20 and 200 nM of LMG-N2-G at pH 9 in wastewater showed exponential decrease of LMG-N2-G, followed by the formation of LMG-N2-G-TP433-Amd.

~ In addition to LMG-N2-G, pH dependent stability of other LMG related compounds showed that LMG and LMG-N2-oxide did not form amidine and guanidine TPs. However, because of different imino tautomer equilibrium both LMG-N2-G and N2-methyl-LMG were susceptible to amidine and guanidine hydrolysis at basic pH.

~ With all the TPs identified a target method based on LC-HRMS and chlorine isotope approach was developed for the quantification of LMG-related compounds in wastewater and surface water samples. Similar to the batch experiments, in three WWTPs investigated the mass balance of LMG-N2-G was closed between 71 and 102 %. In surface water samples, median concentration of all detected LMG-related compound was between 23 and 139 ngL^{-1}. LMG-N2-G abiotic transformation product (LMG-N2-G-TP433-Amd) was only detected in one WWTP influent. However, in the hospital effluent samples which were monitored over a course of one week, this compound was detected in every sample analysed with the median concentration of 134 ngL^{-1}. Although it cannot be excluded that the formation of LMG-N2-G-TP433-Amd occurred during the 24-hour collection in the autosampler (pH range measured was between 8.65 and 8.90), still it was necessary to know its concentration in order to avoid underestimation of LMG-N2-G concentration due to the amidine hydrolysis.

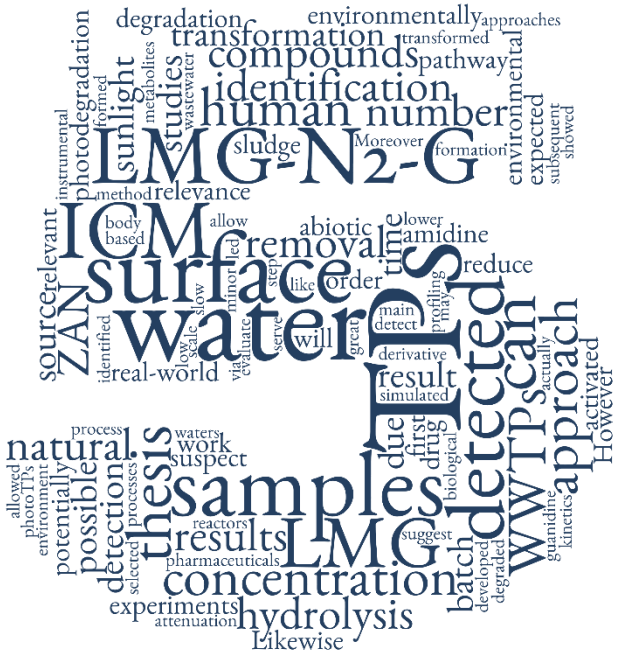

Chapter 5. General Conclusions

Pharmaceuticals can be transformed to TPs as a result of various processes. Studies regarding the fate and occurrence of pharmaceuticals and their TPs have been on the rise over the last decades. However, due to typically lower concentration of TPs in natural waters, it was not until the improvements of instrumental sensitivity and resolution at an affordable price that have allowed to increase significantly the number of reports on their presence in the environment.

In this thesis, the first objective was to evaluate the phototransformation of the antiviral zanamivir by profiling its photoTPs which were generated under natural and simulated sunlight. ZAN was selected because of an outbreak of avian flu at that time. The process was selected due to its relevance to surface water, because ZAN exhibited low metabolism rate in the human body, and equally low elimination in WWTPs. The results have showed that ZAN can be degraded under natural sunlight but following slow kinetics. Likewise, it can be expected that its attenuation in the surface water would be the result of transformation, rather than mineralisation. However, when ZAN and the tentatively identified TPs were retrospectively screened from surface water extracts, none of them were detected. This suggests that the approach of TPs profiling used here, although straightforward, will not automatically translate results of the batch experiments to real-world samples. Likewise, due to time constrains and the question of relevance, it may not be suitable when dealing with a considerably elevated number of TPs formed and detected in batch experiments. The failed detection of both ZAN and its TPs was the main reason why subsequent studies presented in this thesis always started by applying a suspect screening approach, which included a previous step of their TPs prior detection in the environmental samples.

Therefore, as second objective of this thesis, a more sophisticated approach was developed in order to allow to reduce the laborious work of TP identification efforts on those TPs that are actually detected in the real-world samples. Here, the six ICM compounds (iohexol, iomeprol, iopamidol, iopromide, iodixanol and diatrizoate) were photodegraded

under simulated sunlight in surface water. With the optimised approach, it was possible to reduce the number of TPs detected in laboratory studies (108) to a subset of 11, based on their detection frequency in surface water samples which were analysed with a generic SPE method. By setting the 50 % thresholds, the number of compounds potentially detected in the environment was filtered out those that are eventually identified. The identification which was based on UPLC-HRMS (Orbitrap) and NMR, in cases when it was possible to separate the TPs using semipreparative liquid chromatography. Their structural elucidation led to propose that the main photodegradation pathway of ICM will sustain in surface water under natural sunlight is some type of deiodination. This was observed in 10 out of 11 TPs. Due to the availability of the isolation of pure standards for some of the TPs, the target analytical method developed allowed to detect them in 97 % of the surface water samples, and quantified in 70 % of the samples. In addition to the first detection of these TPs in surface water samples, this was the first time concentrations of the dimer ICM (IDX) were reported in environmental samples.

A potential follow-up work would be to characterise the kinetics of formation of these photoTPs in order to assess both: i) the relevance of their removal via photodegradation in surface water, over biodegradation removal during activated sludge process in WWTPs, and ii) identification of photodegradation TPs of known biodegradation TPs formed in activated sludge.

The subsequent objective of the thesis was to evaluate the degradation of the anticonvulsant LMG in WWTPs and identification of its bioTPs. This approach showed that instead of conducting the degradation studies at the early stage, a suspect list that was compiled from literature including LMG human metabolites, TPs and impurities can serve as an informative starting point. Here three human metabolites and a LMG pharmaceutical impurity were detected in influent and effluent WW samples. Semiquantitative analysis suggested that the concentration of OXO-LMG increased while the LMG N2-G concentration was reduced after their passage from the biological WW treatment tank. The combination of suspect and targeted approach led to the discovery of an unexpected transformation pathway of LMG-N2-G. In order to understand this behaviour, the biodegradation batch studies at lab scale were conducted for both LMG and LMG-N2-G showing slow biodegradation of LMG (with only minor biotransformation TPs detected), and LMG-N2-G as the source of OXO-LMG in wastewater.

Moreover, LMG-N2-G can also be transformed by abiotic, pH dependent, amidine and guanidine hydrolysis. Transformation of the glucuronide to its amidine derivative under neutral to basic pH can be an additional source of OXO-LMG due to its possible further hydrolysis in the WWTPs. Other, minor, TPs detected in the abiotic batch reactors were the result of guanidine hydrolysis and can be expected to be less environmentally relevant. For a similar initial concentration of LMG-N2-G, its calculated half-life was much shorter in biological reactors with activated sludge than in any of the abiotic ones. As the result, it is expected that both pathways will compete in the transformation of LMG-N2-G in environments with lower concentration of biomass like surface water. However, in WWTPs, the transformation of LMG-N2-G would proceed via a biotic pathway. Since LMG is extensively metabolised in the human body to LMG-N2-G, it would be possible to reduce the high environmental concentration of LMG by forcing the formation of the LMG-N2-G amidine derivative. This would likely yield OXO-LMG by glucuronide hydrolysis in WWTPs. Additional experiments with the purpose whether OXO-LMG is more easily degraded with AOP like ozonation or UV, or natural attenuation in surface water could demonstrate if this reaction is more convenient for removal.

This study shows an example of a glucuronide drug conjugate that does not exclusively undergo hydrolysis to revert back to its parent compound in wastewater. Instead, it is specifically this human metabolite that is the source of the majority of the LMG-derived TPs in water. It was shown that in this case the human metabolism of a drug is a necessary step in forming novel downstream water contaminants. Likewise, the results of this thesis suggest that glucuronide conjugates of other pharmaceuticals may similarly prove to be sources of yet undiscovered but environmentally relevant compounds.

Finally, the overall results of this thesis suggest that contemporary instrumental techniques allow to work with time-effective approaches which are of great help to detect and identify potentially great number of TPs for a particular drug and could have a potentially wide application in the evaluation of the degradation of variety of polar compounds at real scale. This is a genuine advantage of the approaches described since they dedicate time for the identification of only those TPs that are actually detected in real-world samples, making them environmentally relevant. Moreover, the results of this thesis contribute to a better understanding of removal processes of the compounds investigated here which can serve as basis for development of alternative removal technologies from source waters.


Water
Products
Mass
Analytical
Environ
Res
Sci
Journal
Barceló
Hollender
Richardson
treatment
contrast
Transformation
iodinated
Identification
Wastewater
compounds
emerging
organic
contaminants
drugs
Ternes
waters
Pérez
drug
aqueous
human
Bioanalytical
degradation
Occurrence
Biotransformation
Rapid
Trends
X-ray
kinetics
advanced
tandem
pathways
effluents
oxidation
diclofenac
Talanta

References

Aceña, J., Pérez, S., Gardinali, P., Abad, J.L., Eichhorn, P., Heuett, N. and Barceló, D. (2014) Structure elucidation of phototransformation products of unapproved analogs of the erectile dysfunction drug sildenafil in artificial freshwater with UPLC-Q Exactive-MS. Journal of Mass Spectrometry 49(12), 1279-1289.

Aceña, J., Rivas, D., Zonja, B., Péreza, S. and Barceló́a, D. (2015a) Fast Liquid Chromatography–Mass Spectrometry Methods in Food and Environmental Analysis, pp. 347-377, World Scientific.

Aceña, J., Stampachiacchiere, S., Pérez, S. and Barceló, D. (2015b) Advances in liquid chromatography - High-resolution mass spectrometry for quantitative and qualitative environmental analysis. Analytical and Bioanalytical Chemistry 407(21), 6289-6299.

AEMPS http://www.aemps.gob.es/medicamentosUsoHumano/observatorio/home.htm.

Aguera, A., Perez Estrada, L.A., Ferrer, I., Thurman, E.M., Malato, S. and Fernandez-Alba, A.R. (2005) Application of time-of-flight mass spectrometry to the analysis of phototransformation products of diclofenac in water under natural sunlight. J Mass Spectrom 40(7), 908-915.

Al-Qaim, F.F., Abdullah, M.P., Othman, M.R., Latip, J. and Zakaria, Z. (2014) Multi-residue analytical methodology-based liquid chromatography-time-of-flight-mass spectrometry for the analysis of pharmaceutical residues in surface water and effluents from sewage treatment plants and hospitals. Journal of Chromatography A 1345, 139-153.

Albini, A. and Fasani, E. (2004) Rationalizing the photochemistry of drugs. Photostability of Drugs and Drug Formulations, 67-110.

Alexander, M. (1999) Biodegradation and bioremediation, Gulf Professional Publishing.

Altmann, J., Ruhl, A.S., Zietzschmann, F. and Jekel, M. (2014) Direct comparison of ozonation and adsorption onto powdered activated carbon for micropollutant removal in advanced wastewater treatment. Water Res 55, 185-193.

Andreozzi, R., Marotta, R. and Paxéus, N. (2003) Pharmaceuticals in STP effluents and their solar photodegradation in aquatic environment. Chemosphere 50(10), 1319-1330.

Anumol, T. and Snyder, S.A. (2015) Rapid analysis of trace organic compounds in water by automated online solid-phase extraction coupled to liquid chromatography–tandem mass spectrometry. Talanta 132, 77-86.

Asha, S. and Vidyavathi, M. (2010) Role of Human Liver Microsomes in In Vitro Metabolism of Drugs—A Review. Applied Biochemistry and Biotechnology 160(6), 1699-1722.

Azuma, T., Nakada, N., Yamashita, N. and Tanaka, H. (2012) Synchronous dynamics of observed and predicted values of anti-influenza drugs in environmental waters during a seasonal influenza outbreak. Environ Sci Technol 46(23), 12873-12881.

Babic, S., Perisa, M. and Skoric, I. (2013) Photolytic degradation of norfloxacin, enrofloxacin and ciprofloxacin in various aqueous media. Chemosphere 91(11), 1635-1642.

Barceló, D. and Petrovic, M. (2007) Challenges and achievements of LC-MS in environmental analysis: 25 years on. TrAC Trends in Analytical Chemistry 26(1), 2-11.

Beattie, K., Phadke, G. and Novakovic, J. (2012) Lamotrigine. Profiles Drug Subst Excip Relat Methodol 37, 245-285.

Bedner, M. and MacCrehan, W.A. (2006) Transformation of acetaminophen by chlorination produces the toxicants 1,4-benzoquinone and N-acetyl-p-benzoquinone imine. Environmental Science and Technology 40(2), 516-522.

Beel, R., Lutke Eversloh, C. and Ternes, T.A. (2013) Biotransformation of the UV-filter sulisobenzone: challenges for the identification of transformation products. Environ Sci Technol 47(13), 6819-6828.

Beretsou, V.G., Psoma, A.K., Gago-Ferrero, P., Aalizadeh, R., Fenner, K. and Thomaidis, N.S. (2016) Identification of biotransformation products of citalopram formed in activated sludge. Water Res 103, 205-214.

Bijlsma, L., Boix, C., Niessen, W.M.A., Ibáñez, M., Sancho, J.V. and Hernández, F. (2013) Investigation of degradation products of cocaine and benzoylecgonine in the aquatic environment. Science of The Total Environment 443, 200-208.

Bitton, G. (2005) Wastewater microbiology, John Wiley & Sons.

Bletsou, A.A., Jeon, J., Hollender, J., Archontaki, E. and Thomaidis, N.S. (2015) Targeted and non-targeted liquid chromatography-mass spectrometric workflows for identification of transformation products of emerging pollutants in the aquatic environment. TrAC Trends in Analytical Chemistry 66, 32-44.

Boix, C., Ibáñez, M., Bijlsma, L., Sancho, J.V. and Hernández, F. (2014) Investigation of cannabis biomarkers and transformation products in waters by liquid chromatography coupled to time of flight and triple quadrupole mass spectrometry. Chemosphere 99, 64-71.

Boreen, A.L., Arnold, W.A. and McNeill, K. (2003) Photodegradation of pharmaceuticals in the aquatic environment: A review. Aquatic Sciences 65(4), 320-341.

Borova, V.L., Maragou, N.C., Gago-Ferrero, P., Pistos, C. and Thomaidis, N.S. (2014) Highly sensitive determination of 68 psychoactive pharmaceuticals, illicit drugs, and related human metabolites in wastewater by liquid chromatography–tandem mass spectrometry. Analytical and Bioanalytical Chemistry 406(17), 4273-4285.

Bosch, M.E., Sánchez, A.J.R., Rojas, F.S. and Ojeda, C.B. (2007) Ribavirin: Analytical determinations since the origin until today. J Pharmaceut Biomed 45(2), 185-193.

Bourdat-Deschamps, M., Leang, S., Bernet, N., Daudin, J.-J. and Nélieu, S. (2014) Multi-residue analysis of pharmaceuticals in aqueous environmental samples by online solid-phase extraction–ultra-high-performance liquid chromatography-tandem mass spectrometry: Optimisation and matrix effects reduction by quick, easy, cheap, effective, rugged and safe extraction. Journal of Chromatography A 1349, 11-23.

Brewer, A.J., Ort, C., Banta-Green, C.J., Berset, J.D. and Field, J.A. (2012) Normalized diurnal and between-day trends in illicit and legal drug loads that account for changes in population. Environmental Science and Technology 46(15), 8305-8314.

Bulloch, D.N., Lavado, R., Forsgren, K.L., Beni, S., Schlenk, D. and Larive, C.K. (2012) Analytical and biological characterization of halogenated gemfibrozil produced through chlorination of wastewater. Environmental Science and Technology 46(10), 5583-5589.

Buth, J.M., Arnold, W.A. and McNeill, K. (2007) Unexpected products and reaction mechanisms of the aqueous chlorination of cimetidine. Environmental Science and Technology 41(17), 6228-6233.

Cahill, M.G., Dineen, B.A., Stack, M.A. and James, K.J. (2012) A critical evaluation of liquid chromatography with hybrid linear ion trap-Orbitrap mass spectrometry for the determination of acidic contaminants in wastewater effluents. Journal of Chromatography A 1270, 88-95.

Casado, J., Rodríguez, I., Ramil, M. and Cela, R. (2014) Selective determination of antimycotic drugs in environmental water samples by mixed-mode solid-phase extraction and liquid chromatography quadrupole time-of-flight mass spectrometry. Journal of Chromatography A 1339, 42-49.

CATABOL (2016) CATABOL software (http://oasis-lmc.org/products/models/environmental-fate-and-ecotoxicity/catabol-301c.aspx).

Catalunya, G.d. (2003) Reglament dels serveis públics de sanejament (in catalan), pp. 11143-11158, Diari Oficial de la Generalitat de Catalunya

Celiz, M.D., Tso, J. and Aga, D.S. (2009) Pharmaceutical metabolites in the environment: Analytical challenges and ecological risks. Environmental Toxicology and Chemistry 28(12), 2473-2484.

Cerqueira, M.B.R., Guilherme, J.R., Caldas, S.S., Martins, M.L., Zanella, R. and Primel, E.G. (2014) Evaluation of the QuEChERS method for the extraction of pharmaceuticals and personal care products from drinking-water treatment sludge with determination by UPLC-ESI-MS/MS. Chemosphere 107, 74-82.

Cohen, A.F., Land, G.S., Breimer, D.D., Yuen, W.C., Winton, C. and Peck, A.W. (1987) Lamotrigine, a new anticonvulsant: Pharmacokinetics in normal humans. Clinical Pharmacology & Therapeutics 42(5), 535-541.

Coulter, D.A. (1997) Antiepileptic Drug Cellular Mechanisms of Action: Where Does Lamotrigine Fit In? Journal of Child Neurology 12(1 suppl), S2-S9.

Cunningham, V.L., Binks, S.P. and Olson, M.J. (2009) Human health risk assessment from the presence of human pharmaceuticals in the aquatic environment. Regul Toxicol Pharmacol 53(1), 39-45.

Chan, D., Tarbin, J., Sharman, M., Carson, M., Smith, M. and Smith, S. (2011) Screening method for the analysis of antiviral drugs in poultry tissues using zwitterionic hydrophilic interaction liquid chromatography/tandem mass spectrometry. Anal Chim Acta 700(1-2), 194-200.

Chan, T.W., Graham, N.J.D. and Chu, W. (2010) Degradation of iopromide by combined UV irradiation and peroxydisulfate. J Hazard Mater 181(1–3), 508-513.

ChemAxon-Marvin (2016) Marvin was used for drawing, displaying and characterizing chemical structures, substructures and reactions, Marvin 6.1, 2013, ChemAxon (http://www.chemaxon.com).

Chemaxon (2016) Chemaxon platform, Chemicalize (https://www.chemaxon.com/).

Chiron, S., Gomez, E. and Fenet, H. (2010) Nitration Processes of Acetaminophen in Nitrifying Activated Sludge. Environ Sci Technol 44(1), 284-289.

Chu, W., Wang, Y.R. and Leung, H.F. (2011) Synergy of sulfate and hydroxyl radicals in UV/S2O82−/H2O2 oxidation of iodinated X-ray contrast medium iopromide. Chemical Engineering Journal 178, 154-160.

D'Ascenzo, G., Di Corcia, A., Gentili, A., Mancini, R., Mastropasqua, R., Nazzari, M. and Samperi, R. (2003) Fate of natural estrogen conjugates in municipal sewage transport and treatment facilities. Science of The Total Environment 302(1–3), 199-209.

Deborde, M. and von Gunten, U. (2008) Reactions of chlorine with inorganic and organic compounds during water treatment-Kinetics and mechanisms: A critical review. Water Res 42(1-2), 13-51.

DellaGreca, M., Iesce, M.R., Isidori, M., Nardelli, A., Previtera, L. and Rubino, M. (2007) Phototransformation products of tamoxifen by sunlight in water. Toxicity of the drug and its derivatives on aquatic organisms. Chemosphere 67(10), 1933-1939.

Dettmer, K., Aronov, P.A. and Hammock, B.D. (2007) Mass spectrometry-based metabolomics. Mass spectrometry reviews 26(1), 51-78.

Di Meo, F., Steel, M., Nicolas, P., Marquet, P., Duroux, J.-L. and Trouillas, P. (2013) Acylglucuronide in alkaline conditions: migration vs. hydrolysis. Journal of Molecular Modeling 19(6), 2423-2432.

Diaz, R., Ibáñez, M., Sancho, J.V. and Hernández, F. (2013) Qualitative validation of a liquid chromatography–quadrupole-time of flight mass spectrometry screening method for organic pollutants in waters. Journal of Chromatography A 1276, 47-57.

Dodd, M.C. and Huang, C.H. (2004) Transformation of the antibacterial agent sulfamethoxazole in reactions with chlorine: Kinetics, mechanisms, and pathways. Environmental Science and Technology 38(21), 5607-5615.

Doig, M.V. and Clare, R.A. (1991) Use of thermospray liquid chromatography-mass spectrometry to aid in the identification of urinary metabolites of a novel antiepileptic drug, Lamotrigine. Journal of Chromatography A 554(1-2), 181-189.

Doll, T.E. and Frimmel, F.H. (2003) Fate of pharmaceuticals--photodegradation by simulated solar UV-light. Chemosphere 52(10), 1757-1769.

Doll, T.E. and Frimmel, F.H. (2004) Kinetic study of photocatalytic degradation of carbamazepine, clofibric acid, iomeprol and iopromide assisted by different TiO2 materials—determination of intermediates and reaction pathways. Water Res 38(4), 955-964.

Dray, J., Dray, T. and Ullmann, A. (1972) Hydrolysis of urinary metabolites of different steroid hormones by-glucuronidase from Escherichia coli, p. 853.

DrugBank (2016) The DrugBank Database v5.0 (http://www.drugbank.ca/).

Duirk, S.E., Lindell, C., Cornelison, C.C., Kormos, J., Ternes, T.A., Attene-Ramos, M., Osiol, J., Wagner, E.D., Plewa, M.J. and Richardson, S.D. (2011) Formation of toxic iodinated disinfection by-products from compounds used in medical imaging. Environ Sci Technol 45(16), 6845-6854.

Dunn, W.B., Broadhurst, D., Brown, M., Baker, P.N., Redman, C.W.G., Kenny, L.C. and Kell, D.B. (2008) Metabolic profiling of serum using Ultra Performance Liquid Chromatography and the LTQ-Orbitrap mass spectrometry system. Journal of Chromatography B: Analytical Technologies in the Biomedical and Life Sciences 871(2), 288-298.

Durand, S., Sancelme, M., Besse-Hoggan, P. and Combourieu, B. (2010) Biodegradation pathway of mesotrione: complementarities of NMR, LC-NMR and LC-MS for qualitative and quantitative metabolic profiling. Chemosphere 81(3), 372-380.

Echeverría, S., Herrero, P., Borrull, F., Fontanals, N. and Pocurull, E. (2013) Performance of zwitterionic hydrophilic interaction LC for the determination of iodinated X-ray contrast agents. J Sep Sci 36(23), 3688-3695.

Eichhorn, P., Ferguson, P.L., Pérez, S. and Aga, D.S. (2005) Application of ion trap-MS with H/D exchange and QqTOF-MS in the identification of microbial degradates of trimethoprim in nitrifying activated sludge. Analytical Chemistry 77(13), 4176-4184.

Eichhorn, P., Perez, S., Acena, J., Gardinali, P., Abad, J.L. and Barcelo, D. (2012a) Identification of phototransformation products of sildenafil (Viagra) and its N-demethylated human metabolite under simulated sunlight. J Mass Spectrom 47(6), 701-711.

Eichhorn, P., Pérez, S. and Barceló, D. (2012b) Time-of-Flight Mass Spectrometry Versus Orbitrap-Based Mass Spectrometry for the Screening and Identification of Drugs and Metabolites: Is There a Winner? 58, 217-272.

Emke, E., Sanchís, J., Farré, M., Bäuerlein, P. and de Voogt, P. (2015) Determination of several fullerenes in sewage water by LC HR-MS using atmospheric pressure photoionisation. Environmental Science: Nano 2(2), 167-176.

Emmanuel, E., Keck, G., Blanchard, J.-M., Vermande, P. and Perrodin, Y. (2004) Toxicological effects of disinfections using sodium hypochlorite on aquatic organisms and its contribution to AOX formation in hospital wastewater. Environment International 30(7), 891-900.

Ens, W., Senner, F., Gygax, B. and Schlotterbeck, G. (2014) Development, validation, and application of a novel LC-MS/MS trace analysis method for the simultaneous quantification of seven iodinated X-ray contrast media and three artificial sweeteners in surface, ground, and drinking water. Anal Bioanal Chem 406(12), 2789-2798.

ENVYPY (2016) http://www.eawag.ch/en/department/uchem/projekte/envipy/.

Fabbri, D., Calza, P., Dalmasso, D., Chiarelli, P., Santoro, V. and Medana, C. (2016) Iodinated X-ray contrast agents: Photoinduced transformation and monitoring in surface water. Science of The Total Environment 572, 340-351.

Fatta-Kassinos, D., Hapeshi, E., Malato, S., Mantzavinos, D., Rizzo, L. and Xekoukoulotakis, N.P. (2010) Xenobiotics in the Urban Water Cycle: Mass Flows, Environmental Processes, Mitigation and Treatment Strategies. Fatta-Kassinos, D., Bester, K. and Kümmerer, K. (eds), pp. 387-412, Springer Netherlands, Dordrecht.

Fatta-Kassinos, D., Meric, S. and Nikolaou, A. (2011a) Pharmaceutical residues in environmental waters and wastewater: current state of knowledge and future research. Analytical and Bioanalytical Chemistry 399(1), 251-275.

Fatta-Kassinos, D., Vasquez, M.I. and Kümmerer, K. (2011b) Transformation products of pharmaceuticals in surface waters and wastewater formed during photolysis and advanced oxidation processes – Degradation, elucidation of byproducts and assessment of their biological potency. Chemosphere 85(5), 693-709.

FDA (2016a) Orange Book: Approved Drug Products with Therapeutic Equivalence Evaluations.

FDA (2016b) U. S. Food and Drug Administration (http://www.fda.gov/)

Fedorova, G., Grabic, R., Nyhlen, J., Järhult, J.D. and Söderström, H. (2016) Fate of three anti-influenza drugs during ozonation of wastewater effluents – degradation and formation of transformation products. Chemosphere 150, 723-730.

Fedorova, G., Randak, T., Lindberg, R.H. and Grabic, R. (2013) Comparison of the quantitative performance of a Q-Exactive high-resolution mass spectrometer with that of a triple quadrupole tandem mass spectrometer for the analysis of illicit drugs in wastewater. Rapid Communications in Mass Spectrometry 27(15), 1751-1762.

Fent, K., Weston, A.A. and Caminada, D. (2006) Ecotoxicology of human pharmaceuticals. Aquatic Toxicology 76(2), 122-159.

Ferrer, I. and Thurman, E.M. (2010) Identification of a New Antidepressant and its Glucuronide Metabolite in Water Samples Using Liquid Chromatography/Quadrupole Time-of-Flight Mass Spectrometry. Analytical Chemistry 82(19), 8161-8168.

Ferrer, I. and Thurman, E.M. (2012) Analysis of 100 pharmaceuticals and their degradates in water samples by liquid chromatography/quadrupole time-of-flight mass spectrometry. Journal of Chromatography A 1259, 148-157.

Gago-Ferrero, P., Schymanski, E.L., Bletsou, A.A., Aalizadeh, R., Hollender, J. and Thomaidis, N.S. (2015) Extended suspect and non-target strategies to characterize emerging polar organic contaminants in raw wastewater with LC-HRMS/MS. Environ Sci Technol 49(20), 12333-12341.

Galbavy, E.S., Ram, K. and Anastasio, C. (2010) 2-Nitrobenzaldehyde as a chemical actinometer for solution and ice photochemistry. J Photoch Photobio A 209(2-3), 186-192.

Gallart-Ayala, H., Nuñez, O., Moyano, E., Galceran, M. and Martins, C. (2011) Preventing false negatives with high-resolution mass spectrometry: the benzophenone case. Rapid Communications in Mass Spectrometry 25(20), 3161-3166.

Gao, J., Ellis, L.B.M. and Wackett, L.P. (2010) The University of Minnesota Biocatalysis/Biodegradation Database: Improving public access. Nucleic Acids Research 38(SUPPL.1), D488-D491.

Garcia-Galan, M.J., Fromel, T., Muller, J., Peschka, M., Knepper, T., Diaz-Cruz, S. and Barcelo, D. (2012) Biodegradation studies of N4-acetylsulfapyridine and N4-acetylsulfamethazine in environmental water by applying mass spectrometry techniques. Anal Bioanal Chem 402(9), 2885-2896.

Goldstein, M., Shenker, M. and Chefetz, B. (2014) Insights into the Uptake Processes of Wastewater-Borne Pharmaceuticals by Vegetables. Environ Sci Technol 48(10), 5593-5600.

Gomes, R.L., Scrimshaw, M.D. and Lester, J.N. (2009) Fate of Conjugated Natural and Synthetic Steroid Estrogens in Crude Sewage and Activated Sludge Batch Studies. Environ Sci Technol 43(10), 3612-3618.

Gomez-Canela, C., Ventura, F., Caixach, J. and Lacorte, S. (2014) Occurrence of cytostatic compounds in hospital effluents and wastewaters, determined by liquid chromatography coupled to high-resolution mass spectrometry. Anal Bioanal Chem 406(16), 3801-3814.

Gomez-Ramos Mdel, M., Perez-Parada, A., Garcia-Reyes, J.F., Fernandez-Alba, A.R. and Aguera, A. (2011) Use of an accurate-mass database for the systematic identification of transformation products of organic contaminants in wastewater effluents. J Chromatogr A 1218(44), 8002-8012.

Goncalves, C., Perez, S., Osorio, V., Petrovic, M., Alpendurada, M.F. and Barcelo, D. (2011) Photofate of oseltamivir (Tamiflu) and oseltamivir carboxylate under natural and simulated solar irradiation: kinetics, identification of the transformation products, and environmental occurrence. Environ Sci Technol 45(10), 4307-4314.

Grabic, R., Fick, J., Lindberg, R.H., Fedorova, G. and Tysklind, M. (2012) Multi-residue method for trace level determination of pharmaceuticals in environmental samples using liquid chromatography coupled to triple quadrupole mass spectrometry. Talanta 100, 183-195.

Gros, M., Cruz-Morato, C., Marco-Urrea, E., Longrée, P., Singer, H., Sarrà, M., Hollender, J., Vicent, T., Rodriguez-Mozaz, S. and Barceló, D. (2014) Biodegradation of the X-ray contrast agent iopromide and the fluoroquinolone antibiotic ofloxacin by the white rot fungus Trametes versicolor in hospital wastewaters and identification of degradation products. Water Res 60, 228-241.

Gros, M., Petrovic, M. and Barcelo, D. (2008) Tracing pharmaceutical residues of different therapeutic classes in environmental waters by using liquid chromatography/quadrupole-linear ion trap mass spectrometry and automated library searching. Analytical Chemistry 81(3), 898-912.

Gros, M., Rodríguez-Mozaz, S. and Barceló, D. (2012) Fast and comprehensive multi-residue analysis of a broad range of human and veterinary pharmaceuticals and some of their metabolites in surface and treated waters by ultra-high-performance liquid chromatography coupled to quadrupole-linear ion trap tandem mass spectrometry. Journal of Chromatography A 1248, 104-121.

Gros, M., Rodríguez-Mozaz, S. and Barceló, D. (2013) Rapid analysis of multiclass antibiotic residues and some of their metabolites in hospital, urban wastewater and river water by ultra-high-performance liquid chromatography coupled to quadrupole-linear ion trap tandem mass spectrometry. Journal of Chromatography A 1292, 173-188.

Gros, M., Williams, M., Llorca, M., Rodriguez-Mozaz, S., Barcelo, D. and Kookana, R.S. (2015) Photolysis of the antidepressants amisulpride and desipramine in wastewaters: Identification of transformation products formed and their fate. Sci Total Environ 530-531, 434-444.

Guillarme, D., Veuthey, J.-L. and Smith, R.M. (2012) UHPLC in life sciences, Royal Society of Chemistry.

Gulde, R., Meier, U., Schymanski, E.L., Kohler, H.-P.E., Helbling, D.E., Derrer, S., Rentsch, D. and Fenner, K. (2016) Systematic Exploration of Biotransformation Reactions of Amine-Containing Micropollutants in Activated Sludge. Environ Sci Technol 50(6), 2908-2920.

Gunaydin, H. and Houk, K. (2009) Mechanisms of peroxynitrite-mediated nitration of tyrosine. Chem Res Toxicol 22(5), 894-898.

Gurke, R., Rößler, M., Marx, C., Diamond, S., Schubert, S., Oertel, R. and Fauler, J. (2015a) Occurrence and removal of frequently prescribed pharmaceuticals and corresponding metabolites in wastewater of a sewage treatment plant. Science of The Total Environment 532, 762-770.

Gurke, R., Rossmann, J., Schubert, S., Sandmann, T., Rößler, M., Oertel, R. and Fauler, J. (2015b) Development of a SPE-HPLC–MS/MS method for the determination of most prescribed pharmaceuticals and related metabolites in urban sewage samples. Journal of Chromatography B 990, 23-30.

Helbling, D.E., Hollender, J., Kohler, H.P.E. and Fenner, K. (2010a) Structure-based interpretation of biotransformation pathways of amide-containing compounds in sludge-seeded bioreactors. Environmental Science and Technology 44(17), 6628-6635.

Helbling, D.E., Hollender, J., Kohler, H.P.E., Singer, H. and Fenner, K. (2010b) High-throughput identification of microbial transformation products of organic micropollutants. Environmental Science and Technology 44(17), 6621-6627.

Helbling, D.E., Johnson, D.R., Honti, M. and Fenner, K. (2012) Micropollutant biotransformation kinetics associate with WWTP process parameters and microbial community characteristics. Environ Sci Technol 46(19), 10579-10588.

Hemström, P. and Irgum, K. (2006) Hydrophilic interaction chromatography. J Sep Sci 29(12), 1784-1821.

Hernández, F., Ibáñez, M., Bade, R., Bijlsma, L. and Sancho, J.V. (2014) Investigation of pharmaceuticals and illicit drugs in waters by liquid chromatography-high-resolution mass spectrometry. TrAC - Trends in Analytical Chemistry 63, 140-157.

Hirsch, R., Ternes, A.T., Lindart, A., Haberer, K. and Wilken, -.D.R. (2000) A sensitive method for the determination of iodine containing diagnostic agents in aqueous matrices using LC-electrospray-tandem-MS detection. Fresenius' Journal of Analytical Chemistry 366(8), 835-841.

Hirte, K., Seiwert, B., Schüürmann, G. and Reemtsma, T. (2016) New hydrolysis products of the beta-lactam antibiotic amoxicillin, their pH-dependent formation and search in municipal wastewater. Water Res 88, 880-888.

Hogenboom, A.C., Van Leerdam, J. and De Voogt, P. (2009) Accurate mass screening and identification of emerging contaminants in environmental samples by liquid chromatography–hybrid linear ion trap Orbitrap mass spectrometry. Journal of Chromatography A 1216(3), 510-519.

Holčapek, M., Kolářová, L. and Nobilis, M. (2008) High-performance liquid chromatography–tandem mass spectrometry in the identification and determination of phase I and phase II drug metabolites. Analytical and Bioanalytical Chemistry 391(1), 59-78.

Hopfgartner, G., Varesio, E., Tschäppät, V., Grivet, C., Bourgogne, E. and Leuthold, L.A. (2004) Triple quadrupole linear ion trap mass spectrometer for the analysis of small molecules and macromolecules. Journal of Mass Spectrometry 39(8), 845-855.

Howard, P.H. and Muir, D.C. (2010) Identifying new persistent and bioaccumulative organics among chemicals in commerce. Environ Sci Technol 44(7), 2277-2285.

Hu, Q., Noll, R.J., Li, H., Makarov, A., Hardman, M. and Graham Cooks, R. (2005) The Orbitrap: a new mass spectrometer. Journal of Mass Spectrometry 40(4), 430-443.

Huang, C.H., Dodd, M.C. and Shah, A.D. (2008) Reaction and Transformation of Antibacterial Agents with Aqueous Chlorine Under Relevant Water Treatment Conditions. Fate of Pharmaceuticals in the Environment and in Water Treatment Systems, 261-289.

Huber, M.M., Canonica, S., Park, G.-Y. and von Gunten, U. (2003) Oxidation of Pharmaceuticals during Ozonation and Advanced Oxidation Processes. Environ Sci Technol 37(5), 1016-1024.

Huerta, B., Jakimska, A., Llorca, M., Ruhí, A., Margoutidis, G., Acuña, V., Sabater, S., Rodriguez-Mozaz, S. and Barcelò, D. (2014) Development of an extraction and purification method for the determination of multi-class pharmaceuticals and endocrine disruptors in freshwater invertebrates. Talanta 132, 373-381.

Huntscha, S., Hofstetter, T.B., Schymanski, E.L., Spahr, S. and Hollender, J. (2014) Biotransformation of benzotriazoles: Insights from transformation product identification and compound-specific isotope analysis. Environmental Science and Technology 48(8), 4435-4443.

Ikegami, T., Tomomatsu, K., Takubo, H., Horie, K. and Tanaka, N. (2008) Separation efficiencies in hydrophilic interaction chromatography. Journal of Chromatography A 1184(1), 474-503.

IMSHealth (2015) Global Medicines Use in 2020. 4.

Jelić, A., Petrović, M. and Barceló, D. (2012) Emerging Organic Contaminants and Human Health. Barceló, D. (ed), pp. 47-70, Springer Berlin Heidelberg, Berlin, Heidelberg.

Jelic, A., Rodriguez-Mozaz, S., Barceló, D. and Gutierrez, O. (2015) Impact of in-sewer transformation on 43 pharmaceuticals in a pressurized sewer under anaerobic conditions. Water Res 68, 98-108.

Jeong, J., Jung, J., Cooper, W.J. and Song, W. (2010) Degradation mechanisms and kinetic studies for the treatment of X-ray contrast media compounds by advanced oxidation/reduction processes. Water Res 44(15), 4391-4398.

Jones, O., Voulvoulis, N. and Lester, J. (2002) Aquatic environmental assessment of the top 25 English prescription pharmaceuticals. Water Res 36(20), 5013-5022.

Joss, A., Zabczynski, S., Göbel, A., Hoffmann, B., Löffler, D., McArdell, C.S., Ternes, T.A., Thomsen, A. and Siegrist, H. (2006) Biological degradation of pharmaceuticals in municipal wastewater treatment: Proposing a classification scheme. Water Res 40(8), 1686-1696.

Kagle, J., Porter, A.W., Murdoch, R.W., Rivera-Cancel, G. and Hay, A.G. (2009) Chapter 3 Biodegradation of Pharmaceutical and Personal Care Products. 67, 65-108.

Kaiser, E., Prasse, C., Wagner, M., Broder, K. and Ternes, T.A. (2014) Transformation of oxcarbazepine and human metabolites of carbamazepine and oxcarbazepine in wastewater treatment and sand filters. Environ Sci Technol 48(17), 10208-10216.

Kasprzyk-Hordern, B., Dinsdale, R.M. and Guwy, A.J. (2008) The occurrence of pharmaceuticals, personal care products, endocrine disruptors and illicit drugs in surface water in South Wales, UK. Water Res 42(13), 3498-3518.

Kaufmann, A., Butcher, P., Maden, K., Widmer, M., Giles, K. and Uría, D. (2009) Are liquid chromatography/electrospray tandem quadrupole fragmentation ratios unequivocal confirmation criteria? Rapid Communications in Mass Spectrometry 23(7), 985-998.

Kaufmann, A., Widmer, M. and Maden, K. (2010) Post-interface signal suppression, a phenomenon observed in a single-stage Orbitrap mass spectrometer coupled to an electrospray interfaced liquid chromatograph. Rapid Communications in Mass Spectrometry 24(14), 2162-2170.

Keen, O.S., Ferrer, I., Michael Thurman, E. and Linden, K.G. (2014) Degradation pathways of lamotrigine under advanced treatment by direct UV photolysis, hydroxyl radicals, and ozone. Chemosphere 117(0), 316-323.

Kern, S., Fenner, K., Singer, H.P., Schwarzenbach, R.P. and Hollender, J. (2009) Identification of transformation products of organic contaminants in natural waters by computer-aided prediction and high-resolution mass spectrometry. Environmental Science and Technology 43(18), 7039-7046.

Kind, T. and Fiehn, O. (2007) Seven Golden Rules for heuristic filtering of molecular formulas obtained by accurate mass spectrometry. BMC Bioinformatics 8, 105-105.

Klavarioti, M., Mantzavinos, D. and Kassinos, D. (2009) Removal of residual pharmaceuticals from aqueous systems by advanced oxidation processes. Environment International 35(2), 402-417.

Kleinman, M.H., Baertschi, S.W., Alsante, K.M., Reid, D.L., Mowery, M.D., Shimanovich, R., Foti, C., Smith, W.K., Reynolds, D.W., Nefliu, M. and Ott, M.A. (2014) In Silico Prediction of Pharmaceutical Degradation Pathways: A Benchmarking Study. Molecular Pharmaceutics 11(11), 4179-4188.

Kormos, J.L., Schulz, M., Kohler, H.P.E. and Ternes, T.A. (2010) Biotransformation of selected iodinated X-ray contrast media and characterization of microbial transformation pathways. Environmental Science and Technology 44(13), 4998-5007.

Kormos, J.L., Schulz, M. and Ternes, T.A. (2011) Occurrence of iodinated X-ray contrast media and their biotransformation products in the urban water cycle. Environmental Science and Technology 45(20), 8723-8732.

Kormos, J.L., Schulz, M., Wagner, M. and Ternes, T.A. (2009) Multistep approach for the structural identification of biotransformation products of iodinated X-ray contrast media by liquid chromatography/hybrid triple quadrupole linear ion trap mass spectrometry and 1H and 13C nuclear magnetic resonance. Analytical Chemistry 81(22), 9216-9224.

Kosjek, T., Negreira, N., de Alda, M.L. and Barcelo, D. (2015) Aerobic activated sludge transformation of methotrexate: identification of biotransformation products. Chemosphere 119 Suppl, S42-50.

Kosjek, T., Negreira, N., Heath, E., de Alda, M.L. and Barceló, D. (2016) Biodegradability of the anticancer drug etoposide and identification of the transformation products. Environmental Science and Pollution Research, 1-12.

Kosjek, T., Perko, S., Zupanc, M., Zanoski Hren, M., Landeka Dragicevic, T., Zigon, D., Kompare, B. and Heath, E. (2012) Environmental occurrence, fate and transformation of benzodiazepines in water treatment. Water Res 46(2), 355-368.

Kosjek, T., Zigon, D., Kralj, B. and Heath, E. (2008) The use of quadrupole-time-of-flight mass spectrometer for the elucidation of diclofenac biotransformation products in wastewater. J Chromatogr A 1215(1-2), 57-63.

Kovalova, L., Siegrist, H., von Gunten, U., Eugster, J., Hagenbuch, M., Wittmer, A., Moser, R. and McArdell, C.S. (2013) Elimination of Micropollutants during Post-Treatment of Hospital Wastewater with Powdered Activated Carbon, Ozone, and UV. Environ Sci Technol 47(14), 7899-7908.

Krasner, S.W., Mitch, W.A., McCurry, D.L., Hanigan, D. and Westerhoff, P. (2013) Formation, precursors, control, and occurrence of nitrosamines in drinking water: A review. Water Res 47(13), 4433-4450.

Krauss, M., Singer, H. and Hollender, J. (2010) LC-high resolution MS in environmental analysis: From target screening to the identification of unknowns. Analytical and Bioanalytical Chemistry 397(3), 943-951.

Krkošek, W.H., Koziar, S.A., White, R.L. and Gagnon, G.A. (2011) Identification of reaction products from reactions of free chlorine with the lipid-regulator gemfibrozil. Water Res 45(3), 1414-1422.

Kroutil, W., Mang, H., Edegger, K. and Faber, K. (2004) Biocatalytic oxidation of primary and secondary alcohols. Advanced Synthesis & Catalysis 346(2-3), 125-142.

Kumar, V., Johnson, A.C., Nakada, N., Yamashita, N. and Tanaka, H. (2012) De-conjugation behavior of conjugated estrogens in the raw sewage, activated sludge and river water. J Hazard Mater 227-228, 49-54.

Lam, M.W. and Mabury, S.A. (2005) Photodegradation of the pharmaceuticals atorvastatin, carbamazepine, levofloxacin, and sulfamethoxazole in natural waters. Aquatic Sciences 67(2), 177-188.

Lam, M.W., Young, C.J. and Mabury, S.A. (2005) Aqueous photochemical reaction kinetics and transformations of fluoxetine. Environmental Science and Technology 39(2), 513-522.

Le Roux, J., Gallard, H. and Croué, J.P. (2011) Chloramination of nitrogenous contaminants (pharmaceuticals and pesticides): NDMA and halogenated DBPs formation. Water Res 45(10), 3164-3174.

Lee, H.J., Lee, E., Yoon, S.H., Chang, H.R., Kim, K. and Kwon, J.H. (2012) Enzymatic and microbial transformation assays for the evaluation of the environmental fate of diclofenac and its metabolites. Chemosphere 87(8), 969-974.

Leendert, V., Van Langenhove, H. and Demeestere, K. (2015) Trends in liquid chromatography coupled to high-resolution mass spectrometry for multi-residue analysis of organic micropollutants in aquatic environments. TrAC Trends in Analytical Chemistry 67, 192-208.

Lester, Y., Ferrer, I., Thurman, E.M. and Linden, K.G. (2014) Demonstrating sucralose as a monitor of full-scale UV/AOP treatment of trace organic compounds. J Hazard Mater 280, 104-110.

Lin, A.Y.-C. and Reinhard, M. (2005) Photodegradation of common environmental pharmaceuticals and estrogens in river water. Environmental Toxicology and Chemistry 24(6), 1303-1309.

Lindberg, R.H., Fedorova, G., Blum, K.M., Pulit-Prociak, J., Gillman, A., Järhult, J., Appelblad, P. and Söderström, H. (2015) Online solid phase extraction liquid chromatography using bonded zwitterionic stationary phases and tandem mass spectrometry for rapid environmental trace analysis of highly polar hydrophilic compounds - Application for the antiviral drug Zanamivir. Talanta 141, 164-169.

Loos, R., Carvalho, R., António, D.C., Comero, S., Locoro, G., Tavazzi, S., Paracchini, B., Ghiani, M., Lettieri, T., Blaha, L., Jarosova, B., Voorspoels, S., Servaes, K., Haglund, P., Fick, J., Lindberg, R.H., Schwesig, D. and Gawlik, B.M. (2013) EU-wide monitoring survey on emerging polar organic contaminants in wastewater treatment plant effluents. Water Res 47(17), 6475-6487.

López-Serna, R., Kasprzyk-Hordern, B., Petrović, M. and Barceló, D. (2013) Multi-residue enantiomeric analysis of pharmaceuticals and their active metabolites in the Guadalquivir River basin (South Spain) by chiral liquid chromatography coupled with tandem mass spectrometry. Analytical and Bioanalytical Chemistry 405(18), 5859-5873.

López-Serna, R., Pérez, S., Ginebreda, A., Petrović, M. and Barceló, D. (2010) Fully automated determination of 74 pharmaceuticals in environmental and waste waters by online solid phase extraction–liquid chromatography-electrospray–tandem mass spectrometry. Talanta 83(2), 410-424.

Lopez, A., Mascolo, G., Ciannarella, R. and Tiravanti, G. (2001) Formation of volatile halogenated by-products during chlorination of isoproturon aqueous solutions. Chemosphere 45(3), 269-274.

Lu, W. and Uetrecht, J.P. (2007) Possible bioactivation pathways of lamotrigine. Drug Metab Dispos 35(7), 1050-1056.

Luft, A., Wagner, M. and Ternes, T.A. (2014) Transformation of biocides irgarol and terbutryn in the biological wastewater treatment. Environ Sci Technol 48(1), 244-254.

Macalady, D.L., Tratnyek, P.G. and Wolfe, N.L. (1988) Aquatic Humic Substances, pp. 323-332, American Chemical Society.

Makarov, A. and Scigelova, M. (2010) Coupling liquid chromatography to Orbitrap mass spectrometry. Journal of Chromatography A 1217(25), 3938-3945.

Malchi, T., Maor, Y., Tadmor, G., Shenker, M. and Chefetz, B. (2014) Irrigation of root vegetables with treated wastewater: evaluating uptake of pharmaceuticals and the associated human health risks. Environ Sci Technol 48(16), 9325-9333.

Manning, C.O., Wadsworth, A.H. and Fellows, I. (2002) Synthesis of stable isotopically labelled versions of Lamotrigine and its methylated metabolite. Journal of Labelled Compounds and Radiopharmaceuticals 45(7), 611-618.

Masia, A., Campo, J., Blasco, C. and Pico, Y. (2014) Ultra-high performance liquid chromatography-quadrupole time-of-flight mass spectrometry to identify contaminants in water: an insight on environmental forensics. J Chromatogr A 1345, 86-97.

MassBank (2016) http://www.massbank.jp/?lang=en.

MassFrontier (2016) http://www.highchem.com/index.php/massfrontier.

Meteor (2016) Meteor Nexus (https://www.lhasalimited.org/products/meteor-nexus.htm).

Moschet, C., Piazzoli, A., Singer, H. and Hollender, J. (2013) Alleviating the reference standard dilemma using a systematic exact mass suspect screening approach with liquid chromatography-high resolution mass spectrometry. Analytical Chemistry 85(21), 10312-10320.

MZmine_2 (2016) http://mzmine.github.io/.

Negreira, N., López de Alda, M. and Barceló, D. (2015a) Degradation of the cytostatic etoposide in chlorinated water by liquid chromatography coupled to quadrupole-Orbitrap mass spectrometry: Identification and quantification of by-products in real water samples. Science of The Total Environment 506-507, 36-45.

Negreira, N., Mastroianni, N., Lopez de Alda, M. and Barcelo, D. (2013) Multianalyte determination of 24 cytostatics and metabolites by liquid chromatography-electrospray-tandem mass spectrometry and study of their stability and optimum storage conditions in aqueous solution. Talanta 116, 290-299.

Negreira, N., Regueiro, J., López de Alda, M. and Barceló, D. (2015b) Degradation of the anticancer drug erlotinib during water chlorination: Non-targeted approach for the identification of transformation products. Water Res 85, 103-113.

Negreira, N., Regueiro, J., López de Alda, M. and Barceló, D. (2015c) Transformation of tamoxifen and its major metabolites during water chlorination: Identification and in silico toxicity assessment of their disinfection byproducts. Water Res 85, 199-207.

Negreira, N., Regueiro, J., López de Alda, M. and Barceló, D. (2016) Reactivity of vinca alkaloids during water chlorination processes: Identification of their disinfection by-products by high-resolution quadrupole-Orbitrap mass spectrometry. Science of The Total Environment 544, 635-644.

Nidzworski, D., Dobkowska, J., Holysz, M., Gromadzka, B. and Szewczyk, B. (2014) A multiplex real-time PCR assay for detection of oseltamivir-resistant strains of influenza virus. Open Life Sciences 9(6), 628-633.

Nikolaou, A., Meric, S. and Fatta, D. (2007) Occurrence patterns of pharmaceuticals in water and wastewater environments. Analytical and Bioanalytical Chemistry 387(4), 1225-1234.

Noblet, J.A., Smith, L.A. and Suffet, I.H. (1996) Influence of Natural Dissolved Organic Matter, Temperature, and Mixing on the Abiotic Hydrolysis of Triazine and Organophosphate Pesticides. J Agric Food Chem 44(11), 3685-3693.

Nödler, K., Licha, T., Barbieri, M. and Pérez, S. (2012) Evidence for the microbially mediated abiotic formation of reversible and non-reversible sulfamethoxazole transformation products during denitrification. Water Res 46(7), 2131-2139.

Nováková, L., Vlčková, H. and Petr, S. (2012) Evaluation of new mixed-mode UHPLC stationary phases and the importance of stationary phase choice when using low ionic-strength mobile phase additives. Talanta 93, 99-105.

Núñez, O., Gallart-Ayala, H., Martins, C.P.B. and Lucci, P. (2012) New trends in fast liquid chromatography for food and environmental analysis. Journal of Chromatography A 1228, 298-323.

OECD-Test-N°111 Test No. 111: Hydrolysis as a Function of pH, OECD Publishing.

OECD-Test-N°301 Test No. 301: Ready Biodegradability, OECD Publishing.

OECD-Test-N°302B Test No. 302B: Inherent Biodegradability: Zahn-Wellens/ EVPA Test, OECD Publishing.

OECD (2016) OECD - The Organisation for Economic Co-operation and Development (www.oecd.org).

Ohman, I., Beck, O., Vitols, S. and Tomson, T. (2008) Plasma concentrations of lamotrigine and its 2-N-glucuronide metabolite during pregnancy in women with epilepsy. Epilepsia 49(6), 1075-1080.

Oller, I., Malato, S. and Sánchez-Pérez, J. (2011) Combination of advanced oxidation processes and biological treatments for wastewater decontamination—a review. Science of The Total Environment 409(20), 4141-4166.

Ort, C., Lawrence, M.G., Reungoat, J. and Mueller, J.F. (2010a) Sampling for PPCPs in wastewater systems: Comparison of different sampling modes and optimization strategies. Environmental Science and Technology 44(16), 6289-6296.

Ort, C., Lawrence, M.G., Rieckermann, J. and Joss, A. (2010b) Sampling for pharmaceuticals and personal care products (PPCPs) and illicit drugs in wastewater systems: Are your conclusions valid? A critical review. Environmental Science and Technology 44(16), 6024-6035.

Osorio, V. (2015) Fate, modelling and risk of pharmaceuticals in wastewater treatment plants and Iberian rivers. Universitat de Barcelona.

Osorio, V., Imbert-Bouchard, M., Zonja, B., Abad, J.L., Perez, S. and Barcelo, D. (2014) Simultaneous determination of diclofenac, its human metabolites and microbial nitration/nitrosation transformation products in wastewaters by liquid chromatography/quadrupole-linear ion trap mass spectrometry. J Chromatogr A 1347, 63-71.

Padilla-Sanchez, J.A., Michael Thurman, E., Plaza-Bolanos, P. and Ferrer, I. (2012) Identification of pesticide transformation products in agricultural soils using liquid chromatography/quadrupole-time-of-flight mass spectrometry. Rapid Commun Mass Spectrom 26(9), 1091-1099.

Paíga, P., Lolić, A., Hellebuyck, F., Santos, L.H.M.L.M., Correia, M. and Delerue-Matos, C. (2015) Development of a SPE–UHPLC–MS/MS methodology for the determination of non-steroidal anti-inflammatory and analgesic pharmaceuticals in seawater. J Pharm Biomed Anal 106, 61-70.

Pan, C., Liu, F., Ji, Q., Wang, W., Drinkwater, D. and Vivilecchia, R. (2006) The use of LC/MS, GC/MS, and LC/NMR hyphenated techniques to identify a drug degradation product in pharmaceutical development. J Pharm Biomed Anal 40(3), 581-590.

Panditi, V.R., Batchu, S.R. and Gardinali, P.R. (2013) Online solid-phase extraction–liquid chromatography–electrospray–tandem mass spectrometry determination of multiple classes of antibiotics in environmental and treated waters. Analytical and Bioanalytical Chemistry 405(18), 5953-5964.

PathPred (2016) PathPred: Pathway Prediction server (http://www.genome.jp/tools/pathpred/).

Pavlović, D.M., Babić, S., Horvat, A.J. and Kaštelan-Macan, M. (2007) Sample preparation in analysis of pharmaceuticals. TrAC Trends in Analytical Chemistry 26(11), 1062-1075.

Pellecchia, M., Sem, D.S. and Wuthrich, K. (2002) Nmr in drug discovery. Nat Rev Drug Discov 1(3), 211-219.

Pérez-Carrera, E., Hansen, M., León, V.M., Björklund, E., Krogh, K.A., Halling-Sørensen, B. and González-Mazo, E. (2010) Multiresidue method for the determination of 32 human and veterinary pharmaceuticals in soil and sediment by pressurized-liquid extraction and LC-MS/MS. Analytical and Bioanalytical Chemistry 398(3), 1173-1184.

Pérez-Parada, A., Agüera, A., Gómez-Ramos, M.d.M., García-Reyes, J.F., Heinzen, H. and Fernández-Alba, A.R. (2011) Behavior of amoxicillin in wastewater and river water: identification of its main transformation products by liquid chromatography/electrospray quadrupole time-of-flight mass spectrometry. Rapid Communications in Mass Spectrometry 25(6), 731-742.

Pérez, S. and Barceló, D. (2007a) Application of advanced MS techniques to analysis and identification of human and microbial metabolites of pharmaceuticals in the aquatic environment. TrAC - Trends in Analytical Chemistry 26(6), 494-514.

Pérez, S. and Barceló, D. (2007b) Fate and occurrence of X-ray contrast media in the environment. Analytical and Bioanalytical Chemistry 387(4), 1235-1246.

Pérez, S. and Barceló, D. (2008) First Evidence for Occurrence of Hydroxylated Human Metabolites of Diclofenac and Aceclofenac in Wastewater Using QqLIT-MS and QqTOF-MS. Analytical Chemistry 80(21), 8135-8145.

Perez, S., Eichhorn, P., Ceballos, V. and Barcelo, D. (2009) Elucidation of phototransformation reactions of the X-ray contrast medium iopromide under simulated solar radiation using UPLC-ESI-QqTOF-MS. J Mass Spectrom 44(9), 1308-1317.

Pérez, S., Eichhorn, P., Celiz, M.D. and Aga, D.S. (2006) Structural characterization of metabolites of the X-ray contrast agent iopromide in activated sludge using ion trap mass spectrometry. Analytical Chemistry 78(6), 1866-1874.

Pérez, S., Petrovic, M. and Barceló, D. (2008) Transformation Products of Synthetic Chemicals in the Environment, pp. 43-81, Springer.

Petrie, B., Youdan, J., Barden, R. and Kasprzyk-Hordern, B. (2016) Multi-residue analysis of 90 emerging contaminants in liquid and solid environmental matrices by ultra-high-performance liquid chromatography tandem mass spectrometry. Journal of Chromatography A 1431, 64-78.

Petrovic, M., Farré, M., De Alda, M.L., Perez, S., Postigo, C., Köck, M., Radjenovic, J., Gros, M. and Barcelo, D. (2010) Recent trends in the liquid chromatography–mass spectrometry analysis of organic contaminants in environmental samples. Journal of Chromatography A 1217(25), 4004-4017.

Petrovic, M., Petrovic, M. and Barceló, D. (2007) LC-MS for identifying photodegradation products of pharmaceuticals in the environment. TrAC Trends in Analytical Chemistry 26(6), 486-493.

Plewa, M.J., Wagner, E.D., Richardson, S.D., Thruston Jr, A.D., Woo, Y.T. and McKague, A.B. (2004) Chemical and biological characterization of newly discovered iodoacid drinking water disinfection byproducts. Environmental Science and Technology 38(18), 4713-4722.

Postigo, C. and Richardson, S.D. (2014) Transformation of pharmaceuticals during oxidation/disinfection processes in drinking water treatment. J Hazard Mater 279, 461-475.

Postigo, C., Sirtori, C., Oller, I., Malato, S., Maldonado, M.I., Lopez de Alda, M. and Barcelo, D. (2011a) Photolytic and photocatalytic transformation of methadone in aqueous solutions under solar irradiation: kinetics, characterization of major intermediate products and toxicity evaluation. Water Res 45(16), 4815-4826.

Postigo, C., Sirtori, C., Oller, I., Malato, S., Maldonado, M.I., López de Alda, M. and Barceló, D. (2011b) Solar transformation and photocatalytic treatment of cocaine in water: Kinetics, characterization of major intermediate products and toxicity evaluation. Applied Catalysis B: Environmental 104(1-2), 37-48.

Prakash, C., Shaffer, C.L. and Nedderman, A. (2007) Analytical strategies for identifying drug metabolites. Mass spectrometry reviews 26(3), 340-369.

Prasse, C., Schlüsener, M.P., Schulz, R. and Ternes, T.A. (2010) Antiviral drugs in wastewater and surface waters: a new pharmaceutical class of environmental relevance? Environ Sci Technol 44(5), 1728-1735.

Prasse, C., Wagner, M., Schulz, R. and Ternes, T.A. (2011) Biotransformation of the antiviral drugs acyclovir and penciclovir in activated sludge treatment. Environmental Science and Technology 45(7), 2761-2769.

PubChem (2016) PubChem open chemistry database (https://pubchem.ncbi.nlm.nih.gov/).

Putschew, A., Wischnack, S. and Jekel, M. (2000) Occurrence of triiodinated X-ray contrast agents in the aquatic environment. Science of The Total Environment 255(1–3), 129-134.

Quintana, J.B., Rodil, R., López-Mahía, P., Muniategui-Lorenzo, S. and Prada-Rodríguez, D. (2010) Investigating the chlorination of acidic pharmaceuticals and by-product formation aided by an experimental design methodology. Water Res 44(1), 243-255.

Radjenovic, J., Flexer, V., Donose, B.C., Sedlak, D.L. and Keller, J. (2013) Removal of the X-ray Contrast Media Diatrizoate by Electrochemical Reduction and Oxidation. Environ Sci Technol 47(23), 13686-13694.

Radjenović, J., Pérez, S., Petrović, M. and Barceló, D. (2008) Identification and structural characterization of biodegradation products of atenolol and glibenclamide by liquid chromatography coupled to hybrid quadrupole time-of-flight and quadrupole ion trap mass spectrometry. Journal of Chromatography A 1210(2), 142-153.

Radjenovic, J. and Petrovic, M. (2016) Sulfate-mediated electrooxidation of X-ray contrast media on boron-doped diamond anode. Water Res 94, 128-135.

Radke, M. and Maier, M.P. (2014) Lessons learned from water/sediment-testing of pharmaceuticals. Water Res 55, 63-73.

Ramsay, R.E., Pellock, J.M., Garnett, W.R., Sanchez, R.M., Valakas, A.M., Wargin, W.A., Lai, A.A., Hubbell, J., Chern, W.H., Allsup, T. and Otto, V. (1991) Pharmacokinetics and safety of lamotrigine (Lamictal®) in patients with epilepsy. Epilepsy Research 10(2–3), 191-200.

Rastogi, T., Leder, C. and Kummerer, K. (2014) Qualitative environmental risk assessment of photolytic transformation products of iodinated X-ray contrast agent diatrizoic acid. Sci Total Environ 482-483, 378-388.

Rastogi, T., Leder, C. and Kümmerer, K. (2015) Re-Designing of Existing Pharmaceuticals for Environmental Biodegradability: A Tiered Approach with β-Blocker Propranolol as an Example. Environmental Science and Technology 49(19), 11756-11763.

Redeker, M., Wick, A., Meermann, B. and Ternes, T.A. (2014) Removal of the Iodinated X-ray Contrast Medium Diatrizoate by Anaerobic Transformation. Environ Sci Technol 48(17), 10145-10154.

Renzette, N., Caffrey, D.R., Zeldovich, K.B., Liu, P., Gallagher, G.R., Aiello, D., Porter, A.J., Kurt-Jones, E.A., Bolon, D.N. and Poh, Y.-P. (2014) Evolution of the influenza A virus genome during development of oseltamivir resistance in vitro. Journal of virology 88(1), 272-281.

Richardson, S.D. (2005) New disinfection by-product issues: emerging DBPs and alternative routes of exposure. Global Nest 7(1), 43-60.

Richardson, S.D. (2009) Water analysis: emerging contaminants and current issues. Analytical Chemistry 81(12), 4645-4677.

Richardson, S.D. (2011) Environmental mass spectrometry: emerging contaminants and current issues. Analytical Chemistry 84(2), 747-778.

Richardson, S.D., Fasano, F., Ellington, J.J., Crumley, F.G., Buettner, K.M., Evans, J.J., Blount, B.C., Silva, L.K., Waite, T.J., Luther, G.W., McKague, A.B., Miltner, R.J., Wagner, E.D. and Plewa, M.J. (2008) Occurrence and mammalian cell toxicity of iodinated disinfection byproducts in drinking water. Environmental Science and Technology 42(22), 8330-8338.

Richardson, S.D., Plewa, M.J., Wagner, E.D., Schoeny, R. and DeMarini, D.M. (2007) Occurrence, genotoxicity, and carcinogenicity of regulated and emerging disinfection by-products in drinking water: A review and roadmap for research. Mutation Research - Reviews in Mutation Research 636(1-3), 178-242.

Richardson, S.D. and Ternes, T.A. (2011) Water analysis: Emerging contaminants and current issues. Analytical Chemistry 83(12), 4616-4648.

Richardson, S.D. and Ternes, T.A. (2014) Water analysis: emerging contaminants and current issues. Analytical Chemistry 86(6), 2813-2848.

Rodriguez-Aller, M., Gurny, R., Veuthey, J.-L. and Guillarme, D. (2013) Coupling ultra high-pressure liquid chromatography with mass spectrometry: constraints and possible applications. Journal of Chromatography A 1292, 2-18.

Rodriguez-Caballero, A. and Pijuan, M. (2013) N 2 O and NO emissions from a partial nitrification sequencing batch reactor: exploring dynamics, sources and minimization mechanisms. Water Res 47(9), 3131-3140.

Rosenfeldt, E.J. and Linden, K.G. (2004) Degradation of Endocrine Disrupting Chemicals Bisphenol A, Ethinyl Estradiol, and Estradiol during UV Photolysis and Advanced Oxidation Processes. Environ Sci Technol 38(20), 5476-5483.

Rubirola, A., Llorca, M., Rodriguez-Mozaz, S., Casas, N., Rodriguez-Roda, I., Barcelo, D. and Buttiglieri, G. (2014) Characterization of metoprolol biodegradation and its transformation products generated in activated sludge batch experiments and in full scale WWTPs. Water Res 63, 21-32.

Sanderson, H., Johnson, D.J., Reitsma, T., Brain, R.A., Wilson, C.J. and Solomon, K.R. (2004) Ranking and prioritization of environmental risks of pharmaceuticals in surface waters. Regul Toxicol Pharmacol 39(2), 158-183.

Saracino, M.A., Bugamelli, F., Conti, M., Amore, M. and Raggi, M.A. (2007) Rapid HPLC analysis of the antiepileptic lamotrigine and its metabolites in human plasma. J Sep Sci 30(14), 2249-2255.

Schollée, J.E., Schymanski, E.L., Avak, S.E., Loos, M. and Hollender, J. (2015) Prioritizing Unknown Transformation Products from Biologically-Treated Wastewater Using High-Resolution Mass Spectrometry, Multivariate Statistics, and Metabolic Logic. Analytical Chemistry 87(24), 12121-12129.

Schulz, M., Löffler, D., Wagner, M. and Ternes, T.A. (2008) Transformation of the X-ray Contrast Medium Iopromide In Soil and Biological Wastewater Treatment. Environ Sci Technol 42(19), 7207-7217.

Schürmann, A., Dvorak, V., Crüzer, C., Butcher, P. and Kaufmann, A. (2009) False-positive liquid chromatography/tandem mass spectrometric confirmation of sebuthylazine residues using the identification points system according to EU directive 2002/657/EC due to a biogenic insecticide in tarragon. Rapid Communications in Mass Spectrometry 23(8), 1196-1200.

Schymanski, E.L., Jeon, J., Gulde, R., Fenner, K., Ruff, M., Singer, H.P. and Hollender, J. (2014a) Identifying small molecules via high resolution mass spectrometry: Communicating confidence. Environmental Science and Technology 48(4), 2097-2098.

Schymanski, E.L., Singer, H.P., Longree, P., Loos, M., Ruff, M., Stravs, M.A., Ripolles Vidal, C. and Hollender, J. (2014b) Strategies to characterize polar organic contamination in wastewater: exploring the capability of high resolution mass spectrometry. Environ Sci Technol 48(3), 1811-1818.

Seitz, W., Jiang, J.-Q., Schulz, W., Weber, W.H., Maier, D. and Maier, M. (2008) Formation of oxidation by-products of the iodinated X-ray contrast medium iomeprol during ozonation. Chemosphere 70(7), 1238-1246.

Seitz, W., Weber, W.H., Jiang, J.-Q., Lloyd, B.J., Maier, M., Maier, D. and Schulz, W. (2006) Monitoring of iodinated X-ray contrast media in surface water. Chemosphere 64(8), 1318-1324.

Shen, R. and Andrews, S.A. (2011) Demonstration of 20 pharmaceuticals and personal care products (PPCPs) as nitrosamine precursors during chloramine disinfection. Water Res 45(2), 944-952.

Sidhu, J., Job, S., Bullman, J., Francis, E., Abbott, R., Ascher, J. and Theis, J.G.W. (2006) Pharmacokinetics and tolerability of lamotrigine and olanzapine coadministered to healthy subjects. Br J Clin Pharmacol 61(4), 420-426.

Singer, A.C., Nunn, M.A., Gould, E.A. and Johnson, A.C. (2007) Potential risks associated with the proposed widespread use of Tamiflu. Environmental Health Perspectives, 102-106.

Singer, H.P., Wössner, A.E., McArdell, C.S. and Fenner, K. (2016) Rapid Screening for Exposure to "Non-Target" Pharmaceuticals from Wastewater Effluents by Combining HRMS-Based Suspect Screening and Exposure Modeling. Environ Sci Technol.

Sinz, M.W. and Remmel, R.P. (1991) Isolation and characterization of a novel quaternary ammonium-linked glucuronide of lamotrigine. Drug Metabolism and Disposition 19(1), 149-153.

Slater, F.R., Singer, A.C., Turner, S., Barr, J.J. and Bond, P.L. (2011) Pandemic pharmaceutical dosing effects on wastewater treatment: no adaptation of activated sludge bacteria to degrade the antiviral drug Oseltamivir (Tamiflu®) and loss of nutrient removal performance. FEMS microbiology letters 315(1), 17-22.

Song, W., Chen, W., Cooper, W.J., Greaves, J. and Miller, G.E. (2008) Free-Radical Destruction of β-Lactam Antibiotics in Aqueous Solution. The Journal of Physical Chemistry A 112(32), 7411-7417.

Soufan, M., Deborde, M. and Legube, B. (2012) Aqueous chlorination of diclofenac: Kinetic study and transformation products identification. Water Res 46(10), 3377-3386.

Spraul, M., Freund, A.S., Nast, R.E., Withers, R.S., Maas, W.E. and Corcoran, O. (2003) Advancing NMR Sensitivity for LC-NMR-MS Using a Cryoflow Probe: Application to the Analysis of Acetaminophen Metabolites in Urine. Analytical Chemistry 75(6), 1536-1541.

Statista (2016) Statista - The portal for statistics (https://www.statista.com/).

Steger-Hartmann, T., Länge, R., Schweinfurth, H., Tschampel, M. and Rehmann, I. (2002) Investigations into the environmental fate and effects of iopromide (ultravist), a widely used iodinated X-ray contrast medium. Water Res 36(1), 266-274.

Stierlin, H. and Faigle, J. (1979) Biotransformation of Diclofenac Sodium (Voltaren®) in Animals and in Man.: II. Quantitative determination of the unchanged drug and principal phenolic metabolites, in urine and bile. Xenobiotica 9(10), 611-621.

Stierlin, H., Faigle, J., Sallmann, A., Kung, W., Richter, W., Kriemler, H.-P., Alt, K. and Winkler, T. (1979) Biotransformation of diclofenac sodium (Voltaren®) in animals and in man: I. Isolation and identification of principal metabolites. Xenobiotica 9(10), 601-610.

Stokes, J.M., Davis, J.H., Mangat, C.S., Williamson, J.R. and Brown, E.D. (2014) Discovery of a small molecule that inhibits bacterial ribosome biogenesis. eLife 3, e03574.

Sturini, M., Speltini, A., Maraschi, F., Profumo, A., Pretali, L., Irastorza, E.A., Fasani, E. and Albini, A. (2012) Photolytic and photocatalytic degradation of fluoroquinolones in untreated river water under natural sunlight. Applied Catalysis B: Environmental 119–120, 32-39.

Suárez, S., Carballa, M., Omil, F. and Lema, J.M. (2008) How are pharmaceutical and personal care products (PPCPs) removed from urban wastewaters? Reviews in Environmental Science and Biotechnology 7(2), 125-138.

Suárez, S., Ramil, M., Omil, F. and Lema, J.M. (2005) Removal of pharmaceutically active compounds in nitrifying-denitrifying plants, pp. 9-14.

Taewoo, Y., Willie, F.H. and Tamara, F.-S. (2007) Fate of Pharmaceuticals in the Environment and in Water Treatment Systems, pp. 349-361, CRC Press.

Takanami, R., Ozaki, H., GIRI, R.R., Taniguchi, S. and Hayashi, S. (2012) Antiviral drugs zanamivir and oseltamivir found in wastewater and surface water in Osaka, Japan. Journal of Water and Environment Technology 10(1), 57-68.

Teixeira, S., Gurke, R., Eckert, H., Kühn, K., Fauler, J. and Cuniberti, G. (2016) Photocatalytic degradation of pharmaceuticals present in conventional treated wastewater by nanoparticle suspensions. Journal of Environmental Chemical Engineering 4(1), 287-292.

Ternes, T.A. (1998) Occurrence of drugs in German sewage treatment plants and rivers. Water Res 32(11), 3245-3260.

Ternes, T.A. and Hirsch, R. (2000) Occurrence and Behavior of X-ray Contrast Media in Sewage Facilities and the Aquatic Environment. Environ Sci Technol 34(13), 2741-2748.

Ternes, T.A., Stüber, J., Herrmann, N., McDowell, D., Ried, A., Kampmann, M. and Teiser, B. (2003) Ozonation: a tool for removal of pharmaceuticals, contrast media and musk fragrances from wastewater? Water Res 37(8), 1976-1982.

Tian, F.X., Xu, B., Lin, Y.L., Hu, C.Y., Zhang, T.Y. and Gao, N.Y. (2014) Photodegradation kinetics of iopamidol by UV irradiation and enhanced formation of iodinated disinfection by-products in sequential oxidation processes. Water Res 58, 198-208.

Togunde, O.P., Oakes, K.D., Servos, M.R. and Pawliszyn, J. (2012) Determination of pharmaceutical residues in fish bile by solid-phase microextraction couple with liquid chromatography-tandem mass spectrometry (LC/MS/MS). Environ Sci Technol 46(10), 5302-5309.

Tong, L., Eichhorn, P., Perez, S., Wang, Y. and Barcelo, D. (2011) Photodegradation of azithromycin in various aqueous systems under simulated and natural solar radiation: kinetics and identification of photoproducts. Chemosphere 83(3), 340-348.

Tozuka, Z., Kaneko, H., Shiraga, T., Mitani, Y., Beppu, M., Terashita, S., Kawamura, A. and Kagayama, A. (2003) Strategy for structural elucidation of drugs and drug metabolites using (MS) n fragmentation in an electrospray ion trap. Journal of Mass Spectrometry 38(8), 793-808.

Trautwein, C. and Kummerer, K. (2011) Incomplete aerobic degradation of the antidiabetic drug Metformin and identification of the bacterial dead-end transformation product Guanylurea. Chemosphere 85(5), 765-773.

Trautwein, C. and Kümmerer, K. (2012) Degradation of the tricyclic antipsychotic drug chlorpromazine under environmental conditions, identification of its main aquatic biotic and abiotic transformation products by LC–MSn and their effects on environmental bacteria. Journal of Chromatography B 889–890, 24-38.

Trautwein, C., Kummerer, K. and Metzger, J.W. (2008) Aerobic biodegradability of the calcium channel antagonist verapamil and identification of a microbial dead-end transformation product studied by LC-MS/MS. Chemosphere 72(3), 442-450.

Trovo, A.G., Nogueira, R.F., Aguera, A., Sirtori, C. and Fernandez-Alba, A.R. (2009) Photodegradation of sulfamethoxazole in various aqueous media: persistence, toxicity and photoproducts assessment. Chemosphere 77(10), 1292-1298.

UM-PPS (2016) University of Minnesota Pathway Prediction System (EAWAG Biocatalysis/Biodegradation Database) (http://eawag-bbd.ethz.ch/).

Upton, R., Buskin, J., Williams, R., Holford, N. and Riegelman, S. (1980) Negligible excretion of unchanged ketoprofen, naproxen, and probenecid in urine. Journal of pharmaceutical sciences 69(11), 1254-1257.

USP (2016) United States Pharmacopeia (USP) (http://www.usp.org/sites/default/files/usp_pdf/EN/USPNF/revisions/lamotrigine_tablets.pdf).

van Leerdam, J.A., Vervoort, J., Stroomberg, G. and de Voogt, P. (2014) Identification of Unknown Microcontaminants in Dutch River Water by Liquid Chromatography-High Resolution Mass Spectrometry and Nuclear Magnetic Resonance Spectroscopy. Environ Sci Technol 48(21), 12791-12799.

Vergeynst, L., Langenhove, H., Joos, P. and Demeestere, K. (2014) Suspect screening and target quantification of multi-class pharmaceuticals in surface water based on large-volume injection liquid chromatography and time-of-flight mass spectrometry. Analytical and Bioanalytical Chemistry 406(11), 2533-2547.

Volmajer, J., Toplak, R., Bittner, S., Leban, I. and Le Marechal, A.M. (2003) Novel N-chlorinated derivatives of 2H-1-benzopyran-2-imines. Tetrahedron Letters 44(11), 2363-2366.

Wang, P., He, Y.L. and Huang, C.H. (2010) Oxidation of fluoroquinolone antibiotics and structurally related amines by chlorine dioxide: Reaction kinetics, product and pathway evaluation. Water Res 44(20), 5989-5998.

Watanabe, Y., Bach, L.T., Dinh, P., Prudente, M., Aguja, S., Phay, N. and Nakata, H. (2015) Ubiquitous Detection of Artificial Sweeteners and Iodinated X-ray Contrast Media in Aquatic Environmental and Wastewater Treatment Plant Samples from Vietnam, The Philippines, and Myanmar. Archives of Environmental Contamination and Toxicology, 1-11.

West, C.E. and Rowland, S.J. (2012) Aqueous Phototransformation of Diazepam and Related Human Metabolites under Simulated Sunlight. Environ Sci Technol 46(9), 4749-4756.

Whitacre, D.M. (2012) Reviews of environmental contamination and toxicology, Springer.

Wick, A., Wagner, M. and Ternes, T.A. (2011) Elucidation of the transformation pathway of the opium alkaloid codeine in biological wastewater treatment. Environmental Science and Technology 45(8), 3374-3385.

Wille, K., Noppe, H., Verheyden, K., Vanden Bussche, J., De Wulf, E., Van Caeter, P., Janssen, C.R., De Brabander, H.F. and Vanhaecke, L. (2010) Validation and application of an LC-MS/MS method for the simultaneous quantification of 13 pharmaceuticals in seawater. Analytical and Bioanalytical Chemistry 397(5), 1797-1808.

Willett, K.L. and Hites, R.A. (2000) Chemical Actinometry: Using o-Nitrobenzaldehyde to Measure Light Intensity in Photochemical Experiments. J Chem Educ 77(7), 900-902.

Woche, M., Scheibe, N., von Tümpling, W. and Schwidder, M. (2016) Degradation of the antiviral drug zanamivir in wastewater - The potential of a photocatalytic treatment process. Chemical Engineering Journal 287, 674-679.

Wols, B.A. and Hofman-Caris, C.H.M. (2012) Review of photochemical reaction constants of organic micropollutants required for UV advanced oxidation processes in water. Water Res 46(9), 2815-2827.

Writer, J.H., Antweiler, R.C., Ferrer, I., Ryan, J.N. and Thurman, E.M. (2013a) In-stream attenuation of neuro-active pharmaceuticals and their metabolites. Environ Sci Technol 47(17), 9781-9790.

Writer, J.H., Ferrer, I., Barber, L.B. and Thurman, E.M. (2013b) Widespread occurrence of neuro-active pharmaceuticals and metabolites in 24 Minnesota rivers and wastewaters. Sci Total Environ 461-462, 519-527.

Yan, S. and Song, W. (2014) Photo-transformation of pharmaceutically active compounds in the aqueous environment: a review. Environmental Science: Processes & Impacts 16(4), 697-720.

Yoon, Y., Ryu, J., Oh, J., Choi, B.-G. and Snyder, S.A. (2010) Occurrence of endocrine disrupting compounds, pharmaceuticals, and personal care products in the Han River (Seoul, South Korea). Science of The Total Environment 408(3), 636-643.

Young, R.B., Chefetz, B., Liu, A., Desyaterik, Y. and Borch, T. (2014) Direct photodegradation of lamotrigine (an antiepileptic) in simulated sunlight--pH influenced rates and products. Environ Sci Process Impacts 16(4), 848-857.

Yuan, S., Jiang, X., Xia, X., Zhang, H. and Zheng, S. (2013) Detection, occurrence and fate of 22 psychiatric pharmaceuticals in psychiatric hospital and municipal wastewater treatment plants in Beijing, China. Chemosphere 90(10), 2520-2525.

Zeneth (2016) Zeneth software (https://www.lhasalimited.org/products/zeneth.htm).

Zhang, H., Xie, H., Chen, J. and Zhang, S. (2015) Prediction of Hydrolysis Pathways and Kinetics for Antibiotics under Environmental pH Conditions: A Quantum Chemical Study on Cephradine. Environ Sci Technol 49(3), 1552-1558.

Zhao, C., Arroyo-Mora, L.E., DeCaprio, A.P., Sharma, V.K., Dionysiou, D.D. and O'Shea, K.E. (2014) Reductive and oxidative degradation of iopamidol, iodinated X-ray contrast media, by Fe(III)-oxalate under UV and visible light treatment. Water Res 67, 144-153.

Zhu, B., Zonja, B., Gonzalez, O., Sans, C., Pérez, S., Barceló, D., Esplugas, S., Xu, K. and Qiang, Z. (2015) Degradation kinetics and pathways of three calcium channel blockers under UV irradiation. Water Res 86, 9-16.

Zonja, B., Aceña, J., Jelic, A., Petrovic, M., Pérez Solsona, S. and Barceló, D. (2014a) Transformation Products of Emerging Contaminants in the Environment: Analysis, Processes, Occurrence, Effects and Risks. Nollet, D.A.L.a.L.M.L. (ed), pp. 303-324, John Wiley and Sons Ltd.

Zonja, B., Aceña, J., Pérez, S. and Barceló, D. (2013) Comprehensive Analytical Chemistry. Mira Petrovic, D.B. and Sandra, P. (eds), pp. 593-610, Elsevier.

Zonja, B., Delgado, A., Abad, J.L., Pérez, S. and Barceló, D. (2016a) Abiotic amidine and guanidine hydrolysis of lamotrigine-N2-glucuronide and related compounds in wastewater: The role of pH and N2-substitution on reaction kinetics. Water Res 100, 466-475.

Zonja, B., Delgado, A., Pérez, S. and Barceló, D. (2015) LC-HRMS Suspect Screening for Detection-Based Prioritization of Iodinated Contrast Media Photodegradates in Surface Waters. Environ Sci Technol 49(6), 3464-3472.

Zonja, B., Gonçalves, C., Perez, S., Delgado, A., Petrovic, M., Alpendurada, M.F. and Barcelo, D. (2014b) Evaluation of the phototransformation of the antiviral zanamivir in surface waters through identification of transformation products. J Hazard Mater 265, 296-304.

Zonja, B., Perez, S. and Barcelo, D. (2016b) Human Metabolite Lamotrigine-N(2)-glucuronide Is the Principal Source of Lamotrigine-Derived Compounds in Wastewater Treatment Plants and Surface Water. Environ Sci Technol 50(1), 154-164.

Zubarev, R.A. and Makarov, A. (2013) Orbitrap Mass Spectrometry. Analytical Chemistry 85(11), 5288-5296.

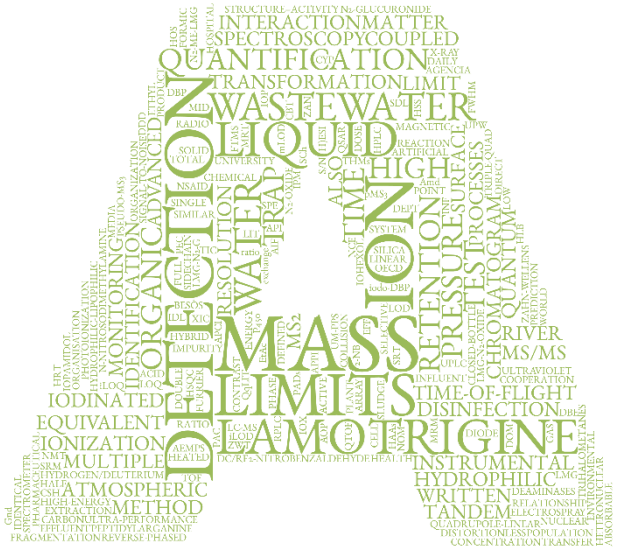

Annex (list of abbreviations)

List of Abbreviations

2-NB	2-NITROBENZALDEHYDE
AEMPS	AGENCIA ESPAÑOLA DE MEDICAMENTOS Y PRODUCTOS SANITARIOS
AFW	ARTIFICIAL FRESHWATER
AIF	ALL ION FRAGMENTATION
Amd	AMIDINE
AOP	ADVANCED OXIDATION PROCESSES
AOR	ADVANCED REDUCTION PROCESSES
AOX	ABSORBABLE ORGANIC HALOGENS
APCI	ATMOSPHERIC PRESSURE CHEMICAL IONIZATION
API	ACTIVE PHARMACEUTICAL INGREDIENT
APPI	ATMOSPHERIC PRESSURE PHOTOIONIZATION
bioTPs	BIOTRANSFORMATION PRODUCTS
BS	BESÒS RIVER
CBT	CLOSED-BOTTLE TEST
CSH	CHARGED SURFACE HYBRID
CYP	CYTOCHROME P450 MONOOXYDASE
DAD	DIODE ARRAY DETECTION
DBE	DOUBLE-BOND EQUIVALENT
DBP	DISINFECTION BY-PRODUCT
DC/RF	DIRECT CURRENT / RADIO FREQUENCY
DD	DATA DEPENDENT
DDD	DEFINED DAILY DOSE
DEPT	DISTORTIONLESS ENHANCEMENT BY POLARIZATION TRANSFER
DOM	DISSOLVED ORGANIC MATTER
DQCOSY	DOUBLE QUANTUM CORRELATION SPECTROSCOPY
DTZ	DIATRIZOATE
EFF	WASTEWATER EFFLUENT WATER
EtAc	ETHYL ACETATE
FA	FORMIC ACID
FTMS	FURRIER TRANSFORMATION MASS SPECTROMETRY
FWHM	FULL WIDTH AT HALF MAXIMUM
GC-MS	GAS CHROMATOGRAPHY COUPLED TO MASS SPECTROMETRY
Gnd	GUANIDINE
H/D exchange	HYDROGEN/DEUTERIUM EXCHANGE
HAAs	HALOACETIC ACIDS
HCD	HIGH-ENERGY COLLISIONAL DISSOCIATION CELL
(H)ESI	(HEATED) ELECTROSPRAY IONIZATION
HILIC	HYDROPHILIC INTERACTION LIQUID CHROMATOGRAPHY
HLB	HYDROPHILIC-LIPOPHILIC BALANCED

HOS	HOSPITAL
HPLC	HIGH PRESSURE LIQUID CHROMATOGRAPHY
HRMS	HIGH RESOLUTION MASS SPECTROMETRY
HRT	HYDRAULIC RETENTION TIME
HSQC	HETERONUCLEAR SINGLE QUANTUM COHERENCE SPECTROSCOPY
HSS	HIGH STRENGTH SILICA
ICM	IODINATED X-RAY CONTRAST MEDIA
ID	IDENTICAL
IDL	IDENTIFICATION DETECTION LIMITS
IDX	IODIXANOL
iLOD	INSTRUMENTAL LIMITS OF DETECTION
iLOQ	INSTRUMENTAL LIMITS OF QUANTIFICATION
IMP	IOMEPROL
INF	WASTEWATER INFLUENT WATER
iodo-DBP	IODINATED DISINFECTION BYPRODUCTS
IOP	IOPROMIDE
IOX	IOHEXOL
IP	IDENTIFICATION POINT
IPM	IOPAMIDOL
IT	ION TRAP
LC-MS	LIQUID CHROMATOGRAPHY COUPLED TO MASS SPECTROMETRY
LIT	LINEAR ION TRAP
LL	LLOBREGAT RIVER
LMG	LAMOTRIGINE
LMG-N2-G	LAMOTRIGINE N2-GLUCURONIDE
LMG-N2-OXIDE	LAMOTRIGINE N2-OXIDE
LOD	LIMIT OF DETECTION
LOQ	LIMIT OF QUANTIFICATION
LRMS	LOW RESOLUTION MASS SPECTROMETRY
MeOH	METHANOL
MID	MULTIPLE ION DETECTION
mLOD	METHOD LIMITS OF QUANTIFICATION
mLOQ	METHOD LIMITS OF DETECTION
MRM	MULTIPLE REACTIONS MONITORING
MRT	MANOMETRIC RESPIROMETRY TEST
MS^2	TANDEM MASS SPECTROMETRY (ALSO WRITTEN MS/MS)
MS/MS	TANDEM MASS SPECTROMETRY (ALSO WRITTEN MS^2)
N2-ME-LMG	N2-METHYL LAMOTRIGINE
NCE	NORMALISED COLLISION ENERGY
NDMA	N-NITROSODIMETHYLAMINE
NMR	NUCLEAR MAGNETIC RESONANCE
NMT	NOT MORE THAN
NOM	NATURAL ORGANIC MATTER
NSAID	HYDROPHILIC INTERACTION CHROMATOGRAPHY

OECD	ORGANIZATION FOR ECONOMIC COOPERATION AND DEVELOPMENT
OXO-LMG	LAMOTRIGINE IMPURITY A
PAC	POWDERED ACTIVATED CARBON
PADs	PEPTIDYLARGANINE DEAMINASES
PE	POPULATION EQUIVALENT
PEC	PREDICTED ENVIRONMENTAL CONCENTRATION
photoTPs	PHOTOTRANSFORMATION PRODUCTS
pMS^3	PSEUDO-MS^3
QSAR	QUANTITATIVE STRUCTURE–ACTIVITY RELATIONSHIP
QqLIT	QUADRUPOLE-LINEAR ION TRAP
QqQ	TRIPLE-QUAD MASS SPECTROMETER
QTOF	QUADRUPOLE TIME-OF-FLIGHT
RPLC	REVERSE-PHASED LIQUID CHROMATOGRAPHY
RT	RETENTION TIME
S/N ratio	SIGNAL-TO-NOISE RATIO
SCh	SIDECHAIN
SDL	SCREENING DETECTION LIMITS
SM	SIMILAR
SPE	SOLID PHASE EXTRACTION
SRM	SELECTIVE REACTION MONITORING
SRT	SLUDGE RETENTION TIME
SW	SURFACE WATER
THMs	TRIHALOMETANES
TIC	TOTAL ION CHROMATOGRAM
TOF	TIME-OF-FLIGHT
TP	TRANSFORMATION PRODUCT
UM-PPS	UNIVERSITY OF MINNESOTA PATHWAY PREDICTION SYSTEM
UPLC	ULTRA-PERFORMANCE LIQUID CHROMATOGRAPHY
UPW	ULTRAPURE WATER
UV	ULTRAVIOLET
WHO	WORLD HEALTH ORGANISATION
WW	WASTEWATER
WWTP	WASTEWATER TREATMENT PLANT
XIC	EXTRACTED ION CHROMATOGRAM
ZAN	ZANAMIVIR
ZWT	ZAHN-WELLENS TEST